Bulletin of the Geological Society of Denmark

VOLUME 73 | 2024 | COPENHAGEN

DGF

Bulletin of the Geological Society of Denmark

is published by the Geological Society of Denmark (DGF, Dansk Geologisk Forening), founded in 1893

The *Bulletin* publishes contributions of international interest in all fields of geological sciences on results of new work on material from Denmark, the Faroes and Greenland. Contributions based on foreign material may also be submitted to the Bulletin if the subject is relevant for the geology of the area of primary interest. The rate of publishing is one volume per year. All articles are published as pdf-files immediately after acceptance and technical production.

Scientific editing and reviewing are done on an unpaid collegial basis; technical production expenses are covered by the membership fees.

The bulletin is freely accessible on the web page of the Geological Society of Denmark:
www.2dgf.dk/publikationer/bulletin/index.html

Cover photo: Underwater photo of tufa columns from Ikka fjord. Columns are vertical and tilt is caused by camera distortion. Photo courtesy by Uli Kunz. See this volume pp. 135–156: Buchardt, B., Stockmann, G., Hansen, M.O. & Sveinbjörnsdóttir, Á.: Isotope hydrology (^{2}H and ^{18}O) of Ikka fjord and its tufa columns, SW Greenland.

A late Oligocene molluscan fauna and Oligocene coastal outcrops from Vilsund, NW Denmark

KAI INGEMANN SCHNETLER, HENRIK MADSEN, KASIA K. ŚLIWIŃSKA, CLAUS HEILMANN-CLAUSEN & KAARE ULLEBERG

Geological Society of Denmark
https://2dgf.dk

Received 16 October 2023
Accepted in revised form
20 December 2023
Published online
09 February 2024

Schnetler, K.I., Madsen, H., Śliwińska, K.K., Heilmann-Clausen, C. & Ulleberg, K. 2024: A late Oligocene molluscan fauna and Oligocene coastal outcrops from Vilsund, NW Denmark. Bulletin of the Geological Society of Denmark, Vol. 73, pp. 1–40. ISSN 2245-7070. https://doi.org/10.37570/bgsd-2024-73-01

A rich late Oligocene molluscan fauna from a coastal cliff at Vilsund on the island of Mors, Jylland, Denmark, was studied. A summary of the upper Palaeogene sedimentary sequence in NW Jylland is given and lithostratigraphical and biostratigraphical correlations are suggested. The molluscan fauna contains 120 species, and the non-molluscs are briefly mentioned. The new species *Mitromorpha (Mitrolumna) danica* n. sp. and *Cerithiopsis vilsundensis* n. sp. are established. *Mitromorpha (Mitrolumna) danica* n. sp. is the first representative of the gastropod genus *Mitromorpha* Carpenter, 1865 and subgenus *Mitrolumna* Bucquoy, Dautzenberg & Dollfus, 1883 from the Cenozoic of Denmark. *Eubela* (s. lat.) *zetes* (Kautsky, 1925) represents the oldest record of the genus *Eubela* Dall, 1889. *Andersondrillia* Schnetler & Beyer, 1990 is considered to be a junior synonym of *Benthomangelia* Thiele, 1925. The bivalve genus *Cubiostrea* Sacco, 1897 is recorded from the upper Oligocene of the North Sea Basin for the first time. In the systematical part, several species are treated, including 16 species which have not been recorded previously from the Danish upper Oligocene; a synopsis of the representatives of the genus *Streptodictyon* Tembrock, 1961 in the Danish Oligocene is also given. *Aphanitoma ingerae* Schnetler & Palm, 2008 is transferred to the genus *Mitromorpha*, subgenus *Mitrolumna*. The fauna is compared with other Danish and German late Oligocene faunas and palaeoecological interpretations are suggested. As many of the mollusc species have not previously been illustrated from the Danish upper Oligocene, the fauna is extensively illustrated.

Dinocyst assemblages have been studied to help date the investigated successions. The assemblages indicate that the glauconitic clay from Vilsund should be assigned to the provisionally named stratigraphical Unit X in Śliwińska *et al.* (2012) or the lowermost Brejning Formation. Unit X was previously only known from the interval 61.5–67.5 m in the Harre-1 borehole. Schnetler & Beyer (1990) assigned the glauconitic clay in the coastal cliff at Mogenstrup to the Brejning Formation, but dinocyst studies herein indicate that these strata should be assigned either to Unit X, most likely the upper part, or the lowermost Brejning Formation (see Appendix). This interpretation is supported by the foraminifers and the pectinid species *Palliolum hausmanni* (Goldfuss, 1835).

The occurrence of other nearby outcrops of differing Oligocene ages is demonstrated. The outcrops are described and dated by means of dinocysts and foraminifers and include a section showing a depositional contact between the lowermost Rupelian Viborg Formation and Chattian Branden Clay. The age of the Mogenstrup section is also demonstrated by means of dinocysts.

Keywords: Mollusca, taxonomy, biostratigraphy, dinocysts, palaeontology, Brejning Formation, Viborg Formation, Oligocene, Denmark, North Sea Basin.

Kai Ingemann Schnetler [ingemann@schnetler.dk], Fuglebakken 14, Stevnstrup, DK-8870 Langå, Denmark. Henrik Madsen [henrik.madsen@museummors.dk], Fossil and Moclay Museum, Museum Mors, Skarrehagevej 8, Nykøbing Mors, DK-7900, Denmark. Kasia K. Śliwińska [kksl@geus.dk], Department of Geo-energy and Storage, Geological Survey of Denmark and Greenland (GEUS), Øster Voldgade 10, DK-1350 Copenhagen K, Denmark. Claus Heilmann-Clausen [claus.heilmann@geo.au.dk], Department of Geoscience, Aarhus University, DK-8000 Aarhus, Denmark. Kaare Ulleberg [ka-ulleb@online.no], Kløverstien 7, N-3074 Sande (Vestfold), Norway.

The Danish land area is situated in the eastern part of the Cenozoic North Sea Basin (*e.g.*, Knox *et al.* 2010). Oligocene sediments from Denmark crop out in cliffs and clay-pits in rather limited parts of Jylland, but they presumably originally had a much wider distribution toward the east, where they have been removed as a result of late Oligocene and Quaternary erosion. To the west, the Oligocene sediments are covered by younger deposits and continue under the North Sea. Recent stratigraphic overviews of the Oligocene in Denmark are given in Ulleberg (1987), Rasmussen & Dybkjær (2005), Rasmussen *et al.* (2010) and Śliwińska *et al.* (2012, 2014).

In the Limfjorden area, Oligocene sediments have been encountered at several localities. Ravn (1907) recognised the Branden Clay, which he considered to be middle Oligocene, at Branden, Lambjerg and Gjærup. The clay at the localities Nordentoft, Silstrup, Agger in Thy and Sundby on Mors was considered to be upper Oligocene. The Branden Clay is now referred to the lower upper Oligocene (Schnetler & Palm 2008, Śliwińska *et al.* 2012), and Agger (Lodbjerg) to the lower Miocene (Rasmussen *et al.* 2010). The non-glauconitic Skive Clay is known from Hesselbjerg near Skive and is considered to be a facies of the Branden Clay (Heilmann-Clausen 2006; Śliwińska *et al.* 2012).

Ravn (1909) described the clay-pit of Vilsund Brickworks on the island of Mors, where two different sedimentary facies were exposed: black micaceous clay with numerous spherical calcitic concretions that contain crab fossils, and greenish, glauconitic clay with sideritic concretions. Based on the molluscs, Ravn (1909) considered both the black micaceous clay and greenish, glauconitic clay to be of late Oligocene age. Beyer (1987) studied upper Oligocene and Miocene localities in NW Jylland for sedimentology and magnetostratigraphy. Schnetler & Beyer (1990) studied the coastal cliff at Mogenstrup, north of Skive, and recorded 197 mollusc species from a greenish, glauconitic clay with sideritic concretions. They assigned this clay to the Brejning Clay Member of the Vejle Fjord Formation (now the Brejning Formation) of late Oligocene (Chattian B) age, based on molluscs and foraminifer zonation (Ulleberg, pers. comm. 1987). Schnetler & Palm (2008) assigned the greenish, glauconitic clay in the clay-pit of the former Vilsund Brickworks to the Branden Clay. The greenish, glauconitic clay at Mogenstrup is either Unit X or the lowermost Brejning Formation (see Appendix), and

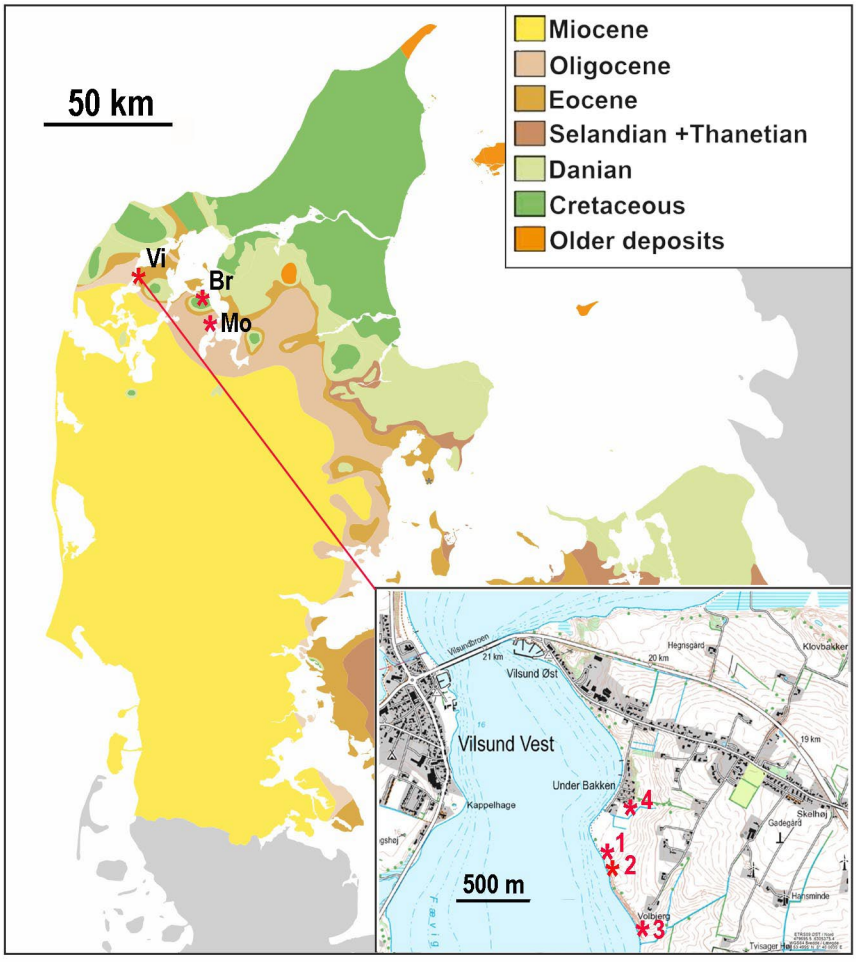

Fig. 1. Pre-Quaternary geology of Denmark. Modified after Jensen (1974) and Håkansson & Pedersen (1992). Inset: Detailed map with the Vilsund localities indicated with asterisks. Vi: the localities near Vilsund. Br: the former Branden Brickworks. Mo: the coastal cliff at Mogenstrup. 1: Vilsund 1 (= Sundby Nord, sampled 2006), 2: Vilsund 2 outcrop, sampled 2022–2023, 3: Vilsund 3, (= Sundby Syd, sampled 2006), 4: Vilsund 4, the location of the former Vilsund Brickworks. © Styrelsen for Dataforsyning og Infrastruktur.

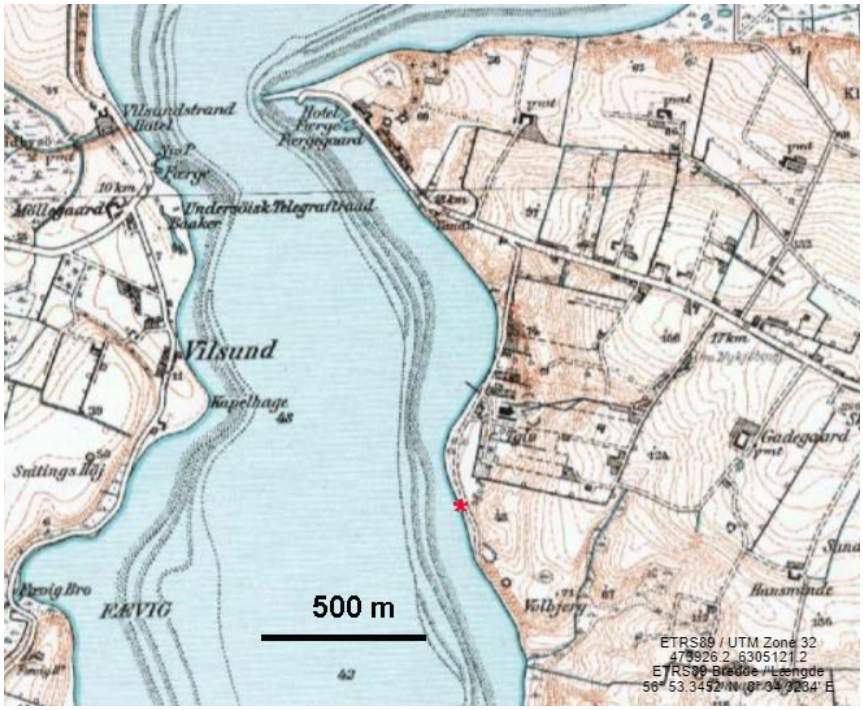

Fig. 2. Map from *c.* 1920, showing the location of the former Vilsund Brickworks (teglværk, Tglv). The studied locality Vilsund 2 is indicated by an asterisk (*). © Styrelsen for Dataforsyning og Infrastruktur.

Fig. 3. An excavated profile 13 m north of Vilsund 2 in 2022, showing the siderite horizons.

the glauconitic clay in the former clay-pit of Vilsund Brickworks is probably of the same age.

Coastal cliffs at northern Vilsund on the west coast of Mors expose Oligocene sediments of varying age (Fig. 1). One of these outcrops has revealed a rich Chattian mollusc fauna. The purpose of the present study is to describe this new fauna and discuss its palaeoecology, stratigraphic context and age, and to compare it with previously known faunas. For this purpose, a dinoflagellate cyst (dinocyst)-based dating of the section as well as of the rich mollusc fauna from Mogenstrup (Schnetler & Beyer 1990) is provided. Another purpose is to describe and biostratigraphically date (dinocysts and foraminifers) other Oligocene outcrops at Vilsund, including a section showing a disconformity (depositional contact) between lowermost Rupelian Viborg Formation and lower Chattian Branden Clay.

Mollusc-bearing locality

The locality Vilsund 2 sampled for molluscs is a low coastal cliff *c.* 1500 m south of the Vilsund Bridge (56°52′22.74″N and 8°38′39.69″E). The locality has been known by one of us (HM) for several years, but the sampling of sediment did not begin until 2022. The outcrop has a length of *c.* 21 m and exposes a stratigraphic thickness of *c.* 1 m. The sediment is glauconitic and greenish, very dark when wet. Fragments of molluscs and brachiopods are visible because of their whitish shells. Three horizons of sideritic concretions occur, and numerous sideritic concretions are scattered on the beach. The section is referred to the middle Chattian (either Unit X or lowermost Brejning Formation, see below). The locality was briefly described by Madsen & Schnetler (2023).

Other Oligocene outcrops at Vilsund

Two other profiles, Vilsund 1 (formerly Sundby Nord) and Vilsund 3 (formerly Sundby Syd), north and south of Vilsund 2, respectively (Fig. 2), were sampled in 2006 for the study of dinocysts and foraminifers; for details, see the appendix. Vilsund 1 was a small outcrop a little north of Vilsund 2, and dinocysts in glauconitic clay at this outcrop indicate assignment to the lower Chattian Branden Clay. Vilsund 3, *c.* 400 m south of Vilsund 2, is a prominent section at Volbjerg exposing the lowermost Rupelian Viborg Formation in depositional contact with the lower Chattian Branden Clay. HM has recently found typical Viborg Formation gastropods here. The section was included in the study by Beyer (1987). The former Vilsund Brickworks and the nearby clay-pit were located *c.* 500 m north of Vilsund 1, but Ravn (1909) gave no information on the exact location of the clay-pit.

Material and methods

The present paper is based on material collected in 2022 and 2023. Numerous fossils have been found, especially molluscs and brachiopods. Almost all mollusc specimens could be identified to genus or species. Larger specimens are very rare and have been collected by handpicking, but the bulk of the material has been obtained by sediment processing. Smaller molluscs are generally well preserved, but many specimens are worn or fragmented, especially thin-walled bivalves such as pectinids. Many species are found in small numbers only.

The bulk of the material was collected in 2022 and a total of approximately 900 kg of clay was processed. The clay was dried, dispersed in water three times, and screen washed through sieves of two different mesh sizes (2.0 mm and 0.5 mm). The residue contains abundant glauconite, some pyrite, grains of sand and fossils. The residues were examined for fossils by HM using a binocular microscope (Euromex). Fossils larger than 5 mm were photographed with a Nikon D7000. Smaller fossils were photographed with a binocular microscope using the Image Stacking Software – Combine ZM.

Among the non-molluscs, abundant specimens and fragments of a terebratulid brachiopod were collected; such remains are frequently visible in the field due to their size and light color. They may be assigned to the family Terebrataliidae Richardson, 1975, subfamily Terebrataliinae Richardson, 1975 (von der Hocht, pers. comm. 2022). The brachiopod genus *Terebratulina* is represented by a few specimens. Teleost otoliths are rather rare, whereas shark teeth are more common. Noteworthy are the teeth of *Pristiophorus* sp., which are also known from Mogenstrup (Schnetler & Beyer 1990). Anthozoa are regularly found (*Ceratocyathus* and *Flabellum*) and serpulids are rather common.

The mollusc taxa from Vilsund are listed in Table 1. The bivalves are arranged following Bouchet & Rocroi (2010), and the gastropods are arranged following Bouchet & Rocroi (2017). WoRMS Editorial Board (2014), World Register of Marine Species, has also been consulted. Taxa recorded from the Danish upper Oligocene for the first time are indicated with an asterisk. Because the fauna is the first recorded from Unit X or the lowermost Brejning Formation, and because many species have not previously been illustrated from the Danish upper Oligocene, almost all species are illustrated on Figs 6–14. The illustrated fossils are housed in the Fossil and Mo-Clay Museum, Nykøbing Mors, and registered in the Specify database with an MM prefix, but some specimens have been declared Danekræ (prefix DK) and will

Table 1. Mollusc taxa from the locality Vilsund 2

Taxon	Number of specimens	New Denmark
Nucula sp.	5 fr.	
Nuculana westendorpi Nyst & Westendorp, 1839	4, 7 fr.	
cf. *Barbatia glimmerodensis* R. Janssen, 1978	1 fr.	*
Acar aff. *dentiens* (Cossmann & Peyrot, 1912)	52, 67 fr.	
Bathyarca bellula (Wiechmann, 1874)	4	
Aspalima chattica (Schnetler & Beyer, 1990)	1	
Limopsis parva Harder, 1913	160, 100 def., 50 fr.	
Cosmetopsis retifera (Semper, 1861)	1, 1 fr.	
Oblimopa vonderhochti (Schnetler & Beyer, 1990)	55, 18 def., 21 fr.	
Ostrea sp.	1	
Cubiostrea sp.	2, 5 fr.	*
Hilberia bifida (Münster, 1835)	4 fr.	
Palliolum limatum (Goldfuss, 1833).	Numerous fr.	
Cyclocardia grossecostata (Koenen, 1884)	18 def.	
Astarte gracilis Goldfuss, 1837	12 def., 3 fr.	
Digitaria koeneni (Speyer, 1866)	1	
Parvicardium kochi (Semper, 1861)	2 fr.	
Varicorbula gibba (Olivi, 1792)	1	
Teredinidae, gen. et sp. indet.	1	
Hiatella arctica (Linnaeus, 1767)	1	
Poromya sp.	1 fr.	
Antalis geminata (Goldfuss, 1841)	2 fr.	
Fissidentalium polypleurum (Seifert, 1959)	Numerous fr.	
Perotrochus aff. *sismondai* (Goldfuss, 1844)	1, 1 fr.	*
Emarginula punctulata (Philippi, 1843)	2, 1 fr.	
Scissurella koeneniana R. Janssen, 1978	1	
Steromphala chattica R. Janssen, 1978	2	*
Collonia troelsi Schnetler & Beyer, 1990	3 fr.	
Homalopoma (Boutillieria) simplex (Philippi, 1843)	141	
Margarites margaritula (Sandberger, 1859)	3	*
Astraea (Lithopoma) pustulosa (Münster, 1844)	61	
Haustator goettentrupensis (Cossmann, 1899)	2	
Cirsotrema insigne (Philippi, 1843)	1	*
Cirsotrema crispata Harder, 1913	2	
Cirsotrema (?Opaliopsis) aff. *koeneni* A.W. Janssen, 1967	1	
Opalia pusilla (Philippi, 1843)	1	
Leptonotis planatus (Speyer, 1864)	2	
Euspira helicina protracta (Eichwald, 1830)	38	
Norephora elatior (Koenen, 1891)	36	
Cerithiopsis henckeliusii (Nyst, 1836)	2	
Cerithiopsis jutensis Schnetler, 1985	1	
Cerithiopsis serrula R. Janssen, 1978	6	
Cerithiopsis aff. *dautzenbergi* Glibert, 1949	5	*
Cerithiopsis (s. lat.) *ariejansseni* R. Janssen, 1978	2	
Cerithiopsis vilsundensis n. sp.	6	*
Cerithiella bitorquata (Philippi, 1843)	6	
Cerithiopsida boelschei (Koenen, 1891)	2	
Laeocochlis supraoligocaenicus Schnetler & Beyer, 1990	13	
Thereitis angusta (Tembrock, 1965)	26	

Table 1 continued

Taxon	Number of specimens	New Denmark
Seila (s. lat.) *koeneni* R. Janssen, 1978	2	
Alvania semperi Wiechmann, 1871	1	
Rissoa karsteni R. Janssen, 1978	1	
Cirsope multicingulata (Sandberger, 1859)	2	
Polygireulima pseudonaumanni (R. Janssen, 1978)	6	
Niso minor Philippi, 1843	11	
Aporrhais speciosa (Schlotheim, 1820)	5	
Echinophoria rondeleti (Basterot, 1825)	3	
Pseudosassia flandrica (Koninck, 1838)	25, 1 fr.	
Onustus scrutarium (Philippi, 1843)	2, 1 fr.	
Euroscaphella siemssenii (Boll, 1851)	2	
Admetula postera (Beyrich, 1856)	2	
Unitas granulata (Nyst, 1845)	2	
Babylonella pusilla (Philippi, 1843)	2	
Searlesia dentifera Vermeij, 1991	1	
Aquilofusus elegantulus (Philippi, 1843)	4	*
Aquilofusus waeli (Nyst, 1852)	5	
Aquilofusus aequistriata (Speyer, 1863)	2	
Boreosiphopsis danicus (Schnetler, 1985)	5	
Streptodictyon cheruscus (Philippi, 1843)	57	
Streptodictyon soellingensis (Tembrock, 1965)	4	
Streptodictyon schnetleri Cadée & Janssen, 1994	24	
Tritia schlotheimi (Beyrich, 1854)	3	
Pterynotus (Pterochelus) tristichus (Beyrich, 1854)	2	
Murexsul kochi (Beyrich, 1854)	2	
Eopaziella deshayesi (Nyst, 1836)	1	
Eopaziella capito (Philippi, 1843)	6	
Trophonopsis angustevaricata (Gripp, 1915)	12	
Siphonochelus sejunctus (Semper, 1861)	11	
Siphonochelus fistulatus (Schlotheim, 1820)	1	*
Lyrotyphis cuniculosus (Nyst, 1836)	2	
Hirtotyphis pungens (Solander, 1766)	1	*
Metula (Daphnobela) scabricula (Philippi, 1843)	4	
Vexillum hastatum (Karsten, 1849)	1	
Conomitra soellingensis (Speyer, 1864)	7	
Ancilla karsteni (Beyrich, 1856)	16	
Conus semperi Speyer, 1862	10	
Bathytoma leunisii (Philippi, 1843)	5	
Drilliola speyeri (Koch & Wiechmann, 1872)	2	
Microdrillia ingerae Schnetler & Beyer, 1990	109	
Orthosurcula regularis (Koninck, 1838)	4	
Cochlespira volgeri (Philippi, 1843)	11	
Fusiturris selysii (Koninck, 1838)	3	
Fusiturris duchastelii (Nyst, 1836)	35	
Fusiturris enodis R. Janssen, 1979	3	
Boreodrillia undatella (Speyer, 1867)	2	
Benthomangelia brejningensis (Schnetler & Beyer, 1990)	2	
Benthomangelia holzapfeli (Koenen, 1890)	1	
Splendrillia koeneni (Speyer, 1867)	16	

Table 1 continued

Taxon	Number of specimens	New Denmark
Stenodrillia obeliscus (des Moulins, 1842)	3	
Amblyacrum roemeri (Koenen, 1867)	1	
Mitromorpha (Mitrolumna) danica n. sp.	1	*
Polystira koninckii (Nyst, 1845)	6	
Glibertturricula ariejansseni Schnetler & Beyer, 1987	8	
Acamptogenotia morreni (Koninck, 1838)	2	
Gemmula geinitzi (Koenen, 1890)	3	
Pleurotomella rappardi (Koenen, 1867)	2	*
Pleurotomella margaritata R. Janssen, 1978	2	
Rimosodaphnella lappanni Schnetler & Beyer, 1990	1	
Eubela (s. lat.) *zetes* (Kautsky, 1925)	1	*
Nipteraxis bimonilifera (Sandberger, 1859)	2	
Graphis hosiusi (Lienenklaus, 1891)	7	
Mathilda bicarinata Koch & Wiechmann, 1872	2	*
Crenilabium terebelloides (Philippi, 1843)	2	
Acteon punctatosulcata (Philippi, 1843)	1	
Odostomia ventriosa (Speyer, 1870)	2	*
Odostomia sp.	2	
Syrnola subcylindrica (Philippi, 1843)	4	
Syrnola laevissima (Bosquet, 1859)	1	
Turbonilla jeffreysi Koch & Wiechmann, 1872	5	
Chrysallida sp.	5	

fr.: fragment, def.: defective

ultimately be stored in the Natural History Museum of Denmark (Copenhagen, NHMD prefix).

A sample of 'glauconitic clay with brachiopods' collected by one of us (IS; 18 March 2022) from the Vilsund 2 locality was analysed for dinocysts. The sample consists of medium grey clay with scattered, well-rounded quartz and quartzite grains ranging from coarse sand to fine sand (up to 3 mm). The sample is very rich (estimated ~50%) in light and dark green, sand-sized glauconite, giving the sediment a greenish colour and grainy texture. The sample is furthermore very rich (estimated ~25%) in shells and shell fragments of molluscs and brachiopods.

For the dinocyst analysis, a sample of 31 g of clean material was processed for palynology at the Department of Geoscience, Aarhus University (as ch-c lab. no. 3283) using a standard technique, which involves successive treatments with HCl, HF, and again HCl and H_2O to dissolve and remove calcium carbonate and siliceous compounds. This procedure was followed by sieving on a 20 μm mesh. The sieved residue was treated briefly (7 min) with cold, concentrated HNO_3 in order to oxidise amorphous organic matter and pyrite. Following oxidisation, the residuum was mounted with gelatine-glycerine on slides for light-microscopy.

Geological setting and stratigraphy

The pre-Quaternary geology of the western Limfjorden area consists of strata ranging from the Danian to the Miocene. The presence of salt diapirs and pillows have resulted in exposure of Upper Cretaceous chalk over the Mors and Batum diapirs (Håkansson & Pedersen 1992), and strata of Danian, Thanetian and Eocene age are found flanking these diapirs. The lowermost Eocene Fur Formation is exposed in several coastal cliffs on Fur and Mors and at Ertebølle north of Hvalpsund and Silstrup south of Thisted. The only existing outcrop in NW Jylland of the lowermost Rupelian Viborg Formation is the high cliff section at Volbjerg (this study Vilsund 3 section, see Appendix). Here the Viborg Formation is in undisturbed depositional contact with the overlying lower Chattian Branden Clay, demonstrating a major intra-Oligocene hiatus in this area. The Oligocene Branden Clay was formerly exposed at Branden near the northern tip of Salling. Originally, Ravn (1907) assigned the Branden Clay to the middle Oligocene, and recently Schnetler & Palm (2008) and Śliwińska *et al.* (2012) stated an early Chattian age. Ravn (1907) also assigned the clay at Gjærup to the middle Oligocene, whereas Schnetler

& Palm (2008) assigned it to the Branden Clay. Ravn (1909) assigned the sediments in Vilsund Brickworks to the upper Oligocene. The uppermost Oligocene Brejning Formation is exposed at Lyby (Beyer 1987; Rasmussen *et al*. 2010) and at Mogenstrup (Beyer 1987; Schnetler & Beyer 1990; Rasmussen *et al*. 2010; present study). The present study indicates that the greenish, glauconitic clay with siderite layers at the Vilsund 2 locality and at Mogenstrup should be assigned to either Unit X (Śliwińska *et al*. 2012) or the Brejning Formation, see Appendix. At Silstrup a depositional contact is exposed between lowermost Eocene Fur Formation and the Brejning Formation (Gry 1979; Heilmann-Clausen 1997; Rasmussen *et al*. 2010; Schulz *et al*. 2020), demonstrating a local *c*. 30 Ma hiatus possibly related to movement in salt diapirs.

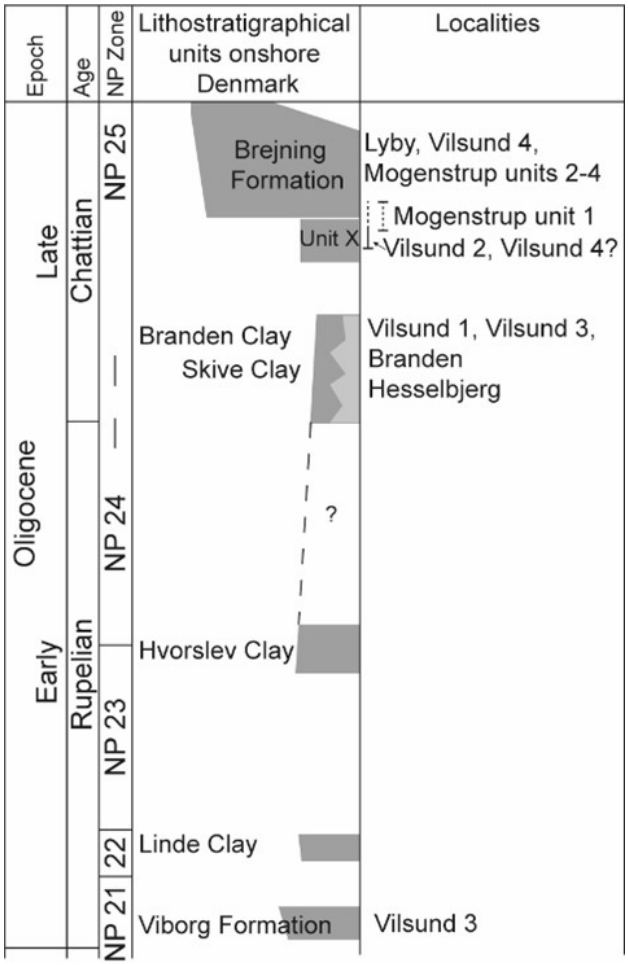

Fig. 4. Composite lithological column illustrating the upper Oligocene sequence in NW Jylland. The stratigraphical positions of the localities at Vilsund, Mogenstrup, Lyby, Branden and Hesselbjerg are indicated. Vilsund 1–3 are coastal exposures, Vilsund 4 is the former Vilsund Brickworks. Modified from Śliwińska *et al*. (2012).

Biostratigraphy and Age

Molluscs

A late Oligocene (Chattian) age is clearly apparent from the molluscan fauna at the Vilsund localities studied herein. Anderson (1958, 1961) and R. Janssen (1979b) suggested a biostratigraphy of the Chattian, based on pectinids. Numerous fragments of pectinids have been collected, viz. abundant *Palliolum limatum* (Goldfuss, 1833) and a few *Hilberia bifida* (Münster, 1835), indicating a Chattian A age. At Mogenstrup, *Hilberia bifida*, *Hilberia soellingensis* (Koenen, 1868) *Palliolum limatum ambignum* and *Palliolum hausmanni* (Goldfuss, 1835) are present (Schnetler & Beyer 1990), and the first two species are probably reworked. The gastropod species *Tritia schlotheimi* (Beyrich, 1854) indicates, according to R. Janssen (1979b), a Chattian B or younger age. This species has been encountered at Mogenstrup, indicating a Chattian B age. However, three specimens were also found at Vilsund.

In the Vilsund fauna, the pectinid *Palliolum hausmanni* is absent, suggesting a Chattian A age. Several species, *e.g. Palliolum limatum*, *Acar* aff. *dentiens*, *Scissurella koeneniana*, *Steromphala chattica*, *Homalopoma simplex* and *Streptodictyon soellingensis* are only known from Chattian A (lowermost upper Oligocene) strata in Germany. The latter species is also known from the lower upper Oligocene (Chattian A) at Branden (Schnetler & Palm 2008), and the occurrence in the Vilsund fauna also supports a Chattian A age.

Ravn (1909) listed the mollusc faunas from the two different sedimentary facies in the clay-pit of Vilsund Brickworks. The senior author studied this material in the Geological Museum, Copenhagen (now NHMD), in 1982 and 2022. The black micaceous clay contained numerous spherical concretions with crabs and a typical late Oligocene fauna. The greenish, glauconitic clay with sideritic concretions contained a rather limited fauna, *e.g. Limopsis goldfussi* (= *Limopsis parva*), *Mitra* sp. (= *Conomitra soellingensis*) and *Parvicardium kochi*. We conclude, based on the molluscs, that both the black micaceous clay and the greenish, glauconitic clay in the clay-pit of the former Vilsund Brickworks are of late Oligocene age. The greenish, glauconitic clay with sideritic concretions is presumably the same unit as the sediments at the Vilsund 2 locality and Mogenstrup, and the black micaceous clay with spherical concretions is assigned to the glauconite-free upper part of the Brejning Formation, as at Mogenstrup.

Dinocysts and foraminifers

Palynofacies. The organic particles in the processed sample from Vilsund 2 ('Glauconitic clay with bra-

chiopods') include palynomorphs (estimated 70–75%), light brown structured woody material (20–25%) and few percent foraminifer-inner linings. Palynomorphs are well preserved and dominated by dinocysts (approximately 50 % of the organic particles). Pollen and spores (mainly bisaccate pollen) make up 20–25% of the organic particles. Non-saccate pollen and spores are underrepresented in residues sieved on 20 μm.

Dinocyst analysis and age of the sample. The dinocyst assemblage is well preserved and diverse. A full account of the assemblage is given in the Appendix. In brief,

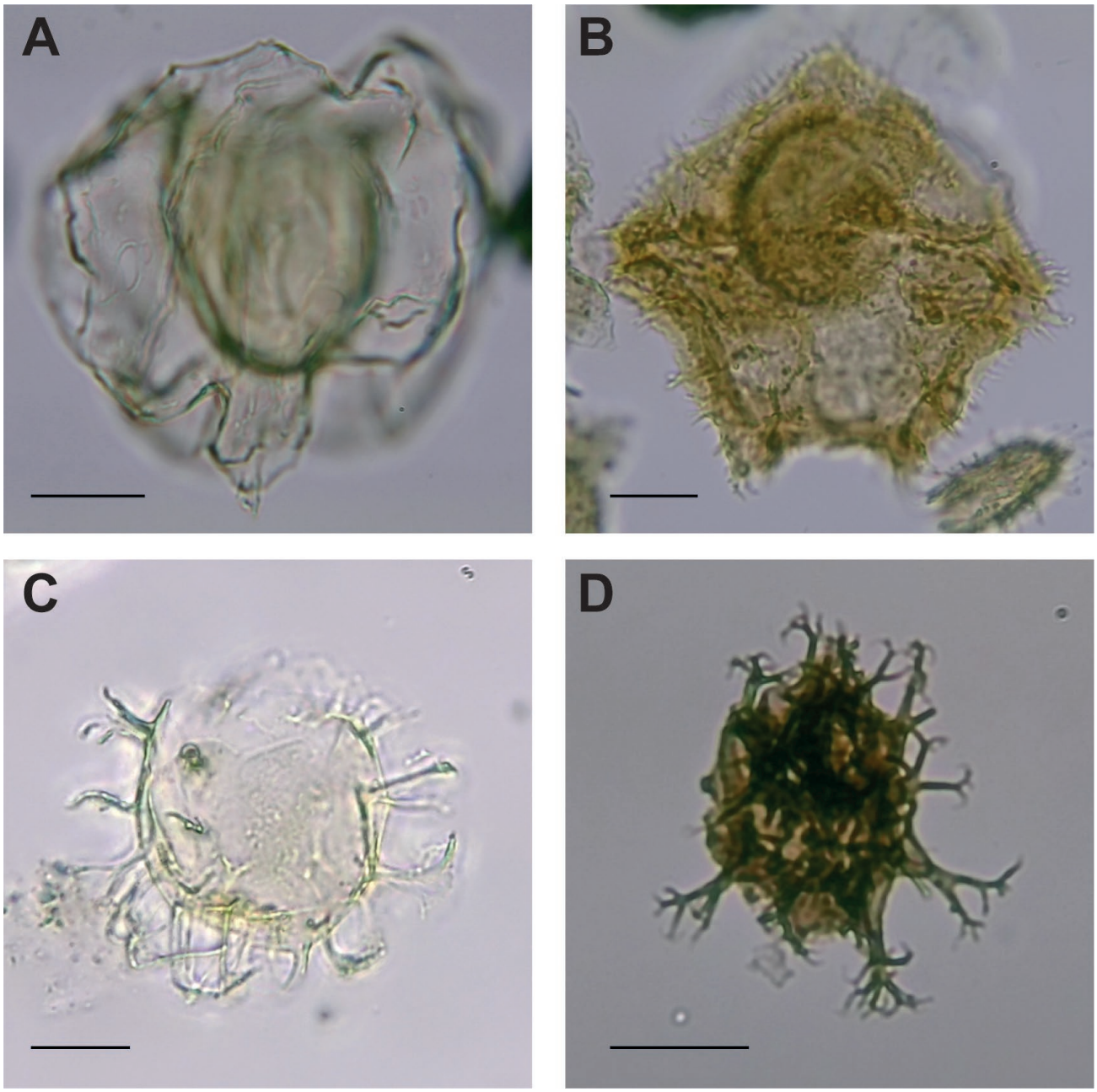

Fig. 5. Selected key dinocysts and an acritarch from the studied outcrops. Scale bars: 20 μm. Microscope coordinates (MC) are taken following the method described by Śliwińska (2019), with A-point coordinates 100.7×0.6. **A,** *Triphragmadinium demaniae* Vilsund 2, Lab. No. 3283, Slide J-2; England Finder Coordinates V19-2. **B,** *Lejeunecysta tenella* Vilsund 2, Lab. No. 3283 Slide J-4, MC 15.5 x 158. **C,** cf. *Licracysta? semicirculata* Vilsund 2, Lab. No. 3283 Slide J-4, MC 20.2 x 152. **D,** acritarch *Artemisiocysta cladodichotoma* Mogenstrup Unit 1, Lab. No. 1143 Slide H-1; MC 18 x 141.

the assemblage contains several long ranging taxa (*e.g.*, *Spiniferites* spp., *Lingulodinium machaerophorum* and *Reticulatosphaera actinocoronata*). The sample yields rare *Chiropteridium galea*, *Lejeunecysta tenella* (Fig. 5 B), the acritarch *Artemisiocysta cladodichotoma* (Fig. 5 D) and cf. *Licracysta*? *semicirculata* (Fig. 5 C, see taxonomic remarks in the Appendix). Notably, several specimens of *Triphragmadinium demaniae* (Fig. 5 A) were recovered, a species (see taxonomic remarks in the Appendix) that has previously only been recorded in the ?upper Eochattian of the Netherlands, Belgium and Germany (Van Simaeys *et al.* 2005; King *et al.* 2016). In the dinocyst zonation of the North Sea Basin (King 2016), the first occurrence of *T. demaniae* indicates the base of dinocyst Subzone DO7b (King 2016, p. 603); note that the base of the subzone is erroneously shown as the *last* occurrence of *T. demaniae* in King (figs 13, 20). The processed sample from Vilsund 2 lacks the following stratigraphically significant taxa: *Deflandrea* spp., *Saturnodinium pansum, Wetzeliella gochtii, W. symmetrica, Rhombodinium draco*, and typical ?*Licracysta semicirculata*. The absence of these taxa, combined with the presence of *T. demaniae*, indicates probable assignment to Subzone DO7b of King (2016), i.e., a late Chattian age. In terms of Danish lithostratigraphic units, the sample should probably be assigned to Unit X of Śliwińska *et al.* (2012), although the lowermost Brejning Formation cannot be excluded (see Appendix).

Systematical part

Abbreviations and repositories. ISL: MNO: Collection of Mogens Stentoft Nielsen, (Odense, Denmark); LSJ: Collection of Lone Sortkjær (Juelsminde, Denmark); MM: Collection of the Fossil and Mo-Clay Museum (Skarrehagevej 8, Nykøbing Mors, Denmark); NHMD: Collection of the Natural History Museum of Denmark (Copenhagen, Denmark); DK: prefix for specimens in the Danekræ Collection (NHMD, Copenhagen). This published work and the nomenclatural acts it contains have been registered in ZooBank: http://zoobank.org:pub

Class Bivalvia Linnaeus, 1758

Autobranchia Grobben, 1894

Infraclass Pteriomorphia Beurlen, 1944

Order Arcida Stolictzka, 1871

Superfamily Arcoidea Lamarck, 1809

Family Arcidae Lamarck, 1809

Genus *Barbatia* Gray, 1842

Type species: *Arca barbata* Linnaeus, 1758 accepted as *Barbatia barbata* (Linnaeus, 1758) (type by subsequent designation).

cf. *Barbatia glimmerodensis* R. Janssen, 1979
Fig. 6f

1979b *Barbatia (Barbatia) glimmerodensis* R. Janssen, p. 24, pl. 1, figs 6–7.

Material. One fragmentary valve. Height 1.7 mm.

Remarks. The sculpture of the fragment matches the description and illustration by R. Janssen well.

Genus *Acar* Gray, 1857

Type species: *Byssoarca divaricata* G. B. Sowerby I, 1833 accepted as *Acar plicata* (Dillwyn, 1817) (type by subsequent designation).

***Acar* aff. *dentiens* (Cossmann & Peyrot, 1912)**
Fig. 6i

1979b *Barbatia (Acar)* aff. *dentiens* Cossmann & Peyrot, 1912 – R. Janssen, p. 25, pl. 1, figs 8–9.
1990 *Barbatia (Acar)* aff. *dentiens* Cossmann & Peyrot, 1912 – Schnetler & Beyer, p. 46, pl. 1, figs 1a–b.

▼ **Fig. 6. a,** *Nuculana westendorpi* Nyst & Westendorp, 1839. Right valve, length 4.2 mm. **a1,** interior view, **a2,** exterior view. MM-13589. **b,** *Aspalima chattica* (Schnetler & Beyer, 1990). Right valve, length 2.8 mm. **b1,** interior view, **b2,** exterior view. MM-13590. **c,** *Cosmetopsis retifera* (Semper, 1861). Right valve, length 2.0 mm. **c1,** interior view, **c2,** exterior view. MM-13591. **d,** *Oblimopa vonderhochti* (Schnetler & Beyer, 1990). Right valve, height 7.2 mm. **d1,** interior view, **d2,** exterior view. MM-13592. **e,** *Limopsis parva* Harder, 1913. Left valve, height 11.0 mm. **e1,** interior view, **e2,** exterior view. MM-13593. **f,** cf. *Barbatia glimmerodensis* R. Janssen, 1979. Fragmentary right valve, height 1.7 mm. NHMD 1651691 (ex MM-13594), DK 1264. **G,** *Bathyarca bellula* (Wiechmann, 1874). Left valve, length 1.6 mm. **g1,** interior view, **g2,** exterior view. MM-13595. **h,** *Ostrea* sp. Height 1.7 mm. **h1,** interior view, **h2,** exterior view. MM-13596. **i,** *Acar* aff. *dentiens* (Cossmann & Peyrot, 1912). Left valve, height 6.0 mm. **i1,** interior view, **i2,** exterior view. MM-13597. **j,** *Cubiostrea* sp. Right valve, length 41.0 mm. **j1,** interior view, **j2,** exterior view. NHMD 1651688 (ex MM-13598), DK 1261. **k,** *Palliolum limatum* (Goldfuss, 1833). Left valve, height 28.0 mm. MM-13599.

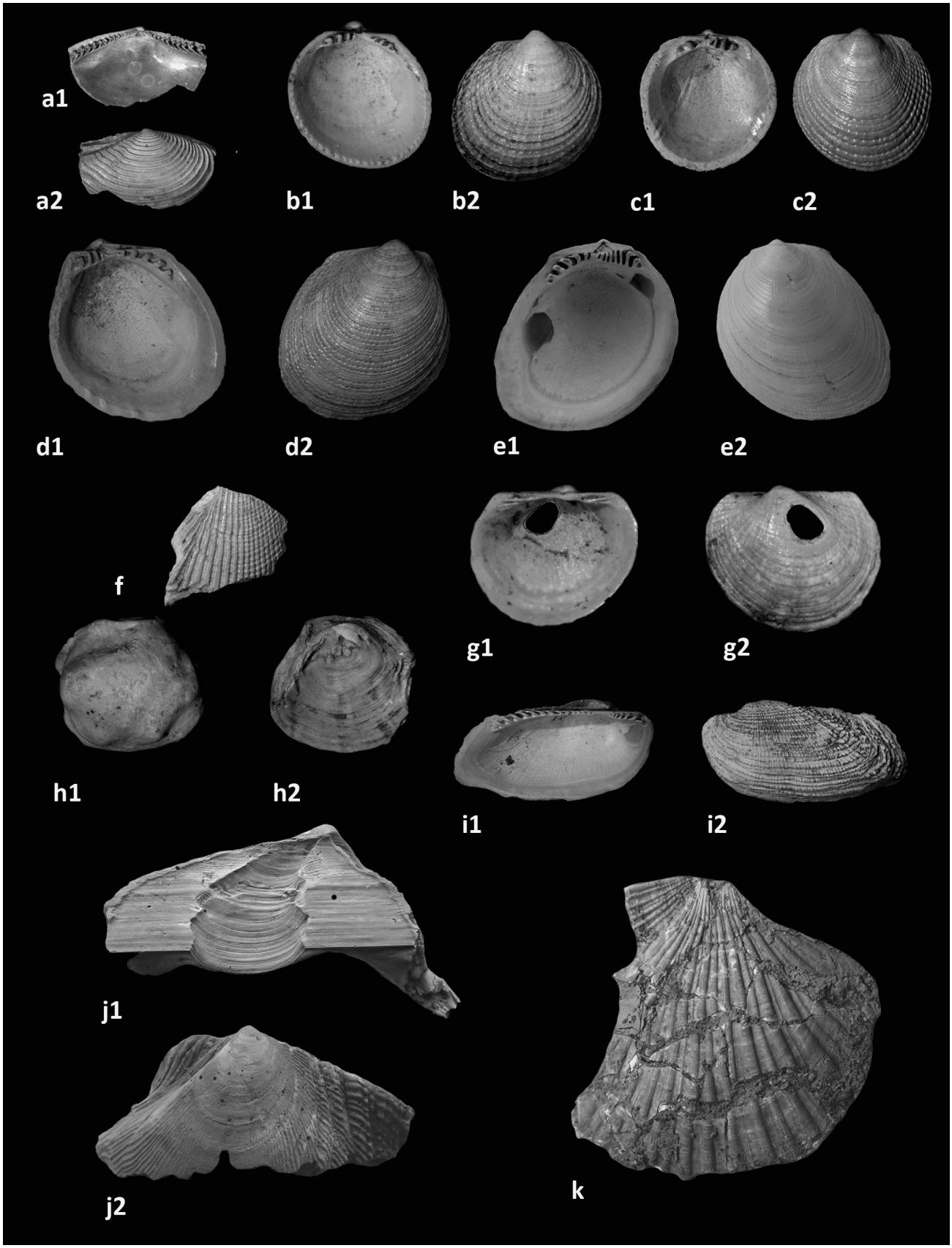
a1
a2
b1
b2
c1
c2
d1
d2
e1
e2
f
g1
g2
h1
h2
i1
i2
j1
j2
k

Material. 52 specimens and 67 fragments.

Remarks. The specimens are generally broken and worn, but the few complete valves match the illustrations in R. Janssen (1979b) well. The species is less common at Mogenstrup (Schnetler & Beyer 1990) and is also found at Brejning (collected by K. Eriksen, unpublished, NHMD). The species is common in the German upper Oligocene at Glimmerode and furthermore reported from Doberg and Söllingen (R. Janssen 1979b).

Order Ostreida

Superfamily Ostreoidea Rafinesque, 1815

Family Ostreidae Rafinesque, 1815

Genus *Cubiostrea* Sacco, 1897

Type species: *Ostrea virginica* Gmelin, 1791 accepted as *Crassostrea virginica* (Gmelin, 1791) (type by original designation).

***Cubiostrea* sp.**
Fig. 6j, Fig. 14a

Material. Three large fragmentary specimens and fragments from the glauconitic clay. A valve in a sideritic concretion has a height of 128 mm and a width of 103 mm.

Description. The illustrated fragmentary right valve has a width of 41.0 mm and a height of 20.3 mm. The other fragmentary specimen has a width of 90 mm. The valve is large and rather fragile. It has numerous rather irregular radial ribs, which are strongest on the margins. There is a large highly triangular and curved ligament pit on the internal of the valve.

Further material. One adult specimen, preserved in a sideritic concretion, one defective valve in clay and a few fragments.

Discussion. The specimen is very similar to the illustration in Cox in Moore 1971 (p. N1141, fig. J117).

Remarks. The species *Cubiostrea digitalina* (Dubois de Montperreux, 1831) was reported from the Hemmoorian at Miste (A.W. Janssen 1984, p. 58, pl. 27, figs 1a–b, 2a–b). The genus is represented in the Eocene of England by three species (*fide* Alan Morton: https://www.dmap.co.uk/index.htm). The Eocene of France contains six species of the genus (*fide* Le Renard & Pacaud 1995). The genus was not previously known from the upper Oligocene of the North Sea Basin.

Class Gastropoda Cuvier, 1795

Subclass Vetigastropoda Salvini-Plawen, 1980

Order Pleurotomariida Cox & Knight, 1960

Superfamily Pleurotomarioidea Swainson, 1840

Family Pleurotomariidae Swainson, 1840

Genus *Perotrochus* P. Fischer, 1885

Type species: *Pleurotomaria quoyana* P. Fischer & Bernardi, 1856, accepted as *Perotrochus quoyanus quoyanus* (P. Fischer & Bernardi, 1856) (type by monotypy).

***Perotrochus* aff. *sismondai* (Goldfuss, 1844)**
Fig. 7h

▼ **Fig. 7. a,** *Hilberia bifida* (Münster, 1835). Length 3.5 mm. MM-13600. **b,** *Cyclocardia grossecostata* (Koenen, 1884). Right valve, height 1.4 mm. **b1,** interior view, **b2,** exterior view. MM-13601. **c,** *Astarte gracilis* Goldfuss, 1837. Right valve, height 1.1 mm. **c1,** interior view, **c2,** exterior view. MM-13602. **d,** *Digitaria koeneni* (Speyer, 1866). Right valve, height 3.5 mm. MM-13603. **e,** *Hiatella arctica* (Linnaeus, 1767). Left valve, height 3.0 mm. **e1,** interior view, **e2,** exterior view. MM-13604. **f,** *Antalis geminata* (Goldfuss, 1841). Length 14.5 mm. MM-13605. **g,** *Fissidentalium polypleurum* (Seifert, 1959). Length 40.3 mm. MM-13606. **h,** *Perotrochus* aff. *sismondai* (Goldfuss, 1844). Height 5.0 cm, width 8.5 cm. MM-13607. **i,** *Emarginula punctulata* (Philippi, 1843). Length 1.8 mm. **i1,** oblique apertural view, **i2,** apical view. MM-13608. **j,** *Scissurella koeneniana* R. Janssen, 1978. Width 1.1 mm. **j1,** lateral view, **j2,** umbilical view, **j3,** apical view. MM-13609. **k,** *Steromphala chattica* (R. Janssen, 1978). Height 0.8 mm. NHMD 1651683 (ex MM-13610), DK 1256. **l,** *Collonia troelsi* Schnetler & Beyer, 1990. Height 1.0 mm. MM-13611. **m,** *Homalopoma simplex* (Sandberger, 1859). Lateral view, height 10.0 mm. MM-13612. **n,** *Homalopoma simplex* (Sandberger, 1859). Specimen with operculum *in situ*. Lateral view, height 3.0 mm. MM-13613. **o,** *Margarites margaritula* (Sandberger, 1859). Apical view, diameter 1.1 mm. NHMD 1651687 A (ex MM-13615), DK 1260. **p,** *Margarites margaritula* (Sandberger, 1859). Height 1.0 mm. **p1,** umbilical view, **p2,** lateral view. NHMD 1651687 B (ex MM-13616), DK 1260. **q,** *Astraea (Lithopoma) pustulosa* (Münster, 1844). Height 2.0 mm. MM-13617.

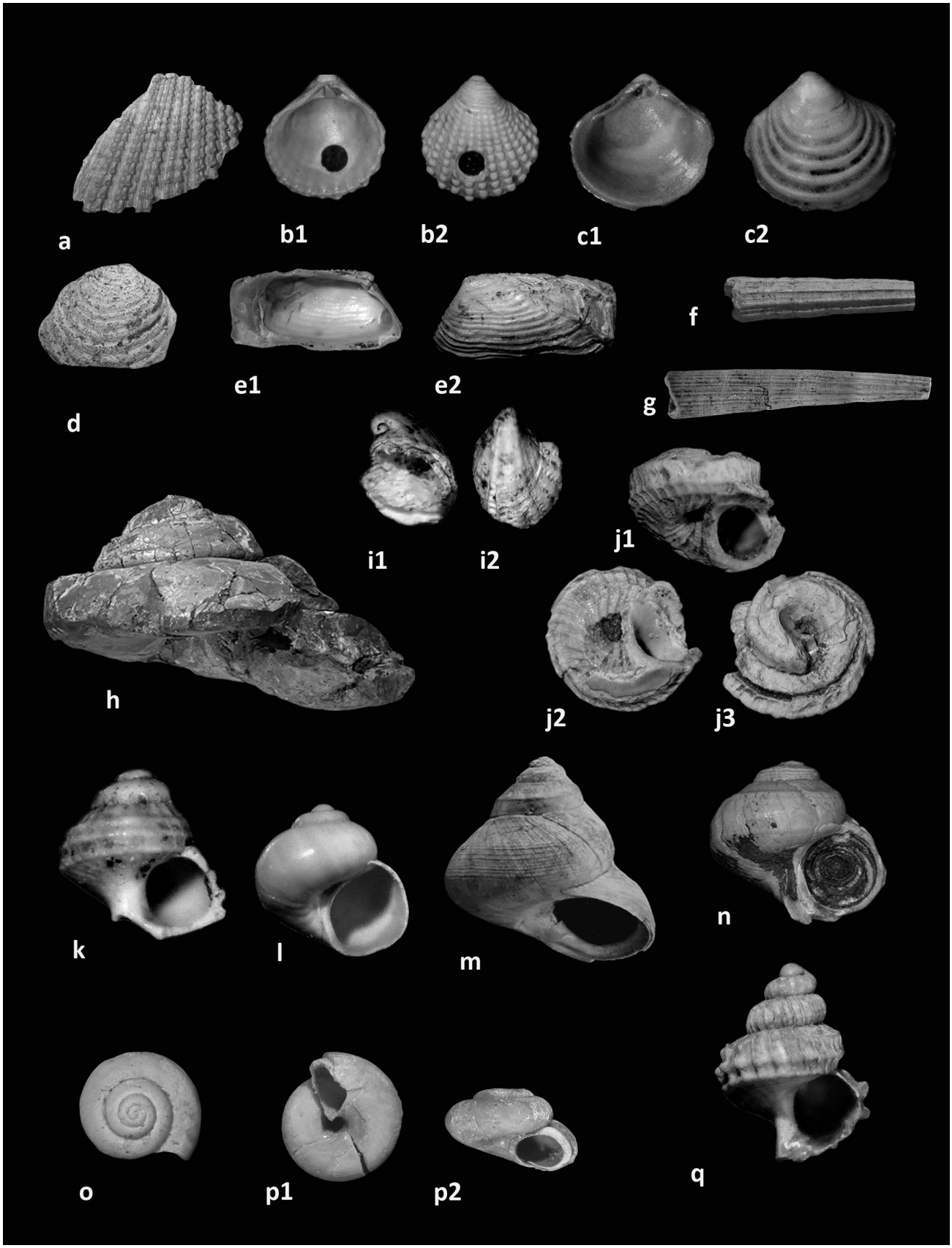
a
b1
b2
c1
c2
d
e1
e2
f
g
i1
i2
j1
h
j2
j3
k
l
m
n
o
p1
p2
q

1978b *Pleurotomaria* aff. *sismondai* (Goldfuss, 1844) – R. Janssen, p. 141.

Description. The large almost complete specimen has a height of 50 mm and a width of 85 mm. The H/W ratio is 0.59. The shell has *c.* 3.5 whorls preserved as internal molds with parts of the nacreous layer preserved. The whorls are almost flat with a narrow shoulder and are separated by a deep suture. The aperture is rather large and almost ellipsoidal, and the umbilicus is rather narrow and deep. No ornament is visible.

Remarks. The species was not recognised by Schnetler & Beyer (1990). Later, several incomplete specimens have been found at Mogenstrup, some of them rather large. The species is elsewhere only known from the upper Oligocene at Doberg (Germany).

Family Scissurellidae Gray, 1847

Genus *Scissurella* d'Orbigny, 1824

Type species: *Scissurella laevigata* d'Orbigny, 1824, accepted as *Scissurella costata* d'Orbigny, 1824 (type by subsequent designation).

***Scissurella koeneniana* R. Janssen, 1978**
Fig. 7j

1978a *Scissurella (Anatoma) philippiana* – R. Janssen, p. 17 [*non* Semper].
1978b *Scissurella (Anatoma) koeneniana* R. Janssen, p. 142, pl. 9, fig. 6.

Remarks. The only specimen found has a coarser sculpture than the illustrated holotype. However, as the range of variation of the taxon is unknown, the specimen has been assigned to this species, which is also known from Mogenstrup.

Order Trochida

Family Trochidae Rafinesque, 1815

Subfamily Cantharidinae Gray, 1857

Genus *Steromphala* Gray, 1847

Type species: *Trochus strigosus* Gmelin, 1791, accepted as *Gibbula cineraria* (Linnaeus, 1758), accepted as *Steromphala cineraria* (Linnaeus, 1758) (type by original designation).

***Steromphala chattica* (R. Janssen, 1978)**
Fig. 7k

1978a *Jujubinus (Strigosella) chatticus* n. sp. R. Janssen, p. 23, pl. 1, fig. 8, pl. 4, fig. 2.
1978b *Jujubinus (Scrobiculinus) chatticus* R. Janssen, 1978 – p. 147, pl. 10, fig. 14.

Material. One juvenile specimen, NHMD 1651683 (ex MM-13610), DK 1256.

Description. The shell is very small and conical, a little higher than wide. The last whorl equals 0.85 of the total shell height, the aperture about 0.46. The aperture is rounded quadratic, the columella concave and the labrum is broken.

The protoconch is paucispiral and consists of one smooth whorl. The nucleus is small and depressed and the protoconch whorl is planspiral. There are 2½ teleoconch whorls, which are separated by a deep suture. On the first medium whorl there is a rather distinct edge on the middle of the whorl, which divides the whorl into an adapical flat part and an abapical part. On the next teleoconch whorl a further spiral appears below the edge, which also becomes a distinct spiral. On the flat adapical part of the whorl an indistinct spiral appears. The flat base is demarcated by a distinct spiral rib. There are *c.* 20 weak axial ribs which gradually get weaker on the terminal whorl. The axial ribs continue on the base, where they are very weak.

Discussion. The specimen is similar to the juvenile specimen illustrated by R. Janssen (1978a, pl. 1, fig. 8), but the aperture on the German specimen is more rectangular. According to WoRMS Editorial Board (2014), *Jujubinus (Strigosella)* Sacco, 1896 is a junior synonym of *Steromphala* Gray, 1847.

Remarks. The species is very common in the fauna from Glimmerode (R. Janssen 1978a), but only two additional specimens are known from Doberg (R. Janssen 1978b).

Genus *Margarites* Gray, 1847

Type species *Margarites diaphana* Gray, 1847 accepted as *Margarites helicinus* (Phipps, 1774) (type by monotypy).

***Margarites margaritula* (Sandberger, 1859)**
Fig. 7o, 7p

1959 *Tiburnus (margaritula) margaritula* (Sandberger, 1859) – Anderson, p. 55, pl. 2, fig. 4.
1978a *Margarites margaritula* (Sandberger, 1859) – R. Janssen, p. 23 [here extensive synonymy].

1978b *Margarites margaritula* (Sandberger, 1859) – R. Janssen, p. 146, pl. 9, fig. 12.

Material. The poor material of five specimens includes only defective and fragmentary remains.

Description. The shell is small and low conical. The height/ width ratio is *c.* 0.8. The protoconch consists of 1½ smooth whorls and the nucleus is small. There are *c.* 3½ convex and smooth teleoconch whorls, which are separated by a deep suture and quickly increasing in diameter. The height of the last whorl equals more than half the shell height. The transition into the slightly convex base is gradual. The umbilicus is deep and rather narrow. The labrum is broken, and the columella is thickened. Neither sculpture nor growth lines could be observed due to poor preservation.

Remarks. The specimens match the description and illustrations in the literature well.

Subclass Caenogastropoda Cox, 1960

Order Caenogastropoda Cox, 1960

Superfamily Triphoroidea Gray, 1847

Family Cerithiopsidae H. Adams & A. Adams, 1853

Genus *Cerithiopsis* Forbes & Hanley, 1850

Type species: *Murex tubercularis* Montagu, 1803, accepted as *Cerithiopsis tubercularis* (Montagu, 1803) (type by monotypy).

***Cerithiopsis* aff. *dautzenbergi* Glibert, 1949**
Fig 8p

1978a *Cerithiopsis (Cerithiopsis) 'henckeliusi'* auct. (pars) sp. 3 – R. Janssen, p. 57, pl. 5, fig. 8.
1978b *Cerithiopsis* (s. lat.) aff. *dautzenbergi* Glibert, 1949 – R. Janssen, p. 167, pl. 12, fig. 43.

Material. Three fragmentary specimens.

Remarks. The rather poor specimens match the descriptions and illustrations well (R. Janssen 1978 a, b). The medium whorls have three spiral cords, of which the adapical two are more narrowly spaced. On the base a weak spiral is situated close to the demarcating spiral rib.

***Cerithiopsis vilsundensis* n. sp.**

Fig. 8n

Type material. Holotype: Fig. 7o, NHMD 1177238 (ex MM-13631), DK-1202. leg. Henrik Madsen.
Additional material. ISL, three defective specimens.

Etymology. This species is named after the type locality.

Type locality. Coastal cliff at Vilsund.

Type strata. Unit X, upper Oligocene.

Diagnosis. A *Cerithiopsis* with three primary spirals and 16 slightly opisthocline axial ribs without knobs. The suture is slightly undulating.

Description. The shell is slender turriculate with a height/width ratio of 3.5. The largest specimen has the last 3½ protoconch whorls and six teleoconch whorls preserved. The last whorl equals 0.33 of the total shell height, the aperture and canal 0.20. The aperture is rounded ovate, with a rather short canal, which is turned to the left. The columella is slightly concave. The first three teleoconch whorls are very convex, the following medium convex.

The initial 1½ protoconch whorls are broken off. The terminal three whorls are convex and separated by a deep suture. They have about 25 axial ribs on the two first whorls and 20 on the terminal whorl. These ribs are slightly flexuous and become stronger on the terminal protoconch whorl. Two very delicate spiral ribs are present on the abapical part of the whorl, and they continue as the abapical two primary spirals. The transition into the teleoconch is gradual.

There are three primary spiral cords; the adapical is placed immediately under the suture, the second at one third of the whorl, and the third at one quarter above the abapical suture. On the following whorls this number continues. The spiral cords are weaker than their interspaces and are sharpest adapically. On the last whorl a fourth distinct spiral demarcates the flat base, which has a few weak spiral ribs at the transition of the neck of the canal.

The teleoconch whorls have slightly opisthocline axial ribs, which are of almost the same width as their interspaces. On the first two teleoconch whorls there are about 18 ribs, on the following 16 ribs. On the last whorl the ribs are more indistinct. The spiral cords run slightly undulating across the axial ribs but cause no knobs.

Discussion. The new species has some resemblance to *Cerithiopsis serrula* R. Janssen, 1978, but differs by having no knobs on the spirals, opisthocline and stronger

axial ribs, a more ovate aperture, and a relatively higher last whorl.

Superfamily Epitonioidea Berry, 1910 (1812)

Family Epitoniidae Berry, 1910 (1812)

Genus *Cirsotrema* Mörch, 1852

Type species: *Scalaria varicosa* Lamarck, 1822, accepted as *Cirsotrema varicosum* (Lamarck, 1822) (type by monotypy).

***Cirsotrema insigne* (Philippi, 1843)**
Fig. 8b

1978b *Cirsotrema (Cirsotremopsis) insigne* (Philippi, 1843) – R. Janssen, p. 175, pl. 13, fig. 61 [here extensive synonymy].

Material. One defective specimen.

Remarks. The specimen matches the description and illustrations in the literature well.

Genus *Pseudosassia* Vicián & Kovács, 2022

Type species: *Triton flandricum* Koninck, 1838 by original designation.

***Pseudosassia flandrica* (Koninck, 1838)**
Fig. 9i

1913 *Tritonium flandricum* – Harder, p. 75, pl. 6, fig. 3.
1979b *Charonia (Sassia) flandrica* (Koninck, 1837) – R. Janssen, p. 199 [herein extensive synonymy].
1987 *Charonia (Sassia) flandrica* (Koninck, 1837) – Schnetler & Beyer, p. 204.
1990 *Charonia (Sassia) flandrica* (Koninck, 1837) – Schnetler & Beyer, p. 48.
2022 *Pseudosassia flandrica* (Koninck, 1838) – Vicián & Kovács, p. 29.

Remarks. Vicián & Kovács (2022) assigned this species to their new genus and selected it as the type species.

The year of the publication of the paper by Koninck is in literature given as 1837 or 1838. Koninck (1838) dated it as "Liege, 29. January 1837', but the paper was first published 1838 in Nouveaux Mémoires de l'Académie des Sciences et Belles-Lettres de Bruxelles. Consequently, 1838 is the correct year.

Order Neogastropoda Wenz, 1938

Superfamily Buccinoidea Rafinesque, 1815

Family Buccinidae Rafinesque, 1815

Genus *Aquilofusus* Kautsky, 1925

Type species: *Fusus waeli* Nyst, 1852 by original designation.

***Aquilofusus elegantulus* (Philippi, 1843)**
Fig. 10a

1843 *Fusus elegantulus* Philippi, p. 59, 76, pl. 4, figs 16, 16a.
1968 *Scalaspira (Scalaspira) elegantula elegantula* – Tembrock, p. 216, pl. 1, figs 2–5. pl. 3, figs 2–7, pl. 5, figs 6–7, pl. 6, figs 7–7a, pl. 7, fig 11.
1967 *Aquilofusus elegantulus* – Rasmussen, p. 187, fig. 171, 12 [*non* Philippi, 1843].
1968 *Aquilofusus elegantulus* – Rasmussen, p. 72, fig. 12 [*non* Philippi, 1843].
1979 *Scalaspira (Scalaspira) elegantula elegantula* (Philippi 1843) – R. Janssen, p. 286, pl. 286, pl. 15, fig. 7 [here extensive synonymy].

Material. Four specimens.

▼ **Fig. 8. a,** *Haustator goettentrupensis* (Cossmann, 1899). Height 14.0 mm. MM-13618. **b,** *Cirsotrema insigne* (Philippi, 1843). Height 3.0 mm. NHMD 1651689 (ex MM-13619), DK 1262. **c,** *Cirsotrema crispata* Harder, 1913. Height 3.8 mm. MM-13620. **d,** *Cirsotrema (?Opaliopsis)* aff. *koeneni* A.W. Janssen, 1967. Height 3.2 mm. MM-13621. **e,** *Opalia pusilla* (Philippi, 1843). Height 3.5 mm. MM-13622. **f,** *Leptonotis planatus* (Speyer, 1864). Length 5.8 mm. **f1,** apertural view, **f2,** apical view. MM-13623. **g,** *Euspira helicina protracta* (Eichwald, 1830). Height 5.5 mm. MM-13624. **h,** *Norephora elatior* (Koenen, 1891). Height 2.1 mm. MM-13625. **i,** *Norephora elatior* (Koenen, 1891). Height 4.0 mm. MM-13626. **j,** *Cerithiella bitorquata* (Philippi, 1843). Height 1.5 mm. MM-13627. **k,** *Cerithiopsis henckeliusii* (Nyst, 1836). Height 2.4 mm. MM-13628. **l,** *Cerithiopsis serrula* R. Janssen, 1978. Height 4.8 mm. MM-13629. **m,** *Cerithiopsis* (s. lat.) *ariejansseni* R. Janssen, 1978. Height 6.3 mm. MM-13630. **n,** *Cerithiopsis vilsundensis* n. sp. Height 3.0 mm. Holotype, NHMD 1177238 (ex MM-13631), DK 1202. **o,** *Cerithiopsis jutensis* Schnetler, 1985. Height 1.4 mm. MM-13632. **p,** *Cerithiopsis* aff. *dautzenbergi* Glibert, 1949. Height 1.0 mm. NHMD 1651690 (ex MM-13633), DK 1263. **q,** *Laeocochlis supraoligocaenicus* Schnetler & Beyer, 1990. Height 5.0 mm. MM-13634. **r,** *Thereitis angusta* (Tembrock, 1965). Height 3.5 mm. MM-13635. **s,** *Seila* (s. lat.) *koeneni* R. Janssen, 1978. Height 1.7 mm. MM-13636.

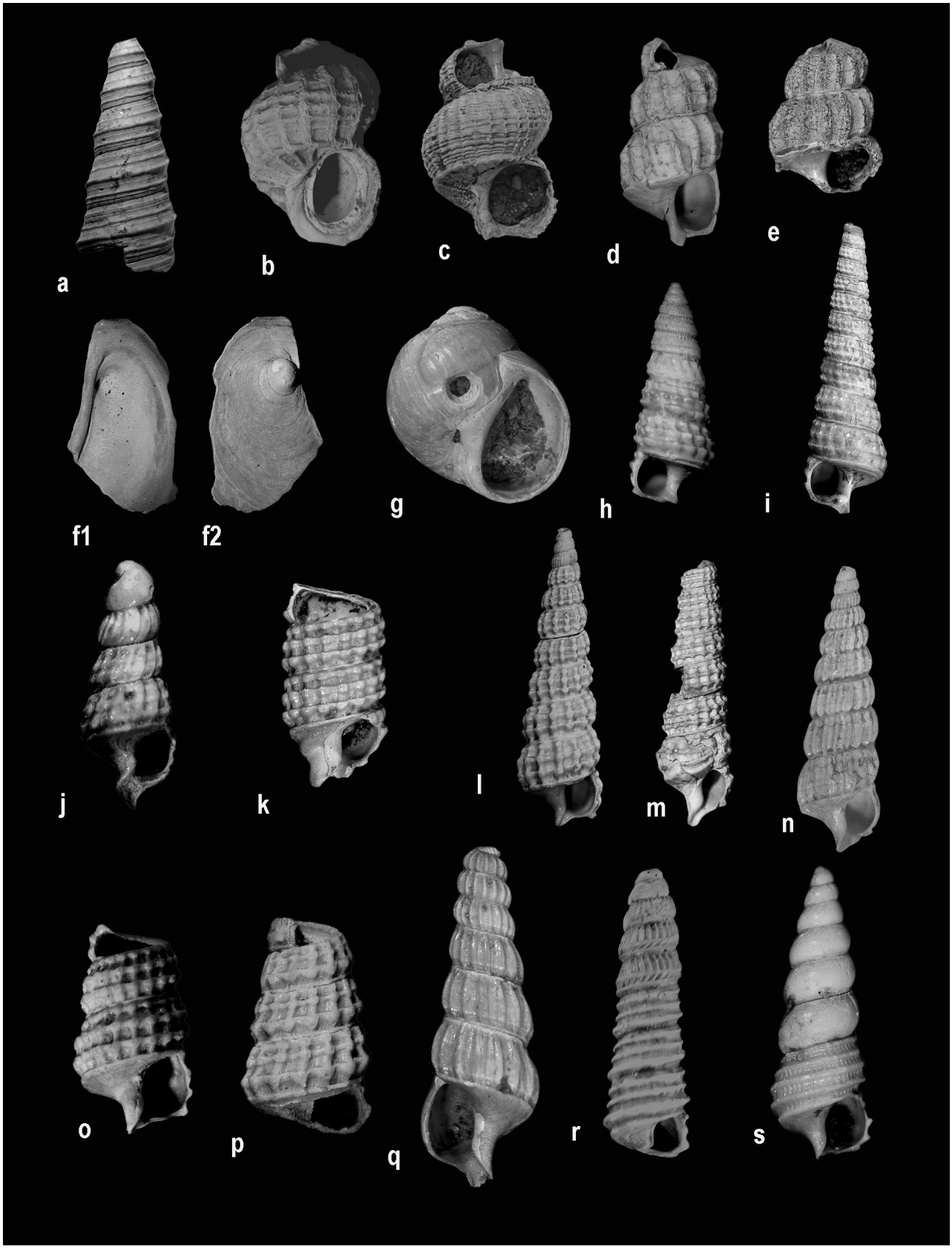
a
b
c
d
e
f1
f2
g
h
i
j
k
l
m
n
o
p
q
r
s

Remarks. The species is characterised by two strong spirals on the first teleoconch whorls. R. Janssen (1979, p. 287) considered *Aquilofusus cochleata* (Speyer, 1863) and *A. tricarinata* (Koch & Wiechmann, 1872) to be extreme forms of *A. elegantulus*. *A. elegantulus* has not previously been recorded from the Danish upper Oligocene. The species illustrated in popular scientific books has a spiral ornament, consisting of many spirals of the same strength. These features thus match *Aquilofusus elegantulus aequistriatus*, which R. Janssen (1979, p. 287) interpreted as an independent species, although he did not exclude an assignment to *A. elegantula*.

Superfamily Buccinoidea Rafinesque, 1815

Family Fasciolariidae Gray, 1853

Subfamily Fusininae Wrigley, 1927

Genus *Streptodictyon* Tembrock, 1961

Type species: *Streptochetus (Streptodictyon) elongatus* Tembrock, 1961 [*non* Nyst = *Streptodictyon sowerbyi* (Nyst, 1836) emend].

The Danish Oligocene species of *Streptodictyon*
Ravn (1907) and Harder (1913) assigned all specimens of *Streptodictyon* fom the middle Oligocene (= the lower Oligocene Viborg Formation and the lower upper Oligocene Branden Clay), as well as in the upper Oligocene (= the upper Oligocene Brejning Formation) to *Fusus elongatus* Nyst, 1836.

Cadée & Janssen (1994) assigned the early Oligocene specimens to *Streptodictyon subelongatus* (d'Orbigny, 1852) or *Streptodictyon impiger* Cadée & Janssen, 1994, both with a query. Almost all late Oligocene specimens were assigned to *Streptodictyon cheruscus* (Philippi, 1843). They introduced the new species *Streptodictyon schnetleri* and assigned two specimens (from Nørre Vissing and Brejning) to *Streptodictyon cheruscus* forma *fascilaroides* (Nyst, 1861), which was predominantly found in the Miocene. They considered *S. soellingensis* and *S. schnetleri* as parts of a lineage, as the latter species was only known from Chattian B at that time.

Schnetler & Palm (2008) monographed the lower upper Oligocene (Chattian A) Branden Clay fauna and found *S. soellingensis* (Tembrock, 1965) and *S. schnetleri*. As these species co-occur a lineage relationship is not supported. *S. cheruscus* is very common in the Brejning Formation but absent in the Branden Clay.

The present study has recorded *S. cheruscus*, *S. soellingensis* (Tembrock, 1965) and *S. schnetleri* from Unit X of early late Oligocene age. *S. cheruscus* is very common, but all specimens except one are juvenile. Only one juvenile specimen of *S. soellingensis* and 11 specimens of *S. schnetleri* have been found.

Family Muricidae Rafinesque, 1815

Subfamily Muricopsinae Radwin & D'Attilio, 1971

Genus *Murexsul* Iredale, 1915

Type species: *Murex octogonus* Quoy & Gaimard, 1833 (type by original designation).

***Murexsul kochi* (Beyrich, 1854)**
Fig. 10m

1854 *Murex kochi* Beyrich, p. 759.
1872 *Murex kochi* – Koch & Wiechmann, p. 13, pl. 1, figs 2a–c.
1963 *Coralliophila (Hirtomurex) kochi* Beyrich, 1854 – Tembrock, p. 323, pl. 2, fig. 9, pl. 3, figs 12–13, pl. 4, fig. 9.
1990 *Coralliophila (Hirtomurex) kochi* Beyrich, 1854 – Schnetler & Beyer, pl. 2, figs 15a–b.

Remarks. Lozouet (1998) questioned the assignment to *Coralliophila* because of the smooth, multispiral protoconch and suggested an assignment to *Murexsul* (P. Lozouet, pers. comm. 2023). The species was not mentioned by Merle *et al.* (2022).

▼ **Fig. 9. a,** *Alvania semperi* Wiechmann, 1871. Height 1.3 mm. MM-13637. **b,** *Rissoa karsteni* R. Janssen, 1978. Height 1.7 mm. MM-13638. **c,** *Cirsope multicingulata* (Sandberger, 1859). Height 3.0 mm. MM-13639. **d,** *Graphis hosiusi* (Lienenklaus, 1891). Height 2.2 mm. MM-13640. **e,** *Polygireulima pseudonaumanni* (R. Janssen, 1978). Height 4.0 mm. **e1,** apertural view, **e2,** lateral view. MM-13641. **f,** *Niso minor* Philippi, 1843. Height 3.1 mm. MM-13642. **g,** *Aporrhais speciosa* (Schlotheim, 1820). Height 4.4 mm. MM-13643. **h,** *Echinophoria rondeleti* (Basterot, 1825). Height 18.0 mm. MM-13644. **i,** *Pseudosassia flandrica* (Koninck, 1838). Height 20.0 mm. MM-13645. **j,** *Onustus scrutarium* (Philippi, 1843). Height 2.5 mm. **j1,** lateral view, **j2,** apical view, **j3,** umbilical view. MM-13646. **k,** *Euroscaphella siemssenii* (Boll, 1851). Height 36.0 mm. MM-13647. **l,** *Admetula postera* (Beyrich, 1863). Height 2.8 mm. MM-13648. **m,** *Unitas granulata* (Nyst, 1845). Height 2.0 mm. MM-13649. **n,** *Babylonella pusilla* (Philippi, 1843). Height 1.5 mm. MM-13650.

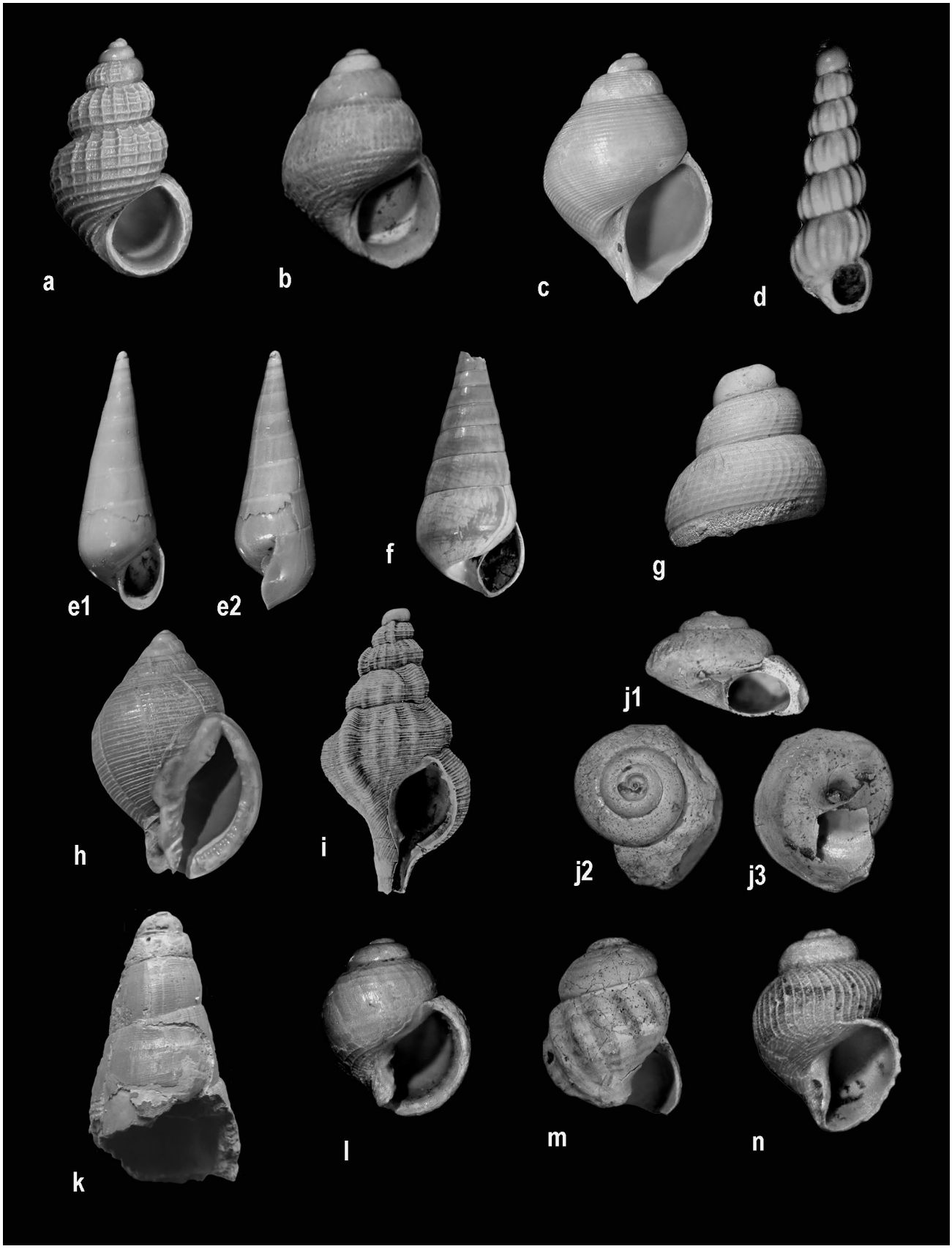
a
b
c
d
e1
e2
f
g
h
i
j1
j2
j3
k
l
m
n

Subfamily Typhinae Cossmann, 1903

Genus *Siphonochelus* Jousseaume, 1880

Type species: *Typhis arcuatus* Hinds, 1843 (type by original designation). Synonym: *Eotyphis* Tembrock, 1963; type species *Typhis sejunctus* Semper, 1861 (type by original designation).

***Siphonochelus fistulatus* (Schlotheim, 1820)**
Fig. 10s

1963 *Lyrotyphis (Lyrotyphis) fistulatus* (Schlotheim, 1820) – Tembrock, p. 318, pl. 7, fig. 3, pl. 8, figs 6, 12a–b, 13, pl. 10, figs 5–6.
1979a *Lyrotyphis (Eotyphis) fistulatus* (Schlotheim, 1820) – R. Janssen, p. 283 [here extensive synonymy].

Material. One defective specimen.

Remarks. R. Janssen (1979a, p. 284) suggested that this form might be a hybrid of *Lyrotyphis sejunctus* and *L. cuniculosus*, as it co-occurs with these species, which are also present in the Vilsund fauna. The species is very rare at German localities and has not previously been recorded from the Danish upper Oligocene, because the predominantly juvenile specimens have been confused with *L. cuniculosus*. *Siphonochelus fistulatus* is now known from Nørre Vissing, Jensgård, Kirstinebjerg Skov and the localities Boestholt and Fakkegrav on the northern coast of Vejle Fjord, Denmark (all occurences unpublished, coll. ISL, MNO and LSJ). Houart *et al.* (2021) stated that *Eotyphis* Tembrock, 1963 is a junior synonym of *Siphonochelus* Jousseaume, 1880.

Genus *Hirtotyphis* Jousseaume, 1880

Type species: *Murex horridus* Brocchi, 1814 (type by original designation).

***Hirtotyphis pungens* (Solander, 1766)**
Fig. 10t

1963 *Typhis (Typhis) pungens* (Solander, 1766) – Tembrock, p. 328, pl. 7, figs 9–10; pl. 8, figs 8, 17a–b; pl. 10, figs 9a–b.
1979a *Typhis (Typhis) pungens* (Solander, 1766) – R. Janssen, p. 282 [here extensive synonymy].

Material. One defective specimen.

Remarks. Lozouet (2023) discussed the genus *Hirtotyphis*, especially the different protoconchs, and questioned the distribution from the Eocene to the late Miocene of the species *Hirtomurex pungens*. The late Oligocene and Miocene species from the North Sea Basin have traditionally been assigned to this species. The only specimen found at Vilsund is defective and has no protoconch preserved but matches the descriptions and illustrations in the literature well. The species is very rare in Denmark and only known from Boestholt (coll. LSJ).

Superfamily Conoidea J. Fleming, 1822

Family Mitromorphidae T.L. Casey, 1904

Genus *Mitromorpha* Carpenter, 1865

Type species: *Daphnella filosa* Carpenter, 1864, *non* Dujardin, 1837 (= *Mitromorpha carpenteri* Glibert, 1954) by monotypy.

Subgenus *Mitrolumna* Bucquoy, Dautzenberg & Dollfus, 1883

Type species: *Mitra columbellaria* Scacchi, 1836 [*Mitra olivoidea sensu* Bucquoy, Dautzenberg & Dollfus, 1883, *non* Cantraine, 1835] by original designation.

***Mitromorpha (Mitrolumna) danica* n. sp.**
Fig. 12j

Type material. Holotype: NHMD 1177239 (ex MM-13692), DK-1203 (Fig. 10). Leg. Ulla Marcussen.

▼ **Fig. 10. a,** *Aquilofusus elegantulus* (Philippi, 1843). Height 20.0 mm. NHMD 1651692 (ex MM-13651), DK 1265. **b,** *Aquilofusus waeli* (Nyst, 1852). Height 8.2 mm. MM-13652. **c,** *Aquilofusus waeli* (Nyst, 1852). Height 3.2 mm. MM-13939. **d,** *Aquilofusus aequistriata* (Speyer, 1863). Height 22.0 mm. MM-13653. **e,** *Searlesia dentifera* Vermeij, 1991. Height 35.0 mm. MM-13614. **f,** *Boreosiphopsis danica* (Schnetler, 1985). Height 6.3 mm. MM-13654. **g,** *Streptodictyon cheruscus* (Philippi, 1843). Height 40.0 mm. MM-13657. **h,** *Streptodictyon cheruscus* (Philippi, 1843). Height 2.8 mm. MM-13655. **i,** *Streptodictyon schnetleri* Cadée & Janssen, 1994. Height 3.1 mm. MM-13656. **j,** *Streptodictyon soellingensis* (Tembrock, 1965). Height 2.3 mm. MM-13789. **k,** *Tritia schlotheimi* (Beyrich, 1854). Height 3.2 mm. MM-13658. **l,** *Pterynotus (Pterochelus) tristichus* (Beyrich, 1854). Height 6.5 mm. MM-13659. **m,** *Murexsul kochi* (Beyrich, 1854). Height 4.5 mm. MM-13660. **n,** *Eopaziella deshayesi* (Nyst, 1836). MM-13661. Height 41.0 mm. **o,** *Eopaziella capito* (Philippi, 1843). Height 9.5 mm. MM-13662. **p,** *Trophonopsis angustevaricata* (Gripp, 1915). Height 11.0 mm. MM-13663. **q,** *Siphonochelus sejunctus* (Semper, 1861). Height 6.4 mm. MM-13664. **r,** *Lyrotyphis cuniculosus* (Nyst, 1836). Height 1.5 mm. MM-13665. **s,** *Siphonochelus fistulatus* (Schlotheim, 1820). Height 8.5 mm. MM-13666. **t,** *Hirtotyphis pungens* (Solander, 1766). Height 4.0 mm. MM-13667.

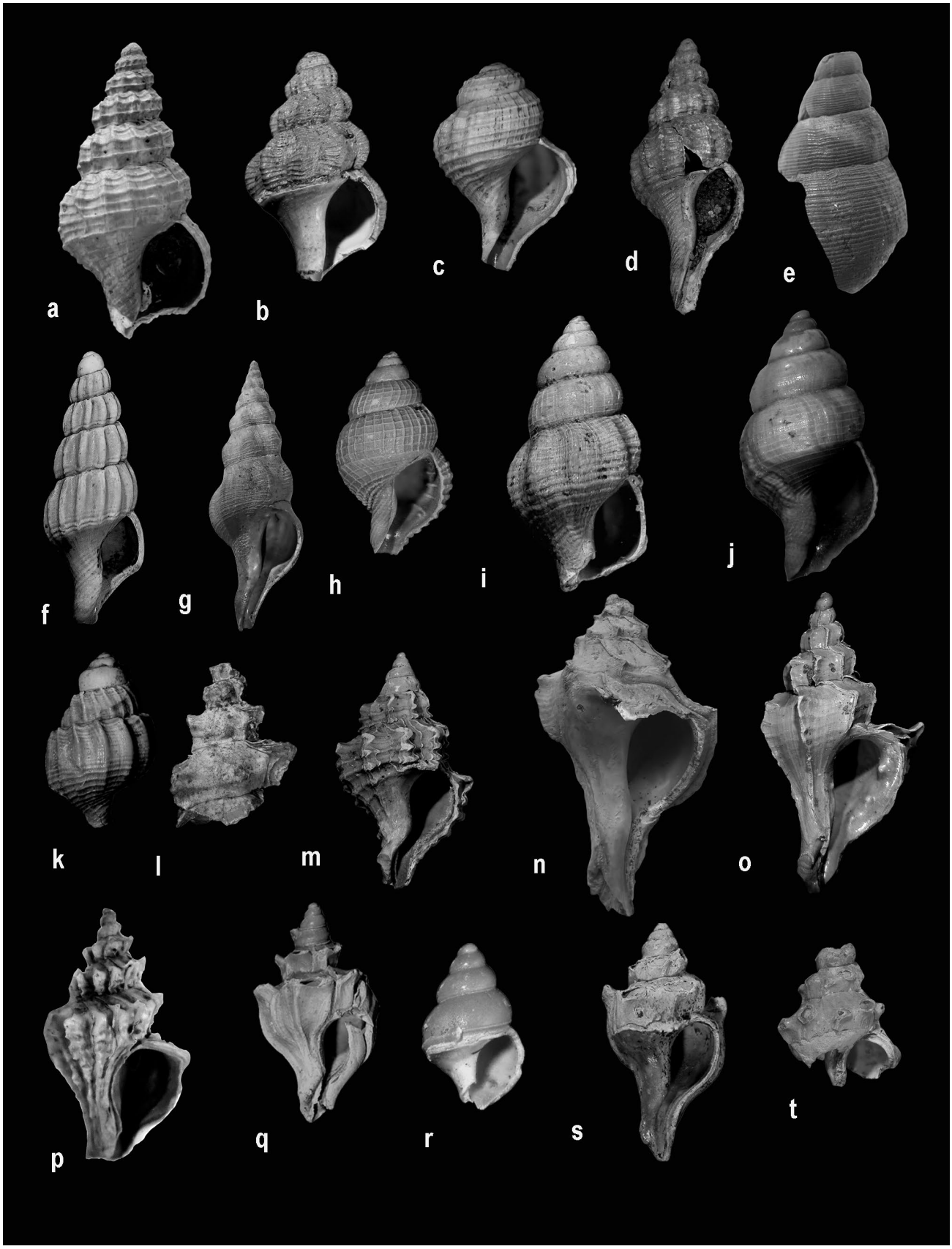
a
b
c
d
e
f
g
h
i
j
k
l
m
n
o
p
q
r
s
t

Etymology. Danica (latin) = Danish.

Type locality. Coastal cliff at Vilsund.

Type strata. Unit X, upper Oligocene.

Diagnosis. A *Mitromorpha (Mitrolumna)* with three primary spirals, 12–14 slightly opisthocline axial ribs and almost flat whorls. The spiral cords and axial ribs are fading gradually out on the teleoconch.

Material. Only the holotype. Height 5.3 mm.

Description. The shell is small and subfusiform. The height/width ratio is 2.3. The protoconch is paucispiral and has 1½ smooth and convex whorls, which are separated by a deep suture. The nucleus is large and almost semiglobular and the transition into the teleoconch is sharp and opisthocline.

The only specimen provides a little more than three almost flat whorls, which are separated by a distinct and slightly undulating suture. The last whorl equals 0.75 of the total shell height, the aperture 0.58. The base is slightly concave and regularly constricted into a rather short siphonal canal. There is a small pseudoumbilicus. The narrow aperture is elongated oval and acute posteriorly and goes into the rather short and straight canal. The columella is oblique to the axis and has two folds near the middle. The callus is well defined. The labrum is slightly thickened and partly broken. Growth lines are visible. They are slightly flexuous adapically and prosocyrt across the whorl, with a wide sinus.

The spiral ornament starts with three spiral bands, separated by much narrower interspaces. The abapical band is the strongest. On the next whorl a secondary spiral band is inserted and demarcated by deep spiral furrows on the following whorls. On the last whorl the spiral furrow between the middle and the anterior spiral bands is almost invisible, and the most prominent spiral ornament are the two spiral furrows demarcating the secondary spiral band, which remains narrow. The adapical spiral equals about one quarter of the whorl height, the middle and abapical spiral bands together a little more than the half. The spirals run slightly undulating across the axial ribs. On the neck of the canal there are about 15 rather distinct spirals.

The axial sculpture consists of 12–14 slightly opisthocline ribs, separated by interspaces of almost the same width. The axial ribs fade out on the last whorl. The shell has a rather smooth appearance because of the fading out of the sculptural elements.

Discussion. *Mitrolumna raulini septemtrionalis* R. Janssen, 1978 from the upper Oligocene of Glimmerode (Germany) is less slender and has more convex whorls with 25–30 weak axial ribs, which continue on the last whorl. The spiral cords are prominent on all teleoconch whorls. *Mitrolumna rupeliensis* Moths, 2000 (p. 28, pl. 10, fig. 5) from the lower Oligocene at Malliss (North Germany) has 7–10 spiral ribs and *c.* 20 opisthocline axial ribs. The aperture is wider and the folds on the columella are weaker. *Mitrolumna hortiensis* Lozouet, 1999 from the upper Oligocene at Peyrehorade (France) has a similar outline as the new species, but differs by having four narrow and sharp spirals, which run across 17–18 slightly opisthocyrt axial ribs. At the intersections between the spiral ornament and the axial ribs there are rather sharp knobs. The interior of the labrum has seven lirae. *Mitromorpha (Mitrolumna) panaulax* Cossmann, 1901 from the lower Pliocene of northwest France (see Ceulemans *et al*. 2018) is less slender and has narrow spiral cords, separated by groves, 7–8 on the penultimate whorl, axial sculpture restricted to the first two teleoconch whorls, outer lip arcuated in profile and denticulate within. Lozouet (2015) established four *Mitrolumna* species from the Oligocene and lower Miocene of Aquitaine (southwest France). *Mitrolumna ventriosa* Lozouet, 2015 has five primary spirals, 17–18 slightly opisthocline axial ribs, which together with spiral cords cause granules. The adapical spiral cord is wider than the other spiral cords and form a cord without granules. Furthermore, the columellar folds are stronger. *Mitrolumna peyroti* Lozouet, 2015 has 6–7 spiral cords on the first teleoconch whorl and 10–12 on the following whorls. The spiral cords run over numerous flattened axial ribs, which fade out on the last whorls, so the spiral ornament is dominating. *Mitrolumna oligomiocaenica* Lozouet, 2015 has three spiral cords, crossed by 16 opisthocyrt axial ribs on the first teleoconch whorl, and five cords, crossed by 20–21 axial ribs. The cords are granulated.

Mitrolumna? *atypica* Lozouet, 2015 has five spiral cords, and 14 slightly opisthocyrt axial ribs.

Schnetler & Palm (2008, p. 51; pl. 7, figs 15a–b, 16a–b, pl. 9, fig. 12) established *Aphanitoma ingerae* from the upper Oligocene Branden Clay of Denmark. We cannot maintain this generic assignment, as the species in outline, sculpture and aperture fits the subgenus *Mitrolumna* much better. Thus, we transfer the Branden Clay species to *Mitrolumna* and suggest the name *Mitromorpha* (*Mitrolumna) ingerae* (Schnetler & Palm, 2008) for it. This species has four primary spiral cords, arising to seven on the following whorls. There are 18–20 opisthocline axial ribs, which fade out on the last whorl.

According to Landau & Harzhauser (2022), species in the subgenus *Mitromorpha* lack well defined columellar folds, whereas species in *Mitrolumna* have two

columellar folds. *Mitrolumna* was relegated to being a subgenus of *Mitromorpha* Carpenter, 1865 by Kilburn (1986) and Drivas & Jay (1986), based on having similar radula formulae.

Family Mangeliidae P. Fischer, 1883

Genus *Benthomangelia* Thiele, 1925

Type species: *Surcula trophonoidea* Schepman, 1913, accepted as *Benthomangelia trophonoidea* (Schepman, 1913) (type by original designation).

***Benthomangelia brejningensis* (Schnetler & Beyer, 1990)**
Fig. 11p

1990 *Microdrillia (Andersondrillia) brejningensis* n. sp. Schnetler & Beyer, 1990, p. 66, pl. 3, figs 9a–b, 10.

Material. Two juvenile specimens.

Discussion. The material consists of a specimen with a complete protoconch and one half of the first teleoconch whorl and a specimen with two teleoconch whorls and the protoconch broken off. Both specimens match the description and illustrations in Schnetler & Beyer 1990 completely. The type species of *Andersondrillia* n. subgen. Schnetler & Beyer, 1990 is *Microdrillia grippi* Anderson, 1964. This species was assigned by Wienrich (2007) to the genus *Benthomangelia*, and Moths *et al*. (2010, p. 694, pl. 111, fig. 10, pl. 146, figs 3a–b, 4–5) discussed and illustrated the species. Lozouet (2017, p. 50) stated that *Andersondrillia* is a junior synonym of *Benthomangelia* and briefly discussed the Danish species. He questioned the assignment to *Benthomangelia* because of the more shouldered whorls and the muricoid outline. However, the Danish species has a protoconch with axial riblets and carinated whorls with growth lines having their sinus above the carina. It has some resemblance to *Benthomangelia venusta* (Peyrot, 1931) as illustrated by Lozouet (2017, pl. 21, figs 1–9). The Danish species differs from species of *Benthomangelia* by having a more concave adapical ramp and knobs on the intersections between spirals and axial ribs. However, we find the assignment to *Benthomangelia* most suitable.

Family Raphitomidae Bellardi, 1875

Genus *Eubela* Dall, 1889

Type species: *Pleurotoma limacina* Dall, 1881, accepted as *Eubela limacina* (Dall, 1881) (type by original designation, 1889, p. 102).

***Eubela* (s. lat.) *zetes* (Kautsky, 1925)**
Fig. 13a

1925 *Daphnella (Eubela) Zetes* Kautsky, p. 190, pl. 12, figs 19a–b.
1958 *Eubela* sp. – Sorgenfrei, p. 293.
2010 *Eubela zetes* (Kautsky, 1925) – Moths *et al*., p. 68, pl. 42, figs 6a–b.

Material. One specimen. NHMD 625416, DK-1176. Ex MM-13695.

Measurements. Heigh 3.9 mm, width 2.2 mm.

Description. The shell is rather small and biconical and the teleoconch whorls are carinated and separated by a distinct suture. The height/width ratio is 1.8, the last whorl equals 0.67 of the total shell height, the aperture and canal 0.45 of the total shell height. The only specimen available has a well preserved protoconch and almost three teleoconch whorls. The last whorl has a fracture, but the aperture is well preserved, except for the labrum, which is broken off. There are *c.* four protoconch whorls, which are medium convex and separated by a distinct suture. The nucleus is small. The last three protoconch whorls have a diagonally cancellated sculpture. At the transition into the teleoconch this sculpture disappears. The terminal protoconch whorl has its greatest diameter abapically and the adapical part of the whorl is flat. On the first teleoconch whorl an unsharp carina appears on the abapical part of the whorl and on the following teleoconch whorls the carina is situated a little above the middle of the whorl. The carina divides the whorls into an adapical concave part and a straight to convex abapical part. The aperture is lengthened ovate, with a very short canal, which is slightly turned to the left. The smooth columella is almost straight. The spiral ornament is very weak. There are no spirals on the adapical concave part of the whorls, but a weak subsutural band is suggested. Another very weak spiral demarcates the concave part of the whorl from the smooth carina. Under the carina there are c. 10 very weak spiral bands, of which one is wider and indistinctly demarcated and situated, where the following whorl is attached. On the neck of the canal there are c. 8 spiral bands, which are decreasing in strength abapically and separated by narrow spiral furrows. An axial sculpture is absent, except for the growth lines, which are most prominent on the concave adapical part of the whorl. On the subsutural band they cause small knobs, in a number of c. 40 on each whorl. In the concave part of the whorls the growth lines have a rather swallow sinus and, on the carina, they run almost horizontal and then, below the carina, they have a wide sinus. The shell has a glossy look because of the very weak ornament.

Discussion. The illustration in Kautsky (1925, pl. 12, figs 19a–b) is poor. Moths *et al.* (2010, p. 68, pl. 42, figs 6a–b) described and illustrated a specimen from the Hemmoorian in the gravel-pit Krinke. They stated that there was in fact a very weak spiral ornament, whereas Kautsky found no spiral ornament. The Danish specimen has a slightly more prominent spiral ornament and the carina situated above the middle of the whorl. On the German specimens, the carina is situated almost at mid-whorl, and the adapical ramp is concave from the first teleoconch whorl. However, these differences are small and, as the range of variation of the two populations is not known, we consider them to be conspecific.

Wenz (1943, p. 1456) mentioned only a few Recent species of *Eubela* from the Atlantic Sea and considered the fossil records as very dubious. Powell (1966) stated that the Recent species of Eubela live at depths of 250–1270 fathoms and have been recorded from Florida to Brazil, off Panama, and in the Indo-Pacific from East Africa to Japan and Hawaii. He stated two miocene species from New Zealand and *Eubela* ? *zetes* from Germany.

A literature review provides the following results: *Eubela limacina* (Dall, 1881) (p. 55), the type species of the genus, from the Western Atlantic, is rather slender and has only 16 subsutural knobs. *E. aequatorialis* Thiele, 1925 (p. 253, pl. 29, figs 13, 13a) 191 is rather slender and has no carina and *c.* 25 subsutural knobs. *E. distincta* Thiele, 1925 (p. 253, pl. 29, figs 15, 15a) is slender and has almost flat whorls and *c.* 30 subsutural knobs. *E. plebeja* Thiele, 1925 (p. 253, pl. 29, figs 16, 16a) has rather convex whorls and no subsutural knobs visible. *Eubela* sp. (Thiele 1925, p. 253, fig. 14) has *c.* 15 subsutural knobs. *E. mcgintyi* Schwengel, 1943 (p. 76, pl. 7, figs 4, 5) from Florida has rather convex whorls, no carina and no subsutural knobs visible. *E. nipponica* Kuroda, 1938 from Japan is slender and has a narrow ramp, and *c.* 25 subsutural knobs.

Eubela woodrowi Ladd, 1982 (p. 69, pl. 23, figs 7, 8) from the Pliocene of Fiji (Western Pacific Islands) is not carinated and has only 12 knobs on the subsutural band. *E. monile* Marwick, 1931 (p. 146, figs 310, 311) from the lower Miocene of New Zealand has a weaker shoulder.

All Recent species and the species from the lower Miocene of New Zealand and the Pliocene of Fiji are not carinated. As the species from the lower Miocene of Germany and the upper Oligocene of Denmark are carinated, they might belong to a separate genus. For the time being, we prefer to use the denomination s. lat.

Sorgenfrei (1958) assigned *Clinura trochlearis* (Hörnes, 1854) from the lower Miocene Klintinghoved Formation to the genus *Eubela*, and furthermore assigned a specimen from the Arnum Formation to the same species. According to his description and illustrations, these specimens have a biconical outline and distinct spirals under the carina and thus cannot be assigned to the genus *Eubela*. Sorgenfrei furthermore described another specimen as *Eubela* sp., one that seems to be conspecific with *Eubela* (s. lat.) *zetes*. The specimen from the Arnum Formation may be assigned to *Clinura circumfossa* (Koenen, 1872) (p. 100, pl. 2, figs 11a–b).

Genus *Pleurotomella* A.E. Verril 1872

Type species: *Pleurotomella packardii* A. E. Verrill, 1872 (type by monotypy).

***Pleurotomella rappardi* (Koenen, 1867)**
Fig. 12g

1979a *Pleurotomella (Pleurotomella) rappardi* (Koenen, 1867) – R. Janssen, p. 327, pl. 18, fig. 74 [here extensive synonymy].

Material. One juvenile specimen.

Description. The specimen has the protoconch and half of the first teleoconch whorl preserved. The protoconch is multispiral with *c.* 4½ whorls, which are medium to very convex and separated by a distinct suture. The nucleus is small and the last four whorls have a diagonally cancellated microsculpture. On

▼ **Fig. 11. a,** *Metula (Daphnobela) scabricula* (Philippi, 1843). Height 2.7 mm. MM-13668. **b,** *Vexillum hastatum* (Karsten, 1849). Height 6.8 mm. MM-13669. **c,** *Conomitra soellingensis* (Speyer, 1864). Height 6.0 mm. MM-13670. **d,** *Ancilla karsteni* (Beyrich, 1856). Height 12.0 mm. MM-13671. **e,** *Conus semperi* Speyer, 1862. Height 5.5 mm. MM-13672. **f,** *Bathytoma leunisii* (Philippi, 1843). Height 20.6 mm. MM-13673. **g,** *Drilliola speyeri* (Koch & Wiechmann, 1872). Height 3.0 mm. MM-13674. **h,** *Microdrillia ingerae* Schnetler & Beyer, 1990. Height 2.3 mm. MM-13675. **i,** *Orthosurcula regularis* (Koninck, 1838). Height 15.2 mm. MM-13676. **j,** *Glibertturricula ariejansseni* Schnetler & Beyer, 1987. Height 4.0 mm. **j1,** apertural view, **j2,** rear view. MM-13688. **k,** *Cochlespira volgeri* (Philippi, 1843). Height 2.2 mm. MM-13677. **l,** *Fusiturris selysii* (Koninck, 1838). Height 7.7 mm. MM-13678. **m,** *Fusiturris duchastelii* (Nyst, 1836). Height 5.9 mm. MM-13679. **n,** *Fusiturris enodis* R. Janssen, 1979. Height 8.0 mm. MM-13680. **o,** *Boreodrillia undatella* (Speyer, 1867). Height 5.0 mm. MM-13681. **p,** *Benthomangelia brejningensis* (Schnetler & Beyer, 1990). Height 4.8 mm. MM-13682. **q,** *Benthomangelia holzapfeli* (Koenen, 1890). Height 4.4 mm. MM-13683.

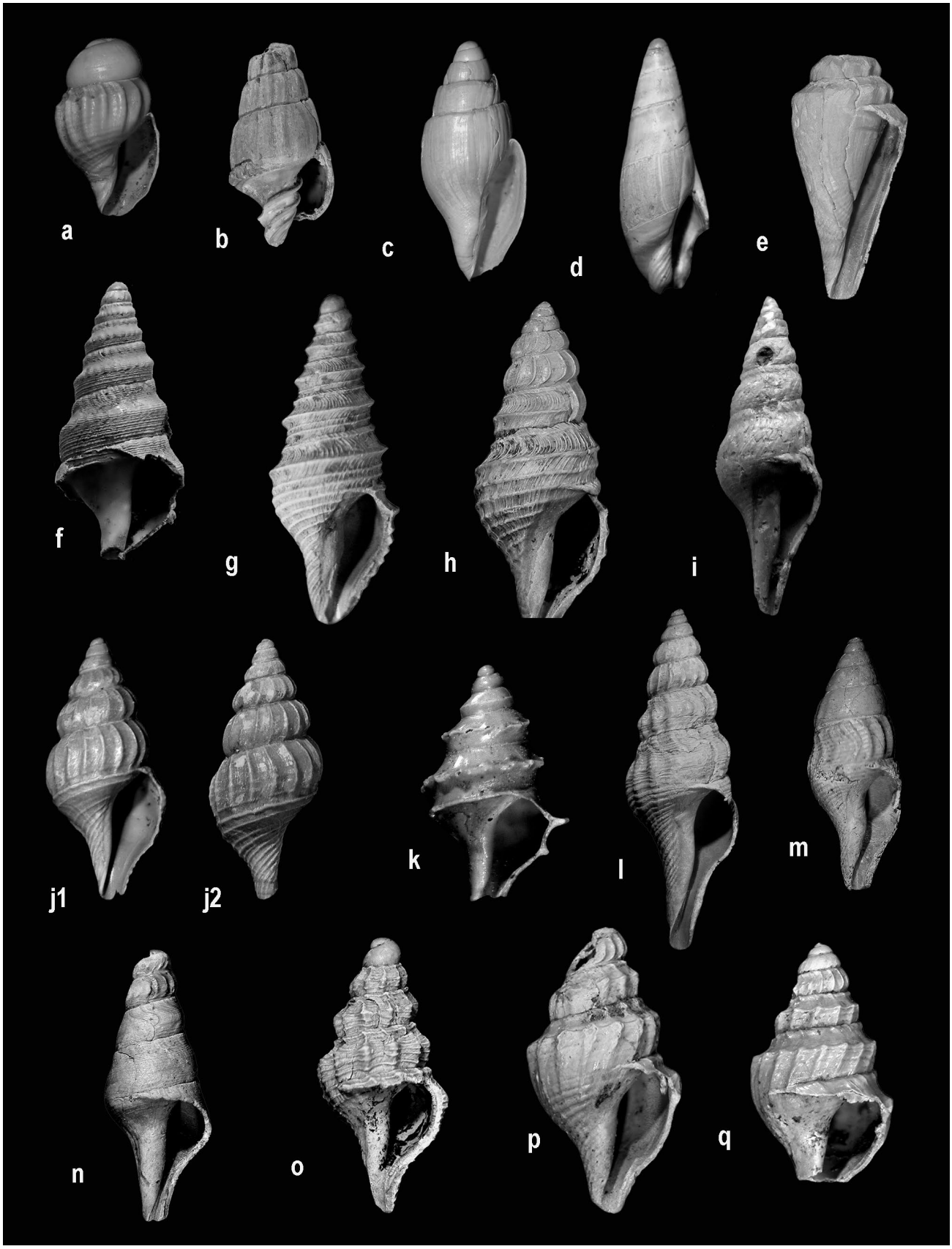
a
b
c
d
e
f
g
h
i
j1
j2
k
l
m
n
o
p
q

the terminal protoconch whorl a distinct spiral keel occurs below the middle of the whorls and soon a further spiral keel occurs below the first. These two keels continue as the primary spirals. On the terminal half of the protoconch fine axial riblets occur below the adapical suture and the transition into the teleoconch whorl is indicated by the disappearance of the diagonal cancellation. A secondary spiral rib is inserted between the two primary spirals and soon is of the same strength as the primary spirals. Fine knobs occur at the intersections between the spiral ribs and the axial ribs. On the slightly convex base and the neck of the canal an additional eight spirals are present, and they are diminishing in strength towards the end of the canal. The aperture is rounded oval and constricted into the rather short canal, which is slightly turned to the left.

Remarks. The species has not previously been recorded from the Danish upper Oligocene. Two juvenile specimens have been found in material from a glacial floe at Skanderborg and three juvenile specimens at Kirstinebjerg Skov (coll. ISL, unpublished). In the German upper Oligocene, the species is rather common at Söllingen, Niederkaufungen and in Sternberger Gestein, but elsewhere very rare or absent (R. Janssen 1979a).

Subclass Heterobranchia Burmeister, 1837

Grade 'Lower Heterobranchia'

Superfamily Mathildoidea Dall, 1889

Family Mathildidae Dall, 1889

Genus *Mathilda* Semper, 1865

Type species: *Turbo quadricarinatus* Brocchi, 1814, accepted as *Mathilda quadricarinata* (Brocchi, 1814) (type by subsequent designation).

***Mathilda bicarinata* Koch & Wiechmann, 1872**
Fig. 13d

1872 *Mathilda bicarinata* Koch & Wiechmann, p. 107, pl. 2, figs 5, 5a–c.
1978b *Mathilda (Fimbriatella) bicarinata* Koch & Wiechmann 1872 – R. Janssen, p. 183, pl. 13, fig. 69.

Material. One very juvenile specimen and one fragment.

Remarks. The species was not previously recorded from the Danish upper Oligocene. A single complete adult specimen is known from Kirstinebjerg Skov (coll. ISL, unpublished).

Family Pyramidelliidae Gray, 1840

Genus *Odostomia* J. Fleming, 1813

Type species: *Turbo plicatus* Montagu, 1803, accepted as *Odostomia plicata* (Montagu, 1803) (type by subsequent designation).

***Odostomia ventriosa* (Speyer, 1870)**
Fig. 13f

1870 *Odontostoma ventriosum* Speyer, p. 53, pl. 10, fig. 7.
1978a *Odostomia (Cyclodostomia) ventriosum* – R. Janssen, p. 141.
1979 *Odostomia (Cyclodostomia) ventriosa* – R. Janssen, p. 333, pl. 18, fig. 83.

Material. Two specimens.

Remarks. The specimens have a characteristic angulated last whorl, a rather thick walled shell and a distinct columellar fold and match the description in R. Janssen 1979 well. The species is very rare in the German upper Oligocene. R. Janssen (1979) only mentioned one specimen each from Glimmerode and Ahnetal.

▼ **Fig. 12. a,** *Splendrillia koeneni* (Speyer, 1867). Height 10.8 mm. MM-13684. **b,** *Stenodrillia obeliscus* (des Moulins, 1842). Height 17.0 mm. MM-13685. **c,** *Amblyacrum roemeri* (Koenen, 1867). Height 3.6 mm. MM-13686. **d,** *Polystira koninckii* (Nyst, 1845). Height 3.0 mm. MM-13687. **e,** *Acamptogenotia morreni* (Koninck, 1838). Height 18.5 mm. MM-13689. **f,** *Gemmula geinitzi* (Koenen, 1890). Height 5.4 mm. MM-13690. **g,** *Pleurotomella rappardi* (Koenen, 1867). Height 2.2 mm. **g1,** apertural view, **g2,** rear view. NHMD 1651684 A (ex MM-13691), DK 1257. **h,** *Pleurotomella margaritata* R. Janssen, 1978. Height 3.8 mm. MM-13693. **i,** *Rimosodaphnella lappanni* Schnetler & Beyer, 1990. Height 1.3 mm. MM-13694. **j,** *Mitromorpha* (*Mitrolumna) danica* n. sp. Height 5.3 mm. **j1,** apertural view, **j2,** rear view, **j3,** lateral view. Holotype, NHMD 1177239 (ex MM-13692), DK-1203.

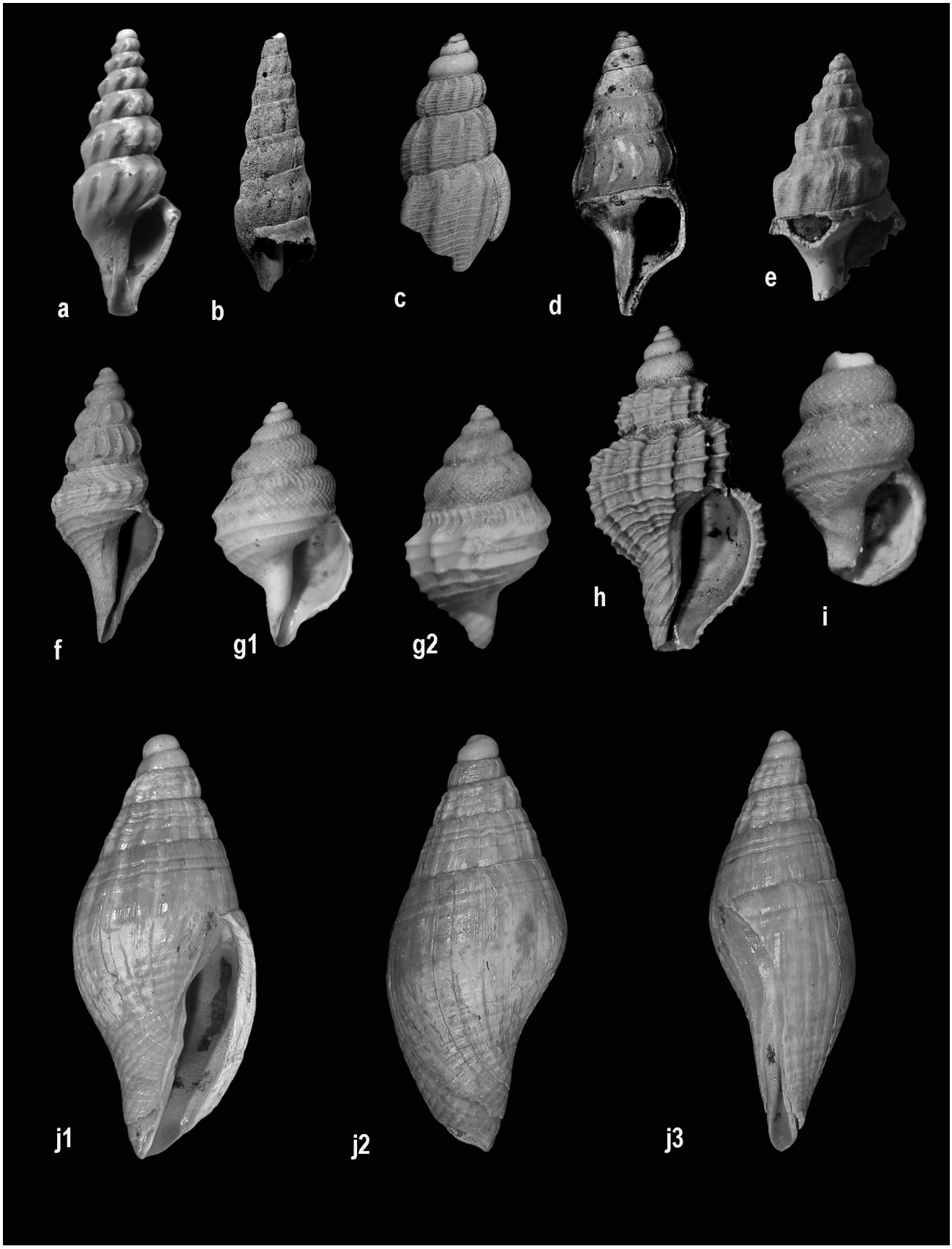
a
b
c
d
e
f
g1
g2
h
i
j1
j2
j3

Comparisons with other late Oligocene mollusc faunas

Mogenstrup (Schnetler & Beyer 1990)
The fauna contains 197 species and the Vilsund fauna shares 109 (80.9 %) with it. However, there are some differences in the frequencies of Limopsidae species. The two small species *Aspalima chattica* and *Cosmetopsis retifera* are very common in the Mogenstrup fauna, but extremely rare at Vilsund, and *Limopsis parva* is generally much larger at Vilsund (maximum size 20 mm). The gastropod species *Homalopoma simplex* is very common at Vilsund and represented by full-grown specimens as well as juvenile specimens but is very rare at Mogenstrup. There is a higher diversity of Muricidae at Vilsund. *Gemmula* species are only represented by a single *Gemmula geinitzi* at Vilsund but are more common at Mogenstrup. Pteropods are absent in the Vilsund fauna but present in the Mogenstrup fauna. *Laeocochlis supraeoligocaenicus* is present, but not as common as in the Vilsund fauna. This species is only known from Mogenstrup and Vilsund.

Nørre Vissing (Schnetler & Beyer 1987)
The fauna contains 144 species and the Vilsund fauna shares 73 species (60.3 %) with it. Of the Limopsidae only *Limopsis parva* is common, whereas *Cosmetopsis retifera* and *Aspalima chattica* are rare and *Oblimopa vonderhochti* absent. Typical Vilsund species such as *Acar* aff. *dentiens*, *Homalopoma simplex* and *Astraea pustulosa* are absent, as are several Cerithiopsidae species. Muricidae are less diverse and *e.g., Trophonopsis angustevaricata* and *Murexsul kochi* are absent.

Aarhus (Harder 1913)
The classical Danish fauna contains 87 species and the Vilsund fauna shares 50 (41.3 %) with it. The family Muricidae is less diverse and many small species, *e.g.* Cerithiopsidae, are absent. Characteristic Vilsund species such as *Acar* aff. *dentiens*, *Homalopoma simplex*, *Astraea pustulosa*, *Trophonopsis angustevaricata* and *Murexsul kochi* are absent. The pteropod species *Ireneia tenuistriata* (Semper, 1861) is rather common. The number of species from Aarhus is somewhat lower, as the clay samples were not processed.

Cilleborg (Ravn 1907)
The classical fauna contains 49 species and the Vilsund fauna shares 28 (22.6 %) with it. The occurrence of the species *Searlesia dentifera* is noteworthy.

Brejning (Eriksen 1937 and unpublished material in coll. ISL, coll. MNO and NHMD)
The fauna contains *c.* 100 species and the Vilsund fauna shares 67 species (55.0 %) with it. The occurrence of the species *Oblimopa vonderhochti*, *Acar* aff. *dentiens*, *Aspalima chattica, Searlesia dentifera* and *Benthomangelia brejningensis* are noteworthy.

Skanderborg (highway excavation 1976, unpublished, coll. ISL)
The fauna contains *c.* 120 species and the Vilsund fauna shares 77 species (63.6 %) with it. The occurrence of the species *Pleurotomella rappardi* and *Trophonopsis angustevaricata* are noteworthy. The pteropod species *Ireneia tenuistriata* (Semper, 1861) is very common, but is absent in the Vilsund fauna.

Kirstinebjerg Skov (coastal cliff, unpublished, coll. ISL and coll. MNO)
The fauna contains *c.* 120 species and the Vilsund fauna shares 63 species (52.1 %) with it. Noteworthy species are *Pleurotomella rappardi* and *Mathilda bicarinata*. The pteropod species *Ireneia tenuistriata* (Semper, 1861) is rather common, but is absent in the Vilsund fauna.

Branden (Denmark)
The fauna of the lower upper Oligocene Branden Clay was studied by Schnetler & Palm (2008). This fauna contains 78 species but shares only 46 species (38.3 %) with the Vilsund fauna.

The mollusc faunas from Vilsund and Mogenstrup are very similar and contain several species which are absent at other Danish localities. However, the noteworthy species mentioned above may suggest that part of the glauconitic clay at the Cilleborg, Brejning, Skanderborg and Kirstinebjerg Skov localities might be of the same age as at Vilsund and Mogenstrup. Unit X is only present at Vilsund, Mogenstrup and in the Harre borehole (Śliwińska *et al.* 2012). Ulleberg (1987, p. 198) presumed, based on Troelsen (1955), that the Branden Clay might be present at Cilleborg. Further studies are necessary.

▼ **Fig. 13. a,** *Eubela* (s. lat.) *zetes* (Kautsky, 1925). Height 3.9 mm. **a1,** apertural view, **a2,** rear view, **a3,** lateral view. NHMD 625416 (ex MM-13695), DK 1176. **b,** *Acteon punctatosulcata* (Philippi, 1843). Height 1.1 mm. MM-13699. **c,** *Nipteraxis bimonilifera* (Sandberger, 1859). Height 3.4 mm. **c1,** lateral view, **c2,** apical view, **c3,** umbilical view. MM-13696. **d,** *Mathilda bicarinata* Koch & Wiechmann, 1872. Height 0.8 mm. NHMD 1651686 A (ex MM-13697), DK 1259. **e,** *Crenilabium terebelloides* (Philippi, 1843). Height 3.4 mm. MM-13698. **f,** *Odostomia ventriosa* (Speyer, 1870). Height 1.5 mm. NHMD 1651685 A (ex MM-13700), DK 1258. **g,** *Odostomia* sp. Height 2.2 mm. MM-13701. **h,** *Syrnola subcylindrica* (Philippi, 1843). Height 4.1 mm. MM-13702. **i,** *Syrnola laevissima* (Bosquet, 1859). Height 4.6 mm. MM-13703. **j,** *Turbonilla jeffreysi* Koch & Wiechmann, 1872. Height 1.6 mm. MM-13704. **k,** *Chrysallida* sp. Height 1.8 mm. MM-13705.

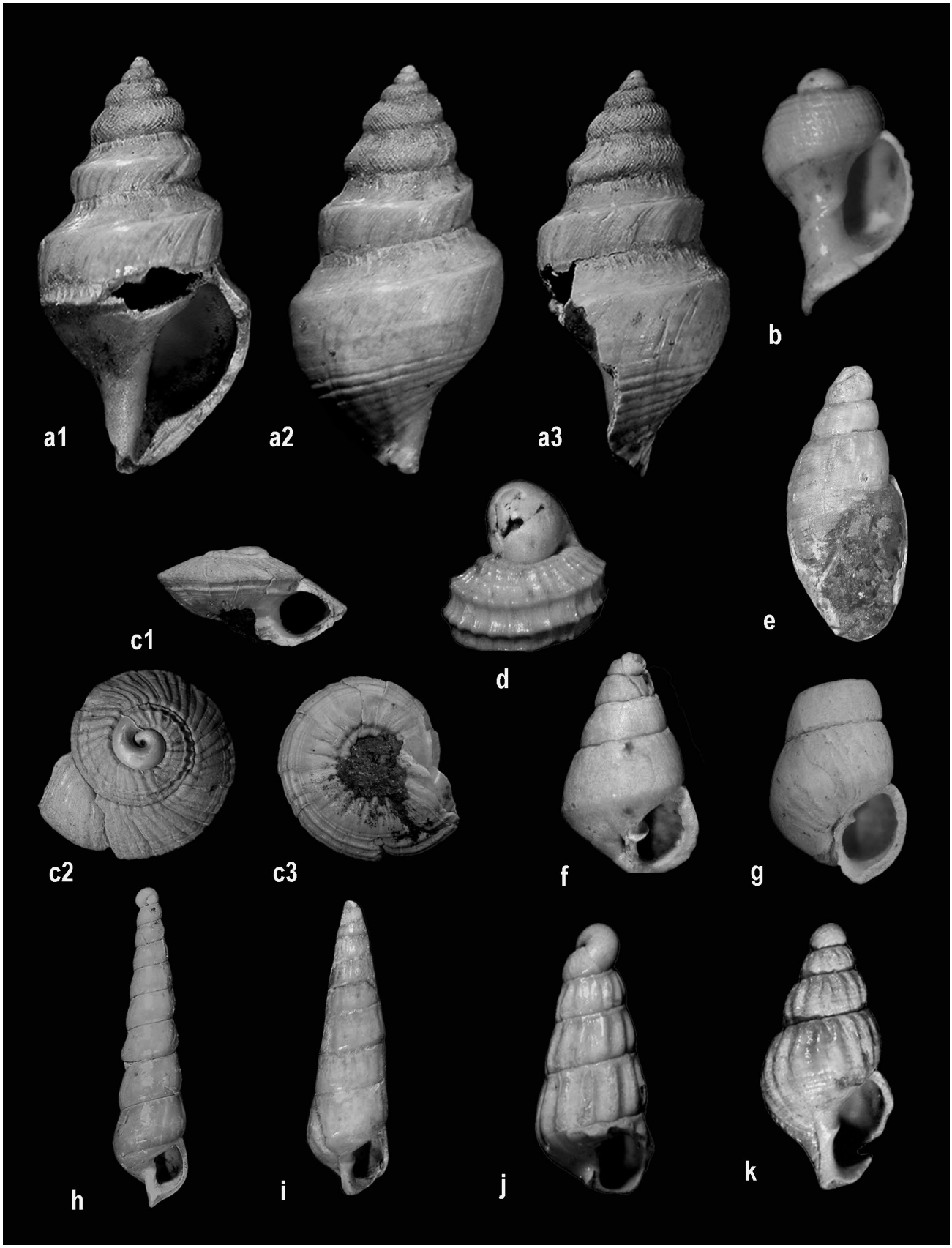
a1
a2
a3
b
c1
d
e
c2
c3
f
g
h
i
j
k

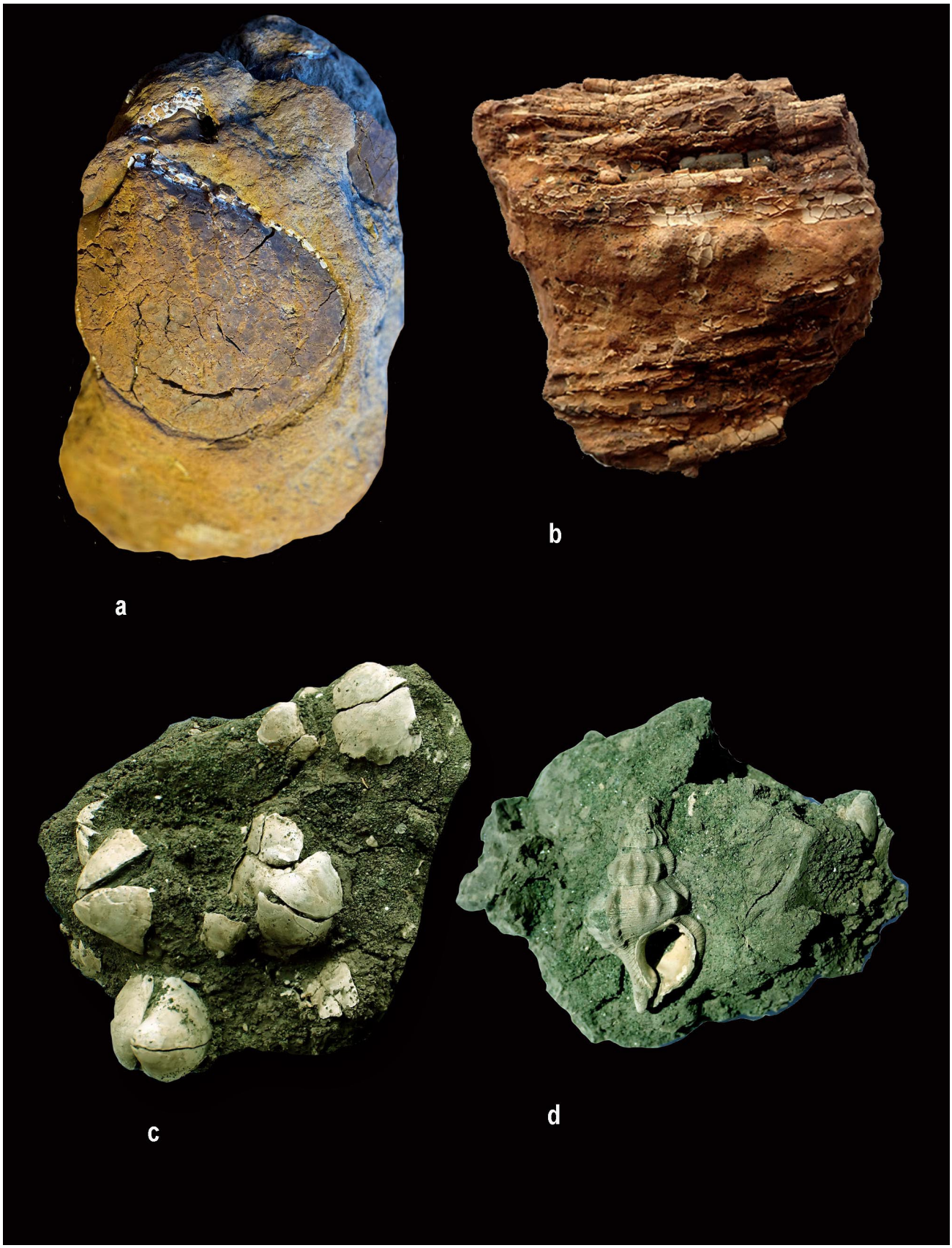

Fig. 14. a, *Cubiostrea* sp. in siderite. Height 128 mm, width 103 mm. MM-13707. **b,** Fossilised wood with borings by Teredinidae. Length of specimen 7 cm. MM-13706. **c,** Glauconitic clay with concentration of Terebrataliidae. Height of largest brachiopod specimen 10 mm. MM-13914. **d,** Glauconitic clay with *Pseudosassia flandrica*. Height of gastropod 35 mm. MM-13915.

Faunas of the same age from Germany have been described by R. Janssen (1978a, 1978b, 1979a, 1979b).

Glimmerode
The Vilsund fauna shares 95 species (77 %) with the fauna from Glimmerode, Germany. Many characteristic species are in common, *e.g.* Cerithiopsidae, *Acar* aff. *dentiens*, *Homalopoma simplex*, *Steromphala chattica* and *Astraea pustulosa*. Of the Limopsidae only *Cosmetopsis retifera* is common, whereas *Aspalima chattica*, *Limopsis parva* and *Oblimopa vonderhochti* are absent.

Freden
77 species (63.6 %) are in common with the Vilsund fauna, among which are *Limopsis parva* and *Astraea pustulosa*. Almost all Cerithiopsidae, *Drilliola speyeri* and *Oblimopa vonderhochti* are absent.

Krefeld
81 species (61.9 %) are in common with the Vilsund fauna. Among these are *Limopsis parva*, *Oblimopa vonderhochti*, *Cirsope multucingulata*, *Cirsotrema crispata*, *Conomitra soellingensis* and *Drilliola speyeri*.

Söllingen
Only 59 species (48.8 %) are in common with the Vilsund fauna. Among these are *Acar* aff. *dentiens*, *Scissurella koeneniana*, *Astraea pustulosa* and *Pterynotus tristichus*.

Palaeoecological interpretation

Many mollusc species are very rare, and several species are represented by juvenile specimens only, whereas others occur as both adults and juveniles. With a few exceptions, larger species are rare. Numerous sharp-edged fragments of *e.g. Limopsis parva* are most likely due to compaction of the sediment.

The bivalve assemblage is dominated by the Limopsidae species *Limopsis parva* and *Oblimopa vonderhochti* and the Arcidae species *Acar* aff. *dentiens*. Limopsidae are epibenthic and byssate and live in a sublittoral environment (Schnetler & Beyer 1990). Fragments of the pectinid species *Palliolum limatum* are abundant. Less common are the endobenthic species *Nuculana westendorpi*, *Cyclocardia grossecostata* and *Astarte gracilis*.

Limopsis parva is found as large specimens when compared to other Danish upper Oligocene localities, *e.g.*, Nørre Vissing, Aarhus and Skanderborg (largest specimen 20.0 mm), This finding suggests that good conditions existed for the species at Vilsund. *Oblimopa vonderhochti* is known from Mogenstrup (Schnetler & Beyer 1990), where large specimens were also found. This species has also been found in unpublished material from Brejning (coll. K. Eriksen, NHMD), but is absent at all other Danish upper Oligocene localities.

Acar aff. *dentiens* is very common and most specimens are rather large. Almost all specimens are worn or crushed. This species has also been recorded with lower frequency from Mogenstrup and a single unpublished specimen was found in the K. Eriksen collection from Brejning (NHMD); the species is absent at all other Danish upper Oligocene localities. The species is very common in the near-shore assemblage at Glimmerode, Germany (R. Janssen 1979b).

The abundant fragments of *Palliolum limatum* and a few of *Hilberia bifida*, as well as the worn specimens of the Limopsidae, indicate reworking or transport. Recent species of *Bathyarca* live in deep water (MolluscaBase 2022) and the presence of *Bathyarca bellula* might indicate deeper water, *e.g.* at least deeper sublittoral. Overall, the bivalve assemblage indicates littoral to deeper sublittoral conditions.

Gastropod species, such as *Microdrillia ingerae*, *Streptochetus cheruscus* and *Fusiturris duchastelii*, are almost exclusively found as juvenile specimens, whereas *Astraea pustulosa*, *Homalopoma simplex* and *Bathytoma leunisii* are found as juveniles and adults. *Astraea pustulosa* and *Steromphala chattica* indicate littoral conditions (R. Janssen 1978a), whereas *Pseudosassia flandrica* indicates deeper water (R. Janssen 1978a). Recent species of the gastropod genus *Homalopoma* are generally sublittoral to bathyal (*e.g. Homalopoma sanguinem* (Linnaeus, 1758): 200 m; *H. eoa* Azuma, 1972: 300–400 m, and *H. laevigata* Sowerby, 1914: 50–200 m, see Poppe 2008). The genus *Eubela* indicates bathyal conditions (Wenz 1943). Species of the families Cerithiopsidae and Triphoridae are generally indicators of shallow water, whereas the family Newtoniellidae is associated with the deep sea (Fernandes & Pimenta 2017). The rather common species *Laeocochlis supraeoligocaenicus* (Newtoniellidae) thus indicates deep water, whereas the diversity of the family Cerithiopsidae and the rather common *Norephora elatior* indicate shallow water. In all, the gastropod assemblage indicates littoral to sublittoral conditions, except for *Eubela* (s. lat.) *zetes*, *Pseudosassia flandrica*, *Laeocochlis supraeoligocaenicus* and *Homalopoma simplex*.

Schnetler & Beyer (1990) studied the fauna from Mogenstrup and found a mixed mollusc fauna with elements indicating deep marine conditions and others indicating more shallow water. They suggested that some species, *e.g.*, the Chattian A pectinids *Hilberia soellingensis* and *Hilberia bifida* and the shallow marine fauna, are most likely reworked. Rasmussen *et al.* (2010) suggested that the shallow marine fauna was transported down the delta or shelf slope to the basin floor. The mixed faunal assemblage from Mogenstrup thus seems to be a thanatocoenosis.

In all, the mollusc assemblage at Vilsund also indicates that the fauna is a thanatocoenosis. The presence of rolled quartz grains in the residues also indicates periods with littoral conditions, and erosion and transport of the molluscs from the littoral zone to the basin floor.

Schwarzhans (pers. comm. 2022) gave a preliminary overview of the otoliths from Vilsund and Mogenstrup and concluded that the Vilsund species indicated rather deep water (100–200 m), deeper than the Mogenstrup species.

Conclusions

A mollusc fauna of 120 taxa has been studied and compared with other faunas of late Oligocene age. Sixteen species have been recorded from the Danish upper Oligocene for the first time, and a synopsis of the representatives of the genus *Streptodictyon* Tembrock, 1961 in the Danish Oligocene is given. Two new species *Mitromorpha (Mitrolumna) danica* n. sp. and *Cerithiopsis vilsundensis* n. sp. are established. The species *Eubela* (s. lat.) *zetes* (Kautsky, 1925) is the oldest representative of a predominantly Recent genus. The bivalve genus *Cubiostrea* Sacco, 1897 has been encountered in the upper Oligocene of the North Sea Basin for the first time. *Andersondrillia* Schnetler & Beyer, 1990 is considered a junior synonym of *Benthomangelia* Thiele, 1925. The environment of the mollusc fauna was most likely sublittoral, but the bivalve species *Bathyarca bellula* (Wiechmann, 1874), the extremely rare gastropod species *Eubela* (s. lat.) *zetes*, the very common gastropod species *Homalopoma simplex*, and the rather common species *Laeocochlis supraeoligocaenicus* and *Pseudosassia flandrica* indicate deeper water (sublittoral to bathyal conditions). The reworked molluscs indicate that the shallow marine fauna was transported down the delta or shelf slope to the basin floor. The mollusc fauna is presumed to be a thanatocoenosis.

The fauna is compared with other upper Oligocene Danish and German faunas and palaeoecological interpretations are suggested. The fauna has the closest affinities to the faunas from Mogenstrup and Glimmerode. As many of the mollusc species have not previously been illustrated from the Danish upper Oligocene, the fauna is extensively illustrated.

Dinocyst and foraminifer studies were carried out on samples from the Oligocene sections at Vilsund and Mogenstrup. The studied assemblages indicate that the greenish, glauconitic clay with siderite at the Vilsund 2 locality and Mogenstrup should be assigned to Unit X in Śliwińska *et al.* (2012) or the lowermost Brejning Formation, whereas a similar lithology at the Vilsund 1 locality is referred to the Branden Clay. The high Vilsund 3 section at Volbjerg exposes an undisturbed depositional contact between the Viborg Formation and Branden Clay, thus demonstrating a 6 Ma hiatus with most of the Rupelian missing in this area. The dark glauconite-free micaceous clay in the former clay-pit of Vilsund Brickworks is referred to the upper part of the Brejning Formation and the greenish, glauconitic clay in the clay-pit should most likely be assigned to Unit X or the lowermost Brejning Formation. The mollusc faunas from Vilsund and Mogenstrup are the first recorded from Unit X or the lowermost Brejning Formation.

Acknowledgements

We are indebted to Erik Skovbjerg Rasmussen (GEUS, Copenhagen) for discussions and advice concerning the stratigraphy and lithology. Ronald Janssen, (Frankfurt a. Main, Germany), Jean-Michel Pacaud (MNHN, Paris), and Thomas Darragh (Victoria, Australia), are thanked for taxonomical advice and help with literature. Pierre Lozouet (MNHM, Paris) kindly gave his opinion of *Murexsul kochi*. Fritz von der Hocht (Kerpen, Germany) kindly commented on the brachiopods. Werner Schwarzhans (Hamburg, Germany) kindly provided his opinion on the otoliths. Mogens Stentoft Nielsen (Odense, Denmark) and Lone Sortkjær (Juelsminde, Denmark) kindly placed material at our disposal.

Samples for foraminifera and dinocysts from Vilsund 1 and 3 were collected during field work in northern Jylland in the summer 2006. The palynological analysis of the samples was carried out by Kasia K. Śliwińska as a part of her PhD project, but the results have not been published before. The PhD project was fully funded by Aarhus University. Annette Ryge and Dorthe Samuelsen prepared the palynological slides.

We are greatly indebted to the reviewers Pierre Lozouet (Paris), Zoltán Kovács (Budapest), and Zelia Pereira (Amadora, Portugal) for valuable suggestions and corrections, which greatly improved the manuscript. Arden Roy Basforth (NHMD, Copenhagen) kindly improved the English text.

Appendix: micropalaeontology of samples from the Vilsund area and Mogenstrup

Mogenstrup

A section (UTM coordinates NH 074 814) in the coastal cliff at Mogenstrup was studied for molluscs by Schnetler & Beyer (1990). According to the authors a *c.* 20 cm thick green glauconite-sand layer at the top of an at least 2 m thick light-greenish clayey silt with three horizons of siderite concretions in the upper meter yielded an abundant and diverse mollusc assemblage. This part of the profile was described as Unit 1 by Schnetler & Beyer (1990), who assigned the unit to the Brejning Clay Member (previously a member in the lower part of the Vejle Fjord Formation, but now defined as the Brejning Formation by Rasmussen *et al.* (2010)). Schnetler & Beyer (1990) assigned the glauconitic sand at the top of Unit 1 to the late Oligocene (Chattian B) based on molluscs. Foraminifers were studied in two samples, one from the glauconitic sand and one from a lower level in Unit 1. The samples were referred to the *Angulogerina gracilis* Zone, previously identified in the Brejning Formation (Ulleberg, pers. comm. 1987).

The mollusc-rich glauconitic layer is overlain, with a sharp boundary, by dark brown micaceous silts and clays, described as units 2-4 by Schnetler & Beyer (1990). This part of the section was referred to an interval of the Vejle Fjord Formation above the Brejning Clay Member and provisionally dated as Chattian C (late Oligocene).

The succession was sampled for palynological analyses in a slightly different position of the coastal cliff in 1987 by C. Heilmann-Clausen and C. Beyer. Palynological preparations ch-c lab. nos. 1141-1142 from Unit 1 below the glauconite-sand, ch-c no. 1143 from the glauconite-sand in the top of Unit 1, and ch-c nos. 1144 and 1145 from Units 2-4 were studied here. Ch-c no. 753 from a spherical calcitic concretion with parts of a skull case from a small cetacean from Lyby Strand (6 km SW of Mogenstrup) was studied as well. The characteristic spherical calcitic concretions at Lyby occur in a similar lithology as Unit 4 at Mogenstrup, and the concretions were also observed by Schnetler & Beyer (1990) within Unit 4. Information on this sample is therefore relevant for the dating of Unit 4 at Mogenstrup. No information based on these dinocyst samples has previously been published.

Palynology

Samples ch-c 1141-1143 (Unit 1). The organic matter in the palynological slides is dominated by terrestrial particles: mainly degraded woody debris and bisaccate pollen. The dinocysts are moderately well preserved, and assemblages are poor in stratigraphically significant species. The most characteristic *in situ* species include *Artemisiocysta cladodichotoma* (Fig. 5 D) and *Distatodinium paradoxum*, both of which are common in all three samples, *Chiropteridium lobospinosum* (1 specimen in slide 1141), questionable *Chiropteridium galea*, *Reticulatosphaera actinocoronata*, *Polysphaeridium zoharyi*, *Dapsilidinium pseudocolligerum*, *Lejeunecysta acuminata*, *Lejeunecysta* cf. *fallax*, *Lejeunecysta tenella*, *Gerlachidinium aechmophorum*, *Selenopemphix nephroides*, *Selenopemphix* cf. *armata*, *Palaeocystodinium teespinosum* or *P. golzowense*, *Homotryblium floripes/plectilum* and *Cordosphaeridium cantharellum*. Mesozoic and older Palaeogene reworked dinocysts are present, but sporadic.

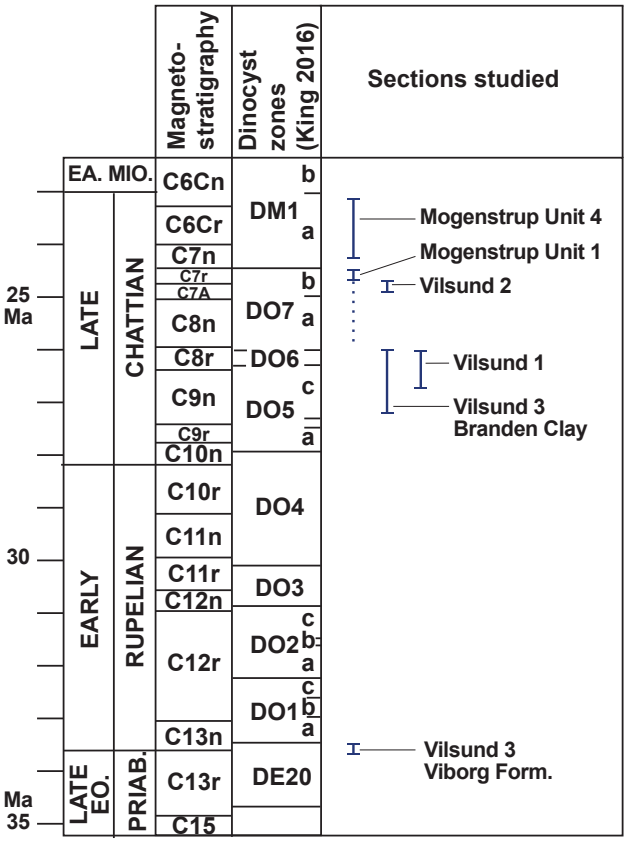

Fig. 15. Age and zonal assignment of sections analysed for dinocysts. Dinocyst zones, magneto- and chronostratigraphy are according to King (2016). Note that the Priabonian/Rupelian boundary definition used in King (2016) differs from the current global definition (see discussion in King 2016, p. 15–16). The Global Time Scale (GTS 2020; Gradstein *et al.* 2020) places the Priabonian/Rupelian boundary slightly deeper, in the upper part of Chron C13r. Following the GTS 2020, the upper part of dinocyst Subzone DE20b (with Viborg Formation in Vilsund 3) is therefore in the basal Rupelian.

Samples ch-c 1144 and 1145 (both from the interval spanning units 2-4). Organic particles consist mainly of brown, degraded lignitic debris. Bisaccate pollen are relatively common. Dinocysts are poorly preserved and very sporadic. The few observed specimens include a significant proportion of reworked Mesozoic and older Palaeogene dinocysts (*e.g, Chatangiella* sp., *Areoligera* sp. and *Enneadocysta pectiniformis*). *In situ* species include, in particular: *Artemisiocysta chladodichotoma*, *Palaeocystodinium golzowense*, a single questionable specimen of *Deflandrea phosphoritica*, *Reticulatosphaera actinocoronata*, *Cleistosphaeridium* cf. *diversispinosum*, *Distatodinium paradoxum* and few fragments of questionable *Chiropteridium galea*.

Sample ch-c 753 (Unit 4 equivalent). The sample includes a well preserved dinocyst assemblage characterised by common *Deflandrea phosphoritica*, *Homotryblium floripes/plectilum* and *Distatodinium paradoxum*, fairly common *Thalassiphora pelagica*, and the presence of *Chiropteridium galea* and *Cordosphaeridium cantharellum*.

Comparison with previous Chattian dinocyst studies from Denmark and age determination

The lower and middle Chattian of Denmark was studied by Sliwinska *et al*. (2012). According to these authors, the distinctive acritarch *Artemisiocysta cladodichotoma* (relatively common in all three samples of Unit 1) is present (but very rare) in Denmark in the lower Chattian (lower part of the Branden Clay). However, its last occurrence is not well constrained in the North Sea Basin. Notably, in the southern North Sea Basin this species ranges at least to near the top of the Oligocene (Van Simaeys *et al.* 2005). Furthermore, a lower Miocene (Aquitanian) reappearance of *Artemisiocysta cladodichotoma* is observed in the North Atlantic (Egger *et al.* 2016), suggesting that the range extends into the Miocene in northern middle latitudes. Accordingly, *A. cladodichotoma* can only have been intermittently present in Danish waters during the Chattian. This may explain its absence in the few previously studied samples from the upper part of the Branden Clay and the overlying Unit X of Śliwińska *et al.* (2012).

As shown by Śliwińska *et al.* (2012), several stratigraphic markers range through the Branden Clay-basal Unit X succession, including *Licracysta*? *semicirculata*, *Wetzeliella* spp., *Rhombodinium draco, Saturnodinium pansum* and *Pentadininum imaginatum*. None of these markers are recorded at Mogenstrup, indicating that the Mogenstrup section should be correlated with a higher level than basal Unit X. This conclusion is supported by the finding of the *Angulogerina gracilis* Zone in Unit 1 (see above). The lowest level for this zone is the upper part of Unit X (Śliwińska *et al.* 2012) and the top of the zone coincides with the top of the Brejning Formation (Ulleberg 1987).

The Oligocene – Miocene transition onshore Denmark (the boundary between the Brejning and the Vejle Fjord formations) was studied by Śliwińska *et al.* (2014). According to these authors, *Deflandrea phosphoritica* is common throughout the Brejning Formation in the Harre-1 borehole, except for the few metres thick, glauconitic basal part of the formation. *D. phosphoritica* is absent in Unit 1 at Mogenstrup. In conclusion, these features suggest a correlation of Unit 1 with the lowermost glauconitic part of the Brejning Formation or upper part of the underlying Unit X. In terms of the North Sea Basin zonation provided by King (2016), Unit 1 can be referred to the upper Chattian Zone DO7, and possibly the upper part, Subzone DO7b as discussed below in connection with the sample from Vilsund 2.

Unit 4 can be confidently correlated with the uppermost Chattian *Deflandrea phosphoritica* Zone of Dybkjær & Piasecki (2010) and DM1a Subzone of King (2016) based on the common *D. phosphoritica* in sample 753. This allows a correlation of Unit 4 to the non-glauconitic upper part of the Brejning Formation in the Harre-1 borehole (cf. above). The *D. phosphoritica* Zone is very thick (33 m) in the Harre-1 borehole and consists of a dark brown micaceous silty clay similar to Unit 4 at Mogenstrup.

Vilsund 2

A sample collected by IS in 2022 from the mollusc-rich strongly glauconitic layer at the Vilsund 2 locality was processed for palynology (ch-c lab.no. 3283). For lithology, preparation and palynofacies, see the main text.

The well-preserved dinocyst assemblage is dominated by *Spiniferites* spp. (including *S. pseudofurcatus*), *Achomosphaera* spp., and *Lingulodinium machaerophorum*. Other common dinocyst taxa include: *Dapsilidinium pseudocolligerum*, *Reticulatosphaera actinocoronata*, *Chiropteridium galea*, and *Cleistosphaeridium diversispinosum*. The acritarch *Cyclopsiella elliptica* is also fairly common. Less common are *Thalassiphora pelagica,* cf. *Licracysta*? *semicirculata* and *Triphragmadinium demaniae* (see Taxonomic remarks to the latter two taxa). Present, but not rare, taxa include *Hystrichokolpoma cinctum* (4 specimens), *Artemisiocysta cladodichotoma* (3, possibly 4 specimens), *Homotryblium floripes/plectilum*, *Distatodinium paradoxum* and *Hystrichokolpma rigaudae*. Rare taxa include *Membranophoridium aspinatum*, *Lejeunecysta tenella* (Fig. 5 B), *Lejeunecysta hyalina* and *Selenopemphix nephroides*.

The diversity is high, which is partly due to a considerable proportion of reworked cysts from the Lower Cretaceous and Palaeogene (Eocene – Oligocene). The most common reworked dinocysts include *Areosphaeridium diktyoplokum* (mainly forms with entire margins of process-platforms from upper Eocene –

lowermost Oligocene) and *Enneadocysta arcuatum/pectiniformis* (middle Eocene – lower Oligocene). Further reworked taxa include, among others *Heteraulacacysta porosa* (several specimens), *Dracodinium* cf. *similis* (1 specimen), *Phthanoperidinium comatum* (1 specimen), several specimens of cf. *Tenua* sp. (Lower Cretaceous). A single questionable *Wetzeliella* sp. is also considered to be reworked.

Comparison with samples from Mogenstrup and age
The palynofacies suggests a more open marine environment than at Mogenstrup, which is heavily dominated by degraded woody material. The dinocyst assemblage shows similarities with Unit 1 at Mogenstrup (presence of *Artemisiocysta cladodichotoma* and *Lejeunecysta tenella*, and absence of the genus *Deflandrea* as well as absence of nearly all stratigraphic markers for the Branden Clay, such as *Saturnodinium pansum*, *Rhombodinium draco* and *Pentadinium imaginatum*). The main difference is the presence of *Triphragmadinium demaniae* and cf. *Licracysta*? *semicirculata* at Vilsund.

According to the data in Van Simaeys *et al.* (2005), *T. demaniae* occurs only in a narrow interval in the lower part of their Zone NSO-8. Zone NSO-8 is identical to Subzone DO7b of King (2016). The Vilsund 2 sample may hence correlate with this narrow interval in the lower part of the upper Chattian Subzone DO7b.

It can be speculated that cf. *Licracysta*? *semicirculata* only occurs a short distance above proper *Licracysta? semicirculata,* the last occurrence of which marks the top of the mid-Chattian Zone DO6 of King (2016) and is absent above the lower part of Subzone DO7b with *T. demaniae*. If so, the Mogenstrup sample, without *Triphragmadinium demaniae* and cf. *Licracysta*? *semicirculata,* should be referred to a higher part of Subzone DO7b than the Vilsund 2 sample.

Sections from the Vilsund area sampled for micropalaeontology in 2006

Two outcrops, Vilsund 1 and Vilsund 3 (during field work named Sundby Nord and Sundby Syd, respectively), were studied for micropalaeontology (dinocysts and foraminifers). The profiles were described, and all samples were collected, during field work in the summer 2006.

Vilsund 1 (formerly Sundby Nord)
The Vilsund 1 section is a *c.* 1.5 m high cliff, which in 2006 was exposed very close to, and probably north of, the Vilsund 2 section. The lower part of the outcrop consists of black, sticky micaceous clay. The middle part exposes a 15–20 cm thick very glauconite-rich layer with siderite concretions. The upper part consists of brown, sticky glauconitic clay. Three sediment samples were collected from the outcrop. Sample no. 1 (GEUS Lab. no. 20.226) was taken *c.* 45 cm below the glauconitic layer with siderite. Sample no. 2 (GEUS Lab. no. 20.227) was collected from the glauconitic unit with siderite. Sample no. 3 (GEUS Lab. no. 20.228) was taken *c.* 70 cm above sample 2. All samples were prepared at the Geological Survey of Denmark and Greenland (GEUS) for dinoflagellate cysts following the methods described in Śliwińska *et al.* (2014). All samples yielded well preserved dinoflagellate cyst assemblages of low to high diversity.

Sample no. 1 (GEUS no. 20.228_6) yields typical early Chattian dinocyst assemblages with *Chiropteridium galea*, *Chiropteridium lobospinosum*, *Pentadinium imaginatum*, *Saturnodinium* cf. *pansum* and *Wetzeliella gochtii*. Sample no. 2 (GEUS no. 20.227_6) has the least diverse dinocyst assemblage. The only useful age indicative dinocyst is *Licracysta? semicirculata*. Sample no. 3 (GEUS no. 20.226_6) yields *Distatodinium biffii*, *Licracysta? semicirculata*, *Saturnodinium* cf. *pansum*, *Wetzeliella symmetrica* and the acritarch *Artemisiocysta cladodichotom*a. *Areosphaeridium diktyoplokum* (with ragged clypeate process terminations, see Śliwińska (2019) for details) and *Areosphaeridium michoudii* (sample no. 3), as well as *Enneadocysta pectiniformis* (sample no. 1), are rare and are considered to be reworked. The dinocyst assemblages in the Vilsund 1 section are typical for the Branden Clay (Śliwińska *et al.* 2012), and can be assigned to the dinocyst D14nb Zone (Köthe 1990), the lower part of the NSO-5b Subzone (Van Simaeys *et al.* 2005) and the upper part of Subzone DO5c or Zone DO6 of King (2016).

Vilsund 3 (formerly Sundby Syd)
The cliff section at Vilsund 3 (registered as the Sundby Syd section in the palynological database at GEUS) is situated at 56° 52′ 12″ N, 8° 38′ 50″ E. at Volbjerg *c.* 2 km south of the Vilsund Bridge. The section was included in a master's thesis on the magnetostratigraphic and sedimentology of the upper Oligocene and Miocene in NW Jylland (Beyer 1987, unpublished). The following description is based on the present study. The site exposes a *c.* 14 m high cliff section, with a thin layer of undifferentiated Quaternary till on top. The interval from the beach level (marked as 0 on Fig. 16) up to *c.* 13.2 m consists of dark brown micaceous silty clay with sporadic lenses of silt and fine sand. From *c.* 10 m above the beach level, the sediments become more sandy. The uppermost *c.* 90 cm of the unit consists of fine sand and silt and is more yellow in appearance. Around level 13.2 m there is a sharp boundary and a shift to green, glauconitic clay. Fifteen sediment samples were collected in total: 14 sediment samples were collected from the lower unit. One sample was collected from the upper unit, *c.* 30 cm above the lithological change.

Seven samples (nos. 1, 4, 7, 10, 12, 14 and 15, see sample position in Fig. 16) were prepared for micropalaeontology (foraminifers) at Aarhus University following methods described in Śliwińska *et al.* (2012). In the interval from 0.0–10.8 m (samples no. 1 to 12), *Turrillina alsatica* is the most dominant species. The other common species are *Nonion affine, Pullenia bulloides, Gyroidinoides* spp. and *Cibicides* spp. The lowermost sample also contains a few *Globigerinacea* spp. The faunal assemblage is typical for the *Turrillina alsatica* Zone. The two uppermost samples (no. 14 and 15) are barren in foraminifers.

All 15 samples were processed at the Geological Survey of Denmark and Greenland (GEUS) for dinoflagellate cysts (sample codes 20.211–20.225) following the method described by Śliwińska *et al.* (2014). Palynological slides are stored at GEUS. All samples yielded well preserved and diverse dinocyst assemblages. The interval from 0.0 m – 12.8 m (sample no. 1 to 14; 20.211-20.224) contains a typical earliest Oligocene dinocyst assemblage with *Areosphaeridium diktyoplokum* (both ragged and entire clypeate process terminations; see Śliwińska 2019), *Cerebrocysta bartonensis, Enneadocysta pectiniformis, Glaphyrocysta semitecta, Lentinia serrata, Phthanoperidinium comatum, Rhombodinum draco,* and *Thalassiphora reticulata* (*e.g.*, Köthe 1990; Van Simaeys *et al.* 2005; Köthe & Piesker 2007; Śliwińska *et al.* 2012). Rare occurrences of *Areosphaeridium michoudii, Eatonicysta ursulae, Diphyes colligerum*, and *Thalassiphora delicata* in the interval are considered to be reworked.

The foraminifera and dinocyst assemblages are very typical for the Viborg Formation (Śliwińska *et al.* 2012), which can be assigned to the dinocyst D12nc Zone (Köthe 1990), the NSO-1 Zone (Van Simaeys *et al.* 2005) and Subzone DE20b of King (2016).

From the uppermost *c.* 1.5 m thick interval only one sample was studied for dinocysts (20.225). The sample contains *Licracysta? semicirculata*, *Chiropteridium galea*, *Chiropteridium lobospinosum*, *Distatodinium biffii* and *Saturnodinium pansum*. The assemblage is typical for the Branden Clay (Śliwińska *et al.* 2012), and can be assigned to the dinocyst D14nb Zone (Köthe 1990), the NSO-5b Subzone (Van Simaeys *et al.* 2005) and DO5c or DO6 of King (2016).

The biostratigraphy shows that the sharp boundary at level 13.2 m is a major disconformity (erosional

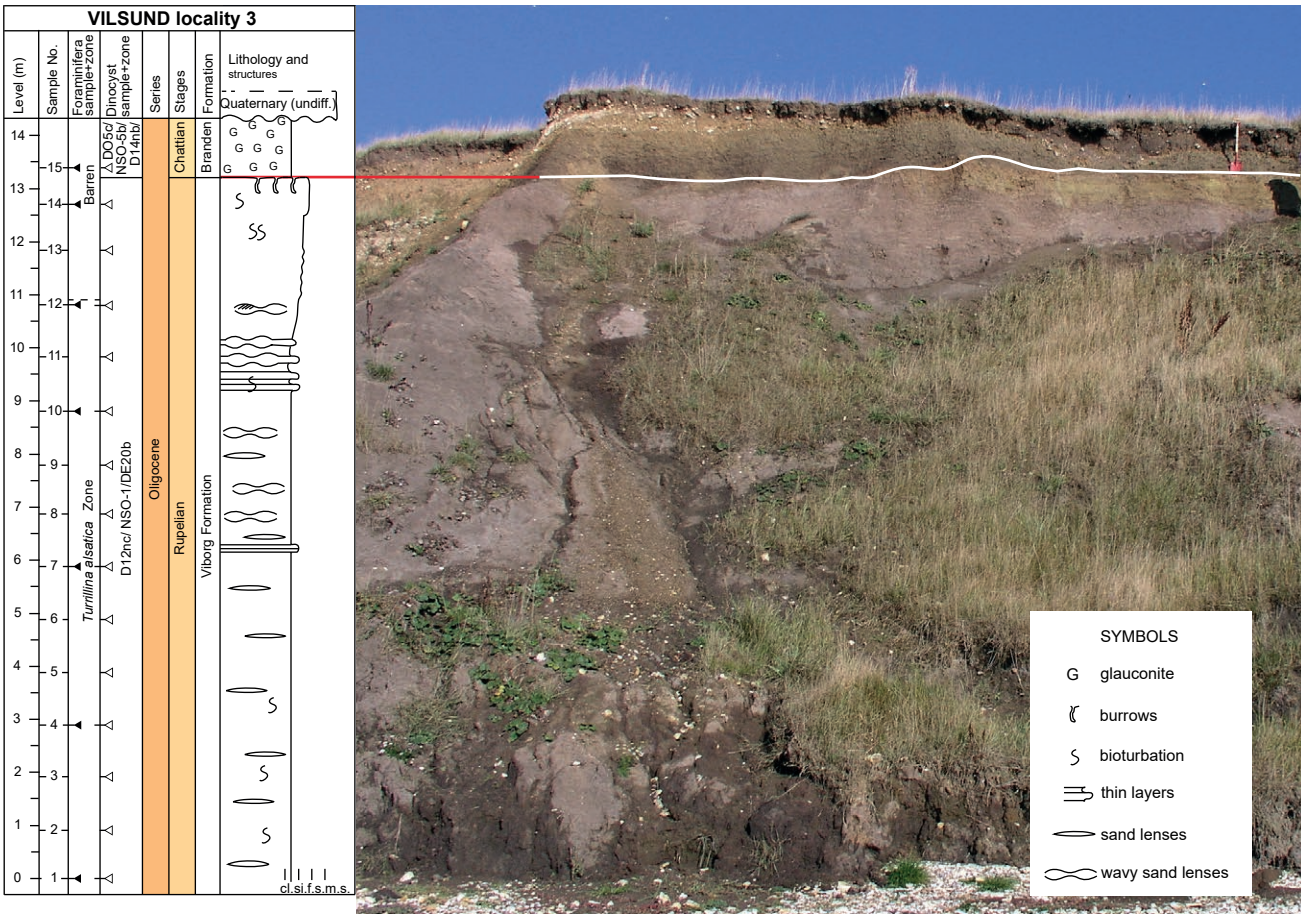

Fig. 16. The Vilsund 3 outcrop section in 2007. cl.: clay; si.: silt; f.s.: fine-grained sand; m.s.: medium-grained sand. Spade for scale. Photo Kasia K. Śliwińska.

unconformity) between the Viborg Formation and the 6 Ma younger Branden Clay. The short section of Branden Clay at Vilsund 1 does not show the contact to the Viborg Formation and must represent a higher level of the Branden Clay.

The Vilsund 3 section is the thickest and most northerly exposure of the Viborg Formation. Accordingly, and because of the sedimentary contact (undisturbed by glacial tectonics) between the Viborg Formation and Branden Clay, the section is of particular interest for education and future research.

Taxonomic remarks

Triphragmadinium demaniae (Fig. 5 A)

This dinocyst was used as a zonal marker by Van Simaeys *et al.* (2005) and King (2016) and is present in the Vilsund sample (ch-c 3283). *Triphragmadinium demaniae* was described relatively recently by Van Simaeys *et al.* (2005) and has rarely been recorded since. Comments on its morphology in the present material are therefore appropriate.

At least 10 specimens were observed. The general shape and structure of the cyst is similar to the type material from the southern North Sea Basin. A number of distinctive characters are also identical to the type material; these include the wrinkled, very thin and hyaline periphragm with a variable number of distinctive small round holes (claustra) in parts of the surface, the antapical invagination of the periphragm surrounding a hollow process (outgrowth of the periphragm), and the contact between peri- and endophragm at the margin of the apical archaeopyle.

The mesophragm described in the type material as a low suturocavate feature on the surface of the endocyst is difficult or impossible to ascertain in our specimens. At least in one specimen (Fig. 5 A) low folds or ridges of thin material on the surface of the endocyst may reflect sutures, thus probably representing the mesophragm. Considering the identity in most characters, we consider the lack of a clearly recognizable mesophragm as an intraspecific variation in *Triphragmadinium demaniae*.

cf. *Licracysta*? *semicirculata* (Fig. 5 C)

This dinocyst is present in the Vilsund sample (ch-c 3283) and may be of stratigraphic significance as discussed above. Approximately 10 specimens were observed; they differ from the type material of *Licracysta*? *semicirculata* by having shorter processes, which are less ribbon-like and more cylindrical.

Storage of palynological preparations

Preparations with ch-c-numbers are stored at the Department of Geoscience, Aarhus University. Preparations with GEUS-numbers are stored at GEUS.

References

Anderson, H.-J. 1958: Die Pectiniden des niederrheinischen Chatts. Fortschritte in der Geologie von Rheinland und Westfalen 1, 297–321.

Anderson, H.-J. 1959: Die Gastropoden des jüngeren Tertiärs in Nordwestdeutschland Teil 1: Prosobranchia, Archaeogastropoda. Meyniana 8, 37–81.

Anderson, H.-J. 1961: Gliederung und palaogeographische Entwicklung der Chattischen Stufe (Oberoligocän) im Nordseebecken. Meyniana 10, 118–146.

Beyer, C. 1987: Ø. Oligocæn – N. Miocæn i Nordvest Jylland. Faciesanalyse & magnetostratigrafi, 164 pp. Unpublished cand. scient. thesis, Aarhus University, Denmark.

Bouchet, P. & Rocroi, J.P. 2010: Nomenclator of bivalve families; with a classification of bivalve families by R. Bieler, J. G. Carter & E.V. Coan. Malacologia 52(2), 1–184. https://doi.org/10.4002/040.052.0201

Bouchet, P., Rocroi, J.-P., Hausdorf, B., Kaim, A., Kano, Y., Nützel, A., Parkhaev, P., Schrödl, M. & Strong, E.E. 2017: Revised classification, nomenclator and typification of gastropod and monoplacophoran families. Malacologia 61(1–2), 1–526. https://doi.org/10.4002/040.061.0201

Cadée, M.C. & Janssen, A.W. 1994: A taxonomic revision of the NW European Oligocene Fasciolariidae traditionally included in the genus Streptochetus (Mollusca, Gastropoda). Contributions to Tertiary and Quaternary Geology 31, 31–107.

Ceulemans, L., van Dingenen, F. & Landau, B.M. 2018: The lower Pliocene gastropods of Le Pigeon Blanc (Loire-Atlantique, northwest France). Part 5 – Neogastropoda (Conoidea) and Heterobranchia (*fine*). Cainozoic Research 18(2), 89–176.

Cox, L.R. & Knight, J.B. 1960: [February], Suborders of Archaeogastropoda. Proceedings of the Malacological Society of London, 33(6): 262–264.

Cox, L.R. *et al.* 1971: Systematic classifications. In: Moore, R.C. (ed.): Treatise on invertebrate palaeontology Part N, Mollusca 6, vol. 3, 953–1224. Geological Society of America and University of Kansas Press.

Dall, W.H. 1881: Reports of the results of dredging by the steamer *Blake*. Bulletin of the Museum of Comparative Zoology at Harvard College 2, 33–144.

Dall, W.H. 1889: Report on the Mollusca (Blake Expedition); Pt. 2, Gastropoda and Scaphopoda: Bulletin of the Museum of Comparative Zoology at Harvard College 18, 492 pp.

Drivas, J. & Jay, M. 1986: Shells of Reunion, 8. Family Turridae Swainson, 1840. Conchiglie 18(208/209), 8–10.

Dybkjær, K. & Piasecki, S. 2010: Neogene dinocyst zonation for the eastern North Sea Basin, Denmark, Review of Palaeobotany and Palynology 161, 1–29. https://doi.org/10.1016/j.revpalbo.2010.02.005

Egger, L. M., Śliwińska, K. K., van Peer, T. E., Liebrand, D., Lippert, P. C., Friedrich, O., Wilson, P. A., Norris, R. D. & Pross, J. 2016: Magnetostratigraphically-calibrated dinoflagellate cyst bioevents for the uppermost Eocene to lowermost Miocene of the western North Atlantic (IODP Expedition 342, Paleogene Newfoundland sediment drifts). Review of Palaeobotany and Palynology 234, 159–185. https://doi.org/10.1016/j.revpalbo.2016.08.002

Eriksen, K. 1937: En foreløbig meddelelse om Tertiæret ved Brejning på sydsiden af Vejle Fjord. Meddelelser fra Dansk Geologisk Forening 9 (2), 137–150.

Fernandes, M.R. & Pimenta, A.D. 2017: Synopsis of the deep-sea groups of Triphoroidea (Gastropoda), Journal of Natural History. https://doi.org/10.1080/00222933.2017.1293181

Gradstein, F.M., Ogg, J.G., Schmitz, M.D. & Ogg, G.M. 2020 (eds): The geologic time scale 2020, 1357 pp., 2 volumes. Amsterdam: Elsevier.

Gry, H. 1979: Beskrivelse til geologisk kort over Danmark. Kortbladet Løgstør. Kvartære aflejringer. Danmarks geologiske Undersøgelse I Række 26, 58 pp. https://doi.org/10.34194/raekke1.v26.6782

Håkansson, E. & Pedersen, S.A.S. 1992: Et nyt undergrundskort. Copenhagen: Varv.

Harder, P. 1913: De oligocæne Lag i Jærnbanegennemskæringen ved Århus Station. Danmarks Geologiske Undersøgelse II Række 22, 140 pp. https://doi.org/10.34194/raekke2.v22.6807

Heilmann-Clausen, C. 1997: How one diatomite led to the development of another diatomite - the Oligocene section at Silstrup, NW Denmark. Tertiary Research 18, 31–34.

Heilmann-Clausen, C. 2006: Oligocæn og den antarktiske forbindelse. In: Larsen, G. & Sand-Jensen, K. (eds): Naturen i Danmark, 552 pp. Copenhagen: Gyldendal.

Houart, R., Buge. B. & Zuccon, D. 2021: A taxonomic update of the Typhinae (Gastropoda: Muricidae) with a review of New Caledonia species and the description of new species from New Caledonia, the South China Sea and Western Australia. Journal of Conchology 44(2), 103–147.

Janssen, A.W. 1984: Mollusken uit het Mioceen van Winterswijk-Miste. Een inventarisatie, met beschrijvingen en afbeeldingen van alle aangetroffen soorten. Koninklijke Nederlandse Natuurhistorische Vereniging, Nederlandse Geologische Vereniging, Rijksmuseum van Geologie en Mineralogie, 451 pp.

Janssen, R. 1978a: Die Scaphopoden und Gastropoden des Kasseler Meeressande von Glimmerode (Niederhessen). Geologisches Jahrbuch A 41, 3–195.

Janssen, R. 1978b: Die Mollusken des Oberoligozäns (Chattium) im Nordseebecken, 1. Scaphopoda, Archaeogastropoda, Mesogastropoda. Archiv für Molluskenkunde 109(1/3), 133–221.

Janssen, R. 1979a: Die Mollusken des Oberoligozäns (Chattium) im Nordseebecken, 2. Neogastropoda, Euthyneura, Cephalopoda. Archiv für Molluskenkunde 109(4/6), 277–376.

Janssen, R. 1979b: Revision der Bivalvia des Oberoligozäns (Chattium, Kasseler Meeressand). Geologische Abhandlungen Hessen 78, 181 pp.

Jensen, E.S. 1974: Nyt undergrundskort. Varv 1974 (2), 47–49. https://doi.org/10.1108/eb017784

Kautsky, F. 1925: Das Miozän von Hemmoor und Basbeck-Osten. Abhandlungen der Preussischen Geologischen Landesanstalt, neue Folge 97, 1–255.

Kilburn, R.N. 1986: Turridae (Mollusca: Gastropoda) of southern Africa and Mozambique, 3. Subfamily Borsoniinae. Annals of the Natal Museum 27, 633–720.

King, C., Gale, A. S. & & Barry, T. L. 2016: A revised correlation of Tertiary rocks in the British Isles and adjacent areas of NW Europe. Geological Society of London. https://doi.org/10.1144/SR27. https://doi.org/10.1144/SR27

Knox, R.W.O'B. *et al*. 2010. Cenozoic. In: Dornenbaal, H. & Stevenson, A. (eds): Petroleum geological atlas of the southern Permian Basin area. EAGE Publications b.v., Houten, the Netherlands, 211–223.

Koenen, A. von 1872: Das Miocaen Nord-Deutschlands und seine Mollusken-Fauna I. Schriften der Gesellschaft zur Beförderung den gesammten Naturwissenschaften zur Marburg 10(3), 262 pp.

Koninck, L. de 1838: Description des coquilles fossiles de l'argile de Basele, Boom, Schelle, etc. Nouveaux Mémoires de l'Académie des Sciences et Belles-Lettres de Bruxelles. 11 [23]: 1-37, pl. 1-4.

Köthe, A. 1990: Paleogene Dinoflagellates from Northwest Germany – Biostratigraphy and Paleoenvironment. Geologisches Jahrbuch Reihe A, Heft 118, 1–111.

Köthe, A. & Piesker, B. 2007: Stratigraphic distribution of Paleogene and Miocene dinocysts in Germany. Revue de Paleobiologie 26, 1–39.

Landau, B. & Harzhauser, M. 2022: The Pliocene Gastropoda (Mollusca) of Estepona, southern Spain. Part 15: Borsoniidae, Clathurellidae, Mitromorphidae, Pseudomelatomidae (Gastropoda, Conoidea). Cainozoic Research 22(2), 103–156.

Larsen, G. & Dinesen, A. 1959: Vejle Fjord Formationen ved Brejning. Sedimenterne og foraminiferfaunaen. Danmarks Geologiske Undersøgelser II Række 82, 114 pp. https://doi.org/10.34194/raekke2.v82.6872

Le Renard, J. & Pacaud, J.-M. 1995 : Revision des Mollusques Paléogènes du Bassin de Paris II – Liste des Réfèrences primaires des Espèces. Cossmanniana 3, 65–132.

Lozouet, P. 1998: Nouvelles espèces de gastéropodes (Mollusca : Gastropoda) de l'Oligocène et du Miocène inférieur d'Aquitaine (sud-Ouest de la France). Cossmanniana 5(3–4), 61–102.

Lozouet, P. 1999: Nouvelles espèces de gastéropodes (Mollusca : Gastropoda) de l'oligocène et du miocène inférieur d'Aquitaine (Sud-Ouest de la France). Partie 2. Cossmanniana 6(1–2), 1–68.

Lozouet, P. 2015: Nouvelles espèces de gastéropodes (Mollusca: Gastropoda) de l'Oligocène et du Miocène inférieur d'Aquitaine (Sud-Ouest de la France). Partie 5. Cossmanniana 17, 15–84.

Lozouet P. 2017: Les Conoidea de l'Oligocène supérieur (Chattien) du bassin de l'Adour (Sud-Ouest de la France). Cossmanniana 19, 3–179.

Lozouet, P. 2023: Muricidae (Gastropoda, Neogastropoda) de l'Oligocène (Chattien) du bassin de l'Adour (Sud-Ouest de la France). Cossmanniana 24, 3–161.

Madsen, H. & Schnetler, K.I. 2023: Geologien fortæller: Glimmerler og krabbeboller. What geology tells: The mica clay and crab-nodules, 144 pp. Museum Mors.

Merle, D., Pointier, J.-P. & Garrigues, B. 2022: Fossil and Recent Muricidae of the World - Part Muricopsinae, 528 pp. ConchBooks.

MolluscaBase: *Bathyarca pectunculoides* (Scacchi, 1835). Accessed through: World Register of Marine Species at: https://www.marinespecies.org/aphia.php?p=taxdetails&id=138799 on 2022-08-11.

Morton, A.: A Collection of Eocene and Oligocene Fossils. https://www.dmap.co.uk/index.htm

Moths, H. 2000: Die Molluskenfauna im Rupelton der Ziegeleigrube Malliß im Wanzeberg (südwestl. Mecklenburg-Vorpommern). Kaliß (Regionalmuseum des Amtes Malliß), 1–103.

Moths, H., Albrecth, F. & Stein, G. 2010: Die Molluskenfauna (Hemmoorium, Untermiozän) aus der Kiesgrube Krinke bei Werder (Nordwest-Niedersachsen). Palaeofocus 3. 155 pp.

Nielsen, O.B., Friis, H. & Korsbech, U. 1994: Lithology and lithostratigraphy of the Harre borehole, Denmark. In: Nielsen, O.B. (ed.): Lithostratigraphy and biostratigraphy of the Tertiary sequence from the Harre borehole, Denmark. Aarhus Geoscience 1, 5–14. Department of Earth Sciences, Aarhus University.

Poppe, G.T. 2008: Philippine marine mollusks. Vol. 1 (Gastropoda – Part 1). ConchBooks, 759 pp.

Powell, A.W.P. 1966: The molluscan families Speightiidae and Turridae: an evaluation of the valid taxa, both recent and fossil, with lists of characteristic species. Bulletin of the Auckland Institute and Museum 5, 1–184.

Rasmussen, E.S. & Dybkjær, K. 2005: Sequence stratigraphy of the Upper Oligocene – Lower Miocene of eastern Jylland, Denmark: role of structural relief and variable sediment supply in controlling sequence development. Sedimentology 52, 25–63. https://doi.org/10.1111/j.1365-3091.2004.00681.x

Rasmussen, E.S., Dybkjær, K. & Piasecki, S. 2010: Lithostratigraphy of the Upper Oligocene – Miocene succession of Denmark. Geological Survey of Denmark and Greenland Bulletin 22, 92 pp. https://doi.org/10.34194/geusb.v22.4733

Rasmussen, L.B. 1967: Tertiærperioden. In: Nørrevang, A. & Meyer, T.J. (eds): Danmarks natur vol. 1, Landskabernes opståen, 161–198. Copenhagen: Politikens Forlag.

Rasmussen, H.W. 1968: Danmarks geologi, 2. Udgave, 176 pp. Copenhagen: Gjellerups liniebøger.

Ravn, J.P.J. 1907: Molluskfaunaen i Jyllands Tertiæraflejringer. Det Kongelige Danske Videnskabernes Selskabs Skrifter VII Række 3, 217–384. København.

Ravn, J.P.J. 1909: Om nogle nye Findesteder for Tertiærforsteninger. Meddelelser fra Dansk Geologisk Forening 3, 258–264.

Schnetler, K.I. & Beyer, C. 1987: A Late Oligocene (Chattian B) mollusc fauna from the clay-pit at Nørre Vissing, Jylland, Denmark. Mededelingen van de Werkgroep voor Tertiaire en Kwartaire Geologie 24, 193–224.

Schnetler, K.I. & Beyer, C. 1990: A Late Oligocene (Chattian B) molluscan fauna from the coastal cliff at Mogenstrup, north of Skive, Jutland, Denmark. Contributions to Tertiary and Quaternary Geology 27, 39–81.

Schnetler, K.I. & Palm, E. 2008: The molluscan fauna of the Late Oligocene Branden Clay, Denmark. Palaeontos 15, 1–92.

Schwengel, J.S. 1943: New marine shells from Florida. The Nautilus 56(3), 75–78.

Schulz, B.P., Vickers, M.L., Huggett, J., Madsen, H., Heilmann-Clausen, C., Friis, H. & Suess, E. 2020: Palaeogene glendonites from Denmark. Bulletin of the Geological Society of Denmark 68. 23–35. https://doi.org/10.37570/bgsd-2020-68-03

Śliwińska, K.K. 2019: Early Oligocene dinocysts as a tool for palaeoenvironment reconstruction and stratigraphical framework – a case study from a North Sea well. Journal of Micropalaeontology 38, 143–176. https://doi.org/10.5194/jm-38-143-2019

Śliwińska, K.K., Abrahamsen, N., Beyer. C., Brünings-Hansen, T., Thomsen, E., Ulleberg, K. & Heilmann-Clausen, C. 2012: Bio- and magnetostratigraphy of Rupelian–mid Chattian deposits from the Danish land area. Review of Palaeobotany and Palynology 172, 48–69. https://doi.org/10.1016/j.revpalbo.2012.01.008

Śliwińska, K.K., Dybkjær, K., Schoon, P.L., Beyer, C., King, C., Schouten, S. & Nielsen, O.B. 2014: Paleoclimatic and paleoenvironmental records of the Oligocene–Miocene transition, central Jylland, Denmark. Marine Geology 350, 1–15. https://doi.org/10.1016/j.margeo.2013.12.014.

Sorgenfrei, T. 1958: Molluscan assemblages from the marine Middle Miocene of South Jutland and their environments. Danmarks Geologiske Undersogelse II Række 79, 503 pp. https://doi.org/10.34194/raekke2.v79.6869

Tembrock, M.-L. 1963: Muriciden aus dem Mittel- und Oberoligozän und den Vierlandschichten des Nordseebeckens. Paläontologische Abhandlungen 1(4), 299–351.

Tembrock, M.L. 1968: Taxionomisch-stratigraphische Studie zur Scalaspira-Gruppc (Gastropoda, Tertiar). Palaontologische Abhandlungen (A) 3(2), 193–366.

Thiele, J. 1925: Gastropoden der Deutschen Tiefsee-Expedition. II Teil. Wissenschaftliche Ergebnisse der Deutschen Tiefsee-Expedition auf dem Dampfer "Valdivia" 1898–1899, 17(2). 37–382.

Troelsen, J.C. 1955: Studies on Ceratobuliminidae (Foraminifera). Meddelelser fra Dansk geologisk Forening 12, 448–478.

Ulleberg, K. 1987: Foraminiferal zonation of the Danish Oligocene sediments. Bulletin of the Geological Society of Denmark 36, 191–202. https://doi.org/10.37570/bgsd-1988-36-02

Van Simaeys, S., Munsterman, D. & Brinkhuis, H. 2005: Oligocene dinoflagellate cyst biostratigraphy of the southern North Sea Basin, Review of Palaeobotany and Palynology 134, 105–128. https://doi.org/10.1016/j.revpalbo.2004.12.003

Vicián Z. & Kovács Z. 2022. Middle Eocene Tonnoidea (Cae-

nogastropoda) from the Hungarian Paleogene Basin. Fragmenta Palaeontologica Hungarica, 37 ["2021"], 13–47. https://doi.org/10.17111/FragmPalHung.2021.37.13

Wenz, W. 1943: Gastropoda, Teil 1: Allgemeiner Teil und Prosobranchia, 1201–1506. In: Schindewolf, O.H. (ed.): Handbuch der Paläozoologie, Band 6. Berlin: Bornträger.

Wienrich, G. 2007. Die Fauna des marinen Miozäns von Kevelaer (Niederrhein), 4. Gastropoda ab Mitridae; Turridae: Janssen & Wienrich, 640–954, pls 108–173; Leiden (Backhuys Publishers).

WoRMS Editorial Board 2014. World Register of Marine Species. http://www.marinespecies.org/

Serpula? *alicecooperi* sp. nov. – a new serpulid from the Lower Jurassic (Pliensbachian) Hasle Formation of Bornholm, Denmark

TOMÁŠ KOČÍ, JESPER MILÀN, STEN LENNART JAKOBSEN & ARDEN R. BASHFORTH

Geological Society of Denmark
https://2dgf.dk

Received 10 January 2024
Accepted in revised form
1 February 2024
Published online
02 March 2024

Kočí, T., Milàn, J., Jakobsen, S.L. & Bashforth, A.R. 2024. *Serpula*? *alicecooperi* sp. nov. – a new serpulid from the Lower Jurassic (Pliensbachian) Hasle Formation of Bornholm, Denmark. Bulletin of the Geological Society of Denmark, Vol. 73, pp. 41–56. ISSN 2245-7070. https://doi.org/10.37570/bgsd-2024-73-02

Serpulid remains are very rare in the Lower Jurassic Hasle Formation of Bornholm, Denmark. A historical specimen mentioned, but not figured by Malling & Grönwall (1909) was reexamined and attributed to *Pentaditrupa quinquesculcata* and here figured for the first time. New finds of additional well-preserved serpulid tubes are described as *Serpula*? *alicecooperi* sp. nov, which show adaptations for a lifestyle on fine-grained sediment in a nearshore environment.

Keywords: Early Jurassic, Pliensbachian, *Serpula*, *Pentaditrupa*, Bornholm, Denmark.

Tomáš Kočí [protula@seznam.cz], Ivančická 581, Prague 9 – Letňany, 19900, Czechia, and Palaeontological Department, Natural History Museum, National Museum, Cirkusová 1740, 193 00 Praha 20 - Horní Počernice, Czechia. Jesper Milàn [jesperm@oesm.dk], Geomuseum Faxe/Østsjællands Museum, Østervej 2, DK-4640 Faxe, Denmark. Sten Lennart Jakobsen [stenlennart@yahoo.dk], Geomuseum Faxe/Østsjællands Museum, Østervej 2, DK-4640 Faxe, Denmark. Arden R. Bashfort [bashforth@snm.ku.dk], Natural History Museum of Denmark, Øster Voldgade 5-7, DK-1350 København K, Denmark.

Serpulids are polychaetes forming calcareous tubes. They represent an important part of the marine benthic communities encrusting hard substrates, both in the recent seas and in the fossil record, and they are classified as sclerobionts (Taylor & Wilson 2003; Schlögl *et al.* 2008; Sanfilippo *et al.* 2013; Guido *et al.* 2017; Breton *et al.* 2020; Kočová *et al.* 2021). Calcareous tubes are developed in all known serpulid genera (Vinn *et al.* 2008b, c; Vinn 2019, 2020), in a single genus of sabellids (*Glomerula*; Vinn *et al.* 2008a; Vinn & Wilson 2010; Vinn & Hosgör 2023; Słowiński *et al.* 2023) and in some cirratulid species of the genus *Dodecaceria* (Kočí *et al.* 2021). Calcareous tubeworms first appeared in the Permian (Sanfilippo *et al.* 2017, 2018), and they greatly diversified from the Jurassic (Goldfuss 1831; Ippolitov 2007a, b, 2010; Vinn & Wilson 2010; Jäger & Lang 2017; Kočí *et al.* 2019; Ippolitov & Martill 2020; Kočí & Fözy 2022; Slovinski *et al.* 2022) and onwards to recent (ten Hove & Kupriyanova 2009; Kupriyanova *et al.* 2020, 2023a, b; Rouse *et al.* 2022 and many references herein). The research on tube-bearing polychaetes from the Jurassic of Europe is limited, if compared to the far more extensive research of Cretaceous tube-dwelling polychaetes (Jäger 1983; Sklenář *et al.* 2013; Ippolitov *et al.* 2014; Kočí *et al.* 2017; Kočová *et al.* 2021 and many references herein).

The knowledge of serpulid tubeworms from Jurassic deposits in Denmark is poor, when compared to the research and amount of material on Cretaceous and Paleocene tubeworms (Ravn 1921, 1923; Ødum 1926; Nielsen 1931; Jäger *et al.* 2018; Milán *et al.* 2021, 2022). The first record of Jurassic serpulids from Bornholm, as *Serpula quinquesulcata* Münster, was mentioned by Malling & Grönwall (1909); it was collected from the Liassic (Lower Jurassic) *Myoconcha* bed at Stampen Å. These authors cited Moberg (1888) who described and figured *S. quinquesulcata* and *S. terquemi* Moberg, 1888 from Lower Jurassic deposits in Sweden. Today the species *Serpula quinquesulcata* is considered to belong to the genus *Pentaditrupa* Regenhardt, 1961 and is named *Pentaditrupa quinquesulcata* (Münster in Goldfuss, 1831), and *Serpula terquemi* may be considered a subjective synonym of either *Pentaditrupa quinquesulcata*, as stated by Jäger (2005) or of *Mucroserpula quinquecristata* (Münster in Goldfuss, 1831), which has sharper keels and an angular pentagonal instead of rounded

pentagonal cross-section. The known occurrence of *S. quinquesulcata* Münster from Bornholm, Sweden, north-western and southern Germany as well as England was compiled by Malling & Grönwall (1909, Table 1). *Pentaditrupa quinquesulcata* is widespread in the Pliensbachian of central and western Europe; for more details, see Jäger & Schubert (2008). Cretaceous (Cenomanian to Senonian) serpulids from Bornholm were mentioned by Ravn (1921, 1923).

The aim of this paper to describe the find of a second, new species of serpulid from the Early Jurassic Hasle Formation of Bornholm, and to taxonomically revise the previous report on serpulids from the Hasle Formation by Malling & Grönwall (1909).

Geological setting

The Lower Jurassic (Pliensbachian) Hasle Formation is exposed along coastal cliffs south of the town of Hasle on the Danish island of Bornholm, located in the Baltic Sea, south of Sweden (Fig. 1). The geology of Bornholm is a complex fault block system related to movements of the NW–SE-trending Sorgenfrei–Tornquist Zone, which separates the Danish Basin from the Baltic Shield (Surlyk & Noe-Nygaard 1986; Donovan & Surlyk 2003). During the Mesozoic, the movements of the Sorgenfrei–Tornquist Zone strongly affected the sedimentation and depositional environments, and the eastern border of the fault is located only a short distance inland from the west coast of Bornholm where the Hasle Formation was deposited (Gravesen *et al.* 1982; Surlyk & Noe-Nygaard 1986; Michelsen *et al*. 2003). The Hasle Formation is a reddish-brown sandstone with hummocky and swaley cross-stratified coarse-grained siltstone and very fine-grained sandstone (Fig. 1c). Single horizons show trough cross-bedding or planar lamination, and at the base of these, the individual swales are draped with a fossiliferous conglomeratic layer of clasts of basement rocks (Surlyk &

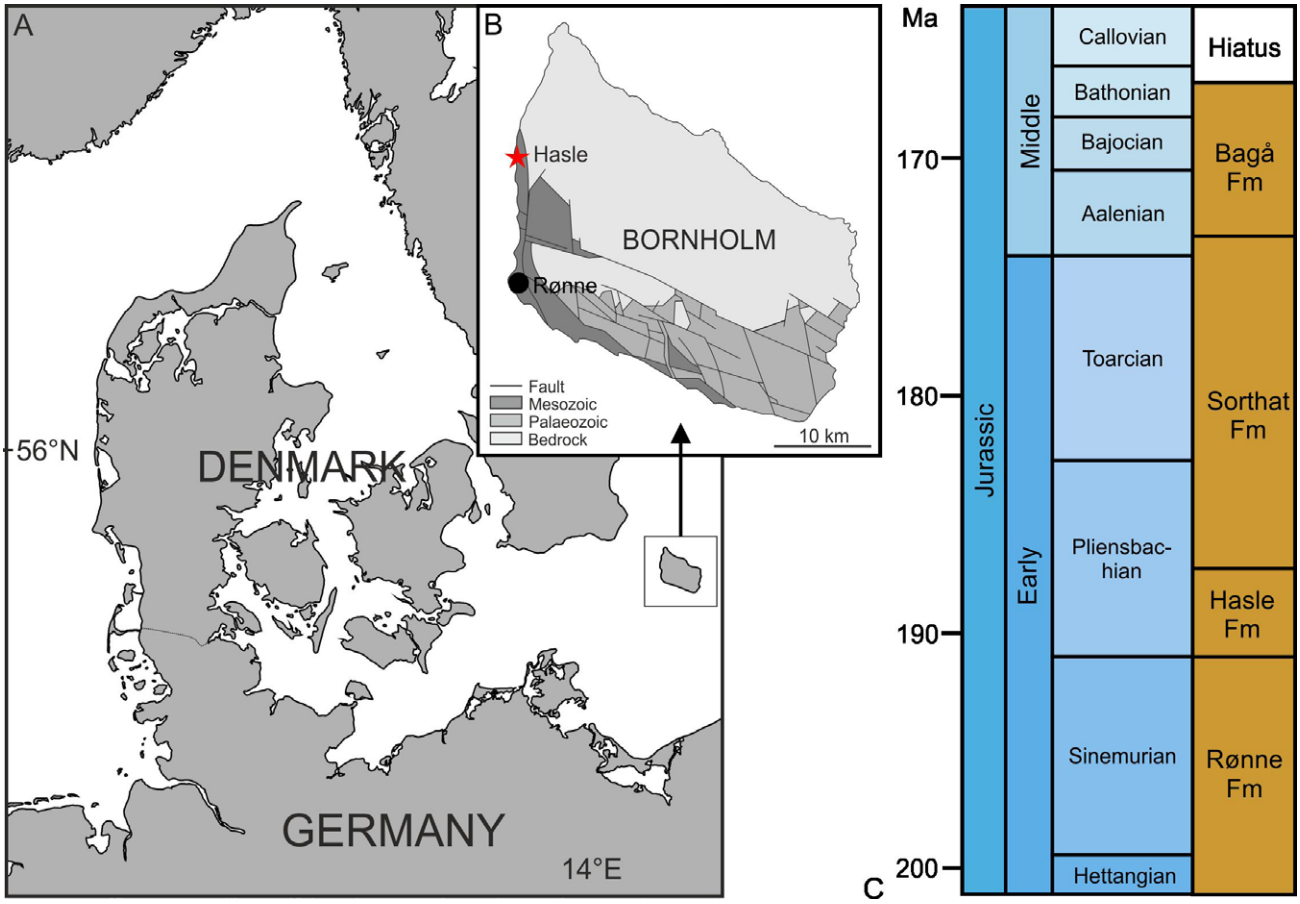

Fig. 1. Location of Bornholm and the type locality of the Hasle Formation. Further exposures of the Hasle Formation exist around Rønne, farther south at Sose Odde. **a.** Location map showing the position of Bornholm in the Baltic Sea. **b.** Outline geological map of Bornholm, showing the location of Hasle, the asterisk indicates the exposure of the Hasle Formation where the specimen was found (Duffin & Milàn 2022). **c.** Late to Middle Jurassic stratigraphy of Bornholm, modified after Sandersen *et al.* (2014).

Noe-Nygaard 1986; Larsen & Friis 1991). The Hasle Formation has been interpreted as shallow marine and has yielded a diverse marine invertebrate and vertebrate fauna. The invertebrate fauna comprises 11 species of ammonites, scaphopods, rare belemnites and several species of bivalves (Malling & Grönwall 1909; Malling 1911, 1914, 1920; Höhne 1933; Donovan & Surlyk 2003). However, due to the coarse-grained nature of the sediment at Hasle (more fine-grained at Rønne), at the type locality at Hasle, most invertebrates are poorly preserved. Condrichthyan remains are common in the form of abundant selachian teeth comprising hybodont and neoselachian species of sharks (Rees 1998), and at least two species of holocephalians (Duffin & Milàn 2017, 2022). Fish remains are abundant and represented by numerous undescribed scales. Skeletal remains and especially teeth of marine reptiles show the presence of at least three plesiosaurian taxa (Milàn & Bonde 2001; Smith 2008), in addition an osteroderm from a thallatosuchian crocodile has been found (Milàn & Mueller-Töwe 2019). Rare remains of terrestrial vertebrates are known by a theropod footprint (Milàn & Surlyk 2015), dinosaurian bone fragments and a mammaliform tooth (Molin 2021), and an isolated dinosaur tooth from? a turiasaurian sauropod (Milàn & Mateus 2024).

Material and methods

A block containing several specimens of the new serpulid species was found by amateur geologist Mette Agersnap Grejsen Hofstedt in 2023 at the type locality of the Hasle Formation, south of the Hasle harbour, Bornholm, Denmark (Fig. 1). The specimens are curated in the collections of the Natural History Museum of Denmark in Copenhagen (MGUH 34317 and MGUH 34318). The original specimen collected by Malling and mentioned by Malling & Grönwall (1909) was located in the collections of the Natural History Museum of Denmark and here taxonomically revised (MGUH 34319).

One piece of the new specimen was polished at a natural break through the tube, to show the structure of the tube wall. This section was made with an electric saw in the Palaeontological Department of the National Museum (PD NM) in Prague with the kind help of Jan Sklenář. The section was hand polished using gradually finer carborundum powder paper (200–2000 units) with water and finally Microlite powder with water. Photographs of the polished sections were made using a light microscope SZX 1200 with Canon EOS 7R camera, and SEM images were taken by using a scanning electron microscope -Hitachi S-3700 N in the Palaeontological Department of the National Museum at Prague. A digital caliper was used for measurements. All figures were prepared using the Corel Draw 20 program.

This published work and the nomenclatural acts it contains have been registered in ZooBank: http://zoobank.org:pub.

Systematic palaeontology

Class Polychaeta Grube, 1850

Subclass Sedentaria Lamarck, 1818

Infraclass Canalipalpata Rouse and Fauchald, 1997

Order Sabellida Levinsen, 1883

Family Serpulidae Rafinesque, 1815

Subfamily Serpulinae Rafinesque, 1815

'Clade AI *Serpula*-group' *sensu* Lehrke *et al*. (2007), Kupriyanova *et al*. (2008) and Ippolitov *et al*. (2014)

Tribe Serpulini Rafinesque, 1815

Genus *Serpula* Linnaeus, 1758

***Serpula? alicecooperi* sp. nov.**
(Figs 2, 3, 6)

Diagnosis. The tubes are straight or very slightly curved in one direction. Circular tube of moderate size, 4–5 mm in diameter. Tube-wall is two-layered, inner surface shows densely-spaced annular rings, the outer surface is unknown. There are no traces of former attachment to a substrate visible; all studied specimens seem to represent free tubes. There are no hints of longitudinal keels visible.

Derivation of name. In honor of musician Alice Cooper for his lifelong dedication to music as a performing artist.

Zoobank ID. LSIDurn:lsid:zoobank.org:act:733CE7CD--3B89-4BAC-A142-E28937EC8101

Type locality. Hasle sandstone, Hasle Formation, Bornholm, Denmark.

Material. One well-preserved tube and several fragmentary tubes, preserved in fine-grained sandstone block found loose on the beach below the cliff section, The tube wall is re-crystallised.

Holotype. The sample consists of two specimens preserved lying side by side in a block and its counterplate (MGUH 34317), deposited in the collections of the Natural History Museum of Denmark in Copenhagen, Fig. 2a.

Paratype. The paratype is visible in polished cross-section (MGUH 34318), Fig. 3.

Description. All studied tubes are fragments of the free anterior portion, straight or slightly curved in one direction and increase in diameter gradually. The tube is circular in cross-section, 4–5 mm in diameter, and the thickness of the tube wall is moderate. No keels are observed, but due to the firmly adhering coarse grains of the surrounding sandstone, the outer surface of the tube appears to be coarse, too, and details of the original surface ornamentation, if such had ever been present, remain unknown. The inner tube surface shows densely-spaced transverse striation, which at regular intervals form annular rings (Fig. 3).

Structure and microstructure of the tube-wall. The cross-sections show that the tube wall consists of a moderately thick dark-coloured outer layer and a very thin bright inner layer, and the longitudinal fractures show that the interior surface of the tube shows densely-spaced delicate annular striation. However, the tubes are recrystallised, and the microstructure of the tube-wall seen in Fig. 3a and 3b does not provide much information.

Remarks and relationships. Due to the relatively few characteristic morphological features of the specimens, it is difficult to state its systematic position within Serpulinae. Beside some superficial similarities to some equally poorly ornamented and hardly determinable Early Jurassic species, for example '*Serpula*' *cylindrica* Terquem & Piette, 1865 and '*Serpula*' *capitata* Phillips, 1829 (see also Tate & Blake 1876), *Serpula*? *alicecooperi* shows close similarities to the genus *Pentaditrupa* Regenhardt, 1961 as well as to '*Serpula*' *etalensis* (Piette, 1856). However, it lacks the most characteristic morphological features of both taxa.

Originally, Piette (1856) erroneously considered his '*Ancyloceras*? *etalensis*' to be a heteromorph ammonite and also compared it with scaphopods. However, according to its tube structure, '*Serpula*' *etalensis* is a true serpulid (Vinn *et al.* 2008c) and belongs to a group of Early Jurassic species representing a still unnamed genus (Jäger 1996). '*Serpula*' *etalensis* is the most typical species of this group and is characterised by many strongly developed but short annular rings on its outer tube surface which, however, are lacking in *Serpula*? *alicecooperi*; in the longitudinal fractures (Fig. 2) no such rings are visible on the outer surface of the tubes. Terquem (1855), Piette (1856) and Terquem & Piette (1865) described and figured several Early Jurassic serpulid tubes from the Lower Jurassic of France, Luxembourg and Belgium. Among these, '*Serpula*' *strangulata* Terquem (1855) is similar to '*S.*' *etalensis*; the strong rings are densely-spaced. The only difference is that the spaces between the strong rings are filled with weak rings, and it seems questionable if this small difference justifies distinguishing two species. Also '*Serpula*' *nodifera* Terquem & Piette (1865: Pl. 14, figs 9, 17, 18) belongs to the same genus as '*Serpula*' *etalensis*; it corresponds relatively well in shape and size, but the annular rings may be weaker than in '*Serpula*'' *etalensis* and may be less densely and less regularly spaced (Piette (1865: Pl. 14, fig. 17). Nevertheless, even such weak and wider spaced annular rings should be visible in the longitudinal sections of the tubes of *Serpula*? *alicecooperi*, if they have such rings. On the contrary, the inner tube surface of *Serpula*? *alicecooperi* shows relatively densely-spaced delicate annular striations. '*Serpula*' *cylindracea* Terquem & Piette (1865: Pl. 14, fig. 10) corresponds rather well by its slender, only slightly curved shape, but its tube diameter is very small, only *c.* 1 mm.

Serpula? *alicecooperi* lacks the five rounded keels and pentagonal cross-section characteristic of the genus *Pentaditrupa* (although occasionally also in *Pentaditrupa* perfectly circular tubes occur; Jäger (1983)). Moreover, the tube diameter of *Serpula*? *alicecooperi* is somewhat larger and the tube wall is somewhat thinner than usual for *Pentaditrupa*. The overall structure of the tube wall of *Serpula*? *alicecooperi* seen at low magnification – thick dark outer layer, very thin bright inner layer; interior surface showing densely-spaced annular striation – is similar to that of the genus *Pentaditrupa*. Therefore, it cannot be excluded that the species *alicecooperi*, in spite of its circular cross-section, lack of keels and somewhat larger tube diameter, may belong to the genus *Pentaditrupa* instead of *Serpula*.

The species *Serpula*? *alicecooperi* was adapted to a life on a soft sandy bottom (according to Jäger & Schubert (2008); Seilacher *et al.* (2008)), because the overal outer space curvature of the tube provide stability to its freely living position or it was attached to some hard substrate by a posterior fixed part that is not preserved. Surlyk & Noe-Nygaard (1986) suggested a

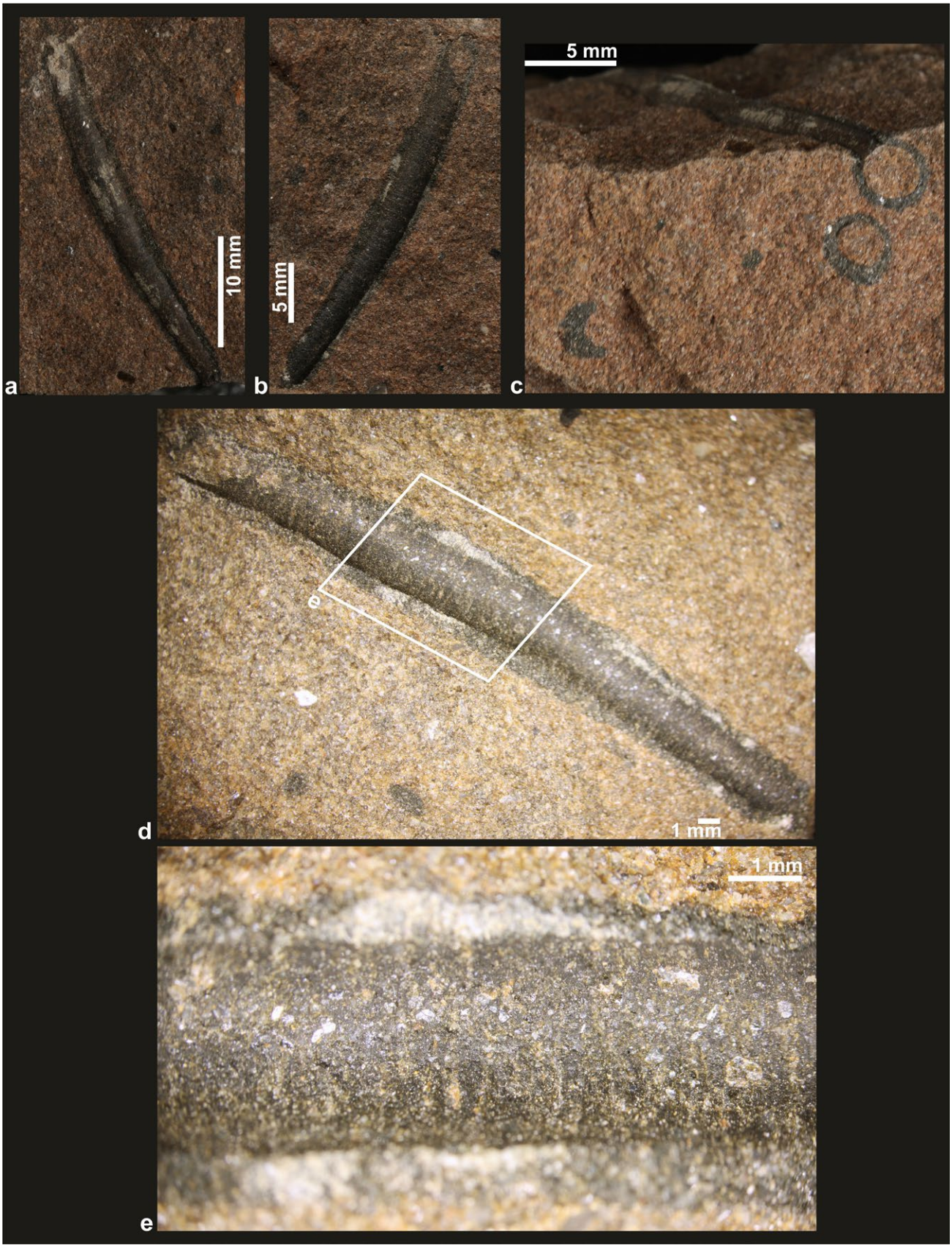

Fig. 2. a. *Serpula? alicecooperi* sp. nov., positive imprint of tube, the transverse rings are visible, Hasle sandstone, Hasle Klint, Bornholm island, Danmark. **b.** Negative imprint of tube. **c.** Circular transverse cross-section of the tube. **d.** Positive imprint showing densely spaced annular rings on the inner tube wall, the figure corresponds with fig a1. **e.** Detailed view of the densely spaced annular rings.

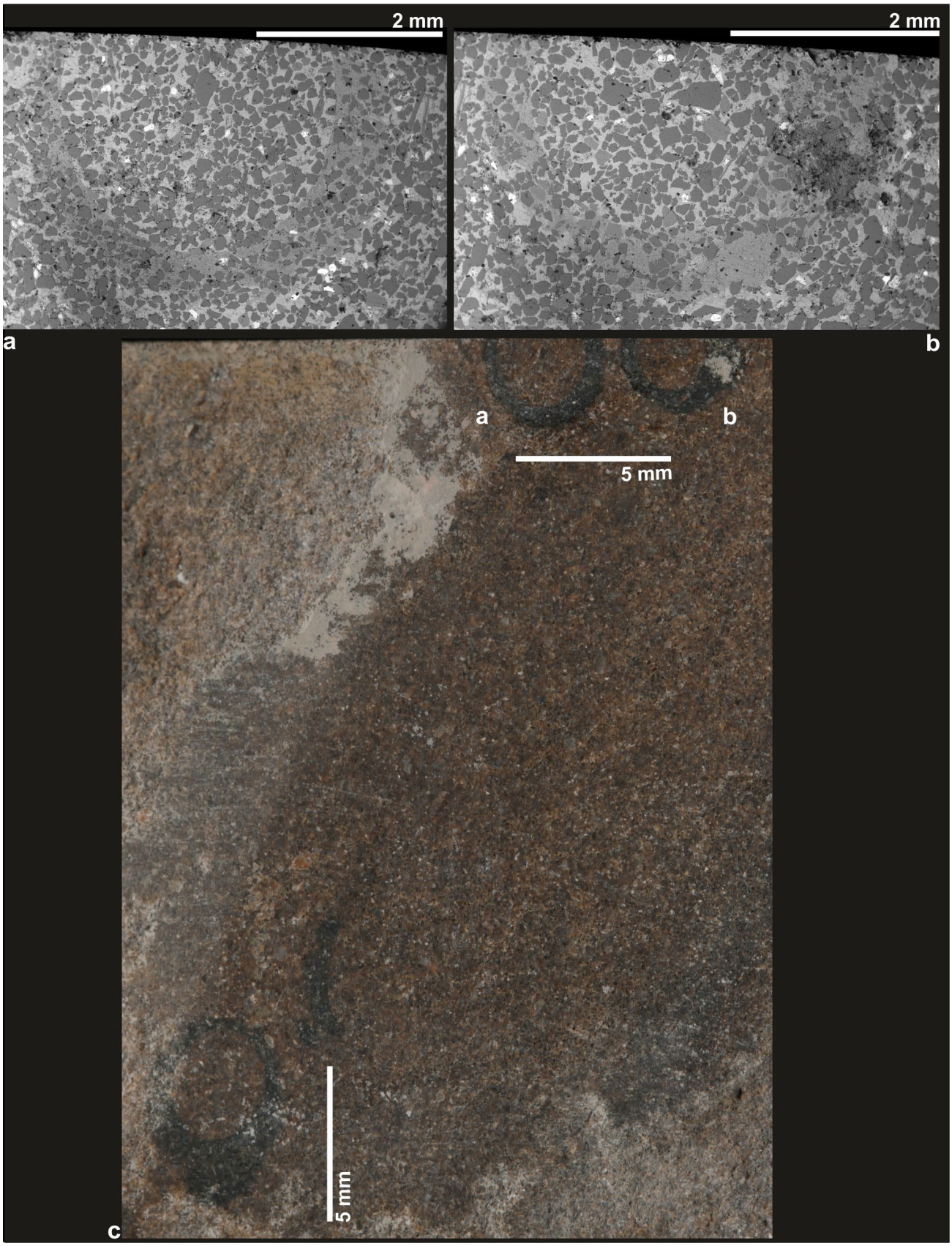

Fig. 3. *Serpula? alicecooperi* sp. nov., small piece from the large specimen. **a.** Transverse cross-section of the tube, SEM image. **b.** Transversal cross-section of the tube, SEM image. **c.** Overall view of transverse section.

palaeo-water depth of 10–40 m and an open marine shelf 1–2 km from the fault-controlled coast. These authors interpreted the Hasle sandstone as a fairly high-energy environment (sandstone and granule conglomerates, very little bioturbation).

'Clade AII *Spirobranchus*-group' *sensu* Lehrke *et al*. (2007), Kupriyanova *et al*. (2008, 2023)

Tribe Ficopomatini Pillai, 1960

Genus *Pentaditrupa*, Regenhardt, 1961

***Pentaditrupa quinquesulcata* (Münster in Goldfuss, 1831)**

(Figs 4, 5)

1831 *Serpula quinque-sulcata* Münster – Goldfuss, p. 226, pl. 67, fig. 8a–d. 1865 *Serpula pentagona*, Terq. et Piette – Terquem & Piette, p. 118, pl. 14, figs 13, 14. 1870 *Serpula subpentagona*, Tate – Tate, p. 402. (pars?) 1876 *Ditrypa quinquesulcata*, Münster – Tate & Blake, p. 438. 1888 *Serpula quinquesulcata* Münster – Moberg, p. 28, pl. 1, fig. 11. ? 1888 *Serpula Terquemi* n. sp. – Moberg, pp. 28–29, pl. 1, figs 12–13. 1909 *Serpula quinquesulcata*, Münster – Malling & Grönwall, p. 275. pars 1956 *Serpula* (*Pentaserpula*) *quinquesulcata* Münster 1831 – Parsch, pp. 228–229. 2008 *Pentaditrupa quinquesulcata* (Münster in Goldfuss, 1831) – Jäger & Schubert, pp. 57 –58, pl. 3, figs 6–13. 2010 *Pentaditrupa quinquesulcata* (Münster in Goldfuss, 1831) – Schubert, p.15, pl. 5, fig. 5.

Material. Two tubes, collected by C. Malling, MGUH 34319, from the Hasle Formation (middle part of early Pliensbachian, *Tragophylloceras ibex* zone, *Beaniceras centaurus* subzone) of Bornholm, Denmark. The tubes were described but not figured by Malling & Grönwall (1909).

Description. The tubes from Bornholm are fragments of the free anterior tube portion. The tube is rounded pentagonal in cross-section. The first tube fragment is at least 10.2 mm long but continues hidden by the adhering sediment; its diameter is 2.3 mm, a diameter of the lumen is 1.9 mm. The thickness of the tube wall may reach up to 0.8 mm. The second tube is compressed to 2 × 2.6 mm due to compaction of the sediment (Fig. 4a). The tubes bear five longitudinal keels, which are low and rounded and appear rather like rounded edges, separated by wide and shallow longitudinal depressions. Transverse ornamentation consists of delicate incremental striations, which run a bit wavy by slightly curving backward at the keels and slightly protruding between the keels, resulting in a chevron-shaped pattern (in Fig. 5 marked by arrows). The tube wall consists of two layers: The external layer is thick, and the internal layer is very thin and bright (Fig. 5a1, a2) and shows densely-spaced delicate annular striations, which are visible in the somewhat oblique cross-section through the second tube (Fig. 5a1).

Remarks and relationships. The tubes from Bornholm match those of the same species from the Pliensbachian of north and south Germany well by shape and ornamentation and by details of the tube wall. The tube diameter is comparable with measurements of tubes from Germany provided by Jäger & Schubert (2008), who stated up to 3 mm. The tube diameter, the only very slight curvature and the rounded, low keels of the tubes from Bornholm indicate that these are fragments of the anterior portions of adult specimens. The geological age (middle part of early Pliensbachian) of the Bornholm tubes matches the hitherto known age of *P. quinquesulcata*. *P. quinquesulcata* is widespread in the Pliensbachian of central and western Europe: Münster's original specimen from Theta near Bayreuth in Franconia in south Germany is from the *Gryphaea*-rich marlstone in the lower part of lower Pliensbachian. Ammon in von Gümbel (1891: 692, 697) mentioned specimens from the upper Pliensbachian and Kuhn (1947: 66, 67) from lower and upper Pliensbachian of Franconia in south Germany. The specimens studied by Jäger & Schubert (2008) are from the *valdani* subzone of lower Pliensbachian near Herford and *stokesi* subzone of upper Pliensbachian at Bielefeld-Jöllenbeck in the Herford Liassic depression, and the specimens studied by Schubert (2010) are from the lower Pliensbachium of Sommersell near Höxter; all these localities are located in Northrhine-Westphalia in northwest Germany. Jäger (unpublished) has collected tubes in lower part of lower Pliensbachian and around the boundary between the lower and upper part of upper Pliensbachian at several places in the foreland of the Swabian Alb in south Germany. Moberg (1888) described it from Kurremölla in Scania in south Sweden. Gallois (1988) mentioned it from the *Beaniceras luridum* subzone of the *ibex* zone of Soham borehole in England. In summary, there is no doubt that the two tubes from Bornholm belong to *Pentaditrupa quinquesulcata* and that this species is the characteristic representative of its genus during more or less the entire Pliensbachian.

The tubes from the Hettangian are too few in number of specimens to state anything about the geologically earliest history of the genus *Pentaditrupa*. Terquem & Piette (1865) introduced their new species '*Serpula*' *pentagona* and figured a beautiful,

Fig. 4. The specimen labelled by C. Malling, Inventory Number 1909. 36, *Centaurus* zone and described as the species *Serpula quinquesulcata* Münster in Goldfuss, 1831. The specimen is now referred to *Pentaditrupa quinquesulcata* (Münster in Goldfuss, 1831). It represents the first find of the serpulid, which was collected on Bornholm, but unfortunately not figured. **a.** Not coated with ammonium chloride. **b**. Coated with ammonium chloride.

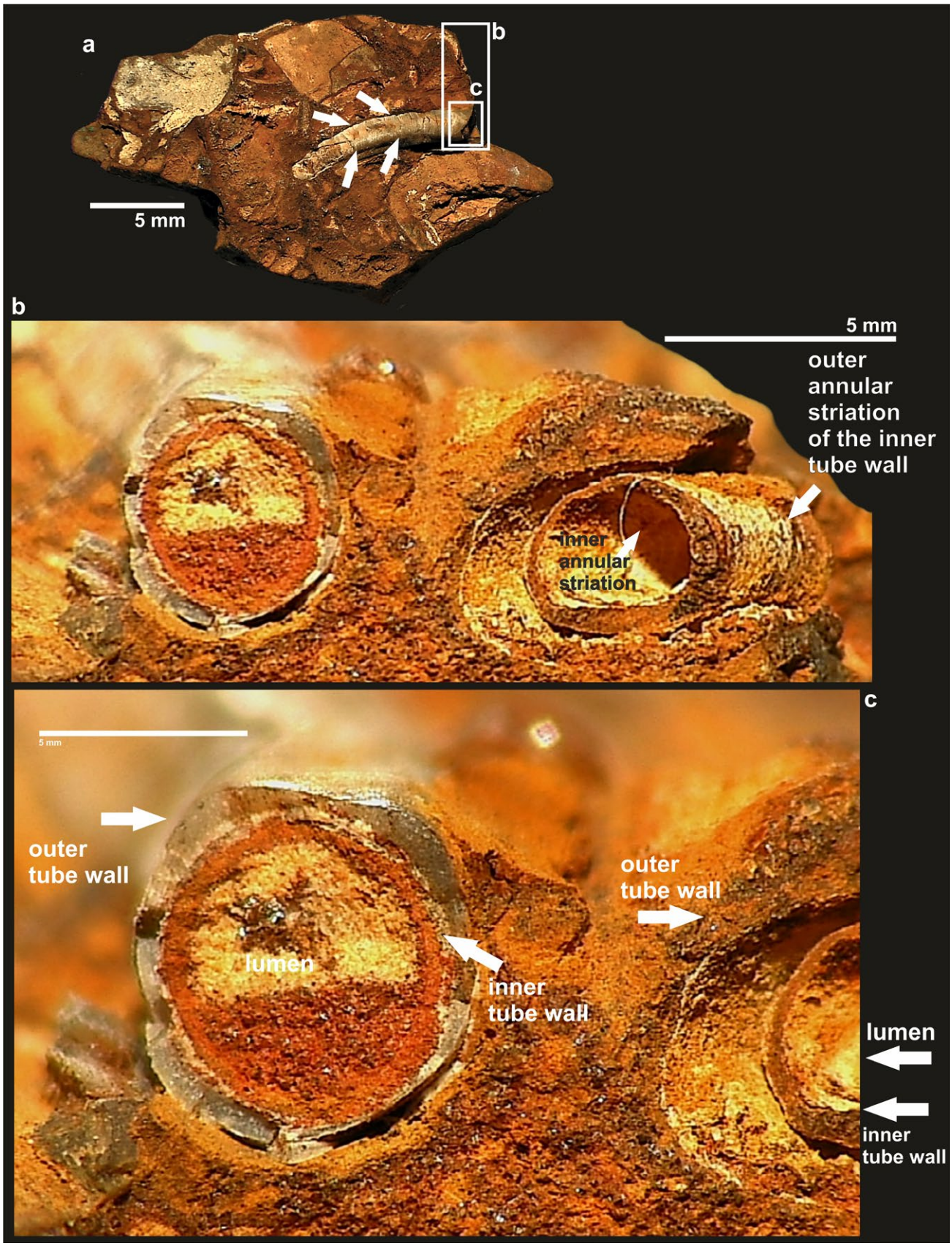

Fig. 5. a. The same specimen of *Pentaditrupa quinquesulcata* (Münster in Goldfuss, 1831). **b.** Transverse cross-section. The white arrows show external tranverse annular striation, left arrow show superficial furrows between rounded ridges. **c.** Detailed view of the pentagonal cross-section.

relatively large tube (diameter up to 4 mm) from the early Sinemurian 'Calcaire à *Ammonites bisulcatus*' of Fleigneux in Département Ardennes in northeast France. Although this is a true *Pentaditrupa* and hardly distinguishable by its morphology from a large specimen of *P. quinquesulcata*, Jäger (2005) preferred to keep it a separate species. Anyway, Terquem & Piette's species name *pentagona* is invalid, because it is a junior homonym of two older versions of the combination '*Serpula pentagona*'. The first homonymy with *Serpula pentagona* Goldfuss, 1831, a valid species name of a Late Jurassic serpulid, was already noticed by Tate (1870) who substituted Terquem & Piette's *pentagona* by uniting all *Pentaditrupa* tubes from lower Sinemurian to upper Pliensbachian under a new name '*Ditrypa*' *subpentagona* Tate, 1870. However later, in Tate & Blake (1876), Tate considered his *subpentagona* a subjective synonym of *P. quinquesulcata*, thereby he widened the stratigraphic range of *P. quinquesulcata* backwards in geological time to lower Sinemurian – upper Pliensbachian. While this is an acceptable solution, an equally acceptable alternative solution is to keep the Sinemurian and Pliensbachian tubes separate by reviving the formally valid name *subpentagona* for the former and restricting *quinquesulcata* for the latter. Anyway, this species, respectively these two species, is/are the most characteristic and most widespread Early Jurassic species of the genus *Pentaditrupa*.

Parsch (1956) stated a much longer stratigraphical range for *P. quinquesulcata* reaching from late Sinemurian ('Lias beta') to Callovian ('Dogger zeta'); very probably not only the similarities among Late Jurassic *Pentaditrupa* species had been the reason for his opinion, but also Parsch's erroneous inclusion of Middle Jurassic pentagonal tubes which, however, belong to a different genus for which later Regenhardt (1961) introduced the name *Mucroserpula*.

The second homonymy with Late Cretaceous *Serpula pentagona* Alth, 1850 was mentioned by Jäger (1983), who considered Alth's invalid species a subjective synonym of *Pentaditrupa subtorquata* (Münster in Goldfuss, 1831).

Several more Early Jurassic *Pentaditrupa* species have been named, some of which are mainly dis-

Fig. 6. Lifelike reconstruction of *Serpula? alicecooperi* sp. nov. Drawing by Lykke Bianca.

tinguished by their small or large size. In the lower Sinemurian, but in and around Rosenfeld in the foreland of the Swabian Alb in south-west Germany, Jäger (unpublished) collected many small to moderately sized pentagonal tubes whose keels vary considerably between specimens. Tubes with rounded keels may be considered small specimens of *P. subpentagona* (Tate, 1870), whereas tubes with sharp keels should rather be referred to the genus *Mucroserpula*. In these geologically relatively old samples from the early Sinemurian, distinguishing between *Pentaditrupa* and *Mucroserpula* is less obvious than in late Sinemurian, Pliensbachian and younger samples, although in the Pliensbachian of south Sweden this problem re-appears. Hence one may wonder if the sharper pentangular and slightly bilateral symmetric '*Serpula Terquemi*' Moberg, 1888 is only a variation and thus a subjective synonym of *P. quinquesulcatus* or belongs to the genus *Mucroserpula*. This question cannot be solved from Moberg's description and figures alone, but we have no fossils from the Pliensbachian of Sweden available for study. Anyway, when sorting tubes from the Pliensbachian of Germany, it is usually possible to differentiate between the rounded-keeled, usually radially symmetrical *Pentaditrupa quiquesulcata* and sharp-keeled, often slightly bilaterally symmetrical *Mucroserpula quinquecristata* (Münster in Goldfuss, 1831). It may be speculated if the similarities of Early Jurassic *Mucroserpula* with *Pentaditrupa* are due to close distance in time to a hypothetical point of phylogenetic bifurcation between the two genera. It seems obvious that fossil *Pentaditrupa* is closely related to recent *Ditrupa* and that fossil *Mucroserpula* and similar fossil *Propomatoceros* are closely related to recent *Spirobranchus* Blainville, 1818. While in the past, only few or vague details of the phylogenetic relationship between *Ditrupa* and other recent serpulid genera had been known (e.g. ten Hove & Smith 1990), the situation has improved, and in the cladograms provided by Kupriyanova *et al*. (2023) *Ditrupa* and *Spirobranchus* both are assigned to the tribe Ficopomatini, making speculation about a phylogenetic separation between *Pentaditrupa* and *Mucroserpula* somewhere around the Triassic/Jurassic boundary a bit more probable.

In the upper Sinemurian dark claystones in the northern foreland of the Swabian Alb in south-west Germany, *Pentaditrupa globiceps* (Quenstedt, 1856) is common (Jäger, unpublished). The actual position of the Quenstedt locality is uncertain. Quenstedt (1856) mentioned and stated the locality 'Breitenbach', which probably refers to a creek rather than than a village. In Quenstedt's study area several creeks with the name Breitenbach are found, one creek is located near the town Reutlingen, but we do not know if this Breitenbach creek was *sensu* Quenstedt (1856; Jäger, personal communication, 26 October 2023). Jäger collected *Pentaditrupa globiceps* (Quenstedt, 1856) in temporal outcrops near Schömberg next to the B27 road to Rottweil and between Aldingen and Trossingen in the foreland of the western part of the Swabian Alb. Tate in Tate & Blake (1876) mentioned this species also from Redcar in northeast England. *P. globiceps* is distinguishable from other Early Jurassic *Pentaditrupa* species by its small size. Also Parsch (1956) had considered this a valid species, but he was misguided by the original description of Quenstedt (1856) who erroneously stated a quadrangular cross-section similar to *Nogrobs tetragona* (J. de C. Sowerby, 1829), whereas in reality *P. globiceps* is pentagonal, and neither Parsch (1956) nor Jäger (unpublished) had ever detected a quadrangular serpulid tube of the genus *Nogrobs* de Montfort, 1808 in late Sinemurian claystones in south Germany.

In the early Pliensbachian of Yorkshire and Cleveland, the very large *Pentaditrupa gigantea* (Phillips, 1829) occurs. Originally, Phillips had described it as *Dentalium giganteum*, and for circa 170 years it has been erroneously considered a scaphopod, although its tube is calcitic and therefore well preserved at Robin Hood's Bay, where this species is common, whereas the aragonitic shells of co-occurring gastropods, scaphopods and some bivalves are dissolved and leave only imprints and steinkerns in the surrounding sediment, as usual in many Mesozoic marlstone and limestone layers. This difference in preservation between calcitic and aragonitic parts of invertebrates is well-known to geologists and experienced amateur collectors. For example, Jäger during an excursion to Robin Hood's Bay in 1992 (and presumably also other people experienced in different kinds of preservation of fossils) recognised at first sight that the supposed '*Dentalium*' *giganteum* cannot be a scaphopod, but must be a serpulid of the genus *Pentaditrupa*, due to its well-preserved tube, regularly curved shape and rounded pentagonal cross-section. Palmer (2001) was the first author who published that '*Dentalium*' *giganteum* must be a serpulid.

For decision if the spiral and strongly rounded pentagonal '*Ditrypa*' *circinata* Tate in Tate & Blake, 1876, which Tate listed from upper Sinemurian to upper Pliensbachian of Yorkshire is a valid *Pentaditrupa* species or just a subjective synonym of *P. gigantea* or *P. quinquesulcata*, a larger number of tubes from Robin Hood's Bay should be studied in more detail.

Serpula olifex (Quenstedt, 1856) occurs in the Hettangian and Sinemurium of Germany and England and is locally very common in a thin upper Sinemurian oil shale bed in the foreland of the Swabian Alb. Its tube is usually regularly curved in one direction and, if growing long enough, may form a wide open planispiral and thereby may resemble a *Pentaditrupa* tube.

However, almost all tubes of *Serpula olifex* are attached to small ammonite shells, mostly but not always to the periphery of the ammonite, where sometimes their posteriormost tube portion was overgrown by the ammonite's next whorl, proving that the serpulid encrusted a living ammonite. In the oilshale the ammonite shells are preserved totally flattened and their aragonitic shells are completely dissolved; sometimes their remains are hardly visible anymore. The also flattened but otherwise well-preserved calcitic tubes of *Serpula olifex* may erroneously be considered unattached free *Pentaditrupa* tubes. Although Seilacher *et al*. (2008) and unpublished specimens collected by Jäger show that the anteriormost tube portion of *Serpula olifex* may indeed change its direction and grow freely away from the ammonite, normally its posterior portion attached to the ammonite is longer than in *Pentaditrupa*. Moreover, three-dimensionally preserved calcified or pyritised specimens of ammonites with *Serpula olifex* encrusting the ammonite's periphery and being overgrown by the ammonites next whorl (e. g. Lange 1932; Schindewolf 1934; Merkt 1966; Müller 1966; Buys 1973; Jäger 1996; Andrew *et al*. 2011) prove that the cross-section of *Serpula olifex* is circular, not pentagonal. By its circular cross-section and by its pseudoplanktic mode of life attached to a living ammonite, *Serpula olifex* is very different from *Pentaditrupa*.

From a long geological time span ranging from the early Toarcian to the middle Albian no *Pentaditrupa* tube is known. The geological younger set of *Pentaditrupa* includes the small *P. wharfensis* (Wilckens, 1922) and *P.* cf. *wharfensis*, together ranging from upper Albian to middle Cenomanian, and the widespread and locally very common (especially in the Campanian and Maastrichtian) medium-sized *P. subtorquata* (Münster in Goldfuss, 1831), also known from upper Albian but mainly from middle Turonian to upper Danian; see Jäger (2005). *P. subtorquata*, of which many synonyms exist, is very variable in width of curvature and cross-section, which ranges from rounded pentagonal to almost perfectly circular. The 'normal' pentagonal form of *P. subtorquata* is very similar to Pliensbachian *P. quinquesulcata*, but in general, the geologically younger *Pentaditrupa* set differs from the early Jurassic *Pentaditrupa* set by never being attached to a substrate and never showing any attachment scar of a former substrate.

The pentagonal genus *Pentaditrupa* and the tusk-shaped and perfectly circular but otherwise very similar Cenozoic and recent genus *Ditrupa* Berkeley, 1835 (extant species are e. g. *Ditrupa arietina* (O. F. Müller, 1776) and *Ditrupa gracillima* Grube, 1878, which occur widespread on and partly in soft sea-bottom, are closely related. Jäger (2005) stated that the geologically youngest *Pentaditrupa* occurred in the late Danian and that phylogenetic transition from *Pentaditrupa* occurred slightly earlier in the Danian, the exact date depends on the earliest occurrence of *Ditrupa schlotheimi* Rosenkrantz, 1920 (Jäger 1993).

Discussion

The rare occurence of serpulids from the Lower Jurassic of Bornholm could be due to the nearshore, high energy environment of the Hasle Formation (Surlyk & Noe-Nygaard 1986). This environment could be poor in nutrients. The taphonomy of the tube wall in *Serpula ?alicecooperi* was caused by cementation of sandstone grains during its diagenesis and fossilisation of the original calcareous tube, however, the calcitic remains of the tube wall are observed under SEM, but we were unable to figure it, due to its poor preservation. The inner tube wall is relatively well preserved and shows annular striations and rings. The preservation of this feature enables us to distinguish between the calcareous tube of serpulids and the agglutinated tube of terebellid or pectinariid polychaetes, because the tubes of the latter genera are formed from agglutinated grains only. The question mark behind *Serpula* Linnaeus, 1758 shows that some diagnostic features are missing, e.g. the external surface of the tube wall is not preserved. The similarities with external and internal dense anullar striations and rings point to the genus *Neovermilia*. *Pentaditrupa quinquesulcata* is a typical species from the lower Jurassic of Europe, it has been reported from France, Germany, Denmark and Sweden. The two examined and redescribed specimens possess typical features of the genus *Pentaditrupa* such as pentagonal cross-section, fine transverse sculptation and two layered tube-wall.

Conclusion

Serpula quinquesulcata mentioned by Malling & Grönwall (1909) is now referred to *Pentaditrupa quinquesulcata* (Münster in Goldfuss, 1831) and is here re-examined and figured for the first time.

A new species of a serpulid worm *Serpula*? *alicecooperi* sp. nov. is described from the Lower Jurassic (Pliensbachian) Hasle Sandstone of Bornholm. SEM examination of the tube-wall of *S.*? *alicecooperi* shows the tube-wall to be recrystallised and infilled by fine-grained sandstone, however, remains of the original wall is poorly visible under SEM examination.

The morphology of the new species shows that it

was adapted to free life in soft, fine-grained, bottom conditions close to the shoreface, environment with very little bioturbation, similar to the interpreted lifestyle of *Pentaditrupa quinquesulcata*.

Acknowledgments

The authors thank amateur geologist Mette Agersnap Grejsen Hofstedt for her find and for bringing it to our attention. We greatly appreciate help by Dr. Manfred Jäger, Rosenfeld, Germany) who read an early draft of the manuscript and provided helpful suggestions that greatly improved the paper. We thank Dr. Jan Sklenář (Palaeontological Department, National Museum, Prague) who cut the sample with an electric saw and Lenka Váchová (Palaeontological Department, National Museum, Prague) for producing SEM images. Illustrator Lykke Bianca is thanked for her beautiful illustration of *S. alicecooperi*. Referee comments by Olev Vinn and an anonymous person are greatly appreciated. This research was financially supported by the Ministry of Culture of the Czech Republic (DKRVO 2024-2028 2.III.c, National Museum, 00023272).

References

Andrew, C., Howe, P., Paul, C.R.C. & Donovan, S.K. 2011: Epifaunal worm tubes on Lower Jurassic (Lower Lias) ammonites from Dorset. Proceedings of the Geologists' Association 122, 34–46. https://doi.org/10.1016/j.pgeola.2010.09.002

Berkeley, M.J. 1835: Observations upon the Dentalium subulatum of Deshayes. The Zoological Journal. 5: 424-427, plate 19, suppl. plate vol. plate 18., available online at http://biodiversitylibrary.org/page/13381128

Blainville, H.M.D. de 1818: Mémoire sur la classe des Sétipodes, partie des Vers à sang rouge de M. Cuvier, et des Annélides de M. de Lamarck. Bulletin des Sciences, par la Société Philomatique de Paris 1818, 78–85. https://biodiversitylibrary.org/page/4146409

Breton, G., Jäger, M. & Kočí, T. 2020: The sclerobionts of the Bajocian Oolithe ferrugineuse de Bayeux Formationmfrom Calvados (Paris Basin, Normandy, France). Annales de Paléontologie 106, 102361. https://doi.org/10.1016/j.annpal.2019.07.002

Buys, J. 1973: Symbiosen van serpula's met ammonieten uit de Onder Lias van Dorset (Zuid-Engeland). Grondboor & Hammer 27, 62–67.

Donovan, D.T., & Surlyk, F. 2003: Lower Jurassic (Pliensbachian) ammonites from Bornholm, Baltic Sea, Denmark. Geological Survey of Denmark and Greenland Bulletin 1, 555–583. https://doi.org/10.34194/geusb.v1.4684.

Duffin, C.J. & Milàn, J. 2017: A new myriacanthid holocephalian from the Early Jurassic of Denmark. Bulletin of the Geological Society of Denmark 65, 161–170. doi:10.37570/bgsd-2017-65-10.

Duffin, C.J. & Milàn, J. 2022: Further holocephalian remains from the Hasle Formation (Early Jurassic) of Denmark. Bulletin of the Geological Society of Denmark 70, 139–149. doi:10.37570/bgsd-2022-70-10. S2CID 254356926.

Gallois, R.W. 1988: Geology of the country around Ely. Memoir British Geological Survey, Sheet 173. British Geological Survey, Natural Environment Research Council London: Her Majesty's Stationery Office.

Goldfuss, A. 1826–1844: Petrefacta Germaniae: tam eaquae in Museo Universitatis Regiae Borussicae Fridericiae Wilhelmiae Rhenanae servantur quam alia quaecunque in Museis Hoeninghusiano Muensterianoaliis que extant; iconibus et descriptionibus illustrata. Abbildungen und Beschreibungen der Petrefacten Deutschlands und der angränzenden Länder, unter Mitwirkung des Herrn Grafen Georg zu Münster, herausgegeben von August Goldfus[s]. Düsseldorf: Arnz and Co.

Gravesen, P., Rolle, F. & Surlyk, F. 1982: Lithostratigraphy and sedimentary evolution of the Triassic, Jurassic and Lower Cretaceous of Bornholm, Denmark. Danmarks Geologiske Undersøgelse Series B, 51 pp. https://doi.org/10.34194/serieb.v7.7062

Grönwall, K.A. 1912: En Fauna i Bornholms Lias. Geologiska Föreningen i Stockholm Förhandlingar 34, 366–367. https://doi:10.1080/11035891209448698.

Grube, A.-E. 1850: Die Familien der Anneliden. Archiv für Naturgeschichte 16, 249–364.

Grube, A.-E. 1878: Annulata Semperiana. Beiträge zur Kenntniss der Annelidenfauna der Philippinen nach den von Herrn Prof. Semper mitgebrachten Sammlungen. Mémoires l'Académie Impériale des Sciences de St.- Pétersbourg série 7, vol. 25, 1–300. https://biodiversitylibrary.org/page/4537

Guido, A., Jimenez, C., Achilleos, K., Rosso, A., Sanfilippo, R., Hadjioannou, L., Petrou, A., Russo, F. & Mastandrea, A. 2017: Cryptic serpulid-microbialite bioconstructions in the Kakoskali submarine cave (Ciprus, Eastern Mediterranean). Facies 63, 21. https://doi:10.1007/s10347-017-0502-3

Gümbel, C.W. von 1891: Geognostische Beschreibung der Fränkischen Alb (Frankenjura) mit dem anstossenden fränkischen Keupergebiete, 763 pp. Kassel: Theodor Fischer.

Höhne, R. 1933: Beiträge zur Stratigraphie, Tektonik und Paläogeographie des südbaltischen Rhät-Lias, insbesondere auf Bornholm. Abhandlungenaus dem Geologisch-Paläontologischen Institut der Universität Greifswald 12, 1–105.

Hove, H.A. & Kupriyanova, E.K. 2009: Taxonomy of Serpulidae (Annelida, Polychaeta): The state of affairs. Zootaxa, 2036, 126 pp. https://doi.org/10.11646/zootaxa.2036.1.1

Ippolitov, A.P. 2007a: Contribution to the revision of some late Callovian serpulids (Annelida, Polychaeta) of central Russia, Part 1. Paleontological Journal 41, 260–267. https://doi.org/10.1134/s0031030107030057

Ippolitov, A.P. 2007b: Contribution to the revision of some late Callovian serpulids (Annelida, Polychaeta) of central Russia, Part 2. Paleontological Journal 41, 429–436. https://doi.org/10.1134/s0031030107040090

Ippolitov, A.P. 2010: Serpulid (Annelida, Polychaeta) evolution and ecological diversification patterns during Middle-Late Jurassic. Earth Science Frontiers 17, 207–208.

Ippolitov, A.P. 2011: Features of serpulid (Annelida, Polychaeta) stratigraphical distribution in the Jurassic of Russian Platform. In: Zakharov, V.A., Rogov, M.A. & Ippolitov, A.P. (eds): Jurassic System of Russia: Problems of Stratigraphy and Paleogeography, 80–83. Saint-Petersburg: LEMA. [in Russian]

Ippolitov, A.P. & Martill, D.M. 2020: 5. Annelids. In: Martill, D.M., Etches, S. & Loveridge, R.F. (eds): Fossils of the Kimmeridge Clay Formation, Vol. 1, Introduction, geology and invertebrate palaeontology. London: The Palaeontological Association.

Ippolitov, A.P., Vinn, O., Kupriyanova, E.K. & Jäger, M. 2014: Written in stone: history of serpulid polychaetes through time. Memoirs of Museum Victoria 71, 123–159.

Jäger, M. 1983: Serpulidae (Polychaeta sedentaria) aus der norddeutschen höheren Oberkreide – Systematik, Stratigraphie, Ökologie. Geologisches Jahrbuch A68, 3–219.

Jäger, M. 1993: Danian Serpulidae and Spirorbidae from NE Belgium and SE Netherlands: K/T boundary extinction, survival, and origination patterns. Contributions to Tertiary and Quaternary Geology, 29, 73–137.

Jäger, M. 1996: 'Serpula etalensis'. Fossilien 13, 38–40.

Jäger, M. 2005. Serpulidae und Spirorbidae (Polychaeta sedentaria) aus Campan und Maastricht von Norddeutschland, den Niederlanden, Belgien und angrenzenden Gebieten. Geologisches Jahrbuch, Reihe A, 157, 121–249.

Jäger, M. & Lang, F. 2017: Serpuliden und Sabelliden aus dem oberen Kimmeridgium von Saal bei Kelheim. In Lang, F. & Simonsen, S. (eds): Fossilien aus dem Riffschuttkalk des Kimmeridgium (Oberjura) von Saal a. d. Donau bei Kelheim (Bayern). Der Steinkern 30, 76–83.

Jäger, M., Kapitzke, M. & Rieter, M. 2001: Neu funde von Pannoserpula pannosa (Quenstedt, 1857) (Polychaeta, Serpulidae) aus den Korallenkalken (Ober-Kimmeridgium) von Nattheimund Gerstetten (Schwäbische Alb). New records of Pannoserpula pannosa (Quenstedt, 1857) (Polychaeta, Serpulidae) from the coral limestones (Upper Kimmeridgian) of Nattheim and Gerstetten (Swabian Alb). Stuttgarter Beiträgezur Naturkunde, Serie B, 308, 17 pp.

Jäger, M. & Schubert, S. 2008: Das Ober-Pliensbachium (Domerium) der Herforder Liasmulde, Teil 2, Serpuliden (Kalkröhrenwürmer). Geologie und Palaeontologie in Westfalen 71, 47–75.

Jäger, M., Kočí, T., Schnetler K.I., Andersen, S.B. & Jacobsen, S.L. 2018: Sabellidae and Serpulidae (Polychaeta, Canalipalpata) from from the Danian of Denmark, with special consideration of specimens from the Faxe quarry – preliminary report. In: Pšenička, J., Frojdová, J., Svobodová, A. & Dašková, J. (eds): Abstract Book 19th Czech-Slovak-Polish Palaeontological Conference & MIKRO 2018 workshop West Bohemian Museum in Pilsen. Folia Musei Rerum Naturalium Bohemiae Occidentalis, Geologica et Palaeobiologica, Special Volume, 32–34. Plzeň.

Kočí, T. & Főzy, I. 2022: Late Jurassic-Early Cretaceous tube-dwelling worms (Sabellidae, Serpulidae) from the Bakony Mountains. In: FŐZY I. (ed.): Fauna, biostratigraphy, facies and paleotectonic evolution of the Late Jurassic-Early Cretaceous formations in the Bakony Mountains (Transdanubian Range, Hungary), 191–199. Institute of Geosciences, University of Szeged, GeoLiteraPublishing House.

Kočí, T., Jäger, M., Šamánek, J. & Hykš, P. 2019: Tube-dwelling polychaetes from the Oxfordian (Late Jurassic) of Hády Quarryat Brno (Moravia, Czech Republic). Neues Jahrbuch für Geologie und Paläontologie-Abhandlungen 294, 311–332.

Kuhn, O. 1947: Gliederungund Fossilführung des Lias und Doggers in Franken. Bericht der naturforschenden Gesellschaft Bamberg 30, 33–89.

Kupriyanova, E.K., Bastida-Zavala, R., Halt, R.M.N., Lee, M.S.Y. & Rouse, G.W. 2008: Phylogeny of the Serpula – Crucigera – Hydroides clade (Serpulidae: Annelida) using molecular and morphological data: implications for operculum evolution. Invertebrate Systematics 22, 425–437. http://dx.doi.org/10.1071/IS08011

Kupriyanova, E.K. & Ippolitov, A.P. 2015: Deep-sea serpulids (Annelida: Polychaeta) in tetragonal tubes: on a tube convergence path from Mesozoic to Recent. Zootaxa 4044, 151–200. https://doi.org/10.11646/zootaxa.4044.2.1

Kupriyanova, E.K., Rzhavsky, A.V. & Hove, H.A. ten 2020: 7.4.7 Serpulidae Rafinesque, 1815. In: Purschke, G., Böggemann, M. & Westheide, W. (eds): Pleistoannelida, Sedentaria II. Handbook of Zoology Annelida 2, 213–275. Berlin: De Gruyter.

Kupriyanova, E., Hove, H.A. ten & Rouse, G.W. 2023a: Phylogeny of Serpulidae (Annelida, Polychaeta) inferred from morphology and DNA sequences, with a new classification. Diversity15, 398, 24 pp. https://doi.org/10.3390/d15030398

Kupriyanova, E., Sun, Y., Wong, E. & Harry, A. 2023b: Hydroides of the World. Csiro Publishing.

Lamarck, J.-B. de 1818: Histoire naturelle des animaux sans vertèbres 5, 612 pp. Paris: Déterville & Verdière.

Lange, W. 1932: Über Symbiosen von Serpula mit Ammoniten im unteren Lias Norddeutschlands. Zeitschrift der Deutschen Geologischen Gesellschaft 84, 229–234.

Larsen, O.H. & Friis, H. 1991: Petrography, diagenesis and pore-water evolution of a shallow marine sandstone (Hasle Formation, Lower Jurassic, Bornholm, Denmark). Sedimentary Geology 72, 269–284.

Lehrke, J., Hove, H.A. ten, Macdonald, T.A., Bartolomaeus, T. & Bleidorn, C. 2007: Phylogenetic relationships of Serpulidae (Annelida: Polychaeta) based on 18S rDNA sequence data, and implications for opercular evolution. Organisms, Diversity and Evolution 7, 195–206. https://doi.org/10.1016/j.ode.2006.06.004

Lundgren, B. 1879: Bidrag til Kännedomen om Jura formationen

paa Bornholm. Festskrift till Universitetet i Köpenhamn vid dess jubileum 1879. Lunds Universitet.
Malling, C. 1911: Hasle-Sandstenens alder. Meddelelser fra Dansk Geologisk Forening 3, 629–631.
Malling, C. 1914: De Jespersenske Buelag i Lias paa Bornholm. Meddelelser fra Dansk Geologisk Forening 4, 265–270.
Malling, C. 1920: Den marine Lias og Wealden-Aflejringer paa Bornholm. Meddelelser fra Dansk Geologisk Forening 5, 55–57.
Malling, C. & Grönwall, K.A. 1909: En Fauna i Bornholms Lias. Meddelelser fra Dansk Geologisk Forening 3, 271–316.
Merkt, J. 1966: Uber Austern und Serpeln als Epoken auf Ammonitengehäusen. Neues Jahrbuch für Geologie und Paläontologie, Abhandlungen 125, 467–497.
Michelsen, O., Nielsen, L.H., Johannessen, P.N., Andsbjerg, J. & Surlyk, F. 2003: Jurassic lithostratigraphy and stratigraphic development onshore and offshore Denmark. In: Ineson, J.R., & Surlyk, F. (eds): The Jurassic of Denmark and Greenland. Geological Survey of Denmark and Greenland Bulletin 1, 145–216. https://doi:10.34194/geusb.v1.4651
Milàn, J. & Bonde, N. 2001: Svaneøgler, nye fund fra Bornholm. Varv 2001, 3–8.
Milàn, J. & Mateus, O. 2024: A turiasaurian (Dinosauria, Sauropoda) tooth from the Pliensbachian Hasle Formation of Bornholm, Denmark, shows an Early Jurassic origin of the Turiasauria. Diversity 16, 12. https://doi.org/10.3390/d16010012
Milàn, J. & Mueller-Töwe, I. 2021: En havkrokodille fra Hasles fjerne fortid. Natur På Bornholm 19, 14–16.
Milàn, J. & Surlyk, F. 2015: An enigmatic, diminutive theropod footprint in the shallow marine Pliensbachian Hasle Formation, Bornholm, Denmark. Lethaia 48, 429–435. doi:10.1111/let.12115.
Moberg, J.G. 1888: Om Lias i Sydöstra Skåne. Geologiska Föreningen i Stockholm Förhandlingar 11, 238-241. https://doi.org/10.1080/11035898909444258
Molin, E. 2021: Rare terrestrial vertebrate remains from the Pliensbachian (Lower Jurassic) Hasle Formation on the island of Bornholm, Denmark. Dissertations in Geology at Lund University, No. 612, 39 pp.
Müller, A.H. 1966: Zur Kenntnis mesozoischer Serpuliden (Annelida, Polychaeta). Geologie 15, 1053–1075.
Müller, O.F. 1776: Zoologiae Danicae prodromus, seu Animalium Daniae et Norvegiae indigenarum: characteres, nomina, et synonyma imprimis popularium, 282 pp. Copenhagen: Typis Hallagerii. http://www.biodiversitylibrary.org/item/47550
Nielsen, K.B. 1931: Serpulidae from the Senonian and Danian deposits of Denmark. Meddelelser fra Dansk Geologisk Forening 8, 71–113.
Ødum, H. 1926: Studier over Daniet i Jylland og paa Fyn. Danmarks geologiske Undersøgelse II. Række, vol. 45, 306 pp. https://doi.org/10.34194/raekke2.v45.6831
Palmer, C.P. 2001: Dentalium giganteum Phillips: a serpulid worm tube. Proceedings of theYorkshire Geological Society, 53, 253–255. https://doi.org/10.1144/pygs.53.3.253
Parsch, K.O.A. 1956: Die Serpuliden-Fauna des südwestdeutschen Jura. Palaeontographica A, Paläozoologie, Stratigraphie 107, 211–240.
Phillips, J. 1829: Illustrations of the geology of Yorkshire; or a description of the strata and organic remains of the Yorkshire coast, 192 pp. York: The author.
Piette, E. 1856: Notice sur les grès d'Aiglemont et de Rimogne. Le Bulletin de la Société géologique de France 2, 188–207.
Pillai, T.G.1960: Some marine and brackish-water serpulid Polychaeta from Ceylon, including new genera and species. Ceylon Journal of Science (Biological Sciences) 3, 1–40.
Quenstedt, F.A. 1856–1858: Der Jura. Tübingen: H. Laupp.
Quenstedt, F.A. 1885: Handbuch der Petrefaktenkunde, 1239 pp. Tübingen: H. Laupp.
Rafinesque, C.S. 1815: Analyse de la nature ou tableau de l'universe et des corps organisés, 224 pp. Palerme: l'Auteur.
Ravn, J.P. J. 1921: Kridtaflejringerne paa Bornholms sydvest kyst og deres Fauna. III. Senonet. IV. Kridt aflejringerne ved Stampe Aa. Danmarks Geologiske Undersøgelse II. Række, vol. 32, 52 pp. https://doi.org/10.34194/raekke2.v32.6817
Rees, J. 1998: Early Jurassic selachians from the Hasle Formation on Bornholm, Denmark. Acta Palaeontologica Polonica 43, 43–439.
Regenhardt, H. 1961: Serpulidae (PolychaetaSedentaria) aus der Kreide Mitteleuropas, ihre ökologische, taxionomische und stratigraphische Bewertung. Mitteilungen aus dem Geologischen Staatsinstitut in Hamburg 30, 5–115.
Rosenkrantz, A. 1920: Craniakalk fra Kjøbenhavns Sydhavn. Danmarks Geologiske Undersøgelse II. Række, vol. 36, 79 pp. https://doi.org/10.34194/raekke2.v36.6822
Rouse, G.W. & Fauchald, K. 1997: Cladistics and polychaetes. Zoologica Scripta 26, 139–204.
Rouse, G.W., Pleijel, F. & Tilic, E. 2022: Annelida, 418 pp. Oxford University Press. http://doi 10. 1093/oso/9780199692309.003.0001
Sandersen, P.B.E., Rasmussen, E.S., Bjerager, M., Jensen, J.B., Schovsbo, N. & Vosgerau, H. 2014: Skitser til opbygningen af en national 3D geologisk model for Danmark, Forslag til legende for den danske del af den nationale 3D geologiske model. Internal GEUS working paper, Rapport 2, 47 pp.
Sanfilippo, R., Rosso, A., Reitano, A. & Insacco, G. 2017: First record of sabellid and serpulid polychaetes from the Permian of Sicily. Acta Palaeontologica Polonica 62, 25–38. https://doi.org/10.4202/app.00288.2016
Sanfilippo, R., Rosso, A., Reitano, A., Viola, A. & Insacco, G. 2018: New serpulid polychaetes from the Permian of western Sicily. Acta Palaeontologica Polonica 63, 579–584. https://doi.org/10.4202/app.00448.2017
Schindewolf, O.H. 1934: Über Epöken auf Cephalopoden--Gehäusen. Paläontologische Zeitschrift 16, 15–31.
Schlögl, J., Michalík, J., Zágorŝek, K. & Atrops, F. 2008: Early Tithonian serpulid-dominated cavity-dwelling fauna, and the recruitment pattern of the serpulid larvae. Journal of Paleontology 82, 351–361.
Schubert, S. 2010: Geologische Erkenntnisse aus den Tongruben

bei Sommersell, Stadt Nieheim. Geologie und Paläontologie in Westfalen 74, 5–37.

Seilacher, A., Olivero, E.B., Butts, S.H. & Jäger, M. 2008: Soft-bottom tube worms: from irregular to programmed shell growth. Lethaia 41, 349–365. https://doi.org/10.1111/j.1502-3931.2008.00092.x

Slowinski, J., Vinn, O., Jäger. M. & Zatoń M. 2022: Middle and Late Jurassic tube dwelling polychaetes from the Polish Basin: Diversity, palaeoecology and comparisons with other assemblages. Acta Palaeontologica Polonica 67, 827–864. https://doi.org/10.4202/app.01006.2022

Słowiński, J., Banasik, K. & Vinn, O. 2023: Insights into the mineral composition and ultrastructure of the Jurassic sabellid tubes (Annelida, Polychaeta): the evolution of sabellid calcification and its palaeoecological implications. Lethaia 56, 1–12. https://doi.org/10.18261/let.56.3.8

Smith, A. S.2008: Plesiosaurs from the Pliensbachian (Lower Jurassic) of Bornholm, Denmark. Journal of Vertebrate Paleontology 48, 1213–1217. https://doi:10.1671/0272-4634-28.4.1213. JSTOR 20491054. S2CID 128999502.

Surlyk, F. & Noe-Nygaard, N. 1986: Hummocky cross-stratification from the Lower Jurassic Hasle Formation of Bornholm, Denmark. Sedimentary Geology 46, 259–273. https://doi:10.1016/0037-0738(86)90062-X

Tate, R. 1870: On the palaeontology of the junction beds of the Lower and Middle Lias in Gloucestershire. Quarterly Journal of the geological Society of London 26, 394–408.

Tate, R. & Blake, J.F. 1876: The Yorkshire Lias, 475 pp. London: John van Voorst.

Taylor, P.D. & Wilson, M.A. 2003: Palaeoecology and evolution of marine hard substrate communities. Earth Science Reviews 62, 1–103. https://doi.org/10.1016/s0012-8252(02)00131-9

Terquem, O. & Piette, E. 1865: Le Lias inférieur de l'Est de la France comprenant la Meurthe, la Moselle, Le Grand-Duché de Luxembourg, la Belgique et la Meuse. Mémoires de la Société géologique de France 8, 1–175.

Vinn, O. 2009: The ultrastructure of calcareous cirratulid (Polychaeta, Annelida) tubes. Estonian Journal of Earth Sciences 58, 153–156. https://doi.org/10.3176/earth.2009.2.06

Vinn, O. & Furrer, H. 2008: Tube structure and ultrastructure of serpulids from the Jurassic of France and Switzerland, its evolutionary implications. Neues Jahrbuch für Geologie und Paläontologie, Abhandlungen 250, 129–135. https://doi.org/10.1127/0077-7749/2008/0250-0129

Vinn, O. & Hosgör İ. 2023: The first record of Middle Jurassic serpulids from SE Turkey, equatorial Tethys. Carnets de Géologie 23, 97–105. https://doi.org/10.2110/carnets.2023.2305

Vinn, O., ten Hove, H.A. & Mutvei, H. 2008a: On the tube ultrastructure and origin of calcification in sabellids (Annelida, Polychaeta). Palaeontology 51, 295–301. https://doi.org/10.1111/j.1475-4983.2008.00763.x

Vinn, O., ten Hove, H.A., Mutvei, H. & Kirsimäe, K. 2008b: Ultrastructure and mineral composition of serpulid tubes (Polychaeta, Annelida). Zoological Journal of the Linnean Society 154, 633–650. https://doi.org/10.1111/j.1096-3642.2008.00421.x

Vinn, O., Jäger, M. & Kirsimäe, K. 2008c: Microscopic evidence of serpulid affinities of the problematic fossil tube 'Serpula' etalensis from the Lower Jurassic of Germany. Lethaia 41, 417–421. https://doi.org/10.1111/j.1502-3931.2008.00093.x

Vinn, O. & Wilson, M.A. 2010: Sabellid-dominated shallow water calcareous polychaete tube worm association from the equatorial Tethys Ocean (Matmor Formation, Middle Jurassic, Israel). Neues Jahrbuch für Geologie und Paläontologie, Abhandlungen 258, 31–38. https://doi.org/10.1127/0077-7749/2010/0080

Wilckens, O. 1922: The Upper Cretaceous gastropods of New Zealand. Paleontological Bulletin. New Zealand Geological Survey 9, 1–42.

Euendolith borings in *Chancelloria* and *Nisusia* from the middle Cambrian (Miaolingian) of North Greenland (Laurentia)

JOHN S. PEEL

Geological Society of Denmark
https://2dgf.dk

Received 5 February 2024
Accepted in revised form
6 March 2024
Published online
24 March 2024

Peel, J.S. 2024. Euendolith borings in *Chancelloria* and *Nisusia* from the middle Cambrian (Miaolingian) of North Greenland (Laurentia). Bulletin of the Geological Society of Denmark, Vol. 73, pp. 57–66. ISSN 2245-7070.
https://doi.org/10.37570/bgsd-2024-73-03

Borings of microscopic organisms (euendoliths) are described from the Henson Gletscher Formation (middle Cambrian, Miaolingian Series, Wuliuan Stage) of Peary Land, North Greenland (Laurentia). Partially phosphatised sclerites of *Chancelloria* and valves of the brachiopod *Nisusia* reveal abundant casts of borings following dissolution of skeletal calcium carbonate in weak acetic acid. Threads referred to *Scolecia* dominate, occurring together with coccoids (*Planobola*) and the branching *Fascichnus*, in a suite comparable to a lower Cambrian assemblage from the Maidiping Formation of Sichuan, China.

Keywords: Euendoliths, *Chancelloria* spicules, *Nisusia*, Cambrian (Miaolingian Series, Wuliuan Stage), North Greenland, Laurentia.

John S. Peel [john.peel@pal.uu.se], Department of Earth Sciences (Palaeobiology), Uppsala University, Villavägen 16, SE-75236 Uppsala, Sweden.

Microorganisms including algae, Cyanobacteria and Fungi that bore actively into hard substrates or the calcareous shells and skeletons of living and dead organisms are termed euendoliths (Golubic *et al.* 1981) and have a geological record that extends back to the Palaeoproterozoic (Campbell 1982; Zhang & Golubic 1987; Bengtson *et al.* 2017). At the present day, their activities contribute to the diminution of the penetrated calcareous materials to cryptocrystalline textures through the process of micritisation (MacIntyre & Reid 1978).

The starting point for studies of euendoliths in the ancient rocks of Greenland is the description by Green *et al.* (1988) of microfossils in thin sections of Upper Proterozoic oolites and pisolites from the Eleonore Bay Group of North-East Greenland. Cambrian euendoliths were first reported in Greenland from the Henson Gletscher Formation by Larsen (1989) and described subsequently by Stockfors & Peel (2005a). Borings in ooliths from the Henson Gletscher Formation that are coated by calcium phosphate, and phosphate infilled casts of the tunnels etched free in weak acetic acid were referred to the presumed cyanobacterium *Eohyella* Zhang & Golubic, 1987 (Fig. 1). Their description followed studies by Runnegar (1985) and Runnegar in Bengtson *et al.* (1990) of calcium phosphate infilled borings in the shells of early Cambrian molluscs from Australia, while Li (1997) recorded an assemblage of phosphatised euendolith casts of borings in fragments of the shells of several groups of invertebrates from the lower Cambrian of China.

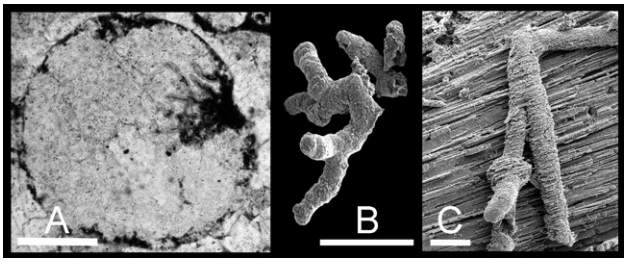

Fig. 1. Preservation of euendoliths in GGU sample 271718, Henson Gletscher Formation, Cambrian (Miaolingian Series, Wuliuan Stage), Løndal, North Greenland. A, *Fascichnus* isp. (*Eohyella* sp). penetrating oolith, MGUH 27656. B, *Fascichnus* isp., internal cast of boring, MGUH 27654. C, calcium phosphate infilled euendolith boring retaining the fine microstructure of the dissolved shell that is reflected in the coarse phosphatic replication of diagenetic aragonite needles now comprising the underlying internal mould. PMU 21439. Scale bars: 10 μm (C); 100 μm (A); 400 μm (B).

Calcium phosphate filled borings formed by euendoliths occur frequently in the calcareous shells of invertebrates from the middle Cambrian Henson Gletscher Formation (Miaolingian Series, Wuliuan Stage) of south-western Peary Land, North Greenland (Fig. 2), although they are uncommon in the helcionelloid molluscs that form the most conspicuous element of the fauna (Peel & Kouchinsky 2022). The mode of preservation is the same as described by Runnegar (1985) and Li (1987), with diagenetic calcium phosphate filling borings within calcareous shells. Routine treatment of limestone samples with weak acetic acid dissolves calcium carbonate, leaving phosphatised casts in the residues.

This paper focusses on the assemblage of euendoliths observed in sclerites of the eumetazoan *Chancelloria* Walcott, 1920 (Figs. 3–6), supplementing the material from the same sample (GGU sample 271718) described by Stockfors & Peel (2005a), but comparisons are made with specimens of the calcareous brachiopod *Nisusia* Walcott, 1905 (Fig. 7). Chancelloriids are a widely distributed problematic group of early–middle Cambrian fossils characterised by a bag-like integument studded with external aragonitic sclerites (Bengtson & Hou 2001; Bengtson 2005; Bengtson & Collins 2015; Randell *et al.* 2005; Yun *et al.* 2021). While their overall form is reminiscent of sponges, chancelloriid sclerites are hollow and formed by mineralisation from within (Bengtson 2005, 2015; Peel in press). Complete specimens of chancelloriids are uncommon, but their dissociated sclerites are widspread and often abundant (Bengtson *et al.* 1990: Moore *et al.* 2014, 2019; Kouchinsky *et al.* 2022) Most are stellate in form, with up to eleven lateral rays surrounding a central ray. However, each ray is a separate entity, without internal connection with neighbouring rays in the sclerite, but a basal foramen connects each ray with the soft tissues of the integument (Bengtson & Hou 2001; Bengtson 2015; Yun *et al.* 2021; Peel in press).

Material and methods

GGU sample 271818 was collected on 15th July 1978 from a thin-bedded, phosphatised, bioclastic, dolo-

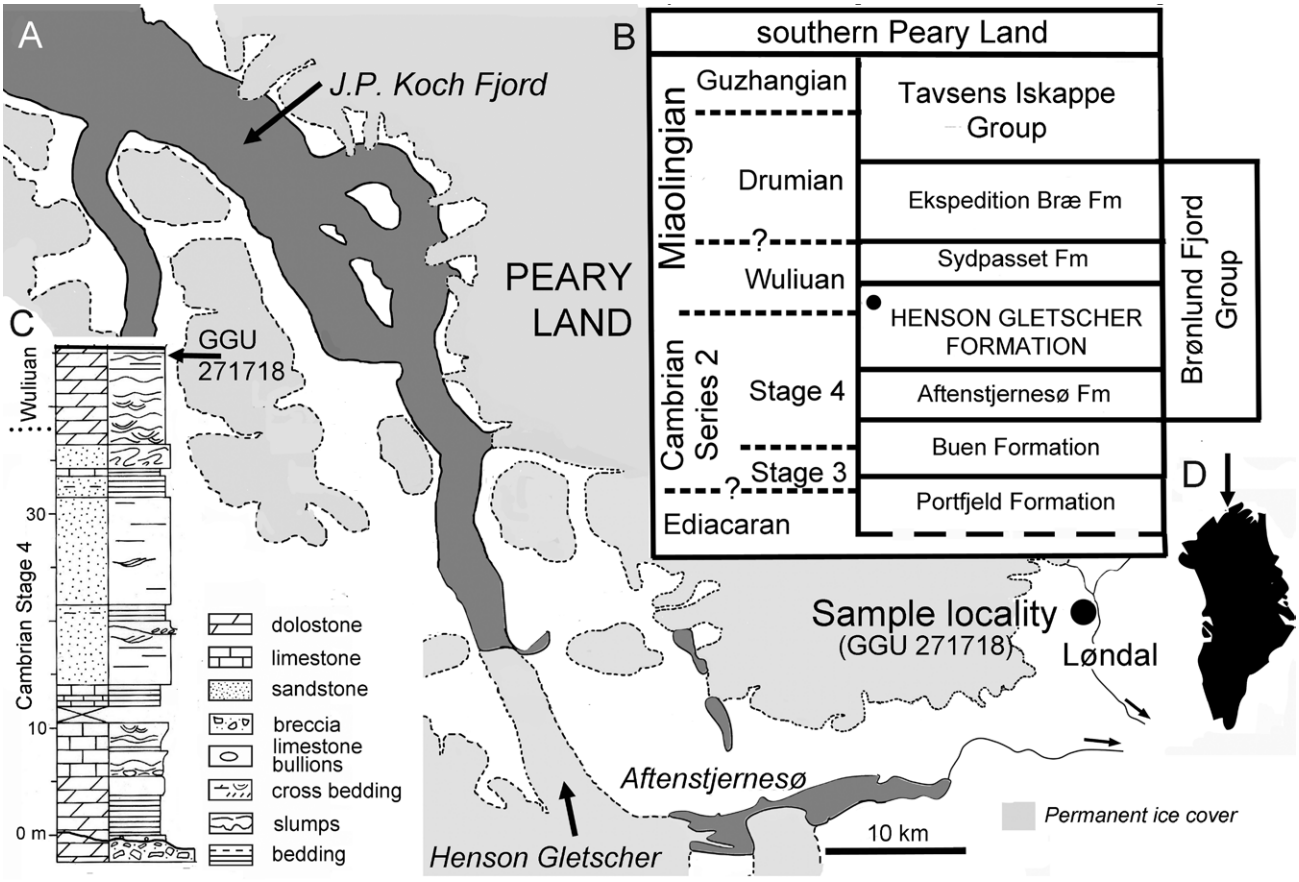

Fig. 2. Geography and geology. **A,** map of the western Peary Land area showing collection locality for GGU sample 271718. **B,** stratigraphic nomenclature in southern Peary Land with location of GGU sample 271718 (black dot). **C,** lithostratigraphic section through the Henson Gletscher Formation in Løndal. **D,** Greenland, arrow locates A.

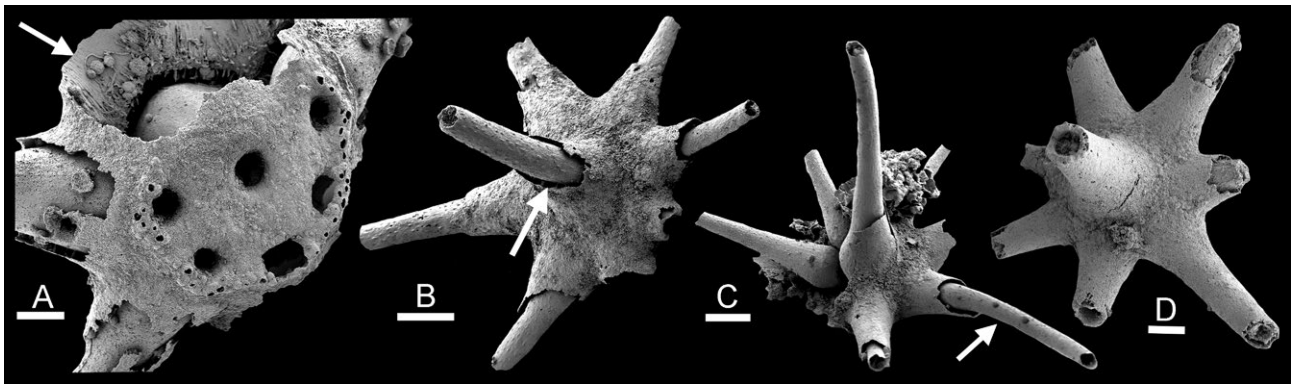

Fig. 3. Phosphatised sclerites of *Chancelloria* from GGU sample 271718, Henson Gletscher Formation, Cambrian (Miaolingian Series, Wuliuan Stage), Løndal, Peary Land. All specimens were treated with weak acetic acid, which dissolved the calcareous shell that is represented by the gap between the internal mould and the external encrustation. **A,** PMU 21440, basal view showing foramina, and the euendolith assemblage (arrow) preserved as internal casts of borings on the phosphatic encrustation of the upper surface of the sclerite. **B,** PMU 21441, upper surface of sclerite showing central ray; arrow locates details in Fig. 5E,G. **C,** PMU 21442, upper surface of sclerite; arrow locates lateral ray with coccoid euendoliths on the internal mould (see Fig. 5B,H). **D,** PMU 21443, upper surface of sclerite. Scale bars: 50 μm (A,D), 100 μm (B,C).

mitic limestone occurring about 1 m below the top of the Henson Gletscher Formation (Higgins *et al*. 1991; Ineson & Peel 1997; Peel 2023) on the west side of Løndal (82°18'N, 37°00'W; Fig. 2). The limestone contains numerous dark, thin, phosphatised layers, some of which formed hardgrounds. The clastic component includes re-deposited calcareous, phosphatised and silicified shells (Peel 2023, fig. 3), together with ooliths. These, and the accompanying bioclasts were frequently bored by euendoliths and covered by calcium phosphate prior to their final deposition.

The Henson Gletscher Formation of western Peary Land, North Greenland, is a highly fossiliferous unit of shelf carbonates and siliciclastic sediments that accumulated within a prograding complex referred to the Brønlund Fjord Group on the present day southern margin of the transarctic Franklin Basin (Higgins *et al*. 1991; Ineson & Peel 1997; Geyer & Peel 2011; Peel *et al*. 2016). The formation is 47 m thick in Løndal and composed mainly of dark, recessive, bituminous and cherty limestones, dolostones and mudstones, but pale fine-grained sandstones form a prominent middle member.

Fossil assemblages from GGU sample 271718 indicate a middle Cambrian age (Miaolingian Series, Wuliuan Stage), although the formation as a whole ranges from Cambrian Stage 4 to the Drumian Stage across North Greenland (Robison 1984, 1994; Higgins *et al*. 1991; Babcock 1994; Blaker & Peel 1997; Ineson & Peel 1997; Geyer & Peel 2011). The rich fauna from GGU sample 271718 and equivalent localities around the front of Henson Gletscher (Fig. 2) was documented by Clausen & Peel (2012), Peel (2021a,b, 2022a,b, 2023), Peel & Kouchinsky (2022, in press).

Methods. The carbonate rock sample was dissolved in acetic acid (10%) and wet sieved into fractions (125 μm and coarser) prior to sorting under a binocular microscope. Selected specimens were gold coated prior to scanning electron microscopy. Images were assembled in Adobe Photoshop CS4.

Preservation. Diagenetic phosphatisation is conspicuous in GGU sample 271718 (Peel 2023). In terms of euendoliths it may be studied in two settings. In thin sections, the diagenetic calcium phosphate is visible as a dark brown coating or the infilling of cavities or borings in calareous ooliths and bioclastic skeletal elements (Fig. 1A). Following dissolution of the calcium carbonate during treatment with weak acetic acid, the calcium phosphate infillings may be etched free (Fig. 1B) or stand in positive relief on phosphatised moulds of the shell interior or encrustations of the exterior (Fig. 1C). Many of the infillings display a fibrous stucture representing traces of the microstructure of the calcareous shells into which the microorganisms bored (Fig. 1C). Golubic *et al*. (1975) noted that this seemed to be mainly a character of Cyanobacteria whereas euendolithic fungi often produced smooth tunnels. Radtke & Golubic (2005) and Wisshak (2012) summarised the organisms producing euendolithic borings and their geological range. The affinity of the boring organisms is not known but cyanobacterians may produce ichnospecies within the ichnogenera noted here (Wisshak 2012).

The borings by euendoliths observed by Larsen (1989) and Stockfors & Peel (2005a) were referred to *Eohyella* Zhang & Golubic, 1987 (Green *et al*. 1988; Larsen 1989; Stockfors & Peel 2005a), which is closely

similar in morphology to the present day *Hyella* Bornet & Flahault, 1988. These authors followed biological nomenclature in describing forms characterised by radiating linear cell series (Radtke & Golubic 2005; Fig. 1A) and their casts (Fig. 1B). However the casts are better classified in ichnotaxonomy and referred to the ichnogenus *Fascichnus* Radtke & Golubic, 2005 since similar trace fossils can be produced by a variety of organisms.

Coccoid trace fossils

***Planobola* cf. *macrogota* Schmidt, 1992**

These spherical to slightly oval, coccoid, bodies are in direct contact with the calcium phosphate encrustation of the outer surface of the shell and range in diameter from 7–20 μm. They are common in a *Chancelloria* sclerite with seven radial rays and a central ray (Fig. 3A, 6J–L) and lie closely spaced on the under surface of the calcium phosphate encrustration of the upper surface of the sclerite but are rare on the internal mould. In a specimen of *Nisusia* they occur in abundance on the inner surface of a valve (Fig. 7D). Their surface is fibrous in larger specimens, occasionally granular, irregular, reflecting etching by the borer into the now dissolved aragonitic shell, with strongly aligned crystallites upto about 1 μm in width (Fig. 6L). The interface between the calcium phosphate encrustation (lower surface in Fig. 6J–L located by arrow in Fig. 3A) and the dissolved calcareous shell has the same orientation as the fibrous texture but is composed of much wider crystal laths. The spheres are also present in *Chancelloria* sp. as described by Peel & Kouchinsky (in press) from equivalent strata in the Henson Gletscher Formation on the western side of Henson Gletscher (Fig. 4I).

Infrequently, there appears to be direct connection of the spheres with meandering, occasionally branch-

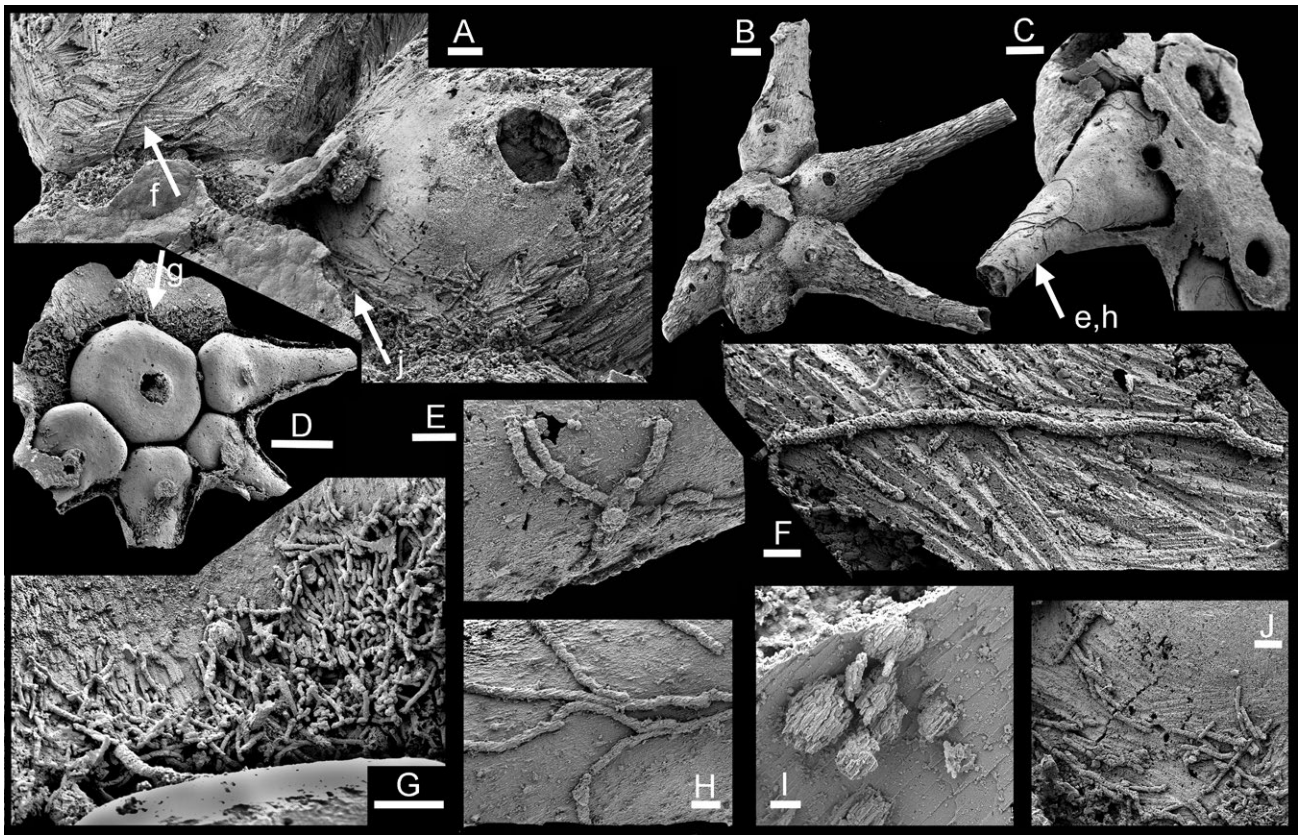

Fig. 4. Euendoliths in *Chancelloria* sclerites. Henson Gletscher Formation, Cambrian (Miaolingian Series, Wuliuan Stage), Løndal, Peary Land. All specimens are preserved as calcium phosphate internal moulds and external encrustations after dissolution of calcium carbonate in weak acetic acid. GGU sample 271718 unless stated. **A,B,F,J,** PMU 21444, basal view with foramina (B), enlarged in (A), to show replicated acicular microstructure of inner shell surface overlain on the internal mould by infilled borings of *Scolecia*, with detail in F and J (located by arrows f and j in A). **C,E,H,** PMU 21445, oblique basal view with internal mould of lateral ray; arrow locates details of *Scolecia* (E,H). **D,G,** PMU 21446, basal view of internal mould; arrow g locates detail of dense mass of *Scolecia* (G). **I,** PMU 21447, infillings of coccoid borings attached to external encrustation of sclerite wall; note microstructure of broad laths on wall. Henson Gletscher Formation at front of Henson Gletscher, after Peel & Kouchinsky (in press). Scale bars: 5 μm (F,H,I); 7 μm (E); 10 μm (J); 20μm (A,G); 50 μm (C); 100 μm (B,D).

ing traces (Figs. 6L, 7D) of both the narrow and wider forms of *Scolecia*. However, both the connected and solitary coccoids occur together (Figs. 5A, 7D).

These spherical microborings are compared to *Planobola macrogota* Schmidt, 1992, which has similar, near perfectly spherical coccoids, although these are typically much larger (Wisshak *et al.* 2008, fig. 5G,H). Illustrations by Wisshak *et al.* (2008) do not show the pronounced fibrous texture inherited from the surrounding substrate seen in most of the Greenland specimens.

A related coccoidal form with widely spaced hemispheres and a more granular texture occurs along the length of the cast of a lateral ray showing the fine fibres and protruberances characteristic of many chancelloriid internal moulds (Fig. 3C, 5B,H; see Yun *et al.* 2021; Peel & Kouchinsky in press, fig. 1). The proximal part of the same ray shows a sphere in contact with the cast but connected to the outer calcium phosphate layer by a broad stalk (Fig. 5G). It resembles *Cavernula coccidia* Glaub, 1994, as illustrated by Wisshak *et al.* (2008, fig. 6A,B)

Li (1997) referred similar spherical coccoids to *Graviglomus* Green, Knoll & Swett, 1988, originally described from ooliths from the Proterozoic Eleonore Bay Formation of North-East Greenland. Green *et al.* (1988, fig. 9.9) illustrated a series of laterally juxtaposed specimens with a U-shaped longitudinal profile in thin section, while recognising that single specimens also occurred. The Henson Gletscher specimens are more perfectly spherical (Figs. 4I, 6L, 7D), as are the specimens illustrated by Li (1997).

Scolecia Radtke, 1991

***Cunicularius* Green, Knoll & Swett, 1988**

Rarely branching borings of uniform width that occur as rounded ridges on internal moulds from the early Cambrian Maidiping Formation of Sichuan, China,

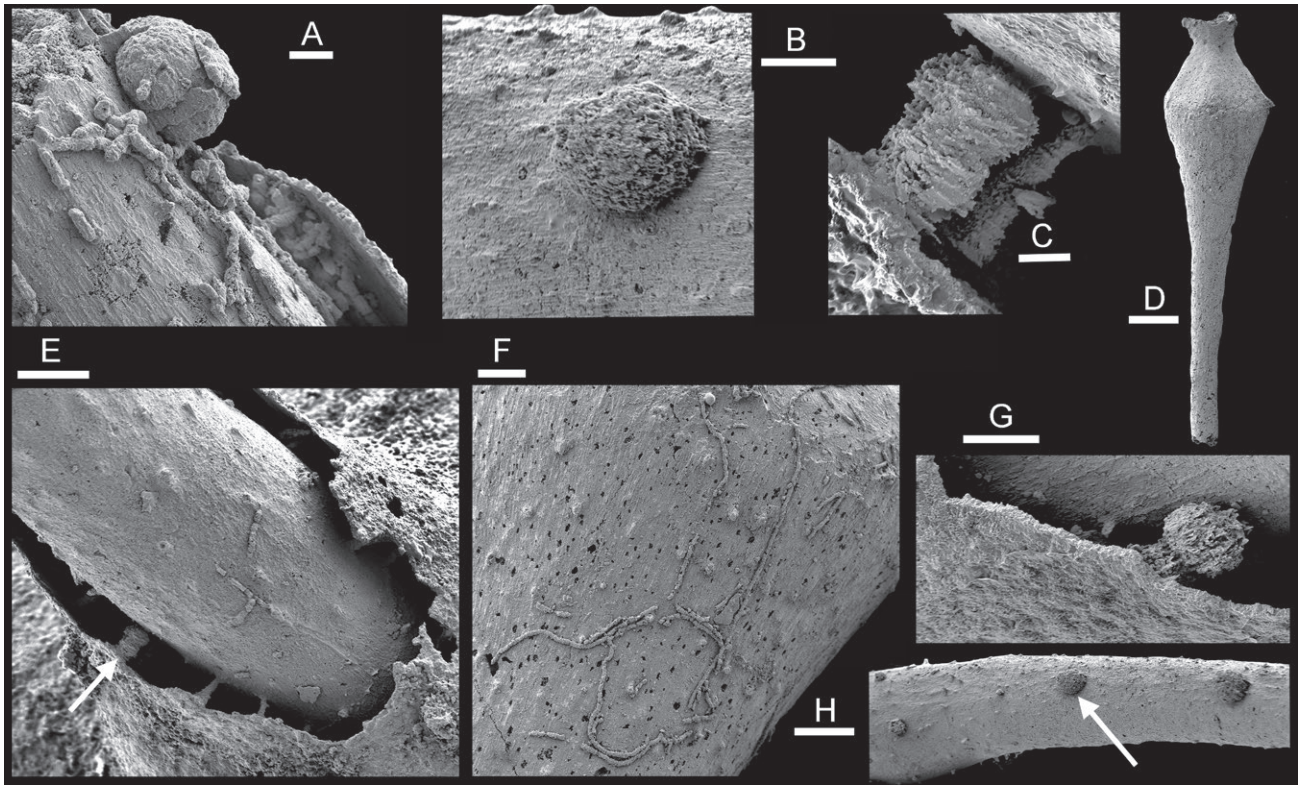

Fig. 5. Euendoliths in *Chancelloria* sclerites, GGU sample 271718. Henson Gletscher Formation, Cambrian (Miaolingian Series, Wuliuan Stage), Løndal, Peary Land. All specimens are preserved as calcium phosphate internal moulds and external encrustations after dissolution of calcium carbonate in weak acetic acid. **A,** PMU 21448, internal mould of cocoid boring and short segments of *Scolecia* on longitudinally striated lateral ray; note internal moulds perpendicular to internal mould surface indicating borings that penetrated the shell (now dissolved). **B,G,H,** PMU 21442, details from Fig. 3C with hemispherical coccoids and stalked coccoid (G). **C,E,** PMU 21441, upper surface of sclerite (Fig. 3B arrow) showing wide perpendicular boring penetrating into the shell (now dissolved) from the outer surface (lower left); note fibrous texture on internal mould reflecting shell microstructure . **D,F,** PMU 21449, internal mould of central ray oriented with base at top (D), with detail of *Scolecia* (F). Scale bars: 5 μm (A,B,C); 10 μm (G); 20 μm(E,F,H); 100 μm (D).

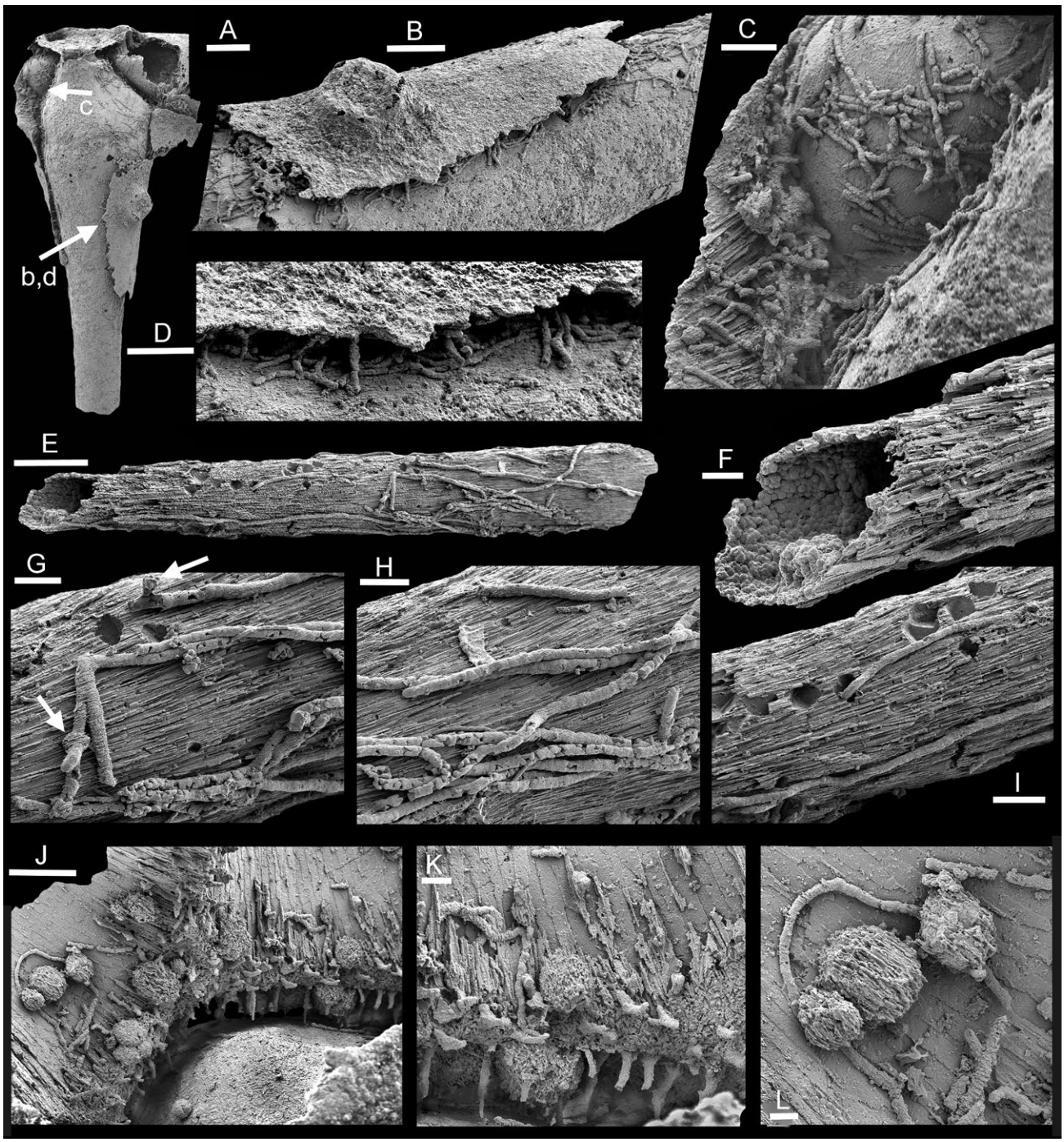

Fig. 6. Euendoliths in *Chancelloria* sclerites, GGU sample 271718. Henson Gletscher Formation, Cambrian (Miaolingian Series, Wuliuan Stage), Løndal, Peary Land. All specimens are preserved as calcium phosphate internal moulds and external encrustations after dissolution of calcium carbonate in weak acetic acid. **A–D,** PMU 21450, internal mould of central ray with patches of external encrustation (A) and with arrows b–d locating B–D; B,D, fragment of outer calcium phosphate encrustation with holdfast of unknown organism; densely packed vertical euendoliths (D) become horizontal and widely spaced along the ray (to left and right in B); C, densely packed, short sections of *Scolecia* on the internal mould and crossing acicular shell structure. **E–I,** PMU 21439, internal mould of lateral ray replicating acicular microstructure of ray interior with longitudinal burrow infillings of *Scolecia*. Note incomplete calcium phosphate deposition within burrows and perpendicular sections (arrows in G) and rare branching. Deep pits in internal mould surface reflect diagenetic crystal growth on inner side of ray prior to calcium phosphate deposition. **J–L,** PMU 21440, details of Fig. 3A, with coccoids and *Scolecia* infilled borings on encrustation of upper surface of sclerite. Note impression of parallel microstructure laths and borings penetrating the shell (now a void) but generally not passing through to the internal mould surface (J). Scale bars: 5 μm (K,L); 20 μm (C,D,F,G,H); 30 μm (I,J);50 μm (B); 100 μm (A,E).

were assigned by Li (1997) to *Cunicularius* Green, Knoll & Swett, (1988), although Moore *et al.* (2019) suggested that they should be placed in the trace fossil *Scolecia* Radtke, 1991.

Tangled masses of short casts about 2–3 μm wide occur mainly on the surface of the internal mould but near vertical borings penetrated through the shell towards the outer surface (Figs. 4G,J, 6A–D,J,K). They tend to form dense groups in local patches, often near the suture between adjacent rays (Fig. 4G), but become more openly spaced and continuous in their length as they pass distally along the rays (Fig. 4A,E,H, and the left and right margins in Fig. 6B), and in *Nisusia* (Fig. 7A,D). Branching is rare, although threads with rounded ends may terminate next to other threads (Fig. 4H). *Cunicularius halleri* Green, Knoll & Swett, 1988 of Li (1997) has filaments of similar diameter. *Cunicularius idiametrus* Li, 1997 also occurs in dense masses, but has wider threads.

***Endoconchia* Runnegar in Bengtson *et al.*, 1990**

As with *Cunicularius*, Moore *et al.* (2019) considered it appropriate to refer *Endoconchia* to the ichnotaxon *Scolecia*.

This second group of threads, preserved on the slender, recrystallised internal mould of a chancelloriid ray (Fig. 6E–I) and in the brachiopod *Nisusia* (Fig. 7B,D) has widely spaced, straight or slightly curved cord-like threads that are about 6 μm in diameter (Fig. 6E–I, 7D) with rounded terminations. As with *Cunicularius*, dense patches of threads occur locally (Fig. 7A). Branching is rare (Fig. 1C). The threads often have a slight beaded form and the boring may not be completely filled with calcium phosphate, creating a pelletoidal effect (Fig. 6H). The surface of the threads is finely ribbed parallel to the much coarser acicular recrystallisation of the underlying internal mould (Figs. 1C, 6G). Rare conical bodies penetrate into the

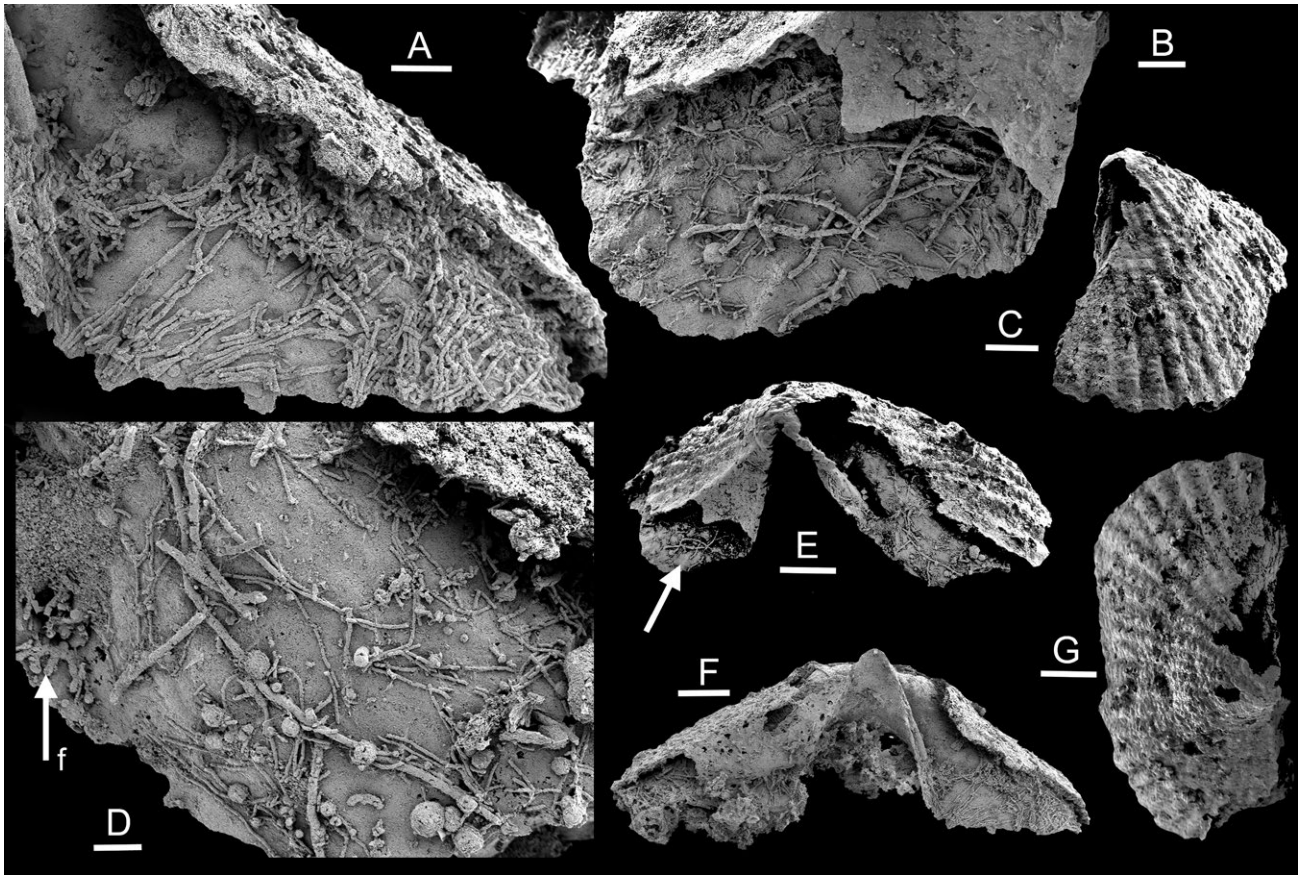

Fig. 7. Incompletely phosphatised valves of the calcareous rhynchonelliformean brachiopod *Nisusia* after decalcification in weak acetic acid, with euendolith assemblages preserved on the calcium phosphate encrustation of the valve interior. GGU sample 271718, Henson Gletscher Formation, Cambrian (Miaolingian Series, Wuliuan Stage), Løndal, Peary Land. **A,F,** PMU 21451 showing entangled mass of *Scolecia* passing vertically through the shell and becoming more linear and widely spaced. **B–E,G,** PMU 39665, showing exterior ribbing (C,G) with inner surface of calcium phosphate encrustation of inner surface (B,D) showing both the narrow and a wide forms of *Scolecia* threads, coccoids (some of which appear to be associated with the threads) and *Fascichnus* (arrow f in D). Scale bars: 30 μm (B–D); 50 μm (A); 200 μm (F); 300 μm (E).

shell (now a void above the internal mould) perpendicular to the threads (arrows in Fig. 6G). Coccoids appear to be associated with the threads in some cases (Fig. 7D) although most are not. Deep, smooth, pits on the *Chancelloria* internal mould represent diagenetic crystal growth on the shell interior prior to formation of the now phosphatised internal mould (Fig. 6I).

Runnegar in Bengtson *et al.* (1990) proposed *Endoconchia* to include two unbranching species from the lower Cambrian of South Australia that are similar to the Henson Gletscher Formation specimens, but one narrower (diameter 3 μm) and one wider (diameter 10 μm). Runnegar (1985, fig. 1E) noted spheroidal and terminal swellings in the narrow species (*Endoconchia angusta* Runnegar in Bengtson *et al.*, 1990) not seen in the Greenland material. Li (1997, pl. 3) described threads with similar swellings from China and speculated that *Endoconchia angusta* might be a synonym of *Cunicularius*. However, it is frequently branched and shows a much less tortuous thread pattern than the original definition of Green *et al.* (1988).

Fascichnus Radtke & Golubic, 2005

Radtke & Golubic (2005) referred borings made by *Hyella*, and by implication also *Eohyella*, to the ichnogenus *Fascichnus*. The calcium phosphate filled borings with radiating branches described in ooliths as *Eohyella* sp. (= *Fascichnus* isp.) by Stockfors & Peel (2005a; Fig. 1A) have not been observed in available chancelloriids from GGU sample 271718, but a single specimen is preserved on the encrustration of the interior surface of a valve of the brachiopod *Nisusia* (Fig. 7D, arrow f). The short branches have a slightly beaded form and are about 6 μm in diameter, which is less than most of the internal moulds described by Stockfors & Peel (2005a; Fig. 3B). A similar specimen was illustrated by Li (1997) from China.

Discussion

There is significant discussion in the literature concerning the occurrence of euendolith microborings and ambient inclusion trails resulting from mineral migration in Cambrian sediments (summary with full references by Yang *et al.* 2017). It is evident that both occur, and that they are often confused. Thus, descriptions of ridged open galleries in late middle Cambrian organophosphatic brachiopods from the Holm Dal Formation by Stockfors & Peel (2005b) are now known to be ambient inclusion trails and not euendolith borings, as originally described, although euendoliths do occur in the same samples. Ambient inclusion trails have not been recognised in the currently described calcareous chancelloriid sclerites and valves of the brachiopod *Nisusia*, but they are present in organophosphatic fossils from the same sample.

Moore *et al.* (2019) noted that calcium phosphate internal moulds of chancelloriid rays from the lower–middle Cambrian boundary region (Delamaran regional stage) of Nevada often preserved rounded threads (diameter 2–6 μm) that they interpreted as the casts of endolithic microborings. They also illustrated a coccoid sphere arising from such a thread (Moore *et al.* 2019, fig. 17L). As in the Greenland material, the unbranching threads are often oriented parallel to the long axes of the chancelloriid rays.

The assemblage of phosphatised euendolith borings described by Li (1997) from the early Cambrian Maidiping Formation of Sichuan, China, includes several taxa proposed by Green *et al.* (1988) from the Proterozoic Eleonore Bay Group of North-East Greenland. The Sichuan assemblage is closely similar in its composition to the middle Cambrian (Miaolingian Series, Wuliuan Stage) assemblage described here from the Henson Gletscher Formation, although the compact multi-sphered *Parenchymodiscus* Green, Knoll & Swett, 1988 described by Li (1997) has not been observed in the Henson Gletscher Formation.

Acknowledgements

The sample was collected during the North Greenland Project (1978–80) of the Geological Survey of Greenland with the assistance of Peter Fryman (Copenhagen). J.R. Ineson (Copenhagen) provided the lithostratigraphic section. Michael Streng (Uppsala) is thanked for guidance with SEM and Artem Kouchinsky (Stockholm) for advice concerning *Chancelloria* microstructure. Comments by Li Guoxiang (Nanjing) and the editor are gratefully acknowledged.

References

Babcock, L.E. 1994: Systematics and phylogenetics of polymeroid trilobites from the Henson Gletscher and Kap Stanton Formations (Middle Cambrian), North Greenland. Bulletin Grønlands Geologiske Undersøgelse 169, 79–127. http://dx.doi.org/10.34194/bullggu.v169.6727

Bengtson, S. 2005: Mineralized skeletons and early animal evolution, 101–124. In: Briggs, D.E.G (ed): Evolving form and function: fossils and development: proceedings of a symposium honoring Adolf Seilacher for his contributions

to paleontology, in celebration of his 80th birthday. Peabody Museum of Natural History, New Haven. http://dx.doi.org/10.1017/s0016756806293051

Bengtson, S. & Collins, D. 2015: Chancelloriids of the Cambrian Burgess Shale: Palaeontologia Electronica 18.1.6A, 1–67. http://dx.doi.org/10.26879/498

Bengtson, S. & Hou, K. 2001: The integument of Cambrian chancelloriids. Acta Palaeontologica Polonica 46, 1–22.

Bengtson, S. & Missarzhevsky, V.V. 1981: Coeloscleritophora — a major group of enigmatic Cambrian metazoans, 19–21. In: Taylor, M.E. (ed.): Short papers from the Second International Symposium on the Cambrian System. US Geological Survey Open-File Report, 81-743, Denver. http://dx.doi.org/10.3133/ofr81743

Bengtson, S., Conway Morris, S., Cooper, B.J.,Jell, P.A. & Runnegar, B.N. 1990: Early Cambrian fossils from South Australia. Memoirs of the Association of Australasian Palaeontologists 9, 1–368.

Bengtson, S., Rasmussen, B., Ivarsson, M, Muhling, J., Broman, C., Marone, F., Stampanoni, M. & Bekker, A. 2017: Fungus-like mycelial fossils in 2.4-billion-year-old vesicular basalt. Nature Ecology & Evolution 1, 041, https://doi.org/10.1038/s41559-017-0141

Blaker, M.R. & Peel, J.S. 1997: Lower Cambrian trilobites from North Greenland. Meddelelser om Grønland, Geoscience 35, 1–145. https://doi.org/10.1017/s0016756898258432

Bornet, É. & Flahault, C. 1888: Note sur deux nouveaux genres d'algues perforantes. Journal de Botanique 2, 161–165.

Campbell, S.E. 1982: Precambrian endoliths discovered. Nature 299, 429–431. http://dx.doi.org/10.1038/299429a0

Clausen, S. & Peel, J.S. 2012: Middle Cambrian echinoderm remains from the Henson Gletcher Formation of North Greenland. GFF 134, 173–200. https://doi.org/10.1080/11035897.2012.721003

Geyer, G. & Peel, J.S. 2011: The Henson Gletscher Formation, North Greenland, and its bearing on the global Cambrian Series 2–Series 3 boundary. Bulletin of Geosciences 86, 465–534. https://doi.org/10.3140/bull.geosci.1252

Golubic, S., Friedmann, I. & Schneider, J., 1981, The lithobiontic ecological niche, with special reference to microorganisms: Journal of Sedimentary Petrology 51, 475–478. http://dx.doi.org/10.1306/212f7cb6-2b24-11d7-8648000102c1865d

Golubic, S., Perkins, R.D. & Lukas, K.J. 1975: Boring microorganisms and microborings in carbonate substrates, 229–259. In: Frey, R.W. (ed.), The study of trace fossils. Springer-Verlag. Berlin–Heidelberg–New York. http://dx.doi.org/10.1007/978-3-642-65923-2_12

Green, J.W., Knoll, A.H. & Swett, K. 1988: Microfossils from oolites and pisolites of the Upper Proterozoic Eleonore Bay Group, Central East Greenland. Journal of Paleontology 62, 835–852. http://dx.doi.org/10.1017/s0022336000030109

Higgins, A.K., Ineson, J.R., Peel, J.S., Surlyk, F. & Sønderholm, M. 1991: Lower Palaeozoic Franklinian Basin of North Greenland. Bulletin Grønlands Geologiske Undersøgelse 160, 71–139. https://doi.org/10.34194/bullggu.v160.6714

Ineson, J.R. & Peel, J.S. 1997: Cambrian shelf stratigraphy of North Greenland. Geology of Greenland Survey Bulletin 173, 1–120. https://doi.org/10.34194/ggub.v173.5024

Kouchinsky, A., Alexander, R., Bengtson, S., Bowyer, F., Clausen, S., Holmer, L.E., Kolesnikov, K.A., Korovnikov, I.V., Pavlov, V., Skovsted, C.B., Ushatinskaya, G., Wood, R. & Zhuravlev, A.Y. 2022: Early–middle Cambrian stratigraphy and faunas from northern Siberia. Acta Palaeontologica Polonica 67, 341–464. http://dx.doi.org/10.4202/app.00930.2021

Larsen, N.H. 1989: Algae from the Lower Palaeozoic Strata of North Greenland. Geological Survey of Greenland Open File Series 89/3, 23 pp.

Li, G. 1997: Early Cambrian phosphate-replicated endolithic algae from Emei, Sichuan. south-west China. Bulletin of National Museum of Natural History 10, 193–216.

MacIntyre, I.G., Reid, R.P. 1978: Micritization. In: Middleton, G.V., Church, M.J., Coniglio, M., Hardie, L.A., & Longstaffe, F.J. (eds): Encyclopedia of Sediments and Sedimentary Rocks. Encyclopedia of Earth Sciences Series. Springer, Dordrecht. https://doi.org/10.1007/978-1-4020-3609-5_136

Moore, J.L., G. Li & Porter, S.M. 2014: Chancelloriid sclerites from the Lower Cambrian (Meishucunian) of eastern Yunnan, China, and the early history of the group. *Palaeontology* 57, 833–878. https://doi.org/10.1111/pala.12090

Moore, J.L., Porter, S.M. Webster, M. & Maloof, A.C. 2019: Chancelloriid sclerites from the Dyeran–Delamaran ('lower–middle' Cambrian) boundary interval of the Pioche–Caliente region, Nevada, USA. Papers in Palaeontology 7, 565–623. https://doi.org/:10.1002/spp2.1274

Peel, J.S. 2021a: Ontogeny, morphology and pedicle attachment of stenothecoids from the middle Cambrian of North Greenland (Laurentia). Bulletin of Geosciences 96, 381–399. https://doi.org/10.3140/bull.geosci.1839

Peel, J.S. 2021b**:** In-place operculum demonstrates that the middle Cambrian *Protowenella* is a hyolith and not a mollusc. Alcheringa 45, 385–394. http://dx.doi.org/10.1080/03115518.2021.2004225

Peel, J.S. 2022a: A priapulid larva from the middle Cambrian (Wuliuan Stage) of North Greenland (Laurentia). Bulletin of Geosciences 97, 445–452. https://doi.org//10.3140/bull.geosci.1865

Peel, J.S. 2022b: The oldest tongue worm: a stem-group pentastomid arthropod from the middle Cambrian (Wuliuan Stage) of North Greenland (Laurentia). GFF 144, 97–105. https://doi.org//10.1080/11035897.2022.2064543

Peel, J.S. 2023: A phosphatised fossil Lagerstätte from the middle Cambrian (Wuliuan Stage) of North Greenland (Laurentia). Bulletin of the Geological Society of Denmark 72, 101–122. https://doi.org/10.37570/bgsd-2022-72-03

Peel, J.S. in press: Sclerite ray canals in the Cambrian coeloscleritophoran *Chancelloria* from North Greenland (Laurentia). PalZ.

Peel, J.S. & Kouchinsky, A. 2022: Middle Cambrian (Miaolingian Series, Wuliuan Stage) molluscs and mollusc-like microfossils from North Greenland (Laurentia). Bulletin of

the Geological Society of Denmark 70, 69–104. https://doi.org/10.37570/bgsd-2022-70-06

Peel, J.S. & Kouchinsky, A. in press: Unusual diagenesis of Cambrian chancelloriids from Greenland and Siberia. Alcheringa

Peel, J.S., Streng, M., Geyer, G., Kouchinsky, A. & Skovsted, C.B. 2016: *Ovatoryctocara granulata* assemblage (Cambrian Series 2–Series 3 boundary) of Løndal, North Greenland. Australasian Palaeontological Memoirs 49, 241–282.

Radtke, G. 1991: Die mikroendolithischen Spurenfossilien im Alt-Tertiär West-Europas und ihre palökologische Bedeutung. Courier Forschungsinstítut Senckenberg 138, 1–185.

Radtke, G., & Golubic, S. 2005: Microborings in mollusk shells, Bay of Safaga, Egypt: Morphometry and ichnology. Facies 51,125–141. http://dx.doi.org/10.1007/s10347-005-0016-02

Randell, R.D., Lieberman, B.S., Hasiotis, T. & Pope, M.C. 2005: New chancelloriids from the Early Cambrian Sekwi Formation with a comment on chancelloriid affinities. Journal of Paleontology 79, 987–996. http://dx.doi.org/10.1666/0022-3360(2005)079[0987:ncftec]2.0.co;2

Runnegar, B. 1985: Early Cambrian endolithic algae. Alcheringa 9, 179–182. http://dx.doi.org/10.1080/03115518508618966

Schmidt, H. 1992: Mikrobohrspuren ausgewählter Faziesbereiche der tethyalen und germanischen Trias (Beschreibung, Vergleich und bathymetrische Interpretation). Frankfurter Geowissenschaften Arbeiten A 12, 1–228.

Stockfors, M. & Peel, J.S. 2005a: Endolithic Cyanobacteria from the Middle Cambrian of North Greenland. GFF 127, 179–185. http://dx.doi.org/10.1080/11035890501273179

Stockfors, M. & Peel, J.S. 2005b: Euendoliths and cryptoendoliths within late Middle Cambrian brachiopod shells from North Greenland. GFF 127, 187–194. http://dx.doi.org/10.1080/11035890501273187

Walcott, C.D. 1905: Cambrian Brachiopoda with descriptions of new genera and species. Proceedings of the United States National Museum 28, 227–337. http://dx.doi.org/10.5479/si.00963801.1395.227

Walcott, C.D. 1920: Cambrian geology and paleontology IV. 6. Middle Cambrian Spongiae. Smithsonian Miscellaneous Collections 67, 261–364.

Wisshak M. 2012. Microbioerosion, 213–243, In: Knaust D. & Bromley R.G. (eds) Trace Fossils as Indicators of Sedimentary Environments. Elsevier, Amsterdam. https://doi.org/10.1016/B978-0-444-53813-0.00008-3

Wisshak, M., Seuss, B. & Nützel, A. 2008: Evolutionary implications of an exceptionally preserved Carboniferous microboring assemblage in the Buckhorn Asphalt lagerstätte (Oklahoma, USA), 21–54, In: Wisshak, M., Tapanila, L. (eds) Current Developments in Bioerosion. Springer Berlin–Heibedlberg–New York. https://doi.org/10.1007/978-3-540-77598-0_2

Yang, X.-G., Han, J., Wang, X., Schiffbauer, J. D., Uesugi , K., Sasaki , O. &% Komiya, T. 2017: Euendoliths versus ambient inclusion trails from early Cambrian Kuanchuanpu Formation, South China. Palaeogeography, Palaeoclimatology, Palaeoecology 476, 147–157. http://dx.doi.org/10.1016/j.palaeo.2017.03.028

Yun, H., Zhang, X., Brock, G.A., Li, L. & Li, G. 2021: Biomineralization of the Cambrian chancelloriids. Geology 49, 623–628. https://doi.org/10.1130/G48428.1

Zhang, Y. & Golubic, S., 1987: Endolithic microfossils (Cyanophyta) from early Proterozoic stromatolites, Hebei, China. Acta Micropalaeontologica Sinica 4, 1–12.

Neotectonic deformations of the lakebeds in Esrum Sø, eastern Denmark, interpreted to indicate a Postglacial pull-apart basin

LARS OLE BOLDREEL & STIG ASBJØRN SCHACK PEDERSEN

Geological Society of Denmark
https://2dgf.dk

Received 21 November 2023
Accepted in revised form
19 April 2024
Published online
18 June 2024

Boldreel, L.O. & Pedersen, S.A.S. 2024. Neotectonic deformations of the lakebeds in Esrum Sø, eastern Denmark, interpreted to indicate a Postglacial pull-apart basin. Bulletin of the Geological Society of Denmark, Vol. 73, pp. 67–88. ISSN 2245-7070. https://doi.org/10.37570/bgsd-2024-73-04

Esrum Sø, with a marked elongation trending N–S, located in the glaciomorphological landscape of north-eastern Sjælland, is one of the biggest lakes in Denmark. The lake is shaped as a large 'sink' with steep sides and a maximum depth of c. 22 m. The present investigation and mapping of the structures of the lakebeds is based on the interpretation of 10 reflectors on 82 acquired high-resolution seismic sections (Chirp III) and correlation to the 8.5 m long Esrum Sø drill core in the northern part of Esrum Sø.

A new formation, the Esrum Formation, with two members, the Fredensborg and Nødebo Members, is erected based on the geological information obtained from the drill core, and traced on the seismic sections over the major part of Esrum Sø. In the northern part of the lake, the seismic sections reveal a number of anti- and synform structures, which we group into five architectural features. The mapping of these structures show N–S trending vertical fractures, fault scarps and fold crests, which in places are bent towards a NW direction. In some, mainly southern, parts of the lake, gas stored in the gyttja (Nødebo Member) and close to the lake floor degrades the seismic signal significantly. The gas is ascribed to seepage and production close to the lake floor. The integration of the seismic interpretation and the Esrum Sø drill core data shows that the Young Baltic till constitutes the base of the depression where Esrum Sø is located. In Bølling to Preboreal time the Esrum Sø was a shallow freshwater lake with no tectonic activity (Fredensborg Member), and the major deformation and subsidence of the lake basin took place in Boreal to Atlantic time (Nødebo Member). Our interpretation favours a model of a Postglacial pull-apart basin related to extension in the wrench-fault tectonic zone aligned with the Sorgenfrei–Tornquist Zone.

Keywords: High-resolution shallow seismic data, wrench-fault tectonics, extensional fractures, calcareous gyttja, shallow gas, Esrum Sø Formation.

Lars Ole Boldreel [lob@ign.ku.dk], Department of Geosciences and Natural Resource Management, Geology Section, University of Copenhagen, Øster Voldgade 10, DK-1350 Copenhagen K, Denmark. Stig A. Schack Pedersen [sasp@geus.dk], Geological Survey of Denmark and Greenland, Øster Voldgade 10, DK-1350 Copenhagen K, Denmark.

In recent years there has been a discussion of neotectonics in Denmark and whether these activities are related to tectonic movements at major fault systems, or if they are related to deglaciation rebound which has triggered reactivation of deep-seated fault systems (e.g. Sandersen & Jørgensen 2015, 2022; Kammann *et al.* 2016; Jensen *et al.* 2017; Brandes *et al.* 2018, 2022; Sandersen *et al.* 2021; Juhlin *et al.* 2022). Most of these studies relate the activities to the Sorgenfrei–Tornquist Zone (STZ, Fig. 1a). These studies are thus concerned with one of the central questions of relevance to the geology of eastern and northern Denmark: "How much influence does the tectonic activity along the Sorgenfrei–Tornquist Zone have on the geomorphology and the Quaternary geological features?". One of the prominent faults crossing the north-eastern part of Sjælland is the Carlsberg Fault (Fig. 1a; e.g. Kammann *et al.* 2016). Satellite radar scanning indicates a recent

displacement causing terrain subsidence in the eastern part of Copenhagen and further to the north in northern Sjælland (Fig. 1a; Jakobsen *et al.* 2013). Kammann *et al.* (2016) investigated the Carlsberg Fault zone (CFZ) onshore Sjælland south of Copenhagen using very high resolution shear (S) wave seismic data to image the upper 30 m of the western part of the CFZ and found that tectonic activity had taken place. They also tentatively suggested that the CFZ continues to the western bank of Furesø (the deepest lake in Denmark) located some 17 km south of Esrum Sø. An overview of Lateglacial and Postglacial faulting in Denmark is given by Sandersen *et al.* (2021) where it is claimed that the CFZ continues south of Copenhagen where it penetrates all the way from the Mesozoic strata at depth to the sea floor (Al Hseinat & Hübscher 2017).

Further to the east in the area of the Bornholm Basin located to the north of Bornholm and east of south Sweden (Fig. 1a), neotectonic activity related to the STZ was suggested by Jensen *et al.* (2017). In the northern part of Jylland (Fig. 1a), neotectonic activity along the north-western segment of the STZ has been documented by Brandes *et al.* (2018) in the area of the Børglum Fault (BF part of the STZ, Fig. 1a) where strike-slip tectonic activity occurred 14 ka to 12 ka ago, with an onset of tectonic activity at 14.5 ka. In Brandes *et al.* (2022) two shear wave seismic sections were acquired and interpreted from the area of northern Jylland; they show that near-surface tectonic activity occurred close to the end of marine isotope stage 6 (MIS 6, 191 ka). They also point out that the northern part of the STZ in their study area

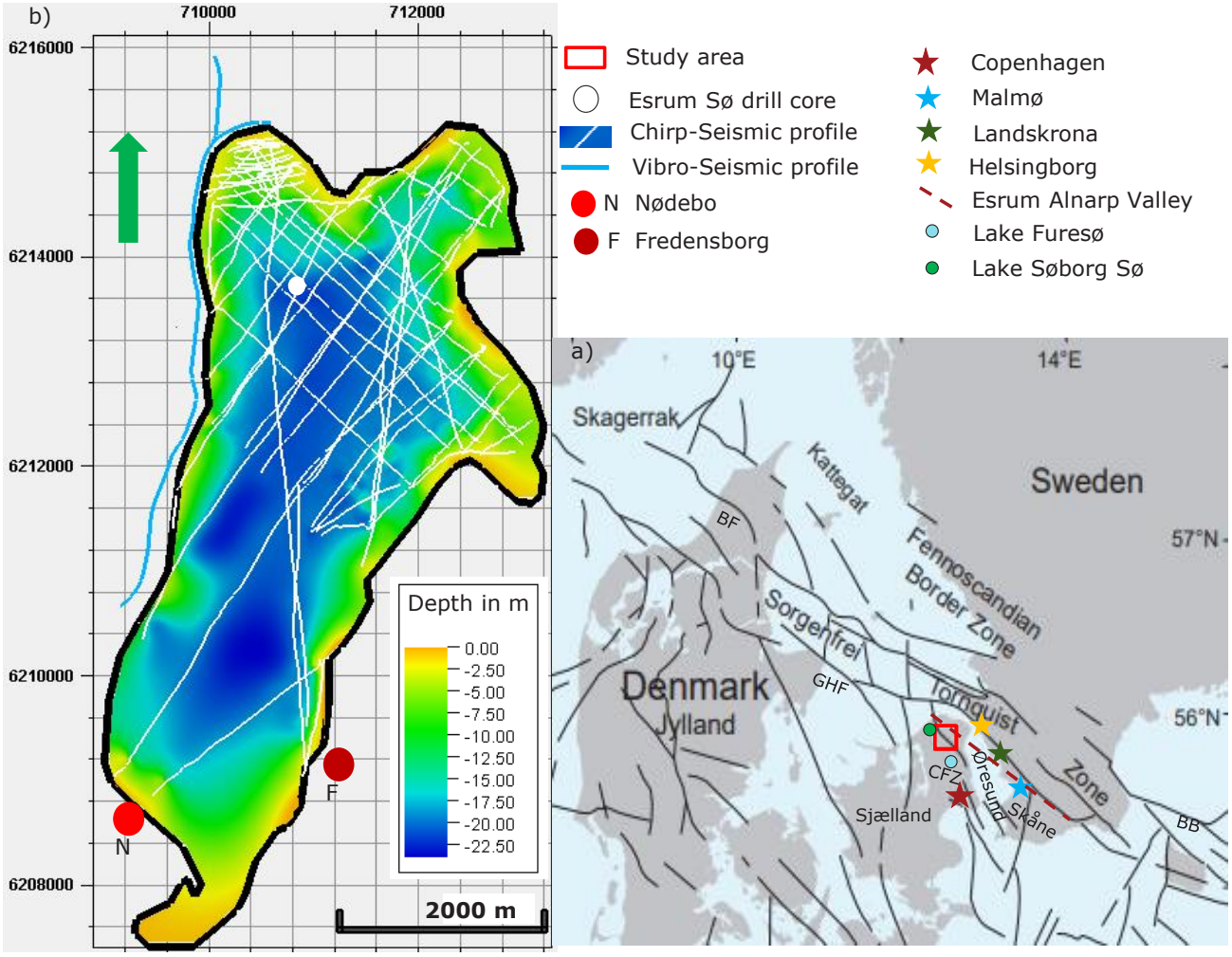

Fig. 1. A: Structural map of Denmark with the location of some of the major faults including the Børglum fault (BF), the Carlsberg Fault (CFZ), the Grenå–Helsingborg Fault Zone (GHF) and the Sorgenfrei–Tornquist Zone (STZ); BB indicates the location of the Bornholm Basin. The red square shows the location of the study area of Esrum Sø. Map modified from Erlström *et al.* (2018). **B**: Map of Esrum Sø showing the depth to the lakebed in metres as interpreted from the seismic sections. White lines show the location of the seismic sections acquired in 2013–2015 and 2022; the white dot shows the location of the Esrum Sø borehole, and the red dots show the location of the two towns Nødebo and Fredensborg. The thick blue line shows the location of the vibro-seismic section along the lake shore from Winsløw *et al.* (2020). The coordinates are shown with reference to UTM zone 32N.

is likely to be a complex fault system with a strike-slip component. Sandersen & Jørgensen (2015) found in their study that a depression in the outwash plain in the southern part of Jylland was related to Holocene strike-slip movements and was not a dead-ice hole, which was the previous interpretation.

Another prominent fault zone is the Grenå–Helsingborg Fault (GHF in Fig. 1a; Kamla *et al.* 2014), which stretches from the eastern part of Jylland to north of Sjælland to Helsingborg in Sweden, and is probably the most regular fault to outline the Sorgenfrei–Tornquist Zone in the north-east Sjælland–Øresund region (Fig. 1a; Håkansson & Pedersen 1992; Winsløw *et al.* 2020). In the subsurface below the Cretaceous chalk, Erlström *et al.* (2018) mapped a number of additional faults, which are notably aligned in an en échelon configuration, but with the same strike paralleling the STZ trend SSE–NNW (Fig. 1a).

Between the Carlsberg Fault and the Grenå–Helsingborg Fault the buried Esrum–Alnarp Valley is located, and this palaeo-valley is interpreted to be the result of geotectonic activity in the Neogene (Sorgenfrei 1945; Schuldt 1981; Konradi 1992). The trend of the valley is controlled by fault structures, which are regarded as being related to the south-western branch of the Sorgenfrei-Tornquist Zone (Håkansson & Pedersen 1992; Winsløw *et al.* 2020). The Esrum–Alnarp Valley extends from the Kattegat sea across the north-eastern corner of Sjælland, below the Øresund strait to Skåne, where it continues in the subsurface of southern Sweden between Landskrona and Malmø (Adrielsson 1984).

Esrum Sø is located in northern Sjælland (Fig. 1a and b) and has the largest volume of water among the lakes in Denmark. The lake is elongated N–S and has an area of 17.3 km^2 with a maximum depth of 22.3 m (Danish Nature Agency 2022). The formation of Esrum Sø has for many years been a subject of discussion, and various models have been suggested for the relatively deep lake located along the nearly 100 m high glaciomorphological landscape of Gribskov. These include speculations of a dead-ice hole (Whiteside 1970), a glaciotectonic hole in a hill-and-hole pair (Gravesen *et al.* 2017), tunnel valley formation and Lateglacial drainage erosion (Winsløv *et al.* 2020), but no seismic data from the lake itself have been published to support the various models.

The position of the lake in a central part of a wrench fault zone (Winsløv *et al.* 2020), the water depth of the lake and its elongated shape with steep sides provoked the question: could it be a neo-tectonic pull-apart basin? Could the lake be related to neotectonic activity in the Sorgenfrei–Tornquist Zone? This question is addressed in this paper. For the first time detailed, shallow high-resolution seismic mapping of the lakebed and *c.* 30 m below it has been carried out. A map of the tectonic features is presented here together with a detailed interpretation of the seismic unit stratigraphy correlated to the drill core in the lakebed.

Geological setting

Bedrock geology and structure

The bedrock geology and the Quaternary geology is summarised in a geological model that shows the evolution (Fig. 2). The bedrock geology below the Quaternary successions in north-eastern Sjælland comprises

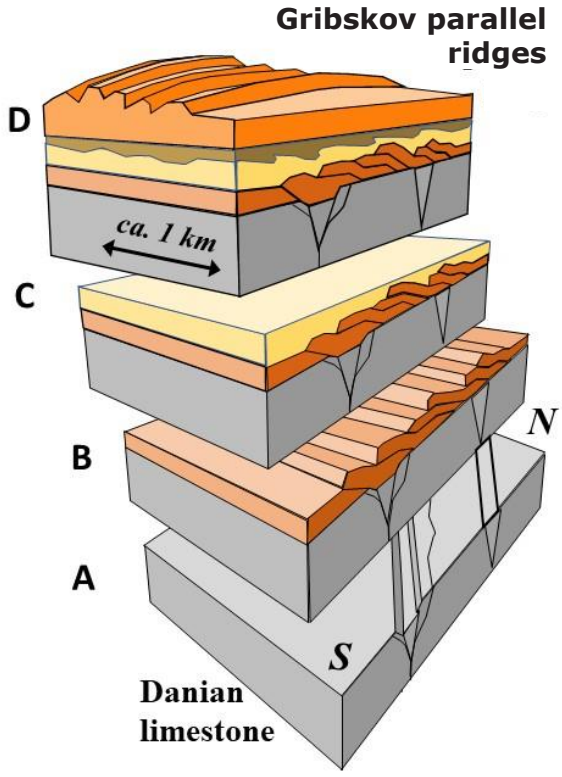

Fig. 2. Model of the geological setting in the Esrum Sø–Gribskov area, interpreted from seismic sections along the western shore of Esrum Sø (Winsløw *et al.* 2020). **A**: Danian limestone including Selandian marl and clay in a negative flower depression related to wrench faulting *c.* 70–60 Ma BP (grey). **B**: Formation of the Norwegian glaciodynamic sequence including glaciotectonised middle Weichselian sand and clay, *c.* 30–28 ka BP (orange). **C**: Proglacial deposition of glacial sediments related to the Swedish glaciodynamic sequence, *c.* 25–21 Ka BP (yellow). **D**: The concluding glaciotectonic deformation in the Swedish glaciodynamic sequence superimposed by the Young Baltic glaciodynamic sequence, *c.* 17 ka BP (orange). The brown unit is the Fændrikvang glaciolacustrine unit of Winsløw *et al.* (2020).

Upper Cretaceous chalk overlain by Danian limestone (Fig. 2A). In a few spots the Selandian marl and clayey units have been preserved in down-faulted 'traps' (Winsløw *et al.* 2020). Wrench-fault structures along the Sorgenfrei–Tornquist Zone, in the form of both positive and negative flower structures, developed during the late Creataceous and early Palaeogene. The negative flowers are the youngest and prevailing features and are regarded to have caused the formation of the buried Esrum–Alnarp Valley (Winsløv *et al.* 2020). The wrench faults creating the extensional basin are the major tectonic features in the region surrounding the Esrum Sø lake basin (Winsløv *et al.* 2020).

Quaternary geology

The Quaternary geology in north-eastern Sjælland can shortly be described as dominated by glaciodynamic sequences of Weichselian age. The oldest preserved units comprise marine deposits from the interglacial Eemian period, which are found at the base of the Esrum–Alnarp Valley (Konradi 1992). The oldest terrestrial unit occupying the landscape in north-eastern Sjælland is the Kattegat Till Formation with intercalations of meltwater clay and glaciolacustrine clay units related to the lowland area fringing the Kattegat depression (Fig. 2B; Houmark-Nielsen 1987; Houmark-Nielsen & Kjær 2003; Pedersen 2005). The Mid Danish Till Formation forms a basal unit in the main part with a general elevation from sea level to 10 m a.s.l. The Mid Danish Till Formation was deposited during the ice advance from central Sweden, which was also responsible for parts of the glaciomorphological features (Fig. 2C; Houmark-Nielsen 1987, 2010; Pedersen & Gravesen 2022). The Baltic Ice Advance is the dominant creator of the formation of a large outwash plain deposited in front of the advancing ice from the south-east (Houmark-Nielsen 1987, 2010). Moreover, a marked system of parallel ridges formed by glaciotectonics created the hilly landscape of Gribskov, the big forest west of the Esrum Sø (Fig. 2D; Winsløv *et al.* 2020). These glaciodynamic deposits are in this paper interpreted to form the base of the lakebeds.

Based on the results from the drill core in the lake, Hansen (1968) found by biostratigraphic dating that the following time span is covered by the sediments in the lake (Fig. 3): The Lateglacial to Holocene time span is represented by lacustrine clay, which comprises the Bølling–Older Dryas–Allerød–Younger Dryas times with colder periods represented by high frequences of silty/fine-sand laminations. The transition to the Preboreal and Boreal times is represented by 4 m of lacustrine calcareous gyttja as reported by Hansen (1968). During the Atlantic time an increase

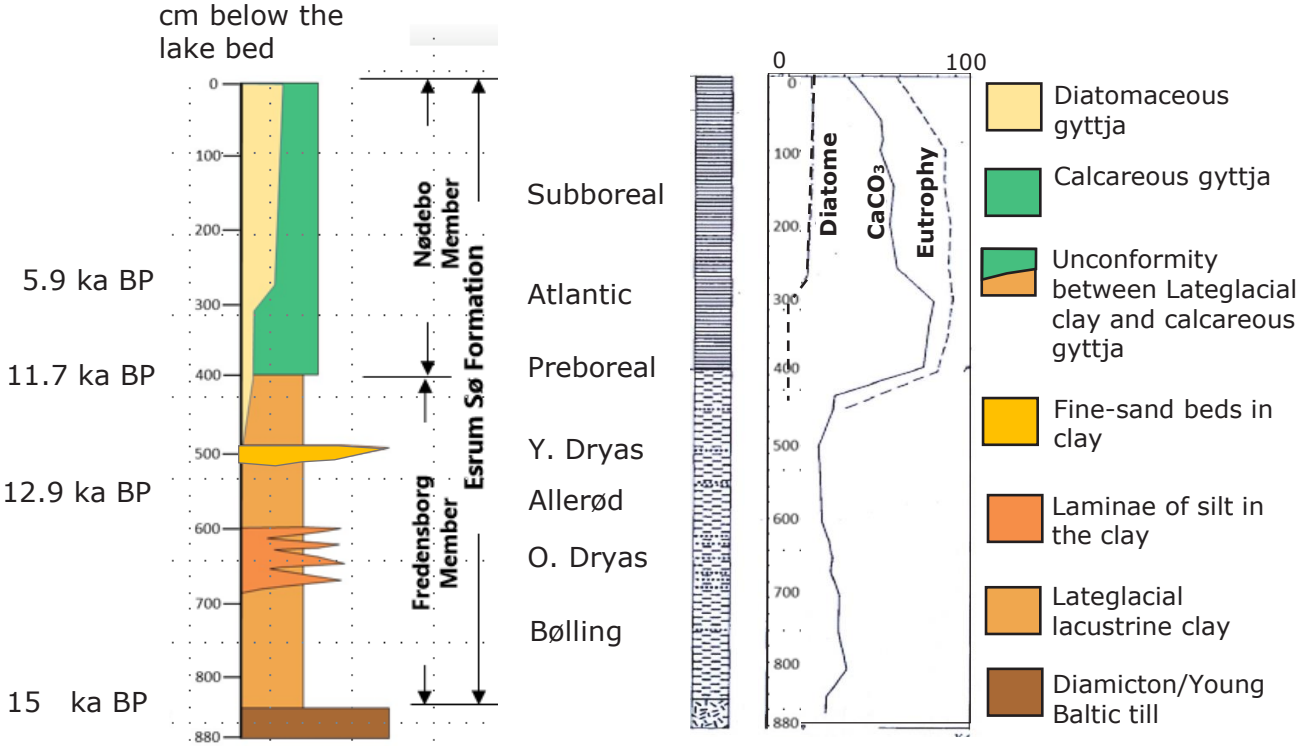

Fig. 3. Stratigraphic log of the Esrum Sø Formation based on the drill core from the *c.* 8 m deep borehole at the location 22 m below the water table in the central northern part of the lake (Fig. 1). The logs in the middle part of the figure are copied from the original description of the drill core by Hansen (1968). At left: ^{14}C ages from Gravesen *et al.* 2017. See the text for descriptions of the log.

of diatomite production occurred as seen in Hansen (1968) and Foged (1968). It is worth noting that the transgressive sequences affecting the lake Søborg Sø (Iversen 1937; Noe-Nygaard *et al.* 2017) just north of Esrum Sø had no influence in Esrum Sø during the Atlantic development. The Atlantic transgression ceased around 6.000 BP and the Subboreal time took over and continued until the Subatlantic time started the modern development of vegetation in the landscape surrounding Esrum Sø.

During the Lateglacial time, Esrum Sø was a relatively shallow lake dominated by sedimentation of silt-rich clay (Whiteside 1970). The laminated glaciolacustrine deposit that is interpreted to represent successive turbidte deposits is about 4.5 m thick, and two sandy intercalations occur at 6.5 m and at 5 m (Fig. 3; Hansen 1968).

The transition from Atlantic to Subboreal time, with generally mild conditions, stimulated diatom blooms, which resulted in a decrease in calcareous gyttja, as seen in the sediments retrieved in the drill core (Fig. 3). According to the chydorid species, found at 370 cm depth in the drill core, the water level in the Preboreal time was relatively low (Whiteside 1970).

No information on gas in Esrum Sø has so far been reported, although information from water wells in nearby areas mention gas in the water (Konradi 1992; Konradi & Laier 1991). However, it is known from studies in many lakes outside Denmark that gas accumulations are found in lakes; the gas delimits the penetration of the seismic signal below the lake floor and sometimes the signal is also strongly dampened, with the result that no geological information is obtained from the seismic sections below the gas. Gas hampering interpretation of seismic data in Danish lakes has been experienced by one of us (LOB) from unpublished seismic sections during fieldwork in two lakes in Jylland. The deterioration of the seismic signal in lakes has been addressed in a number of studies in lakes, where it has been found that this is due to shallow gas occurrences; the phenomenon has been discussed thoroughly by e.g. Lodolo *et al.* (2012), Cukur *et al.* (2013), Visnovitz *et al.* (2015), and Toker & Tur (2021).

Data

Seismic data

A number of 82 high-resolution seismic sections (*c.* 115 km) have been recorded by a Teledyne high-resolution Chirp III subbottom profiler in four field campaigns each lasting one day in 2013 (19 sections, 38 km), 2014 (19 sections, 39 km), 2015 (12 sections, 28 km) and 2022 (32 sections, 10 km) (Figs 1 and 4). In 2013–2015 a large tourist boat named 'Viking' from the company Esrum Bådfart (https://www.baadfarten.com) was hired, whereas in 2022 a small rubber boat was used. The high-resolution recording was carried out by placing the Chirp III at *c.* 50 cm depth in the water in a midship position in order to avoid the air-induced noise in the water from the boat engine.

Vertically above the Chirp a Differential GPS was placed, which recorded the exact position of the seismic instrument with an accuracy of 2 cm. The position of the boat was simultaneously displayed on a computer screen used for recording data and on an iPad for the use of the boat driver to ensure straight lines. A small Honda generator supplied the electricity needed for operating the Chirp, recording computer etc. The Chirp operates with a frequency band (2–20 kHz) for recording, which is split and displayed during the recording of data in two separate windows on the computer screen, a low frequency covering 2–7 kHz and a high frequency covering 10–20 kHz. The two frequencies are written into one SEG-Y file and after recording split into high- and low-frequency data before they are loaded onto a workstation with an interpretation software program (Petrel). In the present work the low-frequency data were used for interpretation of the geological strata between the lake floor and the till (Fig. 3). No frequency filtering or migration was carried out on the seismic data. For vertically recognising a layer in reflection seismic data, normally a thickness of a half wavelength ($\lambda/2$) of the seismic signal is required (e.g. Badley 1985), which ensures that the top of the unit can be separated from the base of the unit (i.e. interference free). The $\lambda/2$ of the 2 kHz signal is 0.35 m and for the 7 kHz signal it is 0.11 m, using a standard water velocity of 1475 m/s. This means that a highly water saturated layer can be recognised below the lake floor if it has a minimum thickness of 0.11–0.35 m. For simplicity, the layers below the water saturated lake floor and the till are attributed a velocity of 2000 m/s. This gives a $\lambda/2$ of the 2 kHz signal of 0.5 m, and 0.14 m for the 7 kHz signal, showing that a sediment layer of 0.25–0.5 m thickness is recognised (interference free) between the lake floor and the till.

The recorded signal is displayed on the figures as a zero phase signal (eg. Badley 1985), and in the template setting (Petrel seismic default), the red-blue-red signature shows an increase in AI (acoustic impedance defined as density×velocity, e.g. Badley 1985) between two units, where the lower unit has a higher AI than the upper; this usually indicates an increase in velocity of the lower unit). A blue-red-blue signature shows a decrease in AI, indicating a decrease of velocity going from the upper unit to the lower unit.

In 2013 a general reconnaissance survey of Esrum Sø was carried out to investigate whether it was possible to acquire high-resolution seismic data in the lake in order to obtain sub-bottom data that could be used for seismic interpretation related to the geological evolution of the lake. It was found that especially in the northern part of the lake it was possible to acquire high-quality data with a penetration of *c.* 30 m below the present lakebed, whereas in the southern part of the lake shallow gas degraded the seismic signal pronouncedly. In 2014 and 2015 the surveying was concentrated in the northern part of the lake to fill in the 2013 seismic grid and to outline the area where high-quality data could be acquired.

In 2022 a small, densely spaced grid in the northwestern part of the lake was acquired (Fig. 1) in order to outline the orientation of some of the antiform structures and the relation between faults, synforms and gas seepage.

The weather conditions were fine for all campaigns, with minor wind. The data is of high quality and reveals the lakebeds in high detail. Working with single-receiver high-resolution seismics, multiples of the lake bottom (interface between water and sediments) and pronounced deeper reflections are present. This especially degrades the data acquired at shallow water depth.

On the displayed seismic sections, interference noise is seen as a number of almost horizontal stripes, most clearly in the water column, a phenomenon also present with other high-resolution seismic instruments. The noise band is probably caused by some type of resonance; as the stripes are slightly dipping, simple processing steps cannot remove it.

The seismic sections are named with a prefix of two digits indicating the year of acquisition, e.g. 15-22 denotes section no 22 acquired in 2015.

Two seismic sections from two different surveys pass close to the location of the Esrum Sø borehole (Figs 1 and 4). From these two sections it is possible to make a correlation between the seismic reflectors and the drill core data (Fig 5). Along the western bank of Esrum Sø, two vibro-seis profiles were acquired in 2014 (Winsløw *et al.* 2020, see Fig. 1 for location), and the profiles were used to obtain the overall structural framework along the western bank of the lake. Jumpties were established between the vibro-seis and the chirp data, although they covered different depth intervals.

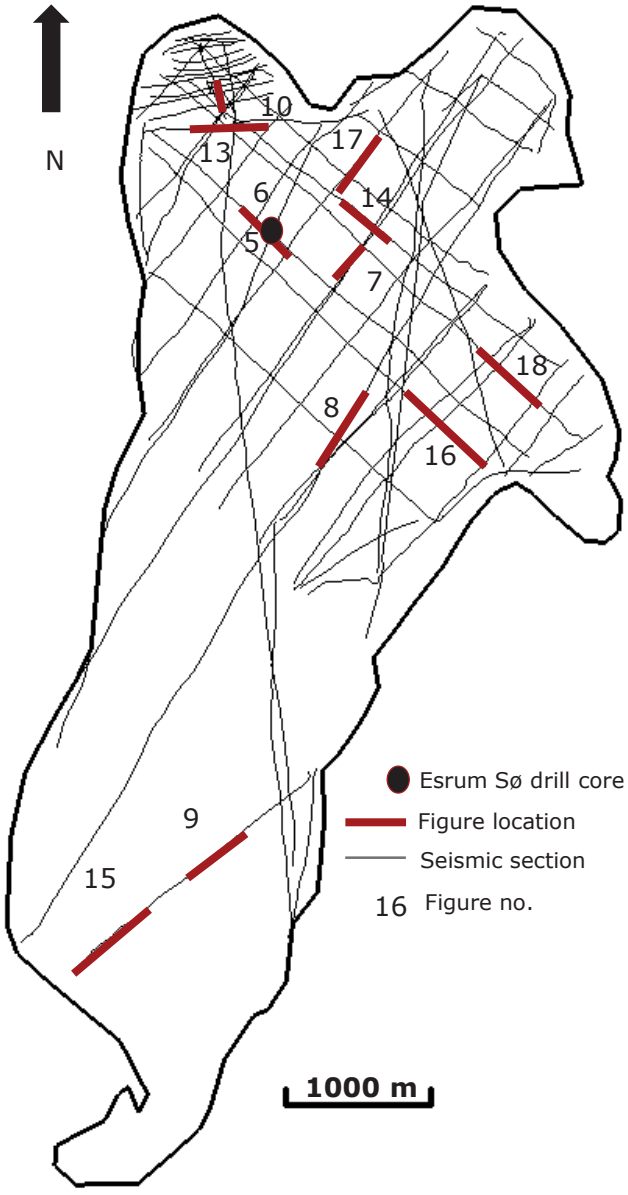

Fig. 4. Location map of the seismic sections investigated for this study. The seismic sections displayed in the following figures are marked with their figure numbers at the lines.

The Esrum Sø drill core

A drill core to a depth of 8.81 m below the lake floor was obtained in 1966 by "Ferskvandsbiologisk Laboratorium" (Hansen 1968; Whiteside 1970). The drill core is not reported to GEUS, and it is not found in the Jupiter database of wells in Denmark. Due to reorganisation of Ferskvandsbiologisk Laboratorium in 2010, the drill core seems only to be documented by Hansen (1968), Whiteside (1970) and Hansen (1981). The position of the drill core (Fig. 1) has been estimated from the description provided by (Hansen 1981) and by integrating the water depth of 22 m at the drill site, the lithological information from the description of the drill core, and the seismic interpretation. The sedimentology of the drill core was described by Hansen (1968), the fauna in the core was investigated by Whitesite (1970), and

analysis of the diatom flora was made by Foged (1968). Further sedimentologic information is provided by Hansen (1981).

The drill site is situated close to two seismic sections recorded in 2013 and 2015. The sections show that the core was drilled on an antiform. Furthermore, the structural interpretation indicates that the drill core misses a smaller part of the sedimentary succession in the middle part of the stratigraphy due to the location of the drill site (Fig. 5).

Five shallow cores in the northern part of the lake covering the interval 0-0.32 m below the lake bottom have been obtained by Danmarks Miljøundersøgelser (2003), and in the eastern part of the lake (southeast of Fredensborg) seven samples up to 0.40 m below lake bottom were achieved by Berg (1938). However, none of these cores and samples contribute to the identification of the lithology and thus they are omitted in this study.

Results and interpretation

The interpretation and correlation of the drill core data and the seismic sections demonstrate the presence of a formation with two distinctive members. Therefore, a new formation, the Esrum Sø Formation, is erected here, following the stratigraphic rules set out by e.g. Murphy & Salvador (1999).

Esrum Sø Formation

New formation

Name and history. The Esrum Sø Formation is named after the lake Esrum Sø (sø is the Danish word for lake) in north-eastern Sjælland, eastern Denmark. The first record of the sediments accumulated in the lake depression became available by drilling in the lake bottom in 1966, as described by Hansen (1968). This record has now been correlated to the seismic sequence architecture adapted in the interpretation of the 2013–2015 seismic data in this study.

Type locality and type profile. The type locality is in the north-western part of the lake, and the type profile is represented by the drill core described by Hansen (1968) (Fig. 3).

Lithology. The formation comprises two markedly different lithologies: a lower unit comprising grey, calcareous clay and fine-sandy/silty clay, and an upper unit comprising gyttja, which at the base is a calcareous gyttja but grades upward into a more and more diatomaceous gyttja towards the top.

Boundaries and thickness. The lower boundary of the formation is the unconformity between the top of the Young Baltic till and the base of the lacustrine grey clay. The top of the formation is the recent lake floor. According to the drill core, the thickness of the formation is 8.40 m. However, in some of the recognised depressions in the lakebeds an extra 1–1.5 m of diatomaceous gyttja may be added, showing that the thickness is up to 10 m.

Extent and correlation. The Esrum Sø Formation covers the *c*. 17 km^2 area of the Esrum Sø lakebed. We refrain from a correlation to neighbouring lakes and bogs. In the nearby former Søborg Sø 4 km north of Esrum Sø. four marine, Postglacial transgressions are documented (Iversen 1937, Noe-Nygaard *et al*. 2017), and these are not recognised in Esrum Sø, which is solely a freshwater basin (Whiteside 1970).

Age. The oldest age of the formation is Bølling in the Lateglacial time (Hansen 1968). Based on various criteria, the melting back of the Young Baltic Ice from Sjælland took place around 16.000 BP (Gravesen *et al*. 2017).

Depositional environment. After the ice melted back from the area, small, shallow ponds started to appear and deposition of calcareous clay began. In the clay, the oldest remnants of aquatic communities (chydorides), which indicate shallow water, were recognised at 4.5 and 5.5 m downhole depth in the drill core (Whiteside 1970). It is thus evident that the water level in the lake from that time on has increased continuously. Whiteside's (1970) analysis demonstrates the presence of 30 species of chydorids, which mainly indicates that Esrum Sø is a clear-water lake. According to the analysis of diatoms, the lake had a relatively high alkalinity throughout the Postglacial time (Foged 1968).

Subdivision. Based on the significant shift in lithology from clay to gyttja at the start of the Preboreal time, the Esrum Sø Formation is subdivided into two members: the Fredensborg Member and the Nødebo Member (Fig. 3). In the drill core this level is marked by a hiatus, where the pollen analysis indicates the absence of at least four pollen zones (IV, V, VI & VII, Hansen 1968). Fig. 5 shows the correlation to a seismic section interpreted as close to the position of the drill core.

Fredensborg Member

New member

Name and history. The Fredensborg Member is named after the town Fredensborg on the eastern bank of Esrum Sø. According to the seismic mapping, the

member crops out dominantly in the lakebed below the bank near Fredensborg town.

Type locality and type profile. The type locality is the same as that of the Esrum Sø Formation, namely in the north-western part of the lake where the borehole is situated, and the type profile is the lower part of the drill core described by Hansen (1968) (Fig. 3).

Lithology. The Fredensborg Member comprises grey, calcareous clay and fine-sandy/silty clay. A fresh sample of the clay is dark grey and soft, but when dry it is hard and light grey. The clay is well laminated with numerous laminae of thin silt and very fine sand. The laminated glaciolacustrine deposit has marked sandy intercalations at 6.5 m and at 5 m (Fig. 3). In the lower part of the member the carbonate content is about 33%, but it decreases towards the top to about 17% (Hansen 1968).

Boundaries and thickness. The lower boundary of the member is the unconformity on the top of the Young Baltic till. The top of the member is marked by the shift from calcareous clay to calcareous gyttja. The thickness of the member in the drill core is 4.40 m.

Extent and correlation. The extent of the Fredensborg Member is similar to that of the Esrum Sø Formation. The seismic survey indicates that the extent corresponds to the coastline of the lake. Although Lateglacial lacustrine beds are well known from various localities on Sjælland, the data background is too uncertain to allow good correlations.

Age. The deposition of the Fredensborg Member started in Bølling time, probably about 15.000 BP. The unconformity at the top of the member coincides with the climatic transition from Lateglacial (Younger Dryas) to Postglacial (Preboreal), which would be the beginning of the Holocene at about 11.700 BP (Noe-Nygaard *et al*. 2017).

Depositional environment. During the Lateglacial time Esrum Sø was a relative shallow lake dominated by sedimentation of silty, calcareous clay in a cold climate. The lamination in the sediment is interpreted to represent successive turbidite deposits and not varvy sedimentation (Hansen 1968).

Nødebo Member

New member

Name and history. The Nødebo Member is named after the town Nødebo on the south-western bank of Esrum Sø.

Type locality and type profile. The type locality corresponds to that of the Esrum Sø Formation, namely in the north-western part of the lake, where the borehole is situated, and the type profile is the upper part of the drill core described by Hansen (1968) (Fig. 3).

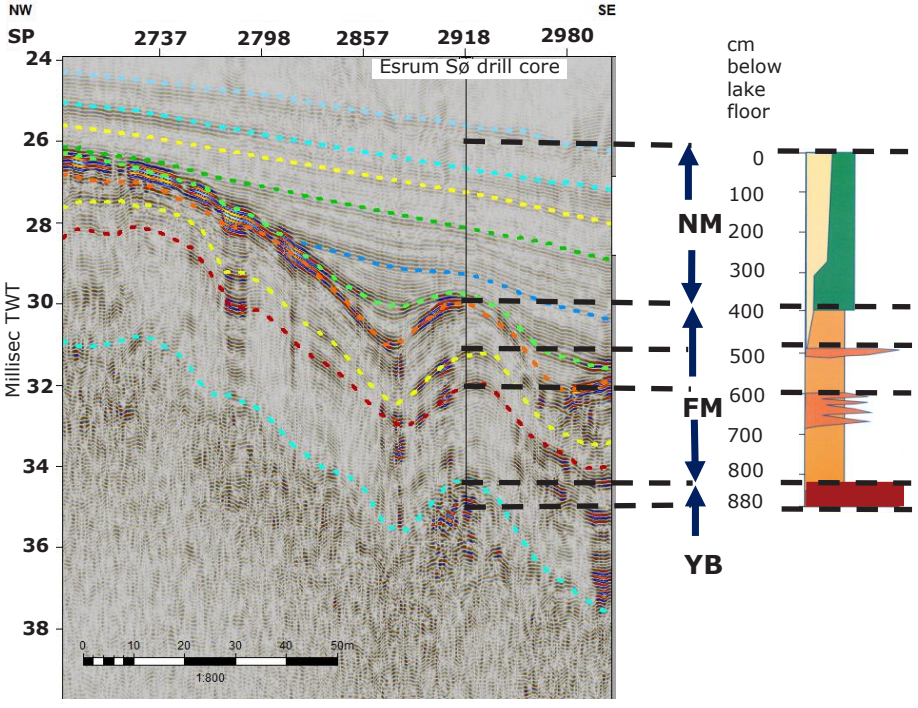

Fig. 5. Correlation between the seismic units and the sediments in the drill core. The dashed black lines show the correlation between the lithology in the drill core and the reflectors on the seismic section intersecting the drill core. The sediment units are Younger Baltic till (YB), Fredensborg Member (FM) and Nødebo Member (NM), which correspond to the seismic architecture units. The dotted lines on the seismic section shows the 10 reflectors interpreted in the survey area. The numbering of the reflectors appears in Fig. 6A. Core depth in centimetres below lake floor according to the core description in Hansen (1968). Seismic section 15-22, vertical exaggeration ×7.5.

Lithology. The Nødebo Member comprises grey, calcareous gyttja which grades up into a more diatomaceous gyttja. A fresh sample of the gyttja is light grey and soft, but a dried sample is brilliant white and stone hard. In contrast to the underlying clay, the gyttja is markedly gritty (Hansen 1968). The carbonate content is about 73–79% at the base of the member. It decreases to 59% at about 2.5 m from the top and to about 50% at the top. The decrease of carbonate is the effect of diatom blooms, which resulted in a relative decrease of the carbonate content (Hansen 1968).

Boundaries and thickness. The lower boundary of the member is the unconformity at the top of the Fredensborg Member. The base of Nødebo Member is marked by a shift from calcareous clay to calcareous gyttja. The drill core has a hiatus at this level, where at least four pollen zones are absent (Hansen 1968). However, in the seismic sections, onlapping beds of the Nødebo Member indicate an additional presence of gyttja at the base of the member (Fig. 5). The thickness of 4 m known from the drill core thus has to be supplemented with the thickness of syntectonically accumulated gyttja beds. The member is therefore regarded to be at least 6–7 m thick.

Extent and correlation. The extent of the Nødebo Member is rather patchy within the area of the Esrum Sø Formation. In some places it is almost absent, whereas in other places it covers large areas with gas-containing gyttja, which hampers the investigations of the structures in the lakebeds.

Age. The deposition of the Nødebo Member began in the Preboreal at about 11.700 BP, and from this time it continued throughout the Holocene (Hansen 1968, 1981).

Depositional environment. The transition from the Atlantic to the Subboreal time was a period with generally mild conditions that stimulated diatom blooming, which resulted in a relative decrease in calcareous gyttja. According to the chydorid species at 370 cm depth, the water level in Preboreal time was relatively low (Whiteside 1970), which clearly indicates increasing Postglacial deepening of the lake basin. According to the seismic survey, the gyttja dominates the lake floor in a large part of the south-western part of the lake. Towards the south, the gyttja transforms into peat, and in the southernmost part the peat was exploited in 4 m deep pits during the world wars. The carbonate in the calcareous gyttja is generally regarded as resulting from dissolution of limestone (glaciotectonite clasts and matrix) in the till, precipitated in the lake water. An instructive example of this dynamic process is the occurrence of tufa at the springs at the toe of the slopes in the wood south of the lake (SASP, unpublished data).

Correlation between seismic sections and the Esrum Sø drill core

Seismic section 15-22 intersects the Esrum Sø borehole (Figs 4 and 5). The borehole is drilled on an antiform. The correlation between the drill core and the seismic section is shown in Fig. 5. In the drill core pronounced lithological boundaries are observed, e.g. the Young Baltic till, the two sand/silt layers within the Fredensborg Member and the unconformity between the Fredensborg and the Nødebo Members (Fig. 5). These pronounced lithological boundaries create a difference in acoustic impedance and thus they are expected to show up as pronounced reflections on the seismic sections. Three pronounced reflections: the top of the basal till, the unconformity separating the Fredensborg and Nødebo Members and the lake floor are marked on the seismic sections, where they are identified by seismic facies and seismic stratigraphy (Fig. 6A reflector no. 1, 4 and 10).

To calculate the seismic velocity of the Fredensborg Member, the formula: Thickness (m) = velocity of the interval (m/s) × thickness (millisec)/2 (e.g. Badley 1985) is used. The thickness (millisec) is read from the seismic section as the distance between the unconformity and the till, while the thickness (m) is measured from the drill core as the distance between the unconformity and the top till. The seismic velocity of the Fredensborg Memebr is thus calculated to 2000 m/s. Use of this velocity places the two sandy intervals in the drill core at depths corresponding to reflectors 2 and 3 (Fig. 6A) according to Hansen (1968). Inspection of the depth interval above the interpreted lake floor (reflector 10) reveals a minor unit characterised by a low reflectivity. Applying a velocity of 1550 m/s this corresponds to 50 cm that has been reported missing at the top of the drill core (Hansen, 1968). This likely reflects that the missing part of the drill core comprised very water-saturated material, e.g. mud, that could have been lost taking the drill core. The interval between the top of the drill core and the unconformity between the Fredensborg and Nødebo Members is 4 m thick, and this corresponds to a velocity of 1900 m/s of the Nødebo Member.

Ten pronounced reflectors are shown in figs 5, 6A and 6B and numbered 1–10 in Fig. 6A. The reflectors can be followed within the whole surveyed area. Reflector 1 is the surface of the Young Baltic till and is a pronounced reflector, likely due to an increase in velocity between the lower part of the Fredensborg Member and the till. In the Fredensborg Member, the

top of the laminated silt in the clay is represented by reflector 2 while the top of the fine sand beds in the clay is named reflector 3. The unconformity between the Fredensborg and Nødebo Members is represented by reflector 4. In the Nødebo Member, five reflectors are mapped; they correspond to minor unconformities and are numbered 5–9. The lowermost part of the Nødebo Member is lacking in the borehole due to its location on an antiform, which is supported by the observation of a hiatus by Hansen (1968). The top of the lakebed is represented by reflector 10.

Analysis of seismic units

Three seismic units are distinguished in the seismic sections and labeled YB (Young Baltic till), FM (Fredensborg Member) and NM (Nødebo Member) (Figs 6A and 6B). The interpretation of the seismic sections is carried out by means of seismic stratigraphy as described by Mitchum *et al.* (1977) and further elaborated by e.g. Badley (1985). Following this method a seismic section is subdivided into a number of units by usage of reflection terminations at the upper unit boundary (toplap, truncation and concordance) as well as at the lower unit boundary (downlap, onlap and concordance), together with the internal reflection pattern, supplemented with the information of reflection continuation and amplitude. In this manner a geological framework is established and a geological evolution is outlined from the seismic section. Combining seismic sections, a 3D model can be established for the evolution of the area in question.

Till (YB). The lower boundary of the unit cannot be observed due to seismic noise and multiples. The upper boundary is marked by a pronounced reflector indicating a transition from a lower into a higher seismic velocity going from FM to YB. The internal pattern of the unit is rather chaotic with no continuity and varying amplitude of the reflections. The transition to FM marks an unconformity, which is somewhat

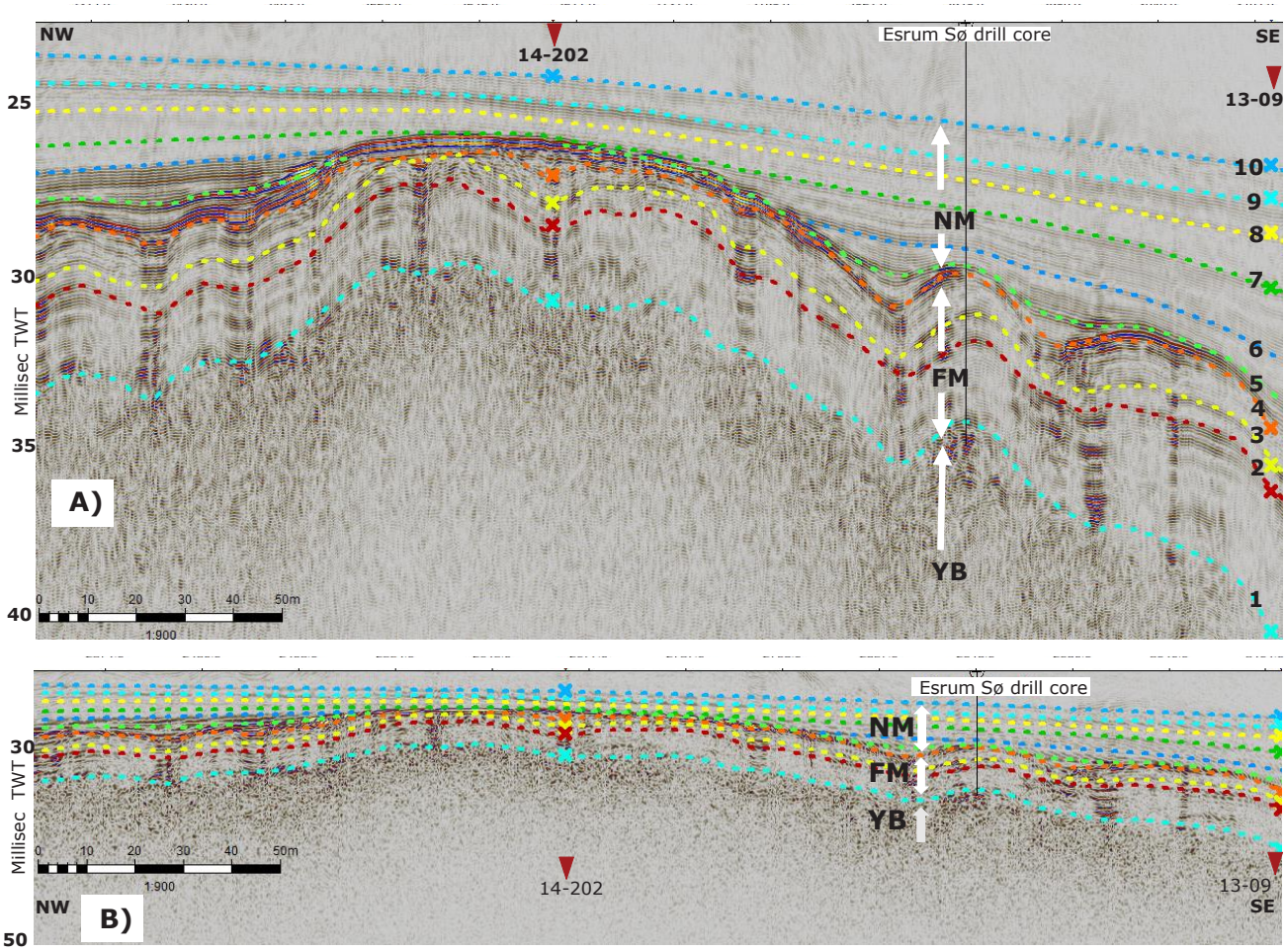

Fig. 6. A: Seismic section 15-22 showing the relation between the mapped seismic reflectors 1 to 10 and the Esrum Sø drill core. The positions of two intersecting seismic section (13-09 and 14-202) are indicated with red triangles at the top of the diagram. Vertical exaggeration ×6. **B**: The same seismic section as in A with lower vertical exaggeration, ×2, and a more realistic appearance. YB: Younger Baltic till; FM: Fredensborg Member; NM: Nødebo Member.

undulating and in places irregular. The unconformity is situated at its deepest level in the middle part of the lake, from where it rises towards the banks of the lake. Jump-tie between the vibro-seis data presented in Winsløw *et al.* (2020) and the Chirp data in the lake show good correspondence between the two data sets. The correlation with the drill core indicates that the till represents the Young Baltic till. The upper part of YB mimics the post-depositional behavior of unit FM, showing tectonic quiescence.

Fredensborg Member (FM). The unit is bounded at the base by an uneven unconformity (reflector 1) representing the top surface of the Young Baltic till. One should note that no outwash deposit is present at the boundary. The upper boundary of FM is a pronounced reflector (reflector 4), which in places forms an erosional unconformity. At the lower boundary, the reflections show onlap towards the transition to YB, indicating that FM at the base 'drowned' the undulating surface of the YB. The internal pattern of FM

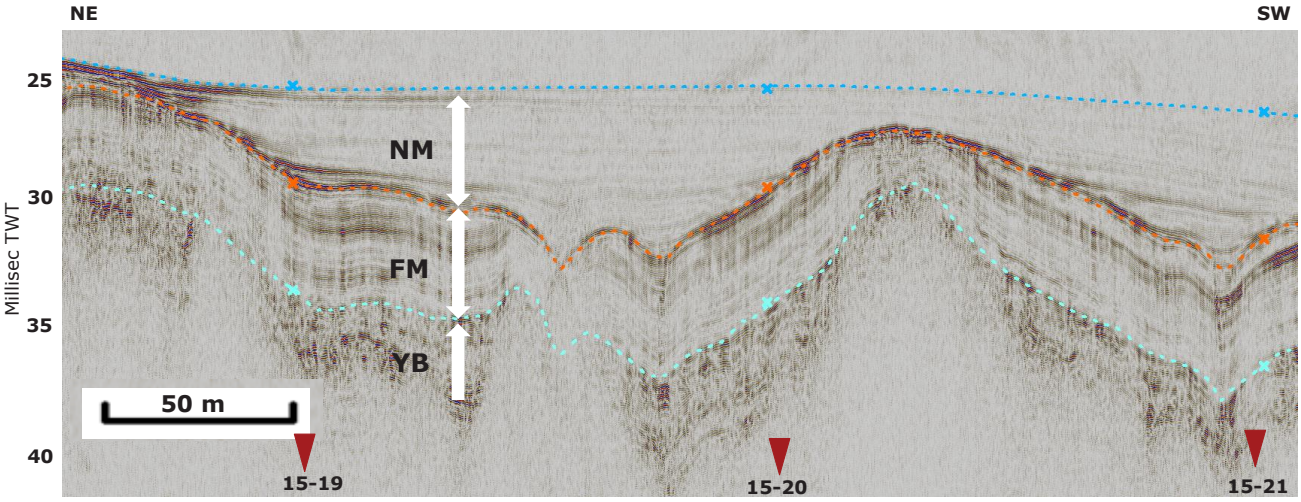

Fig. 7. Seismic section 13-07, illustrating the deformation of seismic units YB (Younger Baltic till) and FM (Fredensborg Member). Note the onlapping relation of unit NM (Nødebo Member) at its lower boundary in the depressions, which contrasts with the erosional development of the top of the antiformal crests. Reflectors showing the boundaries between the lake floor, NM, FM and YB are shown. Intersecting seismic sections are shown by red triangles. Vertical exaggeration ×8.

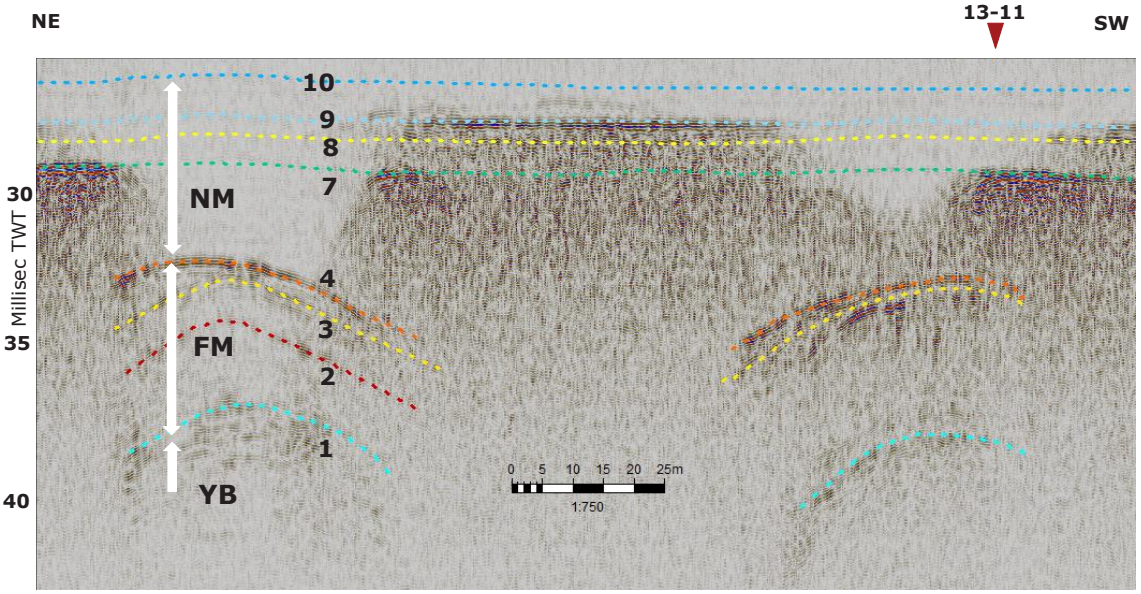

Fig. 8. Seismic section 13-05, illustrating the occurrence of gas stored in the gyttja of **Nødebo Member** (NM). Note that there are three levels of gas saturation, which are indicated with coloured dashed lines (reflectors 7–9). In the windows between the gas-rich areas the deeper units FM Fredensborg Member) and YB (Younger Baltic till) are recognised (reflectors 1–4). Intersecting seismic sections are shown by red triangles. Vertical exaggeration ×5.

shows parallel bedding with high continuity and with a bedding interval of high amplitude. Pronounced reflectors of high continuity and high amplitude, e.g. reflectors 2 and 3, subdivide FM into smaller subunits reflecting changes in the lithology of the unit. The thicknesses of the subunits are constant, which shows that they have been deposited horizontally. The internal reflectors, e.g. 2 and 3, can be correlated to the lithology described in the drill core (Figs 5 and 6A). FM is weakly onlapping the unconformity on top of YB. The post-depositional deformation is clearly identified in FM. In antiform structures, erosion of FM is recognised on the top of the structures (Figs 6A and 7). The thickness of FM is almost constant, indicating horizontal deposition. The thickness may vary due to the uplift and subsidence in the undulating structures but is generally close to about 5 millisec TWT, which is almost identical to the thickness of 4–5 m recorded in the drill core.

Nødebo Member (NM). The base of the unit is an unconformity towards FM (Fig. 6A). The top of the unit is the lake floor (transition between sediment and lake water). The unit shows laminated reflections which mainly diverge from the tilted beds of the top of FM. The continuity of the reflections is high but their amplitude is weak; however some individual reflections are continuous with a high amplitude and form pronounced reflections in the seismic sections. Some reflections show high amplitude close to the onlap of the beds onto the tilted unconformable top surface of FM. The amplitude intensity decreases away from the onlap, which likely reflects proximal coarser grained

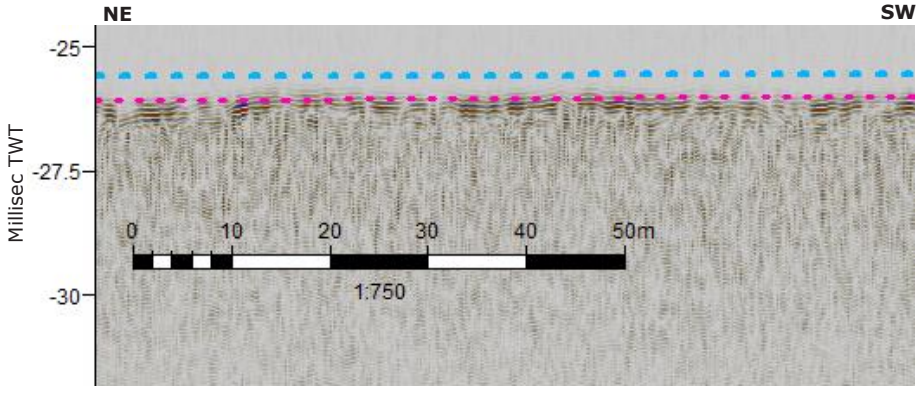

Fig. 9. The general picture of a gas-saturated gyttja mat, which completely prevents the penetration of the seismic signals. The lake floor is marked with blue dashes and the top of the gas-saturated gyttja mat with red dashes. Southern part of the lake, seismic section 13-04, vertical exaggeration ×5.

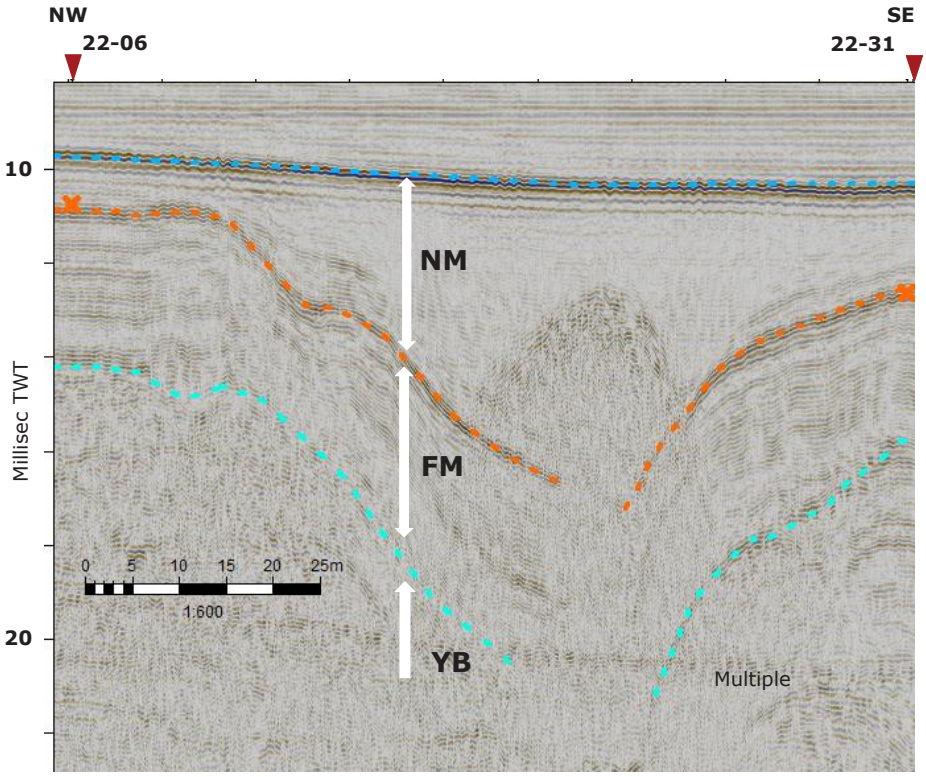

Fig. 10. Subsidence of the sediments into an extensional fracture; this is almost identical to a synform feature. Note the 'cloud' of gas seeping up from the extensional fracture and captured in the Nødebo Member (NM). Intersecting seismic sections are shown by red triangles. Reflectors showing the boundaries between the lake floor, NM, FM and YB are shown. Seismic section 22-13, vertical exaggeration ×5.

sedimentation close to antiformal structures and distal finer grained materials towards a depression (Figs 6A and 7). In the lowermost part of NM, reflections fill up depressions and show onlap towards the tectonically disturbed FM. In the lower half of NM, the reflection pattern shows high continuity and a larger acoustic impedance than in the upper part. This change correlates to the decreasing calcareous content and the increase of diatomaceous gyttja in the deposit.

Three stratigraphic levels in NM (reflectors 7–9) are traced almost all over the lake and are correlated to gas reflections (see below). These levels also represent hiatuses with short durations, reflecting adjustments of the deformed structures (Figs 6A and 8).

Gas seepages

In the seismic sections pronounced reflections at various stratigraphic levels of Nødebo Member outshadow the underlying reflections (Figs 8–10). The shadowing reflectors are characterised by a large acoustic impedance contrast and show a marked change in polarity, indicating that the lithology below the pronounced reflectors has a significantly lower velocity than the lithology above these reflectors. Such shadowing is due to accumulation of gas (Lodolo *et al.* 2012; Cukur *et al.* 2013; Visnovitz *et al.* 2015; Toker & Tur 2021) trapped at various stratigraphic levels (Fig. 8, reflectors 7–9). The gas reflections occur over large parts of the lake, and in the northern part they are located in synforms between antiforms, where the Young Baltic till and Fredensborg Member are folded (Fig. 8). In some areas the gas seepage is related to faulting (Fig.10). In the southern part of the lake, the gas is situated close to the lake floor (the minimum distance is *c.* 10 cm below the lake floor), which results in complete non-transparency so that no information is obtained below the gas-rich zone (Fig. 9).

The observed gas-related reflections are categorised into three types:

1) Continuous pronounced reflections that follow certain stratigraphic horizons and allow part of the energy to be transmitted into the unit below (reflections 7–9 in Fig. 8).
2) Discontinuous pronounced reflections located close to the lake floor, that allow no seismic energy to be transmitted (Fig. 9).
3) Cloud shaped reflections (Fig 10).

Type 1 reflections are found at three different stratigraphic levels in the Nødebo Member (reflections 7–9 on Fig. 8) located above deeper parts of the stratigraphy characterised by depressions that are found in synclinal areas caused by subsidence (illustrated by reflections 2–4 in Fig. 8). The extent of the three reflections varies (see SW and NE part of Fig. 8), but generally the lowermost reflection (reflection 7) has the largest extent compared to the youngest (reflection 9). Seismic energy is commonly transmitted relatively better through the marginal parts of the reflections, which represent the top of the gaseous interval, than through the more gas-rich central parts,

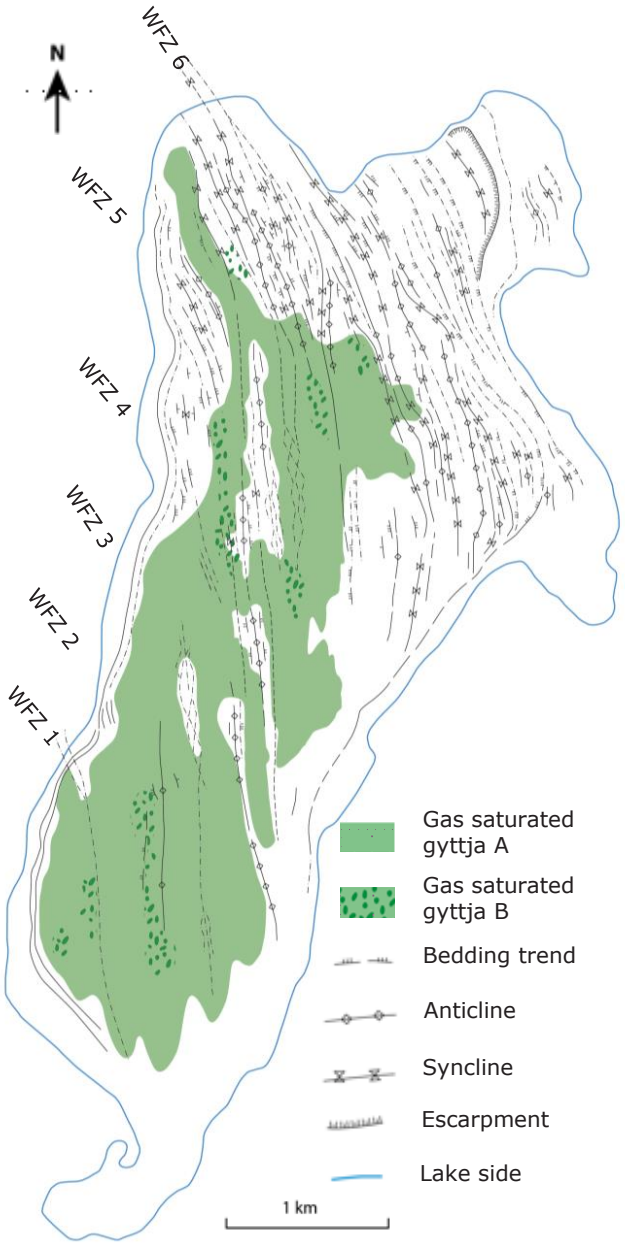

Fig. 11. Structural geological map resulting from the high-resolution seismic survey of Esrum Sø. Note that synclines and anticlines are not folded features but subsidence structures and residual crests between extensional fractures, respectively. The gas saturated gyttja A and B correspond to the gas saturated gyttja illustrated in Fig. 9, and in Figs 8 and 10, respectively. The wrench-fault zones (WFZ 1–6) from Winsløw *et al.* (2020) are marked along the western bank of the lake.

and thus the flanks of the stratigraphically deeper situated antiforms are recognised below the type 1 reflections (Fig. 8). The three reflections (7–9) are correlated to three stratigraphic levels (Fig. 5) and traced over the main part of Esrum Sø. Careful interpretation reveals that the three reflections correlate to weakly developed unconformities on the flanks of antiforms. Seismic windows through the reflections are seen throughout the lake and are persistently located above the antiforms. In the windows, the deeper reflections 1–4 can be correlated even though they are not visible below the strong gas reflections of type 1 (Fig. 8). The three stratigraphic levels are identified at the same depths in all the three seismic surveys. Evidently, the gas depths have not changed in the period 2013–2022 during which the surveys were made.

Type 2 reflections are located in the southern part of the lake and occur near the lake floor (Fig. 9). The reflections marking the top of the gas-rich area are uneven and consist of smaller segments of high-amplitude reflections. The reflection pattern below is chaotic but with moderate amplitude. In this part of the lake the gas-rich areas do not allow any recognition of deeper reflections.

Type 3 reflections show a concave-upwards zone, which is slightly transparent (Fig 10). In several profiles, the deeper reflections in the Young Baltic till and Fredensborg Member can be recognised below the gas-rich area, and the outline of the synforms can also be revealed. This allows the recognition of faulting in these two units, which must have occurred before the capture of gas in the sediments of Nødebo Member.

The gas-rich intervals were grouped into two during the mapping of the units and reflectors. "Gas saturated gyttja type A" gives rise to reflectors of type 2, while "gas saturated gyttja type B" gives rise to reflectors of type 1 and 3. The distribution of the two groups is shown in Fig. 11.

Structural features and deformation development

Based on the high-resolution seismic sections, an interpretation of the deformation affecting the lake sediments has resulted in the recognition of five structural features which are all related to extensional tectonic processes (Fig. 12). They are described from 1 to 5 with increasing complexity due to increasing deformation development.

1. The simplest features are regular, vertical fractures (Fig. 13). Commonly the uppermost beds are bent down towards the vertical fracture, which demonstrates the extensional affiliation of the fractures. Such fractures are widespread. They are regarded as being responsible for seepage of gas from the subsurface, and they are expected to be abundant beneath the shadow zones created by gas-filled gyttja.

2. When the fractures are more widely spaced, subsidence of blocks by normal faulting has taken place within the vertical fractures (Fig. 14). The downthrown displacement is around 0.5–2 m. Due to the drag of the sediments at the top of the lakebeds, the blocks between the fractures appear as gently folded anticlines. These 'anticlines' are easily mapped and can be followed continuously from one seismic section to the next (Fig. 11).

3. A more complex feature is extensional normal listric faults with sub-lacustrine sliding of fault blocks (Fig. 15). This type of deformation is mainly related

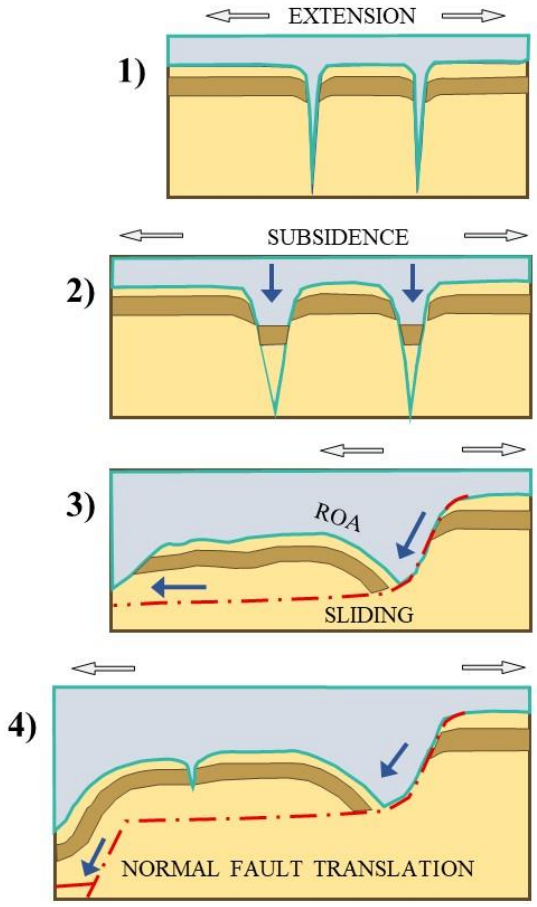

Fig. 12. Structural features related to the extension of the Esrum Sø basin. **1**: Simple extensional vertical fractures. **2**: Vertical extensional fractures with blocks subsided by normal faulting. **3**: Extensional listric fault with slumped fault block at margin-near area of the basin. Note the listric shape of the fault surface and the roll-over-anticline (ROA) at the tail end of the slide block. **4**: Slumped fault block extending into a slide block translated over a steeply dipping normal fault in the deeper part of the basin.

to the nearshore areas, especially in the eastern and north-eastern parts of the lake. Along the listric fault surfaces, roll-over-anticlines are weakly developed in the rear part of the translated blocks, and the sediments in the frontal part are irregularly folded in almost recumbent folds. It might be speculated that this feature could just be interpreted as a lake-slope slumping, but because of the more advanced feature described below, the relation to the extensional subsidence is evident.

4. The advanced stage of extensional, normal fault development is represented by translation of the slide block from the proximal listric fault escarpment and forward over a very shallowly dipping surface to a

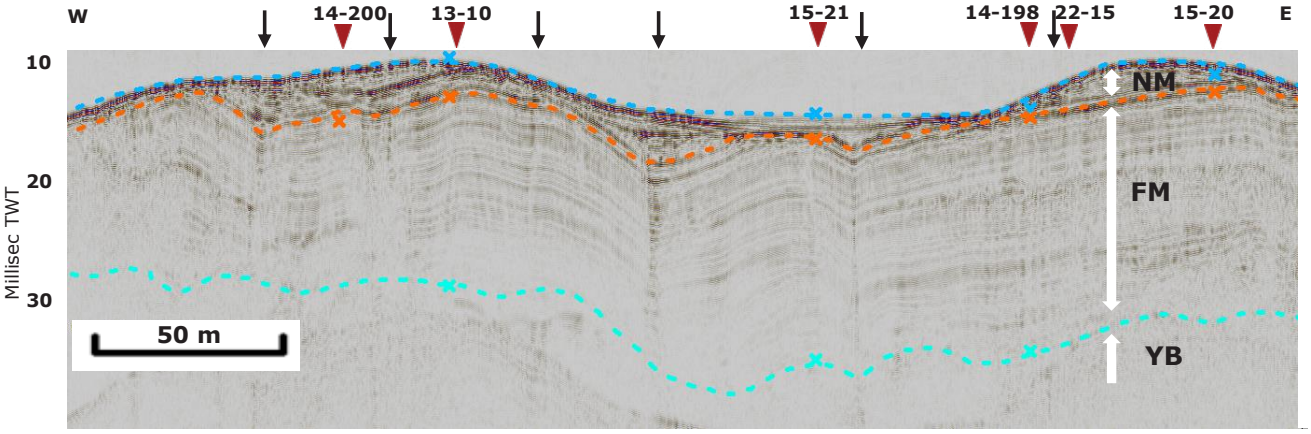

Fig. 13. Simple type 1 extensional fractures recorded in a seismic section from a relatively 'calm' area of the lake. Small black arrows indicate the position of selected fractures. Intersecting seismic sections are shown by red triangles with numbers. Abbreviations and coloured lines as in Figs 5–8. Reflectors showing the boundaries between the lake floor, NM, FM and YB are shown. Seismic section 14-214, vertical exaggeration ×5.

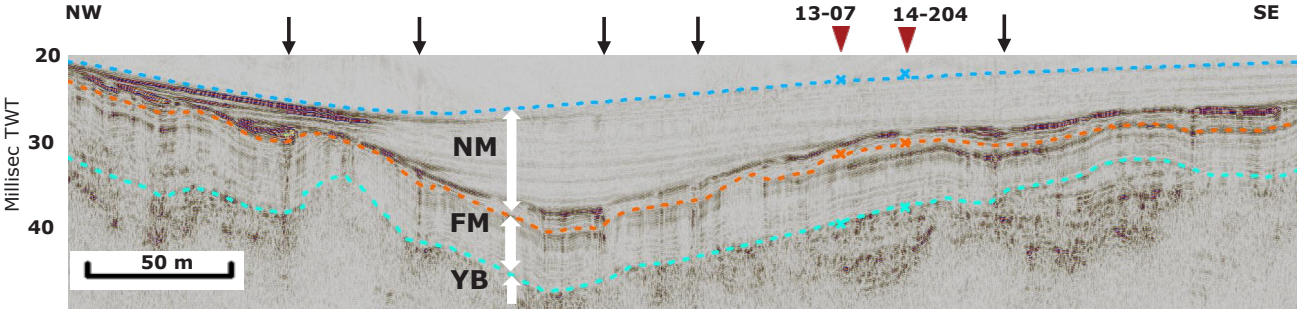

Fig. 14. Subsidence related to fracture features of type 2 recorded in a seismic section over a relatively flat lakebed. Note the sediments of seismic unit NM onlapping onto the rising ground to the left and right. Small black arrows indicate the position of selected type 2 fracture features. Intersecting seismic sections are shown by red triangles with numbers. Abbreviations and coloured lines as in Figs 5–8. Seismic section 15-20, vertical exaggeration ×5.

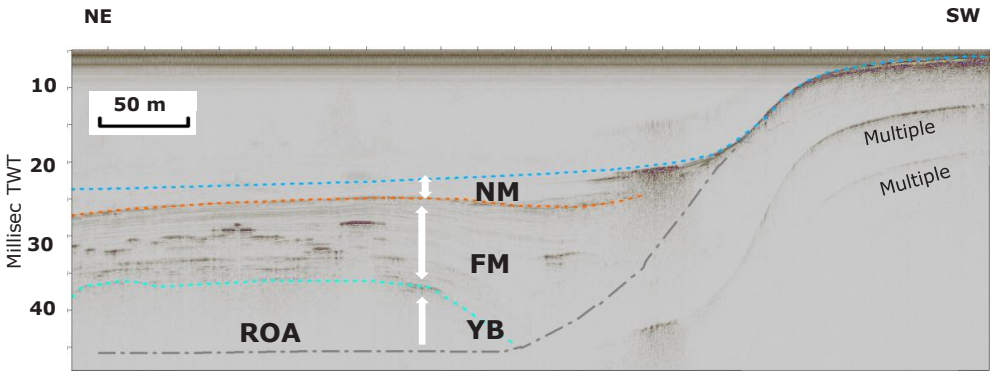

Fig. 15. Fracture feature type 3 comprises a listric fault surface and a related down-faulted block in whose tailing end a roll-over anticline (ROA) has developed. Abbreviations and coloured lines as in Figs 5–8. Seismic section 13-04, vertical exaggeration ×4.

hinge-bend over a steeply dipping normal fault in a more central part of the lake (Fig. 16). The structures in this feature can only be described in a dynamic context of progressively developing fault features and fault block displacement.

5. The progressive development of displacement along faults is furthermore illustrated in places where a part of an initial subsided block is preserved between two later developed extensional fractures (Fig. 17). In this situation the former subsided block is preserved

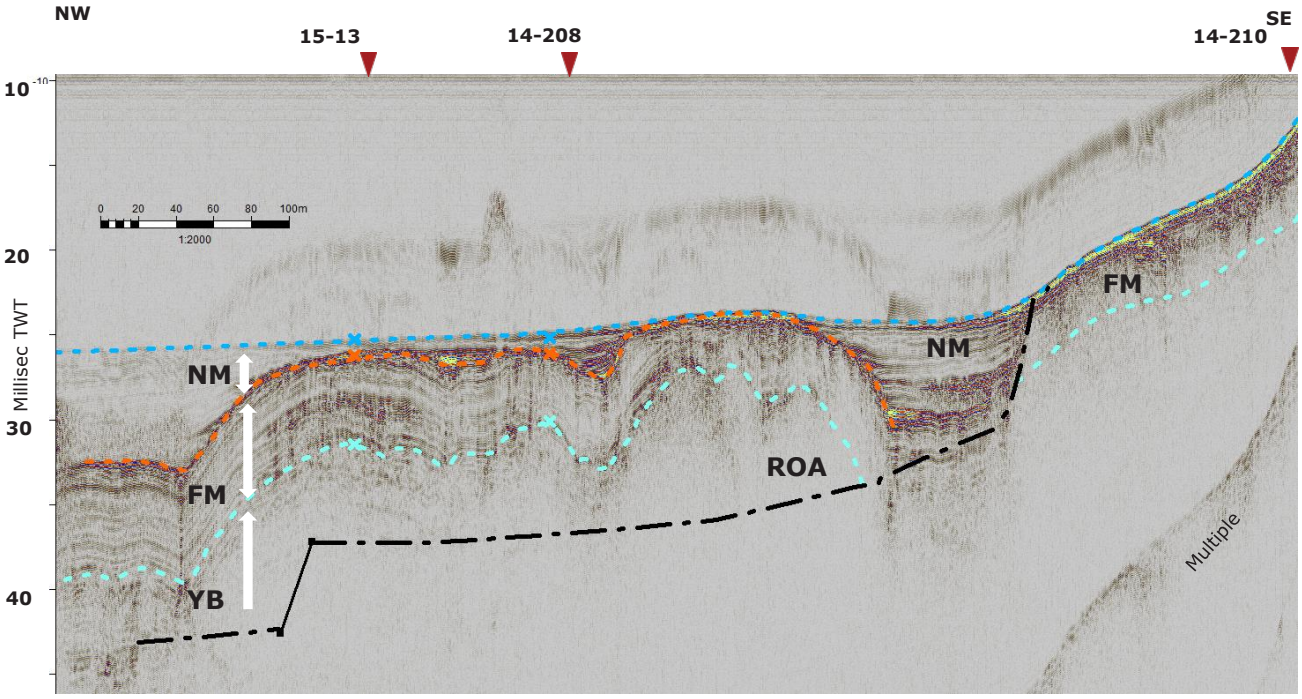

Fig. 16. Fracture feature type 4 is a further development of type 3. Here the slide block has been translated further into the basin and has passed an earlier normal fault in the subsurface, which has resulted in a monoclinal bend of the frontal part of the slide. Intersecting seismic sections are shown by red triangles with numbers. Abbreviations and coloured lines as in Figs 5–8. Seismic section 13-215, vertical exaggeration ×9.

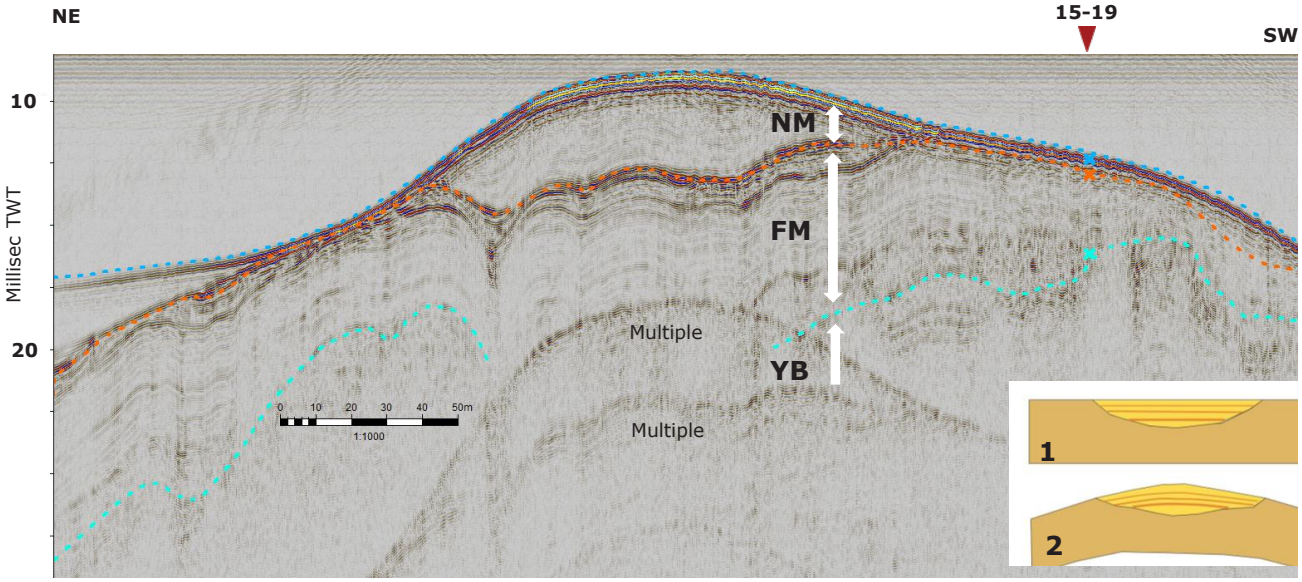

Fig. 17. Superimposed deformation is here illustrated by an early-formed fracture feature of type 2 with related synformal subsidence including syntectonic sedimentation (inset 1). At a proceeding stage, new fractures were formed along the sides of the structure, which led to a relative elevation of the feature into an antiformal crest (inset 2). Intersecting seismic sections are shown by red triangles with numbers. Abbreviations and coloured lines as in Figs 5–8. Seismic section 14-203 Vertical exaggeration ×7.

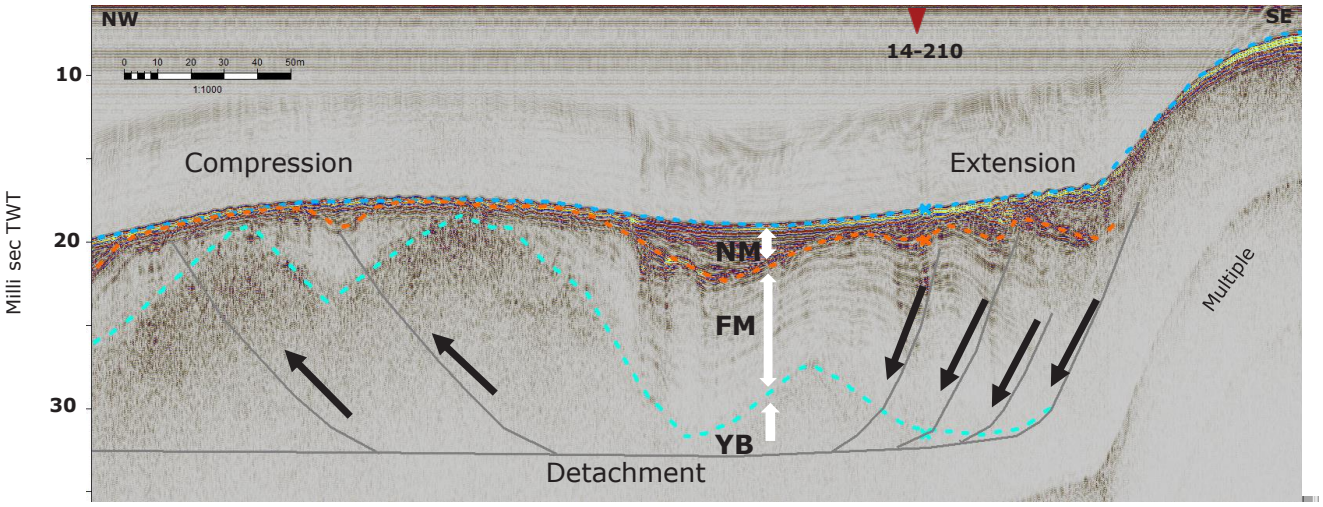

Fig. 18. Seismic section across a subaqueous landslide showing gravity-related slide features (Pedersen 1987). Seismic sections from lake Luzern in Switzerland show similar features (Schnellmann *et al.* 2005). An intersecting seismic section is shown by a red triangle, with number. Abbreviations and coloured lines as in Figs 5–8. Seismic section 15-21, vertical exaggeration ×5.

in the gentle anticline developed in the centre of a fault-bound block.

Gravitational slides are located in the north-eastern corner of the lake, where a number of subaqueous gravitational slides are seen, and among these we have outlined one in Fig. 11 which is marked with an escarpment signature. Another slide is shown in Fig. 18, which is a good example of gravitational gliding with imbricated fault blocks close to the head of slide and overturned folding at the toe.

Compilation of the structural map of Esrum Sø

All the seismic sections have been thoroughly interpreted in terms of mapping of the three seismic units and the occurrence of gas. From the seismic interpretation, all antiforms and synforms (depressions) have been assigned on the shotpoint map (Fig. 11). In areas with closely spaced seismic sections, the process of connecting the observed antiforms and synforms was started by comparing the structures on the intersecting and parallel profiles. The connection of structures was then extended gradually to cover the entire dataset. The structures were found to have an overall NNW–SSE orientation (Fig. 11).

The orientation of the structures was tested in a small area in the north-western corner of Esrum Sø (lines in Fig 1). Here, a number of closely spaced profiles was acquired in 2022 in a grid with a distance between the profiles of minimum 50 m to 100 m over an antiform. The interpreted structures were verified.

Tectonic model for the formation of the Esrum Sø depression

The tectonic model suggested for the formation of the Esrum Sø depression is based on two main evidences: the occurrence of the N–S trending parallel extensional fractures in the lake sediments, and the regional wrench-fault framework in north-eastern Sjælland demonstrated by e.g. Håkansson & Pedersen (1992).

The first evidence is summarised in the map compiled here by the interpretation of the seismic cross sections (Fig. 11). Although the mapping was impeded by the shadowing from the gas captured in the gyttja, trends of fractures are very clear: there is a main strike N–S and an additional twisting at the northern and southern ends towards a dextral drag of the fracture trends.

The second evidence includes the position of the two opposed end points on the two leading en échelon-arranged strike-slip faults south and north of the lake. The southern leading fault is interpreted to be the northern extension of the Carlsberg Fault Zone (Fig. 1). This end point is interpreted to be close to the village Nødebo. Unfortunately, the seismic section interpreted by Winsløw *et al.* (2020) stopped approximately 2 km north of Nødebo, but from the record of wells in the area, displacements of the top-Danian-limestone unconformity demonstrate offsets of up to 10 m downthrow to the NE. Furthermore, a marked topographic ridge parallel to the bank of the lake is located south-south-east of Nødebo, indicating a neotectonically induced topographic element.

The northern leading fault was indicated by

Winsløw *et al*. (2020) as their wrench-fault complex 6 (WFZ 6; for location of their six WFZs see Fig. 11). This is the northernmost negative flower structure covered by their seismic section, which ends just north of the northern lake bank. This wrench fault was interpreted to link up with faults branching up to the Grenå–Helsingborg Fault Zone in the Kattegat sea just north of the northern coastline of Sjælland (Fig. 1). There seems to be a good correlation between the orientation of wrench-fault zones 1, 4, 5, 6 and the trend of the tectonic features in the Nødebo Member, interpreted from the seismic sections. The correlation is less obvious for WFZ 2 and 3 due to the gas occurrences in the lake.

The concept for the model is a dextral, transtensional strike-slip displacement, which formed the depression gap between the two leading faults. In Fig. 19 the model is illustrated, and the transtension is indicated by the strain ellipse deformed by the simple shear between the two leading faults. The following tentative calculation of the strain rate is based on the magnitude of the extensional displacement relative to the area involved in the deformation, calculated with velocity of the displacement. The calculation of strain rate is adapted from Hobbs *et al*. (1976).

The average distance from the eastern to the western bank of the lake is about 2 km. With a distance of 5 km along a N–S strike, a simple figure of 10 km^2 is used for the area. A rough summation of the E–W extension amounts to 10 m. The time of deformation extends from the beginning of the Holocene into the Subtlantic, which is estimated to be about 5000 yr. From this, the strain rate is calculated to be in the order of 6×10^{-15} sec^{-1}. This strain-rate magnitude is in the order of common rock flow magnitudes and almost in the order of strain rates measured in the strike-slip field of the San Andreas Fault in California (Hobbs *et al*. 1976). Plate motion velocities in active mobile belts is 3–10 cm/yr, so the velocity of 0.2 cm/yr calculated for the Esrum Sø depression is pronouncedly less than in

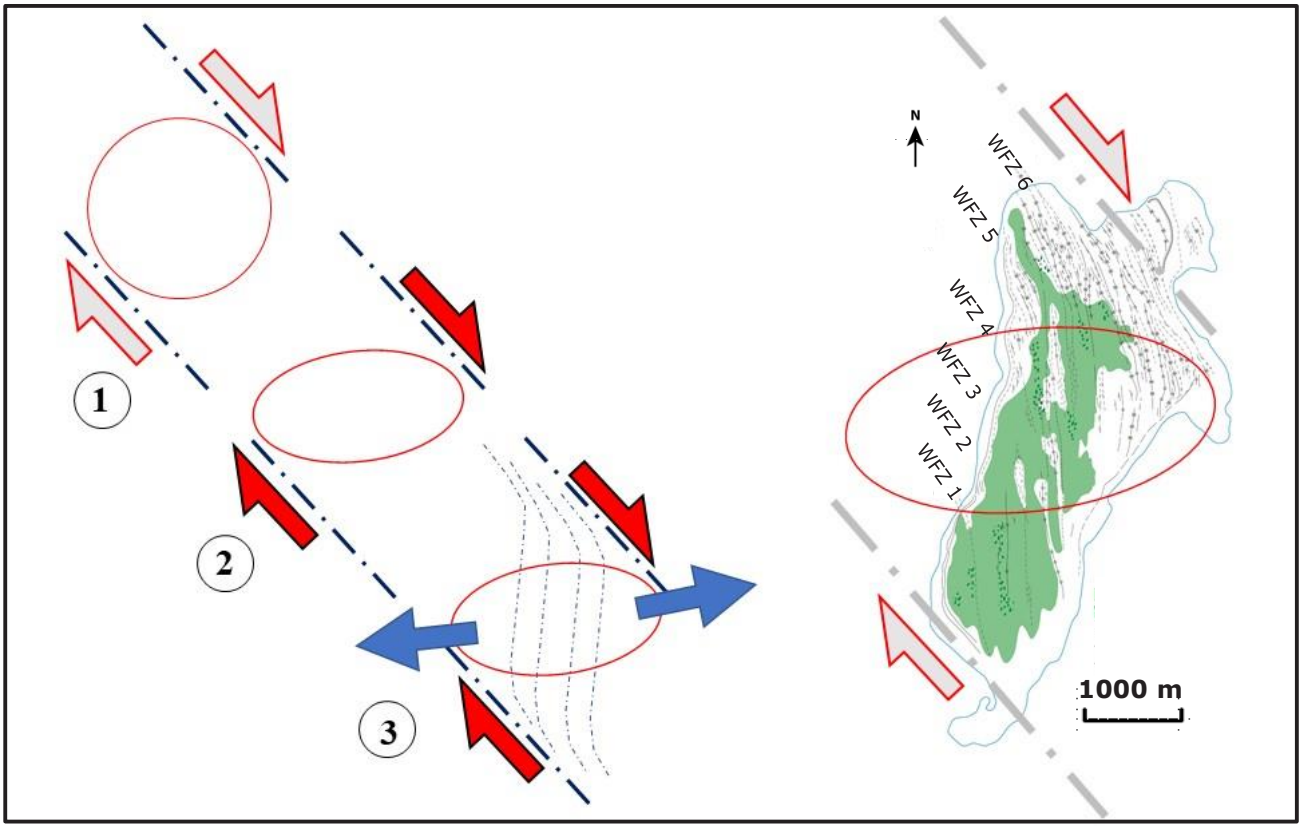

Fig. 19. Tectonic model for the formation of the Esrum Sø pull-part basin. The locations of the wrench-fault zones WFZ 1–6 from Winsløw *et al*. (2020) are marked on the map to the right. Esrum Sø is shown in the position of a pull-apart basin generated by dextral strike-slip wrench faulting. Sketches to the left: **1**: The location of two leading strike-slip faults trending SE–NW with an en échelon jump of the end of the southern fault to the northern fault termination. The circle illustrates the pre-deformational, unstrained situation. **2**: During the dextral strike-slip there is relative extension E–W, as illustrated by the strain ellipse. Note that the strain ellipse is not to scale but only serves to illustrate the extensional relationship to the wrenching. **3**: During the dextral wrenching the N–S striking extensional fractures develop. Note that the fractures are bent at the ends towards the orientation of the wrench faults.

mobile belts but corresponds well with calculation of displacement rates along the Grenå–Helsingborg Fault (0.3 cm/yr) in the upper Cretaceous succession (Kamla 2013). A rough estimate of the depression compared to the extension indicates a maximum subsidence of 30 m for the base level of the lake (top Fredensborg Member). This figure is reasonable compared to the water depth of 22 m and a stratigraphic thickness of 8 m. It cannot be argued that the eastern bank of the lake was separated from the western bank, but a concave depression had to be formed during the extension-created subsidence. One kind of feature formed during this formation of a morphological hole is sub-lake slides such as that shown in Fig. 18. Especially in the north-eastern corner of the lake we mapped several sub-lake slides with escarpments up along the slope to the lake bank, It is evident that the steeply dipping slopes along the lake border and the water-saturated sediments are easily subjected to mass-movement towards the lake bottom.

Discussion

Formation of calcareous gyttja and its relation to the gas seeps

The occurrence of calcareous gyttja in Late- and Postglacial lakes is well known in Denmark. The calcium in the gyttja is commonly considered to derive from the dissolution of limestone and chalk debris in the glacial deposits. The Ca^{++} in solution was transported to well oxygenated lakes, where the carbonate was precipitated and deposited together with suspended clay and organic matter (Noe-Nygaard & Heiberg 2001; Noe-Nygaard *et al.* 2017).

In Esrum Sø the formation of calcareous gyttja took place well into Postgalcial time (Fig. 3). The seismic sections demonstrate gas seepage reflections related to extensional fractures in the Fredensborg Member and gas-storage beds in the overlying Nødebo Member. From wells in the area between Esrum Sø and Søborg Sø Konradi & Laier (1991) reported gas concentrations, which were identified as sourced from the Eemian to Early Weichselian marine Skærumhede series. Therefore, we suggest that the seepage of methan-rich gasses from the extensional fractures stimulated the precipitation of the calcareous gyttja.

Models for the glaciodynamic settings of Esrum Sø

As described in the introduction, models for the formation of the Esrum Sø depression comprise a dead-ice hole (Whiteside 1970), a glaciotectonic hole in a hill-and-hole pair (Gravesen *et al.* 2017) and Lateglacial drainage erosion (Winsløv *et al.* 2020).

The dead-ice hole concept was suggested by Whiteside (1970), who compared the subarctic setting of Esrum Sø to similar Lateglacial lake settings in Canada. A dead-ice hole was normally formed where a block of ice was covered by outwash sediments from a retreating ice margin. When the ice block melted during the following warmer period, a hole was formed in the otherwise relatively planar surface. In the landscape around Esrum Sø there are no signs of a regular plateau intersected by holes. The landscape is an irregular glaciotectonic terrain with intercalations of moraine with hummocky topography.

The hill-and-hole pair concept originally introduced by Aber *et al.* (1989) was suggested by Gravesen *et al.* (2017) for the glaciodynamic setting of the area, where Esrum Sø is compared to the hole from where the material to form the hills in Gribskov has been provided. This glaciomorphological model was also supported by Winsløw *et al.* (2020), and it was regarded to be part of the landscape evolution although at the stage preceding the formation of the deep, N–S elongated Esrum Sø.

It may also be speculated that the lake, like several other elongated lakes in Denmark, is located in a former tunnel valley. However, an examination of the morphological environment adds no support for a tunnel valley formation. There are no clear valley boundaries which fit into an ice advance system, there is no outwash plain deposited either south or north of the elongated lake, and it is difficult to judge from which ice stream the tunnel valley could have formed.

Finally, it could be argued that the lake was part of a drainage system which spilled the meltwater from the central part of north-eastern Sjælland towards the Kattegat sea. This drainage system had to include Søborg Sø north of Esrum Sø. However, it is documented that there was no connection between Søborg Sø and Esrum Sø in the main part of the Postglacial time, as no marine incursions are found in Esrum Sø, while four marine, Postglacial transgressions are documented in Søborg Sø (Iversen 1937; Whiteside 1970; Noe-Nygaard 2017).

Neotectonic activity and the transtensional fault concept

Undoubtedly the area was affected by glaciodynamic processes, but the fracture features in the lake basin clearly suggest a deeper tectonic origin of the depression in Postglacial time. The depression in a wrench-fault setting is classified as a dextral pull-apart basin. This does not mean that the two N–S trending banks

were originally juxtaposed. But in a central zone between the two en échelon leading transtensional faults a relay ramp type of depression developed (Fig. 19). It is not the separation of the ramp slopes to the south-east and to the north-west which are important, but the subsidence of the blocks between the extensional fractures which creates the subsidence of the lake bottom.

The major subsidence of the lake basin took place in Boreal to Atlantic time, and we suggest that this is related to activity on the Sorgenfrei–Tornquist Zone in north-eastern Sjælland. Neotectonic activity along the northern segment of the STZ in northern Jylland (Brandes *et al.* 2018) took place in Allerød and Younger Dryas (14–12 ka) and at the end of the Saalian glaciation (130 ka) (Brandes *et al.* 2022). In southerly direction from Esrum Sø, Kammann *et al.* (2016) show neotectonic activity on seismic sections that extend almost to the surface, and they tentatively suggest that the Carlsberg Fault Zone continues northwards to the lake Furesø. Jensen *et al.* (2017) found pull-apart basins dated to be post Allerød (14 ka) from neotectonic activity offshore northern Bornholm. Thus a number of reports of neotectonic activity are related to the STZ. Other reports of such activity are concerned with structures in Jylland such as the Ringkøbing–Fyn High and the Tønder Graben system (e.g. Sandersen & Jørgensen 2022). The overall pattern of neotectonic activity in southern Scandinavia is still under construction.

Conclusions

A high-resolution seismic survey with 82 lines has been carried out in the lake Esrum Sø in north-eastern Sjælland, Denmark. The sediments investigated comprise a 10 m thick lacustrine formation, the Esrum Sø Formation, which is divided into two members, the lower Fredensborg Member and the upper Nødebo Member. The seismic interpretation is based on correlation between the Esrum Sø drill core and the seismic sections and has led to a total of 10 mapped reflectors in the lake. In large parts of the lake the occurrence of gas in the Nødebo Member degrades the seismic signals. The gas storage is recorded in at least three horizons, indicating a continuous gas seepage.

We suggest a three step evolution of Esrum Sø:

The Young Baltic till is the base of Esrum Sø and formed a small depression in the Postglacial landscape.

During the Bølling to Preboreal time there was a shallow fresh-water lake, where the Fredensborg Member, mainly consisting of Lateglacial lacustrine clay, was deposited horizontally with a constant thickness apart from areas where it onlaps towards the Young Baltic till. At the transition from the Fredensborg Member to the Nødebo Member a hiatus is present that comprises pollen zones IV, V, VI, VII and most of VIII.

In Boreal to Atlantic time the Nødebo Member, consisting of gyttja, was deposited in a syntectonic environment in the lake, where a number of anti- and synform structural features were developed with displacements along fault fractures. The faulting offset the Young Baltic till and the Frendensborg Member which was exposed to erosion at antiforms. The Nødebo Member is influenced by differential subsidence and has variable thickness with onlap towards the deformed boundary to the Fredensborg Member. The mapped faults are aligned parallel, and the fault pattern bends towards a NW direction.

The tectonic model for the subsiding extensional lake basin explains it as a pull-apart basin formed in a dextral, trans-tensional wrench fault setting. The pull-apart basin was created due to E–W extension between two leading SE–NW trending en échelon strike-slip faults located in the subsurface north and south of the lake, respectively. The leading SE–NW faults are parallel with and regarded as connected to the Sorgenfrei-Tornquist Zone.

The tectonic model is supported by our detailed seismic data and the drill core data. For future research we suggest drilling to 30 m depth below the lake floor to obtain further stratigraphic and lithologic information, and a TEM survey of the surrounding geomorphology, which could support the estimation of the fault traces that would be helpful in a renewed classification of the geomorphological environment of Esrum Sø.

Acknowledgement

We thank Peer Jørgensen, who served as technician acquiring the seismic data on all the surveys, and Paul Christiansen for support and boat driving. Lars Nielsen and Lotte Melchior Larsen are thanked for valuable comments on an earlier version of the manuscript. Michael Erlström is thanked for the contribution to Fig. 1. Thanks to an anonymous reviewer for comments on the manuscript.

References

Aber, J.S., Croot, D. & Fenton, M.M. 1989: Glaciotectonic Landforms and Structures; Glaciology and Quaternary Geology

Series Volume 5; Kluwer Academic Publishers: Dordrecht, The Netherlands, 200 pp. https://doi.org/10.1007/978-94-015-6841-8

Adrielsson, L. 1984: Weichselian lithostratigraphy and glacial environments in the Ven–Glumslöv area, Southern Sweden. Lund University, Department of Quaternary Geology. Lundqua Thesis 16, 120 pp.

Al Hseinat, M. & Hübscher, C. 2017: Late Cretaceous to recent tectonic evolution of the north German Basin and the transition zone to the Baltic shield/southwest Baltic Sea. Tectonophysics 708, 28–55. https://doi.org/10.1016/j.tecto.2017.04.021

Badley, M.E. 1985: Practical Seismic Interpretation. 1st edition. 1985: ISBN 0-934634-88-2.

Berg, K. 1938: Studies of the bottom animals in Esrum Lake. Det Kongelige Danske Videnskabernes Selskab Skrifter, Naturvidenskabelig og Mathematisk Afdeling, 9. Raekke, VIII. 1–255.

Brandes, C., Steffen, H., Sandersen, P.B.E., Wu, P. & Winsemann, J. 2018: Glacially induced faulting along the NW segment of the Sorgenfrei-Tornquist Zone, northern Denmark: implications for neotectonics and Lateglacial fault-bound basin formation. Quaternary Science Reviews 189, 149–168. https://doi.org/10.1016/j.quascirev.2018.03.036

Brandes, C., Polom, U., Winsemann, J. & Sandersen, P.B.E. 2022: The near-surface structure in the area of the Børglum fault, Sorgenfrei–Tornquist Zone, northern Denmark: Implications for fault kinematics, timing of fault activity and fault control on tunnel valley formation. Quaternary Science Reviews 289, 1–26. https://doi.org/10.1016/j.quascirev.2022.107619

Cukur, D., Krastel, S., Tomonaga, Y., Çagatay, M.N., Meydan, A.F. & The PaleoVan Science Team 2013: Seismic evidence of shallow gas from Lake Van, eastern Turkey. Marine and Petroleum Geology 48, 341–353. http://dx.doi.org/10.1016/j.marpetgeo.2013.08.017

Danmarks Miljøundersøgelser 2003: Vandrammedirektivet og danske søer. Faglig rapport fra DMU, nr. 476 2003, 68–72.

Danish Nature Agency 2022: Esrum Sø. Ministry of the Environment. https://naturstyrelsen.dk/naturoplevelser/naturguider/esrum-soe

Erlström, M., Boldreel, L.O., Lindström, S., Kristensen, L., Mathiesen, A., Andersen, M.S., Kamla, E. & Nielsen, L.H. 2018. Stratigraphy and geothermal assessment of Mesozoic sandstone reservoirs in the Øresund Basin – exemplified by well data and seismic profiles. Bulletin of the Geological Society of Denmark 66, 123–149. https://doi.org/10.37570/bgsd-2018-66-06.

Foged, N. 1968: Diatoméerme i en postglacial boreprøve fra bunden af Esrom Sø, Danmark. Meddelelser fra Dansk Geologisk Forening 18, 161–180 + 2 plates.

Gravesen, P., Binderup, M., Houmark-Nielsen, M. & Krüger, J. 2017: Geologisk Set – Sjælland og Øerne. Copenhagen, GO Forlag & Geocenter Danmark, 333 pp.

Håkansson, E. & Pedersen, S.A.S. 1992: Geologisk Kort over den Danske Undergrund 1: 500 000. Varv – Bladet med de ældste nyheder 1992(2), 60–63. https://tidsskrift.dk/varv/issue/view/10917/2178

Hansen, K. 1968: En boring i Esrum sø. Meddelelser fra Dansk Geologisk Forening 18, 244–246.

Hansen, K. 1981: Morfologisk-geologiske studier i Nordøst-Sjælland. Geografisk Tidsskrift 81, 1–10.

Hobbs, B.E., Means. W.D. & Williams, P.F. 1976: An Outline of Structural Geology. John Wiley & Sons, New York, 571 pp.

Houmark-Nielsen, M. 1987: Pleistocene stratigraphy and glacial history of the central part of Denmark. Bulletin Geological Society of Denmark 36, 1–189. https://doi.org/10.37570/bgsd-1988-36-01

Houmark-Nielsen, M. 2010: Extent, age and dynamics of Marine Isotope Stage 3 glaciations in the southwestern Baltic Basin. Boreas 39, 343–359. https://doi.org/10.1111/j.1502-3885.2009.00136.x

Houmark-Nielsen, M. & Kjær, K.H. 2003: Southwest Scandinavia, 40–15 ka BP: palaeogeography and environmental change. Journal of Quaternary Science 18, 769–786. https://doi.org/10.1002/jqs.802

Iversen, J. 1937: Undersøgelser over Litorinatransgressioner i Danmark. Meddelelser fra Dansk Geologisk Forening 9, 223–232.

Jakobsen, P.R., Wegmuller, U., Capes, R. & Pedersen, S.A.S. 2013: Terrain subsidence detected by satellite radar scanning of the Copenhagen area, Denmark, and its relation to the tectonic framework. Geological Survey of Denmark and Greenland Bulletin 28, 25–28. https://doi.org/10.34194/geusb.v28.4713

Jensen, J.B., Moros, M., Endler, R. & IODP Expedition 347 Members 2017: The Bornholm Basin, southern Scandinavia: a complex history from Late Cretaceous structural developments to recent sedimentation. Boreas 46, 3–17. https://doi.org/10.1111/bor.12194

Juhlin, C., Erlström, M. Lund, B. & Rosberg, J.-E. 2022: Seismic reflectivity, fracturing and stress field data from the FFC-1 exploratory geothermal project in SW Skåne, Sweden. Geothermics 105, 19 pp. https://doi.org/10.1016/j.geothermics.2022.102521

Kamla, E. 2013: Seismic mapping and structural analysis of an inversion fault complex, Kattegat, Denmark. Interpretation of structural development along the Grenå–Helsingborg Fault Zone from the Permian to Paleogene Period. Unpublished Master's thesis, University of Copenhagen, 88 pp.

Kamla, E., Boldreel, L.O. & Pedersen, S.A.S. 2014: Subsidence and inversion dynamics along the Grenå–Helsingborg Fault Zone during the Mesozoic tectonic development of southern Kattegat, Denmark. Poster presentation in: Geometry and Growth of Normal Faults, The Geological Society, London, 23–25 June 2014, abstract volume, 249–250.

Kammann, J., Hübscher, C., Boldreel, L.O., & Nielsen, L. 2016: High-resolution shear-wave seismics across the Carlsberg Fault zone south of Copenhagen – Implications for linking Mesozoic and late Pleistocene structures. Tectonophysics 682, 56–64. https://doi.org/10.1016/j.tecto.2016.05.043.

Konradi, P.B. 1992: De marine kvartære aflejringer i Esrumdalen. Dansk Geologisk Forening, Årsskrift for 1990–91, 111–115.

Konradi, P. & Laier, T. 1991: Grundvandskemi/groundwater chemistry. Methan i grundvandet. Danmarks Geologiske Undersøgelse, Årsberetning 1990, 47–49.

Lodolo, E., Baradello, L., Darbo, A., Caffau, M., Tassone, A., Lippai, H., Lodolo, A., Zorzi, G. De. &, Grossi, M. 2012: Occurrence of shallow gas in the easternmost Lago Fagnano (Tierra del Fuego). Near Surface Geophysics 2012, 10, 161–169. https://doi:10.3997/1873-0604.2011040

Mitchum, R.M, Vail, P.V. & Sangree, J.B. 1977: Seismic Stratigraphy and Global Changes of Sea Level, Part 6: Stratigraphic Interpretation of Seismic Reflection Patterns in Depositional Sequences. In: Payton, C. (ed.), Seismic Stratigraphy – application to hydrocarbon exploration. AAPG Memoir 26, 117–133. The American Association of Petroleum Geologists Tulsa, Oklahoma, U.S.A. https://doi.org/10.1306/M26490C8

Murphy, M.A. & Salvador, A. 1999: International Stratigraphic Guide – An abridged version. International Subcommission on Stratigraphic Classification of IUGS International Commission on Stratigraphy. Episodes 22(4), 255–271. https://doi.org/10.18814/epiiugs/1999/v22i4/002

Noe-Nygaard N. & Heiberg, E.O. 2001: Lake-level changes in the Late Weichselian Lake Tøvelde, Møn, Denmark: induced by changes in climate and base level. Palaeogeography, Palaeoclimatology, Palaeoecology 174, 351–382. https://doi.org/10.1016/s0031-0182(01)00315-7

Noe-Nygaard, N., Knudsen, K.L. & Houmark-Nielsen, M. 2017: Fra Istid til og med Jægerstenalder. In: Larsen, G. (ed.), Geologien. 3. udgave, 305–334. København: Gyldendal.

Pedersen, S.A.S. 1987: Comparative studies of gravity tectonics in Quaternary sediments and sedimentary rocks related to fold belts. In: Jones, M.E. & Preston, R.M.F. (eds), Sediment Deformation Mechanisms. Geological Society, London, Special Publications 29, 165–180. https://doi.org/10.1144/GSL.SP.1987.029.01.14

Pedersen, S.A.S. 2005: Structural analysis of the Rubjerg Knude Glaciotectonic Complex, Vendsyssel, northern Denmark. Geological Survey of Denmark and Greenland Bulletin 8, 1–192. https://doi.org/10.34194/geusb.v8.5253

Pedersen, S.A.S. & Gravesen, P. 2022: Descriptive text to the Geological map of Denmark, 1:50 000, Møn 1511 I, 1511 IV and 1512 II, GEUS Bulletin 48, 1–53 + inserted geological map. https://doi.org/10.34194/geusb.v48.8293 .

Sandersen, P.B.E. & Jørgensen, F. 2015: Neotectonic deformation of a Late Weichselian outwash plain by deglaciation-induced fault reactivation of a deep-seated graben structure. Boreas 44, 413–431. https://doi.org/10.1111/bor.12103

Sandersen, P.B.E. & Jørgensen, F. 2022: Tectonic impact on Pleistocene and Holocene erosional patterns in a formerly glaciated intra-plate area. Quaternary Science Reviews 293, 21 pp. https://doi.org/10.1016/j.quascirev.2022.107681

Sandersen, P.B.E, Gregersen, S. & Voss, P.H. 2021: Lateglacial and Postglacial Faulting in Denmark. In: Steffen, H., Olesen, O. & Sutinen, R. (eds), Glacially-Triggered Faulting, 263–282. Cambridge: Cambridge Un.iversity Press. https://doi.org/10.1017/9781108779906.020

Schnellmann, M., Anselmetti, F.S., Giardini, D. & McKenzie, J. 2005: Mass movement-induced fold-and-thrust belt structures in unconsolidated sediments in Lake Lucerne (Switzerland). Sedimentology 52, 271–289. https://doi.org/10.1111/j.1365-3091.2004.00694.x

Schuldt, J. 1981: Om Esrumdalens geologi. Dansk geologisk Forening, Årsskrift for 1980, 77–81.

Sorgenfrei, T. 1945: Træk af Alnarp Dalens geologiske Opbygning. Meddelelser fra Dansk Geologisk Forening (Bulletin of the Geological Society of Denmark) 10, 617–627.

Toker, M. & Tur, H. 2021: Shallow seismic characteristics and distribution of gas in lacustrine sediments at Lake Erçek, Eastern Anatolia, Turkey from high-resolution seismic data. Environmental Earth Sciences 80, 727, 23 pp. https://doi.org/10.1007/s12665-021-10039-4

Visnovitz, F., Bodnar, T., Toth, Zs., Spiess, V., Kudo, I., Timar, G. & Horvath, F. 2015: Seismic expressions of shallow gas in the lacustrine deposits of Lake Balaton, Hungary. Near Surface Geophysics 13(5), 433–446. https://doi:10.3997/1873-0604.2015026

Whiteside, M.C. 1970: Danish Chydorid Cladocera: Moderne Ecology and Core Studies. Ecological Monographs 40(1), 79–118. https://doi.org/10.2307/1942442

Winsløw, L.B., Pedersen, S.A.S., Boldreel, L.O. & Nørmark, E. 2020: Wrench-fault structures superimposed by glaciotectonic complexes, interpreted from high-resolution reflection-seismic sections and boreholes along the western bank of Esrum Sø, north-east Sjælland, Denmark. Bulletin of the Geological Society of Denmark 68, 171–193. https://doi.org/10.37570/bgsd-2020-68-08.

The cancellothyridid brachiopod *Terebratulina chrysalis* from the Selandian Kerteminde Marl at Gundstrup, Denmark

ANE ELISE SCHRØDER AND FINN SURLYK

Geological Society of Denmark
https://2dgf.dk

Received 29 May 2024
Accepted in revised form
14 June 2024
Published online
21 June 2024

Schrøder, A.E. & Surlyk, F. 2024. The cancellothyridid brachiopod *Terebratulina chrysalis* from the Selandian Kerteminde Marl at Gundstrup, Denmark. Bulletin of the Geological Society of Denmark, Vol. 73, pp. 89–98. ISSN 2245-7070. https://doi.org/10.37570/bgsd-2024-73-05

The articulate brachiopod *Terebratulina chrysalis* is very common in the Upper Cretaceous chalk of northern Europe and in the Danian chalk, bryozoan limestone and coralline-bryozoan limestone mounds of Denmark. It was one of the few brachiopod species that survived the mass extinction at the Cretaceous–Palaeogene boundary and it belongs to a long-lived group of closely related Cretaceous–Recent species. It represents a non-specialised generalist which with a rootlike pedicle was able to attach itself to a great variety of both hard and soft substrates. The great adaptability is probably the main reason for its evolutionary success. This is the first systematic study concerning brachiopods from the Kerteminde Marl Formation in Denmark. Hitherto *Terebratulina chrysalis* is the only known brachiopod from the Gundstrup blocks, referred to the Kerteminde Marl.

Keywords: Brachiopoda, rootlet pedicle, Cancellothyrididae, Paleocene, Gundstrup gravel pit.

Ane Elise Schrøder [aes@ign.ku.dk], Department of Geosciences and Natural Resource Management, University of Copenhagen, Øster Voldgade 10, 1350 Copenhagen K, Denmark; also Dipartimento di Scienze della Terra, Università degli Studi di Torino, Via Valperga Caluso 35, I-10125 Torino, Italy. https://orcid.org/0000-0001-9371-400X. Finn Surlyk [finns@ign.ku.dk], Department of Geosciences and Natural Resource Management, University of Copenhagen, Øster Voldgade 10, 1350 Copenhagen K, Denmark.

Terebratulina chrysalis (Schlotheim 1813) is one of the most abundant and widespread brachiopod species documented from the Upper Cretaceous chalk of northern Europe. It survived the mass extinction at the Cretaceous–Palaeogene boundary and is also common in the Danian bryozoan mounds at Stevns Klint and the coralline-bryozoan mound complex at Faxe, Denmark (e.g. Steinich 1965; Surlyk 1972; Surlyk & Birkelund 1977; Johansen 1987; Johansen & Surlyk 1990; Simon 1998, 2011; Bjerager & Surlyk 2007; Schrøder & Surlyk 2019, 2020).

Richly fossiliferous erratic blocks of silicified marlstone reworked from the lower Selandian (middle Paleocene) Kerteminde Marl Formation are abundant in the Gundstrup gravel pit, close to the north coast of Fyn, Denmark (Figs 1–3). The fauna includes foraminifers, sponges, bryozoans, brachiopods, molluscs – notably gastropods, cirripeds, annelids, decapod crustaceans, echinoderms, and vertebrates (e.g. elasmobranchs, turtles and birds), but only a few systematic studies relating to certain orders have been conducted (e.g. Schnetler & Nielsen 2018; Myrvold *et al*. 2018; Schwarzhans *et al.* 2021; Vallon & Rindsberg 2022). The brachiopods from the Kerteminde Marl are one of the groups that remains to be systematically treated.

The aim of this paper is to describe and document the presence of *Terebratulina chrysalis* from the lower Selandian Kerteminde Marl Formation of Denmark.

Geological setting and stratigraphy

The type locality of the lower Selandian Kerteminde Marl Formation is situated in the coastal cliff

Lundsgaard Klint, immediately south of Kerteminde close to the north coast of the Danish island of Fyn (Fig. 1; Gry 1935; Sorgenfrei 1957; Dinesen *et al*. 1977). The Gundstrup gravel pit is situated approx. 26 km to the north-west of Lundsgaard Klint and 18 km north of the city of Odense (Figs 1–3). The gravel pit is occasionally also referred as 'Gundstrup (Alex Andersen) Grusgrav' (Lindow 2022a, b). Abundant glaciofluvially transported, erratic boulders found in the gravel pit are derived from the Kerteminde Marl (Fig. 2).

A major eustatic sea-level fall took place at the end of the Danian and large areas of Denmark became emerged and were subject of erosion. This was accompanied by a stop in carbonate deposition and succeeded by a sea-level rise, resulting in flooding of the Danish area (Clemmensen & Thomsen 2005). Deposition changed from chalk and calcisiltite to the Lellinge Greensand Formation in shallower, coastal waters and the Kerteminde Marl Formation in deeper more offshore regions. The marl was deposited in the earliest Selandian (Gry 1935; Thomsen & Heilmann-Clausen 1985; Heilmann-Clausen 1995; Clemmensen & Thomsen 2005; King *et al*. 2016) in nannofossil zones NP5 (Martini 1971) or S1 + S2 (Perch-Nielsen 1979).

Uplift of the Sorgenfrei–Tornquist Zone in the Kattegat sea NE of Fyn (Fig. 1) resulted in exposure and

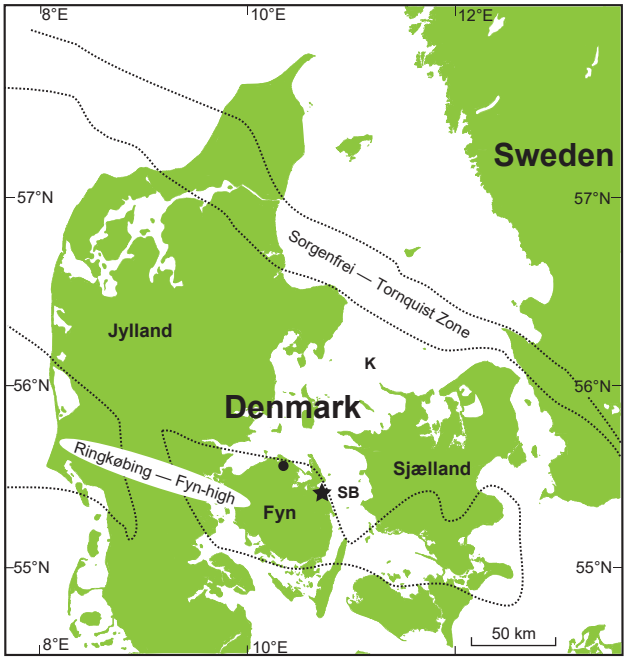

Fig. 1. Map of Denmark showing the main structural features of the Danish Basin at the time of deposition of the Kerteminde Marl Formation (based on figures 1 and 5c in Clemmensen & Thomsen 2005). The position of the Gundstrup gravel pit (55.566°N, 10.353°E) is indicated by a black dot and the type locality of the Kerteminde Marl Formation with a star. K: the Kattegat sea; SB: the Storebælt strait.

erosion of thick layers of Upper Cretaceous chalk. The Kerteminde Marl is thus composed of about equal amounts of clay and reworked chalk derived from erosion of the uplifted Sorgenfrei–Tornquist Zone and deposition is estimated to have taken place in water depths of about 100–150 m (Clemmensen & Thomsen 2005).

The source of the Gundstrup blocks is somewhat enigmatic, but important clues come from the work of fossil hunters Peter Tang Mortensen and colleagues together with geophysical mapping in the northern part of Fyn, where several buried tunnel valleys have been found (Fig. 3) (Sandersen & Jørgensen 2016). The blocks are mainly pebbles and cobbles with only rare boulders. We have used the term block throughout because this is how they are referred to among the fossil hunters. The blocks are all derived from the deeper water-filled parts of the quarry and not from the exposed glacio-fluvial sands (Peter Tang Mortensen and Søren Skibsted, pers. comm. 2024). The blocks are relatively vulnerable to erosion and seem to be restricted to the infill of a system of buried valleys orientated ENE–WSW (see Sandersen & Jørgensen 2016). The blocks could therefore originate from the deep eroded parts of the valleys and afterwards probably transported rather short distances toward WSW within the valley and thus been protected from later glacial reworking. The valley infill is interpreted to relate to an ice advance from ENE (Sandersen & Jørgensen 2016) – presumably the late Weichselian Northeast Ice advance (20–19 ka ago; cf. Houmark-Nielsen 2011, 2021). The source area of the blocks may thus be tentatively identified as an area covering the northern part of the Storebælt strait and southern Kattegat north-east of the island of Fyn. Interestingly, the only offshore locality where the blocks are very common is at Tørresø (more than 40% of all mined blocks in that area) in direct continuation of the buried valley complex in northern Fyn below the Gundstrup gravel pit (Peter Tang Mortensen, pers. comm. 2024). The position of Tørresø submarine gravel extraction area is indicated by a black circle in Fig. 3 in the southernmost part of the Kattegat sea.

The blocks were probably derived from the lowermost part of the Kerteminde Marl, which appears to represent a transitional facies to the lowermost Selandian Lellinge Greensand. This fits well with the results of nannofossil analysis of the blocks, which has given an age corresponding to the lower part of the Lellinge Greensand and the correlative lowermost Kerteminde Marl (Clemmensen & Thomsen 2005). The Lellinge Greensand in cores from Storebælt show a number of silicified layers just like the silicified Gundstrup blocks (Clemmensen & Thomsen 2005, fig. 3). These layers correspond to biofacies 3 of Clem-

mensen & Thomsen (2005), which they interpreted as deposited in a shallow, transgressive sea close to wave base corresponding well with the environmental interpretation of the blocks based on the rich fauna and lithology.

Material

The material forming the basis of the present study was collected by Mette Hofstedt, Peter Tang Mortensen and Mogens Stentoft Nielsen at Gundstrup gravel pit,

Fig. 2. Photographs of the Gundstrup gravel pit. **A,** Overview of the pit seen from the south. The exposed glacio-fluvial sands do not contain any blocks of Kerteminde Marl. The blocks are quarried from the deepest, water-covered parts of the quarry. **B,** Fossil hunting in blocks of Kerteminde Marl. **C**: Peter Tang Mortensen, standing with a boulder of silicified Kerteminde Marl.

Fyn, Denmark in 2023. The specimens are preserved in blocks of slightly silicified marl, the so-called 'Gundstrupblokke' (Heilmann-Clausen & Surlyk 2017). The five specimens were declared Danekræ fossil trove in May 2024. The fossil trove legislation unique to Denmark, covers fossils, meteorites or rare minerals with special exhibition or scientific value. Objects that have been declared fossil trove belong to the Danish state (Christensen & Hald 1990).

The five specimens available for the descriptions presented here are all nested within the same Danekræ collection number, DK-1271. They include five specimen preserved in four individual pieces of marlstone (Fig. 4): 1) NHMD-1758095a (DK-1271), a well-preserved articulated specimen, preserved with the dorsal valve facing outwards (Fig. 4A); 2) NHMD-1758095b (DK-1271), a dorsal valve with the exterior surface of the valve facing outwards (Fig. 4B); 3) NHMD-1758095c (DK-1271), a dorsal valve with the interior part of the valve facing outwards (Fig. 4C); 4) NHMD-1758095d (DK-1271) and NHMD-1758095e (DK-1271), two ventral valves preserved on each side of the same piece of marlstone, with the internal surfaces facing outwards (Figs 4D–E). The specimens are housed in the collections of the Natural History Museum of Denmark.

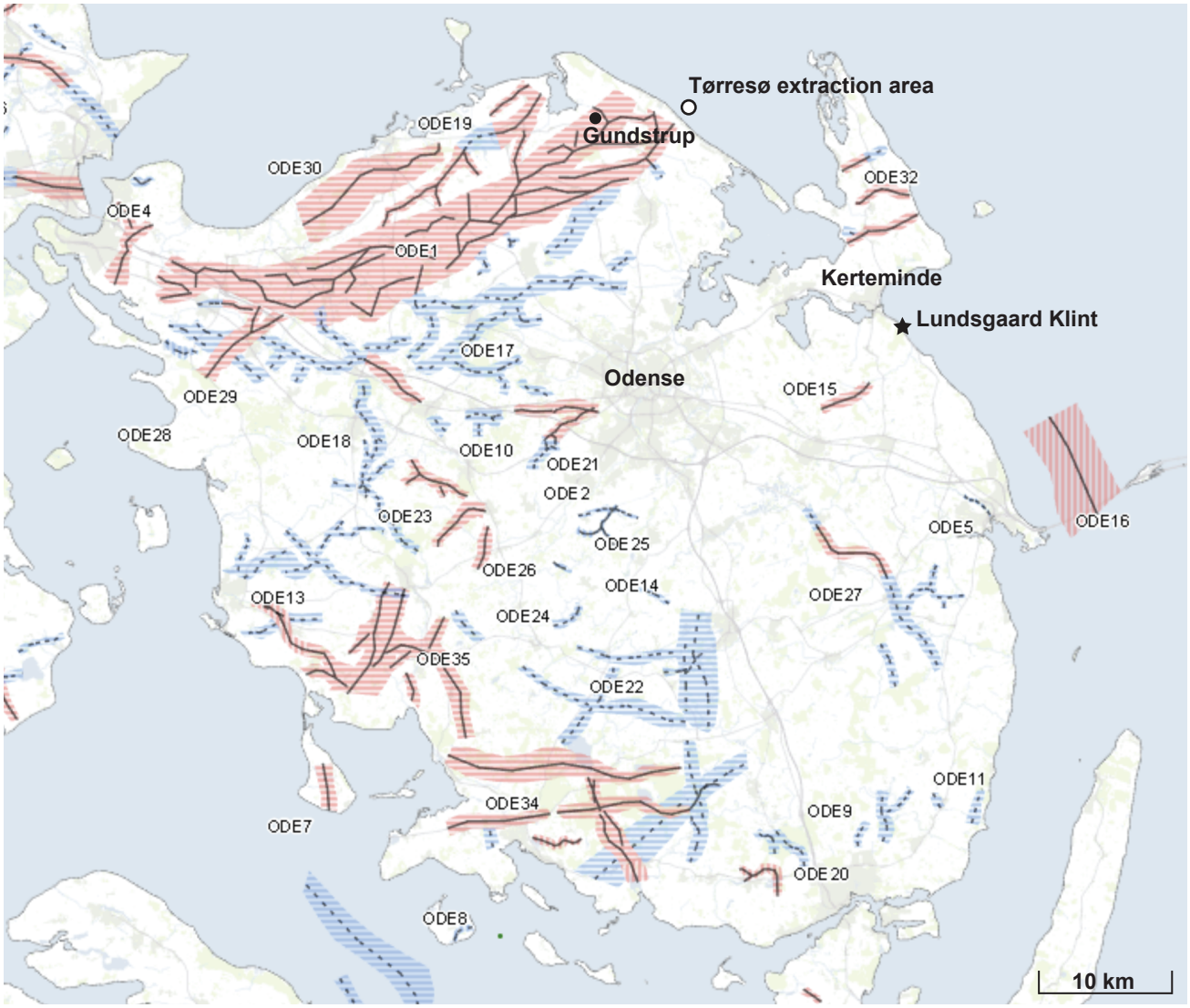

Fig. 3. Map showing the buried Weichselian tunnel valley complex in the northern part of Fyn. A submarine gravel extraction area, approximately 2.5 km north of the small city of Tørresø, is marked by a circle. Note that the Gundstrup gravel pit, indicated by a black dot, is situated above a major WSW–ENE orientated buried valley formed during the advance of the Northeast ice stream (20–19 ka ago). Modified from Sandersen & Jørgensen (2016).

Fig. 4. *Terebratulina chrysalis* from blocks of Selandian Kerteminde Marl. **A,** a well-preserved articulate specimen in a nodule of silicified marl, with the dorsal valve facing outwards NHMD- 1758095a (DK-1271). **B,** a dorsal valve preserved with the exterior surface projecting outwards, NHMD-1758095b (DK-1271). **C,** a dorsal valve with the interior surface of the valve facing outwards, NHMD-1758095c (DK-1271). **D,** 1758095d (DK-1271), ventral valve with the inner surface showing. **E,** 1758095e (DK-1271), the largest specimen, a ventral valve, with the internal surface exposed. The two ventral valves are preserved on each side of the same nodule of silicified marl. Scale bar = 5 mm applies to all.

Institutional Abbreviations

DK, acronym for specimens declared Danekræ fossil trove, and housed in the Danekræ collection of the Natural History Museum of Denmark; **NHMD**, acronym for specimens housed in the collections of the Natural History Museum of Denmark.

Systematic palaeontology

Phylum Brachiopoda Duméril, 1805

Subphylum Rhynchonelliformea Williams, Carlson, Brunton, Holmer & Popov 1996

Class Rhynchonellata Williams, Carlson, Brunton, Holmer & Popov 1996

Order Terebratulida Waagen, 1883

Suborder Terebratulidina Waagen, 1883

Superfamily Cancellothyridoidea Thomson, 1926

Family Cancellothyrididae Thomson, 1926

Subfamily Cancellothyridinae Thomson, 1926

Genus Terebratulina d'Orbigny, 1847

***Terebratulina chrysalis* (Schlotheim, 1813)**
(Fig. 4)

1798 *Térébratules Fossiles*: Faujas de Saint-Fond, pl. XXVI, fig. 9.
1813 *Terebratulites chrysalis*, Schlotheim: Schlotheim, p. 113.
1820 *Terebratulites chrysalis*, Schlotheim: Schlotheim, p. 272.
1834 *Terebratula chrysalis*, Schlotheim: Buch, p. 62.
1841 *Terebratula striatula*, Mantell: Roemer, p. 39, p. 144.
1841 *Terebratula chrysalis*, v. Sehl: Roemer: p. 40, p. 145.
1842 *Terebratula striatula*, Mantell: Hagenow, p. 538.
1847 *Terebratulina striata*, d'Orbigny: d'Orbigny, p. 65.
1909 *Terebratulina striata*, Wahlenberg: Nielsen, p. 159, pl. I, figs 28–32.
1965 *Terebratulina chrysalis* (Schlotheim, 1813): Steinich, p. 53, text-figs 44–61; pl. VIII, fig. 1 a–d; pl. IX, figs. 1–5, 9a, b, 10a, b.
1968 *Terebratulina chrysalis* (Schlotheim, 1813): Popiel-Barczyk, p. 63, pl. XVII, figs 1–3, text-fig. 25.
1972 *Terebratulina chrysalis* (Schlotheim, 1813): Surlyk, p. 21, pl. 4, fig. 5–8, text-figs 12–18.
1979 *Terebratulina chrysalis* (Schlotheim): Bitner & Pisera, p. 73, pl. 3, figs 12–15.
1987 *Terebratulina chrysalis* (Schlotheim, 1813): Johansen, p. 14, pl. 4, figs 1–5, text-figs 14 A–D.
1988 *Terebratulina chrysalis* (Schlotheim, 1813): Johansen, p. 11, figs 7–10.
1989a *Terebratulina chrysalis* (Schlotheim, 1813): Johansen, p. 170, 187, 197–198, tab. 2, figs 23, 37.
1989b *Terebratulina chrysalis* (Schlotheim, 1813): Johansen, p. 246, Fig. 2.
1989 *Terebratulina chrysalis* (Schlotheim, 1813): Popiel-Barczyk, p. 248, pl. CL, fig. 5.
1990 *Terebratulina chrysalis* (Schlotheim, 1813): Johansen & Surlyk, p. 841, pl. 3, figs 1–5.
1990 *Terebratulina chrysalis* (Schlotheim, 1813): Muñoz, p. 67, 76, pl. 2, fig. 1.
1992 *Terebratulina chrysalis* (Schlotheim, 1813): Popiel-Barczyk, p. 27.
1995 *Terebratulina chrysalis* (Schlotheim, 1813): Simon, p. 11.
1998 *Terebratulina chrysalis* (Schlotheim, 1813): Simon, p. 200–201, tab. 1, text-fig. 5, pl. 5, figs 4, 5a–b, 6a–f.
2000 *Terebratulina chrysalis* (Schlotheim, 1813): Simon, tab. 1, text-fig. 5, pl. 1, figs 5a–c, 6a–d, 7, pl. 2, figs 1, 2a–b, 3a–b, 7.
2011 *Terebratulina chrysalis* (Schlotheim, 1813): Simon, text-figs 1–9.
2016 *Terebratulina chrysalis* (Schlotheim, 1813): Engelke *et al*., p. 679, text-fig. 5I1–3.
2019 *Terebratulina chrysalis* (von Schlotheim, 1813): Schrøder & Surlyk, p. 3, 5–8, 10–12, tab. 1–4, figs 3, 4, 6, 8.
2020 *Terebratulina chrysalis* (von Schlotheim, 1813): Schrøder & Surlyk, p. 9–10, 12–13, fig. 9–10, tab. 1.

For a more detailed synonymy see Steinich (1965), Johansen (1987) and Simon (1998).

Material. Five specimens collected from pieces of slightly silicified marlstone from Gundstrup gravel pit. The samples are housed in the collections of the Natural History Museum of Denmark, Copenhagen University.

Stratigraphical range. Upper Campanian – lower Selandian.

Occurrence. *Terebratulina chrysalis* (Schlotheim 1813) is well-known and abundant in the Upper Cretaceous chalk of northern Europe and Danian bryozoan mounds at Stevns Klint and the coralline-bryozoan mound complex at Faxe, Denmark.

Amended diagnosis. Medium-sized; elongate oval to subpentagonal in outline; longer than wide; maximum width slightly anterior to the mid-valve; thin-shelled; flattened ventribiconvex; shell surface costellate with visible growth lines; costellae ornamented with prominent nodules; anterior commissure intermediate between rectimarginate and slightly uniplicate. Beak suberect to erect. Foramen subtriangular to submesothyrid; auricles reduced, and pedicle collar not preserved; deltidial plates triangular and disjunct; brachidium incomplete with only the anterior part of short, stout crura preserved; crural bases fused to inner socket ridges; both inner and outer socket ridges relatively shallow; cardinal process small and ellipsoid.

Description

External morphology. Medium-sized, the largest shell reaching a length of 25.7 mm measured on largest specimen, a ventral valve. Elongate oval to subpentagonal in outline. Relatively thin-shelled. Longer than wide, with the maximum width slightly anterior to the midline of the valves. Flattened ventribiconvex. Shell surface costellate with 41–60 ribs. Up to five prominent growth lines are visible on the dorsal valves. The costellae are ornamented with prominent nodules, most conspicuous close to the anterior margin; ribs are formed by intercalation resulting in an increasing number of costellae towards the margins of the valves. The anterior commissure is rectimarginate to slightly uniplicate. The beak is suberect to erect. The foramen is intermediate between subtriangular and submesothyrid. The auricles are reduced, and the pedicle collar is not preserved in the articulate specimen. The deltidial plates are small, triangular in outline and disjunct.

Internal morphology. The posterior part of the two ventral valves, including their hinge teeth, (NHMD-1758095d, NHMD-1758095e) are not preserved. The remaining part of the valves are smooth, with visible deflection of the costellae. The dorsal valves are also characterized by deflection of the costellae. The brachidium is incompletely preserved with only the posterior part of short, stout crura present. The crural bases are fused to the inner socket ridges. The inner and outer socket ridges are relatively shallow. The cardinal process is small and ellipsoid in outline.

Remarks. The shells are relatively large compared to most specimens, which predominately comprise juvenile individuals, obtained by washing of bulk samples from Cretaceous chalk localities of northern Europe (Surlyk 1972, 1982, 1984), but relatively large, adult individuals have also been described from the Netherlands (Simon 2000, 2011), Rügen (Steinich 1965), and from the Danian bryozoan mounds at Stevns Klint and the coral-bryozoan mound complex at Faxe, Denmark (Bjerager & Surlyk 2007; Schrøder & Surlyk 2019). The five specimens described here appear slightly more robust in terms of shell thickness but can otherwise not be separated morphologically from *Terebratulina chrysalis* from the Danish chalk. The flattened ventribiconvex shape of the articulate specimen (NHMD-1758095a, Fig. 4A) probably reflects flattening by compaction in the soft marl, analogously to flattened individuals of *T. chrysalis* from the soft Maastrichtian chalk (Surlyk 1972; Schrøder *et al*. 2018).

Discussion

The Gundstrup blocks contain an extremely diverse fauna. In addition to the very common gastropods and bivalves described in an impressive monograph by Schnetler & Nielsen (2018), other faunal elements include foraminifers, sponges, anthozoans, serpulids, decapods, cirripedes, bryozoans, brachiopods, asteroids, ophiuroids, crinoids, echinoids, chelonids, ganoids, sharks and even birds (Schnetler & Nielsen 2018; Myrvold *et al*. 2018; Vallon *et al*. 2020).

The brachiopod *Terebratulina chrysalis* is well-known from a variety of different environments in the Late Cretaceous – Danian Chalk Sea of northern Europe. These data have mainly been obtained by investigations based on washing of large bulk samples (Surlyk 1972, 1982, 1984; Johansen 1987; Johansen & Surlyk 1990; Simon 2011). The Selandian specimens from Gundstrup gravel pit were, however, hand-collected from ice-rafted erratic blocks. So far, *T. chrysalis* is the only known brachiopod from the Gundstrup blocks of Kerteminde Marl.

Terebratulina chrysalis is the most abundant brachiopod species of the Maastrichtian–Danian soft-bottom chalk of Denmark and second most abundant of the Danian bryozoan mounds at Stevns Klint and the bryozoan-coral mound complex at Faxe (Surlyk 1972; Bjerager & Surlyk 2007; Schrøder & Surlyk 2019, 2020). It survived the Cretaceous–Palaeogene boundary and was one of the main generalist species of the Chalk Sea able to adapt to, and thrive, in markedly different environments. A close, possibly even conspecific ecotype, *T. striata* is thus well known from the late

early Campanian rocky shore at Ivö Klack in NW Skåne, southern Sweden (Schrøder *et al*. 2018). The success of *T. chrysalis* was probably related to the morphology of the pedicle, interpreted to have been split into a bundle of rootlets, proximally or distally, similar to its extant relatives *T. retusa* (Linnaeus 1758), *T. septentrionalis* (Couthouy 1838), *T. japonica* (Sowerby 1846) and *T. austroamericana* Zezina, 1981, making it able to attach itself to a variety of available substrates on the sea floor, including soft sediment, invertebrate shells of all sizes and rock walls (Surlyk 1972, Curry 1981, 1982). It is therefore not surprising that it was also able to adapt to the fine-grained marly marine seafloor of the early Selandian neritic sea of the Kerteminde Marl.

It is a remarkable example of a 'living fossil'. The extant relative *T. retusa*, the most common brachiopod species in British and Norwegian deeper waters has likewise been recorded from a variety of mainly deep-water substrates including vertical rock wall and attachment to gravels, bivalves and deep-water coral mounds.

Acknowledgements

AES wishes to thank for access to camera setups at the Zoological Museum, the Natural History Museum of Denmark, Copenhagen University. We cordially thank Bent Erik Kramer Lindow for digitizing and assigning collection numbers to the five specimens after they were declared Danekræ fossil trove. AES and FS acknowledge office space and access to other equipment at the Department of Geosciences and Natural Resource Management, University of Copenhagen. We are grateful to Søren Skibsted for discussion and very useful information on the geology of the Gundstrup gravel pit and to the fossil hunters Mette Hofstedt, Peter Tang Mortensen and Mogens Stentoft Nielsen. We thank Claus Heilmann-Clausen, Michael Houmark-Nielsen and Peder Sandersen for information and valuable discussion. Special thanks are directed to Peter Tang Mortensen for useful comments on the occurrence and possible source of the Gundstrup blocks. Journal reviewers Alfréd Dulai and Anne Mehlin Sørensen are thanked for useful comments.

References

Bitner, M.A. & Pisera, A. 1979: Brachiopods from the Upper Cretaceous chalk of Mielnik (eastern Poland). Acta Geologica Polonica 29 (1), 67–88.

Bjerager, M. & Surlyk, F. 2007: Benthic palaeoecology of Danian deep-shelf bryozoan mounds in the Danish Basin. Palaeogeography, Palaeoclimatology, Palaeoecology 250, 184–215. https://doi.org/10.1016/j.palaeo.2007.03.008

Buch, L. von. 1834: Über Terebrateln, mit einem Versuch, sie zu classificiren und zu beschreiben. Gedruckt in der Druckerei der Königlichen Akademie der Wissenschaften, 124 pp.

Christensen, E. F. & Hald, N. 1990: Danekræ – a new concept in Danish Museum legislation. Arkæologiske Udgravninger i Danmark 1990, 7–16.

Clemmensen, A. & Thomsen, E. 2005: Palaeoenvironmental changes across the Danian–Selandian boundary in the North Sea Basin. Palaeogeography, Palaeoclimatology, Palaeoecology 219, 351–394. https://doi.org/10.1016/j.palaeo.2005.01.005

Couthouy, J.P. 1838: Descriptions of new species of Mollusca and shells, and remarks on several Polypii, found in Massachusetts Bay. Boston Journal of Natural History 2, 53–111.

Curry, G.B. 1981: Variable pedicle morphology in a population of the Recent brachiopod *Terebratulina septentrionalis*. Lethaia 14, 9–20. https://doi.org/10.1111/j.1502-3931.1981.tb01068.x

Curry, G.B. 1982: Ecology and population structure of the recent brachiopod *Terebratulina* from Scotland. Palaeontology 25, 227–246.

Dinesen, A., Michelsen, O. & Lieberkind, K. 1977: A survey of the Paleocene and Eocene deposits of Jylland and Fyn. Geological Survey of Denmark, Series B, No. 1, 1–15. https://doi.org/10.34194/serieb.v1.7056

Duméril, A.M.C. 1805: Zoologie analytique ou méthode naturelle de classification des animaux, 344 pp. Paris: Allais.

Engelke, J., Esser, K.J.K., Linnert, C., Mutterlose, J. & Wilmsen, M. 2016: The benthic macrofauna from the Lower Maastrichtian chalk of Kronsmoor (northern Germany, Saturn quarry): Taxonomic outline and palaeoecologic implications. Acta Geologica Polonica 66, 671–694. https://doi.org/10.1515/agp-2016-0036

Faujas de Saint-Fond, B. 1798: Histoire naturelle de la Montagne de St-.Pierre de Maestricht, 263 pp. Paris: J. Jansen. https://doi.org/10.5962/bhl.title.169047

Gry, H. 1935: Petrology of the Paleocene sedimentary rocks of Danmark. Danmarks Geologiske Undersøgelser II Række, 61, 171 pp. https://doi.org/10.34194/raekke2.v61.6849

Hagenow, F. von. 1842: Monographie der Rügen'schen Kreide-Versteinerungen III. Abteilung: Mollusken. Neues Jahrbuch für Mineralogie, Geognosie, Geologie, und Petrefakten-Kunde 1842, 528–579.

Heilmann-Clausen, C. 1995: Palæogene aflejringer over danskekalken. In: Nielsen, O.B. (ed.): Danmarks geologi fra Kridt til i dag, 69–114. Århus: Geologisk Institut, Aarhus Universitet.

Heilmann-Clausen, C. & Surlyk, F. 2017: Koralrev og lerhav: Palæogen. In: Larsen, G. (ed.): Naturen i Danmark: Geologien, 3rd ed., 181–226. Copenhagen: Gyldendal.

Houmark-Nielsen, M. 2011: Pleistocene Glaciations in Denmark: A closer look at chronology, ice dynamics and landforms. Developments in Quaternary Science 15, 47–58. https://doi.org/10.1016/B978-0-444-53447-7.00005-2

Houmark-Nielsen, M. 2021: Istiden i det danske landskab, 392 pp. Copenhagen: Linhardt og Ringhof.

Johansen, M.B. 1987: Brachiopods from the Maastrichtian-Danian boundary sequence at Nye Kløv, Jylland, Denmark. Fossils and Strata 20, 1–99. https://doi.org/10.18261/8200025586-1987-01

Johansen, M.B. 1988: Brachiopod extinction in the Upper Cretaceous to lowermost Tertiary chalk of northwest Europe. In: Lamolda, M.A., Kauffman, E.G. & Walliser O.H. (eds): Revista Espanola De Paleontologia. Palaeontology and evolution: Extinction events. Sociedad Española de Paleontología, Madrid, 41–56.

Johansen, M.B. 1989a: Adaptive radiation, survival and extinction of brachiopods in the northwest European Upper Cretaceous-Lower Paleocene chalk. Palaeogeography, Palaeoclimatology, Palaeoecology 74, 147–204. https://doi.org/10.1016/0031-0182(89)90060-6

Johansen, M.B. 1989b: Background extinction and mass extinction of the brachiopods of the chalk of Northwest Europe. Palaios 4, 243–250. https://doi.org/10.2307/3514772

Johansen, M.B. & Surlyk, F. 1990: Brachiopods and the stratigraphy of the Upper Campanian and Lower Maastrichtian Chalk of Norfolk, England. Palaeontology 33, 823–872.

King, C., Gale, A.S. & Barry, T.L. 2016: A revised correlation of Tertiary rocks in the British Isles and adjacent areas of NW Europe. Special Report 27, 724 pp. London: Geological Society of London. https://doi.org/10.1144/SR27

Lindow, B.E.K. 2022a: NHMD Vertebrate Palaeontology collection. Natural History Museum of Denmark. Occurrence dataset https://doi.org/10.15468/yenbn7

Lindow, B.E.K. 2022b: NHMD Danekrae collection. Natural History Museum of Denmark. Occurrence dataset https://doi.org/10.15468/sbe7zv

Linnaeus, C. 1758: Systema Naturae per regna tria naturae, secundum classes, ordines, genera, species, cum characteribus, differentiis, synonymis, locis. Tomus I. Editio decima, reformata. Laurentii Salvii, Holmiae [Stockholm], 824 pp. https://doi.org/10.5962/bhl.title.542

Martini, E. 1971: Standard Tertiary and Quaternary calcareous nannoplankton zonation. In: Farinacci, A. (ed.): Proceedings of the Second Planktonic Conference, Roma 1970, 739–785.

Muñoz, J. 1990: Microbraquiopodos del Campaniensee Maastrichtiense de los alrededores de Berga (Prepirineo, Provincia de Barcelona). Boletin de la Real Sociedad Espanola de Historia Natural, Seccion Geologica 85, 55–81.

Myrvold, K.S., Milàn, J. & Rasmussen, J.A. 2018: Two new finds of turtle remains from the Danian and Selandian (Paleocene) deposits of Denmark with evidence of predation by crocodilians and sharks. Bulletin of the Geological Society of Denmark 66, 211–218. https://doi.org/10.37570/bgsd-2018-66-11

Nielsen, K.B. 1909: Brachiopoderne i Danmarks Kridtaflejringer. Det Kongelige Danske Videnskabernes Selskab Skrifter, 7. Række. Naturvidenskabelig og Mathematisk Afdeling 6(4), 129–178.

d'Orbigny, A.D. 1847: Paléontologie Française. Description des mollusques et rayonnés fossiles. Terrains Crétacés, 4. Brachiopodes. Paris (Verdière), 1–390.

Perch-Nielsen, K. 1979: Calcareous nannofossils from the Cretaceous between the North Sea and the Mediterranean. In: Weidmann, J. (ed.): Aspekte der Kreide Europas. International Union of Geological Sciences Series A, 6, 223–272.

Popiel-Barczyk, E. 1968. Upper Cretaceous Terebratulids (Brachiopoda) from the Middle Vistula Gorge. Prace Muzeum Ziemi 12, 3–86.

Popiel-Barczyk, E. 1989: Type Brachiopoda. In: Malinowska, L. (ed): Geology of Poland, III, Atlas of Guide and characteristic fossils, 2c, Mesozoic, Cretaceous, 240–251. Warsaw.

Popiel-Barczyk, E. 1992: Mesozoic and Cenozoic Brachiopods. Catalogue of the collection. Polish Academy of Sciences - Museum of the Earth, 55 pp. Warszawa.

Roemer, F.A. 1841: Die Versteinerungen des nord-deutschen Kreidegebirges. Hahn'schen Hofbuchhandlung, p. 146. Hannover. https://doi.org/10.5962/bhl.title.44865

Sandersen, P.B.E. & Jørgensen, F. 2016: Kortlægning af begravede dale i Danmark (Mapping of buried valleys in Denmark). Opdatering 2015 (Update 2015). GEUS Special Publication. December 2016, Volumes 1 & 2 (In Danish), 111 pp. + 628 pp.

Schlotheim, E.F. von. 1813: Beiträge zur Naturgeschichte der Versteinerungen in geognostischer Hinsicht. Leonhard's Taschenbuch für die gesammte Mineralogie 7, 1–134.

Schlotheim, E.F. von. 1820: Die Petrefactenkunde auf ihrem jetzigen standpunkte durch die Beschreibung seiner Sammlung versteinerter und fossiler Überreste des Thier- und Pflanzenreichs. Gotha, 432 pp.

Schnetler, K.I. & Nielsen, M.S. 2018: A Palaeocene (Selandian) molluscan fauna from boulders of Kerteminde Marl in the gravel-pit at Gundstrup, Fyn, Denmark. Cainozoic Research 18, 3–81.

Schrøder, A.E., Sørensen, A.M. & Surlyk, F. 2018: Morphological adaptations of the brachiopods from a Late Cretaceous rocky shore, Ivö Klack, southern Sweden. Palaeogeography, Palaeoclimatology, Palaeoecology 514, 785–799. https://doi.org/10.1016/j.palaeo.2018.09.019

Schrøder, A.E. & Surlyk, F. 2019: Adaptive morphologies of the brachiopod fauna from Danian coral mounds at Faxe, Denmark. Palaeogeography, Palaeoclimatology, Palaeoecology 534, 1–15. https://doi.org/10.1016/j.palaeo.2019.109332

Schrøder, A.E. & Surlyk, F. 2020: Adaptive brachiopod morphologies in four key environments of the Late Cretaceous – Danian Chalk Sea of northern Europe: a comparative study. Cretaceous Research 107, 104288 (20 pages). https://doi.org/10.1016/j.cretres.2019.104288

Schwarzhans, W., Milàn, J. & Carnevale, G. 2021: A tale from the middle Paleocene of Denmark: a tube-dwelling predator documented by the ichnofossil *Lepidenteron mortenseni* n. isp. and its predominant prey, *Bobbitichthys* n. gen. *rosenkrantzi* (Macroridae, Teleostei). Bulletin of the Geological Society of Denmark 69, 35–52. https://doi.org/10.37570/bgsd-2021-69-02

Simon E. 1995. Brachiopods. In: Jagt, J.W.M. *et al*. (eds): Preliminary report of field work at Altembroeck (NE Belgium, Early Maastrichtian). Professional Paper, Service Géologique de Belgique, 276, 11–12.

Simon, E. 1998: Maastrichtian brachiopods from Ciply: palaeoecological and stratigraphical significance. Bulletin de l'Institut royal des Sciences naturelles de Belgique, Sciences de la Terre 68, 181–232.

Simon, E. 2000: Upper Campanian brachiopods from the Mons Basin (Hainaut, Belgium): the brachiopod assemblage from the *Belemnitella mucronata* Zone. Bulletin de l'Institut royal des Sciences naturelles de Belgique, Sciences de la Terre 70, 129–160.

Simon, E. 2011: The late Maastrichtian cancellothyridid brachiopod *Terebratulina chrysalis* (von Schlotheim, 1813) from the type Maastrichtian (southern Limburg, the Netherlands) and elsewhere in Europe. Netherlands Journal of Geosciences 90, 111–127. https://doi.org/10.1017/S0016774600001062

Sorgenfrei, T. 1957: Lexique Stratigraphique International, 1, fasc. 2d. Danemark. Published by the Congres Geologique International. CNRS. Paris, 44 pp.

Sowerby, G.B. 1846: Descriptions of thirteen new species of brachiopods. Proceedings of the Zoological Society of London 14, 91–97.

Steinich, G. 1965: Die artikulaten Brachiopoden der Rügener Schreibkreide (Unter - Maastricht). Paläontologische Abhandlungen, Abteilung A, Paläozoologie 2 (1), 1–220.

Surlyk, F. 1972: Morphological adaptations and population structures of the Danish Chalk brachiopods (Maastrichtian, Upper Cretaceous). Det Kongelige Danske Videnskabernes Selskab. Biologiske Skrifter 19, 1–57.

Surlyk, F. 1982: Brachiopods from the Campanian–Maastrichtian boundary sequence, Kronsmoor (NW Germany). Geologisches Jahrbuch A 61, 259–277.

Surlyk, F. 1984: The Maastrichtian Stage in NW Europe, and its brachiopod zonation. Bulletin of the Geological Society of Denmark 33, 217–233. https://doi.org/10.37570/bgsd-1984-33-20

Surlyk, F. & Birkelund, T. 1977: An integrated stratigraphical study of fossil assemblages from the Maastrichtian White Chalk of northwestern Europe. In: Kauffman, E.G., Hazel, J.E. (eds): Concepts and methods in biostratigraphy, 257–281. Dowden, Hutchinson and Ross Inc., Stroudsburg, Pennsylvania.

Thomsen, E. & Heilmann-Clausen, C. 1985: The Danian–Selandian boundary at Svejstrup with remarks on the biostratigraphy of the boundary in western Denmark. Bulletin of the Geological Society of Denmark 33, 341–362. https://doi.org/10.37570/bgsd-1984-33-28

Thomson, J.A. 1926: A revision of the subfamilies of the Terebratulidae (Brachiopoda). Annals and Magazine of Natural History 18 (9), 523–530. https://doi.org/10.1080/00222932608633548

Vallon, L.H. & Rindsberg, A.K. 2022: Cutting through sponge and time – a new record of *Koptichnus rasmussenae* (trace fossil) from the Kerteminde Marl (middle Paleocene), Denmark. Bulletin of the Geological Society of Denmark 70, 131–137. https://doi.org/10.37570/bgsd-2022-70-09

Vallon, L.H., Milàn, J., Rindsberg, A.K., Madsen, H. & Rasmussen, J.A. 2020: Cutting-edge technology: burrows lined with sponge bioclasts from the Upper Cretaceous of Denmark. Ichnos 27, 317–325. https://doi.org/10.1080/10420940.2020.1744581

Waagen, W.H. 1883: Salt Range fossils. Vol 1, Part 4. Productus limestone fossils, Brachiopoda. Memoirs of the Geological Survey of India. Palaeontologia Indica 2 (13), 391–546.

Williams, A., Carlson, S.J., Brunton, C.H.C., Holmer, L.E. & Popov, L. 1996: A supra-ordinal classification of the Brachiopoda. Philosophical Transactions of the Royal Society of London, Series B, 351, 1171–1193. https://doi.org/10.1098/rstb.1996.0101

Zezina, O.N. 1981: New and rare cancellothyroid brachiopods. Trudy Instituta Okeanologiya 115, 155–164. [in Russian with English summary]

Fish otoliths from the bathyal Eocene Lillebælt Clay Formation of Denmark

WERNER W. SCHWARZHANS & KENT A. NIELSEN

Geological Society of Denmark
https://2dgf.dk

Received 8 September 2023
Accepted in revised form
18 October 2023
Revised version published online
02 July 2024

Schwarzhans, W.W. & Nielsen, K.A. 2024: Fish otoliths from the bathyal Eocene Lillebælt Clay Formation of Denmark. Bulletin of the Geological Society of Denmark, Vol. 73, pp. 99–111. ISSN 2245-7070. https://doi.org/10.37570/bgsd-2024-73-06

Few deepwater otolith associations from the Eocene have been found so far. The small assemblage of aragonitic-preserved otoliths from the Lillebælt Clay Formation described here therefore adds to the understanding of early Palaeogene deep-sea fish faunas. These otoliths were obtained from a level at about the Ypresian/Lutetian interface and may thus be older than the otoliths previously described from Trelde Næs from mold casts from carbonate concretions. Only 14 otoliths were recovered from about 6,000 kg processed bulk samples. The assemblage also differs in the composition and contains three new species and one new genus: *Diaphus*? *duplex* n. sp., *Bregmaceros danicus* n. sp. and the ophidiid *Pronobythites schnetleri* n. gen, n. sp. In addition, the new genus *Treldeichthys* n. gen. in Acanthomorpha incertae sedis is established for *T. madseni* (Schwarzhans, 2007). The small assemblage also differs in composition from comparable associations described from southwest France and northern Italy on the species level but shows some relationship on a higher systematic level. The mechanism and timing of the colonization of the deep sea by selected groups of fishes is discussed, particularly in respect to the depth migration of demersal fishes.

Keywords: otoliths, Eocene, Denmark, new species, Trelde Næs, deepwater colonization.

Werner W. Schwarzhans [wwschwarz@aol.com], Zoological Museum, Natural History Museum of Denmark, Universitetsparken 15, 2100 Copenhagen Ø, Denmark and Ahrensburger Weg 103, 22359 Hamburg, Germany, http://orcid.org/0000-0003-4842-7989. Kent A. Nielsen [kent@ksjm.dk], Tingskoven 22, DK-7330 Brande, Denmark, https://orcid.org/0000-0002-5800-5774.

Few otolith assemblages with bathyal fishes are known from Palaeogene pelagic sediments. The only otolith-based bathyal fish faunas from that time interval are those from the early Oligocene of Italy (Nolf & Steurbaut 1988, 1990, 2004), from the late Eocene of New Zealand (Schwarzhans 2019), and from the late middle Eocene of northern Italy (Schwarzhans & Carnevale 2022). In addition, several otolith associations have been described from Palaeogene sediments on the lower shelf or upper slope. The richest of these are from the middle Eocene of France (Nolf 1988; Lin *et al.* 2016) and from the late Paleocene of Austria (Schwarzhans 2012). These faunas undoubtedly contain otoliths of deepwater fishes. However, it is difficult to assess which species may actually be from deepwater fishes because of the lack of otoliths from time equivalent true pelagic sediments. Moreover, it has been observed that fish groups that today live in the deep sea may in the past have (also) lived in shallow water (Schwarzhans *et al.* 2017; Schwarzhans & Carnevale 2021).

The Lillebælt Clay in Denmark represents a rare opportunity to collect and study otoliths from a bathyal environment of the late early to early middle Eocene. Here, we describe 14 identifiable otoliths collected from Kirstinebjerg East (see Schnetler & Heilmann-Clausen 2011). Because of the unique environment, a description is warranted even though only a few specimens are available due to the scarcity of aragonitic fossils at the Trelde Næs location. In this context, we also reevaluate previously described otoliths from molds from concretions in the Lillebælt Formation (Schwarzhans 2007).

Geology and locality

The Lillebælt Clay Formation crops out along a cliff section for more than 5 km in length at Trelde Næs north of Fredericia, Jylland, Denmark. The outcrop situation and stratigraphy is described in detail by Heilmann-Clausen *et al.* (1984) and Schnetler & Heilmann-Clausen (2011). The otoliths were collected in the cliff section known as Kirstinebjerg East (Fig. 1). In this section, the lower part of the Lillebælt Clay Formation is exposed; that is, the beds L2, L3 and L4 straddling the Ypresian–Lutetian boundary (Schnetler & Heilmann-Claussen 2011). The overall setting is from the deep bathyal zone in the underlying Røsnæs Clay Formation to the outer shelf in the overlying Søvind Marl Formation, gradually shallowing upward (King 2016). The interpretation of the palaeo-water depth of the Lillebælt Clay varies, however, from an undifferentiated bathyal zone (King 2016) to only upper bathyal zone (Thomsen *et al.* 2012) and 100–300/350 m in Schnetler & Heilmann-Clausen (2011) and Carlsen & Cuny (2014). A recent study of a more diverse and prolific association of shark teeth from the same samples from which the otoliths were obtained revealed the presence of numerous deepwater shark representatives (Pollerspöck *et al.* 2023). At Kirstinebjerg, the Lillebælt Clay Formation is capped disconformably by the Brejning Formation of late Oligocene age farther inward from the sea cliff. The dark gray to black shales from the Brejning Formation are sometimes found as slumped blocks in coastal gullies and contain fossils, albeit of a completely different composition from that of the otoliths described here, the shark teeth by Pollerspöck *et al.* (2023), or the mollusks by Schnetler & Heilmann-Clausen (2011).

The otoliths were sampled from a variety of sediments at the foot of Kirstinebjerg East (GPS coordinates: 09°48′09.03″E, 55°35′52.6″N) in an area where the L2 and L3 beds are outcropping but without a detailed stratigraphic position (Fig. 1). It is noteworthy, however, that Schnetler & Heilmann-Clausen (2011) identified a 'mussel layer' in bed L2 just below the Ypresian–Lutetian boundary, from which a few gastropods and bivalves were recovered with preserved aragonite. Elsewhere, aragonite is dissolved throughout the Lillebælt and Søvind formations. It is therefore reasonable to assume that the otoliths stem from the same level even though Schnetler & Heilmann-Clausen (2011) apparently did not find otoliths in their study. This level is positioned within the *Azolla* event, which forms a tool for regional correlation in the North Sea and the Norwegian Sea (see Schnetler & Heilmann-Clausen 2011 and literature cited therein). *Azolla* is a free-floating freshwater fern that lives in warm climates. Its temporary occurrence in the Norwegian Sea and the North Sea is explained by Brinkhuis *et al.* (2006) as a spill-over from a then enclosed warm Arctic Ocean with fresh surface water conditions. Heilmann-Clausen *et al.* (2010) suggested that the *Azolla* spores could have been transported to the sea by rivers from coastal swamps during a time of major transgression and supposed flooding of the coastal marshlands. In Trelde Næs, the *Azolla* spores are enriched in the black sapropelic layers, "indicating a generally reduced oxygen content in the bottom waters during this time" (Heilmann-Clausen *et al.*

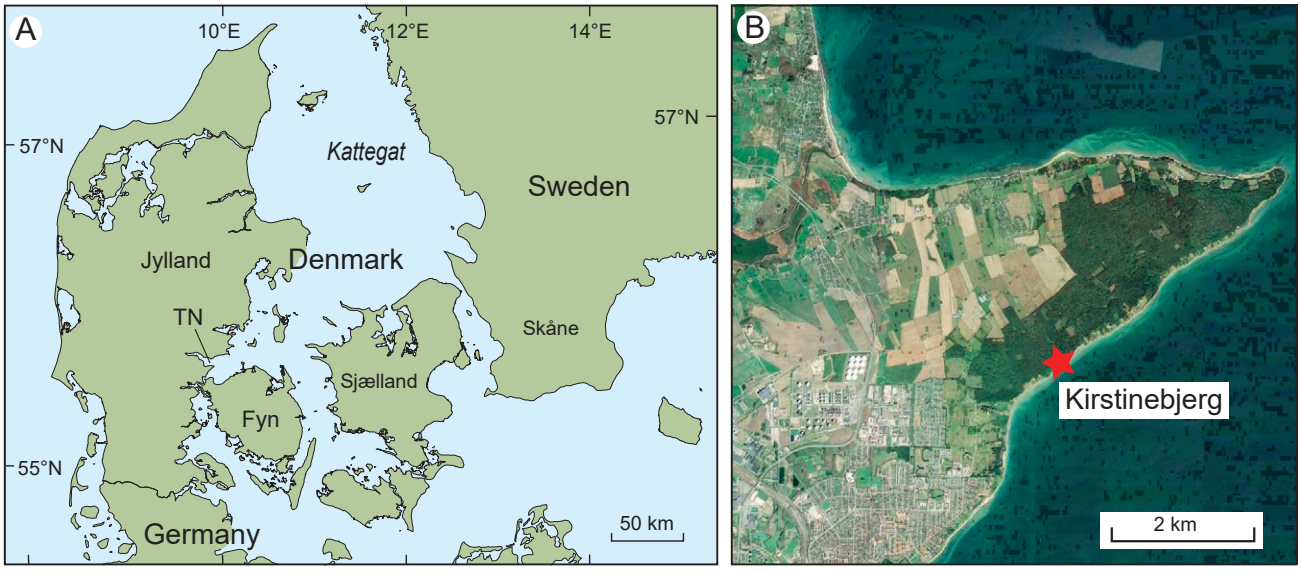

Fig. 1. Location map (after Pollerspöck *et al.* 2023). **A**, Map of Denmark showing Trelde Næs (TN). **B**, Google Earth image showing the Kirstinebjerg sample location on Trelde Næs.

2010). The 'mussel layer' described by Schnetler & Heilmann-Clausen (2011) is positioned within one of the sapropelic layers in Bed L2. They found the mollusk shells sometimes speckled with precipitation of pyrite. The recovered otoliths also exhibit small pyrite speckles, which would support their association with or origin from the 'mussel layer'. The cliff section depicted by Schnetler and Heilmann-Clausen (2011) eroded away some years ago due to the constant wave action of the Baltic Sea. It is still possible to distinguish the layers L2 and L3. However, L2 is unique due to the black sapropelic layers and L3 due to the reddish intervals. The cliff section today is steeper causing sections each winter to slide down, and the result is a mixing of layers at the base of the cliff. Due to the color difference between the layers—L2 being gray-green and L3 reddish—it is still possible, to some extent, to distinguish the individual layers with L2 having the highest fossil content.

Material and methods

Over four years, approximately 6000 kg of material was disaggregated and sieved on the shore of Trelde Næs. The procedure involved the following steps. Soft clay samples collected during the wintertime (15 kg) were placed in a plastic bucket (20 L) and ocean water added. Mechanical stirring of the mixture was performed using an electric screwing machine fitted with a paddle mixer. The dissolved material was poured through double nylon stockings. The process was repeated for 6000 kg until all the material was dissolved and processed as described. Generally, three buckets (approximately 45 kg) of material were reduced each to 1–2 kg before the nylon stocking was replaced. The reduced material was further processed in the following steps. The material was rinsed with cold water while the nylon stocking was gently massaged until clear water was leaving the stocking. The material was then rinsed with lukewarm water for a few minutes before a small portion of dishwashing detergent was added while the nylon stocking was gently massaged. After soaking for several hours, cold water was used to remove the excess soap. The material was then transferred to a large (7 × 20 × 30 cm) plastic container and water added. The floating organic material was stirred to ensure that no inorganic material was attached. The organic material was then slowly emptied from the plastic container. This process was repeated until all the organic material was removed. The remaining water was decanted from the container before the material was dried in an oven at 90°C until completely dry. The final clean fossil material was sorted using a binocular microscope.

The terminology of the morphology of sagittae otoliths follows the nomenclature established by Koken (1884) and amendments by Chaine & Duvergier (1934) and Schwarzhans (1978). Abbreviations used are OL = otolith length; OH = otolith height; OT = otolith thickness; OsL = ostium length; OCL = length of ostial colliculum; OCH = height of ostial colliculum; CaL = cauda length; CCL = length of caudal colliculum; CCH = height of caudal colliculum; SuL = sulcus length.

The otoliths were photographed with a Canon EOS 1000D mounted on a Wild M400 photomacroscope and remotely controlled from a computer. Individual images of every view of the objects taken at ranges of field of depths were stacked using the Helicon Focus software of Helicon Soft (Kharkiv, Ukraine). Adjustment of exposure and contrast and retouching was done in Adobe Photoshop where necessary to improve the images but without altering any morphological features. All otoliths shown are from the right side; left otoliths are reversed for comparison.

The described otoliths are deposited in the collections of the Natural History Museum of Denmark (NHMD), Universitetsparken 15, DK-2100 Copenhagen, collection numbers NHMD-1651020–1651026.

This published work and the nomenclatural acts it contains have been registered in ZooBank: https://zoobank.org/75190823-F060-4278-9839-510A51F-BA5BD

Systematic palaeontology

Order Anguilliformes

Family Congridae Kaup, 1856

Genus *Smithconger* Carnevale, Schwarzhans, Schrøder & Lindow, 2022

Smithconger treldeensis (Schwarzhans, 2007)

Fig. 2A, 3A

2007 *Pseudoxenomystax treldeensis*; Schwarzhans: fig. 3C–E.
2022 *Smithconger treldeensis* (Schwarzhans, 2007); Carnevale *et al.*: fig. 2, 3A, 4–5.

Material. 1 specimen, NHMD-1651020.

Discussion. Smithconger treldeensis was originally described from two mold casts of large otoliths of about 10 to 11 mm in length, one of which was found within a skull fragment. The skull fragment with the otolith (mold) *in situ* is the holotype and in combination with a further, more complete skull, was

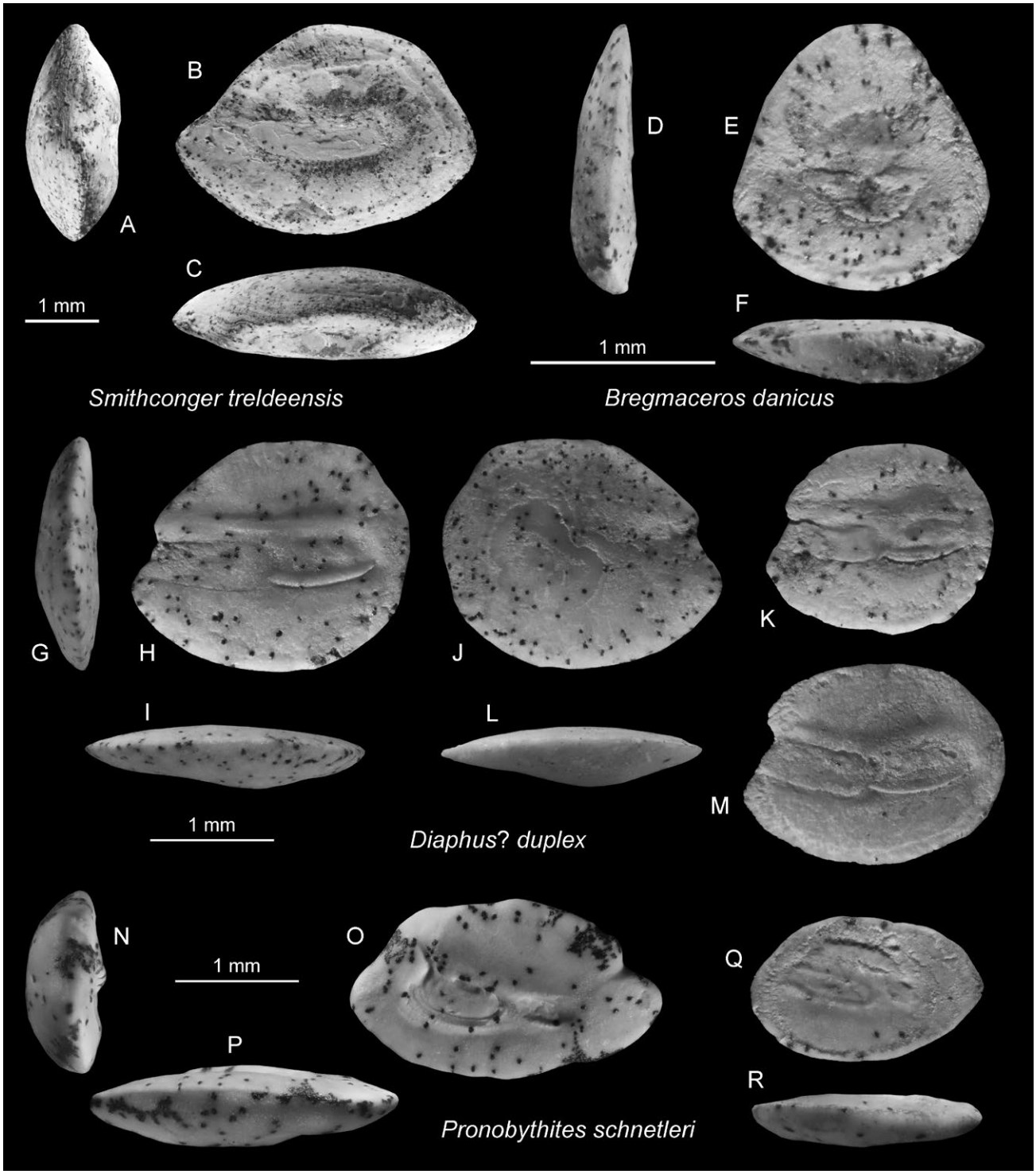

Fig. 2. Photographs of otoliths from Kirstinebjerg. **A–B**, *Smithconger treldeensis* (Schwarzhans, 2007), NMHD-1651020, A anterior view, B inner face, C dorsal view. **D–F**, *Bregmaceros danicus* n. sp., holotype, NMHD-1651021, D anterior view, E inner face, F ventral view. **G–M**, *Diaphus*? *duplex* n. sp., G–H holotype, NMHD-1651023, K–M paratypes, NMHD-1651024, G anterior view, H, K, M inner faces, I, L ventral view, J outer face. **N–R**, *Pronobythites schnetleri* n. gen. et n. sp., N–P holoytpe, NMHD-1651025, Q–R paratype, NMHD-1651026, N anterior view, O, Q inner faces, P, R ventral views.

later placed in the genus *Smithconger* Carnevale *et al.* (2022), a fossil monospecific genus with *S. treldeensis* as type species. We now have the first specimen of the species in aragonitic preservation, albeit from a much smaller specimen (OL = 4.1 mm in length) that is also somewhat leached. The anterior portion differs slightly from the holotype and paratype (both casts from molds) in a less clearly defined anterior sulcus portion and the lack of an ostial channel. We consider these differences to have been caused by a slight erosion in combination with leaching that obliterated this delicate feature.

A similar otolith in terms of otolith and sulcus shape has been figured as *Bathycongrus* sp. from the Bartonian of Piedmont, Italy, by Schwarzhans & Carnevale (2022). This singular otolith is slightly over 2 mm in length and may not be morphologically mature compared with the known otoliths of *S. treldeensis*. More and larger specimens will be needed from the Italian location for a conclusive comparison with the Danish specimens from Trelde Næs.

Order Myctophiformes

Family Myctophidae Gill, 1893

Subfamily Diaphinae Paxton, 1972 (sensu Martin *et al.*, 2018)

Genus indet.

Diaphus? *duplex* n. sp.

Fig. 2 G–M, 3B

Holotype. Fig. 2 G–J, 3B, NMHD-1651023 Trelde Næs, Kirstinebjerg, Lillebælt Clay Formation, presumably Bed L2.

Paratypes. 8 specimens, NHMD-1651024, same data as holotype.

Name. From duplex (Latin) = doubled, referring to the similar proportions of ostial and caudal colliculi.

Diagnosis. Moderately elongate, oval shape; OL:OH = 1.2–1.3. Dorsal rim with variably developed postdorsal angle. Ventral rim regularly curved, smooth, without denticles. Rostrum slightly longer than antirostrum. Ostium narrow, only slightly longer than cauda; OCL:CCL = 1.35–1.45. Caudal pseudocolliculum long and prominent.

Description. Relatively small, elongate oval otoliths up to 2.3 mm in length (holotype). OH:OT = 3.4–3.7. Ventral rim shallow, regularly curved, smooth without denticles. Dorsal rim smooth, regularly curved (Fig. 2 M) or with moderate postdorsal angle (holotype). Rostrum blunt, slightly longer than antirostrum; antirostrum and excisura feeble. Posterior rim blunt, rounded, smooth.

Inner face slightly convex to nearly flat with axially positioned, shallow, relatively narrow and long sulcus reaching near posterior tip of otolith. Sulcus straight or slightly bent; ostium only slightly longer than cauda (OCL:CCL = 1.35–1.45) and equally wide. Infracaudal pseudocolliculum distinct and very long, slightly extending beyond terminations of caudal colliculum. Dorsal depression wide, poorly defined toward dorsal rim; ventral furrow distinct, running relatively close and parallel to ventral rim of otolith. Outer face slightly convex with small postcentral umbo, with short excisural furrow; otherwise perfectly smooth.

Discussion. The otoliths of *Diaphus*? *duplex* resemble in appearance those of certain *Diaphus* species and the fossil *Oligophus*, particularly in the relatively shallow ventral rim. However, *Oligophus* differs in the strong denticles along the ventral rim and a nearly completely flat inner face. The lack of denticles along the ventral rim is also observed in *Diaphus* otoliths when they are eroded in poorly preserved specimens. The holotype of *D.*? *duplex* (Fig. 2 G–J), however, is well enough preserved to exclude erosion as a cause of the smooth ventral rim. Another diagnostic feature is the long caudal colliculum with the long underlying pseudocolliculum that in combination with a narrow sulcus is not known from *Diaphus* otoliths (see Schwarzhans 2013). *Diaphus* look-alike otoliths are also known from the fossil genus *Eokrefftia*, particularly from *E. sulci* (Nolf, 1988) known from middle Eocene lower shelf to bathyal sediments of southwestern France (Nolf 1988) and northern Italy (Schwarzhans & Carnevale 2022). *Diaphus*? *duplex* differs from *E. sulci* in the comparatively longer cauda (lower ratio OVL:CCL of 1.35–1.45 vs >1.5) and the less prominently developed rostrum. Until more myctophid otoliths become available from Eocene rocks, we are uncertain about the generic allocation of this species and therefore leave *D.*? *duplex* in open generic assignment within the Diaphinae.

Order Gadiformes

Family Bregmacerotidae Gill, 1872

Genus *Bregmaceros* Thompson, 1840

Bregmaceros danicus n. sp.

Fig. 2 D–F, 3 C

Holotype. Fig. 2 D–F, 3 C, NMHD-1651021 Trelde Næs, Kirstinebjerg, Lillebæaelt Clay Formation, presumably Bed L2.

Paratypes. 1 specimen, NHMD-1651022, same data as holotype.

Name. Referring to Denmark, the country of origin.

Diagnosis. Rounded triangular, high-bodied otoliths without denticles or projections along the ventral rim; OL:OH = 0.95–1.0. Inner face flat with shallow, short sulcus with narrowly placed oval and equally sized colliculi. Pseudocolliculum well developed, distinctly convex and large. Ventral furrow distinct and very close to ventral rim of otolith.

Description. Small, thin, high-bodied otoliths with rounded triangular outline, up to 1.4 mm in length (holotype). OH:OT = 4.2. Dorsal rim very high, with rounded central culmination. Anterior and posterior rims steeply inclined and symmetrical to broadly rounded inferior angles. Ventral rim shallow, regularly curved without denticles or projections, smooth.

Inner face completely flat with small, inframedian positioned sulcus oriented symmetrical to vertical axis. Sulcus very slightly deepened with two slightly elevated, well-defined oval and nearly symmetrical colliculi with a narrow space between them. Deep and convex pseudocolliculum well developed, large and positioned slightly asymmetrical towards posterior. Dorsal depression large, very poorly defined; ventral furrow distinct along central portion of ventral field, very close to ventral rim of otoliths and becoming closer anteriorly and posteriorly. Outer face very slightly convex, smooth.

Discussion. The two specimens are slightly eroded, and the paratype is particularly eroded on the inner face, an observation often made with fossil *Bregmaceros* otoliths. However, *B. danicus* is readily distinguished from all extant and fossil *Bregmaceros* otoliths by the

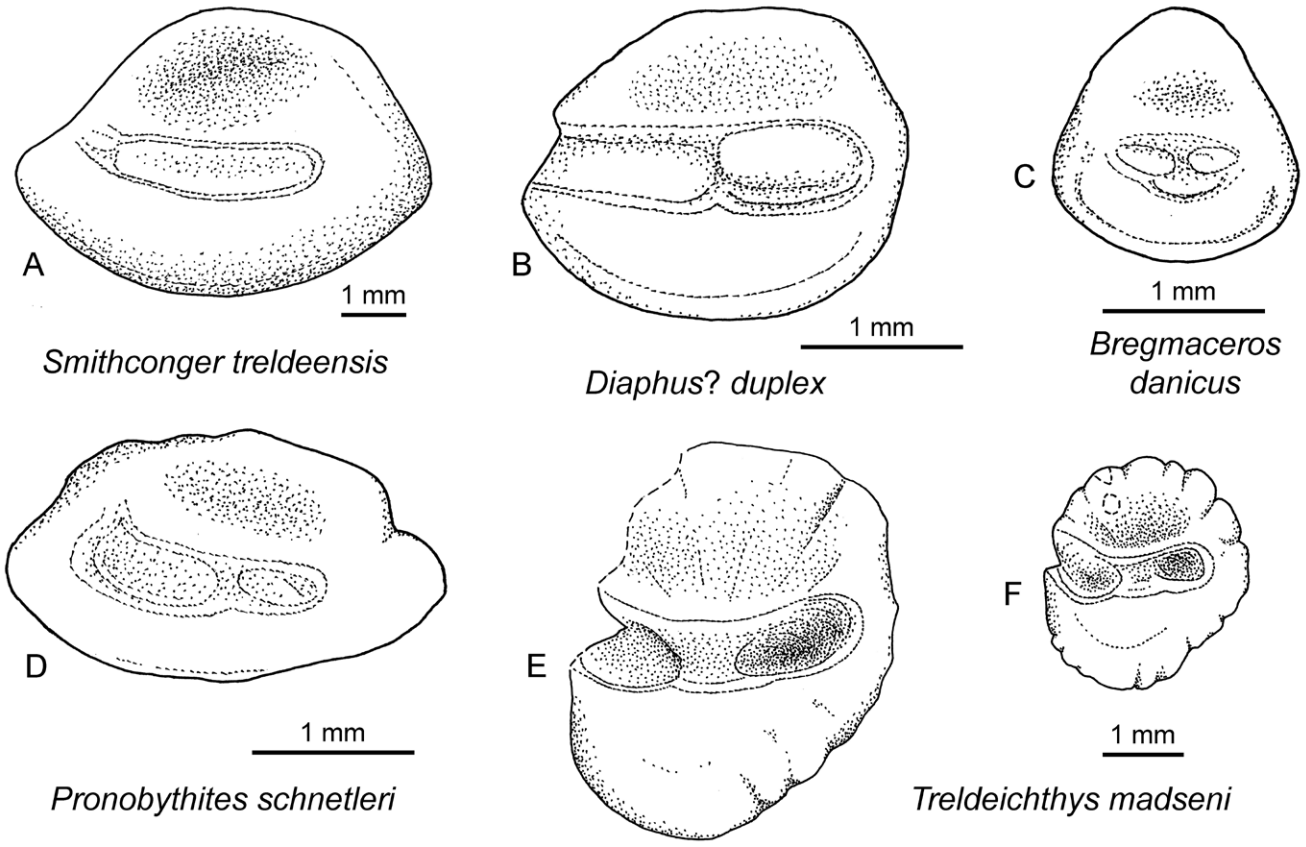

Fig. 3. Drawings of inner faces of otoliths from Kirstinebjerg (A–D) and reproduction from Schwarzhans (2007) (E–F). **A**, *Smithconger treldeensis* (Schwarzhans, 2007), NMHD-1651020. **B**, *Diaphus*? *duplex* n. sp., holotype, NMHD-1651023. **C**, *Bregmaceros danicus* n. sp., holotype, NMHD-1651021. **D**, *Pronobythites schnetleri* n. gen. et n. sp., holoytpe, NMHD-1651025. **E–F**, *Treldeichthys* n. gen. *madseni* (Schwarzhans, 2007), E holotype, MGUH 28344, F paratype, MGUH 28342.

rounded triangular shape without any denticles or projections at the ventral rim and the deeply curved, long and convex pseudocolliculum. It shares the smooth outline with *B. rappei* Nolf, 1988, from the middle Eocene of France, but *B. rappei* has a flattened dorsal rim and a straight pseudocolliculum. It is possible that *B. danicus* represents an extinct bregmacerotid genus, subject, however, to a detailed study of extant otoliths of that family.

Order Ophidiiformes

Family Ophidiidae Rafinesque, 1810

Genus *Pronobythites* n. gen.

Type species. Pronobythites schnetleri n. sp.

Name. From pronus (Latin) = inclined, referring to the inclined orientation of the sulcus on the inner face in combination with the genus name *Bythites*.

Diagnosis. A fossil otolith-based genus of the family Ophidiidae, possibly subfamily Neobythitinae with the following combination of characteristics: moderately elongate otoliths with a ratio OL:OH of 1.6–1.9. Inner face relatively flat with sulcus distinctly inclined against otolith axis between 5° and 15°. Sulcus long, anteriorly closed, its ostium wider and longer than cauda and relatively shallow; cauda slightly deepened. OCL:CCL = 1.7–2.7.

Discussion. Pronobythites otoliths are readily recognized by the distinctly inclined sulcus, which is also clearly divided into an ostium and a cauda. The anteriorly closed ostium is an early advanced feature, while the deepened cauda is considered a primitive feature (Schwarzhans 1981). *Pronobythites* resembles the, mostly extinct, genera in the *Hoplobrotula* group of the Neobythitinae, for instance *Ampheristus* König, 1825, except for the distinctly inclined sulcus. *Pronobythites* seems to represent a first venturing of ophidiid fishes into the deep sea during late early and middle Eocene, but it did not lead to a persistent deepwater establishment of the family.

Species. Pronobythites schnetleri n. sp. from the Lillebælt Clay Formation (upper Ypresian to lower Lutetian) of Trelde Næs, Denmark, *P. bozzolo* (Lin, Nolf, Steurbaut & Girone, 2016) originally described as *'Neobythites' bozzolo* and *P. leonardi* (Lin, Nolf, Steurbaut & Girone, 2016) originally described as *'Neobythites' leonardi*, both from the Lutetian of the Aquitaine Basin in southwest France.

***Pronobythites schnetleri* n. sp.**

Fig. 2 N–R, 3 D

Holotype. Fig. 2 N–P, 3 D, NMHD-1651025 Trelde Næs, Kirstinebjerg, Lillebæaelt Clay Formation, presumably Bed L2.

Paratypes. 2 specimens, NHMD-1651026, same data as holotype.

Name. In honor of Ingemann Schnetler (Aarhus) for his many contributions to the understanding of the fossil fauna from the Cenozoic of Denmark.

Diagnosis. Oval, moderately elongate otoliths; OL:OH = 1.7–1.8. Sulcus inclined at 5–10° against sulcus axis. Sulcus relatively short, OL:SuL = 1.7–1.9. Ostium and cauda clearly divided; cauda deepened.

Description. Relatively small, moderately elongate and robust otoliths reaching 2.7 mm in length (holotype, 2.6 mm). OH:OT = 2.3–2.7. Dorsal rim regularly curved, somewhat undulating in larger specimens (Fig. 2 O) smooth in the smallest specimen of 1.9 mm in length (Fig. 2 Q), with broadly rounded predorsal angle and shallow postdorsal region. Ventral rim shallow, gently and regularly curved, smooth. Anterior tip of otolith bluntly rounded; posterior tip slightly projecting, rounded.

Inner face nearly flat with moderately long sulcus, distinctly inclined at 5–10° against otolith axis. Ostium and cauda clearly divided. Ostium relatively short but longer, shallower and wider than cauda, anteriorly closed, with indication of short ostial channel. OCL:OCH = 1.7–2.7; OCH:CCH = 1.7–2.0; OL:SuL = 1.7–1.9. Dorsal depression wide but with indistinct margins; ventral furrow absent or weak and then close to ventral rim of otolith. Outer face slightly convex, smooth.

Discussion. The smooth outline and more generalized morphology of the small specimen of 1.9 mm in length (Fig. 2 Q–R) is typical for a juvenile, while the holotype of 2.6 mm in length is considered morphologically mature. The largest specimens of the two species from the Lutetian of France described by Lin *et al.* (2016) also do not exceed 3 mm in length (based on 51 specimens), which indicates that the species of *Pronobythites* were relatively small. *Pronobythites schnetleri* differs from the two species from France in the relatively short sulcus (OL:SuL = 1.7–1.9 vs 1.3–1.4). Furthermore, the anterior rim is more rounded (vs blunt and near vertically cut). Otoliths of *P. leonardi* have an even more strongly ventrally inclined sulcus than *P. schnetleri* (10–15° vs 5–10°).

Unidentifiable otoliths from Kirstinebjerg East

Material. The otoliths collected from Kirstinebjerg East also contained seven specimens that were not identifiable due to being fragmented, representing small juveniles or being too poorly preserved. One of the specimens may possibly represent a juvenile haemulid or acropomatid.

Reviewed record from Schwarzhans (2007)

Remarks. The otoliths described from casts of molds in Schwarzhans (2007) came from carbonate concretions, some of them formed in stomatopod living tubes. These concretions were collected from the beach, and therefore, could not be related to specific stratigraphic levels; they had probably fallen off the Trelde Næs cliffs and been washed by the sea. According to Schnetler & Heilmann-Clausen (2011), such concretions occurred primarily in higher levels of the sequence, particularly in Beds L4 to L6 of the Lillebælt Formation; that is, of Lutetian age. Interestingly, the otoliths retrieved from the concretions differ substantially from those body-preserved specimens described here with only a single overlapping species: *Smithconger treldeensis*. The otolith-based fauna from the Lillebælt Clay Formation now comprises 15 species (Table 1).

Table 1. Otolith-based species from the Lillebælt Clay FM

Species	Molds in concretions (2007)	Aragonitic otoliths (this study)
Pterothrissus angulatus	X	
Smithconger treldeensis	X	X
Arius sp.	X	
Argentina tricrenulata	X	
Saurida recta	X	
Diaphus? duplex		X
Bregmaceros danicus		X
Merluccius? sp.	X	
Ampheristus toliapicus	X	
Pronobythites schnetleri		X
Centroberyx sp.	X	
Gephyroberyx hexagonalis	X	
Haemulon? pulcher	X	
Rhombocitharus sp.	X	
Treldeichthys madseni	X	

Acanthopterygii indet.

Genus *Treldeichthys* n. gen.

Type species. *Caproidarum madseni* Schwarzhans, 2007.

Name. Referring to Trelde Næs, the type locality, in combination with ichthys (Greek) = fish.

*Diagnosis***.** A fossil otolith-based genus of uncertain relationship within the Actinopterygii with the following combination of characteristics: compressed high-bodied otolith with OL:OH of 0.80–0.85. Rostrum and antirostrum short, blunt; excisura sharp but not deep. Sulcus markedly turned upward posteriorly with narrow, deep ostium and deepened caudal tip. CaL:OsL = 1.25–1.6. Broad area between ostium and deepened caudal tip rather shallow. Dorsal depression wide; ventral furrow indistinct, far from ventral rim of otolith.

*Discussion***.** *Treldeichthys* was originally described as a member of the family Caproidae of uncertain relationship. However, this allocation can no longer be justified because of the large differences with the highly apomorphic otoliths of the genus *Capros* and the plesiomorphic beryciform-like otoliths of the genus *Antigonia* (see Nolf 2013, for figures). It is also possible that *Treldeichthys* represents a taxon related to certain trachichthyiform families, such as the Diretmidae or Trachichthyidae, or certain Beryciformes. The specific form of the sulcus with the deepened ostium and posterior part of the cauda and the shallower section between, however, is not matched in any of these groups. It is therefore likely that this otolith morphology represents an extinct actinopterygian fish of uncertain relationships, which it is hoped will be better interpreted if otoliths *in situ* are found.

Species. *Treldeichthys* is a monospecific genus with *T. madseni* known exclusively from the Lillebælt Clay Formation.

Faunal comparison

Pollerspöck *et al*. (2023) described teeth of seven shark species from the same samples from which the otoliths were obtained. They all represent deepwater taxa with most of them demersal at bathyal depth. Assuming an at least upper bathyal depositional environment for the sampled rocks, the small otolith association offers a rare view into an early to middle Eocene deepwater fish fauna along with the equally scarce data from Piedmont, Italy (Schwarzhans & Carnevale 2022) and the rich fauna from the Marnes de Donzacq in the Aquitaine Basin, which has been considered bathyal based on shark teeth (Adnet 2006) or lower shelf to upper slope with oceanic influence based on otoliths (Lin *et al*. 2016). Considering only the otoliths from the Lillebælt For-

mation described here, the most remarkable outcome of a correlation with the abovementioned localities is the congruence of taxa at the family level (Congridae, Myctophidae, Bregmacerotidae, and Ophidiidae) but no shared taxa on the species level except possibly in Congridae (see discussion of *Smithconger treldeensis*). In Myctophidae, the otolith association from the Bartonian of Italy is the richest with four species, three of which are shared with the Aquitaine Basin. Bregmacerotid otoliths are also present in all three locations, but in the case of the Italian locality, it is a single unidentifiable specimen. In the Aquitaine Basin, *Bregmaceros rappei* Nolf, 1988, has been identified in the Marnes de Donzacq, while in Denmark, it is *B. danicus*. Both species are very characteristic and greatly differ from each other in otolith shape, colliculi proportions, and the shape and size of the pseudocolliculum. With more information emerging about extant bregmacerotid otoliths, it might be that they each represent separate fossil genera. In ophidiids, finally, only the Lillebælt Clay has yielded a species, *Pronobythites schnetleri*, which is here regarded as the earliest positive record of a deep-sea ophidiiform in the fossil record. Two putatively related species have been described from the Lutetian of the Aquitaine Basin in southwest France by Lin *et al.* (2016) from an upper bathyal to lower shelf transitional environment of the Marnes de Donzacq. The difference in the faunal composition at the species level is thought to have been caused by two factors: (1) the semi-enclosed palaeogeographic position of the North Sea Basin at the time hindering faunal exchange with the localities in France and Italy, and (2) the presumably cooler water in the North Sea Basin compared to the more southerly localities in France and Italy.

Populating the deep sea with fishes

The small number of otoliths described here from the latest Ypresian/earliest Lutetian Lillebælt Formation provide additional rare calibration points for deep-sea fishes, just like the Bartonian Marne di Monte Piano Formation in Piedmont, Italy (Schwarzhans & Carnevale 2022). These calibration points allow for a better understanding of much richer otolith associations from lower shelf to upper bathyal positions like those documented by Lin *et al.* (2016) from the time-equivalent Marnes de Donzacq in the Aquitaine Basin (but bathyal in Adnet 2006) or by Schwarzhans (2012) from the upper Paleocene of Austria. Richer true bathyal faunas are otherwise known from the upper Eocene of New Zealand (Schwarzhans 2019) and the lower Oligocene of northern Italy (Nolf & Steurbaut 1988, 1990, 2004).

Some of the most iconic modern deep-sea bony fishes are the meso- and bathypelagic Stomiiformes and Myctophidae and the bathydemersal Macrouridae and Ophidiidae. Based on the generally held belief that deep-sea fishes migrated into deep water from a shallower habitat during their evolution, a picture is now beginning to emerge about when individual groups submersed into the deep sea and which possible mechanisms were at work. The earliest deep-sea fishes of these four groups may have been the Stomiiformes. There are indications of deep-sea stomiiform skeletal finds since early Late Cretaceous (Carnevale & Rindone 2011), and stomiiform otoliths occur regularly in outer shelf to upper slope environments since at least late Paleocene (Nolf 1988; Schwarzhans 2010, 2012; Lin *et al.* 2016). There are no positive indications yet for deep-sea myctophids, macrourids, or ophidiids prior to the late early Eocene. Schwarzhans & Carnevale (2021) discuss the evolutionary trends in the Myctophidae and postulate that they probably evolved over the outer shelf and upper slope during the latest Paleocene and early Eocene and began to populate true high oceanic environments only during the early Oligocene, triggered by the change from a halothermal deep-ocean circulation to a thermohaline regime. The relative abundance of myctophid otoliths in the bathyal late Eocene sediments of Piedmont, Italy (Schwarzhans & Carnevale 2022), and the bathyal sediments in the Lillebælt Formation now indicates that some clades may have started to move earlier into the deep sea (Fig. 4). In the case of macrourids, a relatively large variety has been observed in the Lutetian of the Aquitaine Basin (Lin *et al.* 2016). Some of these no doubt would represent deepwater taxa, but how many and which remain elusive for now. The earliest macrourid in a true bathyal sediment is *Nezumia morgansi* Schwarzhans, 2019, in the middle Eocene, Bartonian equivalent of New Zealand. The data base is better for the Ophidiidae. True deepwater ophidiid species belonging to persistent genera (*Neobythites*) are known since the late Eocene of New Zealand (Schwarzhans 2019) and a more diverse association from the early Oligocene of northern Italy (Nolf & Steurbaut 2004). Otherwise, ophidiiform otoliths represented a dominant group in shallow and warm seas during the Paleocene and Eocene (Nolf & Stringer 2003; Nolf 2013; Schwarzhans 2012, 2019). The modern deepwater genera such as Neobythites are not identified prior to their first deepwater occurrence in the late Eocene. In the Oligocene of New Zealand, different *Neobythites* species were found at different palaeowater depths, indicating that migration into the deep sea occurred as a depth-related speciation event (Fig. 4). A shallow-water, nearshore fauna from the early to middle Eocene of the Seymour Peninsula,

Antarctica, has yielded several taxa of myctophids, macrourids, and ophidiids, confirming their neritic origin (Schwarzhans *et al.* 2017). The Lillebælt Clay has now shown that deepwater migration may have happened earlier in a few ophidiids; namely, in the newly established fossil otolith-based genus *Prono-*

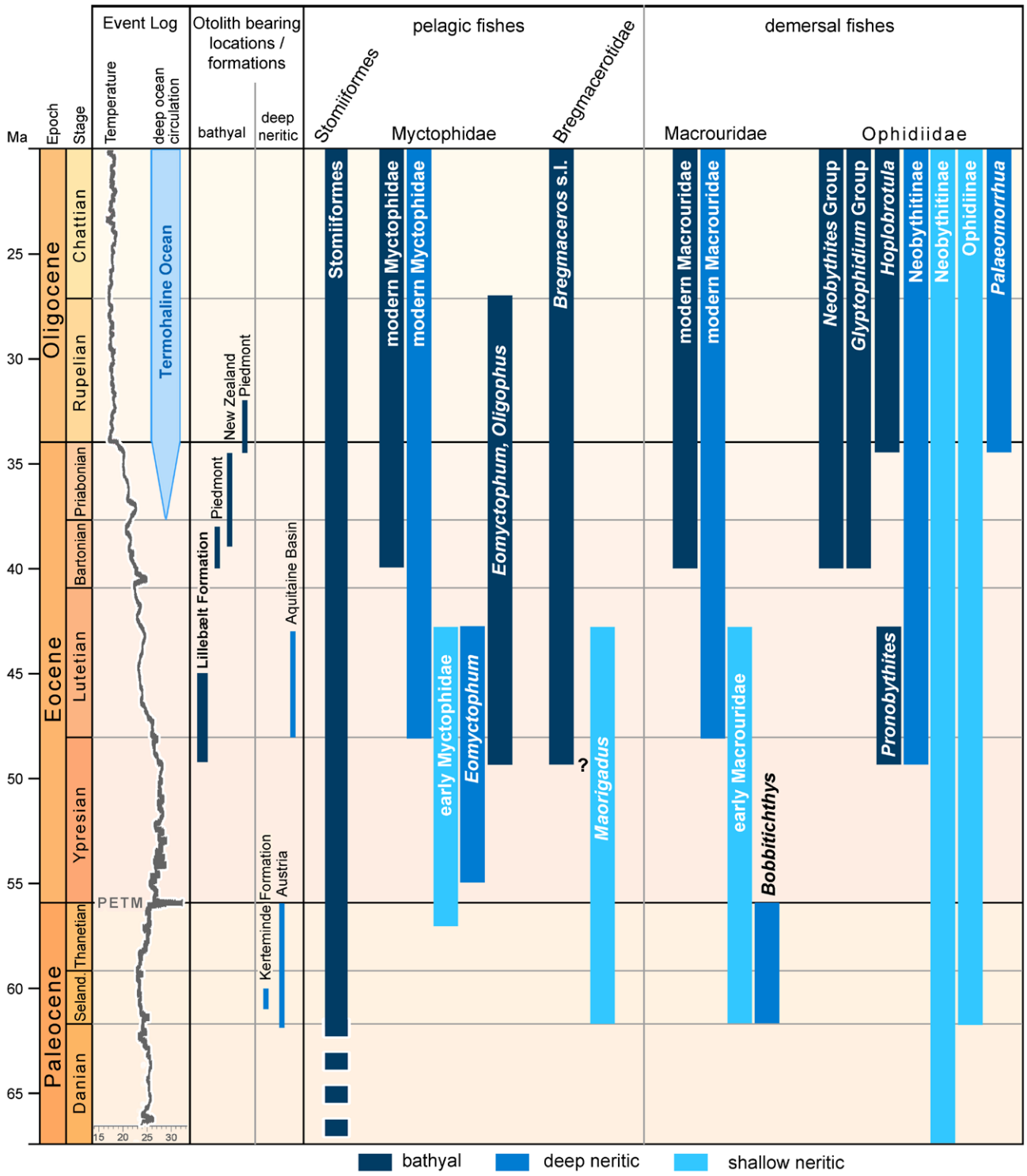

Fig. 4. Distribution and depth migration of certain modern deep-sea fish groups (bathypelagic: Stomiiformes, Myctophidae, and Bregmacerotidae; bathydemersal: Macrouridae and Ophidiidae). The '?' indicates the unclear relationship of the fossil otolith-based genus *Maorigadus* with Bregmacerotidae. Stratigraphic ranges of of locations and formations depicted from cited literature. Water temperature in event log from Rae *et al.* (2021).

bythites. There are two presumably related species in the Lutetian of the Aquitaine Basin reported by Lin *et al.* (2016), *P. bozzolo* and *P. leonardi*, which may have also been bathydemersal. This lineage became extinct in the middle Eocene, however, prior to the migration into the deep sea of another, successful migrant, the genus *Neobythites*.

Our knowledge about the colonization of the deep sea by demersal fishes during the Palaeogene and their evolution is still relatively scarce. Much better known is the history of bathybenthic foraminifera (Miller *et al.* 1992; Thomas 2007), and their fate could serve as a blueprint of what to expect in bathydemersal fish evolution. According to Miller *et al.* (1992), bathybenthic foraminifera survived the K/Pg boundary relatively unscathed in the Paleocene but became the subject of a deep-sea extinction event at the Paleocene–Eocene thermal maximum (PETM), which was presumably caused by the intrusion of warm, low-oxygenated and nutrient-poor water into the deep sea (Thomas 2007). Repopulation of the deep sea started again in the early Eocene at an initially slow pace (Miller *et al.* 1992). A gradual deep benthic foraminiferal turn-over occurred during the late Eocene and early Oligocene well-documented cooling (Miller *et al.* 1992; Thomas 2007), set off by the gradual change in the oceanic circulation from a halothermal to a termohaline regime, increasingly triggering the intrusion of cool, well-oxygenated and nutrient-rich waters into the deep sea.

Little is known about a possible bathydemersal teleost fauna prior to the PETM. The outer shelf/upper slope fauna from the middle and late Paleocene of Kroisbach (Austria) contains some taxa that are tentatively associated with Lophiiformes and Trachichthyiformes (see Schwarzhans 2012). The species of these clades are now predominantly bathydemersal. A small association of otoliths from the middle Paleocene Kerteminde Marl of Denmark was deposited at 100 m to 150 m water depth and contained a macrourid (*Bobbitichthys*) and a bythitid incertae sedis (Schwarzhans *et al.* 2021). Both faunal associations possibly contain deepwater fishes, but it is possible that these groups then (also) lived in shallow water, as evidenced by the observations made in the Eocene of the Seymour Peninsula, Antarctica (Schwarzhans *et al.* 2017). The first unequivocal bathydemersal fishes are now known from the early/middle Eocene transition described here and some probably described in Lin *et al.* (2016) from the Aquitaine Basin, followed by the discussed middle and late Eocene bathyal otolith assemblages from Italy and New Zealand. It appears that the new, post-PETM colonization of the deep sea by bathydemersal macrourids and ophidiids happened through depth-related speciation. This mechanism of migration into deep water may have started relatively early in the Eocene, but it seems that early migrating lineages were not very successful. The first successful/persistent deepwater lineages in the Macrouridae, and Ophidiidae have been identified in the Bartonian and Priabonian. Diversification and radiation of these lineages then accelerated in the early Oligocene. Depth-related speciation, however, has been observed until at least the late Oligocene (Schwarzhans 2019). The current knowledge of teleost deep-sea life during the Palaeogene of the Stomiiformes, Myctophidae, Bregmacerotidae, Macrouridae and Ophidiidae is summarized in Fig. 4. The evolution of deep-sea fishes during the Palaeogene observed so far appears to be congruent with observations made with benthic foraminifera.

Acknowledgements

The authors wish to cordially thank M. Madsen (Fredericia), I. Schnetler (Langå) and C. Heilmann-Clausen (Århus) for important consultation in respect to the geology of the locality and stratigraphic and preservation details. We furthermore wish to thank V. van Hinsbergh (Leiden) and an anonymous reviewer for their constructive reviews, which have helped to improve the article.

References

Adnet, S. 2006: Nouvelles faunes de Sélaciens (Elasmobranchii, Neoselachii) de l'Eocène moyen des Landes (Sud-Ouest France). Implications dans la connaissance des communautés de sélaciens d'eaux profonds. Palaeo Ichthyologica 10, 5–128.

Brinkhuis, H. *et al.* 2006: Episodic fresh surface waters in the Eocene Arctic Ocean. Nature, Letters 441, 606–609. https://doi.org/10.1038/nature04692

Carlsen, A.W. & Cuny, G. 2014: A study of the sharks and rays from the Lillebælt Clay (Early–Middle Eocene) of Denmark, and their palaeoecology. Bulletin of the Geological Society of Denmark 62, 39–88. https://doi.org/10.37570/bgsd-2014-62-04

Carnevale, G. & Rindone, A. 2011: The teleost fish *Paravinciguerria praecursor* Arambourg, 1954 in the Cenomanian of north-eastern Sicily. Bolletino della Società Paleontologica Italiana 50, 1–10.

Carnevale, G., Schwarzhans, W., Schrøder, A.E. & Lindow, B.E.K. 2022: An Eocene conger eel (Teleostei, Anguilliformes) from the Lillebælt Clay Formation, Denmark. Bulletin of the Geological Society of Denmark 70, 53–67. https://doi.org/10.37570/bgsd-2022-70-05-rev

Chaine, J. & Duvergier, J. 1934: Recherches sur les otolithes des poissons. Etude descriptive et comparative de la sagitta des téléostéens. Actes de la Société Linnéenne de Bordeaux 86, 1–254.

Heilmann-Clausen, C. 1984: Lithostratigraphy and depositional environments in the upper Paleocene and Eocene of Denmark. Bulletin of the Geological Society of Denmark 33, 287–323. https://doi.org/10.37570/bgsd-1984-33-26

Heilmann-Clausen, C., Beyer, C. & Snowball, I. 2010: Stratigraphy and paleoenvironment of the Danish Eocene Azolla event. Geophysical Research Abstracts 12, 1 (EGU 2010-12095).

King, C. 2016 (ed. by Gale, A.C. & Barry, T.L.): A revised correlation of Tertiary rocks in the British Isles and adjacent areas of NW Europe. The Geological Society, Special Report 27, 719 pp. https://doi.org/10.1144/SR27

Koken, E. 1884: Über Fisch-Otolithen, insbesondere über diejenigen der norddeutschen Oligocän-Ablagerungen. Zeitschrift der Deutschen Geologischen Gesellschaft 36, 500–565.

Lin, C.-H., Nolf, D., Steurbaut, E. & Girone, A. 2017: Fish otoliths from the Lutetian of the Aquitaine Basin (SW France), a breakthrough in the knowledge of the European Eocene ichthyofauna. Journal of Systematic Palaeontology 15, 879–907. https://doi.org/10.1080/14772019.2016.1246112

Martin, R.P., Olson, E.E., Girard, M.G., Smith, W.L. & Davis M.P. 2018: Light in the darkness: new perspective on lanternfish relationships and classification using genomic and morphological data. Molecular Phylogenetics and Evolution 121, 71–85. https://doi.org/10.1016/j.ympev.2017.12.029

Miller, K.G., Katz, M.E. & Berggren, W.A. 1992: Cenozoic deep-sea benthic foraminifera: A tale of three turnovers. In: Studies in benthic foraminifera, BENTHOS '90, Sendai. Tokai University Press, 67–75.

Nolf, D. 1988: Les otolithes de téléostéens éocènes d'Aquitaine (sud-ouest de la France) et leur intérêt stratigraphique. Mémoire de l'Académie royale de Belgique, Classe des Sciences, 4°, 2e série 19, 1–147.

Nolf, D. 2013: The diversity of fish otoliths, past and present. Royal Belgian Institute of Natural Sciences, Brussels, 222 pp.

Nolf, D. & Steurbaut, E. 1988: Description de la première faune ichthyologique exclusivement bathyale du Tertiare d'Europe: otolithes de l'Oligocène Inférieur du gisement de Pizzocorno, Italie septentrionale. Bulletin de l'Institut Royal des Sciences Naturelles de Belgique 57, 217–230.

Nolf, D. & Steurbaut, E. 1990: Découverte de poissons bathyaux d'âge Oligocène inférieur à Pizzocorno, près de Voghera. Quaderni della sezione di Scienze Naturali del Civico Museo di Voghera 10, 15–31.

Nolf, D. & Steurbaut, E. 2004: Otolithes de poissons de l'Oligocène inférieur du Basssin liguro-piémontais oriental, Italie. Rivista Piemontese di Storia naturale 25, 21–68.

Nolf, D. & Stringer, G.L. 2003: Late Eocene (Priabonian) fish otoliths from the Yazoo Clay at Copenhagen, Louisiana. Louisiana Geological Survey, Geological Pamphlet 13, 1–23.

Paxton, J.R. 1972: Osteology and relationships of the lanternfishes (family Myctophidae). Bulletin of the Natural History Museum of Los Angeles County, Science 13, 1–81.

Pollerspöck, J., Nielsen, K.A., Feichtinger, I. & Straube, N. 2023: New records of fossil deep-sea shark teeth from the Lillebælt Clay (Early–Middle Eocene) of Denmark. Bulletin of the Geological Society of Denmark 72, 153–173. https://doi.org/10.37570/bgsd-2023-72-06

Rae, J.W.B., Zhang, Y.G., Liu, X., Foster, G.L., Stoll, H.M. & Whiteford, R.D.M. 2021: Atmospheric CO_2 over the past 66 million years from marine archives. Annual Review of Earth and Planetary Sciences 49, 599–631. https://doi.org/10.1146/annurev-earth-082420-063026

Schnetler, I. & Heilmann-Clausen, C. 2011: The molluscan fauna of the Eocene Lillebælt Clay, Denmark. Cainozoic Research 8, 41–99.

Schwarzhans, W. 1978: Otolith-morphology and its usage for higher systematical units with special reference to the Myctophiformes s.l. Mededelingen van de Werkgroep voor Tertiaire en Kwartaire Geologie 15, 167–185.

Schwarzhans, W. 2007: Otoliths from casts from the Eocene Lillebælt Clay Formation of Trelde Næs near Fredericia (Denmark), with remarks on the diet of stomatopods. Neues Jahrbuch Geologie und Paläontologie Abhandlungen 246, 69–81. https://doi.org/10.1127/0077-7749/2007/0246-0069

Schwarzhans, W. 2010: Otolithen aus den Gerhartsreiter Schichten (Oberkreide: Maastricht) des Gerhartsreiter Grabens (Oberbayern). Palaeo-Ichthyologica 4, 1–100.

Schwarzhans, W. 2012: Fish otoliths from the Paleocene of Bavaria (Kressenberg) and Austria (Kroisbach and Oiching-Graben). Palaeo Ichthyologica 12, 1–88.

Schwarzhans, W. 2019: Reconstruction of the fossil marine bony fish fauna (Teleostei) from the Eocene to Pleistocene of New Zealand by means of otoliths. Memorie della Società Italiana di Scienze Naturali e del Museo di Storia Naturale di Milano 46, 3–326.

Schwarzhans, W. & Carnevale, G. 2021: The rise to dominance of lanternfishes (Teleostei: Myctophidae) in the oceanic ecosystems: a paleontological perspective. Paleobiology 47, 446–463. https://doi.org/10.1017/pab.2021.2

Schwarzhans,W. & Carnevale, G. 2022: Bathyal fish otoliths from the Bartonian (Eocene) of the Turin Hills (Piedmont, Italy). Rivista Italiana di Paleontologia e Stratigrafia 128, 575–583. https://doi.org/10.54103/2039-4942/17086

Schwarzhans, W., Mörs, T., Engelbrecht, A., Reguero, M. & Kriwet, J. 2017: Before the freeze: otoliths from the Eocene of Seymour Island, Antarctica, reveal dominance of gadiform fishes (Teleostei). Journal of Systematic Palaeontology 15, 147–170. https://doi.org/10.1080/14772019.2016.1151958

Schwarzhans, W., Milàn, J. & Carnevale, G. 2021: A tale from the middle Paleocene of Denmark: A tube-dwelling predator documented by the ichnofossil *Lepidenteron mortensi* n. isp. and its predominant prey, *Bobbitichthys* n. gen. *rosenkrantzi* (Macrouridae, Teleostei). Bulletin of the Geological Society of Denmark 69, 35–52. https://doi.org/10.37570/bgsd-2021-69-02

Thomas, E. 2007: Cenozoic mass extinctions in the deep sea: What perturbs the largest habitat on Earth? The Geological Society of America, Special Paper 424, 1–23. https://doi.org/10.1130/2007.2424(01)

Thomsen, E., Abrahamsen, N., Heilmann-Clausen, C., King, C. & Nielsen, O.B. 2012: Middle Eocene to earliest Oligocene development in the eastern North Sea Basin: Biostratigraphy, magnetostratigraphy and palaeonvironment of the Kysing-4 borehole, Denmark. Palaeogeography, Palaeoclimatology, Palaeoecology 350–352, 212–235. https://doi.org/10.1016/j.palaeo.2012.06.034

Fish otoliths from the basal Oligocene Viborg Formation in Denmark

WERNER W. SCHWARZHANS, KENT ALBIN NIELSEN & KAI INGEMANN SCHNETLER

Geological Society of Denmark
https://2dgf.dk

Received 20 May 2024
Accepted in revised form
16 June 2024
Published online
02 July 2024

Schwarzhans, W.W., Nielsen, K.A. & Schnetler, K.I. 2024. Fish otoliths from the basal Oligocene Viborg Formation in Denmark. Bulletin of the Geological Society of Denmark, Vol. 73, pp. 113–133. ISSN 2245-7070.
https://doi.org/10.37570/bgsd-2024-73-07

The Viborg Formation is the lowest part of the early Oligocene in Denmark and represents the upper part of nannoplankton zone NP21. Here we describe a small assemblage of otoliths from the Viborg Formation obtained from five localities that yielded 88 specimens of nine species. The composition of the otolith-based fish species is transitional between the terminal Eocene (Priabonian) faunas from the Latdorf Formation of northern Germany and its equivalents and the middle and upper Rupelian. The Viborg otolith association witnessed the first arrivals of the subsequently dominant Gadidae (*Trisopterus elegans*) and the migration of certain species of the merlucciid genus *Palaeogadus* from the Eastern Paratethys through the Polish gateway. Furthermore, the otoliths from the Viborg Formation fill an important gap in the previous knowledge of late Eocene and early Oligocene otolith associations in the North Sea Basin and thus facilitate some refinement of their biostratigraphic usage.

Keywords: otoliths, lower Oligocene, Viborg Formation, Denmark, otolith stratigraphy, palaeobiogeography.

Werner W. Schwarzhans [wwschwarz@aol.com], Zoological Museum, Natural History Museum of Denmark, Universitetsparken 15, 2100 Copenhagen Ø, Denmark, and Ahrensburger Weg 103, 22359 Hamburg, German, http://orcid.org/0000-0003-4842-7989. Kent A. Nielsen [kent@ksjm.dk], Tingskoven 22, DK -7330 Brande, Denmark, https://orcid.org/0000-0002-5800-5774; Kai Ingemann Schnetler [ingemann@schnetler.dk], Fuglebakken 14, Stevnstrup, DK - 8870 Langå, Denmark, https://orcid.org/0009-0000-2298-2875.

Oligocene molluscs from Denmark have been studied and findings have been published in several papers, including those by Ravn (1907), Harder (1913), Eriksen (1937), Olsen (1955), Schnetler & Beyer (1987, 1990), Schnetler (2008) and Schnetler *et al*. (2024). Ulleberg (1974, 1987, 1994) studied the foraminifers, and the dinocysts (dinoflagellate cysts) were studied by Śliwińska *et al*. (2012) and King (2016). Otoliths that have commonly been studied from Oligocene deposits in the southern North Sea Basin (e.g., Koken 1884, 1891; Weiler 1942; Schwarzhans 1974, 1994; Nolf 1977; Gaemers & van Hinsbergh 1978), but little is known about Oligocene otoliths from Denmark. Schwarzhans (2008a) studied the otoliths of the Branden Clay (upper Oligocene of Denmark). The present paper comprises the study of the otoliths from the Viborg Formation; a study of the otoliths of the Brejning Formation is being prepared.

Oligocene deposits are found in a rather limited belt through Jutland, but they likely had a greater distribution, as isolated blocks with fossils from the Oligocene have been found further east, such as on Funen. To the west and south of Jutland, the Oligocene deposits are covered by younger deposits, and continue to the west under the North Sea. The rock types, strata, and fossils have been treated in many papers, and several formations and biostratigraphic units have been proposed. Previously, the Oligocene was divided into three units, and Ravn (1907) uses the terms Branden Clay for the middle Oligocene and Cilleborg Clay for the upper Oligocene. Ødum (1936) assigned the Søvind Marl to the lower Oligocene and considered the so-called Katholm blocks from Djursland to be freshwater deposits from the lower Oligocene. The latter are now considered to be from the Jurassic, and the Søvind Marl is assigned to the late Eocene. The Oligocene deposits in the current understanding are the lower Oligocene Viborg Formation (Christensen & Ulleberg 1973, 1974), the lower upper

Oligocene Branden Clay and the upper Oligocene Brejning Formation (Rasmussen 2010). Śliwińska *et al.* (2012) introduced the provisionally stratigraphic Unit X, which underlies the Brejning Formation at two localities in the Limfjorden area (Schnetler *et al.* 2024).

Stratigraphy of the Viborg Formation and previously recorded lower Oligocene otolith assemblages

The Viborg Formation is the earliest lithostratigraphic unit in the lower Oligocene in Denmark (Śliwińska *et al.* 2012; King 2016); it rests unconformably on the late Eocene (Priabonian) Søvind Formation and contains abundant reworked late Eocene micro- and nannofossils which complicates the stratigraphic interpretation (Śliwińska *et al.* 2012). The Eocene–Oligocene (E/O) boundary has been a matter of controversy, and since the Global Stratotype Section and Point (GSSP) in the Massignano Quarry, Italy, was ratified, has been denoted by the stratigraphically highest occurrence (HO) and last appearance datum (LAD) of the planktonic foraminiferal genus *Hantkenina* (see discussion by Berggren *et al.* 2018) at approximately 33.9–33.7 Ma (million years ago). This definition sets the E/O boundary slightly deeper than the LAD of the dinoflagellate cyst *Areospheridium diktyoplokum* at 33.3 Ma, which has been proposed as an alternative marker (see discussion in King 2016). *Areospheridium diktyoplokum* occurs commonly in the Viborg Formation but was considered to have been reworked, while the (rare) presence of the dinoflagellate cyst *Wetzeliella gochtii* would indicate Oligocene age (Śliwińska *et al.* 2012; King 2016). The Viborg Formation is thus considered to be in dinocyst subzone DE20b (Schnetler *et al.* 2024), the upper part of the Chrone C13r (Schnetler *et al.* 2024), the upper part of nannoplankton zone NP21 (Śliwińska *et al.* 2012), and the North Sea Oligocene zone NSO1 (Śliwińska *et al.* 2012), which represents the earliest Oligocene in the North Sea Basin (see also King 2016).

In past literature, various otolith assemblages have been described as being from the early Oligocene or 'Lattorfian' or 'Tongerian' stages (previously considered to be regional stages of the lower Oligocene in the North Sea Basin) from several localities as follows. Koken (1884, 1891) described otoliths from Latdorf, and Müller & Rozenberg (2000) described a large collection of otoliths from time-equivalent strata in nearby Atzendorf locality. Müller & Rozenberg discussed in detail their observations regarding Koken's and von Koenen's historic Latdorf material, which was found to be a mixture of middle Eocene, 'Lattorfian' and Rupelian s.s. (as defined by Müller & Rozenberg 2000) material, as revealed by nannoplankton identified from sediment that was extracted from inside gastropod tests (as cited from Ritzkowski 1968). They also commented on the history and scope of the term 'Lattorfian' and recommended maintaining it as a regional North Sea Basin stage for the lowermost Oligocene and the Rupelian s.s. for the later part of the early Oligocene (but see Müller 2008). Müller & Rozenberg (2000) noted that nannofossils were analyzed from the locality Atzendorf by Andreeva-Grigorovich and indicated zone NP21. They placed the Atzendorf samples in the upper NP21, that is, lower Oligocene, without further explanation, but Müller (2008) proposed that these samples are from the uppermost Priabonian (lower NP21). King (2016) considered the Latdorf Formation to be lower NP21, that is, the uppermost Eocene (Priabonian) based on the presence of *Areospheridium diktyoplokum*. King (2016) also indicated that the Latdorf Formation is in North Sea zone NS27 or NS28 based on the presence of *Uvigerina germanica*, which would be consistent with an upper Priabonian age.

Nolf (1974) described a large otolith association from the Grimmertingen Sand in Belgium as part of the lower Oligocene 'Tongerian.' According to King (2016), the Tongerian comprises Priabonian and early Rupelian strata, and similar to the Lattorfian, the term 'Tongerian' is no longer in use. According to King (2016) the Grimmertingen Sands are in nannoplankton zone NP21; dinocyst zone DE20; and because of the presence of *Uvigerina germanica*, in the North Sea zone NS27 or NS28. Thus, the Grimmertingen Sands are considered late Priabonian in age (King 2016), which is more or less equivalent in time to the Latdorf and Atzendorf localities, although the Grimmertingen Sands were probably deposited in shallower water.

Schwarzhans (1973, 1977) described otoliths from a mine shaft excavation near Hückelhoven, North Rhein-Westfalia, Germany, which at the time were considered to be of early Oligocene age. To the best of our knowledge, no nannoplankton or dinocyst evaluations were performed for these sediments. The otolith association is similar to the one described by Nolf (1974) from the Grimmertingen Sands, and therefore, we now consider them to have originated from the uppermost Priabonian as well.

In a series of articles, Gaemers described otoliths from the lower and middle Oligocene from the Sands of Berg in Belgium (Gaemers 1972), from the 'middle' Oligocene of Poland (Gaemers 1981), from the Basselde Sand in Ruisbroek, Belgium (Gaemers 1984), from the early Rupelian in Heide-Boskant, Belgium

(Gaemers 1985), and in cooperation with van Hinsbergh, from the 'De Vlijt' clay pit near Winterswijk, The Netherlands (Gaemers & van Hinsbergh 1978). Steurbaut & Herman (1978) described otoliths from the Boom Clay in Belgium and established a nannoplankton-based biostratigraphy for the interval. The Berg Sand Member is considered to be from nannoplankton zone NP23. The upper Priabonian Bassevelde Sand was erroneously identified at Ruisbroek; instead, the sediments are now placed in the Ruisbroek Member from nannoplankton zone NP 22 (Steurbaut 1986a, b; King 2016). At Winterswijk, three Rupelian members ('Afzettingen' in Dutch) have been distinguished; from bottom to top, they are the Ratum Member, the Brinkheurne Member, and the Winterswijk Member (van den Bosch *et al.* 1975). The Ratum Member is considered to be from nannoplankton zone NP 22 (King 2016), while the Brinkheurne and Winterswijk

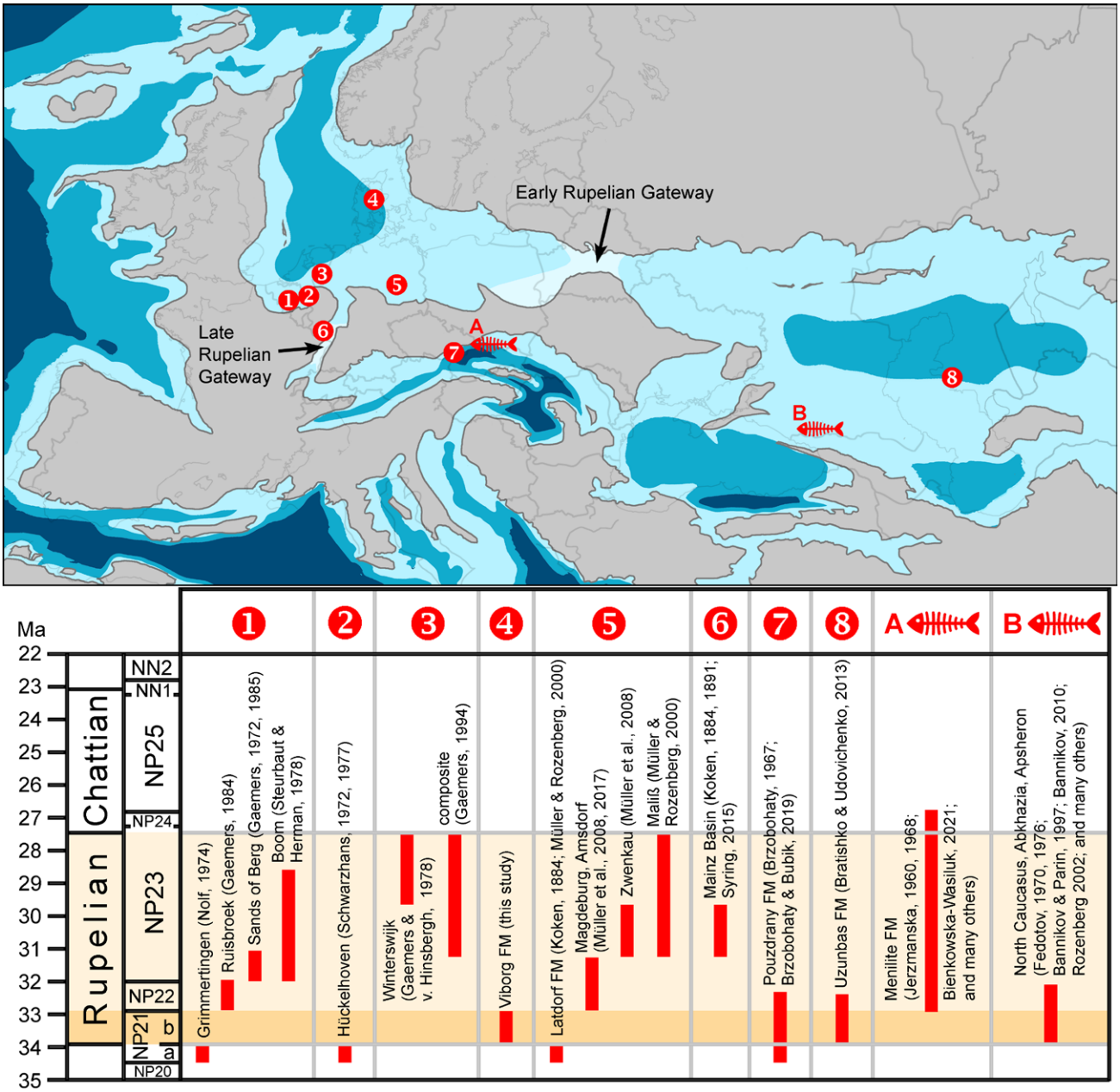

Fig. 1. Early Oligocene (Rupelian) fish database for otoliths (numbers) and articulated skeletons (fish skeleton graph) in the North Sea Basin and the Paratethys. The upper figure portrays the presumed early Oligocene palaeogeographic configuration at approximately 35 Ma (Late Rupelian Gateway at approximately 30 Ma); this is based on Blakey (2020) with alterations that are based on van der Boon *et al.* (2018, 2019). The lower figure shows the approximate stratigraphic ranges of the fish faunas and references thereto. The Viborg Formation is highlighted.

members are from zone NP23. The otoliths described by Gaemers & van Hinsbergh (1978) originate from the Brinkheurne and Winterswijk members.

Syring (2015) described a large otolith-based fish fauna from the Rupelian of the Mainz Basin, Germany. These were obtained from the nearshore Alzey Formation and basinward Bodenheim Formation, both of which are in nannoplankton zone NP23 (middle to late Rupelian, according to literature cited in Syring 2015). This represents the short period during which the North Sea Basin was connected southward to the Western Paratethys through the Mainz Basin and the Upper Rhine Valley.

A rich otolith association was described by Brzobohatý (1967) from the Pouzdrany Formation in the Central Paratethys in the Czech Republic. These otoliths were found in sediments from the *Globigerina oligocenica* and the *Turborotalia ampliapertura* planktonic foraminifer zone, which corresponds to nannoplankton zones NP21–22 (Brzobohatý & Bubik 2019). The recorded otolith-based fish fauna is essentially a deep-water assemblage.

We conclude from this literature review that the Viborg Formation is younger than the Latdorf and Grimmertingen faunas and older than the Rupelian sediments studied in the various articles by Gaemers as well as Gaemers & van Hinsbergh. The Viborg Formation could be time equivalent to the Uzunbas Formation in Western Kazakhstan from where Bratishko & Udovichenko (2013) described a rich otolith association. However, in the North Sea Basin, the otoliths from the Viborg Formation fill a gap between associations from the terminal Priabonian and the Rupelian of NP22–23. Elsewhere, Nolf & Steurbaut (2002) described otoliths from the Rupelian in the Aquitaine Basin in France as being from an interval younger than NP22. They also described otoliths from deep marine, bathyal sediments from the interval NP21 to NP23 in northern Italy (Nolf & Steurbaut 1988, 1990 2004).

Numerous articulated fossil fish skeletons, some with preserved otoliths *in situ*, have been found in the lower Oligocene of the Northern Caucasus (see the check-list of Bannikov & Parin 1997). The key locality is the Belaya River south of Abadzekhskaya in the Maikop district as well as Abkhazia and Azerbaijan on the Apcheron Peninsula (Bannikov & Parin 1997). These fishes originated from the Pshekhian—the lower Khadumian equivalent of the regional Caspian stratigraphy that corresponds to the upper nannoplankton zones NP21 and NP22 (Popov *et al.* 2002, 2004; Vernyhorova & Ryabokon 2020). Bannikov & Parin (1997) posited that certain species occurred throughout the 'Pshekha horizon' (= Pshekhian), while others were found only in the lower or upper part, but they did not provide details. The skeleton-based fish fauna from the Menilite Formation of the Czech Republic, Poland, and Ukraine is slightly younger in age, ranging from NP22 to NP24 (Brzobohatý & Bubik 2019)

The stratigraphic position of the discussed strata and localities are summarised in Figure 1. In the following, we use NP21a for the lower part of nannoplankton zone NP21 in the Eocene (late Priabonian) and NP21b for the upper part of nannoplankton zone NP21 in the Oligocene (early Rupelian). NP21a and NP21b are not formally defined biostratigraphic units, and the usage herein is meant to be for convenience only; no formal meaning is intended.

Materials and methods

The otoliths described herein originated from five localities, four of which were temporary and are no longer accessible, and one that is a coastal outcrop (Kysing). The localities are as follows (Fig. 2).

Ølst *and Hinge* (Larsen & Kronborg 1994)
In the clay pit at Ølst, more than 20 m of the Viborg Formation were exposed. Approximately 1 m of the basal Grundfør Clay Member was exposed and overlaid the Søvind Marl with a sharp boundary; this was followed by approximately 20 m of Viborg Clay Member (Viborg Formation). The Viborg Formation is unconformably overlain by the sandier and more glauconitic Brejning Clay. Molluscs have been collected by KIS since the early 1980s; they were hand-picked from the surface, especially after periods of rain and were easy to recognise because of their whitish colour, which stood out against the dark pyritic clay. Molluscs were not common. The fine-grained, sticky clay was not easy to process by washing and sieving. In 2011, the excavation work in the clay pit ended, and the walls of the pit are now covered by vegetation, so further material cannot be collected. In the clay pit at Ølst, a large landslide in December 2023 was an environmental disaster that has also made further geological observations and collection impossible. Collection of material is still possible in the clay pit at Hinge.

Hadsten (road excavation 1980)
During the first months of 1980, a roadcut was excavated north of Hadsten and exposed a section with Viborg Clay and Brejning Clay, which was observed by KIS in March 1980. During the following months, several molluscs were collected. Since then, the locality has been completely covered by vegetation.

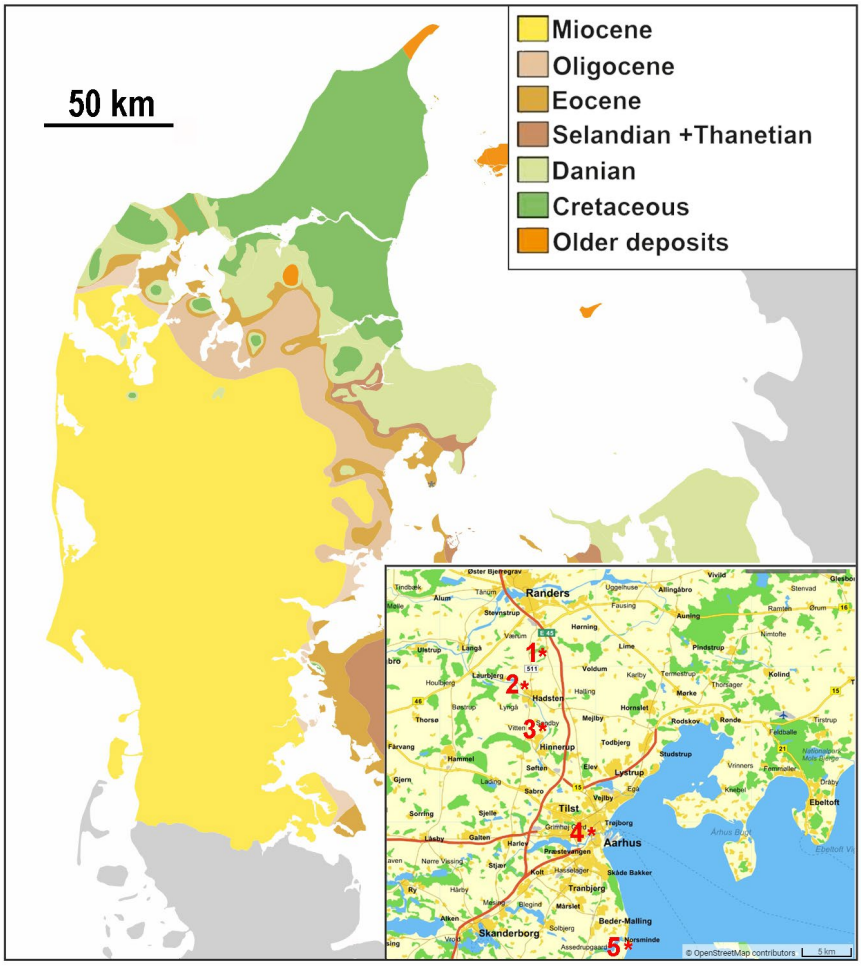

Fig. 2. Sampled localities from the Viborg Formation in Denmark. Geological map after Håkansson & Pedersen 1992 and Jensen 1974. The localities are 1: Ølst, 2: Hadsten, 3: Grundfør, 4: Aarhus, 5: Kysing.

***Grundfør* (Larsen & Kronborg 1994)**

Rasmussen (1968) mentioned specimens of *Fusiturris duchastelii* from Grundfør in his discussion of a Miocene form of this species (now considered to be *Fusiturris flexiplicata*) but offered no details regarding the locality. KIS collected fossils from the clay pit between 1975 and approximately 1985. The brickworks were closed in 1979, and the clay pit is now waterlogged. In the 1970s, a section with a sharp boundary between the Eocene Søvind Marl and the Oligocene Viborg Formation could be observed. In the deepest part of the pit, a few metres of Søvind Marl were exposed; this was unconformably overlain by approximately 1 m of Grundfør Clay, which was followed by approximately 10 m of Viborg Clay. Molluscs were collected directly from the Viborg Clay and from the surface.

***Aarhus* (Ravn 1907; Harder 1913)**

During railway construction between Arhus and Randers in 1860, an excavation occurred west of Aarhus. The railway track followed the Aarhus Å valley. A low hill was excavated for the tracks to the railway station near the old center of Aarhus. Sand and clay layers were exposed in the northern part of this excavation. The lecturer Kristian Erslev examined the layers and collected many molluscs and other fossils, which are housed at the Natural History Museum of Denmark. Ravn (1907) studied this material without describing the sediments in any detail, because Harder had concurrently started a study for the Geological Survey of Denmark of material from a 1906 excavation for the railway tracks. The increasing railway traffic made a wider excavation necessary, and once again, the layers in the northern part were exposed. This material forms the basis for Harder's most important palaeontological paper "De oligocæne Lag i Jærnbanegennemskæringen ved Aarhus" (Harder 1913). This study is still fundamental for our knowledge of the Danish Oligocene molluscs, as the locality yielded faunas from early Oligocene and late Oligocene in age. Both sediments yielded otoliths.

Because of the growth of Aarhus, further extensions of the railway area were needed in the 1920s, and once again, the Oligocene sediments were exposed. Ødum collected several specimens from the early and late Oligocene in 1931, but he did not publish his findings.

As his field diary is no longer available, further data are unknown.

Kysing

The otoliths were sampled from a coastal cliff section at Kysing (GPS coordinates: 10°16′04.1″E, 56°00′40.6″N; see also Thomsen *et al.* 2012). Over three years (2022–2024), approximately 1000 kg of material was processed and sieved on the shore of Kysing. At the Kysing outcrop, about 1 meter of the grey clay from the Viborg Formation was exposed; it was overlain by a lighter grey clay. The procedure involved the following steps. Soft clay samples collected during the wintertime (15 kg) were placed in a plastic bucket (20 L) and ocean water was added. Mechanical stirring of the mixture was performed using an electric screwing machine fitted with a paddle mixer. The disaggregated material was poured through double nylon stockings. The process was repeated for 1000 kg until all the material was processed as described. Generally, three buckets (approximately 45 kg) of material were reduced to approximately 1 to 2 kg before the nylon stocking had to be replaced. The concentrated material was carried home and further processed in the following steps. The material was rinsed with cold water while the nylon stocking was gently massaged until clear water was leaving the stocking. The material was then rinsed with lukewarm water for a few minutes before a small portion of household dishwashing liquid (e.g., 5–15% anionic surfactants, <5% amphoteric surfactants, butylphenyl methylpropional) was added while the nylon stocking was gently massaged. After soaking for some minutes, cold water was used to remove the excess soap. This process removed the last clay from the material. The material was then transferred to a large (7 × 20 × 30 cm) plastic container and water was added. The floating organic material was stirred to ensure that no inorganic material was attached. The organic material was then slowly emptied from the plastic container. This process was repeated until all organic material was removed. The remaining water was decanted from the container before the material was dried in an oven at 90°C. The final clean fossil material was sorted using a binocular microscope.

The otoliths were photographed with a Canon EOS 1000D that was mounted on a Wild M400 photomacroscope and remotely controlled from a computer. Individual images of every view of the objects were taken at ranges of fields of depths and then stacked using the Helicon Focus software from Helicon Soft (Kharkiv, Ukraine). Exposure and contrast adjustments as well as retouching was done in Adobe Photoshop where necessary to improve the images without altering any morphological features. All otoliths presented are depicted from the right side; left-side otoliths are reversed for comparison. The described otoliths are housed in the collections of the Natural History Museum of Denmark (NHMD), Universitetsparken 15, DK-2100 Copenhagen. Comparative otoliths from the Latdorf Formation are figured from the collection of the Römer Museum at Hildesheim, Germany.

https://zoobank.org/D2696DD9-59B3-41D8-8148-B6F4B8CDD851

Systematic palaeontology

In the following section, we discuss the otoliths from the Viborg Formation as compared to data from the earlier Lattorfian/Tongrian and the later Rupelian. Detailed descriptions are not included since all species have previously been described. The systematics follow Nelson *et al.* (2016), whereas the otolith terminology follows Koken (1884) with amendments by Schwarzhans (1978).

Order Albuliformes Jordan, 1923

Family Pterothrissidae Gill, 1893

Genus *Pterothrissus* Hilgendorf, 1877

Pterothrissus umbonatus (Koken, 1884)

Fig. 3A–F

1884 *Otolithus* (*inc. sedis*) *umbonatus* - Koken: pl. 12, fig. 12.
?1884 *Otolithus* (*inc. sedis*) *minor* - Koken: text only, non pl. 11, fig. 14 (*Pterothrissus robustus*).
?1891 *Otolithus* (*inc. sedis*) *minor* Koken, 1884 - Koken: text-fig. 23–24.
?1891 *Otolithus* (*inc. sedis*) *lunaburgensis* - Koken: fig. 26.
1978 *Pterothrissus umbonatus* (Koken, 1884) - Gaemers & van Hinsbergh: pl. 1, fig. 1–4.
1981 *Pterothrissus umbonatus* (Koken, 1884) - Schwarzhans: p. 81.
2000 *Pterothrissus umbonatus* (Koken, 1884) - Müller & Rozenberg: pl. 1, fig. 4, ?5.
2003 *Pterothrissus umbonatus* (Koken, 1884) - Rozenberg: pl. 1, fig. 3 (?fig. 1–2, 4–5).
?2015 *Pterothrissus umbonatus* (Koken, 1884) - Syring: pl. 1, fig. 13–22.

Material. 7 specimens, Viborg Formation: 5 specimens Ølst (NHMD 1758019); 2 specimens Grundfør (NHMD 1758020).

Discussion. *Pterothrissus umbonatus* was described by Koken (1884) based on large specimens from Latdorf, which is now considered to be of latest Priabonian age (see stratigraphy section above). We present two large specimens from the type locality for comparison (Fig. 3G–J). *Pterothrissus. umbonatus* was later recorded from many different localities that range in age from middle Eocene to Late Miocene, although these records were often based on relatively small and thus non-diagnostic juvenile specimens (see discussion in Schwarzhans 1981). Schwarzhans (1981) adopted a rather wide taxonomic and morphological view but stated that specimens smaller than 7 mm to 9 mm in length cannot be convincingly identified to species level. Rozenberg (2003) concluded that the presenta understanding of *P. umbonatus* reflects a 'species basket' (Rozenberg 2003) rather than a discrete species. More recently, Bratishko & Udovichenko (2013) described *P. caspiensis* from time-equivalent strata of the Uzunbas Formation in Western Kazakhstan in the Caspian Basin. They distinguished *P. caspiensis* from *P. umbonatus* (Koken, 1884) by, quote, "the distinct rectangular outline, the well-expressed postdorsal angle and the concave outer face." In fact, the first two characteristics are shared with *P. umbonatus* from the type locality, and only the concave outer face may be distinctive, which is slightly convex-to-flat in *P. umbonatus* and changes with ontogeny.

Koken described another species pertaining to *Pterothrissus* from the Rupelian and Chattian, *P. minor* (Koken, 1884). The specimen figured in his 1884 article originated from the Chattian in Kassel (Koken's fig. 14 on plate 11) but was subsequently assigned to represent *P. robustus* (Koken, 1891); Koken (1891) later depicted small specimens form the Rupelian in the Mainz Basin to represent *P. minor*. Koken (1891) furthermore described a species from the Miocene of Lüneburg, northern Germany, as *Ot.* (*inc. sed.*) *lunaburgensis* that resembles typical specimens of *P. umbonatus* in all pertinent characters. The speci-

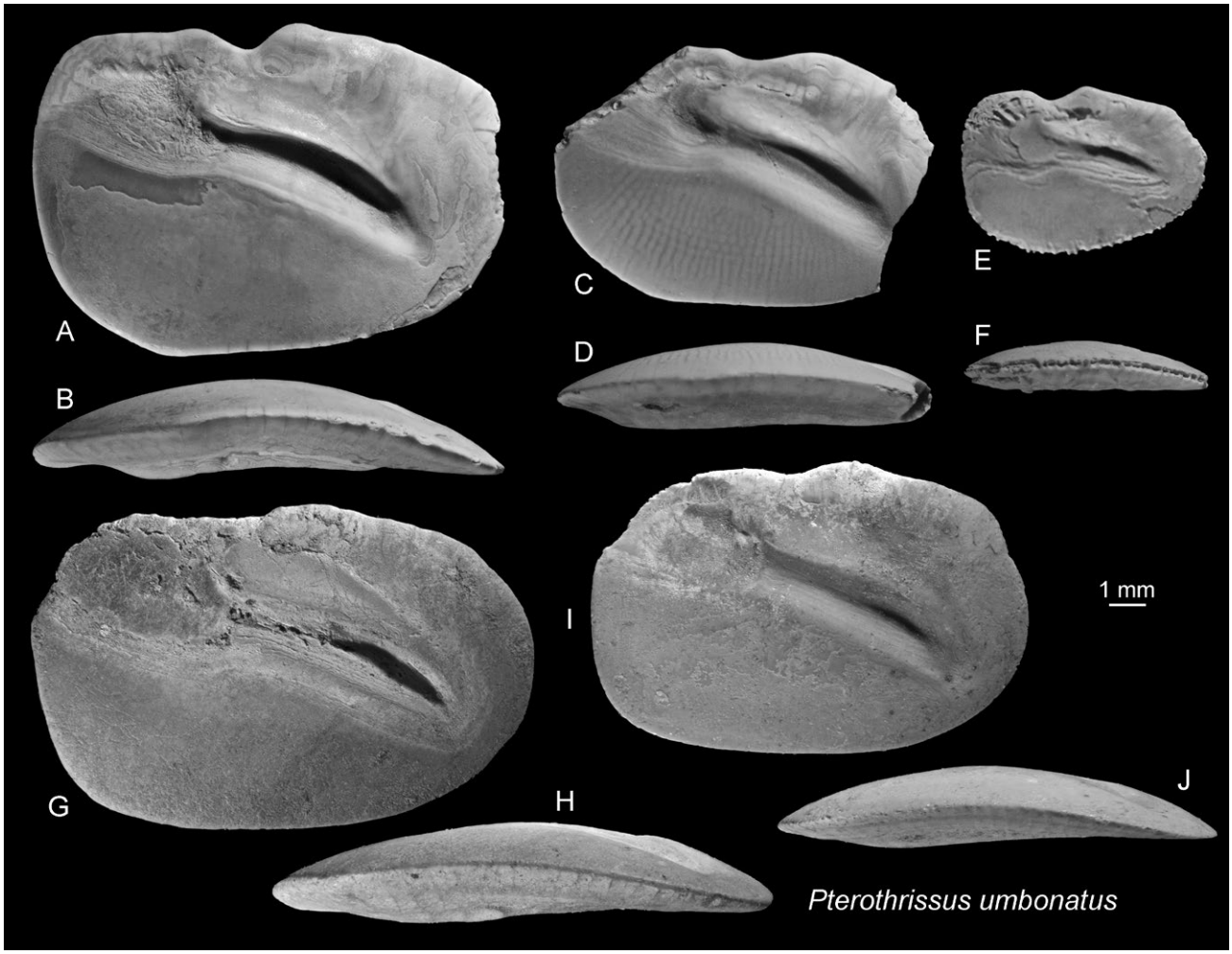

Fig. 3. *Pterothrissus umbonatus* (Koken, 1884). **A–F,** Viborg Formation. **A–D,** Ølst, NHMD 1758019. **E–F,** Grundfør. NHMD 1758020. **G–J,** Latdorf Formation, Latdorf, Germany, Römer Museum Hildesheim. **B,D,F,H,J** ventral views, **G–J** reversed.

men is lost and the stratigraphic allocation appears questionable. Syring (2015) portrayed an ontogenetic sequence of otoliths as *P. umbonatus* from the Rupelian of Waldböckelheim in the Mainz Basin, the largest of which (Syring's fig. 22) is approximately 9.5 mm in length. Syring described a mildly concave outer face, and the figures show a somewhat rounded postdorsal angle and slightly tapering posterior tip. We therefore tentatively allocate his records to *P. umbonatus* as well. Consequently, *P. minor* as redefined by Koken (1891) could be interpreted as a juvenile specimen of *P. umbonatus*. Nevertheless, the *Pterothrissus umbonatus* complex needs to be comprehensively reviewed to incorporate as many of the known large specimens as possible. This task is beyond the scope of this study. We conclude that only specimens from the Priabonian and Rupelian in the North Sea Basin can be safely attributed to *P. umbonatus* and that all other records therefore require revision.

For now, we consider the following traits as diagnostic for *P. umbonatus* s.s.: The ratio of otolith length to height is 1.4–1.6. The sulcus is inclined against the dorsal rim at an angle of 25°–35°. The postdorsal angle is well-developed and nearly rectangular, the preventral angle is well-expressed, and the dorsal and ventral rims are almost straight and nearly parallel, lending the otoliths a nearly rectangular outline. This appearance, however, is only evident in specimens larger than 9–10 mm in length, while smaller specimens have a somewhat posteriorly tapering shape (Fig. 3E). In small specimens, the outer face is slightly convex to flat while the inner face is distinctly convex. *Pterothrissus umbonatus* is very similar to *P. caspiensis* Bratishko & Udovichenko, 2013 but differs mainly in the flat to slightly convex outer face (vs. concave). This subtle distinction in the two nominal species causes us to consider *P. caspiensis* as provisionally valid until a comprehensive review of the *P. umbonatus* complex has been performed. In the current interpretation, *P. caspiensis* is a regional allopatric species that occurred in the early Oligocene in the Caspian Basin. Younger specimens from the late Oligocene and Miocene in European basins seem to consistently differ from the typical specimens of *P. umbonatus* as recorded here, as the posterior rim tapers even in large specimens, the inner face is flatter, and the outer face is more distinctly convex (Schwarzhans 1994, fig. 3–4).

Order Stomiiformes Regan, 1909

Family Sternoptychidae Dumeril, 1806

Genus *Pseudargentina* Schwarzhans, 1994

Pseudargentina parvula (Koken, 1891)

Fig. 4A–G

1891 *Otolithus* (*Berycidarum*?) *parvulus* - Koken: pl. 10, fig. 4–5.
1923 *Gonostoma parvulum* (Koken, 1891) - Posthumus: fig. 58–59.
1942 *Argentina parvula* (Koken, 1891) - Weiler: pl. 1, fig. 20–25, 27–29.
1994 *Pseudargentina parvula* (Koken, 1891) - Schwarzhans: fig. 44–53 (see there for further references).
2000 *Pseudargentina parvula* (Koken, 1891) - Müller & Rozenberg: fig. 5/15–5/16.
2003 *Pseudargentina parvula* (Koken, 1891) - Rozenberg: fig. 5.3/14–15.
2010 *Pseudargentina parvula* (Koken, 1891) - Schwarzhans: pl. 9, fig. 7–10.
2015 *Pseudargentina parvula* (Koken, 1891) - Syring: pl. 1, fig. 6.
2023 *Pseudargentina parvula* (Koken, 1891) - Schwarzhans & von der Hocht: fig. 5.

Material. 52 specimens, Viborg Formation: 2 specimens Grundfør (NHMD 1758021); 49 specimens Kysing (NHMD 1758022); 1 specimen Aarhus (NHMD 1757604).

Discussion. *Pseudargentina parvula* is an easy-to-recognise common species from the North Sea Basin that ranges in age from the late Priabonian (= "Lattorfian"; NP21) to the early Langhian (= Hemmoorian; NN4). This is a species duration of nearly 20 myr (million years duration), which is among the longest ranges observed in fossil otolith-based species. Specimens from the Priabonian and Rupelian appear to be slightly more compressed than those from the late Oligocene and Miocene ones and show a slight undulation of the dorsal rim (vs. smooth). For comparison we present specimens from the Chattian in the North Sea Basin from the collection of WS (Fig. 4H–M). However, we believe that these subtle differences are insufficiently stable and too variable to be of diagnostic value. Nevertheless, the first occurrence date (FOD) of *P. parvula* in nannoplankton zone NP21 and the last occurrence date (LOD) in NN4 are useful otolith markers in the North Sea Basin. To date, *P. parvula* has not been found outside of the North Sea Basin.

Despite its long range, the abundance of *P. parvula* is highly variable. The species is rare at some localities and very common, even dominating at times, at others. Schwarzhans (2008b) noted that *P. parvula* is particularly common in sheltered, nearshore environments of the late Oligocene in the Lower Rhine Embayment in the southern portion of the North Sea Basin. In one locality (early Chattian in Ratingen), it was found to be the dominant species. Schwarzhans (2008b) explained this abundance with *P. parvula*'s a near-surface, epipelagic lifestyle, which contrasts with the present-day occurrence of sternoptychid fishes; alternatively, taphocoensis is a possible explanation, such as from seabird regurgitation products. In the Viborg Formation, *P. parvula* is common only at Kysing where it is the dominant fish species. The lower Oligocene sediments at Kysing were likely deposited at some distance from the shore and in relatively deep water instead of a sheltered nearshore environment as in Ratingen; hence, we now consider an epipelagic, schooling lifestyle as the more likely explanation for this seemingly environmentally independent change in abundance.

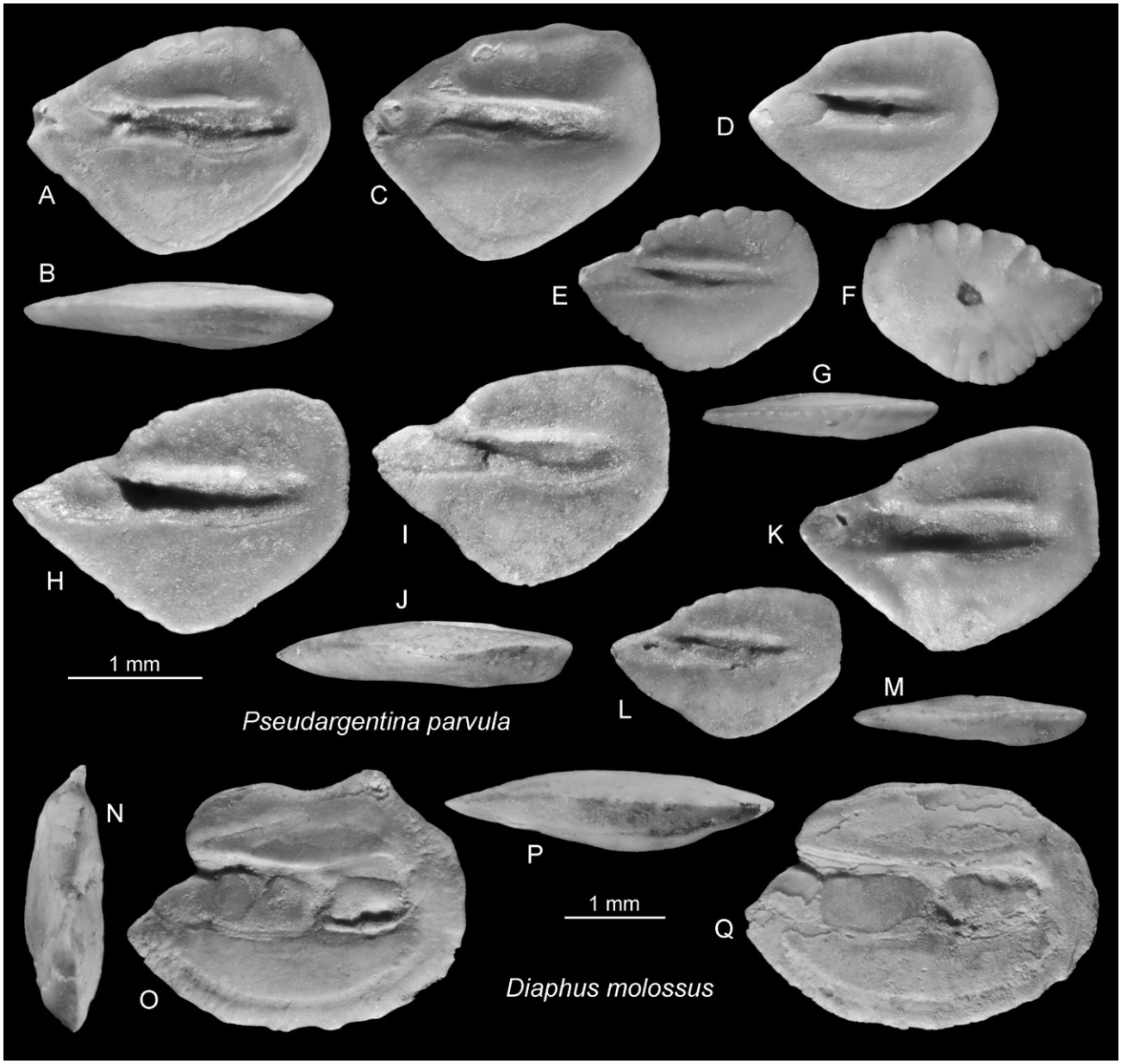

Fig. 4. A-M, *Pseudargentina parvula* (Koken, 1891). **A–G,** Viborg Formation, Kysing, NHMD 1758022. **H–M,** Chattian, Osterholz, Germany, coll. WS; **B,G,J,M** ventral views, **D, K** reversed. **N–Q,** *Diaphus molossus* Nolf & Steurbaut, 1988, Viborg Formation. **N–P,** Grundfør, NHMD 1758024. **Q,** Ølst, NHMD 1758023; **N** anterior view, **P** ventral view, **Q** reversed.

Order Myctophiformes Regan, 1911

Family Myctophidae Gill, 1893

Genus *Diaphus* Eigenmann & Eigenmann, 1890

Diaphus molossus Nolf & Steurbaut, 1988

Fig. 4N–Q

1988 *Diaphus molossus* - Nolf & Steurbaut: pl. 2, fig. 7–11.
1995 *Diaphus molossus* Nolf & Steurbaut, 1988 - Brzobohatý & Nolf: pl. 3, fig. 1–8.
2004 *Diaphus molossus* Nolf & Steurbaut, 1988 - Nolf & Steurbaut: pl. 3, fig. 8.

Material. 2 specimens, Viborg Formation: 1 specimen Ølst (NHMD 1758023); 1 specimen Grundfør (NHMD 1758024).

Discussion. *Diaphus molossus* is one of the large growing early Oligocene otolith-based species of the genus *Diaphus*, which has been used to indicate evolutionary changes in mesopelagic fish that occurred because of the change in the deep-ocean circulation and the establishment of a thermohaline circulation pattern (Schwarzhans & Carnevale 2021). *Diaphus molossus* and *D. stafforaensis* Nolf & Steurbaut, 1988 represent such large growing otolith-based species and have been described from bathyal sediments of the early Oligocene age (NP21) in northern Italy (Nolf & Steurbaut 1988, 2004; Brzobohatý & Nolf 1995). *Diaphus molossus* differs from *D. stafforaensis* in the flatter dorsal rim (vs. rounded) and the strong, massive rostrum. The presence of *D. molossus* in the Viborg Formation in the North Sea Basin signals a wide distribution pattern of the species, as can be expected for mesopelagic fish. Its occurrence also supports the stratigraphic position of the Viborg Formation in the lowermost lower Oligocene.

Order Gadiformes Goodrich, 1909

Family Macruronidae Regan, 1903

Genus *Macrurulus* Schwarzhans, 1980

Macrurulus altus (Nolf, 1974)

Fig. 5C–D

1974 *Raniceps altus* - Nolf: fig. 7–9.
1977 *Palaeogadus altus* (Nolf, 1972) - Schwarzhans: fig. 10–11.
2000 'genus Macrouridarum' *altus* (Nolf, 1972) - Müller & Rozenberg: fig. 9/6–9/9, pl. 3, fig. 11–15.
2003 'genus Macrouridarum' *altus* (Nolf, 1972) - Rozenberg: pl. 9, fig. 10–15.
2008 'genus Macrouridarum' *altus* (Nolf, 1972) - Müller: pl. 1, fig. 52.
?2015 'genus Macrouridarum' sp. - Syring: pl. 3, fig. 9–11.

Material. 1 specimen, Viborg Formation, Ølst (NHMD 1758025).

Discussion. This highly characteristic otolith morphology has been moved around within gadiforms (see references). Müller & Rozenberg (2000) figured a broad assortment of specimens from this species, and the specimen from Ølst fit well into the documented range of variability. This otolith morphology represents a fossil clade with no apparent relationship to extant lineages, as they combine characters found in otoliths of the Merlucciidae, Macruronidae, and Steindachneriidae. We now place it in the fossil otolith-based genus *Macrurulus*, which has been placed in Merlucciidae (Schwarzhans 2019); however, it also bears close resemblance to Macruronidae because of its relatively long ostium and is now placed thereto. To date, *Macrurulus* has been known from three species of the Eocene in New Zealand (Schwarzhans 2019). Thus, *Macrurulus altus* is the only record from the Northern Hemisphere. The origin of *M. altus* in the North Sea Basin remains elusive, as there are no related species known from the region. Müller & Rozenberg (2000) noted that this highly characteristic species is confined to nannoplankton zone NP21, that is, the late Priabonian and early Rupelian. However, Syring (2015) figured similar but somewhat eroded otoliths from the middle Rupelian (NP23) of the Mainz Basin indicating that the stratigraphic range of *M. altus* may have lasted longer than previously thought.

Family Merlucciidae Rafinesque, 1815

Genus *Palaeogadus* von Rath, 1859

Palaeogadus germanus Fedotov, 1970

Fig. 5E–F

?1967 *Palaeogadus emarginatus* (Koken, 1884) - Brzobohatý: pl. 6, fig. 2–4, 10 (non fig. 1).
1970 *Palaeogadus germanus* - Fedotov: fig. 1–2 (skeleton).
1976 *Palaeogadus germanus* Fedotov, 1970 - Fedotov: fig. 6–7 (skeleton), fig. 8 (otolith *in situ*).
2003 *Palaeogadus germanus* Fedotov, 1970 - Rozenberg: pl. 8, fig. 1–2, text-fig. 5.5–5.8.

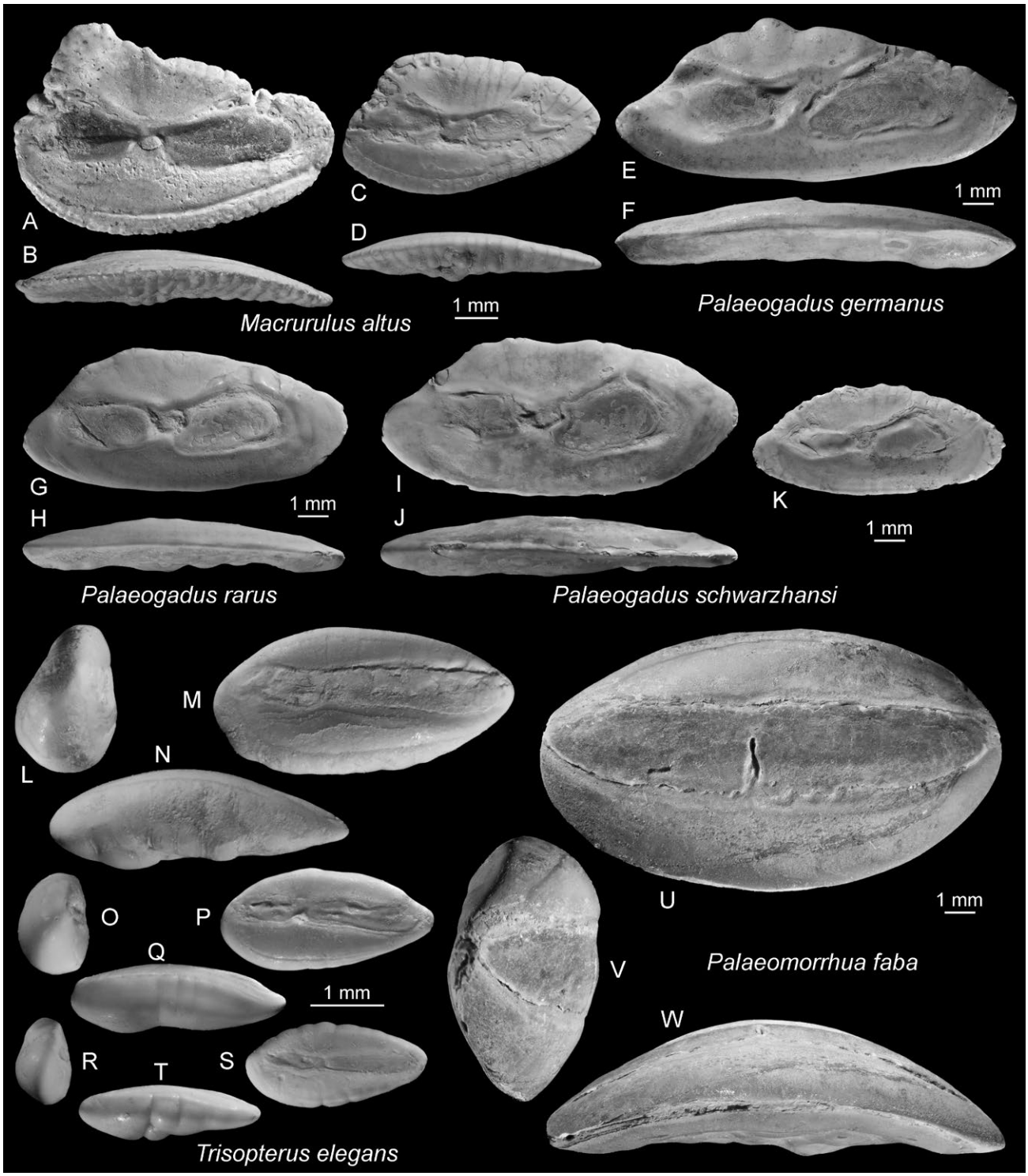

Fig. 5. A–D, *Macrurulus altus* (Nolf, 1974). **A–B,** Latdorf Formation, Latdorf, Germany, Römer Museum Hildesheim. **C–D,** Viborg Formation, Ølst, NHMD 1758025; **B,D**, ventral views. **E–F,** *Palaeogadus germanus* Fedotov, 1970, Viborg Formation, Ølst, NHMD 1758026; reversed, **F** ventral view. **G–H,** *Palaeogadus rarus* Novitskaya, 1961, Viborg Formation, Ølst, NHMD 1758029; **H** ventral view. **I–K,** *Palaeogadus schwarzhansi* Bratishko & Udovichenko, 2013, Viborg Formation. **I–J,** Hadsten, NHMD 1758031; **K** Ølst, NHMD 1758030; **J** ventral view, **K** reversed. **L–T,** *Trisopterus elegans* (Koken, 1884), Viborg Formation. **L–N, R–T,** Grundfør, NHMD 1758032; **O–Q** Kysing, NHMD 1758033; **L,O,S** anterior views, **N,Q,T** ventral views, **L–N** reversed. **U–W,** *Palaeomorrhua faba* (Koken, 1884), Viborg Formation, Aarhus, NHMD 1757602.

Material. 13 specimens, Viborg Formation: 1 specimen Ølst (NHMD 1758026); 5 specimens Grundfør (NHMD 1758027); 6 specimens Kysing (NHMD 1758028), 1 specimen Aarhus (NHMD 1757601).

Discussion. *Palaeogadus germanus* is a moderately elongated otolith with a ratio of otolith length to height of 2.2–2.5 (2.2–2.4 according to Bratishko & Udivichenko 2013) that features the typical low triangular dorsal rim and a relatively wide sulcus with relatively wide colliculi. A further distinctive characteristic is the presence of a notch on the predorsal rim that effectively splits the predorsal lobe into two separate features (see also figures in Bratishko & Udovichenko 2013). This feature is not evident in smaller specimens but appears to be stable in specimens of approximately 6 mm in length or longer. *Palaeogadus germanus* was originally described from the early Oligocene of the Caspian Basin, similar to many other *Palaeogadus* species (see below) and is known to have otoliths *in situ* (Fedotov 1976; Rozenberg 2003). Similar otoliths from the early Oligocene in the Caspian Basin are *P. intergerinus* Daniltshenko, 1947 and *P. latebrosus* Daniltshenko, 1960, all of which have been found with otoliths *in situ* (see Fedotov 1976 and Rozenberg 2003). The otoliths of *P. intergerinus* appear to be more compressed and differ further by their rounded anterior and posterior tips. *Palaeogadus latebrosus* is similar in shape to *P. germanus* but differs in the small, short, and almost equally sized colliculi, and none of them have the notch in the predorsal lobe. The closest resembling species in the North Sea Basin is *Palaeogadus ruisbroekensis* Gaemers, 1984, which differs, however, in the narrower sulcus, its lack of a notch in the predorsal lobe, and its slenderer shape; *P. ruisbroekensis* has a ratio of otolith length to height of 2.8–2.9 (smaller in specimens <3 mm in length) vs. 2.2–2.5.

Palaeogadus germanus has a narrow stratigraphic range in the North Sea Basin in the Viborg Formation only (NP21b). It is not present in Latdorf and coeval sediments (NP21a, uppermost Priabonian). *Palaeogadus germanus* may be closely related to *P. ruisbroekensis* that appears to be confined to the early Rupelian (NP22). Gaemers (1988) established a *Palaeogadus ruisbroekensis* otolith zone for the early Rupelian.

Palaeogadus rarus Novitskaya, 1961

Fig. 5G–H

1961 *Palaeogadus rarus* - Novitskaya: fig. 1–2 (skeleton), 3 (otolith *in situ*).
?1978 *Palaeogadus compactus* - Gaemers & van Hinsbergh: pl. 3, fig. 6, pl. 4, fig. 2–4, pl. 5, fig. 2–6.
2003 *Palaeogadus compactus* Gaemers & van Hinsbergh, 1978 - Rozenberg: pl. 8, fig. 14–15 (see there for further references).
2003 *Palaeogadus rarus* Novitskaya, 1961 - Rozenberg: pl. 8, fig. 10 (*in situ* find), text-fig. 5.5/6, 7, 11.
2013 *Palaeogadus rarus* Novitskaya, 1961 - Bratishko & Udovichenko: fig. 4A–F (see there for further references).
2015 *Palaeogadus compactus* Gaemers & van Hinsbergh, 1978 - Syring: pl. 3, fig. 4–8.

Material. 2 specimens, Viborg Formation: 1 specimen Ølst (NHMD 1758029); 1 specimen Aarhus (NHMD 1757603).

Discussion. When Gaemers & van Hinsbergh (1978) described *Palaeogadus compactus*, they were aware of a potential congruence with a *P. rarus* otolith described *in situ* by Novitskaya (1961). They commented that, quote: "it is not possible to conclude from her (Novitskaya's) pictures that our otoliths (*P. compactus*) belong to *P. rarus* because of the fact that at least some of the pictures do not seem to reflect the true shape." They went on to state, "moreover the dimensions of the otoliths are not given by Novitskaya." Rozenberg (2003) studied the specimens figured by Novitskaya, finding that the specimens originated from a fish that was "not full-grown" and that the otolith and sulcus shapes were not correctly depicted. He extracted and figured an otolith from another, larger *in situ* find, which he interpreted to represent *P. rarus* (Rozenberg's fig. pl. 8, fig. 10). This view was confirmed by Bratishko & Udovichenko (2013) who nevertheless maintained *P. compactus* as a valid species; furthermore, they mentioned as distinctive characterstics a wider cauda and indistinct dorsal depression in *P. rarus* as compared to *P. compactus*. The holotype of *P. compactus* is rather poorly preserved; thus, we cannot verify these subtle differences, especially not in Rozenberg's figures that are denoted to represent the two species. We therefore consider *P. compactus* to potentially represent a junior synonym of *P. rarus*, which then would have a relatively long stratigraphic range throughout the Rupelian.

Palaeogadus schwarzhansi Bratishko & Udovichenko, 2013

Fig. 5I–K

1967 *Palaeogadus emarginatus* (Koken, 1884) - Brzobohatý: pl. 6, fig. 1 (non fig. 2–4, 10).
2003 *Palaeogadus* sp. - Rozenberg: pl. 8, fig. 6–7 (found *in situ*).
2013 *Palaeogadus schwarzhansi* - Bratishko & Udovichenko: fig. 4G–N.

Material. 3 specimens, Viborg Formation: 1 specimen Ølst (NHMD 1758030); 2 specimens Hadsten (NHMD 1758031).

Discussion. *Palaeogadus schwarzhansi* was described from coeval sediments in Western Kazakhstan (Bratishko & Udovichenko 2013) and has also been found *in situ* in an undescribed species from the early Oligocene in the northern Caucasus. *Palaeogadus schwarzhansi* closely resembles *P. rarus* and, according to Bratishko & Udovichenko, differs in the depressed predorsal rim (vs. predorsal lobe) and in being more slender (the ratio of otolith length to height is 2.3–2.6 vs. 2.1–2.25). Additionally, the caudal colliculum is larger and wider in *P. schwarzhansi* as compared to *P. rarus* while the distinction of the ratio of otolith length to height is diminishing.

Family Gadidae Rafinesque, 1810

Genus *Trisopterus* Rafinesque, 1810

Trisopterus elegans (Koken, 1884)

Fig. 5L–T

1884 *Otolithus* (*Gadidarum*) *elegans* - Koken: pl. 11, fig. 2, 4 (non fig. 3 = *Phycis simplex*).
1891 *Otolithus* (*Gadus*) *elegans* Koken, 1884 - Koken: pl. 4, fig. 1.
1972 *Trisopterus elegans* (Koken, 1884) - Gaemers: pl. 2, fig. 1–2.
1984 *Semeniolum rupelense* - Gaemers: pl. 1, fig. 7–13.
1994 *Trisopterus elegans* (Koken, 1884) - Schwarzhans: fig. 88–91.
2000 *Trisopterus elegans* (Koken, 1884) - Müller & Rozenberg: fig. 8/12–16.
2003 *Trisopterus elegans* (Koken, 1884) - Rozenberg: pl. 5, fig. 1–2, text-fig. 5.4/5–9.
2015 *Trisopterus elegans* (Koken, 1884) - Syring: pl. 2, fig. 10–14 (see there for further references).

Material. 7 specimens, Viborg Formation: 2 specimens Grundfør (NHMD 1758032); 5 specimens Kysing (NHMD 1758033).

Discussion. *Trisopterus elegans* represents the earliest species in the genus *Trisopterus* and is known and common throughout the Rupelian and into the lowermost part of the Chattian. Syring (2015) offered an extensive discussion and rationale for references and synonymies.

Order Ophidiiformes Berg, 1937

Family Ophidiidae Rafinesque, 1810

Genus *Palaeomorrhua* Gaemers & Schwarzhans, 1973

Palaeomorrhua faba (Koken, 1884)

Fig. 5U–W

1884 *Otolithus* (*Gadi*) *faba* - Koken: pl. 11, fig. 8.
1891 *Otolithus* (*Morrhua*) *söllingensis* - Koken: pl. 3, fig. 1.
?1891 *Otolithus* (*Morrhua*) *latus* - Koken: pl. 10, fig. 7, 8.
1977 *genus Gadidarum lerichei* - Nolf: pl. 8, fig. 9.
2000 *Palaeomorrhua faba* (Koken, 1884) - Müller & Rozenberg: pl. 10, fig. 19.
2008 *Palaeomorrhua faba* (Koken, 1884) - Schwarzhans: fig. 1H (see there for further references).

Material. 1 specimen, Viborg Formation, Aarhus (NHMD 1757602).

Discussion. The large otoliths of *Plaeomorrhua faba* are highly characteristic. They are mostly uncommon but typical for deepwater environments in the Rupelian and lower part of the Chattian. A single specimen described as by Koken (1891) as stemming from the Miocene of Lüneburg, northern Germany is here considered questionable as for the stratigraphic position. It must be noted that the only other otolith Koken (1891) described from the Miocene of Lüneburg as *Otolithus* (inc. sed.) *lunaburgensis* likely represents a specimen of *P. umbonatus* and gives further doubt to stratigraphic allocation of these otoliths (see above).

Faunal evaluation and palaeobiogeography

The Eocene–Oligocene transition was a time of major change in the deep-ocean circulation and global climate (Corliss *et al.* 1984; Katz *et al.* 2008, 2011; Lear *et al.* 2008; Houben *et al.* 2012; Hutchinson *et al.* 2021; Śliwińska *et al.* 2023). In the North Sea Basin, it was a time of changing seaway connectivity. The westward connection to the Atlantic through the Channel Basin is typically presented as having terminated during the late Eocene in palaeogeographic reconstructions (Popov *et al.* 2004; Knox *et al.* 2010; van der Boon *et al.* 2016, 2018, 2019), with short-lived connections during the later Oligocene and/or Early Miocene. Conversely, the North Sea Basin was connected to the southeast,

that is, the Eastern Paratethys through the Polish gateway during the Priabonian and early Rupelian (Knox *et al.* 2010; van der Boon *et al.* 2016, 2019; Fig. 6). This connection became abandoned later in the Oligocene (Chattian) or at the latest, during Early Miocene. Concurrently, a temporary southward connection was established through the Upper Rhine Valley and Mainz Basin during the middle and late Rupelian (NP23; Syring 2015, and literature cited therein).

The Viborg Formation otolith association represents the peak of the Eocene/Oligocene transition. Although few species have been obtained to date, those that represent the transitional interval demonstrate a clear dominance of taxa that prefer a cool climate (Merlucciidae, Gadidae) and offer a striking similarity to time-equivalent faunas from the Eastern Paratethys (Pterothrissidae, Merlucciidae). The preference of cool-water fishes was probably enhanced by the relatively deep-water depositional environment of the Viborg Formation and hence cooler water temperatures as compared to the earlier otolith associations from Grimmertingen (Nolf 1974) or Hückelhoven (Schwarzhans 1972, 1977) in the shallower southern portion of the North Sea Basin or the later otolith association from the Mainz Basin (Syring 2015). Nine species have been identified in the Viborg Formation; two are distributed throughout the Rupelian and late Priabonian (Latdorf Formation): *Pterothrissus umbonatus* and *Pseudargentina parvula*. *Trisopterus elegans* and *Palaeomorrhua faba* have their FODs in the Viborg Formation. Three *Palaeogadus* species present clear connectivity to the Eastern Paratethys, and two are restricted in the North Sea Basin to NP21b while one, *Palaeogadus germanus*, extends into the later Rupelian. *Diaphus molossus* has, to date, only been recorded from coeval bathyal sediments in northern Italy. As a mesopelagic fish, it probably had a wide superregional, oceanic distribution.

The remarkable diversity of species in the merlucciid genus *Palaeogadus* warrants an in-depth evaluation. Fedotov (1976) listed seven skeleton-based *Palaeogadus* species from the lower Oligocene (Khadumian/Pshekhian) in the Eastern Paratethys, and an eighth is known from otoliths: *P. schwarzhansi*. This is by far the greatest degree of diversity observed in the genus *Palaeogadus* at any time in any region; this diversity probably resulted from a rapid, possibly adaptive endemic evolution in the genus. Danilshenko (as cited in Popov *et al.* 2002) noted a depth segregation in which some species such as *P. intergerinus* occurred in deep water whereas others, such as *P. simionescui*, populated more shallow zones. Popov *et al.* (2002) further commented that the diversity and abundance of the *Palaeogadus* species was highest in the lower Pshekhian (NP21b), while the upper Pshekhian (NP22) experienced a warming phase and change in faunal composition whereby gadids played a less prominent role. Rozenberg (2003) elucidated extensively on the distribution, evolution, and possible dispersal of the species of the genus *Palaeogadus*. His overriding conclusion was

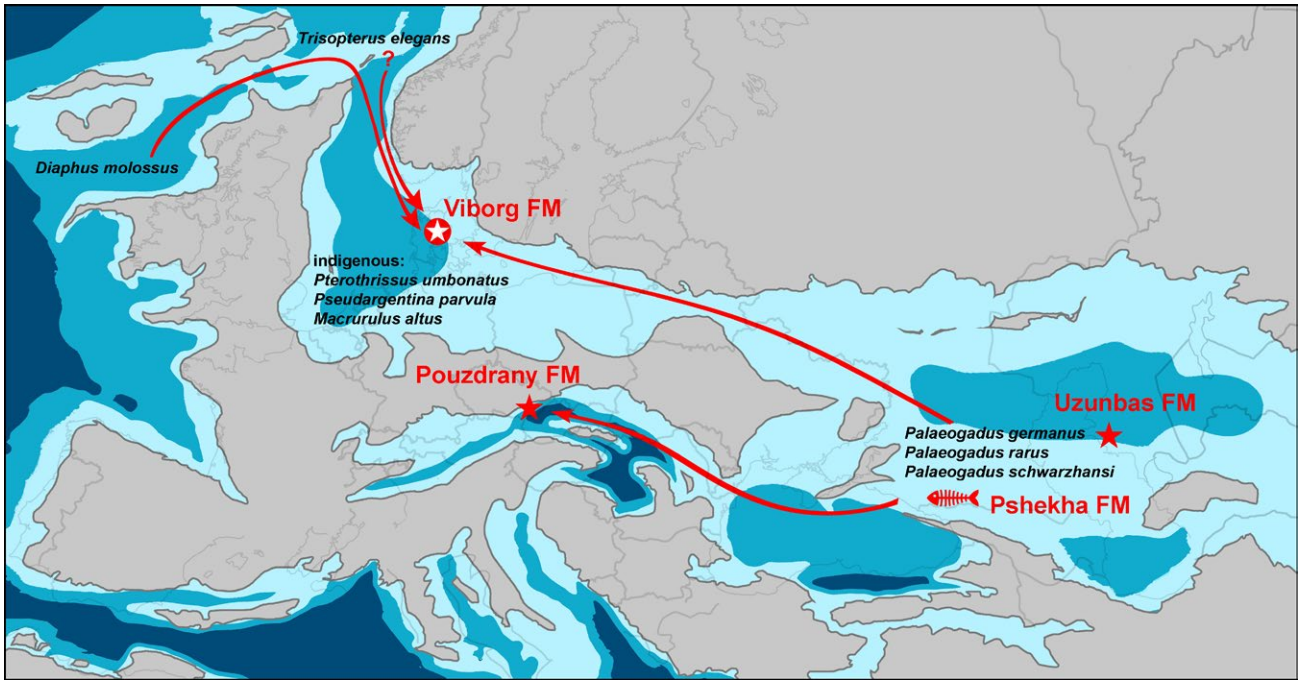

Fig. 6. Assumed migration routes and origin of otolith-based fishes identified in the Viborg Formation. The early Oligocene palaeogeographic configuration at approximately 35 Ma is based on Blakey (2020) with alterations based on van der Boon *et al.* (2018, 2019).

that the genus is of cold water, northerly origin and arrived in the Paratethys, spreading from there to the North Sea Basin in the course of cold-water influence during the Latdorf stage. He postulated that species that lived in deeper water had more elongated otoliths (namely, *P. germanus* and *P. intergerinus*), whereas those living in shallower water had more rounded otoliths (e.g., *P. rarus*). He assumed that *P. rarus* gave rise to *P. compactus* (here considered to be a synonym of *P. rarus*) and *P. obtusus* in the late Oligocene and that the *P. germanus* complex gave rise to the late Oligocene *P. emarginatus* (*P. ruisbroekensis* was considered a doubtful species by Rozenberg 2003). Most of Rozenberg's assumptions are confirmed by our observations. He further assumed that the 'Subparatethys' seaway (Polish gateway) was too shallow for the deep-water Caspian *Palaeogadus* species to effectively migrate into the North Sea Basin. This hypothesis is now falsified due to the occurrence of *P. germanus* in the Viborg Formation and the assumed derivation of the later *P. emarginatus* from the *P. germanus* stock.

The latest Eocene otolith-based fish faunas from Grimmertingen (Nolf 1974) and Hückelhoven (Schwarzhans 1972, 1977), lived in nearshore, shallow-water environments that had a transitional climatic nature with abundant shallow water neobythine taxa (as they are known from the earlier Palaeogene) as well as the initial arrival of a few cold-water gadiform taxa (Rozenberg 2003). The fauna from the Latdorf Formation is more comparable to the one from the Viborg Formation; the latter was deposited at approximately 150 to 300 m water depth (Milàn *et al.* 2018) in a deep-water environment. The composition of otoliths from the Viborg Formation, however, significantly differs from the Latdorf otoliths in the absence of typical warm water neobythitines and the abundance of cold-water gadiforms of the genera *Palaeogadus* and *Trisopterus*. The three *Palaeogadus* species likely migrated from the Eastern Paratethys; the origin of *Trisopterus elegans* is not known, but they presumably immigrated from the north (Fig. 6). Based on these observations we conclude that the Viborg Formation marks a sudden decrease in sea water temperature from the already somewhat cooler Latdorf Formation. The closure of the Polish gateway and the opening of the Upper Rhine Valley/Mainz Basin connection during the middle to late Rupelian once again facilitated the migration of warm-water fishes (Rozenberg 2003; Syring 2015).

Biostratigraphy with otoliths

Several researchers have attempted to establish an otolith biozonation of the Oligocene in the North Sea Basin (Gaemers 1976a,b, 1978, 1984, 1985, 1988, 1994; Schwarzhans 1994; Rozenberg 2003); their efforts have varied from each other: Gaemers followed a strict phylogenetical approach based on his proposal of a novel phylogenetical concept, whereas Schwarzhans and Rozenberg favoured a concept that combines a traditional phylogenetic approach with event stratigraphy. It may be clear from the previous discussion that the FOD of many highly stratigraphically meaningful species in the North Sea Basin is driven by migration events rather than phylogenetic occurrences, but in a strictly regional sense, they are nevertheless very useful. The Viborg Formation now fills an important stratigraphic gap in the otolith record. Therefore, and in combination with data from the cited literature as well as the checklists provided by Müller (2008) and Müller *et al.* (2017), we now refine occurrence dates and arrive at an improved otolith biozonation of the early Oligocene in the North Sea Basin that builds on the status presented by Schwarzhans (1994) and Rozenberg (2003). We do not discuss Gaemers' (1988) phylogenetically based biozonation in any detail, primarily because it cannot be verified, as it contains a plethora of species and genera which are not described, and hence, must be considered *nomina nuda* according to the rules of the ICZN. Furthermore, some of the phylogenetic sequences appear to be equivocal, and Gaemers' otolith zonation is, for the most part is, not formally calibrated with other zonations that are relevant for the North Sea Basin.

The first obstacle is to identify a stratigraphic marker in otoliths at the base of NP21 (Latdorf Formation and equivalents). Rich otolith-based fish faunas are known up to the Bartonian (NP17), but thereafter, a recording gap of approximately 4 myr occurs in the North Sea Basin, which encompasses most of the Priabonian until NP21. Any of the following species may have occurred first in NP21a: *Pseudargentina parvula*, *Macrurulus altus*, *Phycis praecognatus* Schwarzhans, 1977 (syn. *P. magdeburgensis* Müller & Rozenberg, 2000 according to Nolf 2013), *Phycis simplex* (Koken, 1891), *Raniceps tuberculosus* (Koken, 1884), and *Protobrotula ensiformis* (Steurbaut & Herman, 1978), any of which could be considered to represent immigration events and would be subject to testing by otolith assemblages from nannoplankton zones NP18–20 should they ever become available in the North Sea Basin. Müller & Rozenberg (2000) as well as Rozenberg (2003) suggested *M. altus* as an index fossil for a total range zone, and Gaemers (1988) recommended a similar concept for a *Phycis praecognatus* total range zone. However, both species are likely to range into later Rupelian (see Syring 2015, for a potential *M. altus* find in NP23 in the Mainz Basin and Müller 2008, for *P. magdeburgensis* [?syn. *P. praecognatus*] in NP23 as well). *Macrurulus*

altus is also present in the Viborg Formation. However, NP21a apparently does not contain *Trisopterus elegans* or any of the three *Palaeogadus* species found in the Viborg Formation. We therefore propose that the latest Eocene otolith biozone in the North Sea Basin should be redefined as the interval zone between the FOD of *Macrurulus altus* and the FOD of *Trisopterus elegans*, both of which are classified as migration events (Fig. 7).

The FOD of *Trisopterus elegans* qualifies as a marker near the Eocene–Oligocene boundary. The species is well suited because it is easily recognizable and has been a common species since its FOD. Additional useful species are the FOD's of *Palaeogadus germanus*, *P. rarus*, and *P. schwarzhansi*. The top of the biozone is marked by the FOD of *Palimphemus parvus* (Gaemers, 1976), according to Müller's (2008) checklist, as well as the lack of that species in the Viborg Formation. This otolith biozone seems to be coeval with nannoplankton zone NP21b (Fig. 7).

The next FOD is that of *Palaeogadus ruisbroekensis* Gaemers, 1984, which may coincide with the FOD of *Palimphemus parvus*. *Paratrisopterus minutulus* (Gaemers, 1978) appears to have its FOD near that of *P. ruisbroekensis* or slightly higher (Müller *et al*. 2017). *Protobrotula ensiformis* (Steurbaut & Herman, 1978) has its LOD at the top of this interval. We therefore define the next higher otolith biozone as the interval zone between the FOD of *Palaeogadus ruisbroekensis* and the LOD of *Protobrotula ensiformis* in the lower NP23 (Steendorp bed 15 in Steurbaut & Herman 1978; Rozenberg 2003). This otolith zone encompasses nan-

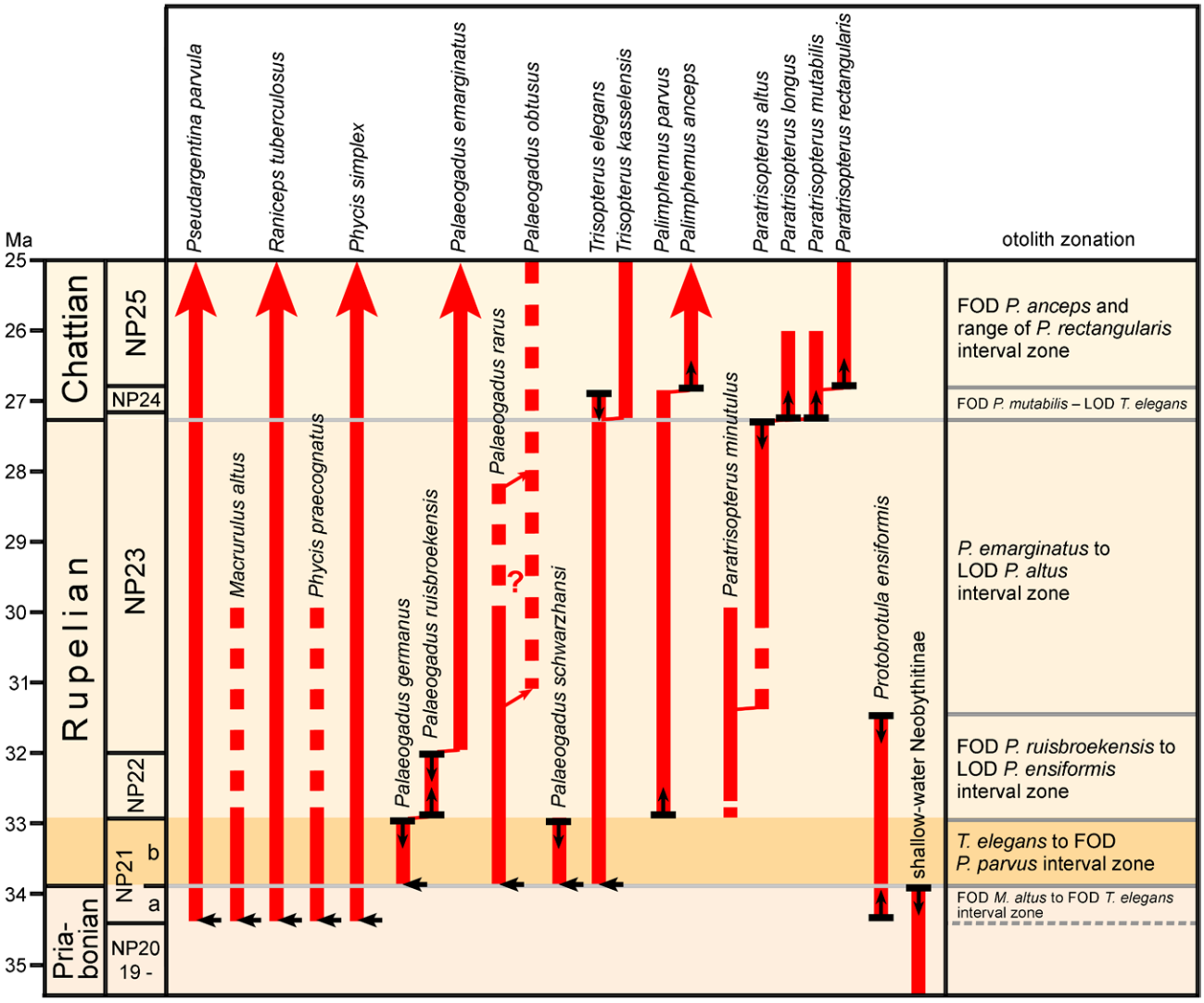

Fig. 7. Otolith-based species range chart for the Rupelian in the North Sea Basin compiled from cited literature and this study. The Viborg Formation is highlighted. Nannoplankton zonation and chronostratigraphy are based on Gradstein *et al*. (2020). Differentiation of zone NP21a and NP21b is informal and for convenience purpose only

noplankton zone NP22 and the lower part of NP23. *Palaeogadus ruisbroekensis* may have derived from *P. germanus* and appears to be restricted to this interval (Fig. 7).

The long-ranging and ubiquitous species *Palaeogadus emarginatus* was first identified from the Brinkheurne Member in Winterswijk, The Netherlands, by Gaemers & van Hinsbergh (1978), which corresponds to the lower part of nannoplankton zone NP23. However, in Rozenberg (2003), the FOD of *P. emarginatus* appears only in NP 24 (Chattian). *Paratrisopterus altus* (Gaemers & van Hinsbergh, 1978) seems to originate slightly later at the interface of the Brinkheurne and the Winterswijk Member. *Palaeogadus emarginatus* may have derived from *P. ruisbroekensis*, which in turn derived from *P. germanus*. Thus, this lineage represents one of the few occasions of phylogenetic succession, while most other occurrences discussed herein appear to be event (migration) driven. A less well-constrained lineage combines *Palaeogadus rarus* (tentatively including *P. compactus* as synonym) and *P. obtusus* (Koken, 1891), the latter having originally been described from the Chattian. We follow Rozenberg's (2003) belief that the distinction of these two nominal species requires a detailed review. Rozenberg (2003) also mentioned *Palaeogadus intergerinus* Daniltshenko, 1947 from the middle Rupelian in the Mainz Basin, whereas Syring (2015) placed these specimens in *P. obtusus*. We are uncertain regarding a possible phasing of *Palaeogadus emarginatus* and *Paratrisopterus altus* and therefore do not distinguish between the apparent FODs of either species. According to Rozenberg (2003), *Paratrisopterus altus* terminated with NP23. This LOD is consistent with Schwarzhans' (1994) assessment of the late Oligocene (Chattian) otolith biozonation in which *P. altus* is no longer present. Therefore, we tentatively assign a *Palaeogadus emarginatus* (FOD) – *Paratrisopterus altus* (LOD) interval zone that corresponds to the middle and higher part of nannoplankton zone NP23 (Fig. 7). This results in a long stratigraphic interval without subdivision, which is primarily due to limited data and the presence of morphologically intermediate forms in supposed lineages that hamper species definitions. Gaemers (1994) attempted to establish a finer otolith biozonation for this interval, but this proposal requires testing and verification.

The early/late Oligocene (Rupelian/Chattian) interface is well documented in otoliths by the FOD of many species around the boundary, most notably *Palimphemus anceps*, *Paratrisopterus mutabilis* (Schwarzhans, 1994; syn. *P. triangularis* Schwarzhans, 1994), and *Paratrisopterus longus* (Schwarzhans, 1974). The LOD of the common species *Trisopterus elegans* seems to be slightly into the lowermost Chattian before it is replaced by *T. kasselensis* Schwarzhans, 1974 (syn. *Trisopterus soellingensis*, nomen nudum, see Schwarzhans 1994).

Conclusions and outlook

The otoliths obtained from the basal Oligocene Viborg Formation are few, but they document interesting aspects for the understanding of the evolution of fishes in the North Sea Basin during this time interval, which was characterised by a major reorganization of the world ocean and global climate. First, a major faunal turnover was eminent. One of the dominant early Palaeogene groups, the warm-water Neobythitinae (Ophidiiformes), which still formed a major faunal element in the Latdorf community, was gone. Instead, the cool-water-adapted Gadiformes became the most diverse group in the Viborg Formation. Here, we identify a remarkable diversity in the Merlucciidae, chiefly in the genus *Palaeogadus*, which mimics the situation known from coeval strata in the Caspian Basin. In fact, all three *Palaeogadus* species are also known from the Caspian Basin; two of them, *P. germanus* and *P. schwarzhansi*, occurred for only a brief time interval in the North Sea Basin – the time of the Viborg Formation. The Caspian connection is further supported by the occurrence of two intimately related species of the genus *Pterothrissus*.

Another interesting aspect is that the faunal turnover from the late Eocene to the early Oligocene was drastic in the North Sea Basin but occurred over a period of time, which may be useful for local biostratigraphic purposes. The first marker to mention is the occurrence of three gadiform species in the late Priabonian of NP21a: *Macrurulus altus, Phycis simplex*, and *Phycis praecognatus*. One of the most iconic and common Rupelian species in the North Sea Basin, *Trisopterus elegans*, had its FOD with the Viborg Formation, which is at the base of the Rupelian (zone NP21b). *Palaeogadus ruisbroekensis* appears to be indicative of zone NP22 where it replaced *P. germanus*, which was known from the Viborg Formation. The occurrence of the mesopelagic *Diaphus molossus* provides an index species for the superregional correlation of zone NP21.

We hope that it will be possible in the future to collect more otoliths from the Viborg Formation to establish a fuller picture of its otolith-based fish fauna. The Viborg otolith assemblage nevertheless demonstrates how new localities and time intervals contribute to a more continuous evaluation of the evolution of fish fauna even in an otherwise extensively studied region such as the North Sea Basin.

Acknowledgements

The authors wish to cordially thank Henrik Madsen, Fossil- og Molermuseet, Mors for information and making specimens from Ølst available. The Römer Museum of Hildesheim is thanked for making otoliths from Latdorf available. Arden Bashfort (NHMD) is thanked for retrieving vintage otoliths collected by P. Harder in 1912, and L. Cotton and B. Lindow (both NMHD) for making them available and registration of the otoliths. Gary Stringer (West Monroe, Louisiana, U.S.A.) and Victor van Hinsbergh (Leiden, The Netherlands) are thanked for their constructive reviews of an earlier version of the manuscript.

References

Bannikov, A.F. 2010: Fossil acanthopterygian fishes (Teleostei, Acanthopterygii). In: Tatarinov, L.P., Vorobyeva, E.I. & Kurochkin, E.N. (eds.): Fossil vertebrates of Russia and adjacent countries, 1–244. Moscow: GEOS. [Russian, with English summary]

Bannikov, A.F. & Parin, N.N. 1997: The list of marine fishes from Cenozoic (upper Paleocene-middle Miocene) localities in southern European Russia and adjacent countries. Journal of Ichthyology 37, 133–146.

Berggren, W.A., Wade, B.S. & Pearson, P.N. 2018: Oligocene chronostratigraphy and planktonic foraminiferal biostratigraphy: historical review and current state-of-the-art. Cushman Foundation Special Publication 46, 29–54.

Bieńkowska-Wasiluk, M. 2021: The fish fauna of the Dynów Marl Member (Menilite Formation, Poland): palaeoenvironment and paleobiogeography of the early Oligocene Paratethys. Bulletin of Geosciences 96, 493–511. https://doi.org/10.3140/bull.geosci.1819

Blakey, R. 2020: Deep time maps. World Wide Web electronic service. (purchased in March 2024).https://deeptimemaps.com

Bratischko, A. & Udovichenko, M. 2013: Fish otoluths from the early Oligocene of Mangyshlak, Kazakhstan. Neues Jahrbuch Geologie Paläontologie Abhandlungen 270, 195–208. https://doi.org/10.1127/0077-7749/2013/0366

Brzobohatý, R. 1967: Die Fisch-Otolithen aus den Pouzdrany-Schichten. Acta Musei Moraviae, Scientiae Naturales 52, 121–168.

Brzobohatý, R. & Bubík M. 2019: Paleogene fish otoliths (Teleostei) from the Subsilesian and Ždánice units in Moravia. Bulletin of Geosciences 94, 101–114. https://doi.org/10.3140/bull.geosci.1715

Brzobohatý, R. & Nolf, D. 1995: *Diaphus* otoliths from the European Oligocene (Myctophidae, Teleostei). Bulletin de l'Institute royal des Sciences Naturelles de Belgique, Sciences de la Terre 65, 257–268.

Corliss, B.H., Aubry, M.-P., Berggren, W.A., Fenner, J.M., Keigwin, L.D. & Keller, G. 1984: The Eocene/Oligocene boundary event in the deep sea. Science 226, 806–810. https://doi.org/10.1126/science.226.4676.806

Christensen, L. & Ulleberg, K., 1973: Sedimentology and micropalaeontology of the Middle Oligocene sequence at Sofienlund, Denmark. Bulletin of the Geological Society of Denmark 22, 283–305.

Christensen, L. & Ulleberg, K. 1974: Sediments and foraminifers of the Middle Oligocene Viborg Formation, Denmark. Bulletin of the Geological Society of Denmark 23, 109–117.

Fedotov, V.F. 1970: Novyi vid roda *Palaeogadus* (Treskovye) iz oligocena Severnovo Kavkaza. Paleontological Journal 1970, 117–119.

Fedotov, V.F. 1976: Gadidae of the Palaeogene-Neogene from the U.S.S.R, 84 pp. Moscow: Nauka.

Gaemers, P.A.M. 1972: Otoliths from the type locality of the Sands of Berg (Middle Oligocene) at Berg, Belgium. Mededelingen van de Werkgroep voor Tertiaire en Kwartaire Geologie 9, 73–85.

Gaemers, P.A.M. 1976a: New gadiform otoliths from the Tertiary of the North Sea Basin and a revision of some fossil and recent species. Leidse Geologische Mededelingen 49, 507–537.

Gaemers, P.A.M. 1976b: New concepts in the evolution of the Gadidae (Vertebrata, Pisces), based on their otoliths. Mededelingen van de Werkgroep voor Tertiaire en Kwartaire Geologie 13, 3–32.

Gaemers, P.A.M. 1978: A biozonation based on Gadidae otoliths for the northwest European younger Cenozoic, with the description of some new species and genera. Mededelingen van de Werkgroep voor Tertiaire en Kwartaire Geologie 15, 141–161.

Gaemers, P.A.M. 1981. Fish otoliths from the Middle Oligocene of Siadło Górne near Szcecin, Poland, and their stratigraphic importance. Mededelingen van de Werkgroep voor Tertiaire en Kwartaire Geologie 18, 109–126.

Gaemers, P.A.M. 1984: Fish otoliths from the Bassevelde Sand (late Tongrian) of Ruisbroek, Belgium, and the stratigraphy of the early Oligocene of Belgium. Mededelingen van de Werkgroep voor Tertiaire en Kwartaire Geologie 21, 13–57.

Gaemers, P.A.M. 1985: Fish otoliths from the Rupelian of sand-pit Roelants at Heide-Boskant (municipality of Lubbeek, Belgium) and the stratigraphy of the early Rupelian, 2. systematic part. Mededelingen van de Werkgroep voor Tertiaire en Kwartaire Geologie 22, 155–172.

Gaemers, P.A.M. 1988: Fishes. In: The Northwest European Tertiary Basin. Results of the IGCP Project No 124. Geolisches Jahrbuch A100, 368–390.

Gaemers, P.A.M. 1994: Refined correlations by means of lithostratigraphy and gadid otolith zonation of the Rupelian of the North Sea Basin: a progress report. Bulletin de la Société belge de Géologie 102, 147–157.

Gaemers, P.A.M. & van Hinsbergh, V. 1978: Rupelian (Middle Oligocene) fish otoliths from the clay pit 'De Vlijt' near Winterswijk, The Netherlands. Scripta Geologica 46, 77 pp.

Gradstein F.M., Ogg J.G., Schmitz M.D. & Ogg G.M. 2020: Geologic time scale 2020, 1357 pp. Amsterdam: Elsevier. https://doi.org/10.1127/nos/2020/0634

Håkansson, E. & Pedersen, S.A.S. 1992: Et nyt undergrundskort (map sheet). Copenhagen: Varv.

Harder, P. 1913: De oligocæne Lag i Jærnbanegennemskæringen ved Århus Station. Danmarks Geologiske Undersøgelse II. Række 22, 140 pp. https://doi.org/10.34194/raekke2.v22.6807

Houben, A.J.P, van Mourik, C.A., Montanari, A., Coccioni, R. & Brinkhuis, H. 2012: The Eocene-Oligocene transition: Changes in sea level, temperature or both? Palaeogeography, Palaeoclimatology, Palaeoecology 335-336, 75–83. https://doi.org/10.1016/j.palaeo.2011.04.008

Hutchinson, D.K. *et al*. 2021: The Eocene-Oligocene transition: a review of marine and terrestrial proxy data, models and model-data comparison. Climate of the Past 17, 269–315. https://doi.org/10.5194/cp-17-269-2021

Jensen, E.S. 1974: Nyt undergrundskort. Varv 1974(2), 47–49. https://doi.org/10.1108/eb017784

Jerzmańska, A. 1960: Ichtiofauna lupkow jaselskikh z Sobnjowa. Acta Palaeontologica Polonica 5, 367–419.

Jerzmańska, A. 1968: Ichthyofaune des couches a menilite (flysch des Karpathes). Acta Palaeontologica Polonica 13, 379–488.

Katz, M.E., Miller, K.G., Wright, J.D., Wade, B.S., Browning, J.V., Cramer, B.S. & Rosenthal Y. 2008: Stepwise transition from the Eocene greenhouse to the Oligocene icehouse. Nature Geoscience 1, 329–334. https://doi.org/10.1038/ngeo179

Katz, M.E., Cramer, B.S., Toggweiler, J.R., Esmay, G., Liu, C., Miller, K.G., Rosenthal, Y., Wade, B.S. & Wright, J.D. 2011: Impact of Antarctic Circumpolar Current development on late Paleogene ocean structure. Science 332, 1076–1079. https://doi.org/10.1126/science.1202122

King, C. 2016 (ed. by Gale, A.C. & Barry, T.L.): A revised correlation of Tertiary rocks in the British Isles and adjacent areas of NW Europe. The Geological Society, Special Report 27, 719 pp. https://doi.org/10.1144/SR27

Knox, R.W.O.B. *et al*. 2010: Cenozoic. In: Doornenbal, J.C. & Stevenson, A.G. (eds): Petroleum Geological Atlas of the Southern Permian Basin area. EAGE Publications b.v. (Houten), 211–22.3.

Koken, E. 1884: Über Fisch-Otolithen, insbesondere über diejenigen der norddeutschen Oligocän-Ablagerungen. Zeitschrift der Deutschen Geologischen Gesellschaft 36, 500–565.

Koken, E. 1891: Neue Untersuchungen an Tertiären Fischotolithen II. Zeitschrift der Deutschen Geologischen Gesellschaft 43, 77–170.

Larsen, G. & Kronborg, C. 1994: Geologisk set: Det mellemste Jylland, 272 pp. Geografforlaget and Skov- og Natyrstyrelsen.

Lear, C.H., Bailey, T.R., Pearson, P.N., Coxall, H.K. & Rosenthal, Y. 2008: Cooling and ice growth across the Eocene-Oligocene transition. Geology 36, 251–254. https://doi.org/10.1130/G24584A.1

Milàn, J., Rasmussen, E.S. & Dybkjær, K. 2018: A crocodilian coprolite from the lower Oligocene Viborg Formation of Sofienlund Lergrav, Denmark. Bulletin of the Geological Society of Denmark 66, 181–187. https://doi.org/10.37570/bgsd-2018-66-09

Müller, A. 2008: Obereozäne bis oligozäne marine Faunen Mitteldeutschlands - eine Übersicht; mit einer lithostratigrafischen Neugliederung des Unteroligozäns im Südraum Leipzig. Zeitschrift der deutschen Gesellschaft der Geowissenschaften 159, 23–85.

Müller, A. & Rozenberg, A. 2000: Fischotolithen (Pisces, Teleostei) aus dem Unteroligozän von Mitteldeutschland. Leipziger Geowissenschaften 12, 71–141.

Müller, A., Martini, E. & Hohndorf, G. 2017: Das Unteroligozän (Rupelium) von Amsdrof bei Röblingen (Mansfelder Land, Sachsen-Anhalt): Lithostratigraphie, Biostratigraphie und Fauna. Mauritiana (Altenburg) 31, 71–151.

Nelson, J.S., Grande, T.C. & Wilson, M.V.H. 2016: Fishes of the World, 707 pp; fifth edition. Hoboken: Wiley. https://doi.org/10.1002/9781119174844

Nolf, D. 1974: Sur les otolithes des Sables de Grimmertingen (Oligocène Inférieur de Belgique). Bulletin de l'Institute Royal des Sciences Naturelles de Belgique 48, 1–22.

Nolf, D. 1977: Les Otolithes des Téléostéens de l'Oligo-Miocène Belge. Annales de la Societé royale de Zoologie Belge 106, 3–119.

Nolf, D. 1988: Les otolithes de téléostéens éocènes d'Aquitaine (sud-ouest de la France) et leur intérêt stratigraphique. Mémoire de l'Académie royale de Belgique, Classe des Sciences, 4°, 2e série 19, 1–147.

Nolf, D. 2013: The diversity of fish otoliths, past and present, 222 pp. Brussels: Royal Belgian Institute of Natural Sciences.

Nolf, D. & Steurbaut, E. 1988: Description de la première faune ichthyologique exclusivement bathyale du Tertiare d'Europe: otolithes de l'Oligocène Inférieur du gisement de Pizzocorno, Italie septentrionale. Bulletin de l'Institut Royal des Sciences Naturelles de Belgique 57, 217–230.

Nolf, D. & Steurbaut, E. 1990: Découverte de poissons bathyaux d'âge Oligocène inférieur à Pizzocorno, près de Voghera. Quaderni della sezione di Scienze Naturali del Civico Museo di Voghera 10, 15–31.

Nolf, D. & Steurbaut. E. 2002: Compléments à l'étude des otolithes de poissons Rupeliens d'Aquitaine méridionale (sud ouest de la France). Revue de Micropaléontologie 45, 297–312. https://doi.org/10.1016/S0035-1598(02)90058-9

Nolf, D. & Steurbaut, E. 2004: Otolithes de poissons de l'Oligocène inférieur du Basssin liguro-piémontais oriental, Italie. Rivista Piemontese di Storia naturale 25, 21–68.

Novitskaya, L.I. 1961: Rod *Palaeogadus* treskovye iz khadumskovo gorizonta Kavkaza. Paleontological Journal 1961, 120–130.

Ødum, H. 1936: Marint Nedre Oligocæn i Danmark. Meddelelser fra Dansk geologisk Forening 9, 88–90.

Olsen, G.V. 1955: Mellem-oligocænet ved Odder. Meddelelser fra Dansk Geologisk Forening 9, 137–150.

Popov, S.V. *et al*. 2002: Biogeography of the Northern Peri-Tethys

from the late Eocene to the early Miocene. Part 2, early Oligocene. Paleontological Journal 36, suppl. 3, 185–259.

Popov, S.V., Rögl, F., Rozanov, A.Y., Steininger, F.F., Shcherba, I.G. & Kovac, M. 2004: Lithological-paleogeographic maps of Paratethys. Courier Forschungsinstitut Senckenberg 250, 1–46.

Posthumus, O. 1923: Bijdragen tot de kennis der tertiaire vischfauna van Nederland. Verhandelingen van het Geologisch-Mijnbouwkundig Genootschap voor Nederland en Kolonien, Geologische Serie 7, 105–142.

Rasmussen, E.S., Dybkjær, K., & Piasecki, S. 2010: Lithostratigraphy of the upper Oligocene–Miocene succession in Denmark. Bulletin of the Geological Survey of Denmark 22, 92 pp. https://doi.org/10.34194/geusb.v22.4733

Rasmussen, L.B. 1968: Molluscan Faunas and Biostratigraphy of the Marine Younger Miocene Formations in Denmark. Part II. Palaeontology. Danmarks Geologiske Undersøgelse II. Række 92, 265 pp. https://doi.org/10.34194/raekke2.v92.6883

Ravn, J.P.J. 1907: Molluskfaunaen i Jyllands Tertiæraflejringer. Det Kongelige Danske Videnskabernes Selskabs Skrifter VII. Række 3, 217–384.

Rozenberg, A. 2003: Otolithen mariner Teleosteer aus dem Obereozän/Unteroligozän des Ostparatethys-Nordseebecken-Raumes: Bestandsaufnahme der auf Otolithen basierenden Fischfaunen sowie biostratigraphische und paläobiogeographische Vergleiche und Analyse, 234 pp. Dissertation, University Leipzig.

Schnetler, K.I. & Beyer, C. 1987: A Late Oligocene (Chattian B) mollusc fauna from the clay-pit at Nørre Vissing, Jylland, Denmark. Mededelingen van de Werkgroep voor Tertiaire en Kwartaire Geologie 24, 193–224.

Schnetler, K.I. & Beyer, C. 1990: A Late Oligocene (Chattian B) molluscan fauna from the coastal cliff at Mogenstrup, north of Skive, Jutland, Denmark. Contributions to Tertiary and Quaternary Geology 27, 39–81.

Schnetler, K.I., Madsen, H., Śliwińska, K.K., Heilmann-Clausen, C. & Ulleberg, K. 2024: A late Oligocene molluscan fauna and Oligocene coastal outcrops from Vilsund, NW Denmark. Bulletin of the Geological Society of Denmark 73, 1–40. https://doi.org/10.37570/bgsd-2024-73-01

Schnetler, K.I. & Palm, E. 2008: The molluscan fauna of the Late Oligocene Branden Clay, Denmark. Palaeontos 15, 1–92.

Schwarzhans, W. 1973: Einige Otolithen aus dem Unteroligozän von Hückelhoven unter besonderer Berücksichtigung der Evolution der Trachinidae. Mededelingen van de Werkgroep voor Tertiaire en Kwartaire Geologie 10, 31–43.

Schwarzhans, W. 1974: Die Otolithen-Fauna des Chatt A und B (Oberoligozän, Tertiär) vom Niederrhein, unter Einbeziehung weiterer Fundstellen. Decheniana 126, 91–132.

Schwarzhans, W. 1977: Otolithen aus dem Unteroligozän (Tertiär) von Hückelhoven (Kreis Heinsberg, Nordrhein-Westfalen). Decheniana 130, 268–292. https://doi.org/10.21248/decheniana.v130.3990

Schwarzhans, W. 1978: Otolith-morphology and its usage for higher systematical units with special reference to the Myctophiformes s.l. Mededelingen van de Werkgroep voor Tertiaire en Kwartaire Geologie 15, 167–185.

Schwarzhans, W. 1981: Die Entwicklung der Familie Pterothrissidae (Elopomorpha: Pisces), rekonstruiert nach Otolithen. Senckenbergiana Lethaea 62, 77–91.

Schwarzhans, W. 1994: Die Fisch-Otolithen aus dem Oberoligozän der Niederrheinischen Bucht. Systematik, Palökologie, Paläobiogeographie, Biostratigraphie und Otolithen-Zonierung. Geologisches Jahrbuch A140, 3–248.

Schwarzhans, W. 2008a: Otoliths from the late Oligocene Branden Clay, Denmark. Palaeontos 15, 93–100.

Schwarzhans, W. 2008b: Otolithen aus küstennahen Sedimenten des Ober-Oligozän der Niederrheinischen Bucht (Northern Germany). Neues Jahrbuch Geologe Paläontlogie Abhandlungen 248, 11–44. https://doi.org/10.1127/0077-7749/2008/0248-0011

Schwarzhans, W. 2010: The otoliths from the Miocene of the North Sea Basin, 352 pp. Leiden: Backhuys Publishers.

Schwarzhans, W. 2019: Reconstruction of the fossil marine bony fish fauna (Teleostei) from the Eocene to Pleistocene of New Zealand by means of otoliths. Memorie della Società Italiana di Scienze Naturali e del Museo di Storia Naturale di Milano 46, 3–326.

Schwarzhans,W. & Carnevale, G. 2021: The rise to dominance of lanternfishes (Teleostei: Myctophidae) in the oceanic ecosystems: a paleontological perspective. Paleobiology 47, 446–463. https://doi.org/10.1017/pab.2021.2

Schwarzhans, W. & von der Hocht, F. 2023: New otolith assemblages from the Miocene of the North Sea Basin and their biostratigraphic significance. Cainozoic Research 23, 189–227.

Śliwińska, K.K., Abrahamsen, N., Beyer, C., Brünings-Hansen, T., Thomsen, E., Ulleberg, K. & Heilmann-Clausen, C. 2012: Bio- and magnetostratigraphy of Rupelian-mid Chattian deposits from the Danish land area. Review of Palaeobotany and Palynology 172, 48–69. https://doi.org/10.1016/j.revpalbo.2012.01.008

Śliwińska, K.K., Coxall, H.K., Hutchinson, D.K., Liebrand, D., Schouten, S. & de Boer, A.M. 2023: Sea surface temperature evolution of the North Atlantic Ocean across the Eocene-Oligocene transition. Climate of the Past 19, 123–140. https://doi.org/10.5194/cp-19-123-2023

Steurbaut, E, 1986a: The Kallo well and its key-position in establishing the Eo-Oligocene boundary in Belgium. In: Pomerol & Premoli-Silva (eds): Terminal Eocene events, 97–100. Amsterdam: Elsevier. https://doi.org/10.1016/S0920-5446(08)70100-6

Steurbaut, E. 1986b: Late middle Eocene to middle Oligocene calcareous nannoplankton from the Kallo well, some boreholes and exposures in Belgium and a description of the Ruisbroek Sand Member. Mededelingen van de Werkgroep voor Tertiaire en Kwartaire Geologie 23, 49–83.

Steurbaut, E. & Herman, J. 1978: Biostratigraphie et poissons fossiles de la formation de l'Argile de Boom (Oligocène moyen du bassin belge). Geobios 11, 297–325. https://doi.org/10.1016/S0016-6995(78)80033-3

Syring, J.C. 2015: Die otolithenbasierten Teleostei-Faunen aus dem Rupelium s.str. des Mainzer Beckens (Unteroligozän, Rheinland-Pfalz, Deutschland) - Systematik, Paläoökologie, Paläobiogeographie und Erstellung einer vorläufigen, otolithenbasierten Biostratigraphie. Dissertation, Humboldt-University, Berlin, 152 pp.

Thomsen, E., Abrahamsen, N., Heilmann-Clausen, C., King, C. & Nielsen, O.B. 2012: Middle Eocene to earliest Oligocene development in the eastern North Sea Basin: Biostratigraphy, magnetostratigraphy and palaeonvironment of the Kysing-4 borehole, Denmark. Palaeogeography, Palaeoclimatology, Palaeoecology 350–352, 212–235. https://doi.org/10.1016/j.palaeo.2012.06.034

Ulleberg, K. 1974: Foraminifera and stratigraphy of the Viborg Formation in Sofienlund, Denmark. Bulletin of the Geological Society of Denmark 23, 269–292.

Ulleberg, K. 1987: Foraminiferal zonation of the Danish Oligocene sediments. Bulletin of the Geological Society of Denmark 36, 191–202. https://doi.org/10.37570/bgsd-1988-36-02

Ulleberg, K. 1994: Oligocene foraminifera and stratigraphy from the Harre borehole, Denmark. Aarhus Geoscience 1, 81–84.

van den Bosch, M., Cadée, M.C. & Janssen, A.W. 1975: Lithostratigraphical and biostratigraphical subdivision of Tertiary deposits (Oligocene-Pliocene) in the Winterswijk-Almelo region (eastern part of the Netherlands). Scripta Geologica 29, 167 pp.

van der Boon, A., Kuiper, K.F., Villa, G., Renema, W., Meijers, M.J.M., Langereis, C.G., Aliyeva, E. & Krijgsman, W. 2016: Onset of Maikop sedimentation and cessation of Eocene arc volcanism in the Talysh Mountains, Azerbaijan. In: Sosson, M., Stephenson, R.A. & Adamia, S.A. (eds): Tectonic evolution of the Eastern Black Sea and Caucasus. Geological Society, Special Publications 428. https://doi.org/10.1144/SP428.3

van der Boon, A., Beniest, A., Ciurej, A., Gaździcka, E., Grothe, A., Sachsenhofer, R.F., Langereis, C.G. & Krijgsman, W. 2018: The Eocene-Oligocene transition in the North Alpine Foreland Basin and subsequent closure of a Paratethys gateway. Global and Planetary Change 162, 101–119. https://doi.org/10.1016/j.gloplacha.2017.12.009

van der Boon, A., van der Ploeg, R., Cramwinckel, M.J., Kuiper, K.F., Popov, S.V., Tabachnikova, I.P., Palcu, D.V. & Krijgsman, W. 2019: Integrated stratigraphy of the Eocene-Oligocene depocits of the northern Caucasus (Belaya River, Russia): intermittent oxygen-depleted episodes in the Peri-Tethys and Paratethys. Palaeogeography, Palaeoclimatology, Palaeoecology 109395. https://doi.org/10.1016/j.palaeo.2019.109395

Vernyhorova, Y.V. & Ryabokon, T.S. 2020: The stratigraphy of the Oligocene-lower Miocene deposits of southern Ukraine. Turkish Journal of Earth Sciences 29, 170–207. https://doi.org/10.3906/yer-1905-24

Weiler, W. 1942: Die Otolithen des rheinischen und nordwestdeutschen Tertiärs. Abhandlung Reichsamt Bodenforschung, NF 206, 140 pp.

Isotope hydrology (^{2}H and ^{18}O) of Ikka fjord and its tufa columns, SW Greenland

BJØRN BUCHARDT, GABRIELLE STOCKMANN, MARC O. HANSEN & ÁRNY SVEINBJÖRNSDÓTTIR

Geological Society of Denmark
https://2dgf.dk

Received 11 April 2024
Accepted in revised form
23 June 2024
Published online
27 September 2024

Buchardt, B., Stockmann, G., Hansen, M.O. & Sveinbjörnsdóttir, Á. 2024. Isotope hydrology (^{2}H and ^{18}O) of Ikka fjord and its tufa columns, SW Greenland. Bulletin of the Geological Society of Denmark, Vol. 73, pp. 135–156. ISSN 2245-7070. https://doi.org/10.37570/bgsd-2024-73-08

From 1995 to 2022, several expeditions have visited the small Ikka fjord in SW Greenland to study growth and stability of the more than 1000 submarine tufa columns build of the metastable, cold-water carbonate *ikaite* ($CaCO_3 \cdot 6H_2O$). The different water types in the area have been sampled for geochemical and stable isotope (^{2}H and ^{18}O) investigations. Here we present the results of more than 300 isotope analyses of water from the fjord and from streams, lakes, springs and tufa columns. Fjord water samples identify a two-component mixing system ($R^2 > 0.99$) between freshwater runoff and sea water entering from the Davis Strait. The freshwater samples have an average composition of –95.4‰ $\delta^{2}H$ and –13.1‰ $\delta^{18}O$. We find both seasonal and altitude effects in fresh water related to early (June–July) or late (August) sampling time. All freshwater samples excluding lakes but including previous precipitation data (GNIP, 1963–1974) can be described by a Local Meteoric Water Line with slope of 6.43 ± 0.12 and offsets between 6.34 and 6.56. Column water samples are mixed with fjord water but extrapolation to a chlorine-free composition defines an endmember composition of –102‰ $\delta^{2}H$ and –14.2‰ $\delta^{18}O$. These compositions identify precipitation on top of the igneous plateau at ~ 500 m altitude as the source for the column water.

Keywords: Hydrogen and oxygen isotopes, meteoric water, fjord water, tufa columns, Ikka fjord, SW Greenland.

Bjørn Buchardt [bjorn.buchardt@mail.dk], Overgaden neden Vandet 5A,1.tv., DK-1414, Copenhagen K, Denmark. Gabrielle Stockmann [gabrielle@hi.is], Jarvik Geoconsulting AB, Gothenburg, Sweden and Department of Earth Sciences, University of Iceland, Reykjavik, Iceland. Marc O. Hansen [marcowater@yahoo.com], Danish Nature Agency, DK-4500, Nykøbing Sjælland, Denmark. Árný Sveinbjörnsdóttir [arny@hi.is], Institute of Earth Sciences, University of Iceland, Reykjavik, Iceland.

The small Ikka fjord in Arctic south-west Greenland (Fig. 1) has been the focus of several multidisciplinary expeditions between 1995 and 2022. The major purpose was to investigate the occurrence and formation of the more than one thousand submarine tufa columns (named *Ikka Columns*, Fig. 2) in the inner part of the fjord (Pauly 1963a; Buchardt *et al*. 1997, 2001; Hansen *et al*. 2011; Seaman & Buchardt 2006; Seaman *et al*. 2022; Stockmann *et al*. 2022). As part of these activities, many additional studies were carried out including zoological, botanical, microbiological, geochemical and geophysical investigations. A hydrological sampling program in and around the fjord collected more than 375 water samples over three decades for geochemical and stable isotope ($^{2}H/^{1}H$ and $^{18}O/^{16}O$) analyses (Table 1). Of this large data base, only a few stable isotope results have been published so far (Buchardt *et al*. 2001).

Stable isotope ratios of water ($^{2}H/^{1}H$ and $^{18}O/^{16}O$ expressed as δ-functions) are valuable tracers of hydrological systems as they are a property of the water molecule itself. Since the pioneering work by Dansgaard (1964), numerous studies have dealt with the stable isotope composition of all types of water from all parts of the Earth. The relationship between $\delta^{2}H$ and $\delta^{18}O$ in meteoric waters is well established and is expressed by the Global Meteoric Water Line (GMWL) equation (Craig 1961; modified by Rozanski *et al*. 1993):

$$\delta^{2}H = 8.17 \times \delta^{18}O + 10.35,\ R^2 = 0.98,\ n = 205$$

Several studies have demonstrated how this relationship is valid only for general use, whereas local conditions may lead to different correlations as expressed by the so-called Local Meteoric Water Lines (LMWL; Clark & Fritz 1997; Darling & Talbot 2003; Darling *et al*. 2003, Leng & Adderson 2003; Tappa *et al*. 2016).

In the present paper, we summarise isotopic results from streams, springs, fjord water and column water in the Ikka fjord area sampled over more than 25 years and compare these to former precipitation data from the Global Network of Isotopes in Precipitation (GNIP) database and to LMWL-data from other areas. The purpose of this paper is: 1) to make the stable isotope results from the Ikka fjord hydrological system available to interested parties, 2) to identify and quantify seasonal and altitude effects affecting the stable isotope composition of fresh water in the Ikka watershed and to establish a local meteoric water line and 3) to give an estimate of the uncontaminated isotopic composition of the so-called column water seeping from the submarine tufa columns in the fjord and to determine its origin. Work is still in progress in the Ikka fjord and further isotopic data may be accumulated over the coming years.

The Ikka Project

The submarine tufa columns in Ikka fjord have been known to science since 1963, when they were first described by the Danish mineralogist Hans Pauly (Pauly 1963a). Pauly identified the tufa material to consist of a new carbonate mineral, a metastable, cold-water (< 7°C, e.g., Bischoff *et al*. 1993) hexahydrate of calcium carbonate ($CaCO_3 \cdot 6H_2O$), which he named *ikaite* after the old spelling of the name of the fjord (Pauly 1963a, b). Renewed interest in the tufa columns was triggered by material brought to Copenhagen by the biologist Henning Thing in 1994 and resulted in the first expedition to Ikka fjord in the summer of 1995. At the same time, a British diving expedition was also active in the fjord. The findings in 1995 were

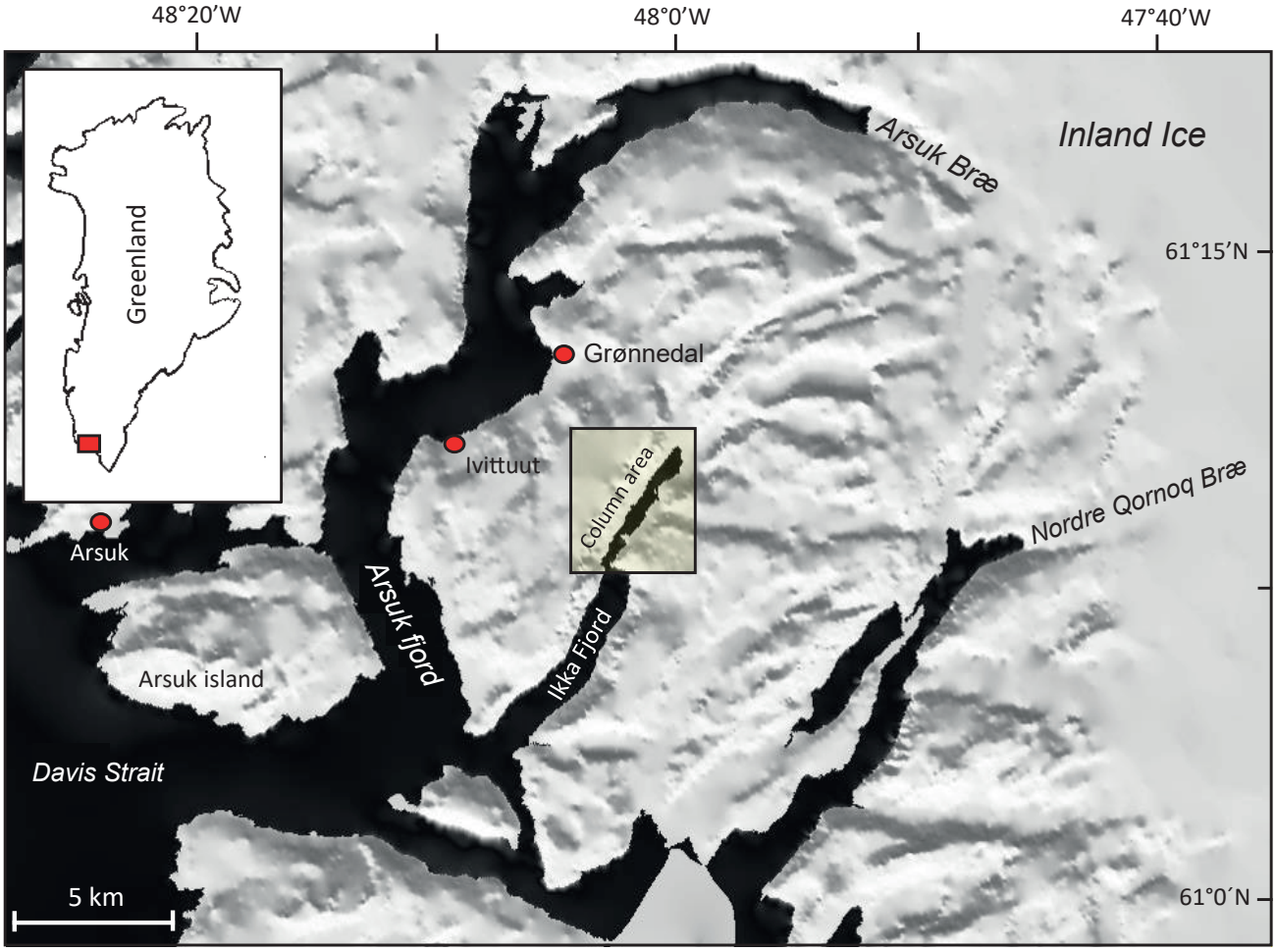

Fig. 1. Map of Ikka fjord and surrounding areas in SW Greenland. The inner part of Ikka fjord (Ikka bund) where the Ikka columns are found, is marked by a rectangle.

so promising that a major project was initiated that led to further expeditions in 1996 and 1997 including British scientists (Buchardt *et al*. 1997). During this period aspects of geology, biology, geochemistry, geophysics and hydrology were included (Kristiansen & Kristiansen 1999; Sørensen & Kristensen 2000; Petersen 2001; Buchardt *et al*. 2001; Thorbjørn & Petersen 2003; Dahl & Buchardt 2006; Stockman & Wilken 2007), and detailed mapping of the columns was achieved by aid of echo sounding and side scan sonar (Seaman 1998; Seaman & Buchardt 2006). Later, from 2006 to 2009, geological and hydrological studies were carried out in the fjord (Hansen *et al*. 2011). Finally, from 2014 to 2022, expeditions investigated the geochemistry of the bedrock geology (Ranta *et al*. 2018; Tollefsen *et al*. 2019) and mineral alterations in the columns (Stockmann *et al*. 2022) and carried out a detailed mapping of the bottom of the fjord (Seaman *et al*. 2022). An overview of expedition periods and number of samples is given in Table 1. The fjord was visited several times in the period from 2002 to 2013 by a group of microbiologists, who sampled the columns for extremophile bacteria occupying the high pH (> 10) environment inside the columns (e.g., Stougaard *et al*. 2002; Schmidt *et al*. 2006; Vester *et al*. 2013; Trampe *et al*. 2016, 2017).

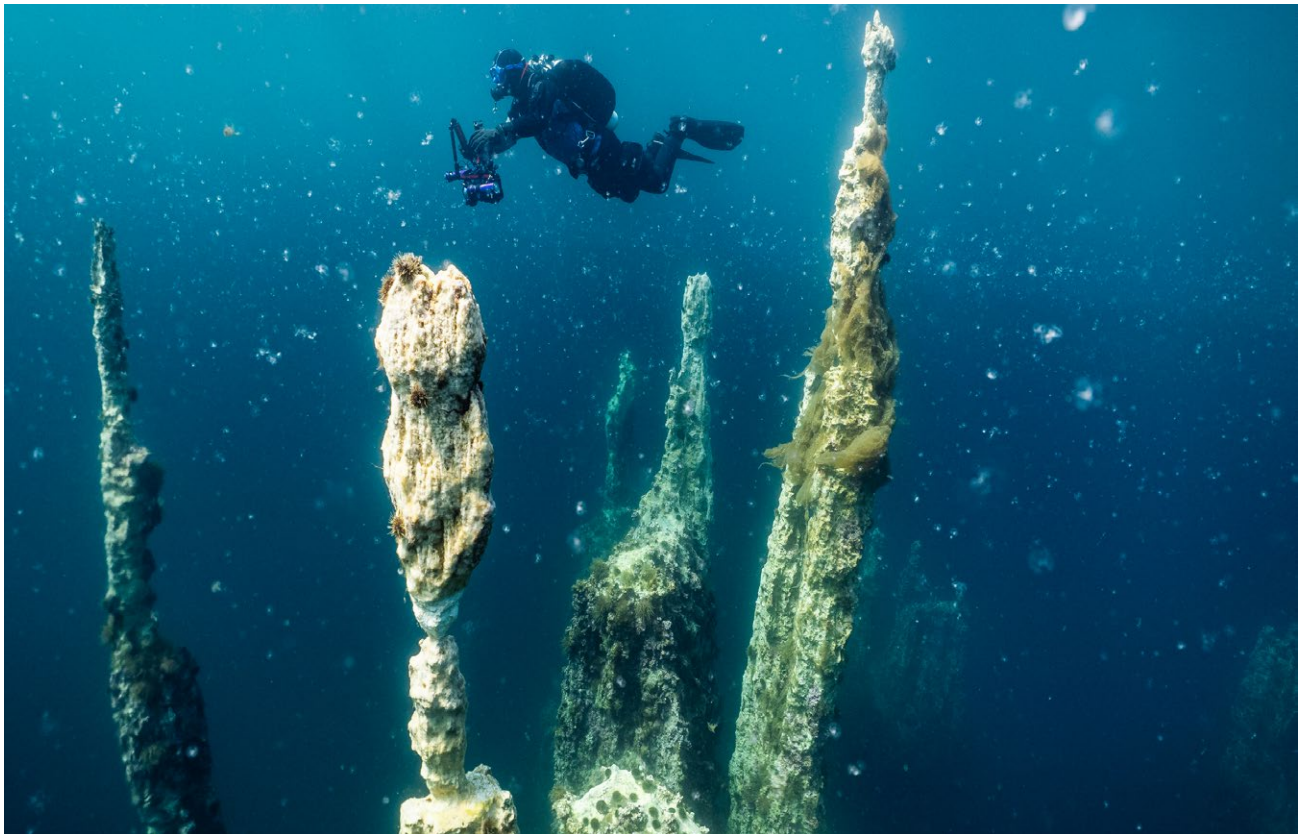

Fig. 2. Underwater photo of tufa columns from the inner part of Ikka fjord. Columns are 12 to 15 m high in this area. Note the cutting surface at the number two column from left. The column above this surface is about 1.3 m high. Columns are vertical and tilt is caused by camera distortion. Photo courtesy by Uli Kunz, SUBMARIS, 2024.

Table 1. Sampling periods and number of samples from individual water types

Year period 1 period 2	1995 early July early Aug.	1996 mid-Aug.	1997 early Aug.	2006 mid-Aug.	2007 early July October	2018 late June	2019 late June	2021 late Aug.
n: $\delta^{18}O$	64	99	39	33	37	10	14	9
n: $\delta^{2}H$	63	66	39	0	0	10	14	9
fjord water	30	54	10	21	9	0	2	0
streams	15	16	2	1	2	1	12	5
springs	3	14	12	4	15	9	0	4
lakes	5	12	1	6	7	0	0	0
columns	8	22	14	0	3	0	0	0

Geology of the Ikka fjord area

The Ikka columns are spatially related to the Grønnedal-Íka igneous ring complex, an alkaline intrusion 8 × 3 km exposed around Ikka fjord (Fig. 3A). It consists of layered nepheline syenites intruded by a xenolithic syenite and a plug of carbonatite (Callisen 1943; Emeleus 1964; Upton 2013; Bartels *et al*. 2015). It formed during the Gardar continental rifting period from 1350 to 1125 Ma ago, when the supercontinent Columbia broke apart (Rogers & Santosh 2002). The igneous complex has a zircon age of 1325 ± 5 Ma (Stockmann *et al*. 2018a) and was intruded into Palaeoproterozoic Ketilidian gneisses (>2700 Ma), which forms the landscape in most of the Ikka fjord area (Allaart 1976). Extensive uplift and erosion took place during Palaeogene time, and major exposures of the igneous complex are found on the Randsletten plateau (500–600 m altitude) north-west of the fjord. Here, syenites, nepheline syenites, and carbonatites of sövite and ankerite compositions are common in the central part (Emeleus 1964; Ranta *et al*. 2018). Syenites are also found in a small area east of the fjord. Major and minor dykes as well as fault systems transect the complex (Emeleus 1964). Economic interest in the iron, phosphate and rare earth contents of the igneous rocks have led to several unsuccessful prospects over the years (Bondam 1992).

Geographical and hydrological overview

The Ikka fjord (61°11´N, 48°01´W) is a submerged glacial valley that emerged from the Inland Ice cover about 11000 years ago (Weidick *et al.* 2004). It is 13 km long, up to 1.6 km wide and 170 m deep at the deepest and empties into the 500 m deep Arsuk fjord to the west over a 20 m deep sill. The fjord is flanked by 500–700 m high plateaus with steep mountain sides towards the fjord and is fringed to the north-east towards the margin of the Inland Ice by up to 900 m high mountains. It can be divided into an outer basin (Yderfjord) and an inner basin (Inderfjord) separated by a 17 m deep sill at Snævringen (the Constriction) that protects the inner

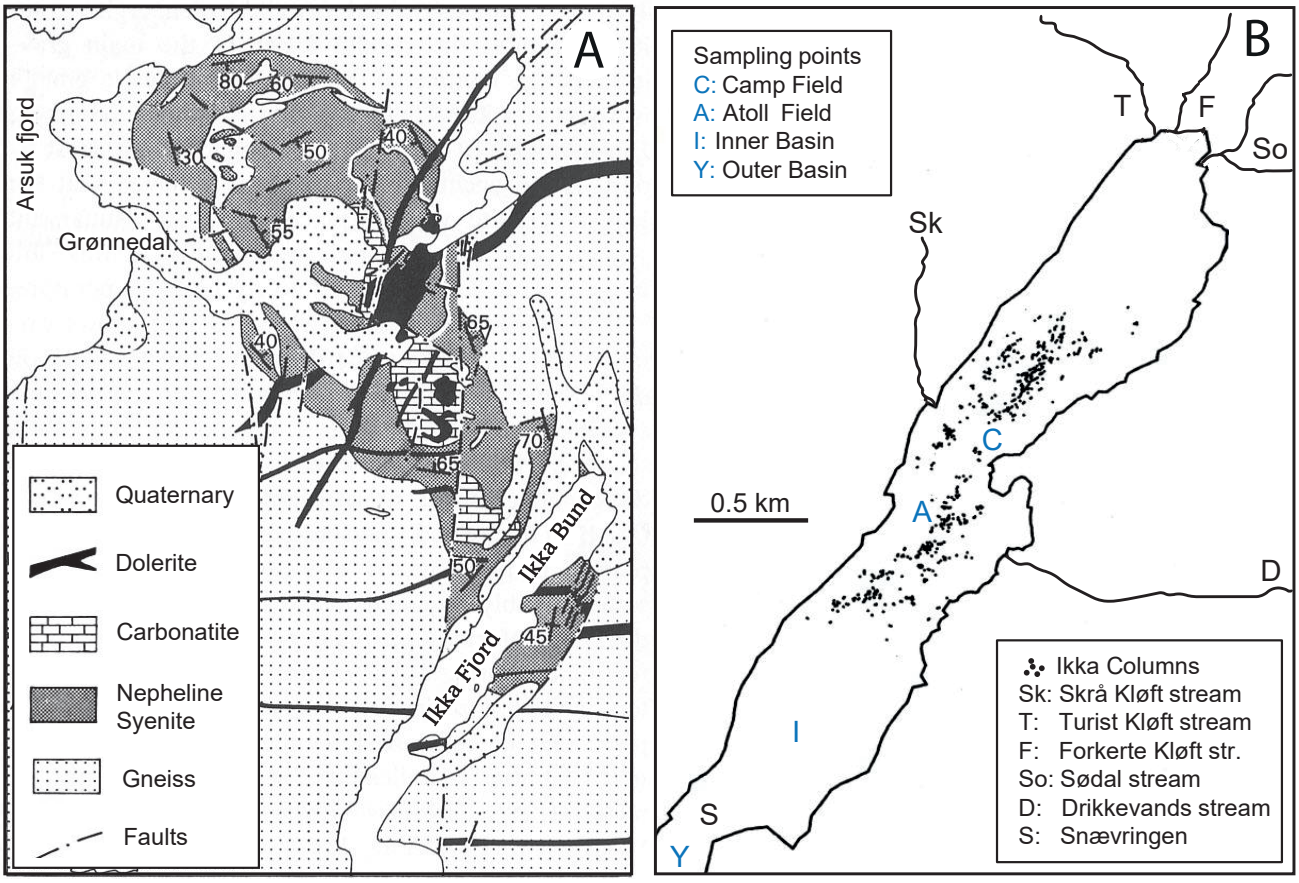

Fig. 3. A. Geological map of the Grønnedal-Íka igneous complex. Modified from Escher & Watt (1976, page 169). **B.** Map of inner part of Ikka fjord with the five sampled streams and the larger tufa columns. Also shown are sampling points for the hydrographic profiles. Modified from Seaman and Buchardt (2006) and Seaman *et al.* (2022).

part of the fjord from larger icebergs. The tufa columns are restricted to a 2 km long area in the innermost part of the inner basin (Fig. 3B; Seaman *et al*. 2022).

Annual precipitation measured at the nearby former naval base at Grønnedal (now Station Grønnedal) are between 600 and 1400 mm with a maximum in October to December and a minimum in May and June (Fristrup 1971; Hansen *et al*. 2011), and no permafrost has been detected. The area is snow-covered at least 140 days a year, and the fjord is frozen from October to May (Hansen *et al*. 2011). Mean annual air temperatures in Ikka fjord between 1961 and 2008 varied from –1.9°C in 1972 to +2.9°C in 1985 (Hansen *et al*. 2011). Bonne *et al*. (2014) gave a mean annual temperature for 2012 to 2013 from Ivittuut close to Grønnedal of +2.7°C. Later data are only available from weather stations farther south-east at Narsarsuaq airport (130 km) and Qaqortoq heliport (125 km; http:// https://www.dmi.dk/vejrarkiv. The latter gave average annual temperatures for the period from 1995 to 2021 between 0.3° (minimum) and 4.4°C (maximum) without any systematic increase over the period.

Four types of water are represented in the Ikka fjord hydrological system: fresh water, sea water, fjord water and column water. Fresh water includes streams, lakes and springs in the local catchment area. Sea water enters from the Davis Strait to the west. Fjord water is the water type formed by mixing of sea water and freshwater run-off. Column water is the highly alkaline spring water sampled by our divers from inside the submarine Ikka columns.

Five major streams named after their ravines flow into the fjord: Skrå Kløft, Turistkløft, Forkerte Kløft, Sødal and Drikkevandselv (Fig. 4; Table 2A). No effort was made to measure the discharge from the streams, but it was clear that Skrå Kløft stream had the smallest discharge and Forkerte Kløft and Sødal streams had the largest. The Skrå Kløft stream is sourced in the alkaline rocks at Randsletten, whereas the other streams all come from gneissic basement rocks. The altitude of the headwaters for the major streams varies from 900 m (Forkerte Kløft) to 300 m (Turistkløft). The catchment area for the streams discharging into Ikka fjord is about 160 km^2. Two glaciers drain the Inland Ice north and south of Ikka fjord: Arsuk Bræ (Arsuk Glacier, Sermeq) to the north and the Qoornoq Bræ system to the south (Fig. 1). As none of the glaciers enter the catchment area around Ikka fjord, the only source of fresh water is local precipitation.

Springs in the areas can be divided into three groups: Springs found outside the intrusive complex, springs on or around the exposures of the Grønnedal-Íka complex at the plateau at 500-metres altitude, and springs discharging at the eastern slopes of the Grønnedal-Íka complex close to the margin of the fjord. The latter springs are marked by a significant luxury of vegetation including orchids and green mosses (Fig. 12C). At least two of the springs are homothermic with all-year temperatures close to 3.4°C (Hansen *et al*. 2011). Springs at the plateau show no vegetation at all.

Lakes in the catchment area (Table 2B) are mainly found at the Randsletten plateau west of Ikka fjord at

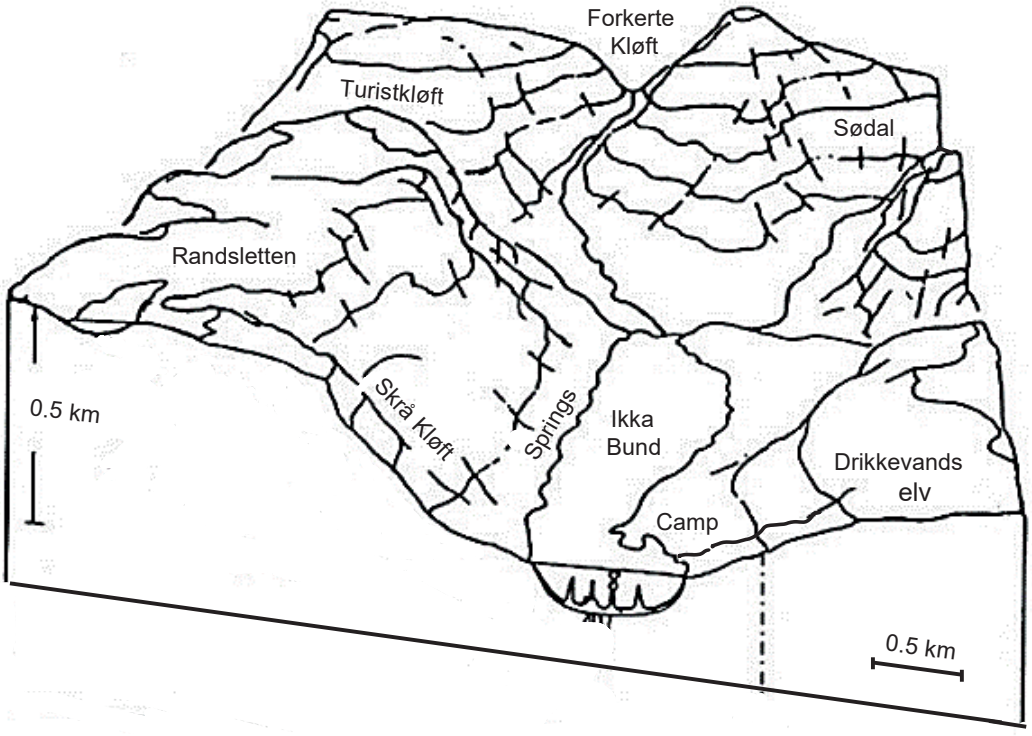

Fig. 4. 3D-rekonstruction of the inner part of Ikka fjord and the surrounding highlands. Also shown are ravine features, where the sampled streams are flowing. Further information on streams, springs and lakes are found in Table 2.

Table 2A. Geographical data for the sampled streams, positions from Google Maps

Name Danish	Name Translated into English	Location mouth	Length (km)	Headwater altitude (m)
Skrå Kløft elv	Oblique Ravine Stream	61°11.66´N, 48°01.86´W	2.2	506
Turist Kløft elv	Turist Ravine Stream	61°12.64´N, 48°00.43´W	2.1	310
Forkerte Kløft elv	Wrong Ravine Stream	61°12.60´N, 48°00.30´W	10.4	900
Sødal elv	Lake Valley Stream	61°12.33´N, 48°00.06´W	6.3	480
Drikkevands elv	Drinking Water Stream	61°09.94´N, 48°02.14´W	1.9	470

Table 2B. Geographical data for the sampled lakes, positions from Google Maps

Name Danish	Name Translated into English	Location	Area km²	Altitude (m)
Lejrsø	Lake Camp	61°13.15´N, 48°01.92´W		10
Xenolitsø	Xenolith Lake	61°09.94´N, 48°02.14´W	0.070	470
Tolvsøer	Twelve Lakes	61°13.45´N, 48°01.92´W	0.027	366
Øvre Radiosø	Upper Radiolake	61°12.65´N, 48°03.32´W	0.022	524
Nedre Radiosø	Lower Radiolake	61°12.62´N, 48°02.74´W	0.057	502
Wilkensø	Lake Wilken	61°12.33´N, 48°02.95´W	0.045	502
Hesteskosø	Horseshoe Lake	61°11.34´N, 47°56.40´W	1.230	470
Drikkevandssø	Drinking Water Lake	61°11.23´N, 47°58.70´W	0.008	467
Bjørnesø	Bear Lake	61°12.94´N, 48°01.79´W	0.004	490

about 500 m altitude (Radiosøerne, Xenolithsø and Bjørnesø). Tolvsøer, a shallow-water group of small lakes have been sampled at 350 m altitude north of the Grønnedal-Íka intrusion. Two major lakes (Hesteskosø and Drikkevandssø) were visited east of the fjord at 470 m altitude, and so was a small lake close to our camp site at sea level.

The fjord water is divided vertically into an upper brackish layer (salinities between 0 and 25 psu) and a deeper marine layer (salinities up to 33 psu; Fig. 5). The halocline between these two layers is typically found at depths between 2 and 5 m. The brackish layer results from mixing between sea water from Arsuk fjord and fresh water from the many streams discharging into the fjord and from precipitation directly onto the fjord and may reach temperatures up to 12ºC during summer. The sea water originates from a side branch of the cold East Greenland Current which turns around the southern tip of Greenland and partly mixes with the warmer Irminger Current in Davis Strait. A tidal range of up to 3 m is responsible for exchange of water in the fjord and mixing between fresh and sea water.

Column water is the non-marine water seeping from springs at the fjord bottom into the Ikka columns, and upon mixing with the cold fjord water precipitates ikaite. Column water is a highly alkaline, sodium-carbonate brine with pH values above 10 (Buchardt *et al*. 1997; Buchardt *et al*. 2001).

Sampling

We sampled the fjord in 1995, 1996 and 1997, again in 2006 to 2007 and finally in 2018, 2019 and 2021. Activities in the fjord took place during the spring and summer seasons when the fjord was ice-free, expect for one winter expedition in April 2008. Earliest in the year were the expeditions in June and beginning of July, later expeditions were in the second half of July, August and in mid-October (see Tabel 1). Therefore – as will be demonstrated later – seasonal variations in water data are expected.

Altogether, more than 372 water samples were collected from the Ikka fjord hydrological system during the 26 years of sampling. Of these, 305 samples were analysed for ^{18}O and 201 for ^{2}H. The types of water samples are shown in Table 1. All samples were stored in polyethylene bottles or in vacutainers and kept refrigerated or frozen until analysis. To avoid exchange with atmospheric CO_2, samples were not filtered in the field. Local precipitation has only been sampled a few times, and precipitation data for comparison have been taken from the Global Network in Isotopes in Precipitation (GNIP) programme at Grønnedal 1961 to 1974 (Rozanski *et al*. 1993) and from Bonne *et al*. (2014).

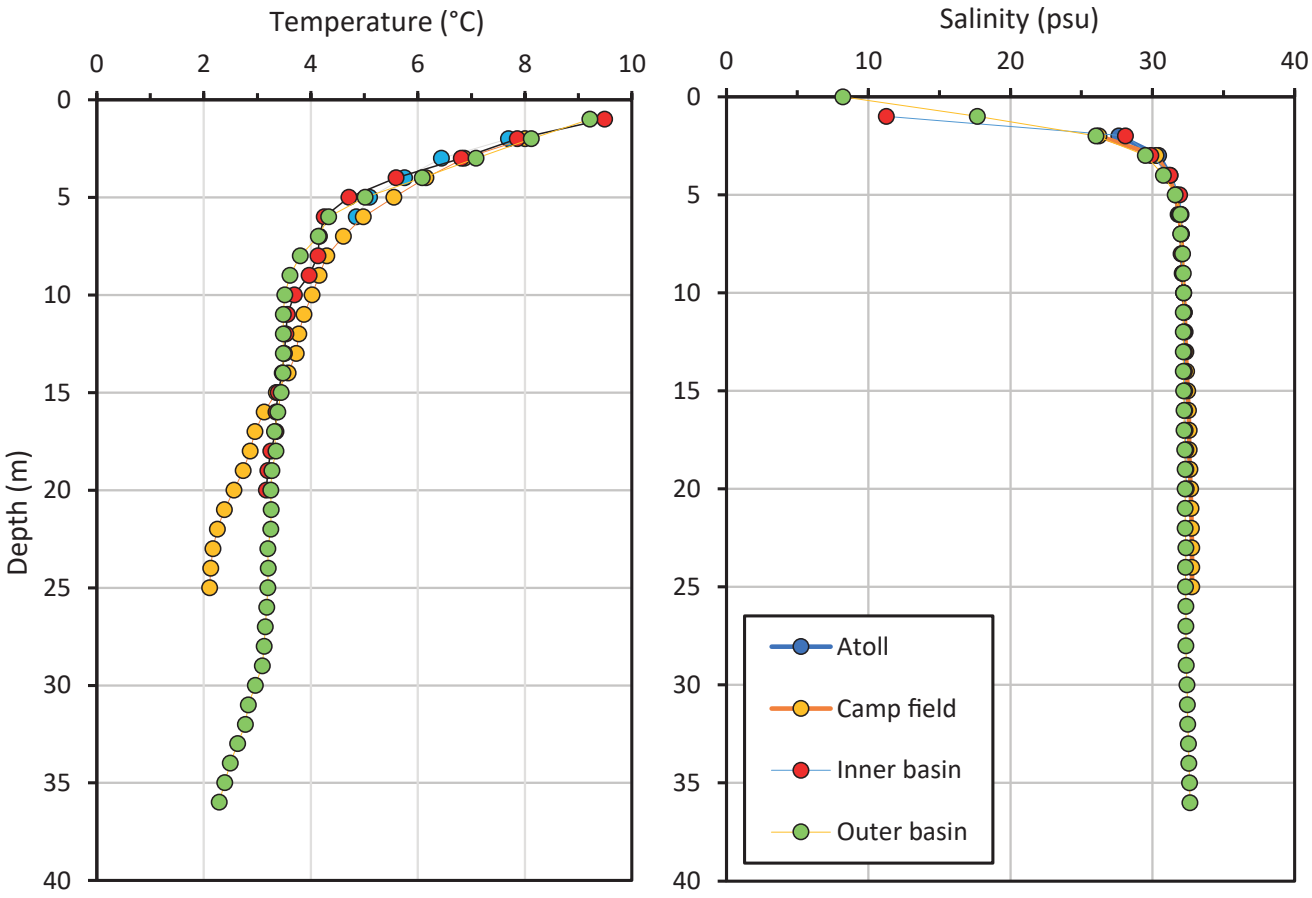

Fig. 5. Hydrographic profiles from Ikka fjord. Sampling stations refer to map on Fig. 3B. The profiles illustrate the mixing between sea water at depth and fresh water at surface. Note the marked halocline at a depth of 2 to 5 m. Data from the Danish Meteorological Institute, pers. com. (1999).

Analytical methods

The long timespan over which we have worked in Ikka fjord means that different analytical methods have been applied over the period. As an example, GPS location of sample sites has evolved from unprecise, differential determinations in 1995 (precision of ± 100 m) to highly precise modern GPS coordinates from 2005 onwards (precision better that 2 m).

Isotope analyses have been carried out by several laboratories over the years (Niels Bohr Institute and Geological Institute, both University of Copenhagen and at the Institute of Earth Sciences, University of Iceland (HÍ)) using different measuring techniques. Comparability have been achieved by application of the same international standards (V-SMOW and GISP). Hydrogen isotope ratios were determined by the zink reduction technique at 700°C on a Finnigan 250 dual inlet mass spectrometer (samples from 1995 to 2007, KU) and by H_2 equilibrium technique, using platinum sticks as catalyst on a Delta V Advantage continuous flow IRMS interfaced with a gasbench II device (samples from 2018, 2019, 2021, HÍ). Oxygen isotope ratios were determined by the CO_2 equilibrium technique on a custom build mass spectrometer at the Niels Bohr Institute, KU (samples from 1995 to 1997), on a Micromass Isoprime continuous flow instrument at GI, KU (samples 2006 and 2007) and by a Delta V Advantage continuous flow IRMS interfaced with a gasbench II device (samples from 2018, 2019, 2021, HÍ). All results are reported as δ-values relative to V-SMOW. General reproducibility is better than ± 2‰ (± 1‰) for hydrogen isotopes and ± 0.5‰ (± 0.1‰) for oxygen isotopes, with numbers in brackets representing the reproducibility of the HÍ samples.

Salinity measurements of water samples were carried out in the field either by thermoconductivity sensors or by a hand-held refractometer and calibrated by conductivity measurements either in the field or later in the laboratory. Hydrographical temperature/salinity depth profiles from selected locations in the fjord system were obtained using CTD-instruments (Conductivity-Temperature-Depth). The best data sets came from a survey in July 1999 performed by the

Danish Meteorological Institute using a Seabird 9-11 sonde and from a survey carried out in 2006 (Hansen *et al*. 2011). The pH and alkalinity were measured in the field or in laboratory facilities in the nearby Ivittuut village. Concentrations of sodium, calcium and chlorine ions were measured by atomic absorption spectrometry and ion chromatography.

Results and discussion

Our water samples represent two different hydrological systems: Meteoric waters including streams, springs lakes and fjord water representing mixing between freshwater run-off and sea water. Column water samples should in principle be included in the meteoric system as spring water but will in practice be a result of mixing between pure column water and fjord water due to sampling contamination and will be treated separately. The results of the isotopic analyses are presented in Fig. 6. Individual results can be found in the Supplementary Material.

Hydrogen and oxygen isotope content of all freshwater samples have δ^2H-values between –114‰ and –84‰ and δ^{18}O-values between –15.8‰ and –10.0‰ (Table 3). These values are markedly depleted in ^{2}H and ^{18}O compared with sea water and reflect the isotopic composition of arctic precipitation. Our freshwater samples have been collected at different

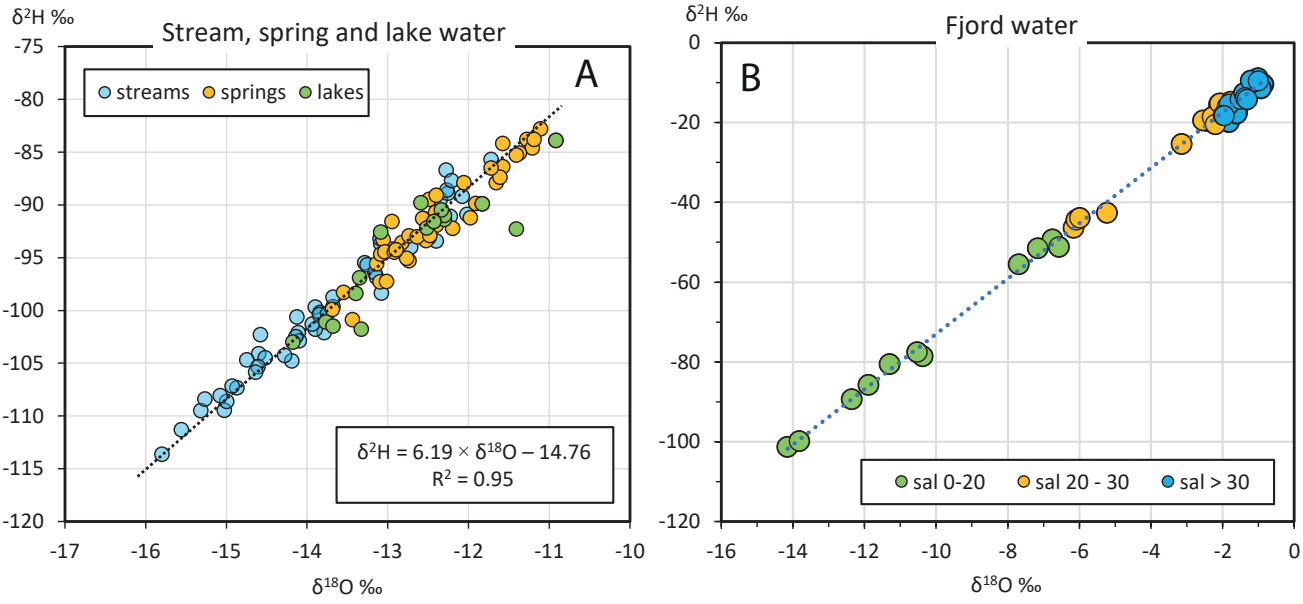

Fig. 6. δ-diagrams for hydrogen and oxygen isotope compositions of fresh water (**A**) and fjord water (**B**) in the Ikka fjord area. Note the more negative (depleted) stream water compositions compared to springs and lakes. Fjord water is divided according to salinity (sal). Green marks: above halocline, orange marks: inside halocline, blue marks: below halocline. Equations based on least square linear regressions.

Table 3. Overview of isotopic results

Type	Parameter	Precipitation*	Streams	Springs	Lakes	Fjord water	Column water
δ^2H‰	n	72	51	38	18	41	44
"	average	–94.1	–99.3	–91.5	–93.4	n.d.	–63.6
"	maximum	–53.3	–85.7	–82.8	–83.9	–8.9	–15.2
"	minimum	–133.3	–113.7	–100.9	–103	–101,3	–95.7
δ^{18}O‰	n	95	55	61	31	130	47
"	average	–12	–13.7	–12.9	–12.6	n.d.	–8.5
"	maximum	–6.5	–11.7	–10.8	–10.0	–0.8	–1.9
"	minimum	–17.5	–15.8	–13.7	–14.2	–14.2	–13.4
LMWL	slope	6.34	6.56	6.37	5.58	6.93	6.96
LMWL	offset	–16.6	–9.51	–12.2	–23.2	–3.62	–2.12
LMWL	R^2	0.87	0.96	0.93	0.85	0.99	0.99

LMWL: Local Meteoric Water Line
*data from GNIP network

times of the year, and streams and springs have been sourced at varying altitudes (0 to 900 m). However, the strong correlation between the isotopic compositions of all the samples ($R^2 = 0.95$, n = 111) suggests that they belong to the same hydrological system as defined by a local meteoric water line (LMWL):

$$\delta^2H = 6.2 \times \delta^{18}O - 14.8 \text{ (least square regression)}$$

Precipitation

The strong correlation between the δ^2H- and $\delta^{18}O$-values from our freshwater samples indicates a common source, in this case local precipitation. Most precipitation in the Ikka area originates from low pressure systems in the North Atlantic either to the south-west or the south-east. Especially the winter 'south-east' gale is known for its ferocity and large amounts of snow (Fristrup 1971). To reach Ikka fjord, most precipitating clouds must pass over 500–700 m high mountain plateaus, and an orographic 'rain-out effect' on the isotopic composition (Dansgaard 1964; Clark & Fritz 1997) must be expected.

As it was not possible to sample local precipitation over a whole year, the limited precipitation data from our expeditions are of little value. Fortunately, a detailed, but rather old, database exists from the GNIP (Global Network of Isotopes in Precipitation) program, including measurements of δ^2H and $\delta^{18}O$ in precipitation from the naval base at Grønnedal (61° 13.9´N; 48° 5.9´W). The base is located only 5 km from Ikka fjord and close to the sea and we use the data as an approximation to conditions in Ikka fjord. Precipitation was sampled from 1963 to 1970 and again from 1973 to 1974 (International Atomic Energy Agency 1969, 1970, 1971, 1973, 1975 & 1979; Rozanski *et al*. 1993). Samples were pooled monthly, but unfortunately only one year (1963) was sampled and analysed in full. Precipitation was mostly in the form of snow for at least 6 months of the year, only July and August were mostly snow-free. δ^2H-values had a range from -133‰ to -53‰ and $\delta^{18}O$-values from -17.5‰ to -6.5‰ with a small seasonal effect between less enriched values during winter (October to March) and more enriched values during summer (May to August; Fig. 7). Pure rain samples (n = 6) are enriched ($\delta^{18}O$-average = -10.4‰) as compared to snow samples (n = 27, $\delta^{18}O$-average = –12.8‰). Samples designated as both rain and snow (n = 29) fall between these values ($\delta^{18}O$-average = –11.4‰). Volume-weighted annual averages for hydrogen and oxygen isotope compositions for the whole period are –94.1‰ and –12.0‰ respectively. The small seasonal effect seen in the Grønnedal precipitation is related to its coastal climate (23 km to Davis Strait), and as all samples were taken close to sea level, any altitude effects can be excluded. Deuterium excess values

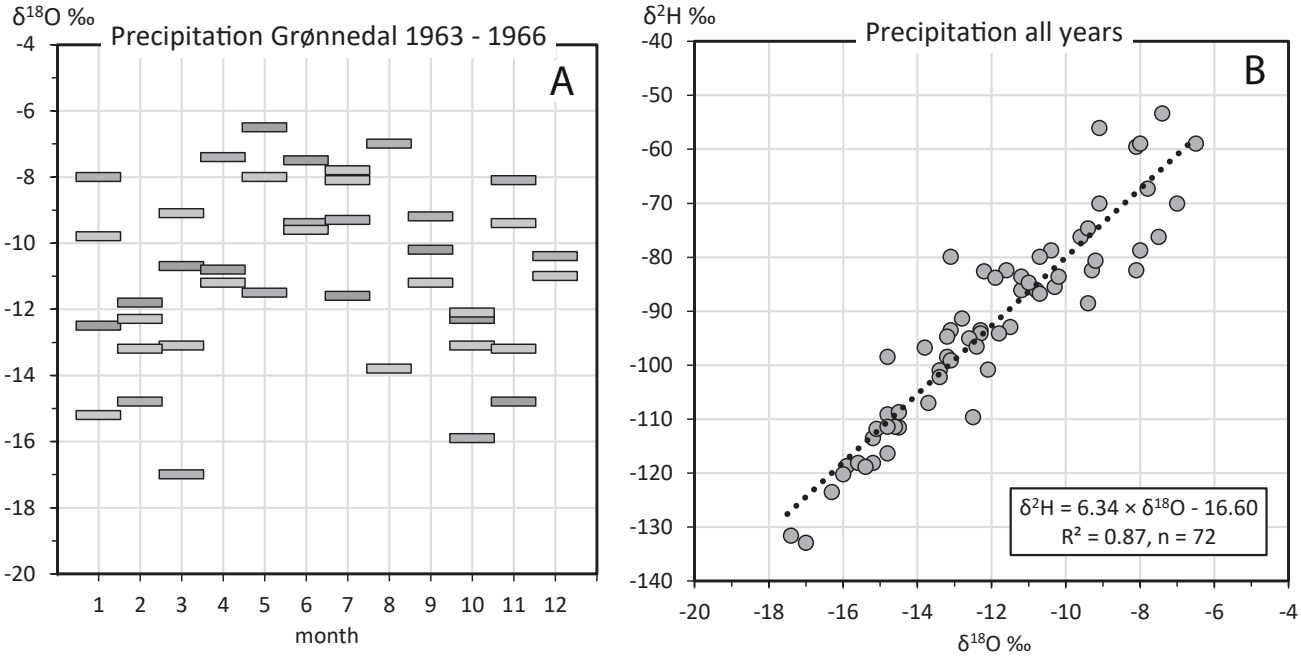

Fig. 7. Precipitation data from the GNIP-database sampled at the former naval base Grønnedal 5 km west of Ikka fjord. Left diagram: Mean $\delta^{18}O$-values for individual months for the period 1963 to 1966. Summer precipitation is more positive (enriched) in ^{18}O compared to the rest of the year, and winter precipitation has a wider range in ^{18}O composition. Right diagram; δ-relation for all precipitation samples (monthly mean) from the periods 1961-1970 and 1973 and 1974. Note the large spread in isotopic compositions. Weighted mean values for all years are –87.7‰ for δ^2H and –11.29‰ for $\delta^{18}O$. Equation based on least square regressions.

(d ‰ = $\delta^2H - 8\times \delta^{18}O$; Dansgaard 1964) vary between –20‰ and +25‰ (average +2.8‰) with no relation to either amount or type of precipitation, only temperature is weakly negatively correlated with d (R^2 = 0.31). Deuterium excess in precipitation is mainly related to relative humidity (RH) at the source areas and is a measure of nonequilibrium fractionation at the sea surface. The large spread suggests varying moisture sources for the precipitation with changing RH conditions.

Since 1974 an increase in summer temperatures of about 1°C has been estimated from meteorological data (Hansen *et al*. 2011). This increase would probably lead to a minor increase in O and H stable isotope compositions of the precipitation. A later study by Bonne *et al*. (2014) includes stable isotope precipitation data from Grønnedal for a period from July 2011 to November 2012. Data from 39 samples of rain and snow have $\delta^{18}O$ values between –20‰ and –6‰ with no mean values given. These numbers are almost identical to the older GNIP dataset.

The relationship between δ^2H and $\delta^{18}O$ from the GNIP data (Fig. 7) is defined by a local meteoric water line (LMWL) given by the equation (Table 3):

$$\delta^2H = 6.3 \times \delta^{18}O - 16.6;\ R^2 = 0.87;\ n = 72$$

This equation is biased by the incomplete dataset missing several monthly results. Taking the values from the only complete year 1963 yields a slightly different LMWL of

$$\delta^2H = 6.7 \times \delta^{18}O - 16.2;\ R^2 = 0.91;\ n = 12$$

The large differences in slope and intercept between the local GNIP-lines and the GMWL ($\delta^2H = 8 \times \delta^{18}O + 10$) reflect differences in evaporative regime in the moisture source areas, also reflected in the deuterium excess variations.

Stream water

Stream water samples were collected from streams in the watershed area, mainly at sea level. Headwater altitude varied from a few metres above sea level to 900 m for the Forkerte Kløft stream (Table 2A). δ^2H- and $\delta^{18}O$-values varied from –114‰ to –86‰ (n = 51) and from –15.8‰ to –11.7‰ (n = 51) respectively (Table 3). Mean values are –99‰ for δ^2H and –13.7‰ for $\delta^{18}O$. Taken together, the stream data define a local meteoric water line (LMWL):

$$\delta^2H = 6.6 \times \delta^{18}O - 9.51,\ R^2 = 0.96,\ n = 51$$

A seasonal effect is evident for our stream data. Samples collected from streams early in the season in June and beginning of July (1995, 2018, 2019) are depleted in both ^2H and ^{18}O as compared to later sampling of the same streams in late July, August, and October (1996, 1997, 2006, 2007 and 2021; Fig. 8). Mean δ-values for samples from the early sampling periods are –105‰ for δ^2H and –14.5‰ for $\delta^{18}O$ and –93‰ and –12.7‰ respectively for the late periods. The Ikka area is snow-covered for more than half of the year, and snow was observed on northerly facing slopes in June and early July. Thus, our early stream samples are probably dominated by melting of isotopically depleted snow from the foregoing winter, whereas the late samples reflect summer precipitation in the form of rain. The most depleted $\delta^{18}O$-composition of all streams (–15.8‰) were found in June 1995 in the stream Forkerte Kløft sourced at the highest altitudes in the area.

When compared, stream and precipitation (GNIP) data reveal interesting aspects. The slopes as defined from the two LMWL´s are almost identical (6.6 versus 6.3) indicating that the two sample sets belong to the same meteoric system. But the range in precipitation data is more than twice as large ($\delta^{18}O$: –17.5‰ to -6.5‰) as that of the stream data (–15.8‰ to –11.7‰), and the stream data – even from the late season samples – are comparable only to the more depleted values of the precipitation data.

Altitude effects

Headwaters of the streams vary from 300 to 900 m altitude (Forkerte Kløft). Samples were collected mainly at the stream mouths at sea level but are here represented by the altitude of their source areas. The altitude plot (Fig. 8) illustrates a combination of seasonal and altitude effects. Viewed individually, both early and late samples are systematically depleted with increasing altitude. An estimate of the $\delta^{18}O$-value of this altitude effect from linear regression amounts to between –3.1‰ (early samples) and –3.6‰ (late samples) for the 900 m difference in source areas or between –0.3‰ and –0.4‰ pr. 100 m. Whether these numbers are results of climatic conditions or reflect a true isotopic orographic effect (e.g., Clark & Fritz 1997) is unclear, but the fact that both early and late stream waters are affected in parallel, points to a general isotopic altitude-related rain-out effect. If all precipitating clouds had to cross the mountains along Ikka fjord, the orographic rain-out effect would probably lead to identical, isotopically depleted rain and snow falling on the back side in the fjord area. As this is obviously not the case, most of the precipitating cloud system must enter from the sea via the Ikka fjord valley before climbing the fjord sides. If so, precipitation from the

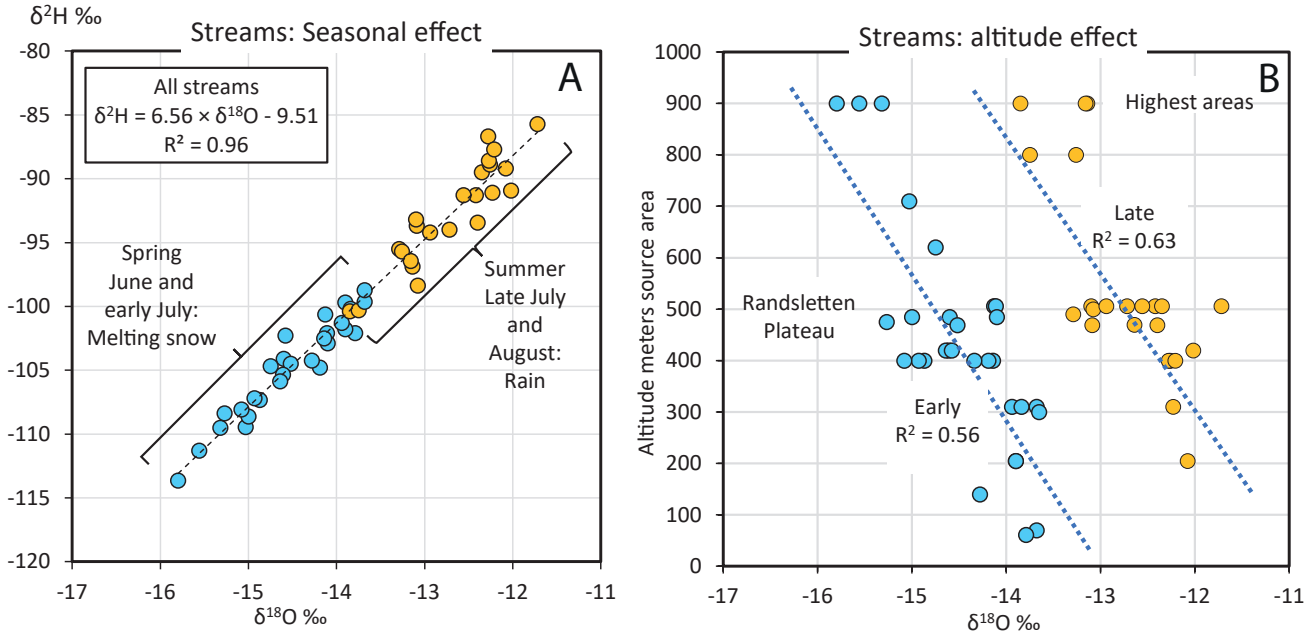

Fig. 8. Hydrogen and oxygen isotope composition data for all streams sampled at different years and from streams sourced at different altitudes. **A.** Seasonal effects in isotopic composition is obvious from differences between early and late sampling related to melting snow or rain as source. **B.** An isotopic altitude effect is suggested when data are treated separately for early and late sampling periods. Lines show linear regressions. Altitude effect amounts to –0.3 to –0.4‰ $\delta^{18}O$ pr. 100 m elevation.

Grønnedal area cannot be the only source of stream water in Ikka fjord.

Our calculated altitude effect of –0.3 to –0.4‰ $\delta^{18}O$ pr. 100 m elevation is comparable to other studies. Darling and Talbot (2003) reported values of –0.2‰ to –0.3‰ $\delta^{18}O$ from Scotland, Tappa *et al*. (2016) gave a value of –0.22‰ $\delta^{18}O$ for a mountainous area in Idaho, US and Clark & Fritz (1997) summarised eight studies to vary between –0.1‰ and –0.5‰ $\delta^{18}O$ pr. 100 m elevation.

Spring water

Over the study period, 61 samples were collected from freshwater springs west and east of Ikka fjord (Fig. 9A). Most samples are enriched in ^{18}O by 1‰ to 2‰ when compared to stream samples from the same year. 55 samples were from eight spring areas close to sea level (< 50 m altitude) at the western side of the fjord below the carbonatite and syenite exposures. This water type had our special attention as a possible source for the column water leaking from the submarine tufa towers in the fjord. Two of these springs were monitored throughout a year (August 2006 to July 2007) and proved to be homothermal with year-long temperatures close to 3.4°C (Hansen *et al*. 2011). Mean annual temperatures in the Ikka area are estimated to no higher than 2.9°C (Hansen *et al*. 2011), so extra heat must be provided for these springs, maybe from radioactive decay in the intrusive complex.

The 2400 m traverse through the eight springs along the western shoreline from Turist Elv in the north to the Skrå Kløft Elv further south (Fig. 4) showed both seasonal and lateral variations in isotopic composition (Fig. 9B). The samples from early July in 1995 were the most ^{18}O-depleted (average $\delta^{18}O$: –13.7‰ ± 0.1‰), whereas the springs sampled at the same time of the year in 2007 were among the most enriched (average $\delta^{18}O$: –11.4‰ ± 0.5‰). Samples from 2018 (June) and from late in the season in 1996, 1997 and 2006 (August) fall between these two extremes. Lateral variations are pronounced between the isotopically depleted springs in the central part of the traverse below the carbonatite exposures (from approx. 600 m to 1500 m, Fig. 9B) and the isotopically enriched springs outside this area, where bedrocks are either syenite or gneiss. The maximal difference amounts to 2.0‰ $\delta^{18}O$ (1996). pH values for these springs vary from 7.1 to 8.2, Ca^{2+} concentrations from 6.0 mg/l to 41.1 mg/l and Sr^{2+} concentrations from 0.3 mg/l to 39.6 mg/l. pH values, Ca- and Sr-concentrations are highest in springs below the exposures of carbonatite, whereas the lowest values are found in the gneissic areas outside the igneous complex. It is thus obvious that the water in the springs below the carbonatite are modified by dissolution of the Ca-rich carbonatitic rocks. Sodium concentrations vary between 2.2 and 5.8 mg/L in the carbonatite-near springs and is higher than those sourced in gneiss (< 3mg/L), but significantly lower than the column water (3900 to 9100 mg/L).

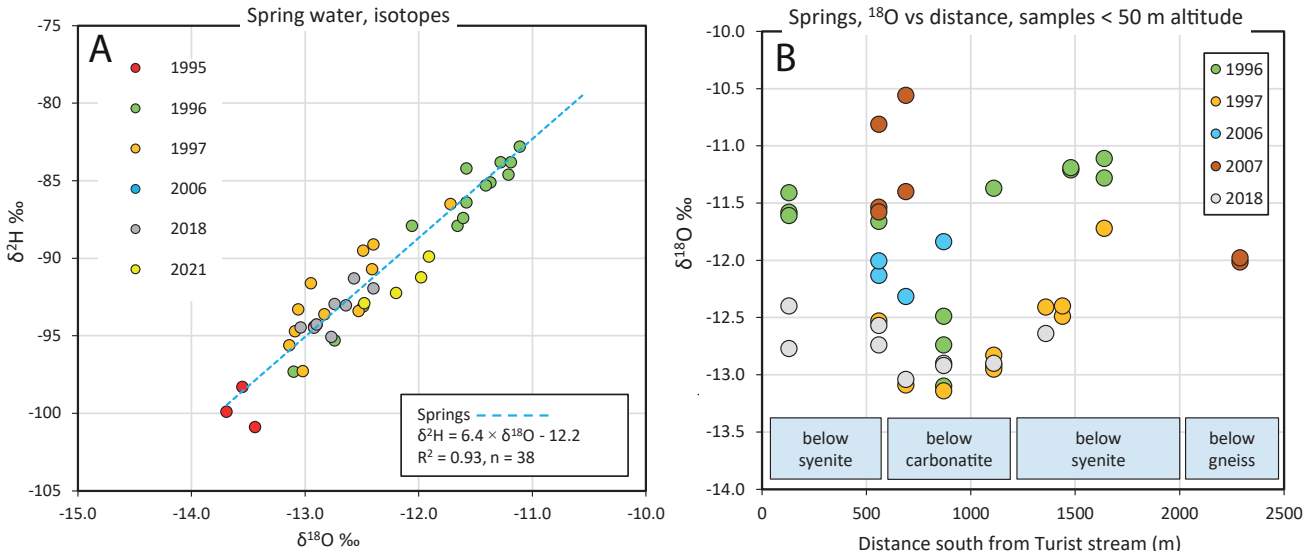

Fig. 9. Hydrogen and oxygen isotope compositions of spring water samples from all years (**A**). The diagram illustrates a seasonal effect where samples from 1995 (early July) are significantly depleted compared to later samples. Samples from 1996 (late August) are the most enriched. Equation based on least square regression. Oxygen isotope composition of spring water sampled at the foot of the igneous exposures along the west side of the fjord (**B**). Note the depletion of samples below the carbonatite. These springs are marked by a luxurious vegetation, whereas springs outside of the carbonatite are free of plants.

The large spread in the spring water isotopic compositions points to a surface-near source with a low residence time – probably local precipitation and melting snow – rather than deep groundwater from the Grønnedal-Íka complex with a more constant isotopic composition. The homothermal character of at least two of the springs below the carbonatite exposures, on the contrary, sems to indicate a deeper source for these springs. The igneous complex is characterised by numerous cracks and fissures and a higher permeability compared to the adjacent homogenic gneissic rocks, which probably result in a more complex source for the spring water below the exposures than the surface-derived water from the gneiss.

Eight spring water samples came from the east side of the fjord and from the Randsletten plateau at altitudes up to 520 m. The samples from 2007 suggest a possible altitude effect estimated to –1.5‰ for ^{2}H and –0.2‰ for ^{18}O comparable to those for the streams.

$\delta^{2}H$-data are not available from spring water in the years 2006 and 2007, but the rest of the samples define a nice LMWL ($R^2 = 0.93$, n = 38) with a slope of 6.4 and an intercept of -12.2. This slope is close to that of the stream data (6.6, $R^2 = 0.96$) and Grønnedal precipitation (6.3, $R^2 = 0.87$) and demonstrate the close relationship between different components of the hydrological system in and around Ikka fjord.

Lake water

31 samples of surface water were collected from six lakes at altitudes between 350 and 520 m at the Grønnedal-Íka plateau inside and outside the margins of the intrusion and from three lakes at the east side of the fjord at 10 and 470 m (Table 2B). Their isotopic values vary from –103‰ to –84‰ ($\delta^{2}H$) and –14.2‰ to –10.0‰ ($\delta^{18}O$; Table 3). Samples from 1995, 1996 and 1997 have been analysed for both ^{2}H and ^{18}O, the remaining from 2006 and 2007 only for ^{18}O. Most of the lake water samples fit the LMWL as defined by stream and spring data, but samples from small and shallow lakes (Bjørnesø, Tolvsøer and Camp Lake) are affected by evaporative enrichment and plot to the right of the LMWL (Fig. 10). The only lake inside the igneous complex (Xenolith Lake at 470 m altitude) is markedly enriched in calcium (Ca-concentration between 14.1 and 16.7 mg/L), magnesium and strontium reflecting the local bed rock geology. Other lakes all have calcium concentrations below 10 mg/L and down to 0.5 mg/L for lakes in the gneissic areas east of the fjord. The bedrock is also reflected in pH, which is slightly higher in Xenolith Lake than in the remaining lakes (pH = 7.9 compared to values between 6.7 and 7.5). The shallow Twelve Lakes (Tolvsøer) at 360 m altitude show a strong annual effect. The more positive oxygen isotope composition in 2006 and 2007 ($\delta^{18}O$ between –10.1‰ and –11.3‰) illustrates evaporation from the shallow lake surface in the summer period, whereas the 1995 sample ($\delta^{18}O$ = –13.3‰) taken at the same time of the year (August) must reflect input of local, depleted precipitation. The few data define a local evaporation line LEL with a slope of 5.6. A comparable study from Kangerlussuaq/Søndre Strømfjord (Leng *et al.* 2003) 650 km to the north in Greenland

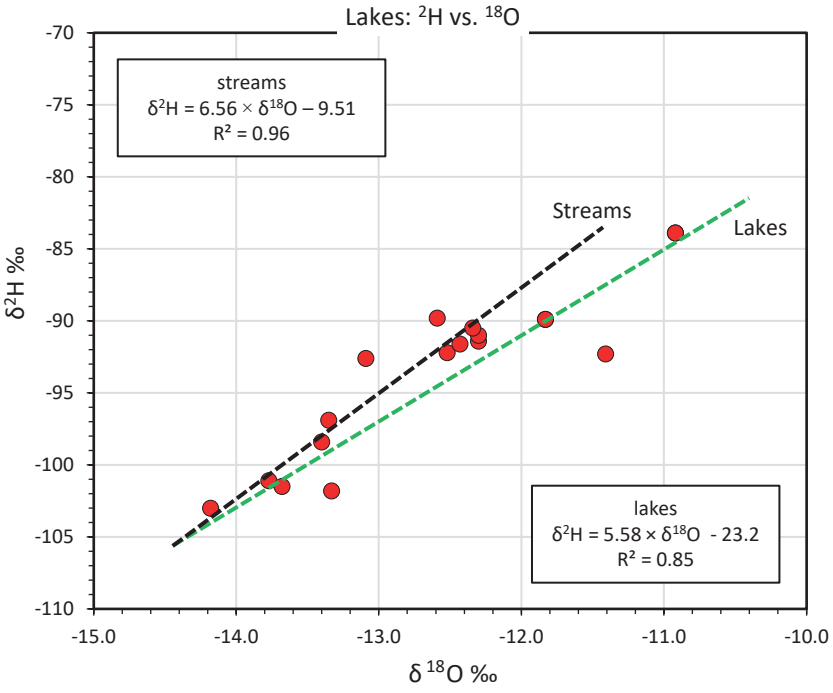

Fig. 10. δ-diagram for lake water samples mainly from the 500 m plateau west of Ikka fjord. Most enriched samples are from small lakes affected by evaporation. Lake samples define a linear regression line LEL with a smaller slope than the shown line for streams caused by preferential evaporation of ^{2}H.

demonstrate similar evaporative effects in small lakes with LEL's lines defined by slopes between 3.9 and 5.8, highest values for the most coast-near lakes.

Fjord water

131 samples from 1995 to 1997, 2006, 2007 and 2019 were measured for ^{18}O-composition and salinity. Of these, 41 samples were also measured for $\delta^{2}H$. Salinity and $\delta^{18}O$ are highly correlated ($R^2 = 0.98$). This correlation reflects the mixing system between sea water from Davis Strait and fresh water from streams and precipitation. When separated into sampling years, an even higher correlation is seen for each individual mixing system ($R^2 > 0.99$; Fig. 11). The varying slopes of the regression lines points to the fact that the end-member compositions of both fresh water and sea water differ from year to year. The 1995 correlation represents samples taken early in the season in early July, whereas samples from 1997 and 2006 were collected in August. When extrapolated to a salinity of 0, the calculated freshwater end member from 1995 has the most depleted $\delta^{18}O$-value of –14.8‰, whereas the 2006 system shows the most enriched $\delta^{18}O$-value of –13.2‰. The 1996 value falls between these with a $\delta^{18}O$ of -13.9‰. It has already been demonstrated how the two major streams entering the fjord early in the season are depleted by 1 to 2‰ in ^{18}O as compared to the late season. These compositions are comparable to the calculated values above.

The stratification of the fjord water column at a halocline between 2 and 5 m depth is nicely illustrated in Fig. 5. Surface water between 0 and 2 m depth has a large spread in both salinity and $\delta^{18}O$. The most enriched surface waters are from samples taken in the outer basin with salinities of 24.6 psu and $\delta^{18}O$-values at –4.6‰ representing only limited mixing with fresh water, part of which probably originated as direct precipitation. Most depleted surface samples have $\delta^{18}O$-values between –13‰ and –14‰ close to that of the streams. Water samples from within the halocline have salinities between 20 and 33 psu and $\delta^{18}O$-values between –4‰ and –1‰. Samples taken below the halocline are all enriched in ^{18}O ($\delta^{18}O > –2‰$) compared to the water masses above and reflect sea water composition.

The sea water entering Ikka fjord is a blend of Polar Water from the cold East Greenland Current and Atlantic Water from the Irminger Current (Buch 1995, 2002). The East Greenland Current originates in the Polar Basin, turns around Cape Farewell and follows the SW Greenland coast northwards and is characterised by salinities below 34 psu, temperatures below 2°C and is depleted in ^{18}O ($\delta^{18}O$ as low as –2‰, e.g., Azetsu-Scott & Tan 1997). The warmer Irminger Current originates in the North Atlantic Ocean and has salinities above 34.8 psu, temperatures around 4°C and is enriched in ^{18}O ($\delta^{18}O > 0‰$, Frew *et al*. 2000). The two water masses merge along the south-west coast of Greenland, and the varying seawater compositions observed in Ikka fjord may well relate to this. It is noteworthy that the year 1995 was characterised by extraordinary large amounts of polar sea ice outside the SW Greenland coast as reflected in the Polar signature of the water in Ikka fjord (Fig. 11).

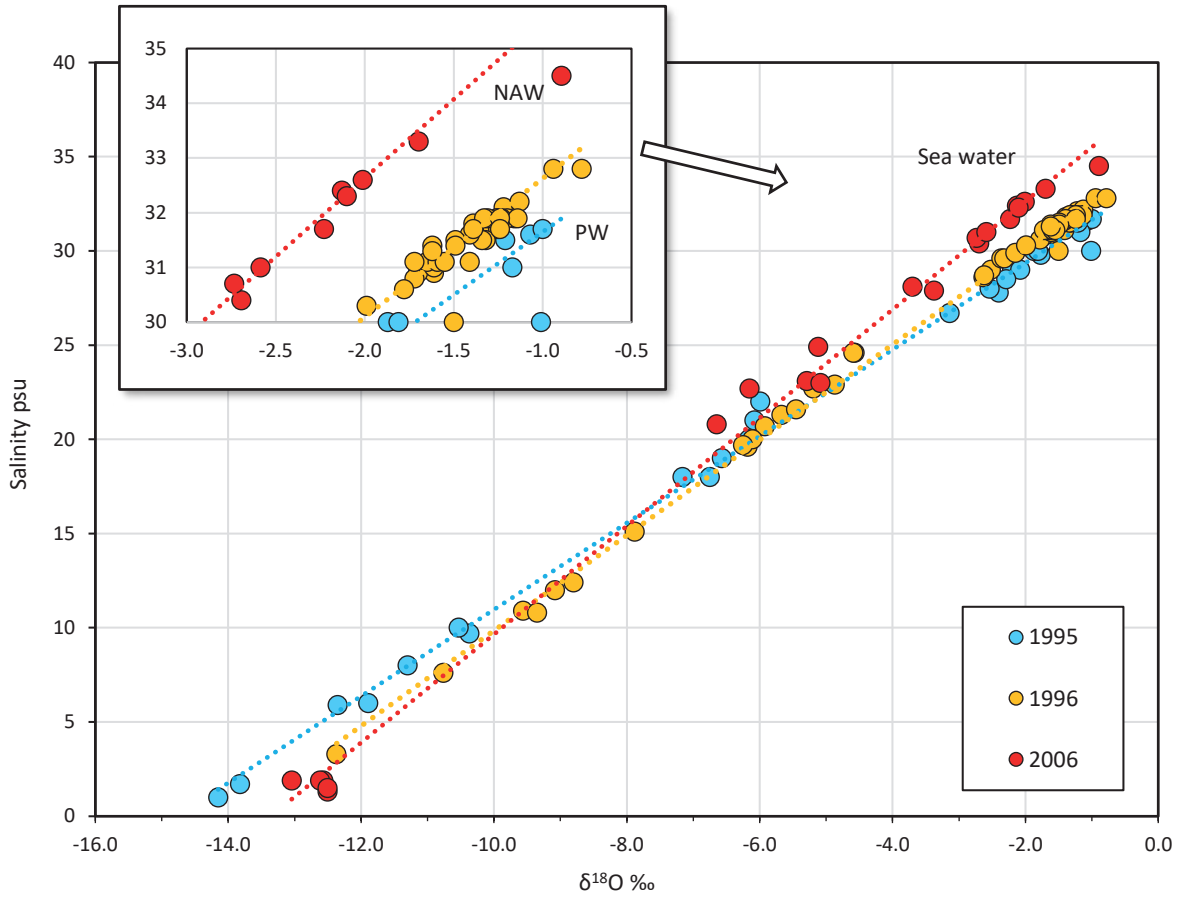

Fig. 11. Salinity/$\delta^{18}O$ diagram showing the variable end members of the seawater/freshwater mixing system. Inserted is an enlargement of the high-salinity part of the plot. Samples from 2006 are closer to the composition of North Atlantic Water (NAW) in the Irminger Current, whereas samples from 1995 and 1996 are influenced by Polar Water (PW) in the East Greenland Current. The year 1995 was characterised by heavy packing of polar ice in Davis Strait.

It is thus not possible to determine a single salinity/$\delta^{18}O$ value-set for the seawater component entering the fjord. Highest salinity values are between 32.8 and 33.3 psu at depths between 25 and 50 m, and corresponding $\delta^{18}O$-values are from –1.7 to –0.8‰. These numbers are taken as best approximations to the local seawater composition.

A smaller number of fjord water samples (41 from 1995, 1997 and 2019) were analysed for hydrogen isotope composition. The combined isotope data define the mixing line between fresh water and sea water described by the equation (Fig. 6, Table 3):

$$\delta^2H = 6.93 \times \delta^{18}O - 3.62,\ R^2 = 0.99,\ n = 41$$

Water samples with higher salinities but 'normal' ^{18}O-concentrations were collected from deeper parts of the inner fjord. These salinities probably reflect 'freezing-out' and brine formation during winter (Bauch *et al*. 2010; Granskog *et al*. 2011). A sample from 100 m depth close to the bottom in the Yderfjord gave surprisingly low values for both salinity (29.6 psu) and oxygen isotope composition ($\delta^{18}O$ = –2.3‰) probably caused by freshwater seeping from bottom springs. Seaman *et al*. (2022) reports pockmarks after submarine springs in the same area.

Column water

This water type is characterised by high carbonate alkalinity (up to 200 meq/L), high pH (up to 10.5), high sodium concentration (up to 6000 mg/L), and depleted hydrogen and oxygen isotope compositions (Buchardt *et al*. 2001). The working hypothesis (Pauly 1963a; Buchardt *et al*. 1997, 2001) for the growth of the submarine Ikka columns is derived from the fact that columns are restricted to the area where the Grønnedal-Íka complex is exposed around the fjord. It was suggested that a confined aquifer under the bottom of the fjord is sourced by precipitation on the 500 m high plateau formed by the Grønnedal-Íka complex west of the Inderfjord. This precipitation dis-

solves carbonates from the carbonatites and sodium from primary and secondary Na-minerals in the syenites (e.g., nepheline) within the alkaline igneous complex and becomes saturated in sodium carbonates (Bondam 1992; Buchardt *et al*. 2001; Ranta *et al*. 2018; Tollefsen *et al*. 2019; Aðalsteinsdóttir 2021). This soda-rich ground water enters the floor of the fjord as submarine springs and precipitates ikaite immediately upon mixing with the cold, calcium-rich fjord water. As the spring water has a lower density than the fjord water, it percolates upwards and leads to growth of the columns. Precipitation of other carbonate minerals is inhibited by high phosphate concentration in the column water (Bishoff *et al*. 1993; Buchardt *et al*. 2001) and by magnesium in the sea water (Stockmann *et al*. 2018b; Tollefsen *et al*. 2018). The metastable ikaite will eventually recrystallise to monohydrocalcite, aragonite, and calcite and thus destabilise the delicate ikaite

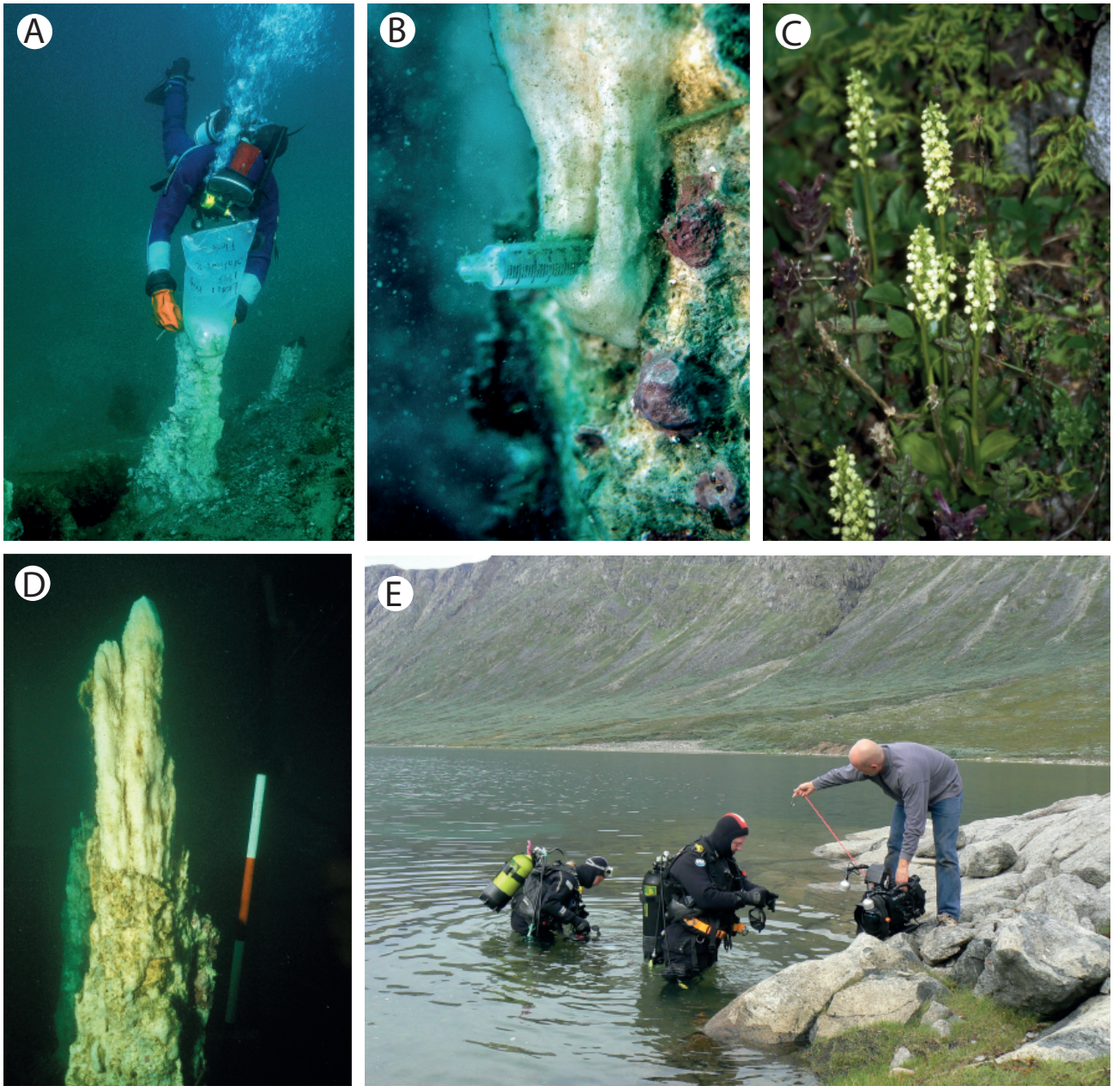

Fig. 12. Photos from Ikka fjord. **A.** The 'bag sampling' method applied by the divers in 1995. **B.** A tapping point drilled into the column in 1996, sample water was pumped out of the column by a syringe handled by the diver. Note the fresh precipitation of ikaite minerals around the tapping point, which was inserted the year before. **C.** Example of impressive vegetation at springs below carbonatite exposure, here orchids (*Psedorchis straminea*). **D.** Column showing a year's growth (appr. 50 cm) over cutting surface. **E.** Divers preparing for a dive in the fjord. Photos by Richard Martin, Gabrielle Stockmann and Bjørn Buchardt.

structure (Dahl & Buchardt 2006; Hansen *et al*. 2011; Stockmann *et al*. 2022).

Sampling of the column water was carried out by scuba divers, and fjord water contamination was a major problem. Sampling stations were placed at columns between 8 and 10 m water depth, where the surrounding fjord water had salinities higher than 25 psu and $\delta^{18}O$-values more positive than –2‰. In 1995, column water was sampled in plastic bags tied above cut columns, so-called bag water (Fig. 12A). This water was clearly contaminated by fjord water (visible precipitation of ikaite inside the bags), but nevertheless demonstrated that column water had a lower density, and much higher pH and alkalinity than the surrounding fjord water. The following years (1996 and 1997), the sampling method was improved by placing tapping ports in drilled holes sealed with linseed puddy in the columns and sucking water out with syringes (Fig. 12B). Two 'tapping stations' were established: The Atoll Station at 10 m water depth close to the so-called Atoll structure (12 samples), and the Camp Field Station at 8 m depth close to the camp (11 samples). By this method samples of column water with only minor fjord-water contamination could be collected.

In 2007, sensors were placed inside a column at the Camp Field Station to monitor pH-, temperature- and conductivity variations over a full year (Hansen *et al*. 2011). Data indicated a long stabilisation period of more than three months before constant values were obtained. Finally, pH settled around 10.3 and conductivity at 6.9 mS cm^{-1} (~ 6.7 psu at 3°C). These values were considered to represent the uncontaminated column water (fjord water in contact with the columns had pH of ~ 8 and conductivity of 31 mS cm^{-1} or 33.2 psu). The long stabilisation period for the pH-sensors makes it unlikely that our syringe samples reflect totally uncontaminated column water.

The stable isotope plot (δ^2H vs $\delta^{18}O$) of column water illustrates the effect of fjord water contamination (Fig. 13). δ^2H- and $\delta^{18}O$-values are highly correlated ($R^2 = 0.99$) because of simple two-component mixing between fjord water and the uncontaminated column water at the sampling points. The linear relation between fjord water and column water as seen in the isotope diagram allows us to calculate the percent of fjord water contamination. Our bag water samples were strongly contaminated (from 55% to 95%), and even the syringe samples contained varying amounts of fjord water (up to 55%) although most samples had less than 20% contamination.

Chemical analyses were carried out to help identify the composition of fully uncontaminated column water. pH was determined for all column water samples and varied between 8.4 pH units for the most fjord-water contaminated samples and 10.5 pH units for the least contaminated samples, whereas pH for the fjord water at the sampling points varied between 7.6 and 8.2. pH seems to stabilise at values of between 10.0 and 10.5 in samples with less than 40% contamination (Fig. 14A). Alkalinity was measured in 14 column water samples (Fig. 14B). Syringe water had the highest alkalinity and varied between 115 and 200 meq/L, bag water had values between 25 and 64 meq/L reflecting the fjord water contamination, whereas fjord water had very low alkalinity (as expected) of 2 meq/L. In

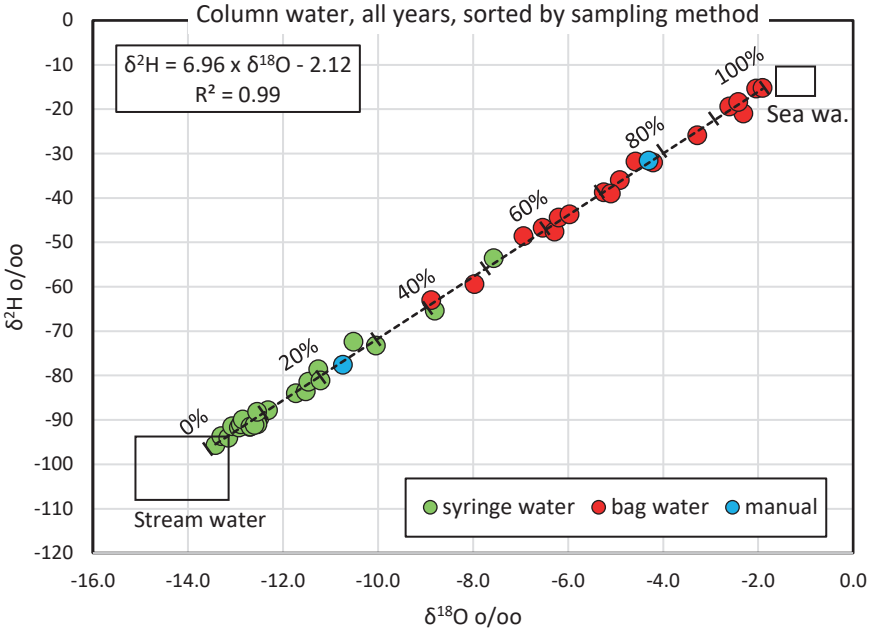

Fig. 13. δ-diagram for column water sampled underwater by different methods. Contamination by sea water during sampling is most pronounced for the bag water, but also water sampled by the syringe method was contaminated to varying degrees. The figure illustrates a simple percentage calculation for the seawater contamination.

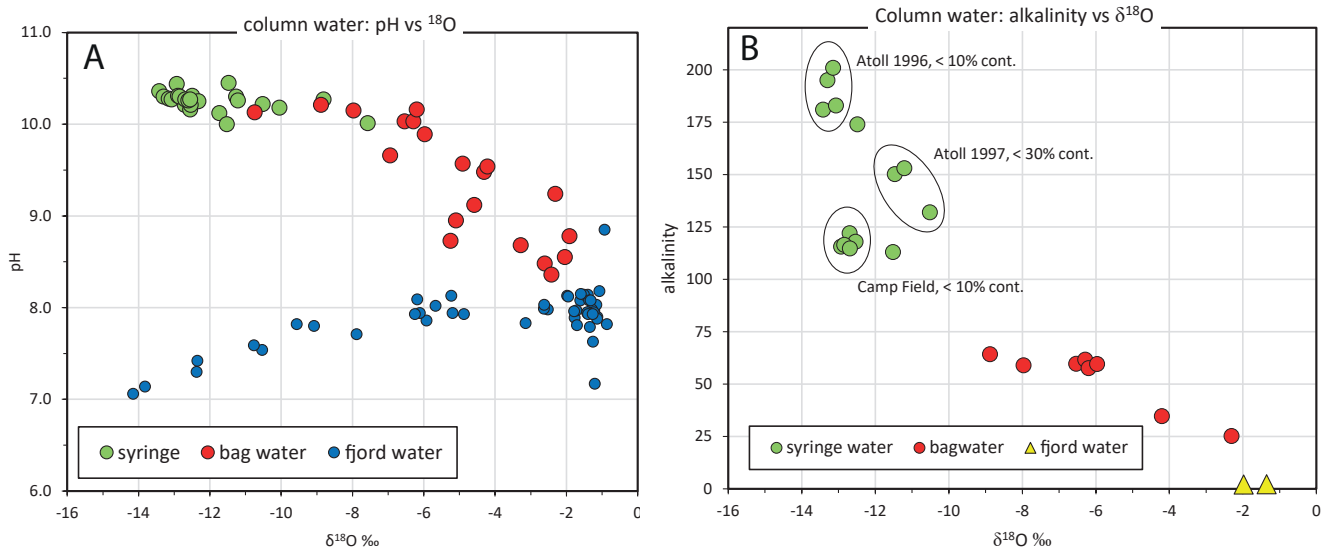

Fig. 14. pH (**A**) and alkalinity (**B**) of column water sampled by the different methods plotted against their $\delta^{18}O$-values. All samples were collected at depths below 8 m. Also shown are the pH-values of fjord water samples ranging from fresh water to sea water. Note the difference in alkalinity for least contaminated water samples from the two sampling stations.

contrast to pH, alkalinity seems to vary between the two sampling stations, even at contaminations less than 10%. Thus, Atoll samples from 1996 were significantly higher in alkalinity (between 180 and 200 meq/L) than Camp field samples (110 to 122 meq/L) probably reflecting true differences.

If the column water originates as precipitation on the Grønnedal-Íka Complex, then its chloride ion concentrations should be neglectable as shown by several analyses of stream and spring water from the complex (all < 0.03 Cl^- mg/L), and no chloride-containing minerals are known from the igneous complex. Thus, chloride ion concentration in column water is a direct measure of fjord water contamination. Column water samples with estimated less than 10% contamination still contain between 750 and 2150 mg/L of chloride ions. The chloride ion concentrations define a linear mixing system between low Cl^- samples from columns and high Cl^- samples from the fjord (R^2 = 0.88, Fig. 15A). If this mixing line is extrapolated to a Cl^- value of zero, the corresponding $\delta^{18}O$-value is –14.18‰. A similar argument can be used for magnesium, and an uncontaminated $\delta^{18}O$-value based on Mg^{2+} concentrations come to –14.11‰. These values let us estimate a general $\delta^{18}O$ value for the uncontaminated column water of approximately –14.2‰, slightly more negative that the least contaminated samples (–13.4‰, Atoll St. and –12.9‰, Camp St.) and the value given by Buchardt *et al*. (2001). A simple percentage calculation between fjord water composition and the suggested uncontaminated column water composition yields a contamination of 4% and 9% for these two samples.

Using the relation (LMWL) between $\delta^{18}O$ and δ^2H in column water samples, the hydrogen isotope composition of uncontaminated column water is estimated at δ^2H = –102‰.

Calcium concentrations stay low in the sample water up to a contamination of at least 75% (Fig. 15B) because of ikaite precipitation in the sample containers. This level represents the end-point of ikaite precipitation (saturation), and more contaminated samples have rapidly increasing calcium concentrations up to fjord water levels of more than 300 mg/L. Strontium behaves in a similar way, as strontium ions from the fjord water (8 to 10 mg/L at 10 m depth) are incorporated into the ikaite crystals.

When the new estimate of the oxygen isotope composition ($\delta^{18}O$ = –14.2‰) of the column water is compared to our stream data, it is evident that its depleted composition is only matched by the most depleted stream data from altitudes above 400 m. This water is likely derived by melting of winter snow on the Ikka plateau. Winter precipitation at Grønnedal (GNIP 1963 to 1974) falling as snow reached $\delta^{18}O$-values as low as –17.5‰. It is also clear that the surface spring water described above belong to another water type as defined by its much more enriched oxygen isotope composition and low pH and alkalinity. The present data thus support the original hypothesis that column water is sourced by precipitation falling on the top of the Grønnedal-Ika igneous complex but provide a better estimation of the composition of uncontaminated column water than those of Buchardt *et al*. (2001). No dating has been obtained for the column water, but

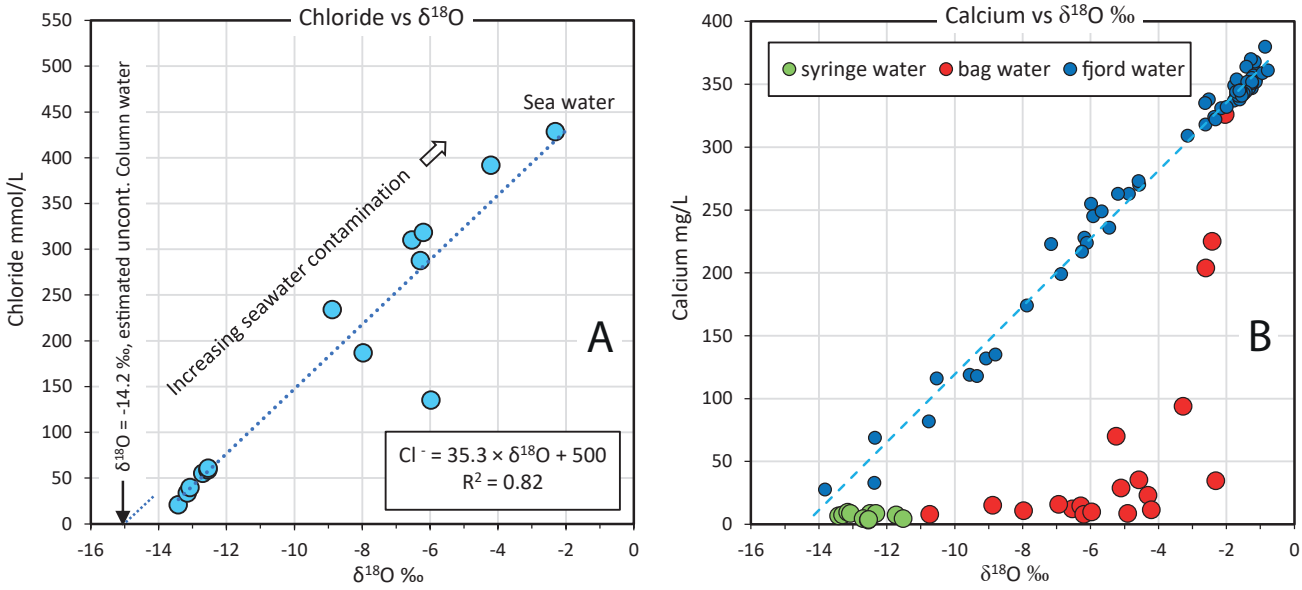

Fig. 15. Chloride ion concentration plotted against oxygen isotope composition for column water samples (**A**). Extrapolation of the linear regression line for the chloride/$\delta^{18}O$ relation leads to a $\delta^{18}O$-value for chloride-free column water of –14.2‰. This value is taken as representing uncontaminated column water. A similar diagram as Fig. 14A for calcium concentration (**B**) illustrates the extraction in the sample containers of calcium ions by ikaite precipitation following mixing of calcium-free column water and calcium-rich fjord water at the sampling sites.

the large altitude difference between source and outflow (~ 500 m) suggests a long residence in cracks and fissures in the igneous complex, probably of several hundred years, and the depleted isotopic composition may well reflect lower air temperatures (Little Ice Age?) at the time of precipitation.

Temporal effects

Our sampling was continued intermittently over a 27-year long period from 1995 to 2021 and temporal effects should be expected. It is evident from our freshwater data that seasonal isotopic effects do exist in the Ikka fjord hydrological system. Streams, springs and lakes sampled early in the summer in June and early July are depleted in ^{2}H and ^{18}O by 14‰ and 2‰ respectively as compared to samples from late July and August. The catchment area for the Ikka fjord freshwater is not affected by meltwater from the ice cap to the east, so local precipitation – either as snow or rain – is the only source. In the Ikka area, snow was seen to persists at the higher altitudes (above 200 m) into early July but had disappeared totally in late July and August. Therefore, melting of isotopically depleted snow early in the summer can easily account for the data. Later in the summer, all precipitation falls as rain enriched in stable isotopes.

Hansen *et al*. (2011) estimated there had been an increase in summer temperatures in Ikka fjord of 0.1°C per decade since 1960, and Seaman *et al*. (2022) reported water temperatures in June 2019 of 6.0° at 13 m depth close to the Atoll structure. Similar measurements in 1995 gave temperatures between 2°C and 3°C. This suggests a pronounced warming of the fjord. As the ikaite mineral is unstable at temperatures above 7°C and dissolves into water and monohydrocalcite, aragonite or calcite (Bischoff *et al*. 1993; Dahl & Buchardt 2006), a continuing warming trend might endanger the survival of the columns.

However, new CTD measurements of the Inderfjord in the summers of 2021 and 2022 combined with continuous temperature recording using a HOBO datalogger in June to August 2021 showed that the warmer (6–9°C) water of 2019 had been exchanged with colder sea water although the top part of taller columns was still exposed to > 7°C (Stockmann *et al*. 2022). None of our isotope data seem to indicate any temporal shift related to increasing temperatures in the fjord area. Climate data from nearby Narsarsuaq and Qaqortoq towns 130 km to the south-east (generated by the Danish Meteorological Institute, https://www.dmi.dk/) do not indicate any significant increase in mean annual temperatures in the area over the 27 years study period. Thus, the higher water temperatures reported by Seaman *et al*. (2022) cannot be explained by a general warming in southern Greenland. Stockmann *et al*. (2022) ascribed the seawater heating of 2019 to the

topographical complexity of the Inderfjord with narrow pathways for sea water in between columns and submarine sills combined with a strong stratification of heated freshwater on top, which requires strong gales from a specific wind direction to exchange the sea water in the Inderfjord.

Summary and conclusions

In this study, we publish hydrogen and oxygen isotope data for a full hydrological cycle including precipitation, lakes, streams and springs flowing into a fjord system, and waters formed by mixing between fjord water and sea water (Table 3). The study deals with a low-Arctic hydrological system not investigated before and covers a period over 27 years, and therefore should provide some new insights.

1) The similarity between the $^{2}H/^{18}O$-relations (Table 3) for the different freshwater types demonstrate that they all belong to the same meteoric water system as shown by the high correlation ($R^2 = 0.95$) between their isotopic compositions as defined by a Local Meteoric Water Line (LMWL):

$$\delta^{2}H = 6.19 \times \delta^{18}O - 14.76$$
(n = 114, least square regression)

This relationship is significantly different from the GMWL (slope of 8) as defined by Craig (1961).

2) Precipitation data are only available from the GNIP-program between 1961 and 1974 sampled at the former Naval Base at Grønnedal. The data show a large spread in both $\delta^{2}H$- and $\delta^{18}O$-values with weighed annual means of –87.7‰ and –11.29‰ respectively and fit a LMWL with slope identical to our stream data.

3) The isotopic composition of stream water is affected by seasonal differences in precipitation and by source altitude. Samples collected in the early field seasons (June to early July) are depleted in ^{2}H by about 14‰ and ^{18}O by about 2‰ when compared to the late field seasons (late July and August). This effect is related to melting of isotopically depleted winter snow and should be considered when comparing data from year to year. Streams sourced at high altitudes are also depleted as compared to streams sources close to sea level, probably reflecting an orographic rain-out effect. This depletion amounts to between –0.2 and –0.3‰ $\delta^{18}O$ pr. 100 m elevation.

4) Spring water is likewise influenced by seasonal variations, the largest $\delta^{18}O$-difference between samples from 1995 (early July) and 1996 (late August) being more than 2.5‰. Moreover, springs below the carbonatite outcrops at the north-western slopes of the fjord are depleted by 1 to 2‰ $\delta^{18}O$ (melting snow) and enriched in calcium as compared to those outside the intrusion. The large differences from year-to-year point to a shallow source for the springs. Springs below the carbonatite outcrops are not the source for the Ikka Column water.

5) Lake waters demonstrate evaporation effects, when shallow lakes are compared to the larger and deeper ones, and thereby define a LEL (lake evaporation line) with a smaller slope than the other water types (Table 3). Seasonal and altitude effects cannot be evaluated owing to the small number of samples.

6) Both salinity and isotopic composition of fjord water in Ikka fjord illustrates well-defined vertical and horizontal mixing between fresh water from streams and precipitation and sea water entering from Davis Strait. The mixing between end members is highly correlated with R^2-values for the $^{2}H/^{18}O$ system of 0.99 and for the ^{18}O/salinity system of 0.98. The latter relation identifies different end member compositions from year-to-year both for inflowing sea water and fresh water. Seawater variations are caused by varying mixing in the Davis Strait between Polar Water from the East Greenland Current and North Atlantic Water from the Irminger Current, whereas freshwater variations reflect the seasonal shifts in precipitation.

7) Column water samples taken under water were contaminated to varying degrees by fjord water at the sampling sites. Least contamination was obtained by the syringe method, where water was extracted from the columns by aid of a syringe pump. Extrapolation to a chloride-free composition defines an uncontaminated column water composition of $\delta^{2}H$ = –102‰ and $\delta^{18}O$ = –14.2‰. This composition is identical to stream water sourced from winter precipitation at 500 m elevation at the carbonatite plateau and thus support the hypothesis that the Ikka columns are depending on a constrained ground water flow down through the igneous complex (Pauly 1963a; Buchardt *et al*. 1997; Buchardt *et al*. 2001).

8) Non-seasonal temporal effects in temperature and isotopic compositions are not clearly defined, and further studies are needed to evaluate the conflicting data reported by Seaman *et al*. (2022) and Stockmann *et al*. (2022).

Acknowledgements

Over the years, many people have contributed to our field work in Ikka fjord, and we can only thank them here collectively for their efforts. But special thanks go to our divers who have made the whole project possible. Of these, extraordinary gratefulness to Rolf Darville and Uffe Wilken, who spent hours sitting on the sea floor pumping water out of columns by aid of small syringes. The Ice Core Laboratory at Niels Bohr Institute, The Chemistry Laboratory at GEUS and Rósa Ólafsdóttir at the University of Iceland are all acknowledged for their help with the analytical work. The different project periods were funded by the following institutions: The Commission for Scientific Surveys in Greenland (DK), Villum Kann Rasmussens Fund (DK), Aage V. Jensens Fonde (DK), Aase and Jørgen Münters Fund (DK), Bolin Center for Climate Research (SE) and the Research Fund of the University of Iceland (IS). We are very grateful to their support. Niels Munksgaard and Anders Svensson are acknowledged for their constructive reviews.

References

Aðalsteinsdóttir, S.M. 2021: The low-temperature weathering of the Grønnedal-Íka Carbonatite Alkaline Silicate Igneous Complex in Southwest Greenland. Master's thesis, Faculty of Earth Sciences, University of Iceland, 82 pp.

Allaart, J.H. 1976: Ketilidian mobile belt in South Greenland. In: Escher, A. & Watt, W.S. (eds): Geology of Greenland, 120–151. Copenhagen: Geological Survey of Greenland.

Azetsu-Scott, K. & Tan, C. 1997: Oxygen isotope studies from Iceland to an East Greenland Fjord: Behavior of glacial meltwater plume. Marine Chemistry 56, 239–251. https://doi.org/10.1016/S0304-4203(96)00078-3

Bartels, A., Nielsen, T.F., Lee, S.R. & Upton, B.G. 2015: Petrological and geochemical characteristics of Mesoproterozoic dyke swarms in the Gardar Province, South Greenland: evidence for a major sub-continental lithospheric mantle component in the generation of the magmas. Mineral Magazine 79, 909–940. https://doi.org/10.1180/minmag.2015.079.4.04

Bauch, D., Hölemann, J., Andersen, N., Dobrotina, E., Nikulina, A. & Heidemarie Kassens, H. 2010: The Arctic shelf regions as a source of freshwater and brine-enriched waters as revealed from stable oxygen isotopes. Polarforschung 80, 127–140.

Bischoff, J.L., Fitzpatrick, J.A. & Rosenbauer, R.J. 1993: The solubility and stabilization of ikaite ($CaCO_3 \cdot 6H_2O$) from 0°C to 25°C: environmental and paleoclimatic implications for thinolite tufa. Journal of Geology 101, 21–33. https://doi.org/10.1086/648194

Bondam, J. 1992: The Grønnedal-Ika alkaline complex in South Greenland: review of geoscientific data relevant to exploration. Open File Serie, Grønlands Geologiske Undersøgelse 92/2, 28 pp.

Bonne, J.-L., Masson-Delmotte, V., Cattani, O., Delmotte, M., Risi, C., H. Sodemann, H. & Steen-Larsen, H.C. 2014: The isotopic composition of water vapor and precipitation in Ivittuut, southern Greenland. Atmospheric Chemistry and Physics 14, 4419–4439. https://doi.org/10.5194/acp-14-4419-2014

Buch, E. 1995: Havstrømme omkring Grønland. In: Gregersen, S. (ed.): Grønlands fysiske natur, 25–32. Copenhagen: Rhodos.

Buch, E. 2002: Present oceanographic conditions in Greenland Waters. Danish Meteorological Institute Scientific Reports 2002-02, 39 pp.

Buchardt, B., Seaman, P., Stockmann, G., Vous, M., Wilken, U., Düwel, L., Kristiansen, A., Jenner, C., Whiticar, M.J. & Kristensen, R.M. 1997: Submarine columns of ikaite tufa. Nature 390, 129–130. https://doi.org/10.1038/36474

Buchardt, B., Israelson, C., Seaman, P. & Stockmann, G. 2001: Ikaite tufa towers in Ikka Fjord, Southwest Greenland: their formation by mixing of seawater and alkaline spring water. Journal of Sedimentary Research 71, 176–189. https://doi.org/10.1306/042800710176

Callisen, K., 1943: Igneous rocks of the Ivigtut region, Greenland; Part 1, the nepheline syenites of the Grønnedal-Ika area. Meddelelser om Grønland 131(8), 74 pp.

Clark, I. D. & Fritz, P. 1997: Environmental isotopes in hydrogeology, 328 pp. New York: Lewis Publishers.

Craig, H. 1961: Isotopic variations in meteoric waters. Science 133, 1702–1703. https://doi.org/10.1126/science.133.3465.1702

Dahl, K. & Buchardt, B. 2006: Monohydrocalcite in the Arctic Ikka fjord, SW Greenland: first reported marine occurrence. Journal of Sedimentary Research 76, 460–471. https://doi.org/10.2110/jsr.2006.035

Dansgaard, W. 1964: Stable isotopes in precipitation. Tellus 16, 436-468. https://doi.org/10.1111/j.2153-3490.1964.tb00181.x

Darling, W.G. & Talbot, J. C. 2003: The O and H stable isotope composition of freshwaters in the British Isles. 1. Rainfall. Hydrology and Earth System Sciences 7, 163–181. https://doi.org/10.5194/hess-7-163-2003

Darling, W., Bath, G.A.H. & Talbot, J.C. 2003: The O and H stable isotope composition of freshwaters in the British Isles. 2. Surface waters and groundwater. Hydrology and Earth System Sciences 7, 183–195. https://doi.org/10.5194/hess-7-183-2003

Emeleus, C.H. 1964: The Grønnedal-Ika alkaline complex, South Greenland. The structure and geological history of the complex. Bulletin Grønlands Geologiske Undersøgelse 45, 75 pp. https://doi.org/10.34194/bullggu.v45.6579

Fristrup, B. 1971: Grønland. Klimatologi og glaciologi. In: Nørrevang, A., Meyer, T.J. & Christensen, S. (eds): Danmarks Natur, 136–176. Copenhagen, Politikens Forlag.

Hansen, M. O., Buchardt, B., Kühl, M., & Elberling, B. 2011: The fate of submarine ikaite tufa columns in southwest Greenland under changing climate conditions. Journal of Sedimentary Research 81, 553–561. https://doi.org/10.2110/jsr.2011.50

Granskog, M. A., Kuzyk, Z. Z. A., Azetsu-Scott, K., & Macdonald, R. W. 2011: Distributions of runoff, sea-ice melt and brine using $\delta^{18}O$ and salinity data – A new view on freshwater cycling in Hudson Bay. Journal of Marine Systems 88, 362–374. https://doi.org/10.1016/j.jmarsys.2011.03.011

International Atomic Energy Agency 1969: Environmental isotope data No. 1: World survey of isotope concentration in precipitation (1953-1963). Technical Reports Series No. 96, 422 pp. Vienna.

International Atomic Energy Agency 1970: Isotope data No. 2: World survey of isotope concentration in precipitation (1964-1965). Technical Reports Series 117, 402 pp. Vienna.

International Atomic Energy Agency 1971: Environmental isotope data No. 3: World survey of isotope concentration in precipitation (1966-1967). Technical Reports Series 29, 402 pp. Vienna.

International Atomic Energy Agency 1973: Environmental isotope data No. 4: World survey of isotope concentration in precipitation (1968-1969). Technical Reports Series 147, 334 pp. Vienna.

International Atomic Energy Agency 1975: Environmental isotope data No. 5: World survey of isotope concentration in precipitation (1970-1971). Technical Reports Series 165, 309 pp. Vienna.

International Atomic Energy Agency 1979: Environmental isotope data No. 6: World survey of isotope concentration in precipitation (1972-1975). Technical Reports Series 192, 187 pp. Vienna.

Kristiansen, J. & Kristiansen, A. 1999: A new species of *Chroomonas* (Cryptophyceae) living inside the submarine ikaite columns in the Ikkafjord, southwest Greenland, with remarks on its ultrastructure and ecology. Nordic Journal of Botany 19, 747–758. https://doi.org/10.1111/j.1756-1051.1999.tb00684.x

Leng, M.J. & Adderson, N.J. 2003: Isotopic variations in modern lake waters from western Greenland. The Holocene 13, 605–611. https://doi.org/10.1191/0959683603hl620rr

Östlund, H.G. & Hut, G. 1984: Arctic Ocean water mass balance from isotope data. Journal of Geophysical Research: Oceans 89(C4), 6373–6381. https://doi.org/10.1029/JC089iC04p06373

Pauly, H. 1963a: Ikait, nyt mineral der danner skær. Naturens Verden 168–192.

Pauly, H. 1963b: "Ikaite", a new mineral from Greenland. Arctic 16, 263–264. https://doi.org/10.14430/arctic3545

Priem, A. & Stougaard, P. 2006: Bacterial diversity in permanently cold and alkaline ikaite columns from Greenland. Extremophiles 10, 551–562. https://doi.org/10.1007/s00792-006-0529-9

Ranta, E., Stockmann, G., Wagner, T., Fusswinkel, T., Sturkell, E., Tollefsen, E. & Skelton, A. 2018: Fluid-Rock reactions in the 1.3 Ga siderite carbonatite of the Grønnedal-Íka alkaline complex, Southwest Greenland. Contributions to Mineralogy and Petrology 173, 1–28. https://doi.org/10.1007/s00410-018-1505-y

Rogers, J.J. & Santosh, M.J.G.R. 2002: Configuration of Columbia, a Mesoproterozoic supercontinent. Gondwana Research 5, 5–22. https://doi.org/10.1016/S1342-937X(05)70883-2

Rozanski, K., Araguás-Araguás, L. & Gonfiantini, R. 1993: Isotopic patterns in modern global precipitation. Climate change in continental isotopic Records 78, 1–36. https://doi.org/10.1029/GM078p0001

Schmidt, M., Priemé, A. & Stougaard, P. 2006: Bacterial diversity in permanently cold and alkaline ikaite columns from Greenland. Extremophiles 10, 551–562. https://doi.org/10.1007/s00792-006-0529-9

Seaman, P.G. 1998: The development of Ikaite in a Fjord environment with special reference to Ikka Fjord. Unpublished. Ph.D. Thesis, Imperial College of Science, Technology and Medicine, University of London, London, UK, 263 pp.

Seaman, P. & Buchardt, B. 2006: The columns of ikaite tufa in Ikka Fjord, Greenland. Meddelelser om Grønland Geoscience 44, 39 pp. https://doi.org/10.7146/moggeosci.v44i.140293

Seaman, P., Sturkell, E., Gyllencreutz, R., Stockmann, G.J. & Geirsson, H. 2022: New multibeam mapping of the unique *Ikaite* columns in Ikka Fjord, SW Greenland. Marine Geology 222, 1–14. https://doi.org/10.1016/j.margeo.2021.106710

Stockmann, G. & Wilken, U. 2007: Ikkasøjlerne – en undersøisk oase i Arktis, 85 pp. Copenhagen: Dansk Polarcenter.

Stockmann G., Karlsson, A., Lewerentz, A., Thomsen, T.B., Kokfelt, T.F., Tollefsen, E., Sturkell, E. & Lundqvist, L. 2018a: New Rb–Sr and zircon U–Pb dating of the Grønnedal-Íka igneous complex, SW Greenland. Nordic geological winter meeting 2018, Copenhagen, Denmark. Abstract volume, p. 38.

Stockmann, G., Tollefsen, E., Skelton, A., Brüchert, V., Balic-Zunic, T., Langhof, J., Skogby, H. & Karlsson, A. 2018b: Control of calcite inhibitor (phosphate) and temperature on ikaite precipitation in Ikka fjord, southwest Greenland. Applied Geochemistry 89, 11–22. https://doi.org/10.1016/j.apgeochem.2017.11.005

Stockmann, G.J., Seaman, P., Balic-Zunic, T., Peternell, M., Sturkell, E., Liljebladh, B. & Gyllencreutz, R. 2022: Mineral changes to the tufa columns of Ikka Fjord, SW Greenland. Minerals 12, 1430. https://doi.org/10.3390/min12111430

Stougaard, P., Jorgensen, F., Johnsen, M.G. & Hansen, O.C. 2002: Microbial diversity in ikaite tufa columns: An alkaline, cold ecological niche in Greenland. Environmental Microbiology 4, 487–493. https://doi.org/10.1046/j.1462-2920.2002.00327.x

Sørensen, M.V. & Kristensen, R.M. 2000: Marine rotifera from Ikka fjord, SW Greenland. Meddelelser om Grønland, Bioscience 51, 46 pp. https://doi.org/10.7146/mogbiosci.v51.142614

Tappa, D. J., Kohn, M. J., McNamara, J. P., Benner, S. G. & Flores, A. N. 2016: Isotopic composition of precipitation in a topographically steep, seasonally snow-dominated watershed and implications of variations from the global meteoric water line. Hydrological Processes 30, 4582–4592. https://doi.org/10.1002/hyp.10940

Thorbjørn L. & Petersen G.H. 2003: The epifauna on the carbonate reefs in the Arctic Ikka Fjord, SW Greenland. Ophelia 57, 177–202. https://doi.org/10.1080/00785236.2003.10409513

Tollefsen, E., Stockmann, G., Skelton, A., Mörth, C.-M, Dupraz,

C. & Sturkell, E. 2018: Chemical controls on ikaite formation. Mineralogical Magazine 82, 1119–1129. https://doi.org/10.1180/mgm.2018.110

Tollefsen, E., Stockmann, G., Skelton, A., Lundqvist, L. & Sturkell, E. 2019: Secondary alteration of the Grønnedal-Ika igneous complex and the genesis of ikaite, $CaCO_3$ $6H_2O$, SW Greenland. Chemical Geology 510, 18–30. https://doi.org/10.1016/j.chemgeo.2019.02.009

Trampe, E.C., Larsen, J.E., Glaring, M.A., Stougaard, P. & Kühl, M. 2016: In situ dynamics of O_2, pH, light, and photosynthesis in ikaite tufa columns (Ikka fjord, Greenland) – a unique microbial habitat. Frontiers of Microbiology 7, 722. https://doi.org/10.3389/fmicb.2016.00722

Trampe, E. C., Castenholz, R.W., Larsen, J.E. & Kühl, M. 2017: Phototrophic microbes form endolithic biofilms in ikaite tufa columns (SW Greenland). Environmental Microbiology 19, 4754–4770. https://doi.org/10.1111/1462-2920.13940

Upton, B.G.J. 2013: Tectono-magmatic evolution of the younger Gardar southern rift, South Greenland. Geological Survey of Denmark and Greenland Bulletin 29, 128 pp. https://doi.org/10.34194/geusb.v29.4692

Vester, J. K., Lylloff, J. E., Glaring, M. A. & Stougaard, P. 2013: Microbial diversity and enzymes in ikaite columns: a cold and alkaline environment in Greenland. Polyextremophiles: Life Under Multiple Forms of Stress, 365–380. https://doi.org/10.1007/978-94-007-6488-0_15

Weidick, A., Kelly, M. & Bennike, O. 2004: Late Quaternary development of the southern sector of the Greenland Ice Sheet, with particular reference to the Qassimiut lobe. Boreas 33, 284–299. https://doi.org/10.1111/j.1502-3885.2004.tb01242.x

Characteristics and formation of natural fractures in a silica-rich chalk, Coniacian Arnager Limestone Formation, Bornholm, Denmark

ASLAUG CLEMMENSEN GLAD, TOBIAS ORLANDER, IDA LYKKE FABRICIUS, OLE RØNØ CLAUSEN & LARS B. CLEMMENSEN

Geological Society of Denmark
https://2dgf.dk

Received 14 November 2023
Accepted in revised form
23 August 2024
Published online
18 October 2024

Glad, A.C., Orlander, T., Fabricius, I.L., Clausen, O.R. & Clemmensen, L.B. 2024. Characteristics and formation of natural fractures in a silica-rich chalk, Coniacian Arnager Limestone Formation, Bornholm, Denmark. Bulletin of the Geological Society of Denmark, Vol. 73, pp. 157–173. ISSN 2245-7070. https://doi.org/10.37570/bgsd-2024-73-09

Natural fractures are abundant and important components in many carbonate sedimentary rocks globally. In hydrocarbon and groundwater reservoirs of carbonate rocks they can form connected networks and thereby influence the permeability and fluid flow significantly. Outcrop studies of fractured carbonate rocks can provide an essential understanding of 3-dimensional fracture networks, thereby aiding in understanding fracture patterns and connectivity in subsurface carbonate reservoirs. The Arnager Limestone Formation is a naturally fractured silica-rich chalk of Coniacian age exposed in a coastal cliff on the island of Bornholm in the Baltic Sea (Denmark). This study examines the natural fractures in the Arnager Limestone Formation from a structural and geomechanical perspective. The Arnager Limestone Formation forms one, 12–20 m thick, main rock mechanical unit; bedding planes acts as weak interfaces and divides it into near-identical, cm- to dm-thick rock mechanical subuits. Flat-lying (horizontal) or low-angle dipping bedding-parallel fractures are intersected by two near-vertical or steeply dipping fracture systems, a major N–S-trending system and a less prominent W–E-trending fracture system. Rock mechanical analysis of the tensile strength and elastic moduli provides the foundation for discussing maximum burial depth of the Arnager Limestone Formation. The tensile strength gives information on the bedding-parallel fractures, which can have formed due to stress relief during uplift and erosion, possible accentuated by glacial processes. The near-vertical fracture sets are interpreted to have formed in response to tectonic movements.

Keywords: Arnager Limestone Formation, silica-rich chalk, natural fractures, rock mechanical properties, Bornholm.

Aslaug Clemmensen Glad [Aslaug.Clemmensen.Glad@Bluenord.com], Bluenord, Lyngbyvej 2, 2100 Copenhagen, Denmark and The Danish Offshore Technology Centre, Technical University of Denmark, Elektrovej 375, 2800, Kgs. Lyngby, Denmark. Tobias Orlander [TOR@geo.dk], The Danish Offshore Technology Centre, Technical University of Denmark, Elektrovej 375, 2800, Kgs. Lyngby, Denmark; present address: Geo – Subsurface Expertise, Maglebjergvej 1, 2800 Kgs. Lyngby. Ida Lykke Fabricius [ilfa@dtu.dk], DTU Department of Environmental and Resource Engineering, Technical University of Denmark, Brovej 118, 2800, Kgs. Lyngby, Denmark. Ole Rønø Clausen [ole.r.clausen@geo.au.dk], Department of Geoscience, Aarhus University, Høegh-Guldbergs Gade 2, 8000 Aarhus. Lars B. Clemmensen [larsc@ign.ku.dk], Department of Geosciences and Natural Resource Management, University of Copenhagen, Øster Voldgade 10, 1350 Copenhagen, Denmark.

A natural fracture forms in response to stress as a mechanical breakage or discontinuity (Wolfsberg 1997; Gudmundsson 2011). Fractures are ubiquitous and prominent constituents of carbonate sedimentary rocks both in the subsurface and in outcrops. They can have a significant influence on the host rock by enhancing the local permeability by orders of magnitude, forming connected pathways for fluid flow, alter the rock strength and impact the petrophysical properties of the rock (Gabrielsen & Koestler 1987; Aguilera 1998; Bratton *et al.* 2006; Lemonnier & Bourbiaux 2010; Ogata *et al.* 2014). Interpretation of fracture patterns, interactions and crosscutting relationships can function as indicator for palaeostress and thereby earlier tectonic episodes (Price & Cosgrove 1990).

Extensive deposition of chalk occurred during the Late Cretaceous across Northwestern Europe with the youngest sediments of Maastrichtian and Danian (Palaeogene) age constituting important reservoirs for both hydrocarbons in the North Sea and groundwater in Denmark, Germany, France, Belgium, the Netherlands, and Britain. Scarce data, based on wells situated kilometers apart, often constrain subsurface understanding of fracture systems, and thus to optimise the understanding of fracture systems in chalk, outcrop studies can provide important insights into the geometry of fractures, their internal relationship, and lithological control on fracture formation.

The Coniacian Arnager Limestone Formation (hereafter Arnager Limestone) is exposed in a coastal cliff at the south coast of Bornholm (Fig. 1). The Arnager Limestone, which is a silica-rich chalk, possesses a well-developed fracture network briefly mentioned by e.g. Hart *et al.* (2012) and Svennevig & Surlyk (2018). However, so far, no detailed characterisation and interpretation of this fracture network have been given. The limestone contains flat-lying (horizontal) to low-angle dipping bedding-parallel fractures intersected by near-vertical to steeply dipping fractures resulting in a block-like appearance of the limestone (Fig. 2).

The purpose of this study is to describe and interpret the origin of the natural fractures in the Arnager Limestone. Bedding-parallel fractures are linked to petrophysical and mechanical properties of the limestone, including porosity, elastic wave velocities, elastic moduli, and tensile strength, and a new estimate of palaeoburial depth of the Arnager Limestone is proposed. Fracture orientation of the near-vertical to steeply dipping fractures are described and their origin discussed in relation to the tectonic evolution of the area.

Geological setting

Structural framework

The island of Bornholm (55°N, 15°E), forms a horst block and is part of the Sorgenfrei–Tornquist Zone that separates the Baltic Shield from the Danish and North German Basins (Graversen 2004, 2009; Fig. 1). Precambrian granites, migmatites and gneisses with ages of approximately 1.4 Ga (Waight *et al.* 2017) are exposed in the northern part whereas faulted Palaeozoic and Mesozoic sedimentary rocks outcrop in the

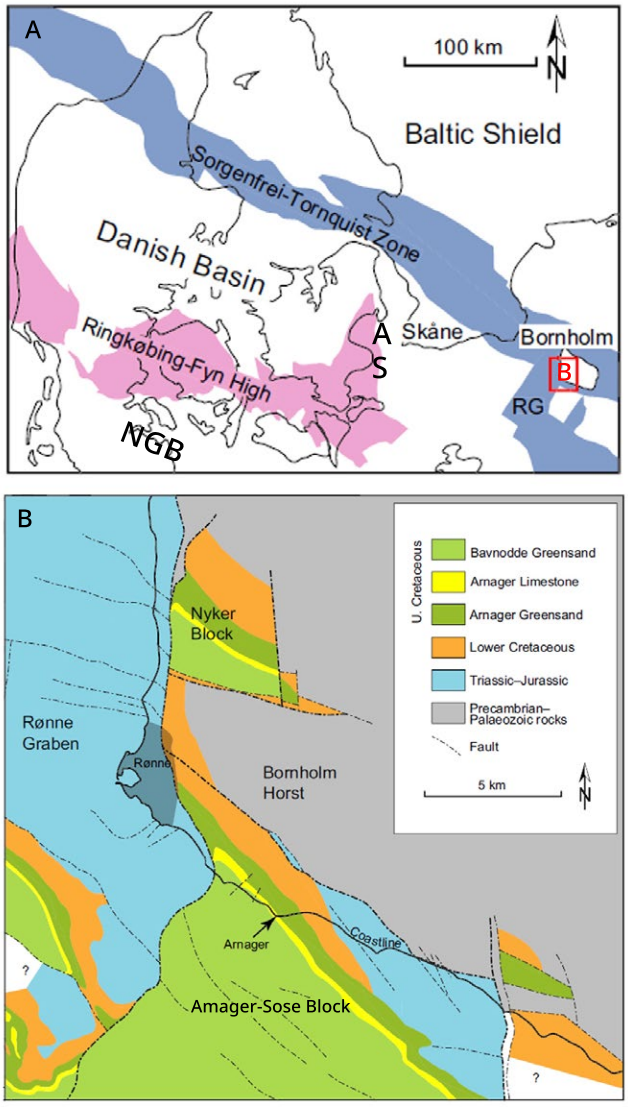

Fig. 1. A, Structural setting of Bornholm in the Sorgenfrei–Tornquist zone; NGB: North German Basin; RG: Rønne Graben; S: Stevns; A: Amager. **B,** Geological map of the south and west coast of Bornholm and nearby coastal areas. The Arnager Limestone Formation is exposed in a coastal cliff at Arnager on the south coast of Bornholm (maps after Svennevig & Surlyk 2018).

southern and south-eastern part. Bornholm is part of the Tornquist lineament at the transition between the Danish-Swedish Sorgenfrei–Tornquist Zone and its southwards continuation towards Poland (Michelsen & Nielsen 1991; Erlström *et al.* 1997; Cotte & Pedersen 2002; Babuska & Plomerova 2004; Lykke-Andersen & Surlyk 2004; Madsen *et al.* 2010). The sedimentary rock exposures are controlled by a series of northwest–southeast striking faults defining the trend of the Tornquist lineament; these major faults are linked by approximately north–south-trending faults running parallel to the Rønne Graben, which is located just offshore the west coast of Bornholm (Vejbæk 1985; Jensen & Hamann 1989).

Late Cretaceous deposits on Bornholm comprise the Arnager Greensand Formation (Cenomanian), the Arnager Limestone Formation (Coniacian), and the Bavnodde Greensand Formation (Coniacian–Santonian) with the Arnager Limestone being confined to the Arnager-Sose Block and a minor exposure on the Nyker Block towards the north. During the Late Cretaceous, Bornholm was situated at a palaeolatitude of 48°N in a boreal realm (Ziegler 1990).

The Mesozoic tectonic evolution of the Bornholm area was characterised by repeated block faulting (Graversen 2009). The geometry of the Mesozoic faults was analysed by Graversen (2009), and the cumulative directions of the faults indicate that most faults on the Mesozoic Arnager-Sose block trend NW–SE (315–135°) with only little variation; a few faults are aligned W–E (275–95°) and NNW–SSE (345–165°). According to Graversen (2009) the Mesozoic fault systems are

Fig. 2. The cliff exposure at Arnager. The Arnager Limestone Formation overlies the Arnager Greensand Formation (green-grey); a complex conglomerate (arrow) occurs at the boundary between the two units. There is a hiatus, but no angular unconformity between the two formations. Both formations have been tilted with identical low angles towards the NW. The Arnager Limestone (exposed thickness here 5–6 m) has a lower unit with mound bedding, and an upper, thinner unit with flat bedding; the bedding in the uppermost part of this unit has been disrupted due to glacial impact. The two formations define two different rock mechanical units. A fracture system composed of two near-vertical and orthogonal fracture sets and a flat-lying to low-angle dipping, bedding-parallel fracture set is seen in the Arnager Limestone Formation; fractures are absent in the Arnager Greensand Formation. Cliff is viewed from the southeast.

related to three-dimensional strain with maximum extension striking NE–SW and secondary extension striking NW–SE. Tectonic activity in the Late Cretaceous and Paleogene caused an inversion of the block and erosion of overlying sediments (Graversen 2004).

Bornholm was covered by the Scandinavian Ice Sheet several times during the Quaternary. In the Weichselian, the ice sheet may have reached a maximum thickness of about 1500 m (Humlum & Houmark-Nielsen 1994; Houmark-Nielsen 2011); the ice retreated 16,000 years ago resulting in the formation of proglacial meltwater deposits at many sites including the Arnager area. These repeated episodes of glacial advance and retreat may have impacted the deformation history of the Arnager Limestone.

Stratigraphy and sedimentology

The Arnager Limestone is of Late Cretaceous (Early to Middle Coniacian) age (Svennevig & Surlyk 2018), and well exposed in a coastal cliff on the south coast of Bornholm immediately to the northwest of the village of Arnager (Figs 1, 2). The Arnager Limestone has here a thickness of 12 to 20 m and overlies the Middle Cenomanian Arnager Greensand Formation (hereafter Arnager Greensand; Svennevig & Surlyk 2018). There is a complex conglomerate of glauconitised and phosphatised pebbles at the boundary between the Arnager Limestone and the underlying Arnager Greensand (Hart *et al.* 2012). The Arnager Limestone is overlain by the up to 180 m thick Late Coniacian to Early Santonian Bavnodde Greensand Formation (hereafter Bavnodde Greensand; Christensen 1985; Packer & Hart 2005; Svennevig & Surlyk 2018); the Bavnodde Greensand rests on the eroded surface of the Arnager Limestone (Packer & Hart 2005). In the studied coastal cliff section, the Arnager Limestone is unconformably overlain by Quaternary deposits.

The Arnager Limestone forms a hard, silica-rich chalk with a macrofauna dominated by siliceous sponges in association with relatively sparse inoceramid bivalves, other bivalves, brachiopods, belemnites and rare ammonites (Svennevig & Surlyk 2018). The chalk is strongly bioturbated with common trace fossils including *Thalassinoides*, *Condrites*, *Zoophycos*, *Planolites* and *Teichichnus* (Noe-Nygaard & Surlyk 1985; Svennevig & Surlyk 2018). No observations of stylolites have been reported.

The matrix of the limestone is composed of fine-grained opal-CT embedded in biogenic partly recrystallised carbonate material (coccoliths, crystallites of coccoliths and shell detritus), SEM images of the latter can be found in Madsen *et al.* (2010). The carbonate content of the sediment typically varies between 45 and 70% by weight (Tröger & Christensen 1991; Noe-Nygaard & Surlyk 1985). Cemented contacts between carbonate particles occur, but no porosity-reducing carbonate cement has been noted as can be seen in the SEM-images in Madsen *et al.* (2010). The silica is diagenetic and probably formed by precipitation of opal-CT sourced by siliceous sponge spicules, which are present as moulds (Madsen *et al.* 2010). The silica content varies between 30 and 50% (Madsen *et al.* 2010). Locally opal-CT has transformed into quartz (Madsen *et al.* 2010). The limestone contains some clay; between 0.4 and 5.4%, with typical values between 1 and 2% (Svennevig & Surlyk 2018).

The Arnager Limestone can be divided into two parts: 1) a lower part with a thickness of 4–5 m which is primarily composed of mound-bedded strata and 2) an upper part comprising the remaining part of the succession primarily composed of flat-bedded strata (Noe-Nygaard & Surlyk 1985); the uppermost part of the limestone has no or poor bedding due to impact by glacial processes. The mounds in the lower part are 6–8 m wide and 1–2 m high; their flanks dip 5–10° (Noe-Nygaard & Surlyk 1985). Individual beds vary between 5 and 30 cm in thickness and are commonly accentuated and dissected by fractures (see later).

In the mound-bedded part of the limestone two microfacies occur: spiculitic wackestone and bioturbated spiculitic wackestone. The former microfacies has porosity of 36–42% with an average of 39%, and permeability of 4–20 mD with an average of 12 mD (Madsen *et al.* 2010). The latter microfacies have porosity values between 12 and 41% with an average of 38%, and permeability of 5–13 mD with an average of 10 mD (Madsen *et al.* 2010). In this study, however, all limestone is treated as one uniform facies.

The complex conglomerate at the boundary between the Arnager Limestone and the Arnager Greensand (Fig. 3) was divided into a number of sedimentary units by Bromley (1979) and Hart *et al.* (2012). According to Hart *et al.* (2012) a lower unit overlies soft glauconitic sand and is composed of somewhat lithified glauconitic sandstone with phosphatised clasts. Hart *et al.* (2012) mentioned a thickness of about 1 m for this unit, however, recent exposures only show a thickness of around 0.3 m. This unit is penetrated by large *Thallassinoides* burrows and is overlain by a surface (hardground) marked by large glauconitised and/or phosphatised clasts (Bromley 1979). Above the hardground associated with large clasts lies a sandy limestone with scattered, relatively small glauconitized and/or phosphatised clasts. Hart *et al.* (2012) suggested that this upper unit has a thickness of around 0.5 m while current exposures are 0.1–0.2 m thick. According to Hart *et al.* (2012), the lower conglomerate unit belongs to the Arnager Greensand Formation, while the upper unit is part of the Arnager

Limestone Formation. Two samples from the boundary conglomerate have a porosity of respectively 29 and 38% and permeability of 1.3 and 1.7 mD (Madsen *et al*. 2010). However, it is unclear which part of the conglomerate these samples represent.

The underlying Arnager Greensand consists of an unconsolidated, poorly sorted, fine-grained quartz sand with abundant glauconite (Solymar & Fabricius 1999). The formation contains a few layers of cemented, coarse-grained sandstone. Laboratory investigation of samples from the uppermost part of this formation gives porosity values between 39 and 44% and permeability between 11 and 29 mD (Solymar & Fabricius 1999).

The overlying Bavnodde Greensand consists of unconsolidated, poorly sorted, glauconitic, fine-grained, silty quartz sand. The formation contains a number of cemented quartz sandstones (Christensen 1985).

In a mechanical stratigraphical framework, the Arnager Limestone is here considered to form one, 12–20 m thick, mechanical unit in agreement with the definition of Cooke *et al*. (2007). However, at a later stage during the Quaternary the uppermost part of the formation has been subjected to glacial forces resulting in disintegration of the bedding. Bedding planes within the limestone act as weak mechanical interfaces and thereby subdivide the limestone into a number almost identical, 0.06 to 0.4 m thick, mechanical subunits. A major mechanical interface is defined by the hardground in the middle of the boundary conglomerate that thereby separates two main rock mechanical units, i. e. the Arnager Greensand and the Arnager Limestone.

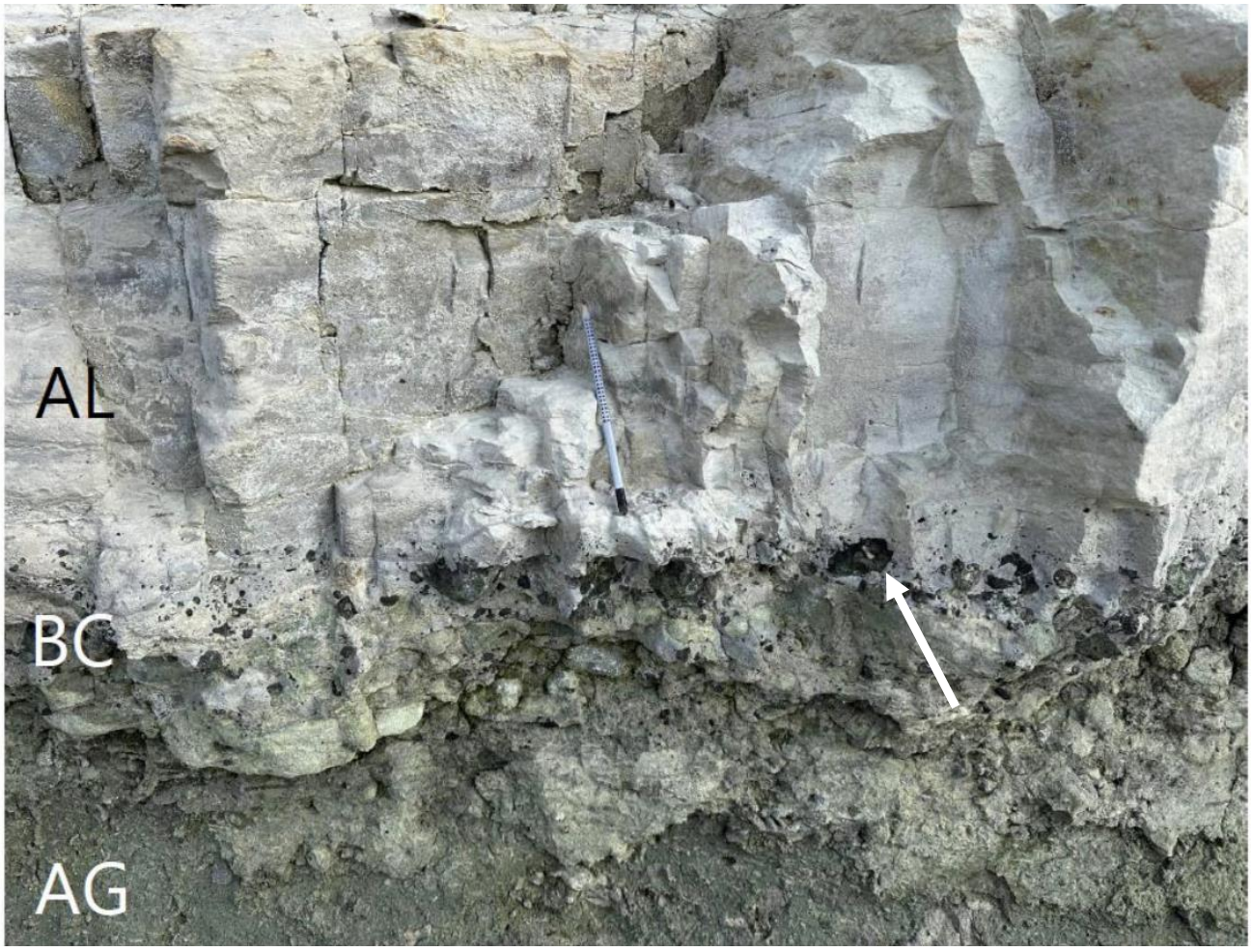

Fig. 3. The boundary conglomerate (BC) forms the transition zone between the Arnager Greensand Formation (AG) and the Arnager Limestone Formation (AL). The boundary conglomerate can be divided into a lower part (belonging to the Arnager Greensand Formation) formed by somewhat lithified glauconitic sandstone with phosphatised clasts and an upper part (belonging to the Arnager Limestone Formation) formed by sandy limestone with scattered, relatively small glauconitised and/or phosphatised clasts; there is a hardground associated with large, dark clasts at the boundary between the two units (arrow). Note that the near-vertical fractures in the Arnager Limestone Formation lose their identity in the upper part of the boundary conglomerate and are absent below the hardground. Pencil for scale.

Methods

Fracture description

The term fracture has been used to describe a range of structures, including faults, joints, veins, dykes, sills, deformation bands, and stylolites (Peacock *et al.* 2017). Fractures that occur within a specific formation/rock unit are termed a fracture system. When individual fractures have similar properties and a well-defined orientation, they can be termed a fracture set (Peacock *et al.* 2017). The spatial arrangement of various fracture sets forms a fracture network; fractures intersect at intersection points (nodes) or intersection lines (Peacock *et al.* 2017).

Six cliff sections in the lowermost mound-bedded part of the Arnager Limestone were selected for this study of fractures. Investigated sections were about 5 m in width and 2 m in height. Moving along the cliff towards the NW the investigated sites represent increasingly higher levels in the stratigraphy. All sites presented a well-developed fracture network in the mound-bedded part of the limestone. The sections were photographed, and fracture types were recorded. The blocky structures of the limestone made it possible to measure strike and dip of the near-vertical to steeply dipping fractures on exposed fracture surfaces. Supplementary investigation of these fractures was carried out on bedding plane exposures seen at low water level on the wave-eroded platform in the beach zone or at the foot of the cliff. On these bedding planes additional data on fracture orientation and spacing was obtained. Flat-lying or low-angle dipping fractures closely follow bedding contacts and are here named bedding-parallel fractures.

Data on spacing of both fracture types were collected along the entire cliff section. At all sampling sites, the spacing of bedding-parallel fractures (bed thickness) was measured in a vertical section of approximately 2 m, while spacing of sub-vertical to steeply dipping fractures was measured in one of the beds. No apparent variation was observed along the cliff exposure.

Rock mechanical testing

Blocks of silica-rich chalk were taken in the lower mound-bedded part of the Arnager Limestone along the cliff section. Samples were taken from different beds of identical visual appearance and considered to have near-identical mechanical properties due to similarity in induration. Around 75 cylindrical plug/disk samples were prepared from the block samples for tensile strength measurements of the vertical (V), horizontal north-west (HNW) and horizontal north-east (HNE) directions (Table 1). The tensile strength was measured using the Brazil test (ISRM 1978), a method suggested for determining the indirect tensile strength, where each disk was loaded between two curved plates until splitting.

The normal splitting load was recorded (P), and the indirect tensile strength (σ_T) calculated as

$$\sigma_T = \frac{2P}{\pi d l} \quad (1)$$

where d and l are the diameter and thickness/length of the disk, respectively.

Five vertical core plugs denoted as S1 to S5 with approximate dimensions of 37 mm diameter and 25 mm length (Table 1) were prepared for advanced testing and cleaned for salt using methanol as the solvent in soxhlet extraction (Dean 1998). Cleaned plug samples were oven-dried at 60˚C before being equilibrated to ambient temperature in a desiccator. Grain density was determined from gas porosimetry by N_2 expansion, and the dry density was derived from dry mass and plug dimensions. In the dry state and at uniaxial stress of 1.5 MPa, we transmitted and recorded one compressional wave (P) and two orthogonal shear waves (S1 and S2) in the longitudinal plug direction. The output frequency of the P- and S-waves is approximately 300 kHz and 600 kHz, respectively. Arrival times corrected for system delay were combined with deformation-corrected plug length to derive elastic P- and S-wave velocities (V_P and V_S).

The elasticity of a porous medium describes the resistance to elastic deformation (strain, ε) and is commonly described in terms of an elastic modulus. By combining the elastic wave velocities with dry density (ρ_{dry}), the dry dynamic compressional (M_{dry}) and shear (G_{dry}) modulus were derived as

$$M_{\mathrm{dry}} = \rho_{\mathrm{dry}} V_{\mathrm{P}}^2 \quad (2)$$

$$G_{\mathrm{dyn}} = \rho_{\mathrm{dry}} V_{\mathrm{S}}^2 \quad (3)$$

Poisson's ratio (ν) defines the ratio of transverse strain (ε_T) (perpendicular to the loading direction) to vertial strain (ε_V) and may be derived through a combination of (M_{dry}) and shear (G_{dry}) as

$$\nu = \frac{\varepsilon_T}{\varepsilon_V} = \frac{M_{dry} - 2G_{dry}}{2M_{dry} - 2G_{dry}} \quad (4)$$

Table 1. Properties of samples from the Arnager Limestone Formation.

ID	Diameter d mm	Length l mm	Dry mass m_{dry} g	Dry density ρ_{dry} g/cm^3	Grain density ρ_s g/cm^3	Porosity ϕ %	Elastic velocity V_p km/s	V_s km/s	Dry dynamic moduli and Poisson's ratio M_{dry} GPa	G_{dry} GPa	v -	Dry tensile strength σ_T[7] MPa
S1[1]	37.32	26.20	42.99	1.50	2.69	44.2[5]	2.26	1.53	7.65	3.54	0.07	
S2[1]	37.22	25.43	37.28	1.35	2.70	50.2[5]	1.84	1.25	4.58	2.10	0.07	
S3[1]	37.35	26.94	43.74	1.48	2.71	45.3[5]	1.72	1.13	4.36	1.89	0.12	
S4[1]	37.31	27.48	45.88	1.53	2.69	43.2[5]	2.23	1.47	7.62	3.28	0.12	
S5[1]	37.28	27.11	45.46	1.53	2.65	42.4[5]	2.22	1.44	7.50	3.19	0.13	
Average					2.69	45.1	2.05	1.37	6.34	2.80	0.10	
Stdandard deviation					0.02	3.1	0.26	0.17	1.71	0.75	0.03	
V1-V22[2]	35.73-37.90	16.16-22.27	26.29-40.85	1.32-1.67		37.9-50.7[6]						3.6-19.2
HNW1-HNW27[3]	37.04-37.91	15.18-21.75	25.25-38.61	1.34-1.72		35.9-50.2[6]						1.7-14.5
HNE1-HNE2[4]	37.55-38.08	15.53-22.68	24.71-38.32	1.34-1.66		38.2-50.1[6]						2.6-12.3 2.6-12.3
Average												8.2
Standard deviation												3.6

[1] Vertical samples used for advanced testing.
[2] Veritial samples used for tensile strength.
[3] Horizotal north-west samples used for tensile strength.
[4] Horizotal north-east samples used for tensile strength.
[5] N_2 porosity.
[6] Calculated from dry density and average grain density.
[7] Indirect dry tensile strength from Brazil testing.
M, *G* and *v* are compressional modulus, shear modulus and Poisson's ratio, respectively.

Results

Fractures

The coastal cliff is 200 m long, beginning just west of the harbour in the village of Arnager (Fig. 2). The cliff has a somewhat irregular appearance with an overall NW–SE-orientation. The Arnager Limestone has an apparent dip of 5° towards the NW (parallel to the cliff) resulting in the lowest stratigraphic levels being exposed towards the SE; from the central part of the cliff exposure and towards the SE, the boundary conglomerate and the uppermost part of the Arnager Greensand are exposed (Fig. 2).

The fracture system of the Arnager Limestone is composed of both bedding-parallel fractures and sub-vertical to steeply dipping fractures; these interacting fractures give the limestone in the cliff exposure a block-like appearance (Fig. 2). In the lower part of the cliff, these blocks have a typical width of 0.07–0.15 m and a typical height between 0.06 and 0.20 m. Towards the top of the cliff (and the Quaternary overburden), these block structures get smaller and smaller, frequently disintegrating into near rubble conditions. Thus, our measurements of fracture characteristics have been carried out in the lower 2 m of the exposed section where the fractures are best defined and easy to study.

At all the six sites studied, the limestone shows a well-defined bedding. All sites were characterised by more or less well-developed mound bedding with flanks that dip 5–10° (Noe-Nygaard & Surlyk 1985). Internally these banks show strata that dip in both directions. Bed boundaries are characterised by thin fractures (bedding-parallel fractures); these are flat-lying or show gentle dips in accordance with the architecture of the mound structure. Rarely, however, there were signs of lithological change along these fractures/bedding planes. In a few cases, mm-thin clay-rich material was observed at the top of a limestone bed supporting the interpretation that the top of this bed is a true bedding plane.

The bedding-parallel fractures, both those associated with the flat-bedded and the mound-bedded

strata, are intersected by two near-vertical to steeply dipping fracture sets; one set is trending N–S (355–175°) and a second set is trending W–E (265–85°; Fig. 4). Fracture orientation and spacing did not show any apparent change along the cliff or across the mound structure. In the middle part of the cliff section wave-eroded platforms with fractures were observed at the cliff foot.

The cliff exposures illustrate the broken-up structure of the limestone with the two orthogonal, steeply dipping fracture sets and the bedding-parallel fracture set (Figs 2, 5). The traces of the N–S fracture set on cliff sides are straight to somewhat undulatory and near vertical. Accordingly, exposed block surfaces controlled by these fractures possess dip angles around 85°. The block surfaces controlled by W–E-trending fractures have less steep dip angles; typically, they vary between 75° and 85°. The traces of these fractures in cliff exposures are straight to somewhat undulatory and have an appearance similar to the N–S-trending fractures.

Visual inspection of the selected sites shows that few N–S-trending fractures are restricted to one bed (mechanical subunit), while most are confined to 2–5 beds and more rarely up to 10 beds (Fig. 5). Many of the fractures show minor sidewards displacement when crossing a bed boundary (weak mechanical interface), and it may therefore be difficult to decide whether such a displaced fracture should be classified as a new fracture or as the original one. A limited number of fractures can be traced from bottom to near the top of the exposure and thereby span the complete mechanical unit of the Arnager Limestone (Fig. 6).

Bedding plane exposures were seen in two levels; one immediately above the boundary conglomerate and one around 1 m above this conglomerate (Fig. 7). On the very low-angle dipping bedding plane exposures, the two sub-vertical to steeply dipping fracture sets are viewed on relatively clean surfaces; it is apparent that one set is trending NNW–SSE and a second set is trending W–E. The two fracture sets are seen to be cross cutting in some places with no or minor offsets at intersection points.

Fracture width of the steeply dipping fractures (aperture) in cliff exposures is typically up to 1 cm; when undisturbed by recent disintegration, fracture width, however, is only a few millimetres. Observations on bedding planes also indicate that the width of these fractures is rarely more than a few millimetres. Fracture coatings or cement were not observed. Fracture width of the bedding-parallel fracture is also up to 1 cm.

Measurement of the spacing of the near-vertical to steeply dipping fractures was carried out at all six sites and confined at each site to one bed. N–S-trending fractures are relatively narrowly spaced with spacing between 0.03 and 0.31 m with most data lying between 0.03 and 0.15 m and with a mean value of 0.12 m (Fig. 8). The spacing of the W–E-trending fractures was more difficult to measure in the field; data obtained, how-

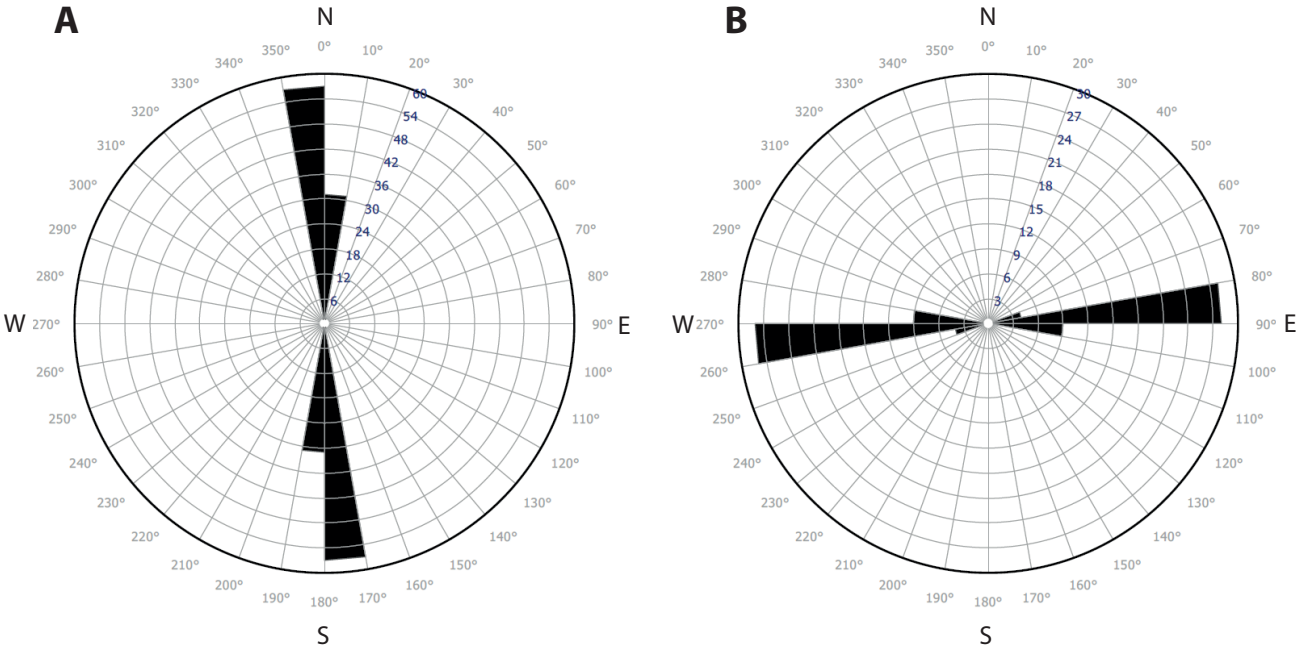

Fig. 4. Rose diagrams showing the orientation of the near-vertical to steeply dipping fractures in the Arnager Limestone Formation. **A,** One fracture set is aligned N–S (combined data from all six study sites). **B,** A second fracture set is aligned W–E (combined data from all six study sites with cliff exposures).

ever, show that most of these fractures have spacing between 0.10 and 0.30 m. Bedding plane exposures in the lowermost part of the limestone show a structure with spacing between the two fracture lines rather similar to those obtained in cliff exposures (Fig. 7).

In the lower part of the limestone, bed thickness (and thereby spacing of bedding-parallel fractures) varies between 0.06 and 0.40 m, with most beds having thicknesses between 0.06 and 0.14 m and a mean value of 0.16 m (Fig. 9).

The two sets of near-vertical to steeply dipping fractures in the Arnager Limestone terminate against the hardground in the middle of the boundary conglomerate (Fig. 7). The basal part of the boundary conglomerate as well as the underlying Arnager Greensand are characterised by a complete lack of these fracture sets.

An important observation of the outcrop is the complete absence of stylolites and polygonal fractures as well as slickenlines that would indicate shear movement. However, plume and hackle marks are observed indicating tensile stress in a zone of compression.

Mechanical properties

New data from the Arnager limestone include porosity, elastic wave velocities, elastic moduli, Poisson's ratio and dry tensile strength. No significant difference in dry tensile strength is found between the investigated orientations (Fig. 10, Table 1). Cross-plotting a calculated bulk density assuming 100% water saturation and tensile strength in the dry state shows a significantly higher tensile strength of the silica-rich Arnager Limestone compared to chalk from København Limestone Formation and from Tor Formation at Stevns (Fig. 10). Voake *et al*. (2019) investigated the difference in tensile strength between dry and water saturated Mons (Belgium) and Kansas (USA) chalk and found 1–2 MPa lower tensile strength of water saturated than dry Mons chalk with porosity similar to the tested Arnager Limestone samples. Because such effects of water saturation mainly are found in calcite-bonded rocks, no significant reduction in the dry tensile strength due to water saturation is expected in the silica bonded chalk of Arnager Limestone.

Fig. 5. Fracture system in lowermost part of the Arnager Limestone Formation. The limestone is well bedded with low-angle dipping mound structures. It has two near-vertical to steeply dipping and orthogonal fracture sets trending N–S and W–E respectively; in addition the limestone displays near-horizontal to gently dipping bedding-parallel fractures. The fractures impose a blocky appearance to the limestone. Length of scale is 50 cm. Cliff is viewed from the southwest. Picture taken at midday Sun.

Discussion

Origin of near-vertical to steeply dipping fracture sets

The near-vertical to steeply dipping fractures in the Arnager Limestone are aligned in two directions, N–S (355–175°) and W–E (265–85°) being perpendicular to each other. The fracture pattern is consistent along the cliff exposure and relatively simple. Bedding plane exposures near the base of the formation, however, display a slightly different fracture pattern with most fractures aligned NNW–SSE (325–145°) and W–E (265–85°). The dominant orientation of major Mesozoic faults bounding the Arnager-Sose block is NW–SE (315–135°); less common fault systems on this block are aligned NNW–SSE (345–165°) and W–E (275–95°; Graversen 2009). Thus, the orientation of the near-vertical to steeply dipping fractures in the Arnager Limestone is in best agreement with the orientation of the less common faults systems on the Arnager-Sose Block. The Arnager fractures also fit reasonably well with measurements of all faults limiting Mesozoic bedrock as these are aligned predominantly N–S (355–175°) and WNW–ESE (285–105°; Graversen 2009). Thus, it is suggested that the near-vertical to steeply dipping fractures are tectonic in origin, although they may have been accentuated during final unloading processes.

The near-vertical to steeply dipping fractures in the Arnager Limestone are opening-mode fractures according to the terminology of Bai & Pollard (2000) and as argued above formed in response to tectonic extension. Experimental results and field observations have shown that opening-mode fractures

Fig. 6. Two closely associated, near-vertical and through-going fractures. The fractures are trending W–E; hammer at base of the cliff for scale. Cliff is viewed from the west. Picture taken at evening Sun.

typically are confined by layer boundaries with their height equal to the height of the fractured layer and their spacing proportional to this thickness (Bai *et al.* 2000). However, in the Arnager Limestone fractures typically cross bed boundaries probably because all beds are of almost identical lithofacies (rock mechanical subunits) and bedding planes thereby only act as weak interfaces. In the Arnager Limestone the average bed thickness is about 0.16 m and the average spacing of near-vertical fractures is about 0.12 m; leading to a ratio between fracture spacing and bed thickness of about 0.8, close to the expected value for a bedded carbonate succession (cf. Bai & Pollard 2000; Cooke *et al.* 2007).

The near-vertical to steeply dipping fractures in the Arnager Limestone are gradually reduced in aperture and finally completely vanish in the upper part of the boundary conglomerate and are absent in the lowermost part of the conglomerate and in the underlying Arnager Greensand. This is explained by a change from brittle conditions in the lithified (coherent) Arnager Limestone to bulk deformation due to grain boundary sliding in the loose, unlithified (loose with no or little cohesion) Arnager Greensand.

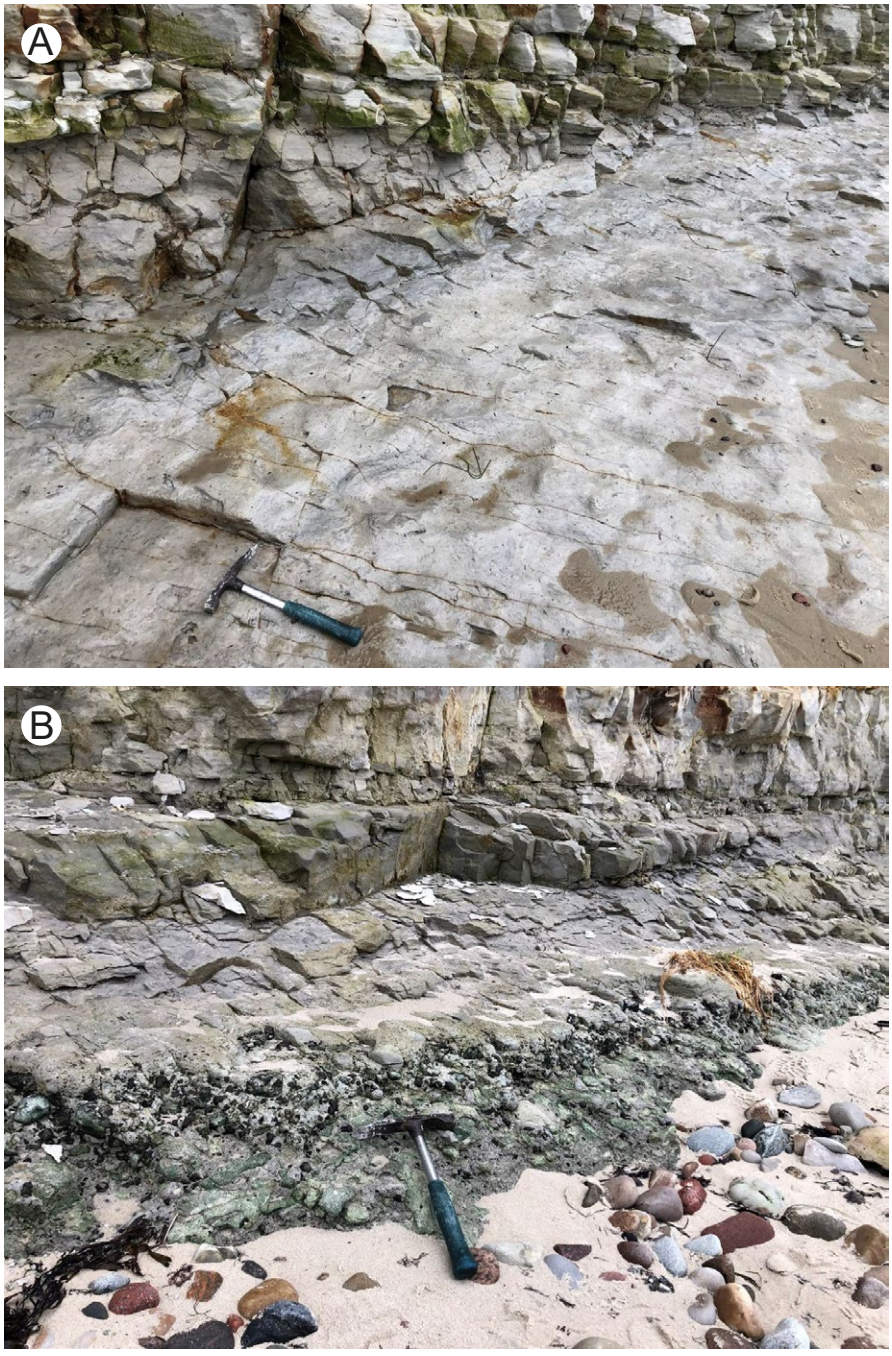

Fig. 7. A, Bedding plane exposures of the near-vertical to steeply dipping fractures in the Arnager Limestone Formation immediately above the boundary conglomerate. One fracture set is trending NNW–SSE (near parallel to hammer shaft) and a second fracture set is trending W–E. Cliff seen in upper part of the picture. Modern beach sand covers the seaward part of the exposure. Exposure is viewed from the west. **B,** The near-vertical to steeply dipping fractures in the Arnager Limestone Formation terminate at the hardground in the middle of the boundary conglomerate. One fracture set is in the Arnager Limestone Formation trending NNW–SSE, a second fracture set is trending W–E. Modern beach sediments cover the seaward part of the sedimentary rocks. Exposure is viewed from the southwest.

Origin of bedding-parallel fracture set

Bedding-parallel fractures are characteristic of the Arnager Limestone outcrop, and can be referred to as unloading fractures. That burial followed by uplift and erosion would result in horizontal fracturing may, at first glance, appear illogical, but the phenomenon is well described in the geotechnical literature (e.g. Santamarina 2003). The fractures arise because the stress geometry during burial and during uplift differ. At maximum burial depth, the vertical stress is likely the major principal stress, and the two principal horizontal stresses are the minor ones. During uplift, the vertical stress approaches zero as it would be at the surface, and the two horizontal stresses become the major principal stresses. This situation corresponds to an extension stress geometry, which would tend to result in horizontal fractures if the tensile strength is exceeded. Whether horizontal fractures form depends on the tensile strength of the rock, and with respect to this property, strain difference on the rock frame over geological time plays a role. As an illustrative case, we define the 1-direction as vertical, and 2- and 3-directions as the horizontals. Further, if we assume that the limestone is isotropic, then the relation between normal strain and normal stress of a representative element volume (REV) is given by Hoek's law as

$$\begin{bmatrix}\varepsilon_1\\ \varepsilon_2\\ \varepsilon_3\end{bmatrix} = \left(\frac{G(3M-4G)}{M-G}\right)^{-1}\begin{bmatrix}1 & -\upsilon & -\upsilon\\ -\upsilon & 1 & -\upsilon\\ -\upsilon & -\upsilon & 1\end{bmatrix}\begin{bmatrix}\sigma_1\\ \sigma_2\\ \sigma_3\end{bmatrix} \quad (5)$$

where ε_1, ε_2, ε_3 are normal strains, σ_1, σ_2, σ_3 are normal stresses, M is the compressional modulus, G is the shear modulus and ν is Poisson's ratio. Inserting $\sigma_1 = 0$

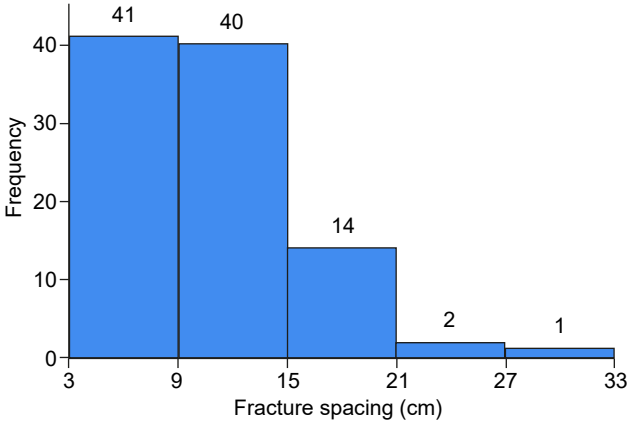

Fig. 8. Histogram showing spacing of near-vertical to steeply dipping fractures in cm. Data represent the N–S-trending fractures. Data were collected in the lowermost, mound-bedded part of the Arnager Limestone Formation.

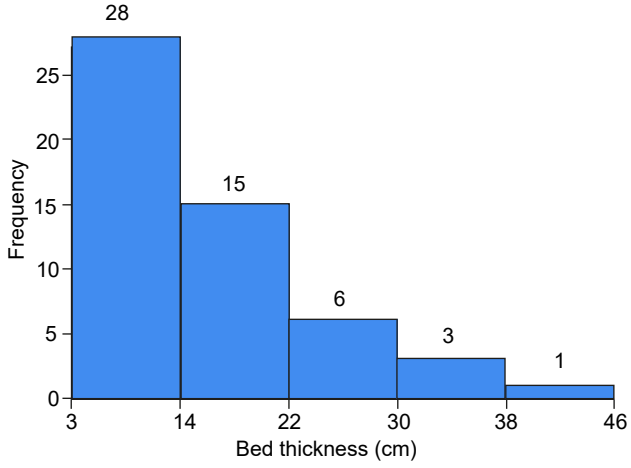

Fig. 9. Histogram of bed thickness in cm. Data were collected in the lowermost part of the Arnager Limestone Formation.

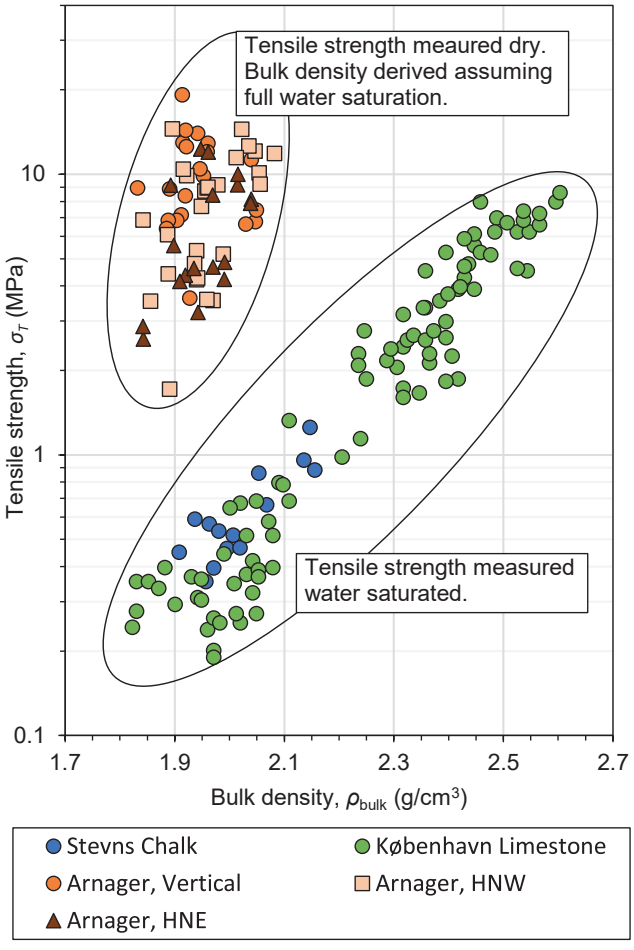

Fig. 10. Cross-plots of bulk density and tensile strength. Blue data points: Stevns chalk (Katić *et al.* 2019), green: København Limestone (Database; Courtesy of Geo). Orange data points: Arnager Limestone where HNW is horizontal north-west direction, and HNE is horizontal north-east direction.

and $\sigma_2,\sigma_3 > 0$ in equation 5, thus representing the time after uplift, we may derive the difference in strain as

$$\begin{bmatrix}\varepsilon_1\\ \varepsilon_2\\ \varepsilon_3\end{bmatrix} = \left(\frac{G(3M-4G)}{M-G}\right)^{-1}\begin{bmatrix}1 & -\upsilon & -\upsilon\\ -\upsilon & 1 & -\upsilon\\ -\upsilon & -\upsilon & 1\end{bmatrix}\begin{bmatrix}0\\ \sigma_2 > 0\\ \sigma_3 > 0\end{bmatrix} \quad (6)$$

from which we see that the vertical normal strain (ε_1) becomes negative during uplift with a magnitude of

$$\varepsilon_1 = \left(\frac{G(3M-4G)}{M-G}\right)^{-1}(-\upsilon(\sigma_2+\sigma_3))\,. \quad (7)$$

The negative vertical strain is caused by the compressive horizontal stresses (σ_2, σ_3), and by assuming that the limestone behaves linear elastic until failure, the negative normal strain may exceed the tensile strength, resulting in horizontal fractures.

The rock may also have reduced tensional strength from a mechanism related to strain difference between particles and cement during uplift. Neglecting temperature increase from burial, the mechanism is that sedimentary particles (in this case, siliceous carbonate ooze) during burial (load increase) are subjected to elastic strain (ε_{fr}), then at a critical strain (ε_{crit}), contact cementation (bonding) takes place, and during subsequent burial, both particles and cement are strained (ε_{fr} and ε_C). The interesting point is that the accumulated strain of the particles is higher than that of the cement. Upon stress relief due to uplift and erosion, the particles relax, causing the cement to endure tensile strain, consequently promoting horizontal fracturing (Fig. 11). This process will likely form micro-cracks from which fractures due to negative (tensional) normal strain may initiate.

It has been argued that bedding-parallel fractures also could be a result from glacial deformation since former glacial deposits directly overlie the Arnager Limestone at the outcrop. If glacial deformation (shearing) was the cause for formation of the bedding-parallel fractures it would have been expected that slicken sides would be present, but these have not been observed. The Arnager Limestone has been subject to unloading due to erosion of overlying deposits and repeated loading/unloading cycles during glaciations since Bornholm was covered by the Scandinavian Ice Sheet during the Quaternary glaciations (Houmark Nielsen & Kjær 2003). The removal of sediments covering the Arnager Limestone (e.g. the Bavnodde Greensand) would create favourable conditions for generating the bedding-parallel fractures described above. A speculative increased fluid overpressure beneath the ice would also favour the formation of fractures, including the bedding-parallel due to the reduction in stress caused by excess pore pressure. However, as horizontal (flat-lying) fractures would, in any case, be expected to form due to the uplift, it is hardly necessary to invoke this extra mechanism.

Comparative studies

Fracture patterns in non-siliceous Upper Cretaceous, Tor Formation chalk deposits exposed at Sigerslev quarry (Stevns), Denmark (Fig. 1) have some similarities to the fracture pattern in the Arnager Limestone. At the Sigerslev quarry, the system consists of closely spaced horizontal fractures and four sets of vertical

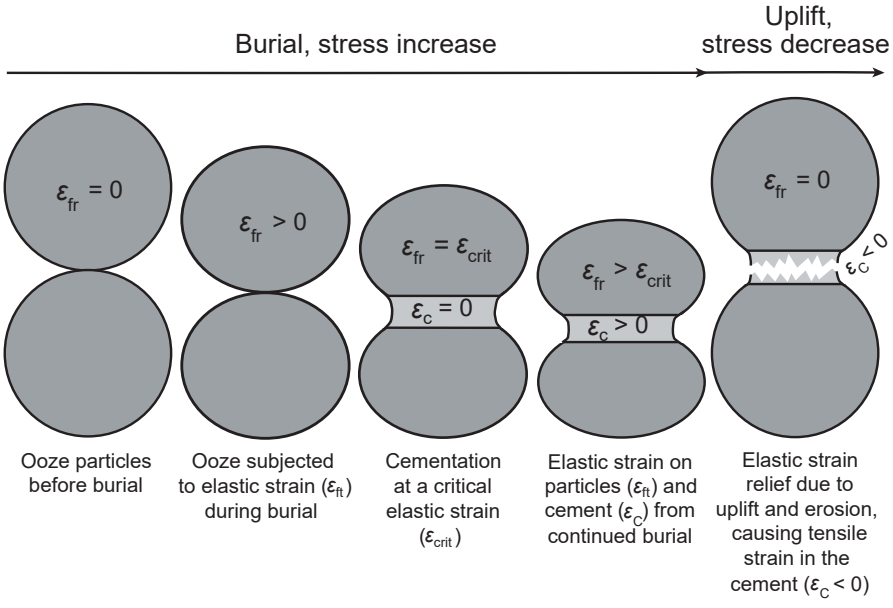

Fig. 11. Conceptual illustration of uniaxial strain development during burial and subsequent uplift on a sedimentary rock frame. Temperature increase from burial is neglected. Positive and negative strain represent compaction and tension, respectively. ε_{fr} is the particle/rock frame strain, and ε_C is the cement strain forming at a critical strain ε_{crit}. Tensile ruptures/fractures are created by tensile strain in the cement ($\varepsilon_C < 0$) due to uplift/ stress decrease and the difference in strain between ε_{fr} and ε_C.

fractures (Rosenbom & Jacobsen 2005). The vertical to steeply dipping fractures are striking 25, 60, 145 and 175°. Unfortunately, no information on fracture spacing is reported, but own observations in the uppermost part of the chalk at Stevns Klint show typical spacings of the steeply dipping fractures rather similar to those observed in the Arnager Limestone. The formation of the vertical fractures at the Sigerslev quarry was related to regional dextral transpressionel stresses along major north-south oriented faults causing partial inversion of the area, while the horizontal fractures would have formed by removal of 500–750 m of overlying sediments by uplift and erosion (Rosenbom & Jacobsen 2005).

The København Limestone Formation (Late Danian) is a partly indurated limestone that has been studied in excavations on Amager (Jakobsen & Klitten 1999; Fig.1); the limestone displays horizontal fractures as well as vertical fractures. The horizontal fractures are typically situated at the boundary between strongly indurated and slightly indurated beds formed during relaxation due to unloading of overlying sediments; loading and unloading of ice during the Quaternary may also have contributed to their formation (Jakobsen & Klitten 1999). The vertical fractures formed in connection with tectonic movements in the Fennoscandian Border (Tornquist) Zone (Jacobsen & Klitten 1999).

Thus, in both the København Limestone and the chalk at Sigerslev two sets of fractures are present: horizontal fractures classified as unloading fractures and vertical to steeply dipping fractures classified as tectonic. In a similar way, the fracture system in the Arnager Limestone is composite. An early tectonic phase created the near-vertical to steeply dipping fracture sets, while the bedding-parallel fractures in the Arnager Limestone most likely formed during a period when the least compressive stress was vertical as they are open fractures that break along bedding planes. Thus, their origin is interpreted to be related to the erosion of overlying sediments. A final phase was most likely tectonic tilting of the complete succession resulting in the present day low-angle dip of 5° towards the NW.

Palaeoburial

The rock mechanical data (table 1), i.e. the tensile strength, elastic moduli and Poisson's ratio, provide the basis for discussing the maximal burial depth of Arnager Limestone. However, a minimum palaeoburial of the Arnager Limestone is constrained by the 180 m thickness of the Bavnodde Greensand (Christensen 1985), whereas a maximum palaeoburial constraint of the Arnager Limestone of 1000 m may be envis-

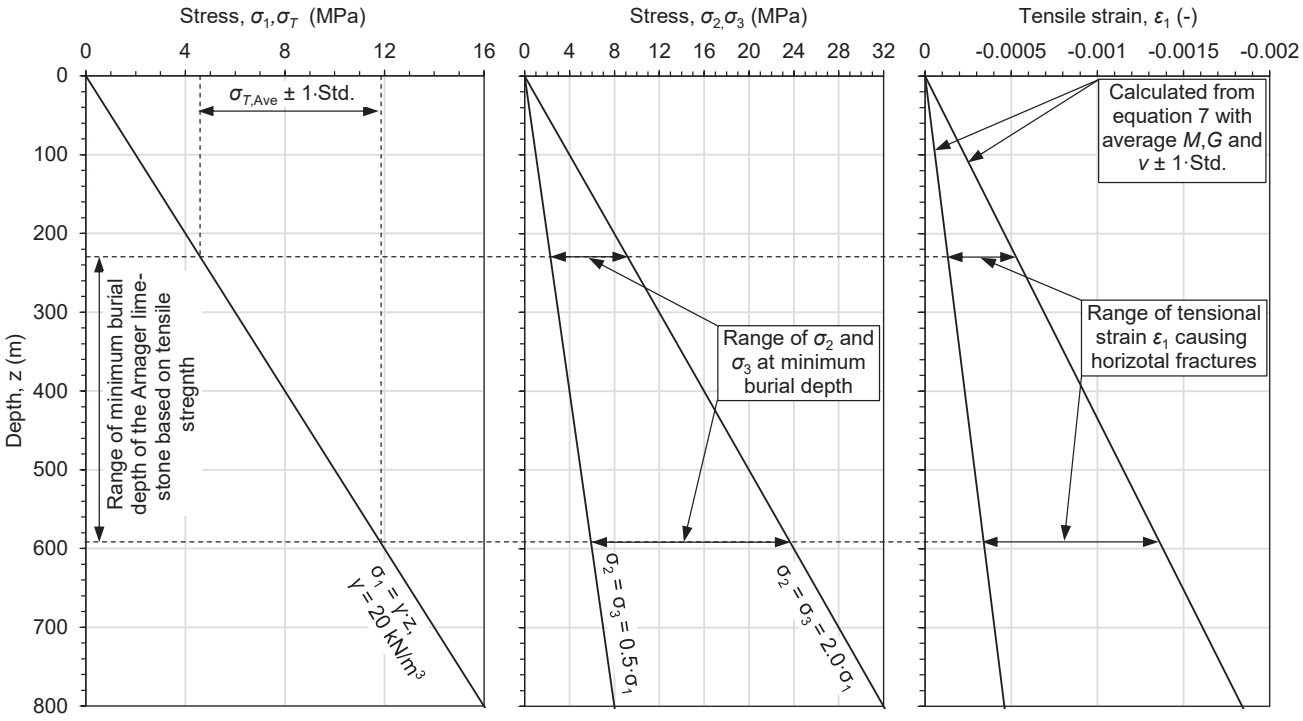

Fig. 12. Stress and strain plots versus depth plots. Left: vertical stress and tensile strength showing the estimated minimum Arnager Limestone burial depth. Middle: horizontal stresses derived from a K0 of 0.5 and 2. Right: vertical tensional strain that is required to generate horizontal fractures from uplift.

aged by the transition from opal-CT to quartz, which requires thermal energy provided by heating through time. In deep chalks of the Ontong Java Plateau the transition is found at 1100 m below sea floor in Eocene sediments, where the present temperature is less than 30˚C (Kroenke *et al*. 1991; Fabricius & Borre 2007). Suppose we assume a higher sea floor temperature on the Coniacian shelf of Bornholm area and take the much longer time into account; even with a low geothermal gradient, burial can hardly have exceeded a maximum of 1000 m, as also indicated by the absence of stylolites in the Arnager Limestone and lack of cementation of Lower Cretaceous and Jurassic sands on Bornholm.

By assuming a linear vertical stress increase with depth from an average unit weight (γ) of 2.0 kN/m^3, the minimum range of palaeoburial of the Arnager Limestone may be estimated from the range of measured tensile strength (Fig. 12). Observations have identified bedding-parallel horizontal fractures (Fig. 2) in the Arnager cliff, meaning that the tensile strength has been exceeded through geological history. Following equation 6 and combining the range of measured tensile strength with estimated vertical stress from burial, the palaeoburial depth is estimated to be approximately 230 to 600 m (Fig. 12). This estimated palaeoburial is thus within the constraints given by the Bavnodde Greensand thickness and the transition from opal-CT to quartz. A guess on the ratio of horizontal to vertical stress (K0) of 0.5 to 2 and assuming equal horizontal stresses ($\sigma_2 = \sigma_3$) illustrates that the vertical tensional strain (ε_1) that is required to generate horizontal fractures from uplift ($\sigma_1 = 0$, $\sigma_2 = \sigma_3 < 0$) and calculated from equation 7 ranges from $4.1{\cdot}10^{-5}$ to $1.4{\cdot}10^{-3}$.

Conclusions

- Exposures of naturally fractured carbonate sedimentary rocks function as analogues for subsurface carbonate reservoirs and can yield insights about the fracture characteristics, patterns, dimensions and cross-cutting relationships and thereby aid interpretations of past tectonic events and burial history.

- The Arnager Limestone shows a system of natural fractures including two near-vertical to steeply dipping orthogonal fracture sets as well as a bedding-parallel, flat-lying to gently dipping fracture set.

- The Arnager Limestone forms a 12–20 m thick, main rock mechanical unit subdivided into near-identical, cm- to dm-thick, mechanical subunits separated by bed boundaries that act as weak interfaces.

- Most of the near-vertical to steeply dipping fractures are confined to 2–5 beds; some span the complete outcrop (main mechanical unit). This pattern underlines the relative constant mechanical properties of the Arnager Limestone, and the weak nature of the interfaces along bedding planes.

- The near-vertical to steeply dipping fracture sets are oriented north–south and west–east respectively. The observed fracture pattern agrees with the overall Mesozoic block fault pattern on Bornholm supporting a tectonic origin of the vertical fracture sets. This type of fractures is not present in the underlying Arnager Greensand as this unit forms a ductile mechanical unit.

- The flat-lying to gently dipping fractures developed along bed boundaries and formed as a result of unloading due to uplift and erosion of covering sediments, possibly accentuated by glacial processes.

- Based on rock mechanical laboratory data and comparative studies, the palaeoburial for the Arnager Limestone is estimated to be 230–600 m.

Acknowledgements

The authors would like to thank Peter Frykman and an anonymous reviewer for their constructive reviews of the manuscript. Ole Bennike and Henrik Tirsgaard are thanked for handling the editorial process. The authors are very grateful to Michael John Welch and Emil Mejlhede Kinslev (DTU) for constructive input to the manuscript and valuable discussions on natural fractures in chalk. Catherine Chagué is thanked for constructive comments on an early version of the manuscript. Joakim Korshøj (GEO) is thanked for assisting with preparation of core plug samples.

References

Aguilera, R. 1998: Geologic aspects of naturally fractured reservoirs. The Leading Edge 17(12), 1667–1670. https://doi.org/10.1190/1.1437912

Babuska, V. & Plomerova, J. 2004: The Sorgenfrei–Tornquist Zone as the mantle edge of Baltica lithosphere: new evidence from three-dimensional seismic anisotropy. Terra Nova 16, 243–249. https://doi.org/10.1111/j.1365-3121.2004.00558.x

Bai, T. & Pollard, D.D. 2000: Fracture spacing in layered rocks: a new explanation based on the stress transition. Journal of Structural Geology 22, 43–57. https://doi.org/10.1016/S0191-8141(99)00137-6

Bourbiaux, B. 2010: Fractured Reservoir Simulation: a Challenging and Rewarding Issue. Oil & Gas Science and Technology – Rev. IFP 65, 227–238. https://doi.org/10.2516/ogst/2009063

Bromley, R.G. 1979: Field meeting in southern Scandinavia 18–28 September 1975. Proceedings of the Geologists' Association 90, 181–191. https://doi.org/10.1016/S0016-7878(79)80004-8

Chaika, C. & Dvorkin, J. 1997: Ultrasonic velocities of opaline rocks undergoing silica diagenesis. Geophysical Research Letters 24, 2039–2042. https://doi.org/10.1029/97GL01959

Christensen, W.K. 1985: The Albian to Maastrichtian of southern Sweden and Bornholm, Denmark; a review. Cretaceous Research 5, 313–327. https://doi.org/10.1016/S0195-6671(84)80027-0

Cooke, M.L., Simo, J.A., Underwood, C.A. & Rijken, S. 2006: Mechanical stratigraphical control on fracture patterns within carbonates and implications for groundwater flow. Sedimentary Geology 184, 325–339. https://doi.org/10.1016/j.sedgeo.2005.11.004

Cotte, N., Pedersen, H.A. & the TOR Working Group 2002: Sharp contrast in lithospheric structure across the Sorgenfrei–Tornquist Zone as inferred by Rayleight wave analysis of TOR1 project data. Tectonophysics 360, 75–88. https://doi.org/10.1016/S0040-1951(02)00348-7

Dean, J.R. 1998: Extraction methods for environmental analysis, 225 pp. Chichester: Wiley.

Erlström, M., Thomas, S.A., Deeks, N. & Sivhed, U. 1997: Structure and tectonic evolution of the Tornquist Zone and adjacent sedimentary basins in Scania and the southern Baltic Sea area. Tectonophysics 271, 191–215. https://doi.org/10.1016/S0040-1951(96)00247-8

Fabricius, I.L. & Borre, M.K. 2007: Stylolites, porosity, depositional texture, and silicates in chalk facies sediments. Ontong Java Plateau – Gorm and Tyra fields, North Sea. Sedimentology 54, 183–205. https://doi.org/10.1111/j.1365-3091.2006.00828.x

Gabrielsen, R.H. & Koestler, A.G. 1987: Description and structural implications for fractures in late Jurassic sandstones of the Troll Field, northern North Sea. Norsk Geologisk Tidsskrift 67, 371–381.

Glad, A.C., Amour, F., Welch, M.J., Clausen, O. R., Anderskouv, K., Ineson, J. R., Sheldon, E. & Nick, H.M. 2022: Natural fractures in a Lower Cretaceous chalk-marlstone reservoir, Valdemar Field, Danish North Sea. Marine and Petroleum Geology 136, 105445. https://doi.org/10.1016/j.marpetgeo.2021.105445

Graversen, O. 2009: Structural analysis of superposed fault systems of the Bornholm horst block, Tornquist Zone, Denmark. Bulletin of the Geological Society of Denmark 57, 25–49. https://doi.org/10.37570/bgsd-2009-57-02

Graversen, O. 2004: Upper Triassic – Lower Cretaceous seismic sequence stratigraphy and basin tectonics at Bornholm, Denmark, Tornquist Zone, NW Europe. Marine and Petroleum Geology 21, 579–612. https://doi.org/10.1016/j.marpetgeo.2003.12.001

Hart, M.B., Bromley, R.G. & Packer, S.R. 2012: Anatomy of the stratigraphical boundary between the Arnager Greensand and Arnager Limestone (Upper Cretaceous) on Bornholm, Denmark. Proceedings of the Geologists Association 123, 471–478. https://doi.org/10.1016/j.pgeola.2011.11.006

Houmark-Nielsen, M. 2011: Pleistocene glaciations in Denmark: a closer look at chronology, ice dynamics and landforms. In: Ehlers, J., Gibbard, P.L. & Hughes, P.D. (eds): Quaternary glaciations – extent and chronology – a closer look. Developments in Quaternary Sciences 15, 47–58. https://doi.org/10.1016/B978-0-444-53447-7.00005-2

Houmark-Nielsen, M. & Kjær, K.H. 2003: Southwest Scandinavia, 40–15 kyr BP: palaeogeography and environmental change. Journal of Quaternary Science 18, 769–786. https://doi.org/10.1002/jqs.802

Humlum, O. & Houmark-Nielsen, M. 1994: High deglaciation rates in Denmark during the Late Weichselian – implications for the palaeoenvironment. Geografisk Tidsskrift 94, 26–37. https://doi.org/10.1080/00167223.1994.10649349

ISRM Commission on Testing Methods 1978: Suggested methods for determining tensile strength of rock materials. International Journal of Rock Mechanics and Mining Sciences & Geomechanics 15, 99–103. http://dx.doi.org/10.1016/0148-9062(78)90003-7

Jakobsen P.R. & Klitten, K. 1999: Fracture systems and groundwater flow in the København Limestone Formation. Nordic Hydrology 30, 301–316. https://doi.org/10.2166/nh.1999.0017

Jensen, J.B. & Hamann, N.E. 1989: Geological mapping of Mesozoic deposits along the eastern margin of the Rønne Graben, offshore Bornholm, Denmark. Bulletin of the Geological Society of Denmark 37, 237–260. https://doi.org/10.37570/bgsd-1988-37-19

Katić, N., Korshøj, J.S., Christensen, H.F. 2019: Bryozoan limestone experience – the case
of Stevns Klint. AIMS Geosciences 5,163–183. https://doi.org/10.3934/geosci.2019.2.163

Kroenke, L.W. *et al.* 1991: Proceedings of the Ocean Drilling Program, Initial Reports 130, 1240 pp. College Station, Texas. https://doi.org/10.2973/odp.proc.ir.130.1991

Lemonnier, P. & Bourbiaux, B. 2010: Simulation of naturally fractured reservoirs. state of the art – part 2 – matrix-fracture transfers and typical features of numerical studies. Oil & Gas Science and Technology – Rev. IFP 65, 263–286. https://doi.org/10.2516/ogst/2009067

Lykke-Andersen, H. & Surlyk, F. 2004: The Cretaceous–Palaeogene boundary at Stevns Klint, Denmark: inversion tectonics or sea-floor topography? Journal of the Geological Society of London 161, 343–352. https://doi.org/10.1144/0016-764903-021

Madsen, H.B., Stemmerik, L. & Surlyk, F. 2010: Diagenesis of silica-rich mound-bedded chalk, the Coniacian Arnager limestone, Denmark. Sedimentary Geology 223, 51–60. https://doi.org/10.1016/j.sedgeo.2009.10.002

Mavko, G., Mukerji, T. & Dvorkin, J. 2009: The rock physics handbook: Tools for seismic analysis of porous media, 329

pp. Cambridge University Press. https://doi.org/10.1017/CBO9780511626753

Noe-Nygaard, N. & Surlyk, F. 1985: Mound bedding in a sponge rich Coniacian chalk, Bornholm, Denmark. Bulletin of the Geological Society of Denmark 34, 237–249. https://doi.org/10.37570/bgsd-1985-34-19

Ogata, K., Senger, K., Braathen, A., Tveranger, J. & Olaussen, S. 2014: The importance of natural fractures in a tight reservoir for potential CO_2 storage: a case study of the upper Triassic-middle Jurassic Kapp Toscana Group (Spitsbergen, Arctic Norway). In: Spence, G.H. *et al.* (eds): Advances in the study of fractured reservoirs. Geological Society of London, Special Publications 374, 395–415. https://doi.org/10.1144/SP374.9

Packer, S.R. & Hart, M.B., 2005: Coniacian–Santonian Radiolaria from the Upper Cretaceous of Bornholm, Denmark. A preliminary investigation. Bulletin of the Geological Survey of Denmark 52, 141–157. https://doi.org/10.37570/bgsd-2005-52-11

Peacock, D.C.P., Nixon, C.W., Rotevatn, A., Sanderson, D.J. & Zuluaga, L.F. 2016: Glossary of fault and other fracture networks. Journal of Structural Geology 92, 12–29. https://doi.org/10.1016/j.jsg.2016.09.008

Rosenbom, A.E. & Jacobsen, P.R. 2005: IR thermography and fracture analysis of preferential flow in chalk. Vadose Zone Journal 4, 271– 280. https://doi.org/10.2136/vzj2004.0074

Santamarina, J.C. 2003: Soil behavior at the microscale: particle forces. In: Germaine, J.T., Sheahan, T.C. & Whitman, R.V. (eds): Proceedings of the Symposium on Soil Behavior and Soft Ground Construction, in honor of Charles C. Ladd - October 2001. American Society of Civil Engineers Special Publication 119, 25–56. https://doi.org/10.1061/40659(2003)2

Solymar, M. & Fabricius, I.L. 1999: Image analysis and estimation of porosity and permeability of Arnager Greensand, Upper Cretaceous, Denmark. Physics and Chemistry of the Earth Part A – solid Earth and Geodesy 24, 587–591. https://doi.org/10.1016/S1464-1895(99)00084-8

Svennevig, K. & Surlyk, F. 2018: A high-stress shelly fauna associated with sponge mud-mounds in the Coniacian Arnager Limestone of Bornholm, Denmark. Lethaia 52, 57–76. https://doi.org/10.1111/let.12290

Tröger, K.A. & Christensen, W.K. 1991: Upper Cretaceous (Cenomanian Santonian) inoceramid bivalve faunas from the island of Bornholm, Denmark. Danmarks Geologiske Undersøgelse A28, 47 pp. https://doi.org/10.34194/seriea.v28.7048

Vejbæk, O.V. 1985: Seismic stratigraphy and tectonics of sedimentary basins around Bornholm, southern Baltic. Danmarks Geologiske Undersøgelse A8, 30 pp. https://doi.org/10.34194/seriea.v8.7027

Voake, T., Nermoen, A., Ravnås, C., Korsnes, R.I. & Fabricius, I.L. 2019: Influence of temperature cycling and pore fluid on tensile strength of chalk. Journal of Rock Mechanics and Geotechnical Engineering, 11, 277–288. https://doi.org/10.1016/j.jrmge.2018.12.004

Waight, T.E., Serre, S.H., Naesby, S.H. & Thomsen, T.B. 2017: The ongoing search for the oldest rock on the Danish island of Bornholm: new U-Pb zircon ages for a quartz-rich xenolith and country rock from the Svaneke Granite. Bulletin of the Geological Society of Denmark 65, 75–86. https://doi.org/10.37570/bgsd-2017-65-06

Welch, M.J., Souque, C., Davies, R.K. & Knibe, R.J. 2015: Using mechanical models to investigate the controls on fracture geometry and distribution in chalk. In: Agar, S.M & Geiger, S. (eds): Fundamental controls on fluid flow in carbonates: current workflows to emerging technologies. Geological Society of London, Special Publications 406, 281–309. https://doi.org/10.1144/SP406.5

Ziegler, P.A. 1990: Geological atlas of western and central Europe, 2nd edition, 239 pp. The Hague: Shell International Petroleum Maatschappij B.V.

Insights into the K–Pg extinction aftermath: The Danish Cerithium Limestone Member

TJÖRDIS STÖRLING, ISALINE DEMANGEL, ANDERS LINDSKOG, JACOB ANDERSSON, MIKAEL CALNER, DANIEL J. CONLEY & SYLVAIN RICHOZ

Geological Society of Denmark
https://2dgf.dk

Received 12 January 2023
Accepted in revised form
10 July 2024
Published online
13 November 2024

Störling, T., Demangel, I., Lindskog, A., Andersson, J., Calner, M., Conley, D.J. & Richoz, S. 2024. Insights into the K–Pg extinction aftermath: The Danish Cerithium Limestone Member. Bulletin of the Geological Society of Denmark, Vol. 73, pp. 175–191. ISSN 2245-7070. https://doi.org/10.37570/bgsd-2024-73-10

The Cretaceous–Palaeogene (K–Pg) mass extinction about 66 Ma ago was one of Earth's largest mass extinction events. The demise of calcifiers, among others, influenced biogeochemical cycles and changed the conditions for carbonate deposition in the global ocean. This study addresses the sedimentology and carbonate microfacies of the Cerithium Limestone Member of the Rødvig Formation within the renowned Stevns Klint succession in Denmark. The limestone was deposited in the earliest Danian Stage, immediately after the K–Pg mass extinction. It is a pale yellow, partly cemented unit with a dense network of *Thalassinoides* burrows and numerous flint nodules. Studies of the thin sections revealed that the Cerithium Limestone Member is more variable than expected from its overall homogeneous appearance at the macroscopic scale. The thin sections and scanning electron microscope (SEM) images showed that the highly bioturbated limestone consists of four principal microfacies: a mudstone, a wackestone and two different packstones. The 30 to 120-cm thick Cerithium Limestone Member fills depressions between low-amplitude mounds in the Maastrichtian chalk. The lowermost part constitutes a thin layer of a bryozoan-rich packstone, probably reworked from the crests of the Maastrichtian mounds. The successive part of the member is dominated by wackestone with mainly foraminifera (planktic and benthic), molluscs and echinoderm debris, and in some areas an abundance of peloids. The foraminifera- and mollusc-rich packstone appears in lenses. The mudstone contains few foraminifera and is linked to burrows and syn-sedimentary fractures. SEM observations revealed that the Cerithium Limestone Member corresponds to a dispersed micrite, with small calcite crystals ~1–4 μm in size. The general shape of these calcite crystals suggests precipitation from cyanobacterial activity and, thus, a microbial genesis for the micrite of the Cerithium Limestone Member.

Keywords: Cerithium Limestone Member, Stevns Klint, Cretaceous–Palaeogene boundary, carbonate microfacies, thin sections, Danian, microbial micrite.

Tjördis Störling [tjordis.storling@geol.lu.se], Isaline Demangel [isaline.demangel@geol.lu.se], Anders Lindskog [anders.lindskog@geol.lu.se], Mikael Calner [mikael.calner@geol.lu.se], Jacob Andersson [ja0503an-s@student.lu.se], Daniel J. Conley [daniel.conley@geol.lu.se], Sylvain Richoz [sylvain.richoz@geol.lu.se], Department of Geology, Lund University, Sölvegatan 12, 223 62 Lund, Sweden.

The Cretaceous–Palaeogene (K–Pg) mass extinction at 66 Ma represents one of the five largest extinctions in the past 500 million years, with the disappearance of ~75% of marine species (e.g., Alvarez *et al.* 1980; Schulte *et al.* 2010). This extinction event was triggered by the impact of a large asteroid (e.g., Alvarez *et al.* 1980; Schulte *et al.* 2010; Hull *et al.* 2020) in the Yucatán Peninsula of Mexico (Fig. 1) and, within a broader time frame, by the massive Deccan flood basalt volcanism (e.g., Chenet *et al.* 2009; Schoene *et al.* 2019). It resulted in catastrophic changes of the Earth's climate and ecosystem disruptions (Schulte *et al.* 2010). In the marine realm, ocean acidification, darkening and cooling had a significant impact on primary producers (Hull *et al.* 2020), particularly calcifiers living in the photic zone (Olsson *et al.* 1999; Bown 2005; MacLeod *et al.* 2007; Bralower *et al.* 2020).

This disturbance of the food chain enabled the emergence of a new ecological equilibrium, with diatoms and dinoflagellates dominating over calcareous nannoplankton (Katz *et al.* 2004; Knoll & Follows 2016). Consequently, the carbon cycle underwent significant transformations (Birch *et al.* 2016), with changes in the export, burial and accumulation rates of organic carbon (e.g., Zachos & Arthur 1986; D'Hondt 2005; Henehan *et al.* 2016; Alvarez *et al.* 2019; Sepúlveda *et al.* 2019).

Extensive research has been conducted on the extinction interval, yet the understanding of the recovery processes in the earliest Paleocene has received less focus. Palaeontological and geochemical studies have provided an increasingly detailed record of the biotic and climatic/environmental development through the early Paleocene (e.g., Rasmussen *et al.* 2005; Gilleaudeau *et al.* 2018; Alvarez *et al.* 2019; Westerhold *et al.* 2020; Frederiksen *et al.* 2024). To date few detailed and systematic studies of the microfacies characteristics in thin sections from lower Paleocene strata have been published. Studies in sedimentology and carbonate microfacies can be used to better understand the sea-floor environment, including surface and intra-sediment processes, in the earliest aftermath of the K–Pg event. The coastal cliffs along Stevns Klint in south-eastern Denmark (Figs 1B, 2) provide an excellent succession that spans the upper Cretaceous to the lower Palaeogene (Fig. 3) and the opportunity to investigate the development of non-tropical carbonate depositional systems throughout this time interval. There, the Cerithium Limestone Member of the Rødvig Formation is found in the lowermost part of the local Palaeogene succession.

This study aims to clarify the genesis and palaeoenvironmental conditions of the deposition of the limestone by providing a detailed analysis of the microfacies and microfossil content of the Cerithium Limestone Member in the Rødvig section of Stevns Klint.

Geological setting and stratigraphy

Stevns Klint is a 14.5 km long coastal cliff in eastern Denmark (Fig. 2A). The cliffs rise up to 20 m above sea level, and the exposed succession exhibits the transition from the white chalks of the Maastrichtian (*c.* 72–66 Ma) to the bryozoan-rich mounds of the lower Danian (e.g., Surlyk 1997; Hart *et al.* 2005; Surlyk *et al.* 2006). The Stevns Klint succession (Fig. 3) is well known for the iridium anomaly documented by a thin but distinct clay bed known as the Fiskeler Member (Rødvig Formation), which gave rise to the hypothesis that an asteroid impact caused the mass extinction at the K–Pg boundary (Alvarez *et al.* 1980).

The Maastrichtian chalk of the Møns Klint Formation is divided into the Sigerslev Member and the Højerup Member (Fig. 3). The Sigerslev Member corresponds to a white mound-bedded chalk (Surlyk *et al.* 2006), which is exposed to a maximum of 32 m along the cliff. The overlying unit, the Højerup Member, is a 4–5 m thick bryozoan-rich grey chalk of the uppermost Maastrichtian (Surlyk *et al.* 2006). The lower Danian limestones are subdivided into two formations: the Rødvig Formation with the Fiskeler and the Cerithium Limestone members, and the Ste-

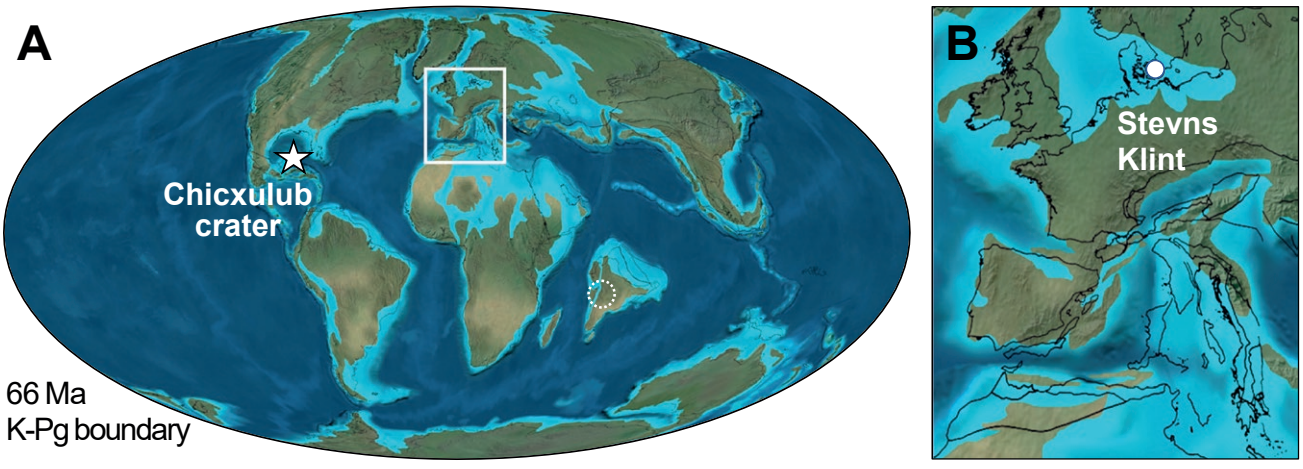

Fig. 1. Palaeogeographical maps during the Cretaceous–Palaeogene boundary interval (*c.* 66 Ma). **A**: Global palaeogeographical reconstruction with the Chicxulub impact site (white star) and the Deccan traps (white, dashed line). **B**: Map of the palaeogeography of Europe with the study site at Stevns Klint (white dot, palaeolatitude 44.53°N). Green: land, light blue: shallow seas, dark blue: open oceans. © 2016 Colorado Plateau Geosystems Inc. Modified from Sepúlveda *et al.* (2019).

vns Klint Formation with the Korsnæb Member (Fig. 3). The Danian Fiskeler Member with the iridium anomaly at its base (Alvarez *et al.* 1980), is a stratified clay-marl layer typically 5–10 cm thick lying just above the K–Pg boundary (e.g., Surlyk *et al.* 2006). It reaches a maximum thickness of ~ 45 cm at Kulstirenden in the northern part of Stevns Klint (Hart *et al.* 2005; Fig. 2B). This thin unit passes gradually or, in certain places, abruptly upwards into the lower Danian Cerithium Limestone Member (Surlyk *et al.* 2006; Rosenkrantz *et al.* 2021).

The sampling location for the present study, called the Rødvig section, is situated at the southern end of Stevns Klint, immediately east of Rødvig at Korsnæb (55.25403°N, 12.39624°E; Fig. 2B).

The Cerithium Limestone Member

The Cerithium Limestone Member is named after the gastropod genus *Cerithium* (Forchhammer 1825). Despite numerous studies (e.g., Forchhammer 1825; Nielsen 1917; Rosenkrantz 1924; Bernecker & Weidlich 2005; Heinberg 2005; Machalski & Heinberg 2005; Surlyk *et al.* 2006; Gilleaudeau *et al.* 2018; Rosenkrantz *et al.* 2021) the depositional conditions of the Cerithium Limestone Member are not completely understood.

The Cerithium Limestone Member has a typical thickness of about 30–60 cm (Surlyk *et al.* 2006). In northern sections, such as Korsnæb and Kulstirenden, its thickness can reach up to 80 cm and 120 cm, respectively (Hart *et al.* 2005; Surlyk *et al.* 2006). A dense network of *Thalassinoides* burrows and flint nodules in the upper part form a striking characteristic of the unit (Surlyk *et al.* 2006). The *Thalassinoides* burrows are concentrated horizontally and form an important local marker horizon below a syn-sedimentary hardground (e.g., Ekdale & Bromley 1984; Surlyk 1997). This hardground surface reflects a fall in sea level coupled with submarine erosion and a hiatus (e.g., Rosenkrantz 1924; Surlyk *et al.* 2006). The prominent erosion surface truncates both the Cerithium Limestone Member and the crests of the Maastrich-

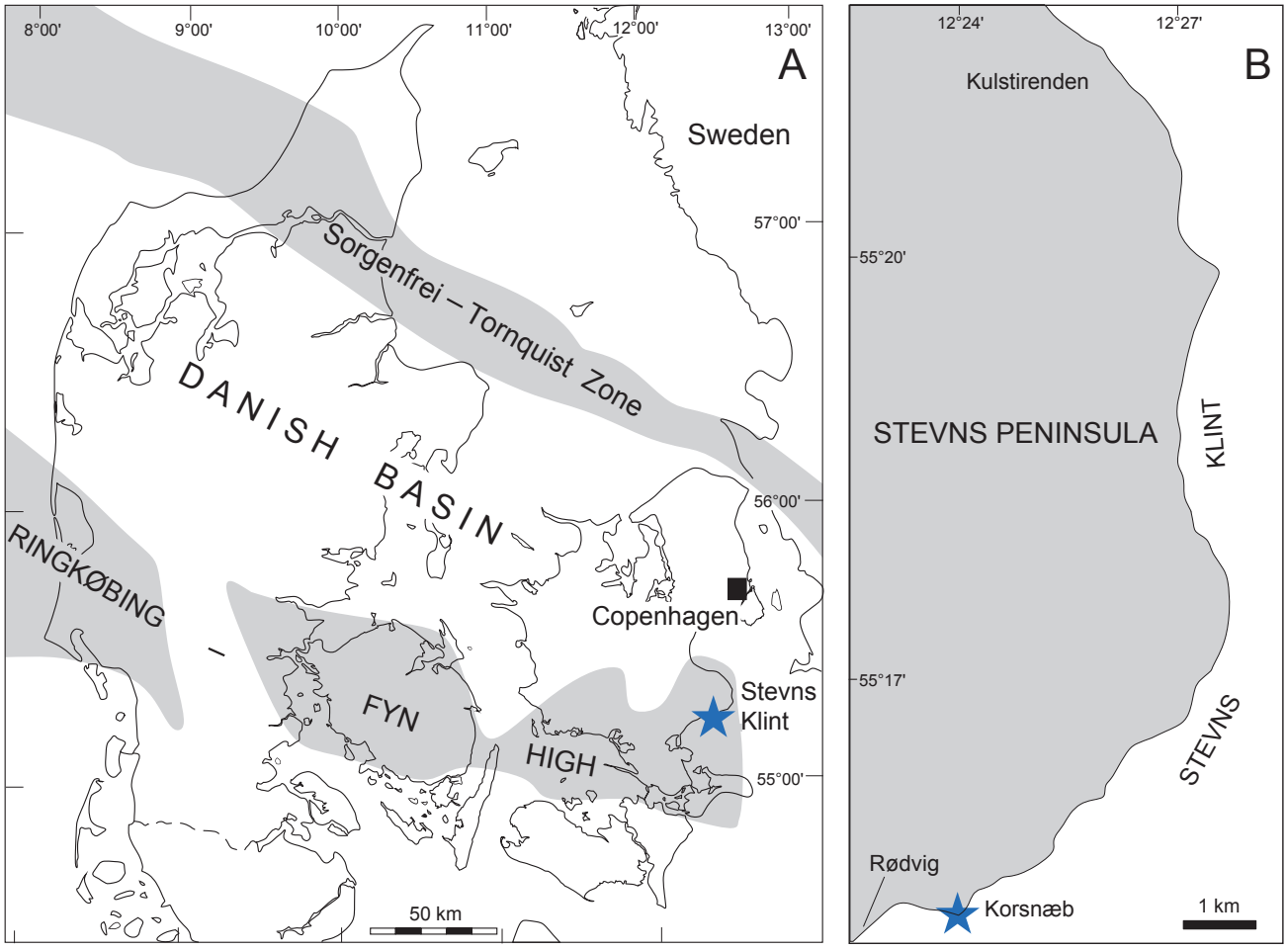

Fig. 2. A: Map of Denmark showing the major structural elements and the position of the studied section at Stevns Klint (blue star). **B**: Map of Stevns peninsula showing the location of the studied section at Korsnæb (55.25403°N, 12.39624°E), east of Rødvig. Modified from Rosenkrantz *et al.* (2021).

tian mounds of the Højerup Member and forms the base for the lower Danian bryozoan mounds of the Korsnæb Member (Stevns Klint Formation; Surlyk *et al.* 2006; Rosenkrantz. *et al.* 2021).

A wavy relief of the erosion surface suggests that the original sea-floor topography was formed by WNW-flowing bottom currents (Surlyk & Lykke-Andersen 2007). After erosion, the remaining Cerithium Limestone Member is preserved as a disjointed series of small depression fills, which are separated by truncated Maastrichtian mounds (Surlyk *et al.* 2006). The Cerithium Limestone Member shows thinning, condensation, or even erosion in the northern part of the Stevns Klint area (e.g., Surlyk *et al.* 2006). The depositional environment of the unit was marine and ranged from mid-neritic (30–100 m water depth) to a deeper milieu, as suggested by a high proportion of planktic foraminifera (e.g., Rasmussen *et al.* 2005; Surlyk *et al.* 2006).

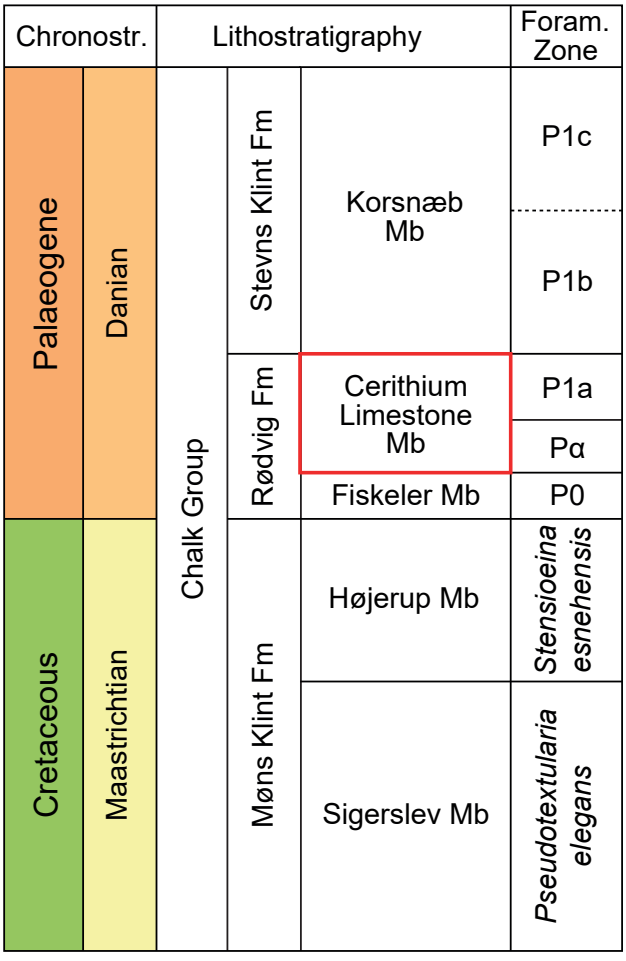

Fig. 3. Chronostratigraphy of the Cretaceous-Palaeogene interval along with the lithostratigraphy and the foraminiferal zonation at Stevns Klint. The Cerithium Limestone Member is indicated by a red rectangle (modified from Surlyk *et al.* 2006).

The Cerithium Limestone Member has been described both as fossil-poor, with only gastropods, echinoderms and crinoids (Rosenkrantz 1939), and as fossil-rich, with additional foraminifera (e.g., Schmitz *et al.* 1992; Hart *et al.* 2005; Rasmussen *et al.* 2005), bivalves (Heinberg 1999), siliceous sponges (Bernecker & Weidlich 2005), ammonites (Machalski & Heinberg 2005) and rare bryozoans (Heinberg 2005). Several species surviving the K–Pg event have been documented from the Cerithium Limestone Member, with the most remarkable discovery being several ammonites (Machalski & Heinberg 2005). Biostratigraphic studies have resulted in contrasting evidence and opinions concerning the age and duration of the Cerithium Limestone Member (Rasmussen *et al.* 2005).

Materials and methods

Two sampled profiles across the Cerithium Limestone Member at Rødvig were analysed. The initial profile is a 60 cm thick block that encompasses the entire vertical extent of the unit. To gain comprehensive insights into microfacies and the fossil content, twelve samples were selected for thin section production. The samples were chosen based on distinct characteristics of the limestone, such as burrows, colour changes or textural variations. Seventeen samples were prepared for scanning electron microscope (SEM) analyses, representing the various microfacies of the Cerithium Limestone Member. These samples were used to analyse the microfacies at the micro- and nanometre scales. Following the observation of diverse microfacies, seven additional samples were collected from a 60 cm vertical profile, with number 2 at the base until number 8 at the top of the section (Fig. 4). These samples were prepared for quantitative analyses of bioclast content and microfacies variability in the stratigraphic succession. From these seven samples, a total of fifteen thin sections were produced, with one per sample along the main vertical profile and duplicates for certain samples: two for sample 3, three for sample 4, one for sample 5 and two for sample 7.

During the thin section preparation, due to the brittle and soft nature of the Cerithium Limestone Member, the samples were embedded in epoxy, using a vacuum chamber to prevent any damage. Subsequently, the samples were manually ground and polished. Observations were conducted using an Olympus BX50 petrographic microscope equipped with a digital camera (Olympus SC50) and an electronic stepping stage for point counting, at the Department of Geology, Lund University. Lithologies

were classified according to the Dunham classification (Dunham 1962) and the modified scheme of Embry & Klovan (1971). Analyses of the microfacies (e.g., composition, fabrics and textures) were carried out according to Wilson (1975) and Flügel (2010).

The characteristics of the thin sections were quantified using Petrog 5 software. A random grid of points was selected, with the number of counts per thin section set at 250, as the threshold for statistical significance is considered to be at around 200 counts (Galehouse 1971). The bioclasts were classified at the order level, distinguishing between benthic and planktic foraminifera. Bioclasts were typically counted only if the pointer of the crosshair hit their shells, although complete shells were included in the count if the crosshair hit inside them. Variations in matrix colouration were divided into three groups: dark, intermediate and light matrix.

The samples for the SEM study were cut, polished and sputter-coated with platinum-palladium (Cressington sputter coater 108 auto, 20 mA, 20 seconds). The selection of seventeen samples was studied using a Tescan Mira3 High-Resolution Schottky field emission-scanning electron microscope equipped with an Oxford energy dispersive X-ray spectroscopy (EDS) at the Department of Geology, Lund University. Samples were imaged and analysed for microstructures related to sediment-influencing/-producing organisms and diagenetic processes. EDS was used for elemental analyses and to determine the chemical composition of the main components. Additionally, calcareous nannofossils were quantified along one

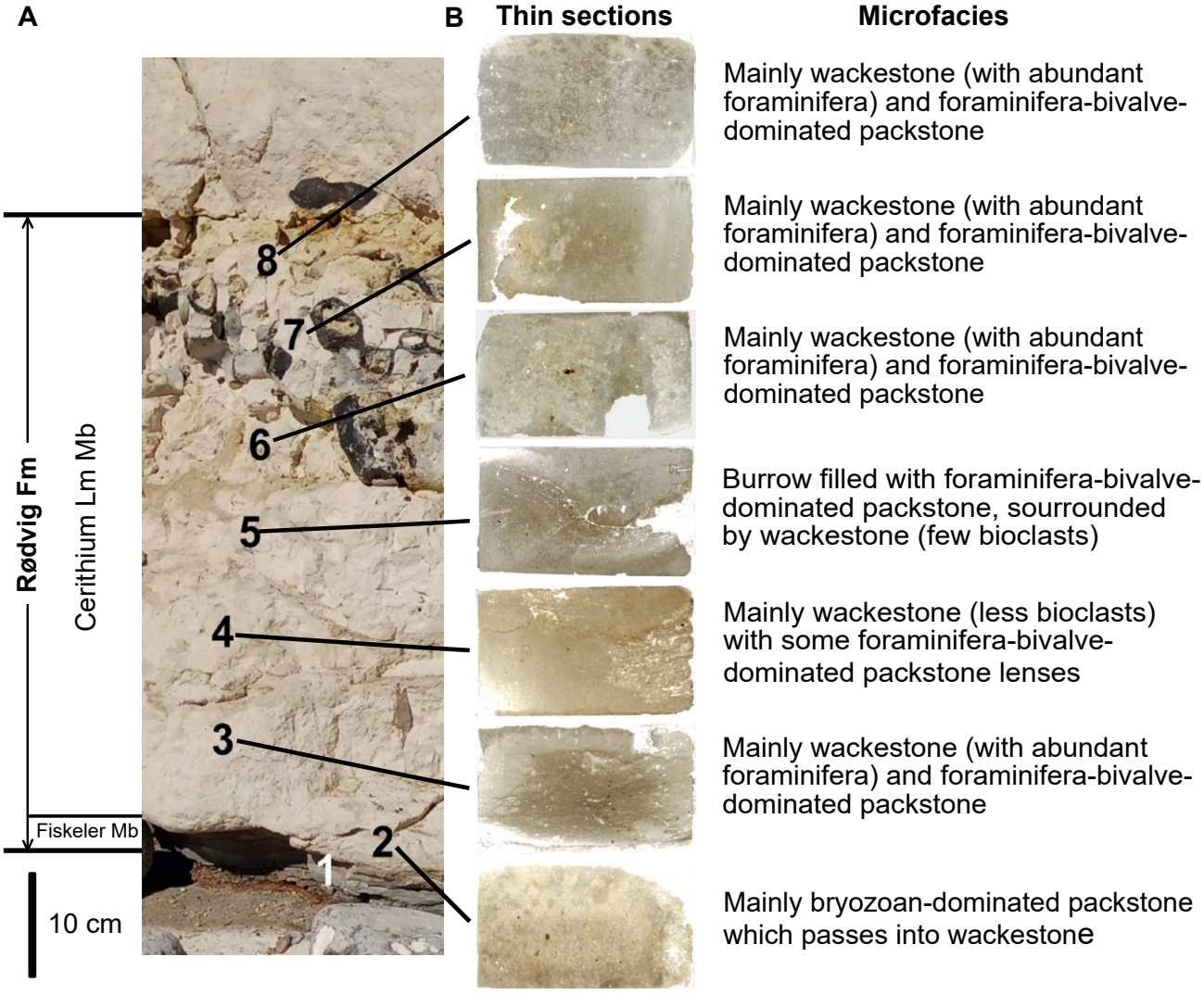

Fig. 4. Representation of the studied Rødvig section. **A**: Outcrop photograph of the K–Pg boundary strata east of Rødvig, indicating the sample levels. The Rødvig Formation includes the lowermost Danian Fiskeler Member, recording the iridium anomaly, and the overlying Cerithium Limestone Member studied in detail herein. **B**: Scanned images of seven thin sections from the vertical profile of the Cerithium Limestone in stratigraphic order with a description of their microfacies.

transect of ~1 cm in three samples: one at the base, one at the middle and one at the top of the section. All sample materials and thin sections are stored at the Department of Geology, Lund University, Sweden.

Results

The Cerithium Limestone Member in our section is ~ 0.6 m thick, beige-yellowish with an unevenly exposed surface (Figs 4, 5). The relatively soft lower part exhibits a beige colour, while the more cemented upper part appears pale yellow. At the macroscopic scale, the lithology appears homogeneous, with brown bioturbation tracks scattered throughout the section. Macrofossils occur locally and observed specimens include gastropods that are preserved as moulds.

Thin sections analyses – sedimentary microfacies

The position, overview image, microfacies and bioclast content of the thin sections along the vertical

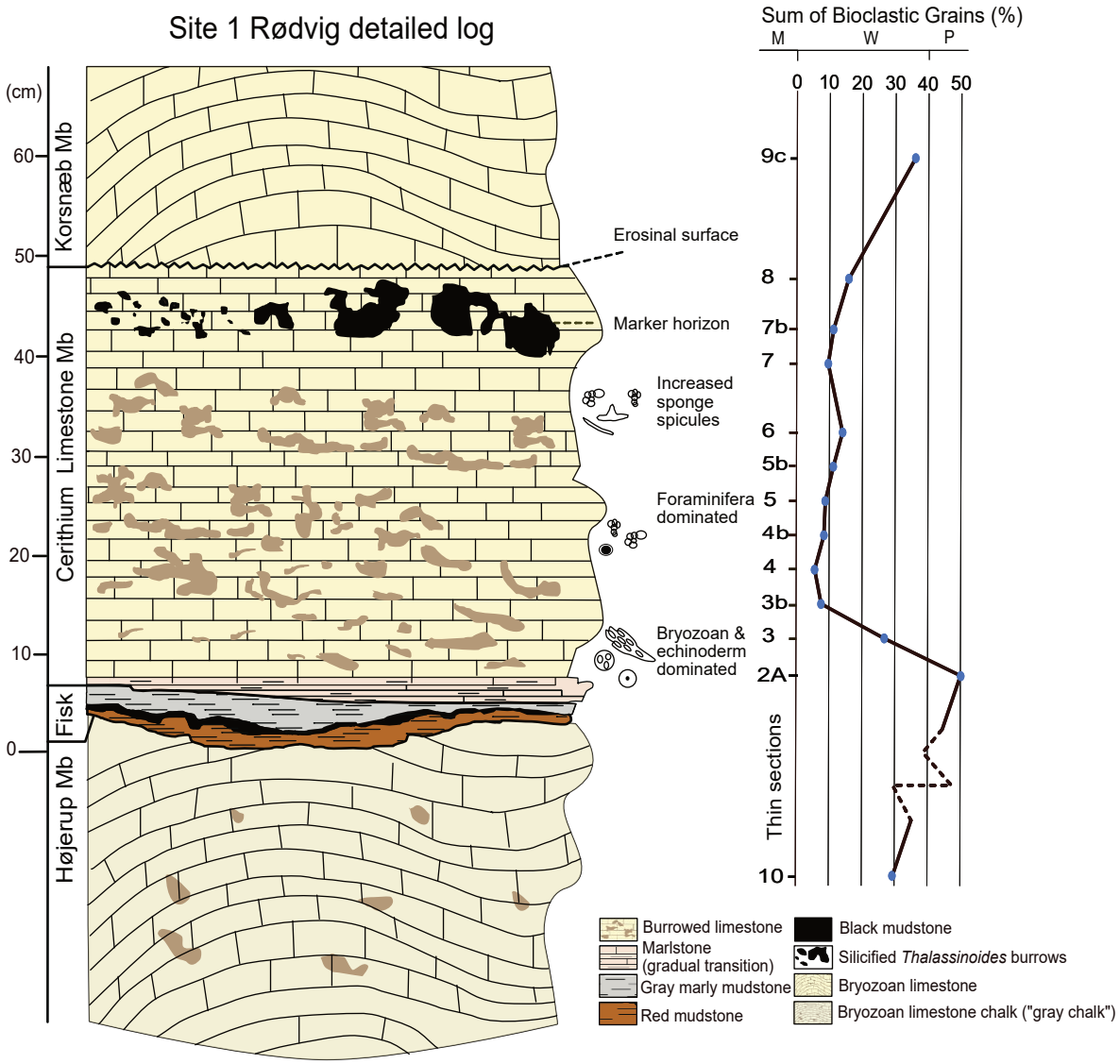

Fig. 5. Schematic representation of the Rødvig section, including the height, members and lithology, along with the total abundance of bioclasts in percentages. The different members of the sample site at Rødvig are on the left, Fisk: Fiskeler Member. Point counting results with bioclastic amounts are shown to the right of the log with the samples matched with the log's vertical scale. The percentage bioclastic amounts are grouped according to Dunham's classification with mudstone (M), wackestone (W) and packstone (P) respectively. The 0 in the section is the base of the Rødvig Formation, located approximately 1 m above sea level at the studied site. Highlights of the general fossil content from the samples are shown next to the log.

profile are summarised in Figs 4 and 5. Thin section analyses show that the Cerithium Limestone Member is composed of four distinct microfacies: a carbonate mudstone (Fig. 6A), a predominant wackestone (Fig. 6B), a foraminifera-bivalve-dominated packstone (Fig. 6C) and a bryozoan-dominated packstone (Fig. 6D).

Mudstone. The mudstone (Figs 6A1, A2) has less than 10% grains and is dominantly beige. The mud-sized matrix is mixed with few dark grey peloids, red iron oxides and yellowish pyrite. Recognisable fossils are scarce in this microfacies, with only a few bivalves, gastropods and foraminifera. Scattered benthic and planktic foraminifera are present with either the test preserved (Fig. 6A1) or just as a mould (Fig. 6A2). Most foraminifera tests or moulds are filled with black or brownish sediment. Small burrows are present within the mudstone and are filled with a foraminifera-bivalve-dominated packstone. The burrows are rich in bioclasts, including planktic and benthic foraminifera, ostracods, bivalves, gastropods, echinoderms and sponge spicules.

*Wackestone***.** The light grey wackestone contains iron-oxides and a larger number of pyrite and bioclasts compared to the mudstone (Fig. 6B1). In certain places, it contains large amounts of small dark grey peloids. Most fossils are planktic and benthic foraminifera, presenting a relatively broad range of sizes and species. Bivalves, ostracods, gastropods, echinoderms and bryozoans are also commonly observed. Calcareous dinoflagellates occur sparsely. The wackestone shows burrows with an infilling of a foraminifera-bivalve-dominated packstone (Figs 4B, 5). Abundant and relatively diverse bioclasts, with different sizes of planktic and benthic foraminifera, ostracods, bivalves, gastropods, echinoderms and sponge spicules, are identified in the burrows. Upon examination under a fluorescence light microscope, one of the burrows exhibits a white outline, indicating the presence of organic matter. Smaller burrows within the wackestone are filled with a fossil-rich packstone or wackestone. This packstone is rich in bioclasts including planktic and benthic foraminifera, ostracods, bivalves, gastropods, echinoderms and sponge spicules. Overall, the two described types of burrows show a high abundance of fossil assemblages, whereas a third type of burrows with a fine-grained mudstone infilling nearly lacks bioclasts as only a few scattered foraminifera are visible (Fig. 6E). These small-scale or micro-burrows with a diameter range <1 mm have multiple branching points and show in certain cases a connection to larger vertical shafts (Fig. 6E). They show an irregular margin and a branched distribution pattern in thin sections. They might represent thin *Chondrites* (Baucon *et al.* 2020). Note that due to significant differences in hardness and lithification, some parts of the fine-grained burrow infills were lost during the polishing of the thin sections (Fig. 4).

*Foraminifera-bivalve-dominated packstone***.** This packstone (Fig. 6C1) is dark brownish with a fine-grained matrix, iron oxides, pyrite, clay particles and peloids of different sizes. This microfacies is richer in bioclasts, including abundant and diverse planktic and benthic foraminifera, gastropods, bivalves, corals, ostracods, echinoderms and calcified sponge spicules. Bryozoans are scarce and skeletal grains often appear in clusters. The above-mentioned small-scale or micro-burrows with a fine-grained mudstone are also present in this packstone.

*Bryozoan-dominated packstone***.** This packstone (Fig. 6D) contains a large amount of bryozoan debris, broken mollusc shells, small foraminifera, calcite crystals, small oxides and small to large pyrites. The micrite has a beige colour with abundant, minute bioclastic debris and peloids. In certain areas, it could be referred to as a wackestone. No burrows were seen in this microfacies. The bryozoan-dominated packstone is only present in sample 2 (Figs 4, 5, 6D), just above the Fiskeler Member. The transition to the dominating wackestone microfacies is observed in sample 3.

Vertical stratigraphic development

Along the vertical profile, the first 7–12 cm above the Fiskeler Member are mainly composed of the bryozoan-rich packstone (sample 2; Figs. 4, 5, 6D). Above this, a progressive transition over several centimetres into the dominant wackestone microfacies is visible, marked by the disappearance of bryozoan components. Throughout the Cerithium Limestone Member, foraminifera-bivalve-dominated packstone forms isolated concentrations, mostly associated with burrowing activity. The mudstone microfacies is frequently observed in small fractures and burrows (Fig. 6E).

Except for the lowermost bryozoan-dominated layer, the most abundant fossils in the Cerithium Limestone Member (under light microscope) are planktic and benthic foraminifera, with a predominance of the latter. Transitions between microfacies are either sharp, especially between burrows and the surrounding rock, or gradual, with a progressive increase in the number of bioclasts.

Bioclast abundance

The point counting results (Fig 5, supplementary material, Table S1) indicate the highest abundance of bioclasts, reaching up to 50% of bioclastic grains, in

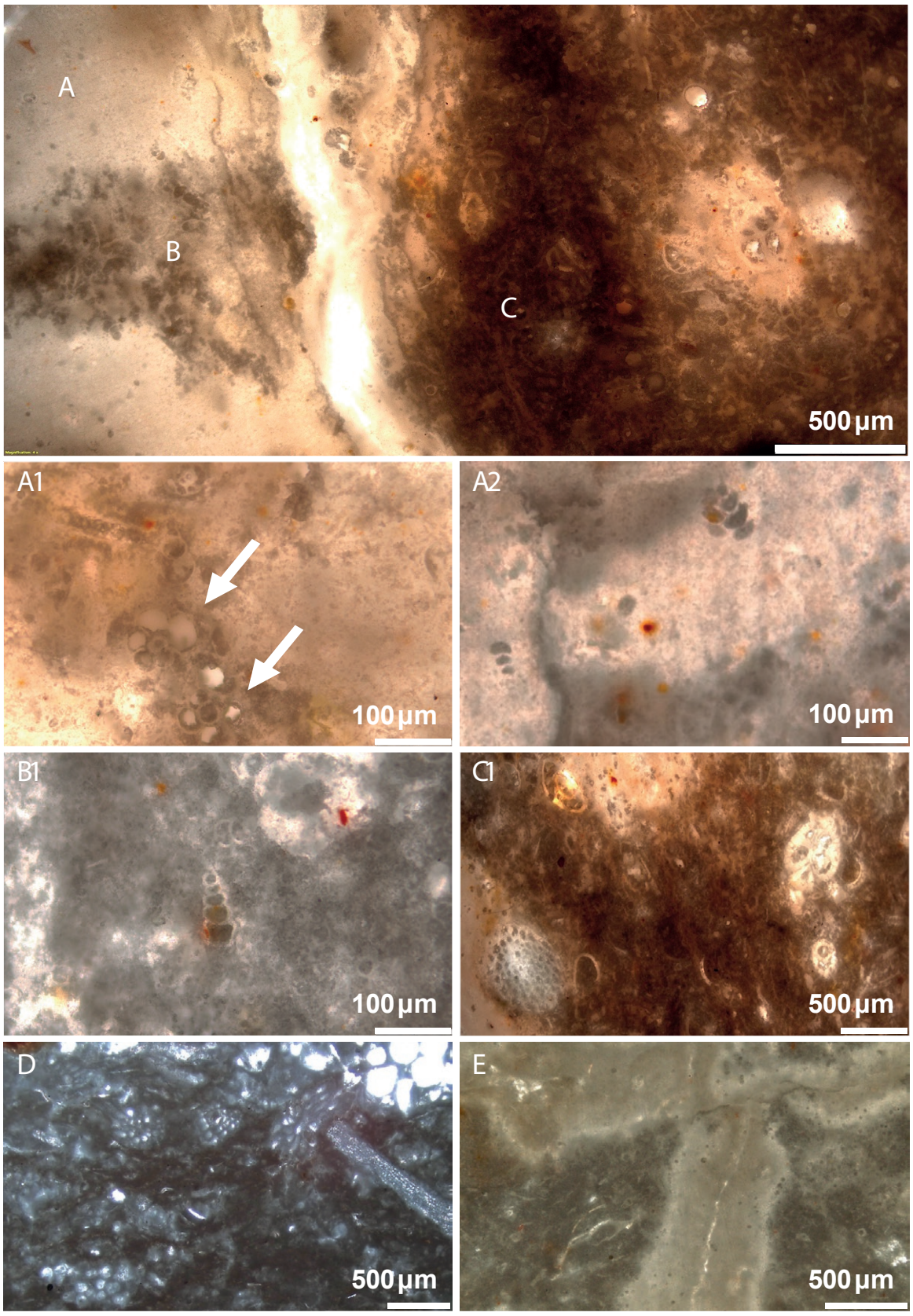

Fig. 6. Optical microscope images of thin sections from the Cerithium Limestone show four different microfacies with A: mudstone, B: wackestone, C: foraminifera-bivalve-dominated packstone and D: bryozoan-dominated packstone. **A1,2**: Mudstone including preserved foraminifera test (A1) and filled moulds of foraminifera (A2). **B1**: Wackestone with foraminifera. **C1**: Foraminifera-bivalve-dominated packstone with abundant fossil content. **D**: Bryozoan-dominated packstone with abundant bryozoans. **E**: A burrow in wackestone filled with mudstone.

the basal sample 2 corresponding to the bryozoan-rich packstone microfacies. The grain abundance gradually decreases to around 10% in the main part of the Cerithium Limestone Member through samples 3 to 7. The uppermost part of the Cerithium Limestone Member is characterised by an increase in abundance with around 15% bioclastic grains, mainly calcified sponge spicules and rare bryozoans.

SEM analyses

Microfacies analyses under SEM

Under the SEM, the mudstone and wackestone exhibit the highest porosity (Figs 7, 8). The freshly cut and polished samples show deep and elongated holes in the matrix. Cementation occurs sparsely in those two microfacies and consists of low-Mg-calcite crystals without silica, as indicated by elemental mapping. The matrix of the wackestone and mudstone microfacies is composed of small crystalline calcite with a dominance of 1–4 μm crystals (Fig. 7). Very small, equant crystals below 1 μm in size occur in clusters and crystals up to 10 μm are also present. Calcite spar crystals of up to 15 μm were occasionally observed. In general, the shape of the crystals shows a variety of polyhedral forms with reduced corners but edges visible. Dissolution attributed to early diagenetic alterations is apparent on both the matrix and crystals in all microfacies (Fig. 7 A, B). Observations reveal cracks and dissolution pits, along with crystals with reduced corners and edges, leading to the transformation of rhombohedral shapes into polyhedral forms (Fig. 7 A, B).

Changes in microfacies are either gradual (Fig. 8A), with a progressive increase in the number of bioclasts, or sharp, especially between burrows and the surrounding rock. In the wackestone, bioclasts are loosely packed, with few in close contact with each other (Fig. 8B). Sharp boundaries are most commonly found in the transition zone from the mudstone to the foraminifera-bivalve-dominated packstone (Fig. 8F). A change from the mudstone and wackestone to the foraminifera-bivalve-dominated packstone is clearly visible through a significant increase in bioclasts (Figs 8A, C, F). Densely packed bioclasts are present in both packstone varieties (Figs 6C1, D, 8D, E). The packstones

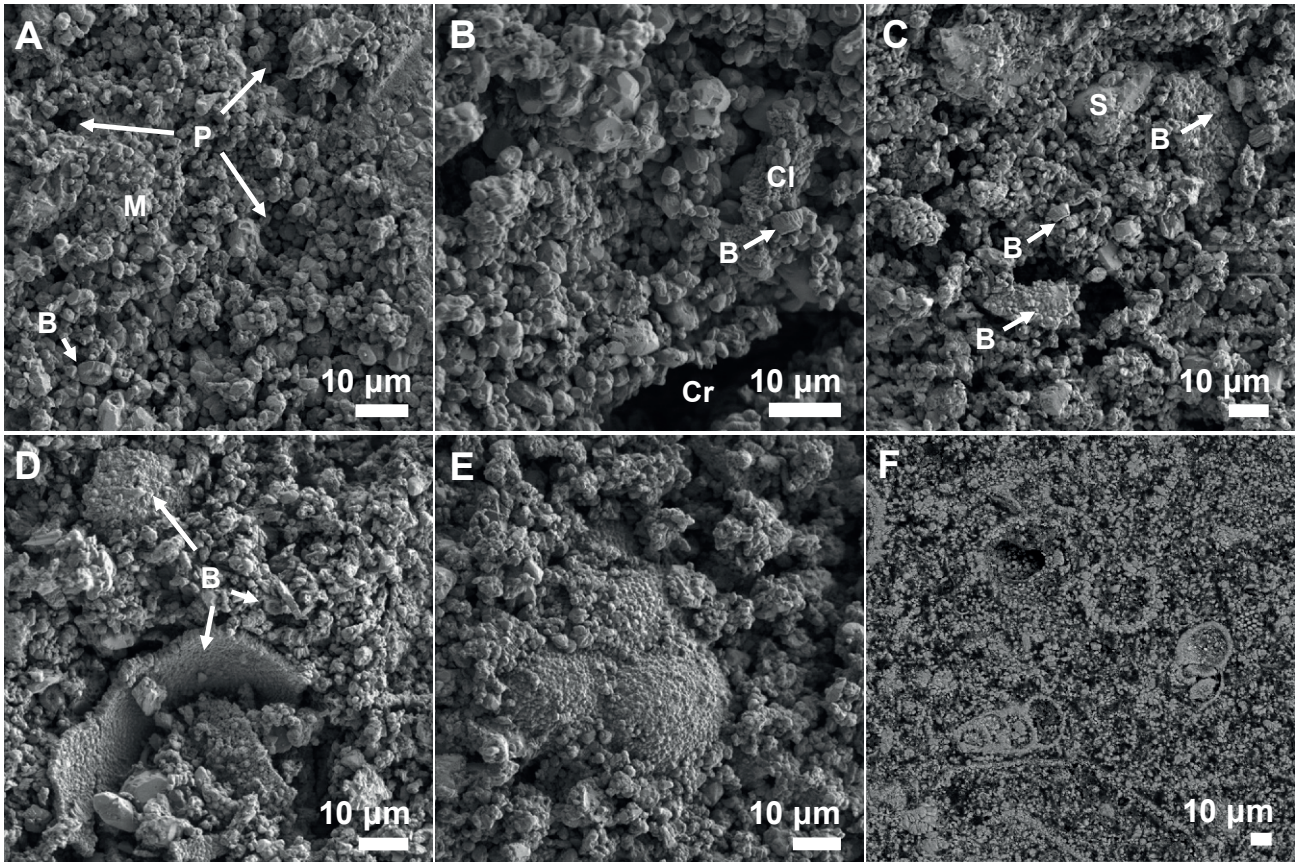

Fig. 7. Scanning electron microscopy images of the four different microfacies in the Cerithium Limestone. **A**: Mudstone. **B**: Wackestone with cracks and clusters. **C**: Foraminifera-bivalve-dominated packstone with bioclasts and spar. **D**: Foraminifera-bivalve-dominated packstone with bioclasts. **E**: Foraminifera covered in fine microcrystals in the wackestone. **F**: Bryozoan-dominated packstone, B: bioclasts, Cl: cluster, Cr: crack, M: micrite, P: porosity, S: spar.

are less porous than the other two microfacies (Figs 7C, D, F). Deep and elongated cracks are absent, and crystals have more contact surfaces in between. The size and shape of the calcite crystals are highly variable, with increasingly larger crystals including some exceeding 15 μm (Fig. 7C). However, as for the other microfacies, micrite with crystals smaller than 4 μm is dominant. Most crystals show a rough surface with many cracks. Cement is present in the foraminifera-bivalve-dominated packstone and consists of low Mg-calcite and no silica, as indicated by element mapping (see supplement Fig. S1).

Microfossil analyses under SEM

Studies of the microfossil content under the SEM show a few scattered foraminifera and calcareous nannofossils in the mudstone, while the wackestone shows more abundant fossils (Figs. 7B, E, 8B, D). Foraminifera were observed as fragments or complete with either the tests preserved covered by calcite microcrystals (Fig. 7E) or as imprints (Fig. 8B). Additionally, numerous calcareous nannofossils (Fig. 7D) with mainly coccoliths and few calcareous dinoflagellate cysts (see supplement Pl. S1) were observed in all microfacies with different abundances. Sample 2, at the base of the section, shows the poorest preservation and records the lowest abundance of calcareous nannofossils with ~ 8×10^2 nannofossils/cm^2 (Table S2). Sample 4 exhibits very good preservation with entire coccospheres and coccoliths preserved. This sample presents the highest abundance of calcareous nannofossils with ~ 1×10^4 nannofossils/cm^2 (Table S2). Sample 8, at the top of the section, exposes fewer calcareous nannofossils with ~ 3×10^3 nannofossils/cm^2 (Table S2). The coccolith assemblage comprises 10–15 (Pl. S1) species with a dominance of *Arkhangelskiella cymbiformis* (Vekshina 1959), *Biscutum castrorum* (Black & Barnes 1959), *Biscutum harrisonii* (Varol 1989), *Neocrepidolithus neocrassus* (Perch-Nielsen 1968; Romein 1979) and *Neocrepidolithus* spp. Rare *Ahmuellerella regularis* (Górka

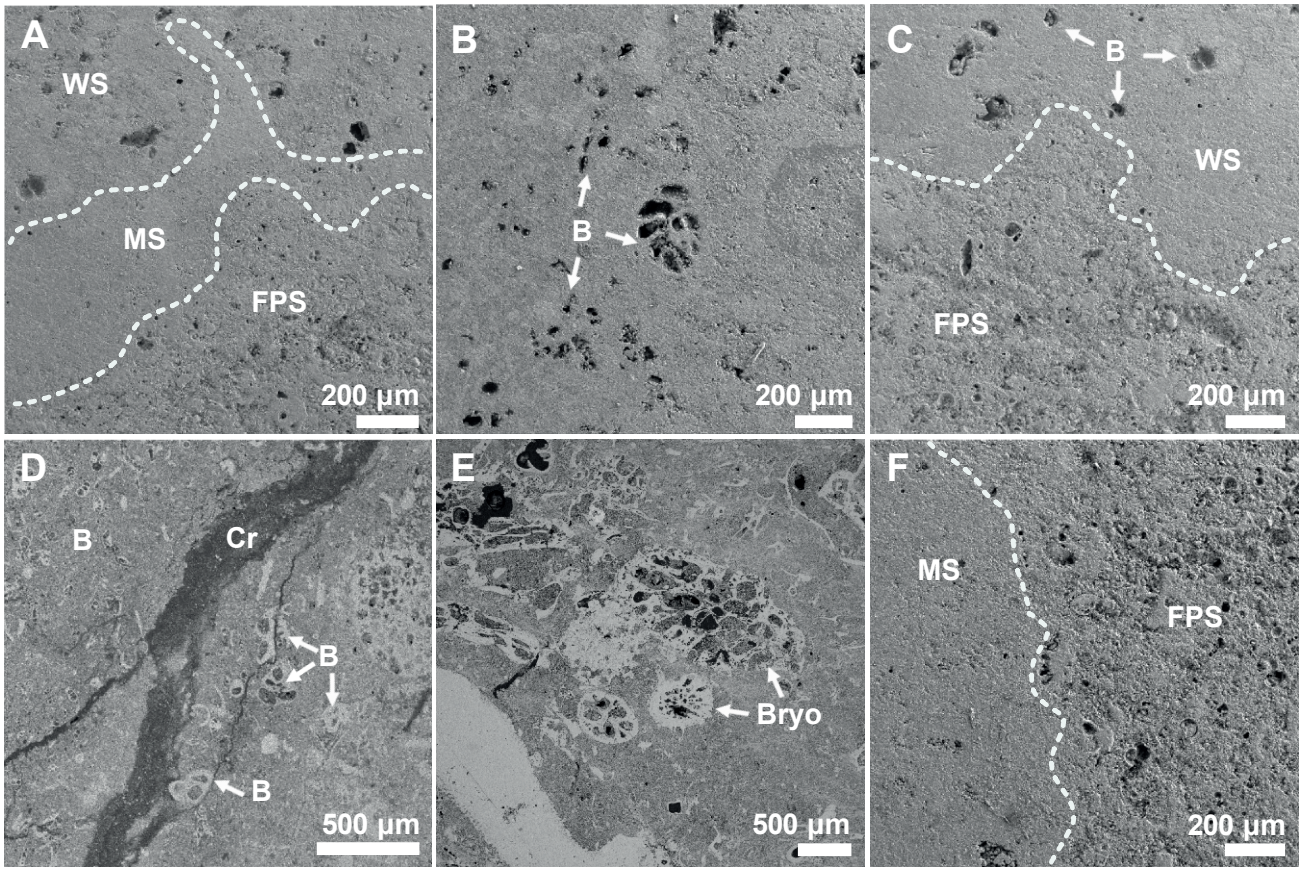

Fig. 8. Scanning electron microscopy images of thin sections from the Cerithium Limestone. **A**: Three microfacies of the upper part of the limestone with their boundaries illustrated in dashed lines. **B**: Wackestone with bioclasts including imprints of dissolved tests of foraminifera. **C**: Transition from wackestone to the foraminifera-bivalve-dominated packstone. **D**: Foraminifera-bivalve-dominated packstone with a high amount of preserved tests of foraminifera. **E**: Bryozoan-dominated packstone with bryozoans. **F**: Transition zone from foraminifera-bivalve-dominated packstone to mudstone. B: bioclasts, Bryo: bryozoans, Cr: crack, FPS: foraminifera-bivalve-dominated packstone, MS: mudstone, WS: wackestone. The white dashed line shows the transition between the microfacies.

1957; Reinhardt & Górka 1967), *Kamptnerius magnificus* (Deflandre 1959), *Nephrolithus frequens frequens* (Górka 1957), *Watznaueria fossacincta* (Black 1971; Bown & Cooper 1989), *Zeugrhabdotus sigmoides* (Bramlette & Martini 1964; Bown & Young 1997), *Markalius apertus* (Perch-Nielsen 1979), *Markalius inversus* (Deflandre & Fert 1954; Bramlette & Martini 1964), *Prediscosphaera stoveri* (Perch-Nielsen 1968; Shafik & Stradner 1971) and *Cyclagelosphaera alta* (Perch-Nielsen 1979) were observed. Calcareous dinoflagellates are mostly preserved as half-broken but well-preserved specimens of *Cervisiella operculata* (Bramlette & Martini 1964; Streng *et al.* 2004) with a size of up to 20 μm (Pl. S1).

Different fragments of bioclasts such as fish teeth, broken shells of macrofossils, bryozoans and microfossils were observed, with the highest amount in the packstone microfacies.

Discussion

Fossil content

The Cerithium Limestone Member is described as a fossil-rich unit with gastropods, echinoderms, crinoids, foraminifera, bivalves, calcified siliceous sponges, ammonites and occasionally bryozoans (e.g., Machalski & Heinberg 2005; Rasmussen *et al.* 2005). In our thin section analyses, we find two different parts within the Cerithium Limestone Member that may have stratigraphic significance. The lowermost part, in contact with the Fiskeler Member, consists of a bryozoan-dominated packstone with bivalves, foraminifera and gastropods (Figs 4, 5, 6D, 8E). This bryozoan-dominated packstone does not re-appear higher up in the Cerithium Limestone Member. The high amount of bryozoans and broken bioclasts, the presence of calcite crystals, and the low amount of micrite compared to the rest of the Cerithium Limestone Member, suggest reworking of older sediments. These may have originated from the crest of the Maastrichtian mounds surrounding the depression where the Cerithium Limestone Member has been preserved (Surlyk *et al.* 2006).

The upper, main part of the Cerithium Limestone Member is dominated by the wackestone microfacies with foraminifera, bivalves, gastropods, echinoderms, crinoids, calcified siliceous sponges and rare bryozoans. Despite poor preservation, Rasmussen *et al.* (2005) reported an abundant but low-diversity assemblage of foraminifera in the 40–125 μm fraction from the Cerithium Limestone Member. Standard foraminiferal biostratigraphy from different studies (e.g., Heinberg 2005; Rasmussen *et al.* 2005) indicates that the Cerithium Limestone Member belongs to the Pα and the P1a zones (Fig. 3). The section at Rødvig represents mainly the Pα foraminiferal zone and was possibly deposited within 400 ka (Heinberg 2005; Rasmussen *et al.* 2005; Ogg *et al.* 2016), with both the Pα and the P1a zones representing less than 800 ka (Ogg *et al.* 2016). These findings suggest that the wackestone was deposited during an initial stage of the post-extinction recovery interval during the earliest Danian, rather than being a result of reworking of older sediments.

Fossils have also been impacted by dissolution, as indicated by the visible internal and external moulds of test fragments of foraminifera, resulting from the dissolution of the original tests (Fig. 6A2). The random occurrence of those foraminifera moulds, both horizontally and vertically, suggests widespread dissolution affecting the entire section. Species-specific resistance or weakness to dissolution seems unlikely as both benthic and planktic species were affected. Imprints in the sediment suggest that the dissolution of the tests occurred after the lithification of the host rock. Poor preservation and issues such as dissolution and fragmentation of foraminifera have been reported previously (Hart *et al.* 2005; Rasmussen *et al.* 2005). Any (re-)evaluation of foraminiferal zonation along the cliff exposure should take into account the very local changes in the type of preservation of the foraminifera, which evidently can vary within a few centimetres.

The SEM observations revealed the presence of calcareous nannofossils, including dinoflagellate cysts in low abundance and coccoliths in higher abundance in all microfacies (Fig. 7). In contrast to the foraminifera, dissolution was not apparent in the calcareous nannofossils, which occur with good preservation; even coccospheres are preserved. Only the calcareous nannofossils in sample 2, just above the K–Pg extinction interval, show slight dissolution features. Quantification indicates an abundance of calcareous nannofossils ranging between 8×10^2 and 1×10^4 nannofossils/cm^2. Just prior to the K–Pg mass extinction, the latest Cretaceous recorded the highest abundance and diversity of calcareous nannofossils of the entire Mesozoic Era, with up to 149 recognised species and a yearly deposition on the order of 10^7 nannofossils/cm^2 (Bown *et al.* 2004; Suchéras-Marx *et al.* 2019). The low abundance and diversity (10–15 species) of calcareous nannofossils in the Cerithium Limestone Member attest to the K–Pg mass extinction event affecting calcifying nannoplankton.

Among the calcareous dinoflagellate cysts, *Cervisiella operculata* (Pl. S1) dominates the assemblage but does not occur in high abundance. *C. operculata* is abundant in low-latitude successions (Guerra *et al.* 2021) and is used as a marker for the earliest Danian

(McLachlan & Pospelova 2021). This species is described as a 'disaster taxon', flourishing in stressed environmental conditions (Wendler & Willems 2002; Hildebrand-Habel & Streng 2003; Bralower *et al*. 2020; Guerra *et al*. 2021; Mahanipour *et al*. 2022) due to reduced competition (Guerra *et al*. 2021) and the sudden appearance of vacant niches (Smit 2005). *C. operculata* is suggested to indicate warm water environments (Egger *et al*. 2009; Mohamed *et al*. 2012) and decreased primary productivity (Guerra *et al*. 2021).

In our samples, coccoliths were found in higher abundance than the calcareous dinoflagellate cysts. Using the terminology of Bernaola & Monechi (2007), the assemblage contains a few Cretaceous-vanishing (C-vanishing) species, such as *A. cymbiformis, A. regularis, K. magnificus, N. frequens frequens, P. stoveri* and *W. fossacincta*. The C-vanishing species include all Cretaceous species that became extinct at or below the boundary and species that progressively disappeared in the lowest metres of the Danian (Bernaola & Monechi 2007). The evolution of the calcareous nannoplankton across the K–Pg transition is not fully understood, but most studies explain the presence of the rare C-vanishing species by reworking (e.g., Bown 2005; Minoletti *et al*. 2005).

The Cretaceous-persistent (C-persistent) species are, on the contrary, considered survivors from the Mesozoic into the Cenozoic era (Bernaola & Monechi 2007). C-persistent species include Cretaceous species found in low abundance in the uppermost Maastrichtian but persist well into the Palaeogene, where their relative abundance increases (Bernaola & Monechi 2007). In our samples, C-persistent species are represented by *Biscutum* spp., *Markalius* spp., *Neocrepidolithus* spp., *Z. sigmoides* and *C. operculata*. They are relatively more abundant than the C-vanishing species, but our quantification results show a low total abundance, arguing in favour of the persistence of harsh environmental conditions during the deposition of the Cerithium Limestone Member. Finally, the presence of *C. alta* in sample 4 marks the appearance of a new Paleocene taxon.

Origin of the micrite

In the aftermath of the K–Pg event, oceanic productivity recovered rapidly in terms of biomass (Alegret *et al*. 2012) with hypothetical eutrophication supporting the plankton blooms (Alegret *et al*. 2012). Global post-impact 'whitings' caused by cyanobacterial blooms may have contributed to the formation of the pale grey marly chalk of the Fiskeler Member, directly underlying the Cerithium Limestone Member (Bralower *et al*. 2020). In certain localities, these global whiting events might have persisted for thousands of years after the K–Pg event (Bralower *et al*. 2020) and continued until the deposition of the Cerithium Limestone Member. Cyanobacterial blooms in whitings require $CaCO_3$ supersaturation in seawater (Jones *et al*. 2019). The abrupt extinction of calcifiers (Bown 2005) and a lowered $CaCO_3$-to-organic carbon rain ratio (Henehan *et al*. 2016) possibly resulted in supersaturated surface waters (Bralower *et al*. 2020).

The presence of cyanobacteria in the Fiskeler Member at Stevns Klint has been inferred on the basis of organic biomarkers for bacterial productivity (Sepulveda *et al*. 2009; Schaefer *et al*. 2020). A high abundance of steranes and hopanes (in the Fiskeler Member) reflects a rapid recovery (*c.* 10^2–10^3 years) of bacterial and algal production in the area (Sepúlveda *et al*. 2009), suggesting thriving cyanobacterial communities (Schaefer *et al*. 2020). The survival of cyanobacteria without significant losses in the extinction event (Sepulveda *et al*. 2009; Alegret *et al*. 2012) and their possibly unique adaptation to the extreme post-extinction environments may have contributed to micrite precipitation (Robbins & Blackwelder 1992; Thompson 2000; Obst *et al*. 2009; Bralower *et al*. 2020).

Although different microfacies occur in the Cerithium Limestone Member, the rock matrix is consistently dominated by small calcite crystals in the micron size range (< 4 μm; Fig. 7). In this respect, our observations confirm those of Hansen (1990). Hansen (1990) defined the rock unit as extremely loose, with no or little attachment between crystals and with a richness of small grains ranging between 1 and 5 μm in size. The dominance of calcite crystals smaller than 4 μm in size, with rare or absent microbioclast debris, suggests a microbial origin of the Cerithium Limestone Member, possibly from cyanobacteria (Flügel 2010). Moreover, EDS analyses of the four microfacies indicate a low-Mg-calcite composition, as also reported by Hansen (2019). Low-Mg calcite with microcrystals in the 1–9 μm size range is globally characteristic of Phanerozoic limestones (Kaczmarek *et al*. 2015) and is typical of cyanobacterial whiting (Bralower *et al*. 2020). Thus, we suggest that the micrite of the Cerithium Limestone Member was formed due to the high abundance of cyanobacteria. Abundant cyanobacteria would entail strong photosynthetic activity, leading to an increase in alkalinity that ultimately triggered whiting events, enabling the precipitation of micrite.

Microfacies types and environmental conditions

Our study reveals that the Cerithium Limestone Member mainly consists of two relatively distinct stratigraphic parts: the first is the lowermost part of the unit and likely constitutes a thin layer of Maastrichtian reworked material. The second and major part is a burrowed limestone comprising mudstone,

wackestone and foraminifera-bivalve-dominated packstone microfacies. These microfacies types are typical for open marine, mid–outer carbonate ramps/shelves (Flügel 2010). The bioclastic wackestone and packstone with diverse, common to abundant fossils and peloids (which occur as mudstone peloids in outer ramps), are characteristic of the outer ramp microfacies type RMF 3 (Flügel 2010). Notably, the microfacies occur randomly; in the vertical profile (Fig. 4), above sample 3, all three microfacies occur in each sample and no distributional pattern or depositional succession of the microfacies is discernible. An explanation for the random distribution of the microfacies might be a high degree of bioturbation as exemplified by *Thalassinoides*, *Spongeliomorpha*-type burrows (Ekdale & Bromley 1984) and other ichnofossils (Rasmussen 1971). The bioturbation can be partly described as endichinal (common) and exichnial (from above) with the toponymic classification system after Martinsson (1970). Burrows typically occur across the ramp but are particularly abundant below the wave base and storm wave base (Flügel 2010).

Deposition of the Cerithium Limestone Member in cooler, deeper waters was suggested by the finding of shark teeth belonging to species living in deeper waters (Adolfssen & Ward 2015). These conditions confirm the interpretation of an open marine, outer ramp setting for the deposition of the Cerithium Limestone Member as suggested by our detailed microfacies analyses. The deposition and accumulation of carbonate mud clouds from the water surface implies generally low-energy conditions in a calm marine area. However, it is plausible that seasonal and relatively strong winds or storm events resulted in periodic bottom currents (Bjerager & Surlyk 2007) and facilitated the transportation of fossils, which accumulated in previously formed burrows. In summary, we suggest that the Cerithium Limestone Member was deposited in an open marine, outer-ramp-like setting in a dominantly low-energy environment.

Conclusions

This study reports detailed descriptions of thin sections of the Cerithium Limestone Member (Rødvig Formation) at Stevns Klint, Denmark. Four main microfacies were identified during microscopic investigations: a carbonate mudstone, a wackestone and two types of packstones. Our study confirms that the Cerithium Limestone Member is composed of two stratigraphically distinct parts, as previously assumed. The lowermost part consists of a thin layer of a bryozoan-rich packstone, interpreted as reworked material from the crests of the underlying Maastrichtian mounds. The second major part of the rock unit is an intensely burrowed limestone consisting of wackestone with predominantly foraminifera, mudstone with few foraminifera and foraminifera-bivalve-dominated packstone microfacies. A random spatial distribution of the microfacies suggests a high degree of bioturbation, as indicated by a variety of burrows. It is possible that the Cerithium Limestone Member had previously shown some stratigraphic development in its (micro-)facies characteristics, but this was erased due to bioturbation. SEM and light microscopy observations enabled the identification of various fossils, including planktic and benthic foraminifera, gastropods, bivalves, corals, ostracods, echinoderms, calcified sponge spicules and nannofossils. The predominance of small calcite crystals (1–4 μm) and the general shape of these crystals indicate that a significant portion of the micrite might have been formed through precipitation driven by microbial activity. The Cerithium Limestone Member is interpreted as formed in a mainly low-energy, open-marine, outer ramp-like sedimentary environment. In conclusion, the thin sections of the Cerithium Limestone Member at Stevns Klint provided new insights into the genesis of this famous rock unit.

Acknowledgements

This research received funding from the European Research Council (ERC) under the European Union's Horizon 2020 Research and Innovation Programme (Grant agreement No. 833454) and by a grant from the Knut and Alice Wallenberg Foundation to Daniel J. Conley. Anders Lindskog acknowledges funding from the Birgit and Hellmuth Hertz' Foundation and the Royal Physiographic Society in Lund. We received a sample permit for this protected area from the Geo-Museum Faxe, thanks to Jesper Milàn. We thank Carl Alwmark and Josefin Martell for their help with the SEM. Constructive reviews by Morten Bjerager and Finn Surlyk are gratefully acknowledged.

References

Adolfssen, J.S. & Ward, D.J. 2015: Neoselachians from the Danian (early Paleocene) of Denmark. Acta Palaeontologica Polonica 60, 313–338. https://doi.org/10.14202/app.2012.0123

Alegret, L., Thomas, E. & Lohmann, K.C. 2012: End-Cretaceous marine mass extinction not caused by productivity collapse. Proceedings of the National Academy of Sciences

of the United States of America 109, 728–732. https://doi.org/10.1073/pnas.1110601109

Alvarez, L.W., Alvarez, W., Asaro, F. & Michel, H.V. 1980: Extraterrestrial cause for the cretaceous-tertiary extinction. Science 208, 1095–1108. https://doi.org/10.1126/science.208.4448.1095

Alvarez, S.A., Gibbs, S.J., Bown, P.R., Kim, H., Sheward, R.M. & Ridgwell, A. 2019: Diversity decoupled from ecosystem function and resilience during mass extinction recovery. Nature 574, 242–245. https://doi.org/10.1038/s41586-019-1590-8

Baucon, A. *et al*. 2020: Ethology of the trace fossil Chondrites: Form, function and environment. Earth-Science Reviews 202, 102989. https://doi.org/10.1016/j.earscirev.2019.102989

Bernaola, G. & Monechi, S. 2007: Calcareous nannofossil extinction and survivorship across the Cretaceous-Paleogene boundary at Walvis Ridge (ODP Hole 1262C, South Atlantic Ocean). Palaeogeography, Palaeoclimatology, Palaeoecology 255, 132–156. https://doi.org/10.1016/j.palaeo.2007.02.045

Bernecker, M. & Weidlich, O. 2005: Azooxanthellate corals in the Late Maastrichtian Early Paleocene of the Danish basin: bryozoan and coral mounds in a boreal shelf setting. In: Bernecker, M. & Weidlich, O. (eds): Cold-water corals and ecosystems, 3–25. Berlin: Springer. https://doi.org/10.1007/3-540-27673-4_1

Birch, H.S., Coxall, H.K., Pearson, P.N., Kroon, D. & Schmidt, D.N. 2016: Partial collapse of the marine carbon pump after the Cretaceous-Paleogene boundary. Geology 44, 287–290. https://doi.org/10.1130/G37581.1

Bjerager, M. & Surlyk, F. 2007: Benthic palaeoecology of Danian deep-shelf bryozoan mounds in the Danish Basin. Palaeogeography, Palaeoclimatology, Palaeoecology 250, 184–215. https://doi.org/10.1016/j.palaeo.2007.03.008

Black, M. 1971: Coccoliths of the Speeton Clay and Sutterby Marl. Proceedings of the Yorkshire Geological Society 38, 381–424. https://doi.org/10.1144/pygs.38.3.381

Black, M. & Barnes, B. 1959: The structure of coccoliths from the English chalk. Geological Magazine 96, 321–328. https://doi.org/10.1017/S0016756800062294

Bown, P. 2005: Selective calcareous nannoplankton survivorship at the Cretaceous-Tertiary boundary. Geology 33, 653–656. doi:10.1130/G21566.1

Bown, P.R. & Cooper, M.K. E. 1989: New calcareous nannofossils from the Jurassic. Journal of Micropalaeontology 8, 91–96. https://doi.org/10.1144/jm.8.1.91

Bown, P.R. & Young, J.R. 1997: Mesozoic calcareous nannoplankton classification. Journal of Nannoplankton Research 19, 21–36. https://doi.org/10.58998/jnr2027

Bown, P.R., Lees, J.A. & Young, J.R. 2004: Calcareous nannoplankton evolution and diversity through time. In: Thierstein, H.R. & Young, J.R. (eds): Coccolithophores: from molecular processes to global impact, 481–508. Berlin: Springer. https://doi.org/10.1007/978-3-662-06278-4_18

Bralower, T.J. *et al*. 2020: Origin of a global carbonate layer deposited in the aftermath of the Cretaceous-Paleogene boundary impact. Earth and Planetary Science Letters 548, 116476. https://doi.org/10.1016/j.epsl.2020.116476

Bramlette, M.N. & Martini, E. 1964: The great change in calcareous nannoplankton fossils between the Mastrichtian and Danian. Micropaleontology 10, 291–322. https://doi.org/10.2307/1484577

Chenet, A.L., Courtillot, V., Fluteau, F., Gerard, M., Quidelleur, X., Khadri, S.F.R., Subbarao, K.V. & Thordarson, T. 2009: Determination of rapid Deccan eruptions across the Cretaceous-Tertiary boundary using paleomagnetic secular variation: 2. Constraints from analysis of eight new sections and synthesis for a 3500-m-thick composite section. Journal of Geophysical Research-Solid Earth 114, B06103. https://doi.org/10.1029/2008JB005644

D'Hondt, S. 2005: Consequences of the cretaceous/paleogene mass extinction for marine ecosystems. Annual Review of Ecology Evolution and Systematics 36, 295–317. https://doi.org/10.1146/annurev.ecolsys.35.021103.105715

Deflandre, G. 1959: Sur les nannofossiles calcaires et leur systématique. Revue de Micropaléontologie 2, 127–152.

Deflandre, G. & Fert, C. 1954: Observations sur les coccolithophoridés actuels et fossiles en microscopie ordinaire et électronique. Annales de Paléontologie 40, 115–176.

Dunham, R.J. 1962: Classification of carbonate rocks according to depositional texture. In: Ham, W.E. (ed.): Classification of carbonate rocks – A symposium. American Association of Petroleum Geologists Memoir 1, 108–121. https://doi.org/10.1306/M1357

Egger, H., Koeberl, C., Wagreich, M. & Stradner, H. 2009: The Cretaceous-Paleogene (K/Pg) boundary at Gams, Austria: Nannoplankton stratigraphy and geochemistry of a bathyal northwestern Tethyan setting. Stratigraphy 6, 333–347. https://doi.org/10.29041/strat.06.4.04

Ekdale, A.A. & Bromley, R.G. 1984: Sedimentology and ichnology of the Cretaceous-Tertiary boundary in Denmark – implications for the causes of the terminal Cretaceous extinction. Journal of Sedimentary Petrology 54, 681–703. https://doi.org/10.1306/212F84D6-2B24-11D7-8648000102C1865D

Embry, A. & Klovan, J. 1971: A late Devonian reef tract on northeastern Banks Island, N.W.T. Bulletin of Canadian Petroleum Geology 19, 730–781.

Flügel, E. 2010: Microfacies of carbonate rocks, 2nd edition, 976 pp. Berlin: Springer. https://doi.org/10.1007/978-3-642-03796-2

Forchhammer, G. 1825: De geognostostiske forhold i en Deel af Sjelland og Naboeöerne. Det Kongelige Danske Videnskabers Selskab, physiske og mathematiske Skrifter 1, 248–280.

Frederiksen, A., Thibault, N., Gilleaudeau, G.J., Bjerrum, C.J., Moreau, J. & Frei, R. 2024: Combined cadmium and chromium isotopes record a collapse of bioproductivity across the Cretaceous–Paleogene boundary in the Danish basin. Chemical Geology 654, 122058, https://doi.org/10.1016/j.chemgeo.2024.122058

Galehouse, J.S. 1971: Sedimentation analysis. In: Carver, R.E. (ed.): Procedures in sedimentary petrology, 69–94. London: Wiley.

Gilleaudeau, G.J., Voegelin, A.R., Thibault, N., Moreau, J., Ullmann, C.V., Klaebe, R.M., Korte, C. & Frei, R. 2018: Stable isotope records across the Cretaceous-Paleogene transition, Stevns Klint, Denmark: New insights from the chromium isotope system. Geochimica et Cosmochimica Acta 235, 305–332. https://doi.org/10.1016/j.gca.2018.04.028

Górka, H. 1957: Les Coccolithophoridés du Maestrichtien supérieur de Pologne. Acta Palaeontologica Polonica 2, 239–284.

Guerra, R. M., Concheyro, A., Kochhann, K. G. D., Bom, M. H. H., Ceolin, D., Musso, T., Savian, F.F. & Fauth, G. 2021: Calcareous microfossils and paleoenvironmental changes across the Cretaceous-Paleogene (K-Pg) boundary at the Cerro Azul Section, Neuquen Basin, Argentina. Palaeogeography, Palaeoclimatology, Palaeoecology 567, 110217. https://doi.org/10.1016/j.palaeo.2021.110217

Hansen, H.J. 1990: Diachronous extinctions at the K/T boundary – a scenario. In: Sharpton, V.L. & Ward, P.D. (eds): Global catastrophes in Earth history: An interdisciplinary conference on impacts, volcanism, and mass mortality. The Geological Society of America, Special Papers 247, 417–423. https://doi.org/10.1130/SPE247-p417

Hansen, T. 2019: Gastropods from the Cretaceous-Palaeogene boundary in Denmark. Zootaxa 4654, 196 pp. https://doi.org/10.11646/zootaxa.4654.1.1

Hart, M. B., Feist, S.E., Håkansson, E., Heinberg, C., Price, G.D., Leng, M.J., Watkinson, M.P. 2005: The Cretaceous-Palaeogene boundary succession at Stevns Klint, Denmark: Foraminifers and stable isotope stratigraphy. Palaeogeography, Palaeoclimatology, Palaeoecology 224, 6–26. https://doi.org/10.1016/j.palaeo.2005.03.029

Hashim, M.S. & Kaczmarek, S.E. 2021: Evolution of calcite microcrystal morphology during experimental dissolution. Journal Of Sedimentary Research 91, 229–242. https://doi.org/10.2110/jsr.2020.154

Heinberg, C. 1999: Lower Danian bivalves, Stevns Klint, Denmark: continuity across the K/T boundary. Palaeogeography, Palaeoclimatology, Palaeoecology 154, 87–106. https://doi.org/10.1016/S0031-0182(99)00088-7w

Heinberg, C. 2005: Morphotype biostratigraphy, diachronism, and bivalve recovery in the earliest Danian of Denmark. Bulletin of the Geological Society of Denmark 52, 81–95. https://doi.org/10.37570/bgsd-2005-52-07

Henehan, M.J., Hull, P.M., Penman, D.E., Rae, J.W. & Schmidt, D.N. 2016: Biogeochemical significance of pelagic ecosystem function: an end-Cretaceous case study. Proceedings of the Royal Society B: Biological Sciences 371, 20150510. https://doi.org/10.1098/rstb.2015.0510

Hildebrand-Habel, T. & Streng, M. 2003: Calcareous dinoflagellate associations and Maastrichtian-Tertiary climatic change in a high-latitude core (ODP Hole 689B, Maud Rise, Weddell Sea). Palaeogeography, Palaeoclimatology, Palaeoecology 197, 293–321. https://doi.org/10.1016/S0031-0182(03)00470-X

Hull, P. M. *et al.* 2020: On impact and volcanism across the Cretaceous-Paleogene boundary. Science 367, 266–272. https://doi.org/10.1126/science.aay5055

Jones, H.L., Lowery, C.M. & Bralower, T.J. 2019: Delayed calcareous nannoplankton boom-bust successions in the earliest Paleocene Chicxulub (Mexico) impact crater. Geology 47, 753–756. https://doi.org/10.1130/G46143.1

Kaczmarek, S.E., Fullmer, S.M. & Hasiuk, F.J. 2015: A universal classification scheme for the microcrystals that host limestone microporosity. Journal of Sedimentary Research 85, 1197–1212. https://doi.org/10.2110/jsr.2015.79

Katz, M.E., Finkel, Z.V., Grzebyk, D., Knoll, A.H. & Falkowski, P.G. 2004: Evolutionary trajectories and biogeochemical impacts of marine eukaryotic phytoplankton. Annual Review of Ecology, Evolution, and Systematics 35, 523–556. https://doi.org/10.1146/annurev.ecolsys.35.112202.130137

Knoll, A.H. & Follows, M.J. 2016: A bottom-up perspective on ecosystem change in Mesozoic oceans. Proceedings of the Royal Society B: Biological Sciences 283, 20161755. https://doi.org/10.1098/rspb.2016.1755

Machalski, M. & Heinberg, C. 2005: Evidence for ammonite survival into the Danian (Paleogene) from the Cerithium Limestone Member at Stevns Klint, Denmark. Bulletin of the Geological Society of Denmark 52, 97–111. https://doi.org/10.37570/bgsd-2005-52-08

MacLeod, K.G., Whitney, D.L., Huber, B.T. & Koeberl, C. 2007: Impact and extinction in remarkably complete Cretaceous-Tertiary boundary sections from Demerara Rise, tropical western North Atlantic. Geological Society of America Bulletin 119, 101–115. https://doi.org/10.1130/B25955.1

Mahanipour, A., Mutterlose, J. & Parandavar, M. 2022: Integrated bio- and chemostratigraphy of the Cretaceous – Paleogene boundary interval in the Zagros Basin (Iran, central Tethys). Palaeogeography, Palaeoclimatology, Palaeoecology 587, 110785. https://doi.org/10.1016/j.palaeo.2021.110785

Martinsson, A. 1970: Toponomy of trace fossils. In: Crimes, T.P. & Harper, J.C. (eds): Trace fossils. Geological Journal Special Issue 3, 323–330. Liverpool: Seel House Press.

McLachlan, S.M.S. & Pospelova, V. 2021: Calcareous dinoflagellate cyst distribution across the K/Pg boundary at DSDP site 577, Shatsky Rise, western North Pacific Ocean. Marine Micropaleontology 168, 102057. https://doi.org/10.1016/j.marmicro.2021.102057

Minoletti, F., de Rafelis, M., Renard, M., Gardin, S. & Young, J. 2005: Changes in the pelagic fine fraction carbonate sedimentation during the Cretaceous-Paleocene transition: contribution of the separation technique to the study of Bidart section. Palaeogeography, Palaeoclimatology, Palaeoecology 216, 119–137. https://doi.org/10.1016/j.palaeo.2004.10.006

Mohamed, O., Piller, W.E. & Egger, H. 2012: The dinocyst record across the Cretaceous/Palaeogene boundary of a bathyal mid-latitude Tethyan setting: Gosau Group, Gams Basin, Austria. Cretaceous Research 35, 143–168. https://doi.org/10.1016/j.cretres.2011.12.007

Nielsen, K.B. 1917: Cerithiumkalken i Stevns Klint. Danmarks

Geologiske Undersøgelse IV. Række, Vol. 1(7), 14 pp. https://doi.org/10.34194/raekke4.v1.6954

Obst, M., Wehrli, B. & Dittrich, M. 2009: $CaCO_3$ nucleation by cyanobacteria: laboratory evidence for a passive, surface-induced mechanism. Geobiology 7, 324–347. https://doi.org/10.1111/j.1472-4669.2009.00200.x

Ogg, J.G., Ogg, G.M. & Gradstein, F.M. 2016: A concise geologic time scale, 240 pp. Amsterdam: Elsevier.

Olsson, R.K., Berggren, W.A., Hemleben, C. & Huber, B.T. 1999: Atlas of Paleocene planktonic foraminifera. Smithsonian Contributions to Paleobiology 85, 1–252. https://doi.org/10.5479/si.00810266.85.1

Perch-Nielsen, K. 1968: Der Feinbau und die Klassifikation der Coccolithen aus dem Maastrichtien von Danemark. Biologiske Skrifter, Kongelige Danske Videnskabernes Selskab 16, 1–96.

Perch-Nielsen, K. 1979: Calcareous nannofossil zonation at the Cretaceous/Tertiary boundary in Denmark. In: Birkelund, T. & Bromley, R.G. (eds): Proceedings of the Cretaceous-Tertiary Boundary Events Symposium, 115–135. Copenhagen.

Rasmussen, H.W. 1971: Echinoid and crustacean burrows and their diagenetic significance in the Maastrichtian-Danian of Stevns Klint, Denmark. Lethaia 4, 191–216. https://doi.org/10.1111/j.1502-3931.1971.tb01289.x

Rasmussen, J.A., Heinberg, C. & Håkansson, E. 2005: Planktonic foraminifers, biostratigraphy and the diachronous nature of the lowermost Danian Cerithium Limestone Member at Stevns Klint, Denmark. Bulletin of the Geological Society of Denmark 52, 113–131. https://doi.org/10.37570/bgsd-2005-52-09

Reinhardt, P. & Górka, H. 1967: Revision of some Upper Cretaceous coccoliths from Poland and Germany. Neues Jahrbuch für Geologie und Paläontologie, Abhandlungen 129, 240–256.

Robbins, L.L. & Blackwelder, P.L. 1992: Biochemical and ultrastructural evidence for the origin of whitings – a biologically induced calcium-carbonate precipitation mechanism. Geology 20, 464–468. https://doi.org/10.1130/0091-7613(1992)020<0464:BAUEFT>2.3.CO;2

Romein, A.J.T. 1979: Lineages in Early Paleogene calcareous nannoplankton. Utrecht Micropaleontological Bulletin 22, 1–231.

Rosenkrantz, A. 1924: Nye Iagttagelser over Cerithiumkalken i Stevns Klint med Bemærkninger om Grænsen mellem Kridt og Tertiær. Meddelelser fra Dansk Geologisk Forening 6, 28–31.

Rosenkrantz, A. 1939: Faunaen i Cerithiumkalken og det hærdnede Skrivekridt i Stevns Klint. Meddelelser fra Dansk Geologisk Forening 9, 509–514.

Rosenkrantz, A., Surlyk, F., Anderskouv, K., Frykman, P., Stemmerik, L. & Thibault, N. 2021: The K-T boundary strata north of Korsnæb, Stevns Klint, Denmark – evolution and geometry revealed in a long, horizontal profile. Bulletin of the Geological Society of Denmark 69, 233–244. https://doi.org/10.37570/bgsd-2021-69-10

Schaefer, B. *et al.* 2020: Microbial life in the nascent Chicxulub crater. Geology 48, 328–332. https://doi.org/10.1130/G46799.1

Schmitz, B., Keller, G. & Stenvall, O. 1992: Stable isotope and foraminiferal changes across the Cretaceous Tertiary boundary at Stevns-Klint, Denmark – arguments for long-term oceanic instability before and after Bolide-Impact Event. Palaeogeography, Palaeoclimatology, Palaeoecology 96, 233–260. https://doi.org/10.1016/0031-0182(92)90104-D

Schoene, B., Eddy, M.P., Samperton, K.M., Keller, C.B., Keller, G., Adatte, T., Khadri, S.F.R. 2019: U-Pb constraints on pulsed eruption of the Deccan Traps across the end-Cretaceous mass extinction. Science 363, 862–866. https://doi.org/10.1126/science.aau2422

Schulte, P. *et al.* 2010: The Chicxulub asteroid impact and mass extinction at the Cretaceous-Paleogene boundary. Science 327, 1214–1218. https://doi.org/10.1126/science.1177265

Sepúlveda, J., Wendler, J.E., Summons, R.E. & Hinrichs, K.U. 2009: Rapid resurgence of marine productivity after the Cretaceous-Paleogene mass extinction. Science 326, 129–132. https://doi.org/10.1126/science.1176233

Sepúlveda, J., Alegret, L., Thomas, E., Haddad, E., Cao, C. & Summons, R.E. 2019: Stable isotope constraints on marine productivity across the Cretaceous–Paleogene mass extinction. Paleoceanography and Paleoclimatology 34, 1195–1217. https://doi.org/10.1029/2018PA003442

Shafik, S. & Stradner, H. 1971: Nannofossils from the Eastern Desert, Egypt. Jahrbuch der Geologischen Bundesanstalt, Sonderband 17, 69–104.

Smit, J. 2005: The section of the Barranco del Gredero (Caravaca, SE Spain): a crucial section for the Cretaceous/Tertiary boundary impact extinction hypothesis. Journal of Iberian Geology 31, 179–191.

Streng, M., Hildebrand-Habel, T. & Willems, H. 2004: A proposed classification of archeopyle types in calcareous dinoflagellate cysts. Journal of Paleontology 78, 456–483. https://doi.org/10.1666/0022-3360(2004)078<0456:APCOAT>2.0.CO;2

Suchéras-Marx, B., Mattioli, E., Allemand, P., Giraud, F., Pittet, B., Plancq, J. & Escarguel, G. 2019: The colonization of the oceans by calcifying pelagic algae. Biogeosciences 16, 2501–2510. https://doi.org/10.5194/bg-16-2501-2019

Surlyk, F. 1997: A cool-water carbonate ramp with bryozoan mounds: Late Cretaceous-Danian of the Danish basin. In: James. N.P. & Clarke, J.A.D. (eds): Cool-Water Carbonates. SEPM Special Publication 56, 293–307. https://doi.org/10.2110/pec.97.56.0293

Surlyk, F. & Lykke-Andersen, H. 2007: Contourite drifts, moats and channels in the Upper Cretaceous chalk of the Danish Basin. Sedimentology 54, 405–422. https://doi.org/10.1111/j.1365-3091.2006.00842.x

Surlyk, F., Damholt, T. & Bjerager, M. 2006: Stevns Klint, Denmark: Uppermost Maastrichtian chalk, Cretaceous-Tertiary boundary, and lower Danian bryozoan mound complex. Bulletin of the Geological Society of Denmark 54, 1–48. https://doi.org/10.37570/bgsd-2006-54-01

Thierstein, H.R. 1980: Selective dissolution of late cretaceous and earliest tertiary calcareous nannofossils: Experimen-

tal evidence. Cretaceous Research 1, 165–176. https://doi.org/10.1016/0195-6671(80)90023-3

Thompson, J.B. 2000: Microbial whitings. In: Riding, R.E. & Awramik, S.M. (eds): Microbial Sediments, 250–260. Berlin: Springer. https://doi.org/10.1007/978-3-662-04036-2_27

Varol, O. 1989: Palaeocene calcareous nannofossil biostratigraphy. In: Crux, J.A. & van Heck, S.E. (eds): Nannofossils and their applications, 267–310. British Micropalaeontological Society.

Vekshina, V.N. 1959: Coccolithophoridae of the Maastrichtian deposits of the West Siberian lowlands. Siberian Science Research Institute of Geology, Geophysics, Mineralogy and Raw Materials 2, 56–81.

Wendler, J. & Willems, H. 2002: Distribution pattern of calcareous dinoflagellate cysts across the Cretaceous-Tertiary boundary (Fish Clay, Stevns Klint, Denmark): Implications for our understanding of species-selective extinction. In: Koeberl, C. & MacLeod, K.G. (eds): Catastrophic events and mass extinctions: Impacts and beyond. Geological Society of America, Special Papers 356, 265–275. https://doi.org/10.1130/0-8137-2356-6.265

Westerhold, T. *et al.* 2020: An astronomically dated record of Earth's climate and its predictability over the last 66 million years. Science 369, 1383-1387. https://doi.org/10.1126/science.aba6853

Wilson, J.L. 1975: Carbonate facies in geologic history, 471 pp. Berlin: Springer. https://doi.org/10.1007/978-1-4612-6383-8

Zachos, J.C. & Arthur, M.A. 1986: Paleoceanography of the Cretaceous/Tertiary boundary event: Inferences from stable isotopic and other data. Paleoceanography 1, 5–26. https://doi.org/10.1029/PA001i001p00005

Tomagnostella tullbergi n. sp. (Agnostidae) from the middle Cambrian *Lejopyge laevigata* Zone of Scandinavia

THOMAS WEIDNER, ARNE THORSHØJ NIELSEN & JAN OVE R. EBBESTAD

Geological Society of Denmark
https://2dgf.dk

Received 22 June 2024
Accepted in revised form
27 September 2024
Published online
13 November 2024

Weidner, T., Nielsen, A.T. & Ebbestad, J.O.R. 2024: *Tomagnostella tullbergi* n. sp. (Agnostidae) from the middle Cambrian *Lejopyge laevigata* Zone of Scandinavia. Bulletin of the Geological Society of Denmark, Vol. 73, pp. 193–198. ISSN 2245-7070. https://doi.org/10.37570/bgsd-2024-73-11

A rare new agnostoid species, *Tomagnostella tullbergi* n. sp., is described from the lower part of the middle Cambrian *Lejopyge laevigata* Zone in Scandinavia, corresponding to the lower part of the Guzhangian global Stage. The species is currently known only from the Andrarum Limestone Bed of Skåne, southernmost Sweden, and coeval strata in the Oslo Region, Norway; it has also been recorded from ice-rafted Andrarum Limestone found in Germany. The material assigned to *T. tullbergi* n. sp. has previously been confused with *Tomagnostella exsculpta*. The new species is characterized by a cephalon with a moderately angular glabellar front (distinctly angular in *T. exsculpta*) and a pygidium with a narrow, pointed axis showing a depressed tip; a small secondary node is located within this depression close to the tip of the axis (in *T. exsculpta* the axis is broad and rounded posteriorly and without a posterior depression; a minute terminal node may or may not be present). *Tomagnostella tullbergi* n. sp. is also comparatively large-sized whereas *T. exsculpta* attains smaller maximum sizes.

Keywords: Agnostoids, *Tomagnostella*, Andrarum Limestone, Miaolingian, Scandinavia.

Thomas Weidner [to.we@paradis.dk], Ravnholtvej 23, Rårup, DK-7130 Juelsminde, Denmark. Arne Thorshøj Nielsen [arnet@ign.ku.dk], Department of Geosciences and Natural Resource Management, University of Copenhagen, Øster Voldgade 10, DK-1350 Kbh K, Denmark. Jan Ove R. Ebbestad [jan-ove.ebbestad@em.uu.se], Museum of Evolution, Uppsala University, Norbyvägen 22, SE-75236 Uppsala, Sweden.

http://zoobank.org/urn:lsid:zoobank.org:pub:5A94A097-6AA3-489E-84A7-C0C2C2CB6067

Angelin (1851) described *Agnostus exsculptus* based on four cephala and two specimens interpreted as pygidia, all stated to derive from the Andrarum Limestone at Andrarum, Skåne (southern Sweden). Later, Tullberg (1880, p. 22) identified the two 'pygidia' as cephala of *Goniagnostus nathorsti*, and he also considered that two of the syntype cephala, although generally similar to *A. exsculptus*, represented an ancestral form, supposedly deriving from bituminous limestone (stinkstone) below the Andrarum Limestone. Westergård (1946) agreed with this interpretation, except that one of the discarded syntype cephala was reassigned to *Hypagnostus exsculptus* (*ibid*., pl. 6, fig. 1a, b, NRM Ar 2006, 5.6 mm long). According to Westergård, this specimen is also preserved in Andrarum Limestone. The syntype cephalon previously illustrated by Tullberg (1880, pl. 1, fig. 10) was selected as lectotype for *H. exsculptus* and re-illustrated (Westergård 1946, pl. 5, fig. 35a, b, NRM Ar 2007, 3.0 mm long; it is here shown in Fig. 1A). Westergård (1946) also figured an additional cephalon, assigned to *H. exsculptus,* from a drill-core obtained at Södra Sandby, Skåne (*ibid*., pl. 6, fig. 2, SGU 4008a, 5.6 mm long; see Fig. 1G), and he further listed six unfigured cephala from Andrarum and Kiviks-Esperöd (Skåne), all deriving from the Andrarum Limestone. Westergård (1946) also illustrated three relatively large pygidia, representing two different morphs, but he was uncertain which of these forms belong to *H. exsculptus*.

Robison (1988), Peng & Robison (2000), Peng *et al*. (2009) and Weidner *et al*. (2023) assigned *exsculpta* to *Tomagnostella* (see also Kobayashi 1939 and Öpik 1979) and described material from Greenland, China, Himalaya and Scandinavia. These authors demonstrated that *T. exsculpta* is a variably scrobiculate species with shields up to 3 mm long, characterized by

a cephalon with an angular glabellar front (Fig. 1A) and a pygidium with a broad axis reaching the border furrow or almost so (Fig. 1B). They synonymized *T. nepos* (Westergård, 1946) with *T. exsculpta* as the exterior sculpture, smooth or scrobiculate, is of no taxonomic significance and intermediate specimens occur. For a detailed discussion on the confused interpretation of *T. exsculpta* through time, see Weidner *et al*. (2023).

Prior to these contributions, Öpik (1979, p. 71) pointed out that both the larger cephalon illustrated by Westergård (1946, pl. 6, fig. 1a, b) with its apparently straight glabellar front and the three tentatively assigned pygidia (Westergård 1946, pl. 6, figs 3–5) with a narrow and pointed axis have features not observed in *T. exsculpta*. Öpik suggested that the cephalon and the two pygidia with a depressed tip (Westergård 1946, pl. 6, figs 3–4) may represent a new species of *Tomagnostella*. We agree with this interpretation (see Weidner *et al*. 2023, pp. 61–62), but new photographs of the cephalon (Fig. 1E1) show that the glabellar front is moderately angular and not straight as stated by Westergård. In recent decades, sparse additional material of this form has been recorded from the Oslo Region (Norway), Skåne (Sweden) and an ice-rafted boulder found in Germany (all occurrences are specified below) which allows formal description of a new species, here named *T. tullbergi* n. sp.

Systematic palaeontology

We follow the generic concept of Shergold & Laurie (1997).

Repositories. NRM (Naturhistoriska Riksmuseet, Swedish Museum of Natural History, Stockholm); PMO (Palaeontological collections of the Natural History Museum, University of Oslo, Norway); PMU (Palaeontological collections, Museum of Evolution, Uppsala University, Sweden); SGU (Geological Survey of Sweden).

This published work and the nomenclatural acts it contains have been registered in ZooBank: http://zoobank.org/urn:lsid:zoobank.org:pub:5A94A097-6AA3-489E-84A7-C0C2C2CB6067

Family Spinagnostidae Howell, 1935

Genus *Tomagnostella* Kobayashi, 1939

Type species (OD). Agnostus exsculptus, Angelin, 1851, from the Andrarum Limestone Bed, lower part of the *Lejopyge laevigata* Zone, Andrarum, Skåne, Sweden.

Diagnosis. See Shergold & Laurie (1997).

Tomagnostella tullbergi n. sp.

Fig. 1E1–M

1946 *Hypagnostus exsculptus* (Angelin, 1851) [*partim*]; Westergård, pp. 50–51, pl. 6, figs 1–2; non pl. 5, fig. 35a, b.
1946 *Hypagnostus exsculptus*? (Angelin, 1851) [*partim*]; Westergård, pp. 50–51, pl. 6, figs 3–4; non pl. 6, fig. 5.
1959 *Tomagnostella exsculpta* (Angelin); Howell, p. O186, Fig. 127:2a, b.
1994 *Tomagnostella exsculpta* (Angelin 1851); Rudolph, pp. 138–139, pl. 7, fig. 15.
2008 *Tomagnostella exsculpta* (Angelin 1851); Høyberget & Bruton, pp. 44–45, pl. 7, figs A–D.

▼ **Fig. 1.** *Tomagnostella exsculpta* and *T. sulcifera* are figured to facilitate comparison with *T. tullbergi* n. sp. **A, B:** *Tomagnostella exsculpta* (Angelin, 1851). **A:** Lectotype cephalon (NRM Ar 2007), from Andrarum, Skåne. Previously illustrated by Tullberg (1880), pl. 1, fig. 10, Westergård (1946), pl. 5, fig. 35a, b and Shergold & Laurie (1997, fig. 226:2a). **B:** Pygidium (PMU 37227/2), from Gislövshammar, Skåne. Previously illustrated by Weidner *et al*. (2023), fig. 33U. Note the minute terminal node. **C, D:** *Tomagnostella sulcifera* (Wallerius, 1895). **C:** Cephalon (PMU 34319/1), from Vilske, Västergötland. Previously illustrated by Weidner *et al*. (2023), fig. 33O. **D:** Pygidium (PMU 38335/2), from Vilske, Västergötland. Note the terminal node. Previously illustrated by Weidner *et al*. (2023), fig. 33P. **E–M:** *Tomagnostella tullbergi* n. sp. **E1, E2:** Cephalon in dorsal and right lateral views (NRM Ar 2006), from Andrarum, Skåne. Previously illustrated by Westergård (1946), pl. 6, fig. 1a, b. **F:** Cephalon (PMO 211.993), from Gjøvik, Norway. Previously illustrated by Høyberget & Bruton (2008), pl. 7C. **G**: Cephalon (SGU 4800a), from Södra Sandby, Skåne. Previously illustrated by Westergård (1946), pl. 6, fig. 2. **H**: Cephalon (PMO 211.992), from Gjøvik, Norway. Previously illustrated by Høyberget & Bruton (2008), pl. 7B. **I**: Paratype cephalon (PMO 211.991), from Gjøvik, Norway. Previously illustrated by Høyberget & Bruton (2008), pl. 7A. **J1, J2:** Holotype pygidium in dorsal view and close up showing secondary node within the axial depression (PMO 211.994), from Gjøvik, Norway. Previously illustrated by Høyberget & Bruton (2008), pl. 7D. **K1, K2:** Pygidium in dorsal view and close up showing secondary node within the depression (NRM Ar 9519), from Andrarum, Skåne. Previously illustrated by Westergård (1946), pl. 6, fig. 4. **L:** Small pygidium (PMU 31777), from Brantevik, Skåne. (M) Pygidium (SGU 4801), from Södra Sandby, Skåne. Previously illustrated by Westergård (1946), pl. 6, fig. 3. Black scale bars: 1 mm; scale bar in A is the same for all except J2 and K2.

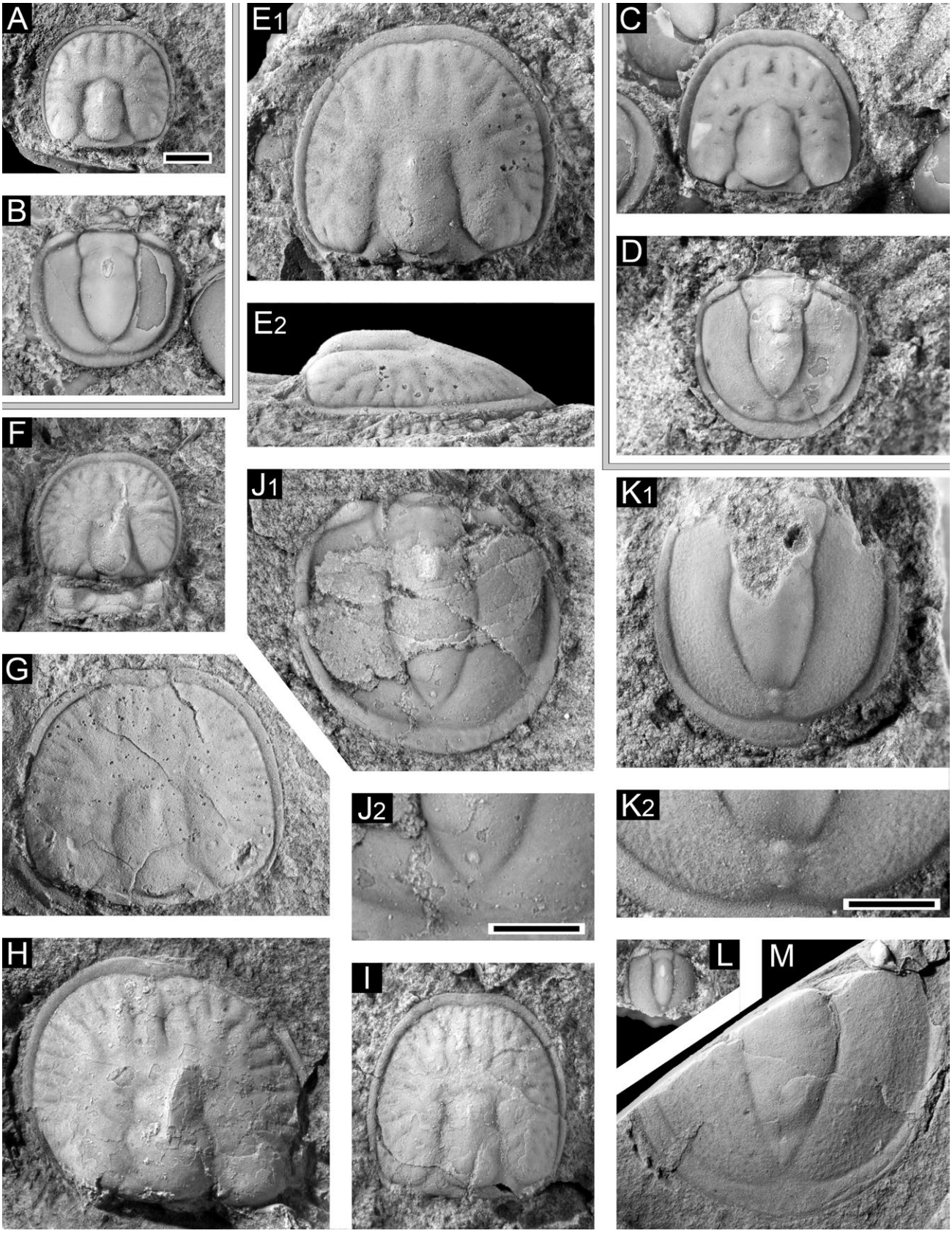
A
B
E1
E2
C
D
F
J1
K1
G
J2
K2
H
I
L
M

Derivation of name. In recognition of the Swedish botanist, palaeontologist and geologist Sven Axel Tullberg (1852–1886). He discarded two of the cephala from Angelin's syntype material of *Agnostus exsculptus* (see Tullberg 1880, p. 22; Westergård 1946, pp. 50–51) and one of these is here assigned to *Tomagnostella tullbergi* n. sp. (illustrated in Fig. 1E1, E2).

Holotype (designated here). Pygidium, PMO 211.994, from the *Lejopyge laevigata* Zone at Gjøvik, Norway, illustrated in Fig. 1J1, J2. It was previously illustrated by Høyberget & Bruton (2008), pl. 7D.

Paratype (designated here). Cephalon, PMO 211.991, from the *Lejopyge laevigata* Zone at Gjøvik, Norway, illustrated in Fig. 1I. It was previously illustrated by Høyberget & Bruton (2008), pl. 7A.

Material and occurrence. All material of the new species illustrated in the literature so far, six cephala and four pygidia, derives from the lower part of the *Lejopyge laevigata* Zone, i.e. the Andrarum Limestone (henceforth AL) and the equivalent level in southern Norway. All of these specimens have been restudied except for the cephalon recorded as *T. exsculpta* by Rudolph (1994), from an ice-rafted boulder of AL found on the island of Rügen, Germany. Measurements and museum numbers of the specimens are listed in Table 1. Material illustrated as *H. exsculptus* by Westergård (1946) includes one cephalon and one pygidium from the AL at Andrarum, and one cephalon and one pygidium from the same horizon in a boring at Södra Sandby, Skåne. One pygidium was collected by H.-J. Schmütz from a block of AL on the shore at Brantevik, Skåne, and donated to PMU. In addition to the holotype pygidium and the paratype cephalon, another two cephala were reported as *T. exsculpta* from a limestone lens at Gjøvik, Norway, by Høyberget & Bruton (2008).

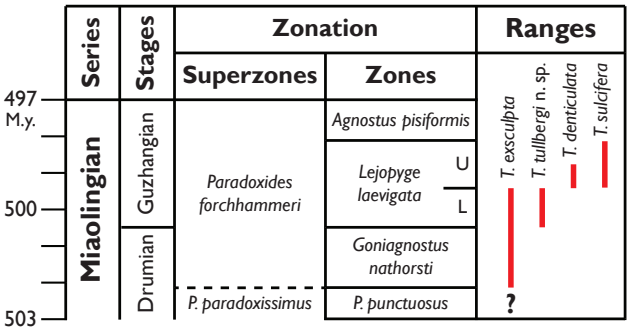

Fig. 2. Stratigraphic distribution of species of *Tomagnostella* in Scandinavia. Data from Westergård (1946), Rudolph (1994), Høyberget & Bruton (2008), Weidner & Nielsen (2014) and present study.

Diagnosis. A comparatively large *Tomagnostella* species with a cephalon having radial scrobiculae and a glabella with faintly indicated and moderately angular F3 forming the glabellar front. Pygidial axis is narrow, pointed, with a depressed tip; a tiny, but distinct secondary node is located within this depression. The axis extends to the border furrow or nearly so.

Description. No complete specimen is at hand. However, all cephala and pygidia derive from the Andrarum Limestone and the equivalent stratigraphic level in Norway and in some cases even from the same sample. They possess features characteristic of *Tomagnostella* but differ from the longer-ranging *T. exsculpta* and the younger *T. sulcifera* as specified below (ranges shown in Fig. 2). We therefore confidently consider the described cephala and pygidia as conspecific.

Tomagnostella tullbergi n. sp. is a comparatively large species. The length of the five studied cephala ranges from 3.2 mm to 6.0 mm, and the three adult pygidia are between 6.2 mm and 6.5 mm long (Table 1). The cephalon is moderately inflated (for a side view, see

Table 1. List of the investigated material of *Tomagnostella tullbergi* n. sp.

Repository no.	Fig. this paper	Part	Length (mm)	Previous illustration	Previous assignment
NRM Ar 2006	E1, E2	cephalon	5.6	Westergård 1946, pl. 6, fig. 1a, b	*Hypagnostus exsculptus*
PMO 211.993	F	cephalon	3.2	Høyberget & Bruton 2008, pl. 7C	*Tomagnostella exsculpta*
SGU 4800a	G	cephalon	5.6	Westergård 1946, pl. 6, fig. 2	*Hypagnostus exsculptus*
PMO 211.992	H	cephalon	6.0	Høyberget & Bruton 2008, pl. 7B	*Tomagnostella exsculpta*
PMO 211.991	I	cephalon	5.1	Høyberget & Bruton 2008, pl. 7A	*Tomagnostella exsculpta*
PMO 211.994	J1, J2	pygidium	6.4	Høyberget & Bruton 2008, pl. 7D	*Tomagnostella exsculpta*
NRM Ar 9519	K1, K2	pygidium	6.2	Westergård 1946, pl. 6, fig. 4	?*Hypagnostus exsculptus*
PMU 31777	L	pygidium	1.7	(New collection)	
SGU 4801	M	pygidium	6.5	Westergård 1946, pl. 6, fig. 3	?*Hypagnostus exsculptus*

Westergård 1946, pl. 6, fig. 1b), has a rounded outline, with approximately equal width/length, and a border only slightly widening anteriorly, delimited by a narrow well-defined border furrow. The glabella is slender and fades out in front of M3; the glabellar front (corresponding to F3) is moderately angular. The F3 furrow is very faintly impressed in all five cephala at hand including the small specimen (Fig. 1F). M1 and M2 appear as one lobe, slightly bowed out, F2 is marked by weak constrictions only; in some specimens F1 is seen as weak indentations (Fig. 1G, I). M3 is narrower than the combined M1–M2 lobe and bears an elongate node, situated almost centrally on the acrolobe. In most specimens the axial furrows are shallow. Basal lobes are simple. The surface sculpture consists of radial scrobiculae.

The pygidium has a border of equal width all the way, except behind the axis where it widens forwards (sag.). The border furrow is narrow. The axis is slender and bounded by moderately deep furrows. M2 bears an elongate node and is narrower (tr.) than both M1 and the posteroaxis. The posteroaxis tapers to a sharp point and reaches the border furrow or nearly so; the tip of the axis is depressed and a small secondary node is located within this depression close to the tip of the axis. The latter features are especially characteristic of the new species and can already be observed in juvenile specimens (Fig. 1L).

Remarks and comparison. In *T. exsculpta* (Fig. 1A), characteristic of the *G. nathorsti* Zone, but also occurring sparsely in the AL (Fig. 2), the axial furrows of the cephalon are distinct and the glabellar front (corresponding to F3) is distinctly angular (moderately angular in *T. tullbergi* n. sp.). The F1 and F2 furrows are typically obsolete, but rarely very faint constrictions are recognizable. The surface is mostly smooth (Høyberget & Bruton 2008, pl. 6O–R, as *T. nepos*; Weidner *et al*. 2023), but scrobiculate cephala are reported from China and Himalaya, and in these specimens the segmentation of the glabella is also better defined (Peng & Robison 2000, fig. 69; Peng *et al*. 2009, fig. 16). All known cephala of *T. tullbergi* n. sp. are scrobiculate. The pygidium of *T. exsculpta* has a wide and inflated axis that has a sharply rounded termination. In material from Scandinavia and Himalaya, a minute terminal node is generally observable (Høyberget & Bruton 2008, pl. 6S–V, as *T. nepos*; Weidner *et al*. 2023, fig. 33; Fig. 1B; Peng *et al*. 2009, fig. 16), but not in material from China (Peng & Robison 2000, pl. 69). The secondary node of *T. tullbergi* n. sp. differs by being located within a transverse depression near the tip of the axis.

Tomagnostella sulcifera (Fig. 1C, D) is common in the upper part of the *L. laevigata* Zone. In the cephalon, the axial furrows are distinct, and the glabellar front is distinctly angular, like in *T. exsculpta*. The segmentation of the glabella is well-defined by constrictions of the F1 and F2 furrows. The surface can be smooth or display scrobiculae. The pygidial axis is short and bears at its extreme end a tiny node, which has been observed in material from Sweden (Weidner *et al*. 2023, fig. 33; Fig. 1D) and China (Peng & Robison 2000, pl. 70). A long postaxial furrow is present.

One of the pygidia figured by Westergård (1946, pl. 6, fig. 5a, b) from the Andrarum Limestone of Skåne (as *H. exsculptus*?) has a strongly incised M2, the axis is narrow and shows a terminal node but lacks the transverse depression characteristic of *T. tullbergi* n. sp., and the axial tip is far from reaching the border. This specimen brings *T. sulcifera* to mind (compare Fig. 1D) but identification remains uncertain.

Conclusions

Four species of *Tomagnostella* are now described from the Miaolingian of Scandinavia (Fig. 2). The common *T. exsculpta* (Angelin, 1851) from the *G. nathorsti* Zone and the lower part of the *L. laevigata* Zone, the rare *T. tullbergi* n. sp. from the lower part of the *L. laevigata* Zone, and the common *T. denticulata* (Westergård, 1946) and *T. sulcifera* (Wallerius, 1895) from the upper part of the *L. laevigata* Zone. These species differ with regard to the outline of the glabellar front, the outline of the pygidial axis (length; pointed or more rounded tip; posterior depression), presence or absence of a postaxial furrow, and presence or absence as well as position of a secondary pygidial node. *Tomagnostella denticulata* (Westergård, 1946) is furthermore distinguished by having short posterolateral spines in the pygidium.

Acknowledgements

We are grateful for help with specimens from various collections and thank Niclas Borinder (SGU), Jonas Hagström (NRM) and Franz-Josef Lindeman (PMO). Hans-Jürgen Schmütz kindly donated a specimen of *T. tullbergi* n. sp. from Brantevik, Skåne. Comments and corrections by referees Per Ahlberg (Sweden) and John Laurie (Australia) improved the original manuscript which is gratefully acknowledged.

References

Angelin, N.P. 1851: Palaeontologia Svecica. P. I. Iconographia Crustaceorum formationis transitionis. Fasc. I, 24 pp. Lund: Berlings.

Howell, B.F. 1935: New Middle Cambrian agnostian trilobites from Vermont. Journal of Paleontology 9, 218–221.

Howell, B.F. 1959: Suborder Agnostina and Eodiscina. In: Moore, R.C. (ed.): Treatise on Invertebrate Paleontology. Part O, Arthropoda 1, O172–O190. New York: Geological Society of America and Lawrence: University of Kansas Press.

Høyberget, M. & Bruton, D.L. 2008: Middle Cambrian trilobites of the suborders Agnostina and Eodiscina from the Oslo Region, Norway. Palaeontographica, Abteilung A 286, 87 pp. https://doi.org/10.1127/pala/286/2008/1

Kobayashi, T. 1939: On the Agnostids (part 1). Journal of the Faculty of Science, Imperial University of Tokyo, Section 2(5), 69–198.

Öpik, A.A. 1979: Middle Cambrian Agnostids: Systematics and Biostratigraphy. Bureau of Mineral Resources, Geology and Geophysics Bulletin 172, 188 pp.

Peng, S.C. & Robison, R.A. 2000: Agnostoid biostratigraphy across the Middle-Upper Cambrian boundary in Hunan, China. Memoirs of the Paleontological Society 53, 104 pp. https://doi.org/10.1666/0022-3360(2000)53[1:ABATMC]2.0.CO;2

Peng, S.C., Hughes, N.C., Heim, N.A., Sell, B.K., Zhu, X.J., Myrow, P.M. & Parcha, S.K. 2009: Cambrian trilobites from the Parahio and Zanskar Valleys, Indian Himalaya. Paleontological Society Memoir 71, 95 pp. https://doi.org/10.1666/08-129.1

Robison, R.A. 1988: Trilobites of the Holm Dal Formation (late Middle Cambrian), central North Greenland. Meddelelser om Grønland, Geoscience 20, 23–103. https://doi.org/10.7146/moggeosci.v20i.139888

Rudolph, F. 1994: Die Trilobiten der mittelkambrischen Geschiebe, 309 pp. Wankendorf: Verlag Frank Rudolph.

Shergold, J.H. & Laurie, J.R. 1997: Introduction to the Suborder Agnostina. In: Kaesler, R.L. (ed.): Treatise on Invertebrate Paleontology. Part O. Arthropoda 1, Trilobita, revised. Volume 1, O331–O383. Boulder: The Geological Society of America and Lawrence: The University of Kansas Press.

Tullberg, S.A. 1880: Om Agnostus-arterna i de kambriska aflagringarne vid Andrarum. Sveriges Geologiska Undersökning C42, 38 pp.

Wallerius, I.D. 1895: Undersökningar öfver zonen med Agnostus laevigatus i Vestergötland, jämte en inledande öfversikt af Vestergötlands samtliga Paradoxideslager, 72 pp. Lund: Gleerupska Universitetsbokhandeln. https://doi.org/10.1080/11035899609444325

Weidner, T. & Nielsen, A.T. 2014: A highly diverse trilobite fauna with Avalonian affinities from the Middle Cambrian Acidusus atavus Zone (Drumian Stage) of Bornholm, Denmark. Journal of Systematic Palaeontology 12, 23–92.

Weidner, T., Nielsen, A.T. & Ebbestad, J.O.R. 2023: Middle Cambrian agnostoids and trilobites from the Lower Allochthon, Swedish Caledonides. Fossils and Strata 68, 121 pp. https://doi.org/10.18261/9788215068022-2023-01

Westergård, A.H. 1946: Agnostidea of the Middle Cambrian of Sweden. Sveriges Geologiska Undersökning C477, 140 pp.

A new helcionelloid mollusc from the Cambrian of Greenland and Idaho (Laurentia)

YEONGJU OH & JOHN S. PEEL

Geological Society of Denmark
https://2dgf.dk

Received 27 September 2024
Accepted in revised form
18 October 2024
Published online
13 November 2024

Oh, Y. & Peel, J.S. 2024. A new helcionelloid mollusc from the Cambrian of Greenland and Idaho (Laurentia). Bulletin of the Geological Society of Denmark, Vol. 73, pp. 199–208. ISSN 2245-7070. https://doi.org/10.37570/bgsd-2024-73-12

Ressericonella gen. nov., a new genus of helcionelloid mollusc, characterized by a narrow shell with a shallowly convex dorsal surface and flat to shallowly concave lateral areas, is described from the Cambrian of Greenland and Idaho. The type species is *Helcionella aequa* Resser, 1939 from the Langston Formation (Naomi Peak Limestone Member) of early middle Cambrian age (Miaolingian Series, Wuliuan Stage, *Albertella* Biozone). *Ressericonella pipalukae* gen. et sp. nov. occurs in the latest early Cambrian (Cambrian Series 2, Stage 4, *Bonnia–Pagetides elegans* Biozone) of southern Freuchen Land, North Greenland. Silicified specimens of *Ressericonella pipalukae* from North Greenland preserve two-layered shell structure in which an inner layer with a transverse fibrous pattern similar to lamello-fibrillar structure is overlain by an outer layer with fine threads radiating from the apex.

Keywords: Mollusca, Helcionelloida, Cambrian, Idaho, North Greenland.

Yeongju Oh [yjoh@kopri.re.kr], Division of Glacier & Earth Sciences, Korea Polar Research Institute, 26 Songdomirae-ro, Yeonsu-gu, 21990, Incheon, Republic of Korea; University of Science and Technology, Daejeon, 34113, Republic of Korea. John S. Peel [john.peel@pal.uu.se], Department of Earth Sciences (Palaeobiology), Uppsala University, Villavägen 16, SE-752 36, Uppsala, Sweden.

Helcionelloids are diverse and widespread during the Cambrian and dominate mollusc assemblages. Their bilaterally symmetrical, slightly coiled, calcareous shells occur from the earliest Cambrian to the Early Ordovician (Gubanov & Peel 2001). Historically, most helcionelloids described before the middle of the last century were based on millimetre-sized hand specimens and assigned to one of three widely-drawn genera: *Helcionella* Grabau & Shimer, 1909, *Scenella* Billings, 1872 or *Metoptoma* Phillips, 1836, although the last-mentioned was originally defined as a Carboniferous gastropod (Phillips 1836). However, researchers subsequently started to describe diverse assemblages from microscopic residues of limestones treated with weak acetic acid, which promoted an explosive increase in helcionelloid taxonomy (Rozanov & Missarzhevsky 1966; Rozanov *et al.* 1969; Yu 1979; Zhou & Xiao 1984; Geyer 1986; Missarzhevsky 1989; Bengtson *et al.* 1990; Parkhaev 2001; Vendrasco *et al.* 2010, 2011; Li *et al.* 2021; Peel & Kouchinsky 2022). Most of this material has been diagenetically phosphatised but significant assemblages of silicified material have also been documented (Runnegar & Jell 1976; Gubanov *et al.* 2004; Jacquet & Brock 2016).

In a Greenland context, embracive descriptions of early Cambrian helcionelloid assemblages from North-East Greenland were given by Skovsted (2004, 2006), while Peel & Kouchinsky (2022) monographed an extensive middle Cambrian (Miaolingian Series, Wuliuan Stage) fauna. Other accounts include Peel (1988, 1989, 1991a,b, 1994, 2021, 2023), Atkins & Peel (2004, 2008), Peel & Skovsted (2005), Peel *et al.* (2016) and Oh *et al.* (2024).

A distinctive helcionelloid species identified during our ongoing studies of the latest early Cambrian of southern Freuchen Land, North Greenland (Fig. 1A, C), compares closely to *Helcionella aequa* Resser, 1939 from the earliest middle Cambrian (Miaolingian Series, Wuliuan Stage) Naomi Park Limestone of Idaho (Fig. 1A) and we establish a new genus, *Ressericonella* gen. nov., to accommodate these two species. The genus is named for Charles Elmer Resser (1889–1943), an American palaeontologist who was a prolific contributor to the taxonomy of Laurentian Cambrian

invertebrates, although his profligacy in introducing new taxonomic names for trilobites is legendary (Sundberg 2007).

Material

Specimens of *Helcionella aequa* Resser, 1939 were collected on the north side of Two Mile Canyon, near its mouth, two miles south-east of Malad, northern Wasatch Mountains, southern Idaho, USA (Fig. 1A). According to Resser (1939, p. 8), the specimens were derived from collections made at locality 54s by F. B. Meek and C. D. Walcott in 1898, and C.D. Walcott and L. D. Burling in 1906. In the collection of the Natural History Museum, Smithsonian Institution, Washington DC, the holotype, USNM 98487, is associated with two additional specimens. *Helcionella aequa* was assigned by Resser (1939) to the "Langston" limestone. Maxey (1958) referred to this limestone as the Naomi Peak Limestone Member of the Langston Formation, which he referred to an *Albertella–Kochaspis* subzone, now the *Albertella* Biozone (Kimmig *et al*. 2019, fig. 1c).

Samples from southern Freuchen Land, North Greenland, were collected from dark thin limestone lenses located 1–2 m above the base of the upper member of the Henson Gletscher Formation (Fig. 2) on the south-western corner of a nunatak (Fig. 1C; 82°09´N, 42°25´W) that was illustrated by Geyer & Peel (2011, fig. 2B). This is locality 1 of Blaker & Peel (1997, figs 8A, 10) and Geyer & Peel (2011, figs 1D, 2B), see also Streng *et al*. (2016, fig. 1E) and represents the reference section (thickness 112 m) of the Henson Gletscher Formation described by Ineson & Peel (1997, figs 21, 32, 33). The limestone samples were collected by J.S.

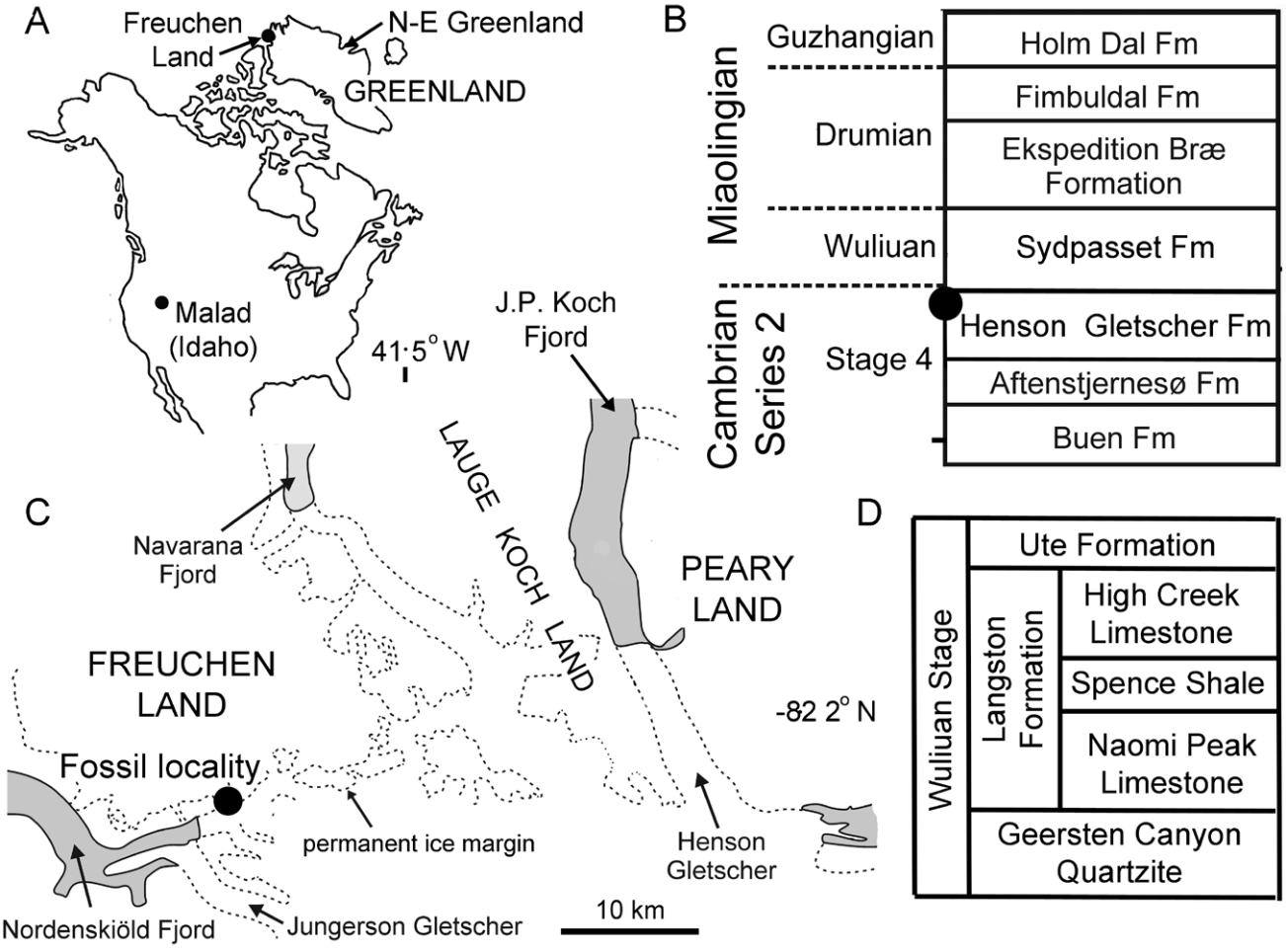

Fig. 1. Stratigraphy and derivation of samples. **A:** location of Freuchen Land (North Greenland) and Malad (Idaho). **B:** Cambrian stratigraphy of southern Freuchen Land showing sample horizon (black dot). **C:** map of Freuchen Land–Peary Land region, North Greenland, showing location of fossil locality (black dot). **D:** simplified stratigraphy of the Malad region in Idaho showing members of the Langston Formation (after Kimmig *et al.* 2019).

Peel and M.R. Blaker on 6th July 1985 (GGU sample 298550) and August 17th 1985 (GGU sample 301346). They were digested in 10% acetic acid and selected silicified specimens were imaged using a Zeiss Supra 35VP scanning electron microscope. All images were assembled using Adobe Photoshop CS4.

Faunas from the Henson Gletscher Formation in southern Freuchen Land, Lauge Koch Land and western Peary Land (Fig. 1C) range in age from early Cambrian (Cambrian Series 2, Stage 4) to middle Cambrian (Miaolingian Series, Wuliuan Stage; *Ptychagnostus gibbus* Biozone), but Drumian Stage strata occur in the Henson Gletscher Formation further to the west, along the northern coast of North Greenland (Higgins *et al.* 1991; Robison 1994; Blaker & Peel 1997; Ineson & Peel 1997; Geyer & Peel 2011).

Fossils from the upper member of the Henson Gletscher Formation in southern Freuchen Land (Figs 1C, 2) comprise the *Bonnia–Pagetides elegans* Biozone of Geyer & Peel (2011) and Sundberg *et al.* (2016, 2022), which is the youngest biozone of Cambrian Stage 4 recognized in the Henson Gletscher Formation in North Greenland. The *Bonnia–Pagetides elegans* Biozone overlies strata referred to the *Eoagnostus roddyi– Oryctocarella duyunensis* Biozone by Sundberg *et al.* (2016, 2022). Note that an inadvertent error in Sundberg *et al.* (2022, fig. 4) places *Oryctocarella duyunensis* within the *Bonnia–Pagetides elegans* Biozone instead of the older eponymous biozone. This stratigraphic position in the figure should be assigned to *Pagetides elegans*. Unfortunately, both *Oryctocarella duyunensis* and *Pagetides elegans* are thereby omitted from their respective biozones in the Greenland column.

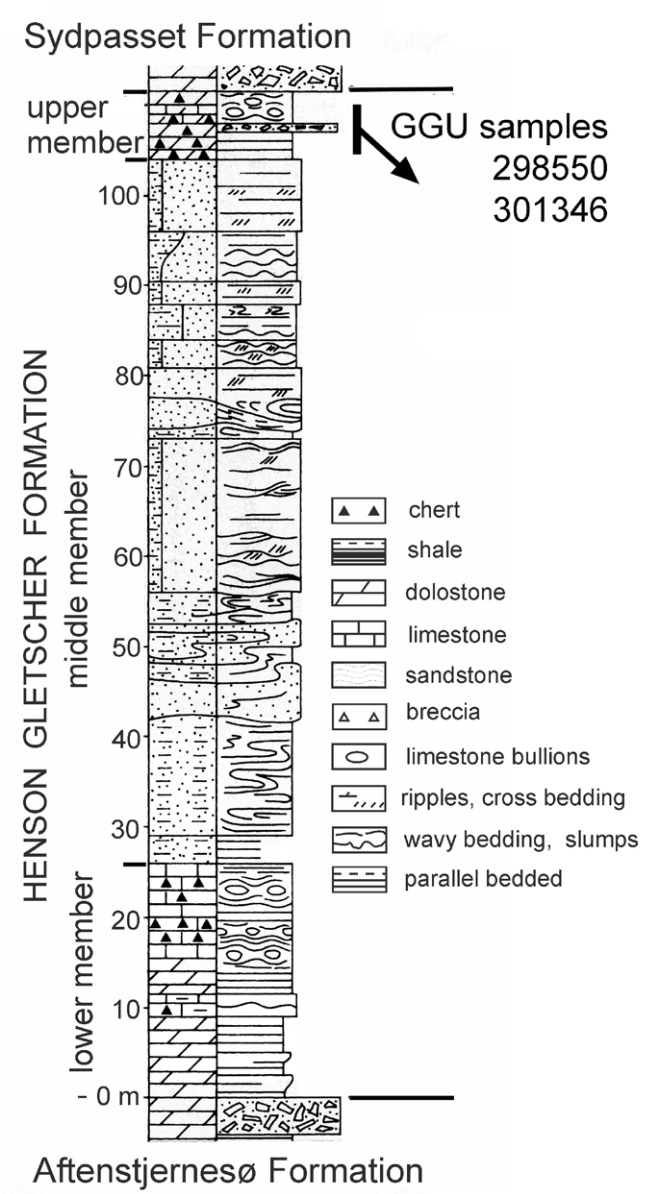

Fig. 2. Stratigraphic section of the Henson Gletscher Formation at the fossil locality in southern Freuchen Land (Fig. 1C) showing derivation of GGU samples. Section measured by J.R. Ineson (after Ineson & Peel 1997, fig. 32).

Systematic palaeontology

Institutional abbreviations and repositories. GGU prefix indicates a sample collected during field work by Grønlands Geologiske Undersøgelse (Geological Survey of Greenland), now part of the Geological Survey of Denmark and Greenland, Copenhagen, Denmark (GEUS). Specimen repositories: palaeontological type collection of the Museum of Evolution, Uppsala University, Sweden (PMU prefix); palaeontological collection of the Natural History Museum, Smithsonian Institution, Washington DC, USA (USNM prefix).

This published work and the nomenclatural acts it contains have been registered in Zoobank: http://zoobank.org/622724FF-49DB-46B9-A232-6BBADFB382BB

Phylum Mollusca Cuvier, 1797

Class Helcionelloida Peel, 1991a

Family Helcionellidae Wenz, 1938

Genus *Ressericonella* gen. nov.

Type species. *Helcionella aequa* Resser, 1939 from the Naomi Peak Limestone, the lowest member of the Langston Formation, Malad, southern Idaho; Cambrian, Miaolingian Series, Wuliuan Stage, *Albertella* Biozone. Here designated.

Derivation of name. *Ressericonella* is named for Charles Elmer Resser (1889–1943), American palaeontologist, combined with conella (Latin), meaning little cone, in the form of *Helcionella*, the eponymous genus of the class and family. Gender is feminine.

Diagnosis. Laterally compressed helcionelloid curved through about three quarters of a whorl such that the tightly coiled apex overhangs the sub-apical margin. Lateral surfaces are shallowly concave to shallowly convex, passing abruptly onto the shallowly convex supra-apical surface. Aperture sub-rectangular. Sub-apical surface arched into an apertural sinus. Ornamentation of numerous spiral cords crossed by comarginal growth lines, sometimes with weak rugae.

Discussion. *Ressericonella* gen. nov. is based on two species: the type species *Ressericonella aequa* (Resser, 1939) from southern Idaho, USA, and a new species, *Ressericonella pipalukae* sp. nov., from southern Freuchen Land, North Greenland. The former species occurs in the Naomi Peak Limestone Member (Miaolingian Series, Wuliuan Stage, *Albertella* Biozone) of the Langston Formation (Resser 1939; Maxey 1958; Kimmig *et al.* 2019). The latter species occurs in slightly older strata of the Henson Gletscher Formation (latest Cambrian Series 2, Stage 4, *Bonnia–Pagetides elegans* Biozone) in southern Freuchen Land (Geyer & Peel 2011).

In dorsal view, the rate of lateral expansion of *Ressericonella* decreases after the initial growth stage, resulting in an unusually narrow shell with sub-parallel lateral surfaces (Figs. 3B, 4C, F, J). In lateral view, the rate of shell expansion decreases with growth, causing smaller specimens (Figs. 3E, 4G) to exhibit a proportionately longer aperture where the apex is less strongly overhanging. Conversely, the large holotype of *Ressericonella aequa* has a relatively shorter aperture with a more pronounced overhang of the apex (Fig. 3A, C).

The coiled shell with flattened lateral surfaces and sub-rectangular aperture of *Ressericonella* gen. nov. recall several Cambrian helcionelloid genera mainly from Cambrian Stage 4 to Wuliuan Stage: *Coreospira* Saito, 1936, *Hampilina* Kobayashi, 1958, *Wakayella* Kruse, 1998, *Eocyrtolites* Yu, 1986, and *Tichkaella* Geyer, 1986. *Coreospira* differs from the cyrtoconic *Ressericonella* in having the lateral margins of the supra-apical (dorsal) surface forming a broad rounded ridge that overhangs the lateral areas, which display prominent rugae. In the type species, *Coreospira rugosa* Saito, 1936, and *Coreospira walcotti* Knight, 1947, the shell is tightly coiled through more than one whorl in the adult shell (Saito 1936; Knight 1947; Oh *et al.* 2021) but *Coreospira carinata* (Rasetti, 1957) has a cyrtoconic form. Geyer (2014) noted the similarity between *Helcionella aequa* [= *Ressericonella aequa*] and *Tichkaella* Geyer, 1986 in terms of the presence of radial ornamentation and laterally compressed shell. But *Ressericonella* differs from *Tichkaella* in the absence of prevailing paired radial ornamentation on dorsum (Geyer, 1986, pl. 4, 52b) and flattened sub-apical surface (Geyer, 1986, pl. 4, 51a). *Ressericonella* has a more strongly coiled shell than *Hampilina* or *Wakayella* but their prominent comarginal rugae are absent or only weakly developed (Kruse 1998; Oh *et al.* 2021). *Ressericonella* also differs from *Eocyrtolites* in having a much narrower sub-apical width relative to the supra-apical width (Yu 1986). Although classified into different genera, the cyrtoconic shells with sub-parallel lateral surfaces observed in *Ressericonella* and other related genera may indicate a close relationship. Their unique morphology distinguishes them from other helcionelloid species, and their occurrences in nearly coeval strata further support this connection. (Cambrian Series 2, Stage 4 to Miaolingian Series, Wuliuan Stage; Kruse, 1986; Yu, 1986, 1996; Oh *et al*., 2021).

A few species of *Dorispira* Parkhaev in Parkhaev & Demidenko, 2010, such as *Dorispira tavsenensis* Peel & Kouchinsky, 2022 and *Dorispira tippik* Peel & Kouchinsky, 2022 from the Henson Gletscher Formation (Wuliuan Stage of North Greenland), also have a sub-rectangular aperture, but *Dorispira* is readily distinguished from *Ressericonella* by its sharp comarginal rugae that cross over the dorsal surface (Parkhaev & Demidenko 2010).

Ressericonella aequa (Resser, 1939)

Fig. 3

1939 *Helcionella aequa* Resser, p. 24, pl. 1, figs 45–47.
1957 *Helcionella aequa* Rasetti, p. 970, 971.
2014 *Helcionella aequa* Geyer *et al*., p. 380.

Figured material. USNM 98487, holotype (Fig. 3A–C) and two additional specimens, USNM98487b and USNM 98487c, in the same museum tray as the holotype (Fig. 3D, E–H). Naomi Peak Limestone Member of the Langston Formation, near Malad, Idaho (Resser 1939; Maxey 1958). Cambrian, Miaolingian Series, Wuliuan Stage (*Albertella* Biozone).

Description. Laterally compressed cyrtoconic shell with bilateral symmetry. Shell width much narrower than length. Adult shell coiled through about three-quarters of a whorl (holotype; Fig. 3A–C). Apex recurved, overhanging the sub-apical surface. Aperture sub-rectangular to trapezoidal, with apertural sinus

at the sub-apical margin mainly evident in juvenile shells. Supra-apical surface shallowly convex; lateral surfaces flat to slightly concave; junction between the supra-apical surface and lateral surfaces relatively prominent, slightly angular. Densely spaced fine spiral cords and comarginal growth lines overprint very shallow rugae mainly developed on lateral surfaces.

Discussion. Resser (1939) illustrated only the holotype, but two additional specimens present in the same box as the holotype are likely conspecific and are also figured (Fig. 3D–H). The lateral surfaces of the holotype are exfoliated such that ornamentation is poorly preserved, except on the supra-apical surface (Fig. 3B), where the finely developed spiral ornamentation and comarginal growth lines are clearly visible, as is also the case in the two accompanying specimens (Fig. 3D, F).

Ressericonella pipalukae gen. et sp. nov.

v?2016 *Coreospira* sp. Peel *et al*. p. 264, fig. 14N, O.
2024 Helcionelloid indet. Oh *et al*. p. 8, fig. 5D, E.

Figs. 4, 5A, B

Holotype. PMU 18380 from GGU sample 301346, upper member of the Henson Gletscher Formation, southern Freuchen Land. Cambrian Series 2, Stage 4, *Bonnia–Pagetides elegans* Biozone.

Additional figured material. PMU 18378 from GGU sample 298550, PMU 18379, PMU 18382 and PMU 18381 from GGU sample 301346 from the same locality and horizon as the holotype.

Derivation of name. For Pipaluk Jette Tukuminguaq Kasaluk Palika Häger Freuchen (1918–1999), Greenland-born daughter of Danish Explorer Peter Freuchen and his wife Navarana, whose names are commemorated in Freuchen Land and Navarana Fjord (Fig. 1).

Diagnosis. Species of *Ressericonella* with smooth transition between the supra-apical surface and the lateral surfaces, and fine spiral (radial) and comarginal ornamentation without rugae.

Description. Moderately expanding, laterally compressed shell coiled through half to twothirds of a whorl. Aperture sub-rectangular, shell length about twice to three times shell width (Fig. 4F, G) with the apertural sinus at the sub-apical margin mainly

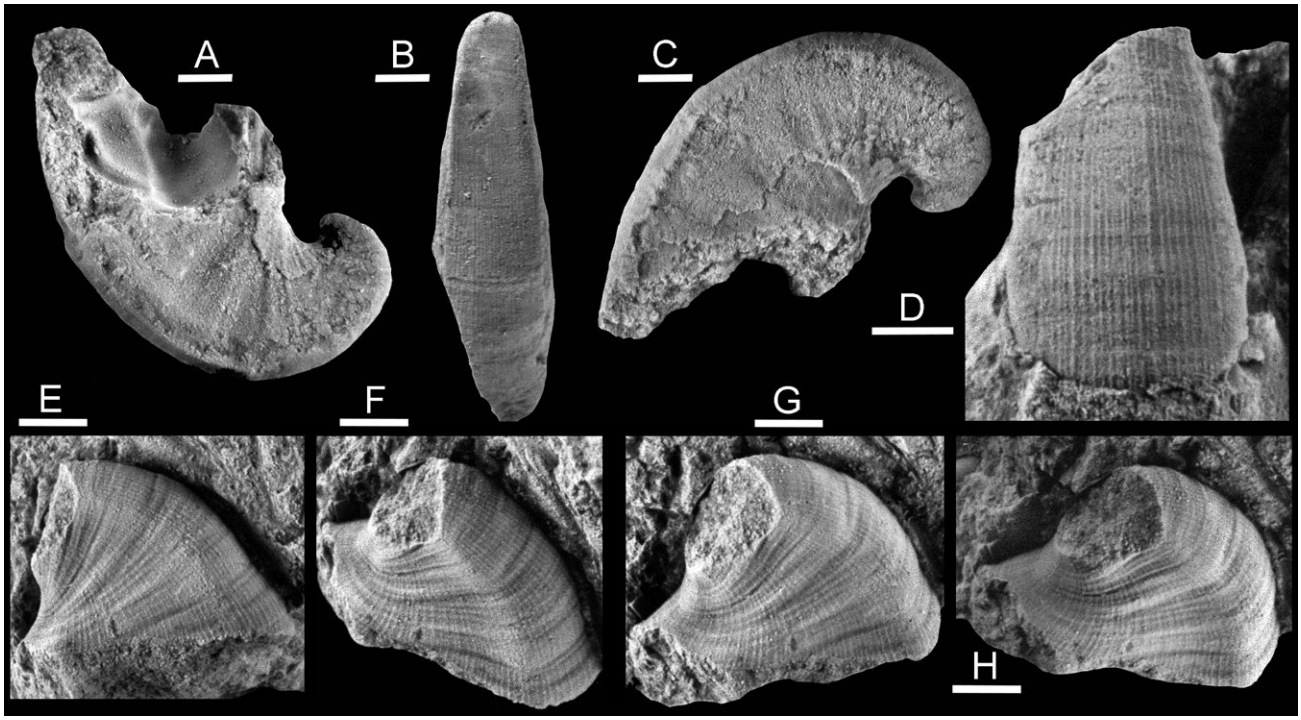

Fig. 3. *Ressericonella aequa* (Resser, 1939), Two Mile Canyon, Wasatch Mountains, Idaho. Langston Formation (Naomi Peak Limestone Member). Cambrian, Miaolingian Series, Wuliuan Stage, *Albertella* Biozone. **A–C:** USNM 98487, holotype, lateral (A,C) and dorsal (B) views. **D:**USNM 98487b, specimen in same museum tray as the holotype, fragment with dorsal ornamentation. **E–H:** USNM 98487c**,** specimen with broken apex in the same museum tray as the holotype, lateral (E) and oblique lateral (F–H) views. Scale bars: 1 mm.

evident in juvenile shells (Fig. 4C, D). The degree of expansion at the earliest growth stage is relatively rapid, but slower at the later growth stage, so that the width of the shell becomes constant in the adults (Fig. 4I, F, J). Apex pointed, recurved, overhanging the sub-apical surface; sometimes with shallow constrictions that possibly delimit the protoconch (Fig. 4C, H, I). Supra-apical surface transversely shallowly convex, becoming flattened in later growth stages (Fig. 4I, L); transition from the supra-apical surface to the lateral surfaces initially smooth (Fig. 4A, C), becoming more abruptly rounded in later growth stage (Fig. 4I, L); sub-apical surface strongly concave, with variable curvature. The shell surface smooth, without comarginal rugae; ornamented by comarginal growth lines and extremely finely spaced spiral cords (Fig. 4B, D). Shell seemingly composed of two shell layers, with an outer spirally (radially) ornamented layer overlying an inner layer with transverse fibrous structure (Figs. 4G, K, 5).

Discussion. *Ressericonella pipalukae* gen. et sp. nov. is variable in form, particularly with regard to the degree of curvature in the early growth stages of preserved shells. This is partly an ontogenetic effect, but may be affected by lateral crushing of the silicified shells, also seen in the holotype (Fig. 4H, L). *Ressericonella pipalukae* lacks the comarginal rugae seen on the lateral areas of *Ressericonella aequa*, from which it differs in the more rounded transition from the dorsum to the lateral areas.

In lateral view (Fig. 4G), *Ressericonella pipalukae* appears much more rapidly expanding than the holotype of *Ressericonella aequa*, but the latter is a larger specimen that markedly reduces the rate of expansion as it

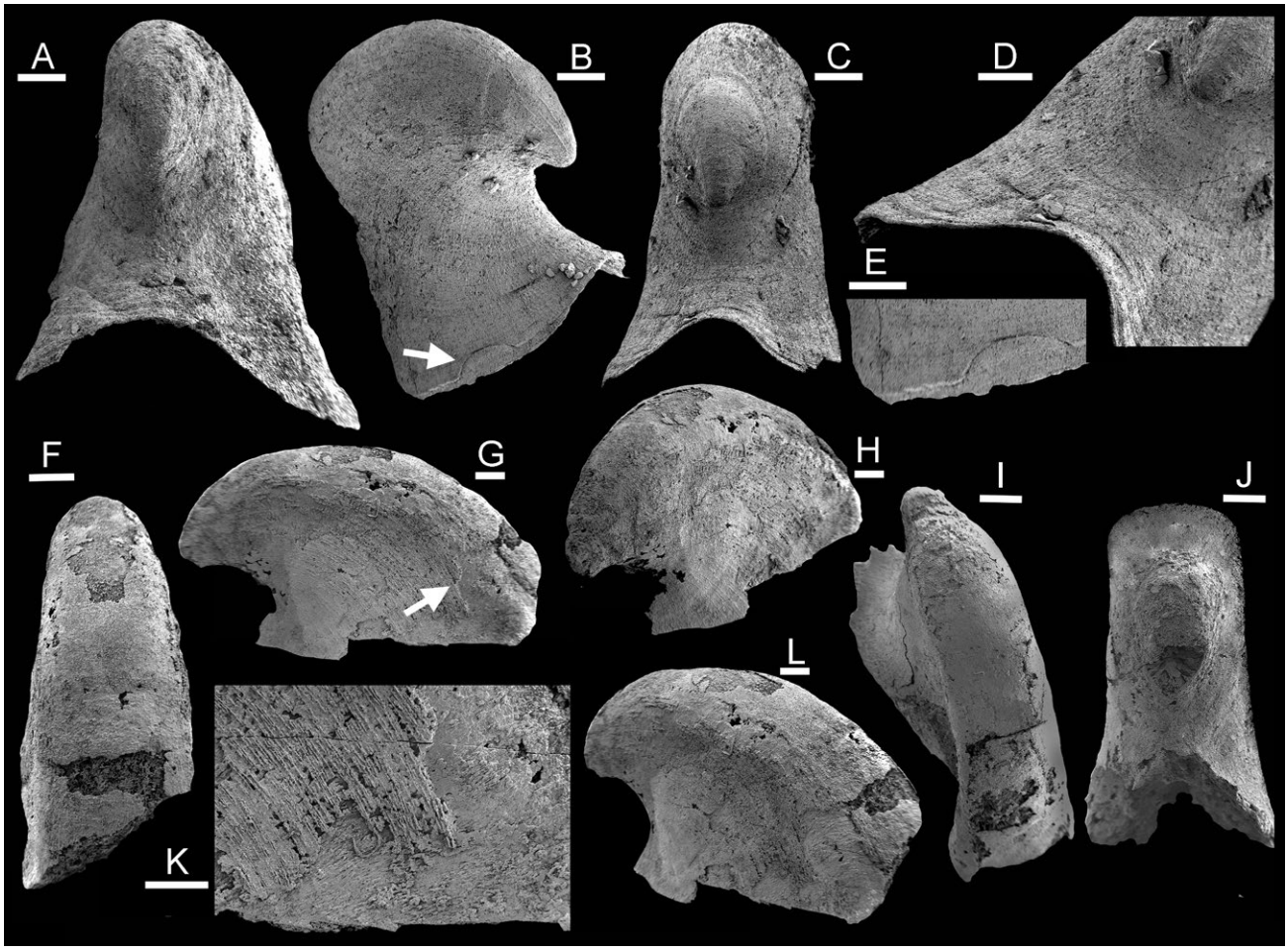

Fig. 4. *Ressericonella pipalukae* gen. et sp. nov. from the upper Henson Gletscher Formation, southern Freuchen Land. Cambrian Series 2, Stage 4, *Bonnia–Pagetides elegans* Biozone. GGU sample 301346 unless stated. **A:** PMU 18378 from GGU sample 298550, sub-apical view. **B–E:** PMU 18379, sub-apical view (C) with detail of apertural emargination showing fine spiral ribs (D) and oblique lateral view (B) with repaired injury in apertural margin (E, arrow in B). **F–H, K, L:** PMU 18380, holotype, dorsal (supra-apical, F), lateral (G) and oblique lateral (H, L) views with surface detail (K, arrow in G). **I, J:** PMU 18381, oblique dorsal (I) and apical (J) views, with broken sub-apical margin. Scale bars: 200 µm (D, E, K); 300 µm (A–C, G–J, L); 400 µm (F).

gets larger. Lateral expansion is reduced with growth in both species such that dorsum almost stops increasing in width (Figs. 3B, 4F).

The silicified holotype of *Ressericonella pipalukae* preserves two-layered shell structure on the dorsolateral area (Fig. 4G, H, K) with an outer spirally (radially) ribbed layer overlying an inner fibrous layer. In detail (Fig. 4K), the fibres appear to lie on imbricated laminae that step down towards the dorsum. In this view, the spiral (radial) cords are narrow and often paired, but their appearance is clearly affected by imperfect silicification during diagenesis. Oh *et al*. (2024) interpreted radial threads on a variety of silicified shells from the Cambrian, inclusive the same samples in southern Freuchen Land, as fossilized periostracal structures.

One fragmented helcionelloid with radial ornaments, previously referred to as Helcionelloid indet. by Oh *et al*. (2024, fig. 5D, E; PMU 21541 from GGU sample 301347), is assigned herein to *Ressericonella pipalukae*. This assignment is justified based on the similar outline of the umbonal region and the same shell structure (see below).

A specimen referred to as *Coreospira* sp. in Peel *et al*. (2016, fig. 14N, O) from the *Ovatoryctocara granulata* assemblage of the Henson Gletscher Formation in the Løndal area (PMU 28970 from GGU sample 218681) is tentatively assigned to *Ressericonella pipalukae*, mainly based on the sub-rectangular aperture and fine radial and comarginal ornamentation, but further study is required based on more complete samples.

A small repaired shell injury (Fig. 4B, E) is likely of non-biogenic origin.

Ressericonella sp.

Fig. 5C–E

Figured material. PMU 18383 from GGU sample 301346, upper member of the Henson Gletscher Formation, southern Freuchen Land. Cambrian Series 2, Stage 4, *Bonnia–Pagetides elegans* Biozone.

Discussion. A single specimen (Fig. 5C–E) is tentatively assigned to *Ressericonella* sp. because it has a much more tightly coiled (rapidly expanded shell), represented by a narrower umbilicus and a more laterally compressed shell profile (compare 4G and 5C), although similar shell structure (see below).

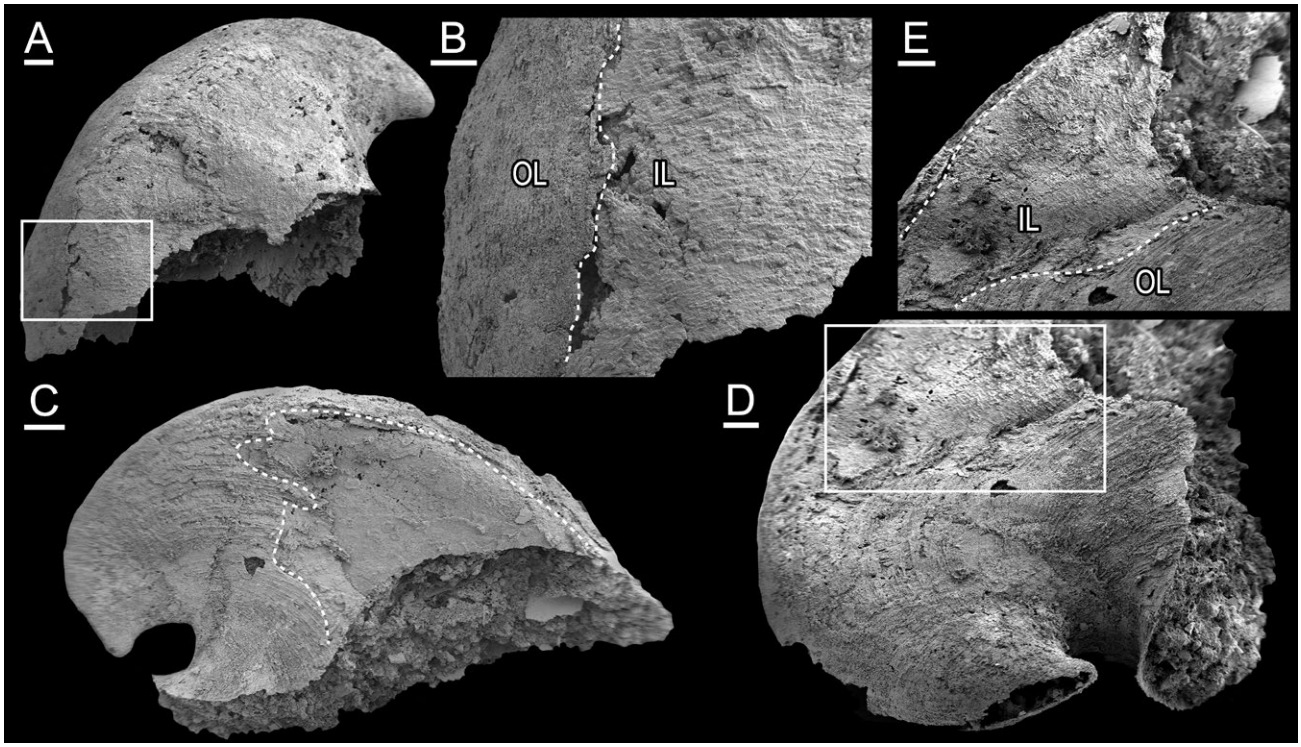

Fig. 5. Shell structures of *Ressericonella* from the upper Henson Gletscher Formation, southern Freuchen Land. Cambrian Series 2, Stage 4, *Bonnia–Pagetides elegans* Biozone. GGU sample 301346. **A, B:** *Ressericonella pipalukae* sp. nov. PMU 18382, lateral view (A) and magnified view showing the outer layer (OL) and the inner layer (IL) (B). **C–E:** *Ressericonella* sp. PMU 18383, lateral view (C), oblique lateral view (D) and magnified view (E) showing the outer layer (OL) and the inner layer (IL) (E). The box in A and D indicates the magnified area in B and E respectively. Dashed lines denote the boundary between the outer and inner layers. Scale bars: 100 μm (B); 200 μm (A, D, E); 300 μm (C).

Remarks on shell structure

Several samples preserve shell structure consisting of outer and inner layers ('OL' and 'IL' in Fig. 5B, E). The outer layer is characterized by radially arranged lineations ('radial threads') originating from the umbonal region, covering the shell surface (Figs. 4B, C, D, G, K, 5C, D). Similar features have been reported in other helcionelloid species with silicified or phosphatized forms, described as 'radial threads' (Runnegar & Jell 1976), 'radial striation' (Gubanov *et al*. 2004), and 'radiating ridges' (Vendrasco *et al*. 2011). According to a recent study (Oh *et al*. 2024), these features possibly represent the molluscan periostracum. The structure observed in a specimen (Fig. 4B–D) reveals closely spaced radial threads resembling fine spiral ribbing, indicating potential variations in periostracal morphology. The outer layer with radial threads may correspond to a thin encrustation on the shell surface, while the original shell, composed of calcareous material (e.g., aragonite), could have been lost during diagenesis or the acid etching process used to obtain the samples.

The underlying inner layer shows a fibrous pattern arranged transversely, perpendicular to the radial threads on the outer layer. This fibrous pattern is similar to lamello-fibrillae, although it has been replaced by coarse silica (Fig. 5B). While the lamello-fibrillar microstructure is uncommon in modern molluscs, it appears to have been common in Cambrian forms [e.g., *Pelagiella deltoides* Runnegar & Jell, 1976, in Vendrasco *et al*. 2010; *Ilsanella* cf. *orectes* (Jiang in Luo *et al*., 1982) in Feng & Sun 2003]. The lamello-fibrillar microstructure of *Pelagiella* is known from the outermost shell layer (Li *et al*. 2017), but it also occurs in the internal mould of *P. deltoides*, representing the innermost surface of the shell (Vendrasco *et al*. 2010).

The recognition of the multi-layered shell structure of *Ressericonella pipalukae* sp. nov. (Fig. 5) can be compared to other Cambrian helcionelloids. Vendrasco & Checa (2015) suggested that *Mackinnonia davidi* (Runnegar in Bengtson *et al*., 1990) [= *Davidonia rostrata* (Zhou & Xiao, 1984)] from the Parara Limestone of South Australia has a two-layered shell consisting of a prismatic outer layer and a calcitic semi-nacre inner layer. They noted the similarity of the shell microstructure of *Davidonia rostrata* with other Cambrian molluscan taxa such as *Mellopegma* Runnegar and Jell, 1976 (a stenothecid helcionelloid), suggesting a possible phylogenetic relationship between them. Ebbestad *et al*. (2024) reported *Davidonia puppis* (Høyberget, Ebbestad, Funke & Nakrem, 2015) from the Gislöv Formation (Cambrian Series 2, Stage 4) in southern Sweden. At least two layers of shell were identified, consisting of the relatively thick, fibrous inner layer and thin outer layer shaping the smooth cap shaped outline enveloping the strongly undulated internal mould (Ebbestad *et al*. 2024, fig. 14I, J).

Li *et al*. (2017) documented five types of shell microstructures in the Cambrian helcionelloid *Pelagiella madianensis*, indicating an aragonitic composition organised into a hierarchical structure with four orders. Their findings included specimens with preserved internal moulds and outermost layers (termed 'acid-etched shell residue') that are similar to the specimens examined here (Li *et al*. 2017, fig. 1A, b; Fig. 5), however it is uncertain whether *Ressericonella* also has the same complex hierarchical shell morphology.

Acknowledgements

The authors are most grateful to two reviewers, Gerd Geyer and Jan Ove R. Ebbestad, for their constructive comments and suggestions. Material from Freuchen Land was collected during the North Greenland regional mapping project (1984–1985) of Grønlands Geologiske Undersøgelse (Geological Survey of Greenland). J.S.P. acknowledges aid during sample collection from Mark Blaker and ongoing collaboration with Jon R. Ineson (GEUS, Copenhagen) concerning North Greenland Cambrian geology. Y.O was supported by a Korea Polar Research Institute (KOPRI) grant funded by the Ministry of Oceans and Fisheries (KOPRI PE24060).

References

Atkins, C.J. & Peel, J.S. 2004: New species of *Yochelcionella* (Mollusca; Helcionelloida) from the Lower Cambrian of North Greenland. Bulletin of the Geological Society of Denmark 51, 1–9. https://doi.org/10.37570/bgsd-2004-51-01

Atkins, C.J. & Peel, J.S. 2008: *Yochelcionella* (Mollusca, Helcionelloida) from the lower Cambrian of North America. Bulletin of Geosciences 83, 23–38. https://doi.org/10.3140/bull.geosci.2008.01.023

Bengtson, S., Conway Morris, S., Cooper, B.J., Jell, P.A. & Runnegar, B.N. 1990: Early Cambrian fossils from South Australia. Memoirs of the Australasian Association of Palaeontologists 9, 1–364.

Billings, E. 1872: On some new species of Palaeozoic fossils. The Canadian Naturalist 6, 213–222.

Blaker, M.R. & Peel, J.S. 1997: Lower Cambrian trilobites from North Greenland. Meddelelser om Grønland, Geoscience 35, 1–145. https://doi.org/10.1017/s0016756898258432

Cuvier, G. 1797: Tableau Élementaire de l'historie Naturelle des Animaux, 710 pp. Paris: Baudouin.

Ebbestad, J.O.R., Cederström, P. & Peel, J.S. 2024. Helcionelloid molluscs from the lower Cambrian (Series 2, Stage 4) of southern Sweden. Historical Biology 36, 1854–1882.

Feng, W.M. & Sun, W.G. 2003: Phosphate replicated and replaced microstructure of molluscan shells from the earliest Cambrian of China. Acta Palaeontologica Polonica 48, 21–30.

Geyer, G. 1986: Mittelkambrische Mollusken aus Marokko und Spanien. Senckenbergiana lethaea 67, 55–118.

Geyer, G., Peel, J.S., Streng, M., Voigt, S., Fischer, J. & PREUßE, M. 2014: A remarkable Amgan (Middle Cambrian, Stage 5) fauna from the Sauk Tanga, Madygen region, Kyrgyzstan. Bulletin of Geosciences 89, 375–400.

Geyer, G. & Peel, J.S. 2011: The Henson Gletscher Formation, North Greenland, and its bearing on the global Cambrian Series 2–Series 3 boundary. Bulletin of Geosciences 86, 465–534. https://doi.org/10.3140/bull.geosci.1252

Grabau, A.W. & Shimer, H.W. 1909: North American index fossils, invertebrates, Volume 1, 853 pp. New York: A.G. Seiler & Company. https://doi.org/10.5962/bhl.title.52120

Gubanov, A.P. & Peel, J.S. 2001: Latest helcionelloid molluscs from the Lower Ordovician of Kazakhstan. Palaeontology 44, 681–694. https://doi.org/10.1111/1475-4983.00198

Gubanov, A., Kouchinsky, A., Peel, J.S. & Bengtson, S. 2004: Middle Cambrian molluscs of 'Australian' aspect from northern Siberia. Alcheringa 28, 1–20. https://doi.org/10.1080/03115510408619272

Higgins, A.K., Ineson, J.R., Peel, J.S., Surlyk, F. & Sønderholm, M. 1991: Lower Palaeozoic Franklinian Basin of North Greenland. Bulletin Grønlands Geologiske Undersøgelse 160, 71–139.

Høyberget, M., Ebbestad, J.O.R., Funke, B. & Nakrem, H.A. 2015. The shelly fauna and biostratigraphy of the lower Cambrian (provisional Series 2, Stage 4) Evjevik Member, Ringstrand Formation in the Mjøsa area, Norway. Norwegian Journal of Geology 95, 23–56.

Ineson, J.R. & Peel, J.S. 1997: Cambrian shelf stratigraphy of North Greenland. Geology of Greenland Survey Bulletin 173, 1–120. https://doi.org/10.34194/ggub.v173.5024

Jacquet, S.M. & Brock, G.A. 2016: Lower Cambrian helcionelloid macromolluscs from South Australia. Gondwana Research 36, 333–358. https://doi.org/10.1016/j.gr.2015.06.012

Kimmig, J., Strotz, L.C., Kimmig, S.R., Egenhoff, S.O. & Lieberman, B.S. 2019: The Spence Shale Lagerstätte: an important window into Cambrian biodiversity. Journal of the Geological Society 176, 609–619. https://doi.org/10.1144/jgs2018-195

Knight, J.B. 1947: Some new Cambrian bellerophont gastropods. Smithsonian Miscellaneous Collections 106, 1–11.

Kobayashi, T. 1958: On some Cambrian gastropods from Korea. Japanese Journal of Geology and Geography 29, 111–118.

Kruse, P.D. 1998: Cambrian palaeontology of the eastern Wiso and western Georgina Basins. Northern Territory Geological Survey Report 9, 68 pp.

Luo, H., Jiang, Z., Wu, X., Song, X. & Ouyang, L. et al. 1982: The Sinian-Cambrian boundary in eastern Yunnan, China, 285 pp. Kunming: P.R. China. (Chinese with English abstract)

Li, L., Zhang, X., Yun, H. & Li, G. 2017: Complex hierarchical microstructures of Cambrian mollusk *Pelagiella*: insight into early biomineralization and evolution. Scientific Reports 7, 1935. https://doi.org/10.1038/s41598-017-02235-9

Li, L., Zhang, X., Skovsted, C.B., Yun, H., Pan, B. & Li, G. 2021: Revisiting the molluscan fauna from the Cambrian (Series 2, stages 3–4) Xinji Formation of North China. Papers in Palaeontology 7, 521–564. https://doi.org/10.1002/spp2.1289

Maxey, G. B. 1958: Lower and Middle Cambrian stratigraphy in northern Utah and southeastern Idaho. Geological Society of America Bulletin 69, 647–688.

Missarzhevsky, V.V. 1989: Drevneyshie skeletnye okamenelosti i stratigrafiya ogranichnykh tolshch dokembriya i kembriya. Trudy Geologicheskogo Instituta, Akademiya Nauk SSSR 443, 1–237.

Oh, Y., Lee, D.-C., Lee, D.-J., & Lee, J.-G. 2021: Cambrian helcionelloids (univalved molluscs) from the Korean Peninsula: systematic revision and biostratigraphy. Alcheringa 45, 127–139. https://doi.org/10.1080/03115518.2021.1929479

Oh, Y., Peel, J.S., Zhen, Y.Y., Smith, P.M., Lee, M. & Park, T.-Y.S. 2024: Periostracum in Cambrian helcionelloid and rostroconch molluscs: comparison to modern taxa. Lethaia 57, 1–17 https://doi.org/10.18261/let.57.1.6

Parkhaev, P.Yu. 2001: Molluscs and siphonoconchs, 133–210. In: Alexander, E.M., Jago, J.B., Rozanov, A.Yu. & Zhuravlev, A.Yu. (eds): The Cambrian biostratigraphy of the Stansbury Basin, South Australia. Transactions of the Palaeontological Institute, Russian Academy of Sciences 282.

Parkhaev, P.Yu. & Demidenko, Yu. 2010: Zooproblematica and Mollusca from the lower Cambrian Meishucun section (Yunnan, China) and taxonomy and systematics of the Cambrian small shelly fossils of China. Paleontological Journal 44, 883–1161. https://doi.org/10.1134/S0031030110080010

Peel, J.S. 1988: Molluscs of the Holm Dal Formation (late Middle Cambrian), central North Greenland. Meddelelser om Grønland, Geoscience 20, 145–168.

Peel, J.S. 1989: A Lower Cambrian *Eotebenna* (Molluscs) from Arctic North America. Canadian Journal of Earth Sciences 26, 1501–1503.

Peel, J.S. 1991a*:* Functional morphology of the Class Helcionelloida nov., and the early evolution of the Mollusca. In: Simonetta, A. & Conway Morris, S. (eds): The early evolution of Metazoa and the significance of problematic taxa, 157–177. Cambridge: Cambridge University Press. https://doi.org/10.1093/sysbio/42.1.106

Peel, J.S. 1991b: The classes Tergomya and Helcionelloidea, and early molluscan evolution. Bulletin Grønlands Geologiske Undersøgelse 161, 11–65. https://doi.org/10.34194/bullggu.v161.6717

Peel, J.S. 1994: An enigmatic cap-shaped fossil from the Middle Cambrian of North Greenland. Bulletin Grønlands geologiske Unders*øgelse* 169, 149–155. https://doi.org/10.34194/bullggu.v169.6729

Peel, J.S. 2021: An outer shelf shelly fauna from Cambrian Series 2 (Stage 4) of North Greenland (Laurentia). Journal of Paleontology 95, Memoir 83, 1–41. https://doi.org/10.1017/jpa.2020.112

Peel, J.S, 2023: Muscle scars in Miaolingian helcionelloids from Laurentia and the diversity of muscle scar patterns in Cambrian univalve molluscs. Alcheringa 47, 221–233. https://doi.org/10.1080/03115518.2023.2243501

Peel, J.S. & Kouchinsky, A. 2022: Middle Cambrian (Miaolingian Series, Wuliuan Stage) molluscs and mollusc-like microfossils from North Greenland (Laurentia). Bulletin of the Geological Society of Denmark 70, 69–104. https://doi.org/10.37570/bgsd-2022-70-06

Peel, J.S. & Skovsted, C.B. 2005: Problematic cap-shaped fossils from the Lower Cambrian of North-East Greenland. Paläontologische Zeitschrift 79, 461–470.

Peel, J.S., Streng, M., Geyer, G., Kouchinsky, A. & Skovsted, C.B. 2016: *Ovatoryctocara granulata* assemblage (Cambrian Series 2–Series 3 boundary) of Løndal, North Greenland. Australasian Palaeontological Memoirs 49, 241–282.

Phillips, J. 1836: Illustrations of the Geology of Yorkshire; or a description of the strata and organic remains: accompanied by a geological map, sections and diagrams, and figures of the fossils. Part II. The Mountain Limestone District. John Murray, London, 370 pp.

Rasetti, F. 1957: Additional fossils from the Middle Cambrian Mt. Whyte Formation of the Canadian Rocky Mountains. Journal of Paleontology 31, 955–972.

Resser, C.E. 1939: The *Ptarmigania* strata of northern Wasatch Mountains. Smithsonian Miscellaneous Collection 98, 1–72.

Robison, R.A. 1994: Agnostoid trilobites from the Henson Gletscher and Kap Stanton formations (Middle Cambrian), North Greenland. Bulletin Grønlands Geologiske Undersøgelse 169, 25–77. https://doi.org/10.34194/bullggu.v169.6726

Rozanov, A.Yu. & Missarzhevsky, V.V. 1966: Biostratigrafiya i fauna nizhnikh gorizontov kembriya. Akademiya Nauk SSSR, Trudy Geologicheskaya Instituta 148, 1–125.

Rozanov A.Yu. *et al*. 1969: Tommotskiy yarus i problema nizhney granitsy kembriya. Akademiya Nauk SSSR, Trudy Geologicheskaya Instituta 206, 1–379.

Runnegar, B. & Jell, P.A. 1976: Australian Middle Cambrian molluscs and their bearing on early molluscan evolution. Alcheringa 1, 109–138. https://doi.org/10.1080/03115517608619064

Saito, K. 1936: Older Cambrian Brachiopoda, Gastropoda, etc., from northwestern Korea. Journal of the Faculty of Science, the Imperial University of Tokyo, Section 2, 4, 345–367.

Skovsted, C.B. 2004: Mollusc fauna of the Early Cambrian Bastion Formation of North–East Greenland. Bulletin of the Geological Society of Denmark 51, 11–37. https://doi.org/10.37570/bgsd-2004-51-02

Skovsted, C.B. 2006: Small shelly fauna from the upper lower Cambrian Bastion and Ella Island formations, North-East Greenland: Journal of Paleontology 80, 1087–1112.

Streng, M., Butler, A.D., Peel, J.S., Garwood, R.J. & Caron, J.-B. 2016: A new family of Cambrian rhynchonelliformean brachiopods (Order Naukatida) with aberrant coral-like morphology. Palaeontology 59, 269–293. https://doi: 10.1111/pala.12226

Sundberg, F.A. 2007: Nightmare on Resser Street – dealing with Resser's trilobite taxonomy. In: Mikulic, D.G., Landing, E. & Kluessendorf, J. (eds): Fabulous fossils – 300 years of worldwide research on trilobites, 213–224. New York State Bulletin 507.

Sundberg, F.A., Geyer, G., Kruse, P.D., McCollum, L.B., Pegel', T.V., Żylińska, A. & Zhuravlev, A.Yu. 2016: International correlation of the Cambrian Series 2-3, Stages 4-5 boundary interval. Australasian Palaeontological Memoirs 49, 83–124.

Sundberg, F.A., Webster, M. & Geyer, G. 2022: Biostratigraphical significance of a new trilobite fauna from the Harkless Formation (upper Stage 4, Series 2, Cambrian), Nevada, USA. Lethaia 55, 1–12. https://doi.org/10.18261/let.55.3.8

Vendrasco, M.J. & Checa, A.G. 2015: Shell microstructure and its inheritance in the calcitic helcionellid *Mackinnonia*. Estonian Journal of Earth Sciences 64, 99–104. http://hdl.handle.net/10481/35706

Vendrasco, M.J., Porter, S.M., Kouchinsky, A., Li, G. & Fernandez, C.Z. 2010: New data on molluscs and their shell microstructures from the Middle Cambrian Gowers Formation, Australia. Palaeontology 53, 97–135. https://doi.org/10.1111/j.1475-4983.2009.00922.x

Vendrasco, M.J., Kouchinsky, A.V., Porter, S.M. & Fernandez, C.Z. 2011: Phylogeny and escalation in *Mellopegma* and other Cambrian molluscs. Palaeontologia Electronica 14: 1–44. palaeo-electronica.org/2011_2/221/index.html

Wenz, W. 1938: Gastropoda. Allgemeiner Teil und Prosobranchia. In: Schindewolf, O.H. (ed.), Handbuch der Paläozoologie 6, 1–240. Berlin: Gebrüder Bornträger.

Yu, W. 1979: Earliest Cambrian monoplacophorans and gastropods from western Hubei with their biostratigraphical significance. Acta Palaeontologica Sinica 18, 233–270 [Chinese with English abstract].

Yu, W. 1986. Lower Cambrian univalved molluscs from Kuruktag, Xinjiang. Acta Palaeontologica Sinica 25, 10–16. [Chinese with English abstract].

Yu, W. 1996. Early Cambrian stenothecoid molluscs from China. Records of the Western Australia Museum 18, 209–218.

Zhou, B. & Xiao, L. 1984: Early Cambrian monoplacophorans and gastropods from Hainan and Huoqiu Counties, Anhui Province. Professional Papers of Stratigraphy and Palaeontology 13, 125–140 [Chinese with English abstract]

Holocene history of Fiskesø, Prinsesse Ingeborg Halvø, eastern North Greenland

BERND WAGNER & OLE BENNIKE

Geological Society of Denmark
https://2dgf.dk

Received 2 April 2024
Accepted in revised form
11 September 2024
Published online
13 November 2024

Wagner, B. & Bennike, O. 2024: Holocene history of Fiskesø, Prinsesse Ingeborg Halvø, eastern North Greenland. Bulletin of the Geological Society of Denmark, Vol. 73, pp. 209–220. ISSN 2245-7070. https://doi.org/10.37570/bgsd-2024-73-13

Sediment cores up to 92 cm in length were recovered with gravity and Russian peat corers from Fiskesø, Prinsesse Ingeborg Halvø, eastern North Greenland, during the summer 2014. The correlated sediment succession consists of clastic sediments that are interspersed in the upper part with layers of organic material and likely record the environmental history of the lake since deglaciation. The paucity of macrofossil remains hampered radiocarbon dating of the sediments from Fiskesø. According to published data, the deglaciation of the region took place *c.* 10 cal. ka BP. Relative sea-level reconstructions from the region suggest that the Fiskesø basin, which is today located at 33 m above sea level, was characterised by marine conditions until *c.* 8.1 cal. ka BP. Marine fossils in the lower part of the sediment succession support the prevalence of marine conditions. A reliable radiocarbon age from 5 cm above the isolation horizon in Fiskesø sediments indicates an age of 6.1 cal. ka BP and supports the isolation of the basin prior to this time. Cooling is indicated in the upper part of the sediment succession and is reported to have taken place in the region stepwise shortly after 6.1 cal. ka BP and at *c.* 4.5–4.0 cal. ka BP. Despite the poor chronology the data from Fiskesø support existing terrestrial and marine reconstructions from the region.

Keywords: Holocene, lake sediments, macrofossils, geochemistry.

Bernd Wagner [wagnerb@uni-koeln.de], University of Cologne, Institute of Geology and Mineralogy, Zülpicher Str. 49a, D-50674 Köln, Germany. Ole Bennike [obe@geus.dk] Geological Survey of Denmark and Greenland (GEUS), Øster Voldgade 10, DK-1350 Copenhagen K, Denmark.

Eastern North Greenland is one of the most remote regions on Earth, which is also expressed in a paucity of environmental records spanning the Holocene history of the region. Such records are needed to gain a better understanding of land-ocean interactions, including changes in temperatures and precipitation, history of local ice caps and sea-ice cover. For example, the shelf area off eastern North Greenland is discussed as one of the source regions of the East Greenland Current (EGC), which exports cold, polar water masses from the Arctic Ocean into the North Atlantic and is strongly interconnected with Atlantic water circulation patterns (e.g. Rudels & Quadfasel 1991; Jeansson *et al.* 2008; Foukal *et al.* 2020).

From the terrestrial perspective, information from North Greenland ice cores is very limited and amplified by large problems in obtaining reliable age control of these cores. The Hans Tausen Iskappe in central North Greenland retreated behind present position around 8.5 cal. ka BP and only the northern part may have survived the early Holocene Thermal Maximum (HTM; Landvik *et al.* 2001; Zekollari *et al.* 2017). Studies of a 345-m-long core from the ice cap revealed that the oldest ice at the coring location may be dated to around 4.0 cal. ka BP (Madsen & Thorsteinsson 2001). The chronological constraints allow interpretation only for the last 2000 years (Hammer *et al.* 2001). In eastern North Greenland, local ice caps may also have survived the HTM (Larsen *et al.* 2019). However, a 425-m-long ice core drilled from Flade Isblink in 2006 may have captured only the last 2800–3300 years of environmental history and chronological constraints are poor (Lemark 2010).

Lacustrine records are also sparsely available from eastern North Greenland and partly exhibit very limited age control. Palynological studies of sediment

records from Klaresø in Peary Land (Fredskild 1969) and Sommersø on Prinsesse Ingeborg Halvø (Funder & Abrahamsen 1988) showed a decline in vegetation during the Middle Holocene around 4.0–4.5 cal. ka BP. In a sediment record from Bliss Lake, Peary Land, 24 samples were used for radiocarbon dating, but only six samples provided reliable ages (Olsen *et al.* 2012). The record from this lake provides a valuable record of environmental change in the region, showing a transition from lacustrine to marine conditions in the earliest Holocene and an isolation from the sea again at 7.2 cal. ka BP. A sediment record from Kaffeklubben Sø in northernmost Peary Land covers the last *c.* 3000 years only (Perren *et al.* 2012). Further to the east, a number of lakes on Finderup Land provided valuable information on relative sea-level (RSL) changes and fluctuations of the Flade Isblink during the Holocene (Strunk *et al.* 2018; Larsen *et al.* 2019). Sediment records from Skallingen, south of Flade Isblink, show various changes in environmental conditions over the last 8000 years in a location further inland, but the age control is also quite limited (Wagner & Bennike 2015; Kusch *et al.* 2019).

We here present data from sediment successions recovered from Fiskesø on Prinsesse Ingeborg Halvø. The data will help to set the existing data from other terrestrial and marine records in a broader regional context and will help to better understand land-ocean interactions in the closer surrounding.

Study area

Fiskesø (81°33'N, 16°14'W) is located at 33 m above sea level (a.s.l.), ~8 km to the southeast of Station Nord on Prinsesse Ingeborg Halvø, Kronprins Christian Land, eastern North Greenland (Fig. 1). The lake has an irregular shape with a maximum extension of ~800 m along the N–S-axis. Fiskesø was visited between 16 and 20 July 2014. At these days, the ice cover on the lake had started to disintegrate, with the formation of a moat and holes of up to ~2 m diameter in the ice cover (Fig. 1C). Measurements with a handheld echosounder at eight sites in the central part of the lake indicated an undulated bathymetry and a maximum water depth of at least 22.2 m (Fig. 1D). According to measurements in early December 2017, the ice cover on Fiskesø was 58 cm thick and the lake water showed a pH of 7.35 and a conductivity of 200 μS/cm (Christoffersen 2018).

The bedrock surrounding the lake is dominated by Upper Permian carbonates and shales, with the latter prevailing north of the lake towards the present marine shoreline (Håkansson & Pedersen 2001, 2015). Lower Permian limestone and tectonic breccia occur south of Fiskesø, but is, as the areas north of the lake, predominantly covered by till (Goodsite *et al.* 2014). The Prinsesse Ingeborg Halvø (peninsula) is bordered by the Flade Isblink ice cap to the east and south and the Wandel Sea to the west and north. The subdued landscape of the peninsula scarcely exceeds 150 m a.s.l. (Håkansson *et al.* 1989). Several beach ridges can be found ~500 m to the north of Fiskesø (Goodsite *et al.* 2014) and document the relative sea-level lowering of the region after deglaciation.

The High Arctic climate on Prinsesse Ingeborg Halvø, with mean annual temperatures of –16.9°C and a mean July temperature of 3.4°C (during the period from 1961 to 1990; Cappelen *et al.* 2001), causes a short snow-free period that lasts from late July to early September (Funder & Abrahamsen 1988). The vegetation cover on the very shallow active layer (probably around 10 cm; Goodsite *et al.* 2014) is extremely sparse and mainly composed of algae, lichens, mosses and very few angiosperms, which classifies the area as a polar desert (Funder & Abrahamsen 1988). The dwarf shrubs *Salix arctica* and *Dryas integrifolia* are the only woody plants, they grow in areas that become snow-free relatively early.

Material and methods

Based on the echosounder measurements, two locations were selected for the recovery of sediment cores from Fiskesø. The first location was in the western central part of the lake, where the maximum water depth of 22.2 m was measured (Fig. 1D). At this location (81°33'33.2''N, 16°14'23.6''W), two deployments of a gravity corer (GC; UWITEC Co.) with a recovery of 21 and 40 cm, respectively, indicated dark silty sediments and a series of small turbidites through the transparent PVC liner. In order to obtain longer and undisturbed sediment successions with the gravity corer and a Russian peat corer with a 100-cm-long and 7.5-cm-wide chamber, a shallower location in the more central part of the lake was selected, where the echosounder revealed a water depth of 8.6 m (Fig. 1D). At this location, two gravity cores of 52 cm (GC1) and 34 cm (GC2) length with an undisturbed sediment surface were recovered. Subsequently, three sediment cores were recovered with the peat corer. Hammering on the peat corer at a sediment depth of ~1 m provided only marginal further penetration. The surfaces of the cores were partly washed out due to incomplete closure of the corer during retrieval through the water column. Immediately after recovery, the cores obtained with the peat corer

were photographed, transferred to PVC half pipes and wrapped in cling film.

Opening of the gravity cores in the laboratories of the University of Cologne revealed a good match between the surface sediments and the sediment successions recovered with the peat corer. Visual correlation of marker layers allowed splicing of the cores and revealed that Russian core (RC) 1 covered 8–92 cm, RC2 0–81 cm and RC3 0–91 cm (appendix).

For grain-size analyses on core RC3 and in order to

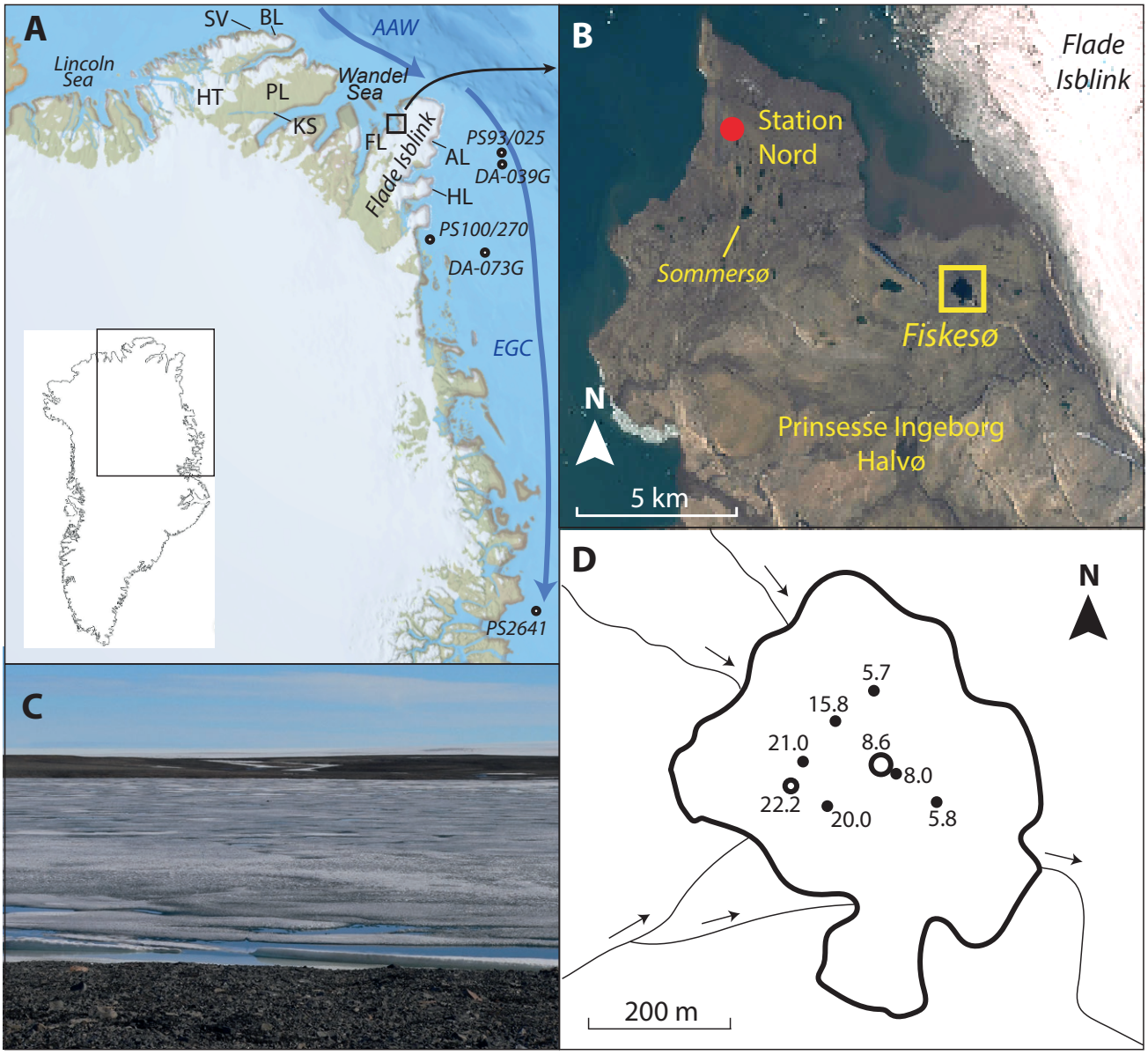

Fig. 1. A, Map of Greenland with zoom in on northeastern Greenland (screenshot from National Geographic Mapmaker) showing the location of Prinsesse Ingeborg Halvø in eastern North Greenland and place names mentioned in the text (PL: Peary Land, HT: Hans Tausen Iskappe, SV: Sifs Valley, BL: Bliss Lake, KS: Klaresø, FL: Finderup Land, AL: Amdrup Land, HL: Holm Land, SK: Skallingen). Blue arrows indicate simplified currents with Arctic Atlantic Water (AAW) and the East Greenland Current (EGC). Locations and names of marine sediment cores mentioned in the text are indicated by black dots with core names in italics (DA-039G=DA17-NG-ST03-039G and DA-073G=DA17-NG-ST03-073G). **B,** Satellite image (Google Earth screenshot, with map data from Maxar Technologies, U.S, Geological Survey, with tonal value modified) of Prinsesse Ingeborg Halvø with the locations of Station Nord and Fiskesø. **C,** Photo of Fiskesø taken on 19 July 2014 with a view from the west. **D,** Close-up of Fiskesø with main inlets in the western part and the outlet at the southeastern corner of the lake. Locations, where the water depth was measured with a handheld echosounder, are indicated by black dots with the respective water depths in metres. Open circles indicate coring locations. Core data shown here are from the central location, where 8.6 m water depth was measured.

remove authigenic matter ~1 g of the sample material taken in 1-cm-intervals was treated with hydrogen peroxide (H_2O_2, 30 %), hydrochloric acid (HCl, 10 %), and sodium hydroxide (NaOH, 1M). Prior to the analyses, the sample material was dispersed with $Na_4P_2O_7$ on a shaker for 12 h and underwent 1 min of ultrasonic treatment. Sample aliquots were then measured three times with a Laser Diffraction Particle Analyser LS 13320 (BECKMANN COULTER Co.) and the individual results were averaged. Data processing was carried out by using the GRADISTATv8 program (Blott & Pye 2001). For geochemical analyses, a spliced sediment succession from GC1 and RC3 was sampled in 1-cm-intervals. The samples were freeze-dried, ground to <63 μm, and homogenised. Total carbon (TC) and total inorganic carbon (TIC) were measured using a DIMATOC 200 (DIMATEC Co.) analyser and allowed calculation of total organic carbon (TOC) by subtraction. Total sulphur (TS) and total nitrogen (TN) were analysed with a Vario Micro Cube combustion CNS elemental analyser (ELEMENTAR Co.).

Macrofossil analyses were carried out on RC2. Macrofossils were recovered from the >0.4, >0.2, and >0.1 mm residues obtained from wet sieving of subsamples, placed onto petri dishes and analysed using a dissecting microscope.

Radiocarbon dating was carried out at the CologneAMS accelerator mass spectrometry facility and followed standard methods (Rethemeyer *et al.* 2013). For radiocarbon dating two horizons of core RC2 were selected. These horizons were at 32–34 cm and 37–38 cm, which was corrected to 30–32 cm and 35–36 cm, when compared with GC1 and RC1 (Table 1, Fig. 2, appendix). The upper horizon contained very few *Salix arctica* remains. The lower horizon did not contain terrestrial macrofossil remains but showed a maximum in TOC. Therefore, bulk organic matter in this horizon was used for radiocarbon dating. The radiocarbon ages were calibrated into calendar years using the Calib 8.2 software (Stuiver & Reimer 1993). Published radiocarbon ages were also calibrated to calendar ages using this software.

Results and discussion

Lake history and terrestrial environment

The restricted progress in penetration with the Russian corer below a sediment depth of ~1 m implies that the sediments underlaying the recovered cores from Fiskesø have likely been deposited during or shortly after deglaciation of the region. This is supported by a few rock fragments and sand, which were found at the base of core RC2, and indicates that the recovered sediment successions contain the complete history of the lake. Radiocarbon dating of the basal sediments of the recovered sediment succession from Fiskesø was not possible, because only very few and tiny macrofossils were found and organic matter (OM) content, which is represented by TOC and TN, was low (Fig. 2). However, former studies provide some information on the timing of the last deglaciation of the Prinsesse Ingeborg Halvø. A marine bivalve shell, which was found 1 km to the southwest of Fiskesø, provided the oldest reliable age in the area and constrains the minimum age of deglaciation at 9.86 cal. ka BP (Funder *et al.* 2011). Finderup Land, which is located ~20 km to the west of Prinsesse Ingeborg Halvø, became ice free shortly before 10 cal. ka BP (Strunk *et al.* 2018). This matches well with deglaciation dates from the eastern margin of Flade Isblink, where the ice retreated between *c.* 11.0–9.4 cal. ka BP to the present margin and thereafter beyond the present margin (Hjort 1997; Funder *et al.* 2011; Larsen *et al.* 2019). These data indicate that the basal sediments of the Fiskesø sediment succession date around 10.0 cal. ka BP (Fig. 2). The timing of the last deglaciation and onset of sedimentation around this period could be triggered by a relatively high temperature anomaly, as derived from oxygen isotope values in the Agassiz and Renland ice cores (Vinther *et al.* 2009, Lecavalier *et al.* 2017). Although this shift in oxygen isotope values is less pronounced in most ice cores from the Inland Ice, the Greenland Ice Sheet likely experienced a substantial thinning around 10.0

Table 1. AMS radiocarbon ages from core RC2, Fiskesø, North Greenland

Laboratory no.	Depth (cm)	Spliced depth (cm)	Material	$\delta^{13}C$ (‰)	^{14}C age (a BP)	Calendar [1] (cal. a BP)
COL3496.1.1	32–34	30–32	*Salix artica*	–28.7	5333 ± 43	5995–6211
COL3497.1.12 [2]	37–38	35–36	bulk sediment	–25.4	17381 ± 86	20779–21332

[1] Calibrated according to the INTCAL20 dataset (Reimer *et al.* 2020). Ages are ± 2 std.

[2] No marine reservoir correction was applied, as the age is regarded as erroneous.

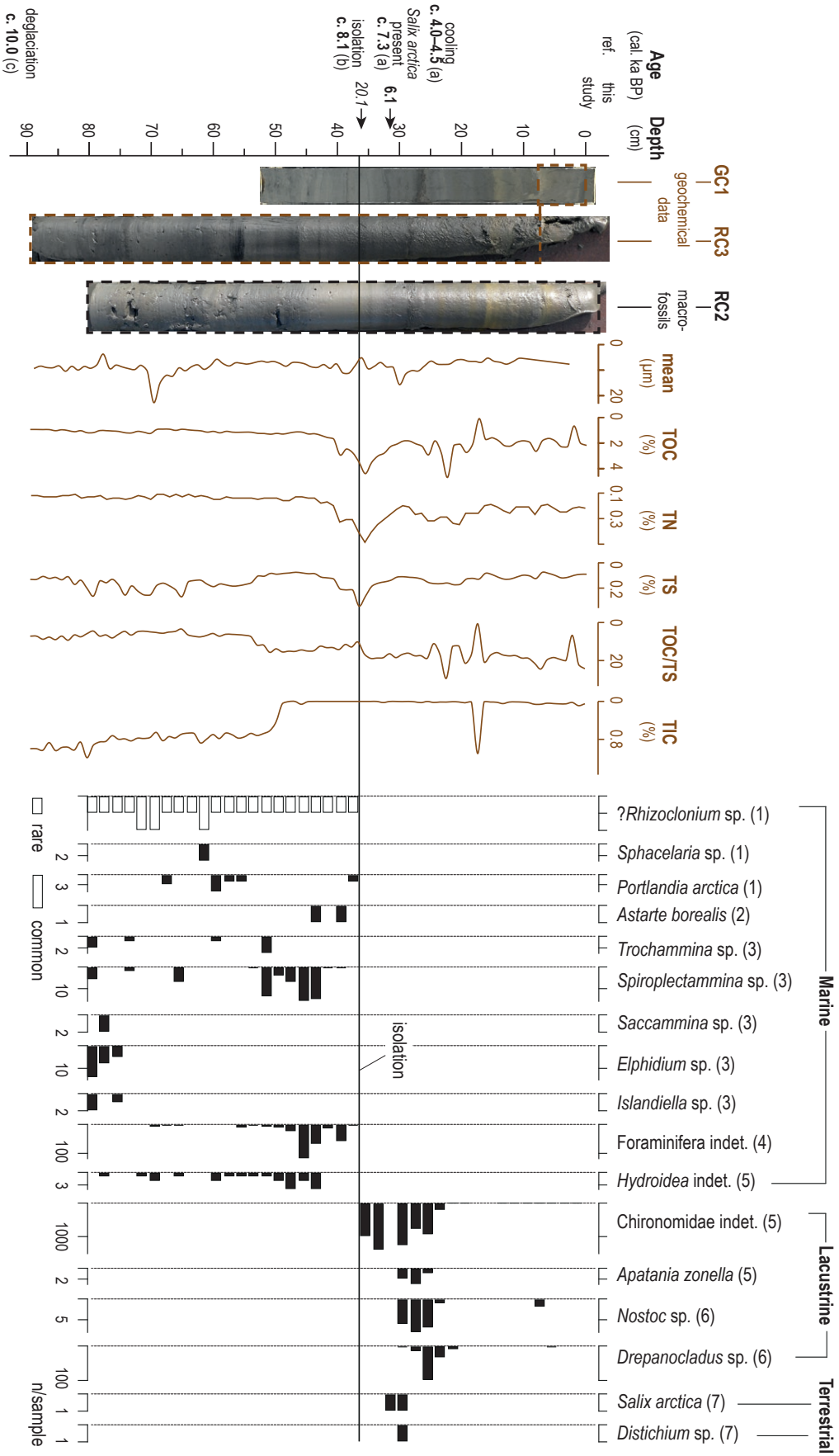

Fig. 2. Photos, grain-size mean, geochemical data and fossils of cores from Fiskesø. Brown dashed lines framing GC1 and RC3 indicate core sections that were used for analyses on a composite sediment succession. Core RC2 was used for macrofossil analyses. Numbers in brackets behind taxa names indicate 1: tallus, 2: periostracum fragments, 3: tests, 4: foraminiferal linings, 5: exo-skeleton parts, 6: colonies, 7: stems, leaves. Radiocarbon dating was performed at samples from two horizons, of which the sample from 36 cm depth (italics) is regarded as erroneous (left). Age and environmental information from literature refer to a: Funder & Abrahamsen (1988), b: Funder *et al.* (2011), c: Strunk *et al.* (2018), see text for further information.

cal. ka BP (Vinther *et al*. 2009), which likely correlates with the deglaciation of the Station Nord region.

The fine-grained, greyish sediments deposited in the lower part of the Fiskesø sediment succession show low OM, relatively high TS and TIC contents, a low TOC/TS ratio, and contain marine macrofossils with very few and tiny fragments of shells and tests of foraminifera below 36 cm depth (Fig. 2). This indicates that marine conditions prevailed in the Fiskesø basin immediately after deglaciation and matches with former studies from eastern North Greenland, where marine waters inundated the lowland areas during and immediately after deglaciation. Marine bivalve shells from Prinsesse Ingeborg Halvø postdating the deglaciation are reported from altitudes up to 58 m a.s.l. (Funder *et al.* 2011), i.e. well above the present altitude of Fiskesø at 33 m a.s.l. On Amdrup Land and Finderup Land (Hjort 1997; Larsen *et al.* 2019) the marine limit is around 80 m a.s.l. Noteworthy is the distinct decrease in TIC at ~50 cm depth in the Fiskesø sediment succession (Fig. 2). This could indicate a change in sediment supply from a larger marine environment to a more local source, particularly the Upper Permian shales to the north of Fiskesø (Håkansson & Pedersen 2015), in the course of ongoing RSL fall during the early Holocene. The RSL fall is, however, only marginally indicated in the grain-size data. A single coarser horizon at 69 cm depth with a mean of ~22 μm might originate from a thin mass flow deposit (Fig. 2). Above, mean values range around 7 μm. A faint increase in grain size mean to ~10 μm around 38 cm depth may indicate slightly shallower waters and more wave action before the isolation of Fiskesø.

The isolation horizon at 36 cm in the Fiskesø sediment succession is characterised by increasing OM, a maximum in TS and an abrupt shift from the occurrence of marine to lacustrine fossils (Fig. 2). The bulk OM sample (COL3497.1.1) from the isolation horizon in the Fiskesø sediment succession gave an age of *c.* 20.1 cal. ka BP (Fig. 2, Table 1). This age is regarded as unreliable because of the supposed much later deglaciation of the region and RSL information from other studies in the vicinity. The study of lake Sommersø located nearby on Prinsesse Ingeborg Halvø at an altitude of 25 m a.s.l. revealed that the lake became isolated between *c.* 7.0 and 8.0 cal. ka BP (Funder & Abrahamsen 1988). A skeleton from a whale that likely stranded at 20 m a.s.l. on Prinsesse Ingeborg Halvø provided an age of 6.7 cal. ka BP (Bennike 1997). Based on radiocarbon dating of marine bivalve shells and driftwood a RSL curve for Prinsesse Ingeborg Halvø was constructed by Funder *et al.* (2011), according to which the isolation of Fiskesø took place at *c.* 8.1 cal. ka BP. The emergence curve for Prinsesse Ingeborg Halvø is in good agreement with RSL reconstructions from the surrounding regions. Radiocarbon dates from Holm Land and Amdrup Land suggest a RSL fall from ~55 to 26 m a.s.l. between *c.* 8.5 and 7.4 cal. ka BP (Hjort 1997), which provides an average rate of ~2.6 cm a^{-1} for the RSL fall. This would place the timing of an isolation of a lake at 33 m a.s.l. as for Fiskesø at *c.* 7.7 cal. ka BP. The average rate of RSL fall is consistent with a RSL reconstruction from Finderup Land, where a RSL fall from ~60 to ~20 m a.s.l. was reconstructed for the period between *c.* 9.5 and 8.0 cal. ka BP (Strunk *et al.* 2018). This would place the timing of the isolation of a basin at 33 m a.s.l. to *c.* 8.5 cal. ka BP. Although there are some differences between the ages constraining the isolation of Fiskesø, all ages are much younger than the age of sample COL3497.1.1 (Table 1) and indicate that the bulk OM from this sample likely contains redeposited material, probably from the Upper Permian shales to the north of Fiskesø. Assuming a deglaciation of Fiskesø around 10 cal. ka BP and an isolation at *c.* 8.1 cal. ka BP, a relatively high sedimentation rate prevailed during the marine phase of the basin.

The maximum in TS and the corresponding minimum in TOC/TS at the isolation horizon in Fiskesø indicate a shift in bottom water redox conditions. A similar shift has been observed in other lakes from Greenland at the transition from marine to brackish or freshwater conditions (e.g. Wagner & Melles 2002; Wagner *et al.* 2010). However, the OM increase below might also indicate increasing productivity promoting oxygen consumption during decomposition. Relatively high temperatures during the Early Holocene may have caused a minimum extent of Flade Isblink after 8.7 cal. ka BP (Larsen *et al.* 2019). This matches well with the regional HTM and a minimum in sea-ice cover between *c.* 8.5 and 6.0 cal. ka BP (Funder *et al*. 2011; Olsen *et al*. 2012; Briner *et al*. 2016) and data from Nioghalvfjerdsfjorden, where glacial recession culminated between 7.7 and 4.5 cal. ka BP (Bennike & Weidick 2001). The maximum in OM proxies and specific macrofossil remains confirm a HTM during and after the isolation of the Fiskesø basin. Chironomid remains can be found in the highest numbers directly after the isolation and document a rapid shift from marine to freshwater conditions. The first occurrence of *Salix arctica* is radiocarbon dated by sample COL3496.1.1, which provides a reliable age of 6.1 cal. ka BP. This age is from only 4–6 cm above the isolation horizon and implies that the sedimentation rate in Fiskesø distinctly lowered directly after the isolation. Taken that the 4–6 cm between the presumed timing of isolation and the dated horizon contains approximately 2000 years, the 2-cm-thick sample might comprise several hundred years. This

could at least partly explain why the first occurrence of *Salix arctica* in the Fiskesø sediment succession is much later than its first occurrence in the area at 7.3 cal. ka BP (Funder & Abrahamsen 1988).

Shortly after 6.1 cal. ka BP, around 30 cm depth, the grain-size mean shows a faint maximum and OM content is low again (Fig. 2). This indicates that the environmental conditions may have slightly changed again. Coarser grain sizes, the occurrence of terrestrial moss remains (*Distichium* sp.) and subsequent occurrence of aquatic mosses (*Drepanocladus* s.l. sp.), algae (*Nostoc* sp.) and caddis fly larvae (*Apatania zonella*) imply that the lake level of Fiskesø lowered shortly after 6.1 cal. ka BP. This lowering might be due to relatively high temperatures and restricted precipitation and might correspond with a glacier retreat that was reconstructed in Sifs Valley, Peary Land, between 6.3 and 5.5 cal. ka BP (Möller *et al.* 2010; Larsen *et al.* 2019). It might also correspond to the time-period when Flade Isblink had a minimum extent, which occurred sometime between ~8.7 to 4.1 cal. ka BP (Larsen *et al.* 2016, 2019).

A distinct decline of lacustrine and terrestrial macrofossils is observed at ~23 cm in the Fiskesø sediment succession. Interpolation of sedimentation rates to the top of the Fiskesø sediment succession suggests that this decline took place *c.* 4.4 cal. ka BP. This matches well with palynological studies from nearby Sommersø, where cooling is reported between *c.* 4.5–4.0 cal. ka BP (Funder & Abrahamsen 1988). Reworked marine shells from the western margin of the Flade Isblink, i.e. from less than 2.5 km from Fiskesø, imply that the margin of the glacier expanded from behind its present position to its present position at 4.1 cal. ka BP (Larsen *et al.* 2019). The readvance might have been promoted by a still existing but dwindling presence of temporarily open water conditions in the marine realm off North Greenland, due to which these open waters could act as a moisture source (Zekollari *et al.* 2017). An increase in precipitation may have led, in combination with a cooling, to longer persisting snow cover during the short summer, which makes the growing conditions for plants less favourable. In the wider vicinity, also Klaresø on Peary Land shows a decline in pollen concentration and particularly *Salix arctica* at this time (Fredskild 1969). Two small lakes in Skallingen, Lille Sneha Sø and Trifna Sø, show maximum macrofossil abundances of warmth-demanding plants (*Salix arctica* and *Dryas integrifolia*) and invertebrates *(Daphnia pulex* and Chironomidae) between *c.* 7.4 and 6.2 cal. ka BP and a decrease of OM contents and increasing minerogenic input at *c.* 4.4 cal. ka BP, which probably also reflects the end of the HTM (Wagner & Bennike 2015; Kusch *et al.* 2019).

In the Fiskesø sediment succession, OM proxies show another small decline at ~18 cm and negligible changes in all studied proxies above. The decline at ~18 cm would correspond to an age of *c.* 3.5 cal. ka BP, when assuming a fairly constant sedimentation rate in the upper, lacustrine part of the succession. It could indicate a further cooling and may correspond with an expansion of a Flade Isblink margin a few kilometres to the south of Fiskesø from a minimum extent to its present position around 3.1 cal. ka BP (Larsen *et al.* 2019). An increase in soil erosion and clastic matter input is also observed to the south of Flade Isblink, in the Lille Sneha Sø and Trifna Sø sediments from Skallingen, around *c.* 3.4 to 3.0 cal. ka BP (Kusch *et al.* 2019). The sediment record from Bliss Lake on Peary Land shows a higher sedimentation rate after *c.* 3.3 cal. ka BP, but this was probably connected to slightly warmer conditions and somewhat reduced winter sea-ice cover (Olsen *et al.* 2012). On the other hand, driftwood data suggest an increase in sea-ice cover at the coast of North and eastern North Greenland around 2.5 cal. ka BP (Bennike 1987; Landvik *et al.* 2001; Funder *et al.* 2011). Overall, the upper 18 cm of the Fiskesø sediment succession suggest that the climatic and environmental conditions remained fairly constant during the late Holocene and similar to those of today, where the region is described as a polar desert (Funder & Abrahamsen 1988).

Marine environment

The environmental history of Fiskesø is closely related to the marine environment. Arctic Atlantic Water (AAW), which is a subsurface water mass (T ~0.8–2 °C, S ~34.8) and underlies cold and low salinity surface waters (T <0 °C, S <31.2), passes the coast to the north of Kronprins Christian Land (e.g. Dmitrenko *et al.* 2017, Hansen *et al.* 2022 and references therein). AAW contributes to the lower section of the EGC (Fig. 1), which conveys cold low-saline (T < 0 °C, S < 34.5), Polar surface waters, together with glacial meltwater and drift ice along the eastern Greenland margin and into the North Atlantic (e.g. Hansen *et al.* 2022 and references therein).

The closest marine sediment records were taken from the Wandel Sea less than 30 km northwest and west of Station Nord (Nørgaard-Pedersen *et al.* 2008; Van Nieuwenhove *et al.* 2020). The core data suggest that a semi-permanent fast-ice cover characterised the sites between 10.0 and 8.9 cal. ka BP and that the deeper troughs in the mouth region of the Independence Fjord system were intruded by subsurface Atlantic water in this period (Nørgaard-Pedersen *et al.* 2008). This is probably in line with modelling data from the southern Lincoln Sea ~500 km to the west, where a widespread transition from perennial to seasonal sea-ice was reconstructed (Detlef *et al.* 2023). The data

from the Wandel Sea cores support a deglaciation of the Fiskesø basin around 10.0 cal. ka BP or slightly earlier. Unfortunately, the cores provide only limited evidence of changes in environmental conditions after *c.* 9.0 cal. ka BP. Extremely low sedimentation rates were tentatively explained by a strongly restricted influx of meltwater-derived sediments (Nørgaard-Pedersen *et al.* 2008) but contradict with relatively high sedimentation rates presumed for marine Fiskesø basin at that time. A higher inflow of subsurface Atlantic water into the Independence Fjord system in the last 2000 years (Van Nieuwenhove *et al.* 2020) seems to have not affected the environmental conditions in the Fiskesø basin.

Marine sediment records from the continental shelf off eastern Kronprins Christian Land show a slightly inconsistent pattern with respect to temperature and sea-ice conditions during the early and middle Holocene. Cores PS93/025 and PS100/270 show prolonged open-water conditions between 10.2 and 9.3 cal. ka BP, which was linked to the HTM and followed by a steady increase in sea-ice conditions in the area during the middle Holocene (Syring *et al.* 2020a, b). Data from neighbouring core DA17-NG-ST03-039G indicated a succession of a cold period with marginal ice zone conditions and enhanced EGC and Atlantic Water advection from 10.2 to 9.4 cal. ka BP, followed by harsher sea-ice conditions and Atlantic Water inflow from 9.4 to 7.5 cal. ka BP (Hansen *et al.* 2020). In contrast to Syring *et al.* (2020a, b), the timing of the HTM was defined to the period from *c.* 7.5 to 6.7 cal. ka BP, when high surface and subsurface water productivity prevailed and as promoted by the enhanced Atlantic Water flow to the shelf (Hansen *et al.* 2022). The transition towards a cold period with increased drift-ice transport via a strong EGC is recorded from *c.* 6.2 cal. ka BP. A bit further to the south, on the Northeast Greenland shelf in front of Nioghalvfjerdsfjorden, core DA17-NG-ST07-73G revealed a highly stratified water column with cold, sea-ice-loaded surface waters and a strong influx of warm Atlantic water in the subsurface between 9.4 and 8.2 cal. ka BP (Pados-Dibattista *et al.* 2022). This period was followed by a strong influence of the Return Atlantic Current and a weakened transport of Polar water in the upper EGC until 6.2 cal. ka BP. The inferred HTM from 8.2 to 6.2 cal. ka BP at this site is quite consistent with the HTM inferred from Fiskesø sediment data.

After the HTM, the marine sediment records from the continental shelf show that the EGC became stronger, with sea-ice-loaded surface waters and relatively warm Atlantic-sourced subsurface waters (Pados-Dibattista *et al.* 2022). Consistent with the reconstruction from Fiskesø, where stepwise harsher conditions are indicated at *c.* 4.4 and 3.5 cal. ka BP, increased Polar water at the surface of the EGC led to freshening and increased drift-ice transport with a (near) perennial sea-ice cover on the continental shelf along the coast of Northeast Greenland to the east and southeast of Flade Isblink between *c.* 4.5 and 4.2 cal. ka BP (Perner *et al.* 2015; Hansen *et al.* 2022; Pados-Dibattista *et al.* 2022). A further strengthening of the EGC at *c.* 3.2 cal. ka BP was characterised by a thick layer of cold and fresh polar water on the surface and a minimum in surface-water productivity (Pados-Dibattista *et al.* 2022). Foraminifera data from core PS2641-4 recovered from the central East Greenland shelf (Fig. 1) revealed that the EGC flow may have peaked between *c.* 2.3 and 1.4 cal. ka BP due to a complex interplay of Atlantic water masses and increased heat advection of the North Atlantic Currents into the Arctic Ocean (Perner *et al.* 2015). The record from Fiskesø, however, cannot provide information about this strengthening, probably because the region around Fiskesø was already too barren to record such environmental changes in the studied proxies.

Conclusions

The studies of sediment successions from Fiskesø on Prinsesse Ingeborg Halvø contributed to a better understanding of the environmental history of the region and linkages to the marine realm. Radiocarbon dating was problematic due to the low abundance of macrofossils in the sediments. According to existing data, the lake basin was deglaciated around 10 cal. ka BP. The isolation of the basin around 8.1 cal. ka BP is likely synchronous with the onset of the regional HTM, which may have lasted until shortly after *c.* 6.1 cal. ka BP. Lake-level lowering is recorded between *c.* 6.0 and 5.0 cal. ka BP. Stepwise cooling is recorded in macrofossils and OM content and likely occurred around 4.4 and 3.5 cal. ka BP. During the Late Holocene, absence of macrofossils and low organic matter contents document a harsh environment with low summer temperatures and long-lasting lake-ice cover.

Overall, the data from Fiskesø support the existing knowledge based on the few marine and terrestrial records in the region. They document the influence of Arctic Atlantic Water masses on the East Greenland Current during the Holocene. New techniques in radiocarbon dating, e.g. compound specific dating, and lower amounts of carbon requested for dating may help to improve the chronologies in sediment succession from such environments. This, however, does not improve other limitations of these sediment successions, such as redeposition of old material and often very low sedimentation rates, which hamper high-resolution studies. The comparison of macrofossil and geochemical data from Fiskesø reveals that macrofossil remains reflect well the general climatic

and environmental settings, whereas geochemical data are more sensitive to lake-internal changes, such as changes in catchment settings, nutrient and redox conditions. The combination of the data provides a reliable basis for a reconstruction of the environmental history and the isolation of the basin from the marine environment.

Acknowledgments

We are grateful to the Joint Arctic Command for transportation to Station Nord. We would like to thank the two reviewers J. Müller and A. Strunk and the editor Nicolaj Krog Larsen for helpful comments and suggestions to improve the manuscript.

References

Bennike, O. 1987: Quaternary geology and biology of the Jørgen Brønlund Fjord area, North Greenland. Meddelelser om Grønland Geoscience 18, 23 pp. http://dx.doi.org/10.7146/moggeosci.v18i.139876

Bennike, O. 1997: Quaternary vertebrates from Greenland: a review. Quaternary Science Reviews 16, 899–909. https://doi.org/10.1016/S0277-3791(97)00002-4

Bennike, O. & Weidick, A. 2001: Late Quaternary history around Nioghalvfjerdsfjorden and Jøkelbugten, North-East Greenland. Boreas 30, 205–227. http://dx.doi.org/10.1080/030094801750424139

Blott, S.J. & Pye, K. 2001: GRADISTAT: A grain size distribution and statistics package for the analysis of unconsolidated sediments, Earth Surface Processes and Landforms 26, 1237–1248, doi:10.1002/esp.261

Briner, J.P., McKay, N.P., Axford, Y., Bennike, O., Bradley, R.S., de Vernal, A., Fisher, D., Francus, P., Frechette, B., Gajewski, K., Jennings, A., Kaufman, D.S., Miller, G., Rouston, C. & Wagner, B. 2016: Holocene climate change in Arctic Canada and Greenland. Quaternary Science Reviews 147, 340–364. http://dx.doi.org/10.1016/j.quascirev.2016.02.010

Cappelen, J., Jørgensen, B.V., Laursen, E.V., Stannius, L.S. & Thomsen, R.S. 2001: The observed climate of Greenland, 1958–99 – with climatological standard normal, 1961-1990. Danish Meteorological Institute, Technical Report 00-18, 149 pp.

Christoffersen, K.S. 2018: Lake Ecology and Monitoring at the Very North: Year-Round Measurements of Life Conditions in Lakes. Villum Research Station, Station Nord, Annual Report 2017, 12–13.

Detlef, H., O'Regan, M., Stranne, C., Jensen M.M., Glasius, M., Cronin, T.M., Jakobsson, M. & Pearce, C. 2023: Seasonal sea-ice in the Arctic's last ice area during the Early Holocene. Communications Earth and Environment 4, 86. https://doi.org/10.1038/s43247-023-00720-w

Dmitrenko, I.A., Kirillov, S.A., Rudels, B., Babb, D.G., Pedersen, L.T., Rysgaard, S, Kristoffersen, Y. & Barber, D.G. 2017: Arctic Ocean outflow and glacier-ocean interactions modify water over the Wandel Sea shelf (northeastern Greenland). Ocean Science 13, 1045–1060. https://doi.org/10.5194/os-13-1045-2017

Foukal, N.P., Gelderloos, R. & Pickart, R.S. 2020: A continuous pathway of freshwater along the East Greenland shelf. Scientific Advances 6, eabc424. https://doi.org/10.1126/sciadv.abc4254

Fredskild, B. 1969: A postglacial standard pollen diagram from Peary Land, North Greenland. Pollen and Spores 11, 573–583.

Funder, S. & Abrahamsen, N. 1988: Palynology in a polar desert, eastern North Greenland. Boreas 17, 195–207. https://doi.org/10.1111/j.1502-3885.1988.tb00546.x

Funder, S., Goosse, H., Jepsen, H., Kaas, E., Kjær, K.H., Korsgaard, N.J., Larsen, N.K., Linderson, H., Lysså, A., Möller, P., Olsen, J. & Willerslev, E. 2011: A 10,000-year record of Arctic Ocean sea-ice variability-view from the beach. Science 333, 747–750. http://dx.doi.org/10.1126/science.1202760

Goodsite, M., Skov, H., Asmund, G., Bennike, O., Feilberg, A., Glasius, M., Gross, A. & Hermanson, M. 2014: Pilot study of contaminants near Station Nord, a military airbase and research station in NE Greenland. In Linkov, I. (ed.): Sustainable cities and military installations, NATO Science for Peace and Security Series C: Environmental Security, 177–198. Springer Science, Dordrecht. https://doi.org/10.1007/978-94-007-7161-1_10

Håkansson, E. & Pedersen, S.A.S. 2001: The Wandel Hav strike-slip mobile belt – a Mesozoic plate boundary in North Greenland. Bulletin of the Geological Society of Denmark 48, 149-158. https://doi.org/10.37570/bgsd-2001-48-08

Håkansson, E. & Pedersen, S.A.S. 2015: A healed strike-slip plate boundary in North Greenland indicated through associated pull-apart basins. Geological Society (London) Special Publications, 413, 143–169. http://dx.doi.org/10.1144/sp413.10

Håkansson, E., Madsen, L. & Pedersen, S.A.S. 1989: Geological investigations of Prinsesse Ingeborg Halvø, eastern North Greenland. Rapport Grønlands Geologiske Undersøgelse 145, 113–118. https://doi.org/10.34194/rapggu.v145.8088

Hammer, C.U., Johnsen, S.J., Clausen, H.B., Dahl-Jensen, D., Gundestrup, N. & Steffensen, J.P. 2001: The paleoclimatic record from a 345 m long ice core from the Hans Tausen Iskappe. Meddelelser om Grønland, Geoscience 39, 87–95. https://doi.org/10.7146/moggeosci.v39i.140226

Hansen, K.E., Lorenzen, J., Davies, J., Wacker, L., Pearce, C. & Seidenkrantz, M.-S., 2022: Deglacial to Mid Holocene environmental conditions on the northeastern Greenland shelf, western Fram Strait. Quaternary Science Reviews 293, 107704. https://doi.org/10.1016/j.quascirev.2022.107704

Hjort, C. 1997: Glaciation, climate history, changing marine levels and the evolution of the Northeast Water Polynya. Journal of the Marine Systems 10, 23–33. https://doi.org/10.1016/S0924-7963(96)00068-1

Jeansson, E., Jutterström, S., Rudels, B., Anderson, L.G., Olsson, K.A., Jones, E.P., Smethie Jr., W.M. & Swift, J.H. 2008: Sources to the East Greenland Current and its contribution to the Denmark Strait Overflow. Progress in Oceanography 78, 12–28. http://dx.doi.org/10.1016/j.pocean.2007.08.031

Kusch, S., Bennike, O., Wagner, B., Lenz, M., Steffen, I. & Rethemeyer, J. 2019: Holocene environmental history in high-Arctic North Greenland revealed by a combined biomarker and macrofossil approach. Boreas 48, 273–286. https://doi.org/10.1111/bor.12377

Landvik, J.Y., Weidick, A. & Hansen, A. 2001: The glacial history of the Hans Tausen Iskappe and the last glaciation of Peary Land, North Greenland. Meddelelser om Grønland. Geoscience 39, 27–44. http://dx.doi.org/10.7146/moggeosci.v39i.140218

Larsen, N.K., Funder, S., Linge, H., Möller, P., Schomacker, A., Fabel, D., Xu, S. & Kjær, K.H. 2016: A Younger Dryas re-advance of local glaciers in north Greenland. Quaternary Science Reviews 147, 47–58. https://doi.org/10.1016/j.quascirev.2015.10.036

Larsen, N.K., Levy, L.B., Strunk, A., Søndergaard, A.S., Olsen, J. & Lauridsen, T.L. 2019: Local ice caps in Finderup Land, North Greenland, survived the Holocene Thermal Maximum. Boreas 48, 551–562. https://doi.org/10.1111/bor.12384

Lecavalier, B.S., Fisher, D.A., Milne, G.A., Vinther, B.M., Tarasov, L., Huybrechts, P., Lacelle, D., Main, B., Zheng, J., Bourgeois, J., & Dyke, A.S. 2017: High Arctic Holocene temperature record from the Agassiz ice cap and Greenland ice sheet evolution. Proceedings of the National Academy of Sciences of the USA, 23, 5952–5957. https://doi.org/10.1073/pnas.1616287114

Lemark, A. 2010: A study of the Flade Isblink ice cap using a simple ice flow model. Master's thesis, Niels Bohr Institute, Copenhagen University. https://nbi.ku.dk/english/theses/masters-theses/andreas-lemark/A_Lemark_Speciale.pdf

Madsen, K.N. & Thorsteinsson, T. 2001: Textures, fabrics and meltlayer stratigraphy in the Hans Tausen ice core, North Greenland – indications of late Holocene ice cap generation? Meddelelser om Grønland, Geoscience 39, 97–114. http://dx.doi.org/10.7146/moggeosci.v39i.140229

Möller, P., Larsen, N.K., Kjær, K.H., Funder, S., Schomacker, A., Linge, H. & Fabel, D. 2010: Early to middle Holocene valley glaciations on northernmost Greenland. Quaternary Science Reviews 29, 3379–3398. http://dx.doi.org/10.1016/j.quascirev.2010.06.044

Nørgaard-Pedersen, N., Mikkelsen, N.& Kristoffersen, Y., 2008: Late glacial and Holocene marine records from the Independence Fjord and Wandel Sea regions, North Greenland. Polar Research 27, 209e221. https://doi.org/10.1111/j.1751-8369.2008.00065.x

Olsen, J., Kjær, K.H., Funder, S., Larsen, N.K. & Ludikova, A. 2012: High-Arctic climate conditions for the last 7000 years inferred from multi-proxy analysis of the Bliss Lake record, North Greenland. Journal of Quaternary Science 27, 318–327. https://doi.org/10.1002/jqs.1548

Pados-Dibattista, T., Pearce, C., Detlef, H., Bendtsen, J. & Seidenkrantz, M.-S. 2022: Holocene palaeoceanography of the Northeast Greenland shelf. Climate of the Past 18, 103–127. https://doi.org/10.5194/cp-18-103-2022

Perner, K., Moros, M., Lloyd, J.M., Jansen, E., Stein, R., 2015: Mid to late Holocene strengthening of the East Greenland Current linked to warm subsurface Atlantic water. Quaternary Science Reviews 129, 296–307. https://doi.org/10.1016/j.quascirev.2015.10.007

Perren, B.B., Wolfe, A.P., Cooke, C.A., Kjær, K.H., Mazzucchi, D. & Steig, E.J. 2012: Twentieth-century warming revives the world's northernmost lake. Geology 40, 1003–1006. https://doi.org/10.1130/G33621.1

Reimer, P.J. *et al*. 2020: The IntCal20 Northern Hemisphere radiocarbon age calibration curve (0–55 cal kB). Radiocarbon 62, 725–757. https://doi.org/10.1017/RDC.2020.41

Rethemeyer, J. *et al*. 2013: Status report on sample preparation facilities for ^{14}C analysis at the CologneAMS center. Nuclear Instruments and Methods in Physics Research B294, 168–172. https://doi.org/10.1016/j.nimb.2012.02.012

Rudels, B. & Quadfasel, D. 1991: Convection and deep-water formation in the Arctic Ocean-Greenland Sea system. Journal of the Marine Systems 2, 435–450. http://dx.doi.org/10.1016/0924-7963(91)90045-v

Stuiver M. & Reimer P.J. 1993: Extended 14C database and revised CALIB radiocarbon calibration program. Radiocarbon 35, 215–230. https://doi.org/10.1017/S0033822200013904

Strunk, A., Larsen, N.K., Nilsson, A., Seidenkrantz, M.-S., Levy, L.B., Olsen, J. & Lauridsen, T.L. 2018: Relative sea level changes and ice sheet history in Finderup Land, North Greenland. Frontiers in Earth Science 6, 129. https://doi.org/10.3389/feart.2018.00129

Syring, N., Stein, R., Fahl, K., Vahlenkamp, M., Zehnich, M., Spielhagen, R.F. & Niessen, F. 2020a: Holocene changes in sea-ice cover and polynya formation along the eastern North Greenland shelf: New insights from biomarker records. Quaternary Science Reviews 231, 106173. https://doi.org/10.1016/j.quascirev.2020.106173

Syring, N., Lloyd, J.M., Stein, R., Fahl, K., Roberts, D.H., Callard, L. & O'Cofaigh, C. 2020b: Holocene interactions between glacier retreat, sea ice formation, and Atlantic Water advection at the nnner Northeast Greenland continental shelf. Paleoceanography and Paleoclimatology 35, e2020PA004019. https://doi.org/10.1029/2020PA004019

Van Nieuwenhove, N., Limoges A, Nørgaard-Pedersen, N., Seidenkrantz, M.-S. & Ribeiro, S. 2020: Episodic Atlantic Water inflow into the Independence Fjord system (eastern North Greenland) during the Holocene and Last Glacial period. Frontiers in Earth Science 8, 565670. https://doi.org/10.3389/feart.2020.565670

Vinther, B.M. *et al*. 2009: Holocene thinning of the Greenland Ice Sheet. Nature 461, 385–388. https://doi:10.1038/nature08355

Wagner, B. & Bennike, O. 2015: Holocene environmental change in the Skallingen area, eastern North Greenland, based on a lacustrine record. Boreas 44, 45–59. https://doi.org/10.1111/bor.12085

Wagner, B. & Melles, M. 2002: Holocene environmental history of western Ymer Ø, East Greenland, inferred from lake sediments. Quaternary International 89, 165–176. http://dx.doi.org/10.1016/s1040-6182(01)00087-8

Wagner, B., Bennike, O., Cremer, H. & Klug, M. 2010: Late Quaternary history of the Kap Mackenzie area, northeast Greenland. Boreas 39, 492–504. https://doi.org/10.1111/j.1502-3885.2010.00148.x

Zekollari, H., Lecavalier, B.S. & Huybrechts, P. 2017: Holocene evolution of Hans Tausen Iskappe (Greenland) and implications for the palaeoclimatic evolution of the high Arctic. Quaternary Science Reviews 168, 182–193. http://dx.doi.org/10.1016/j.quascirev.2017.05.010

Appendix. Photos of sediment cores recovered with a gravity corer (GC) and a Russian peat corer (RC) from Fiskesø, Prinsesse Ingerborg Halvø, in July 2014. Note that the photos of the Russian cores were made in the field and thus show some distortion, particularly in the upper and lower parts. Green foam was used to stabilise the sediment surface of the gravity cores during transport. The black lines show the correlation of the cores based on marker horizons. The age-depth plot at the right side includes tie points at the year of core recovery (2014= 0 cm depth), the two ^{14}C dated horizons (circles; open circle: unreliable age), and the presumed age of deglaciation and onset of sedimentation in the Fiskesø basin at the base of the cores.

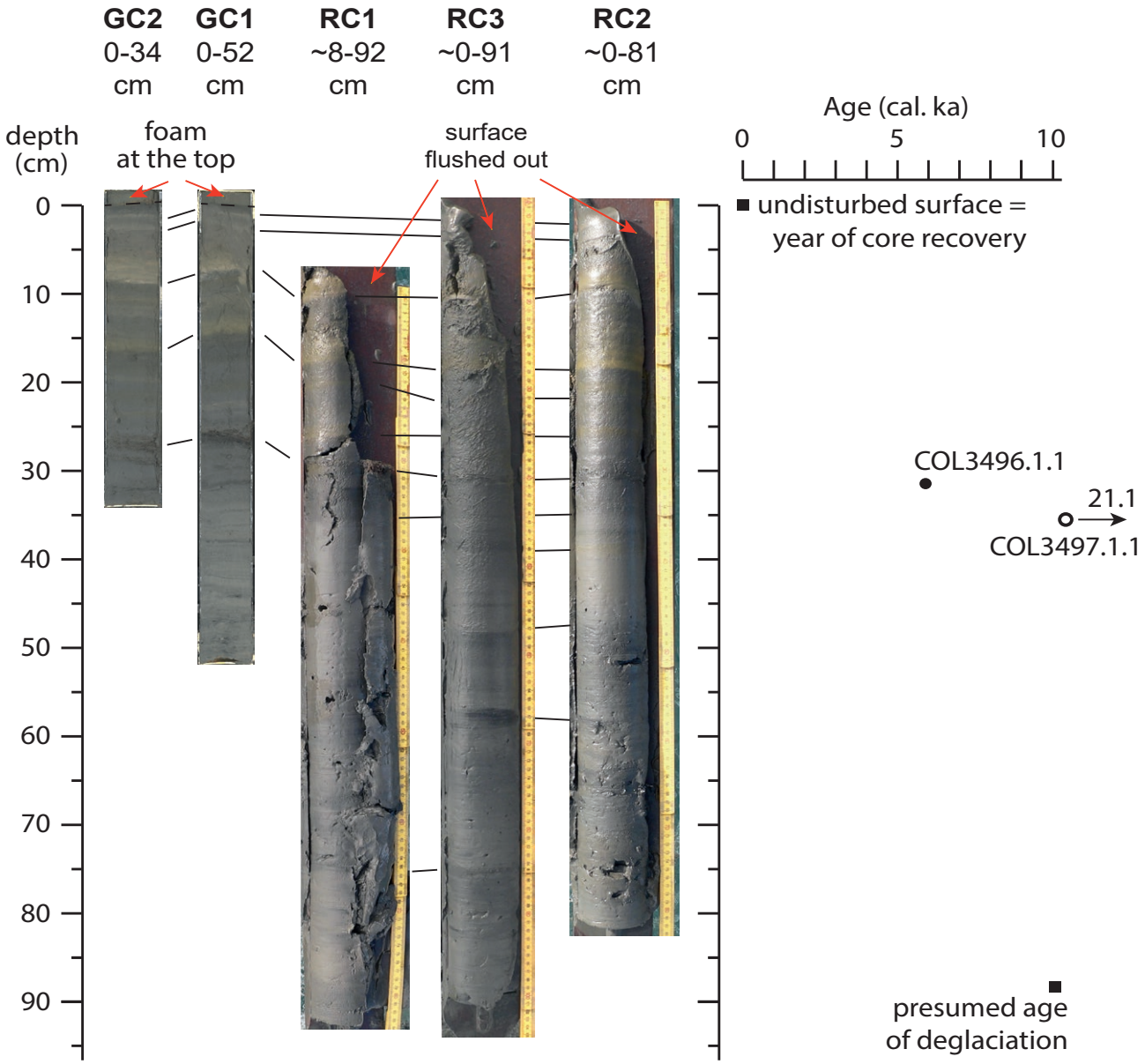

The first tritylodontid (Synapsida, Cynodontia) fossil from Scandinavia

EMMY MOLIN, STEPHEN A. HALL, MIRIAM HEINGÅRD, JESPER MILÀN & JOHAN LINDGREN

Geological Society of Denmark
https://2dgf.dk

Received 29 August 2024
Accepted in revised form
12 December 2024
Published online
19 December 2024

Molin, E., Hall, S. A., Heingård, M., Milàn, J. & Lindgren, J. 2024: The first tritylodontid (Synapsida, Cynodontia) fossil from Scandinavia. Bulletin of the Geological Society of Denmark, Vol. 73, pp. 221–230. ISSN 2245-7070.
https://doi.org/10.37570/bgsd-2024-73-14

Lower Jurassic (Pliensbachian) sand- and siltstones of the Hasle Formation on the Danish Island of Bornholm have yielded a diverse invertebrate and vertebrate assemblage dominated by marine taxa. Recently, dental and skeletal remains of terrestrial animals have also been collected from this rock unit, including the first tritylodontid tooth from Scandinavia. Here we describe the new fossil (NHMD 1725979), identified as a left lower postcanine. Even though precise taxonomic placement within Tritylodontidae is difficult, the preserved morphological characters are shared to varying extent with the Middle Jurassic – Lower Cretaceous genera *Polistodon*, *Montirictus*, *Nuurtherium*, *Stereognathus*, *Xenocretosuchus*, and *Shartegodon*. Hence, NHMD 1725979 may represent the stratigraphically oldest occurrence of a derived tritylodontid.

Keywords: Bornholm, Hasle Formation, Jurassic, Pliensbachian, tooth, Tritylodontidae.

Emmy Molin [emmymolin96@hotmail.com] Department of Geology, Lund University, Sölvegatan 12, SE-223 62 Lund, Sweden; Stephen A. Hall [stephen.hall@solid.lth.se] Department of Construction Sciences, Lund University, Ole Römers Väg 1, SE-223 63 Lund, Sweden; Miriam Heingård [miriam.heingard@gmail.com] Department of Geology, Lund University, Sölvegatan 12, SE-223 62 Lund, Sweden; Jesper Milàn [jesperm@oesm.dk] Geomuseum Faxe, Østsjællands Museum, Rådhusvej 2, DK-4640 Faxe, Denmark; Johan Lindgren [johan.lindgren@geol.lu.se] Department of Geology, Lund University, Sölvegatan 12, SE-223 62 Lund, Sweden.

Tritylodontidae comprises an extinct group of tetrapods that first appear in the fossil record during the Upper Triassic (e.g., Henning 1922; Fedak *et al*. 2015; Sues & Olsen 2015). Even though these animals might have looked superficially like modern rodents when alive, tritylodontids are neither considered to be true mammals nor the direct ancestors of these (Watson 1942). The taxonomic position of tritylodontids within non-mammaliaform cynodonts remains contentious, although most scholars consider them to be a clade of mammaliamorphs phylogenetically close to Mammaliaformes (e.g., Rowe 1993; Luo *et al*. 2002; Ruta *et al*. 2013). Notably, though, some researchers (e.g., Hopson & Barghusen 1986; Hopson & Kitching 2001) place tritylodontids within Cynognathia, and thus further away from true mammals.

Regardless of precise phylogenetic affinity, tritylodontids were extremely successful during the Jurassic, with dental and skeletal elements occurring in terrestrial environments on all continents (e.g., Bonaparte 1970; Kemp 1982; Watabe *et al*. 2007; Hammer & Smith 2008; Fedak *et al*. 2015). Until now, however, no fossil remains have been discovered in Scandinavia. Here, we describe an isolated tooth from the Pliensbachian (Lower Jurassic) Hasle Formation on the Danish island of Bornholm and discuss its affinity within the Tritylodontidae as well as potential implications on the inferred depositional environment of this rock unit.

Geological setting

The type locality of the Hasle Formation is a coastal cliff section just south of the town of Hasle on the Danish Island of Bornholm (Fig. 1). The geology of Born-

holm is a complex fault block system influenced by movements of the NW–SE-trending Sorgenfrei–Tornquist Zone, which separates the Danish Basin from the Baltic Shield (Surlyk & Noe-Nygaard 1986; Donovan & Surlyk 2003). The sediments of the Hasle Formation include yellowish–brownish sandstones with hummocky cross stratification, as well as coarse-grained siltstones. Some beds show trough cross-bedding and, at the base of these, the swales are draped with a fossiliferous conglomeratic layer of basement rock clasts (Surlyk & Noe-Nygaard 1986; Larsen & Friis 1991). The depositional environment has been interpreted as shallow marine, and the Hasle Formation has yielded a diverse invertebrate fauna comprising 11 species of ammonites, belemnites, scaphopods, serpulids, and bivalves (Malling & Grönwall 1909; Malling 1911, 1914, 1920; Höhne 1933; Donovan & Surlyk 2003; Koci *et al.* 2024). However, most of these fossils are poorly preserved due to the coarse-grained fabric of the encasing matrix. Vertebrate remains are common in the Halse Formation, especially teeth of hybodont and neoselachian sharks (Rees 1998), along with tooth plates from at least two species of holocephalians (Duffin & Milàn 2017, 2022). Bony fish remains are also abundant and include numerous (undescribed) body scales. Marine tetrapods are represented by isolated plesiosaurian teeth and bones, which collectively indicate the existence of at least three taxa (Milàn & Bonde 2001; Smith 2008). In addition, an incomplete osteoderm from a thalattosuchian crocodile has recently been collected

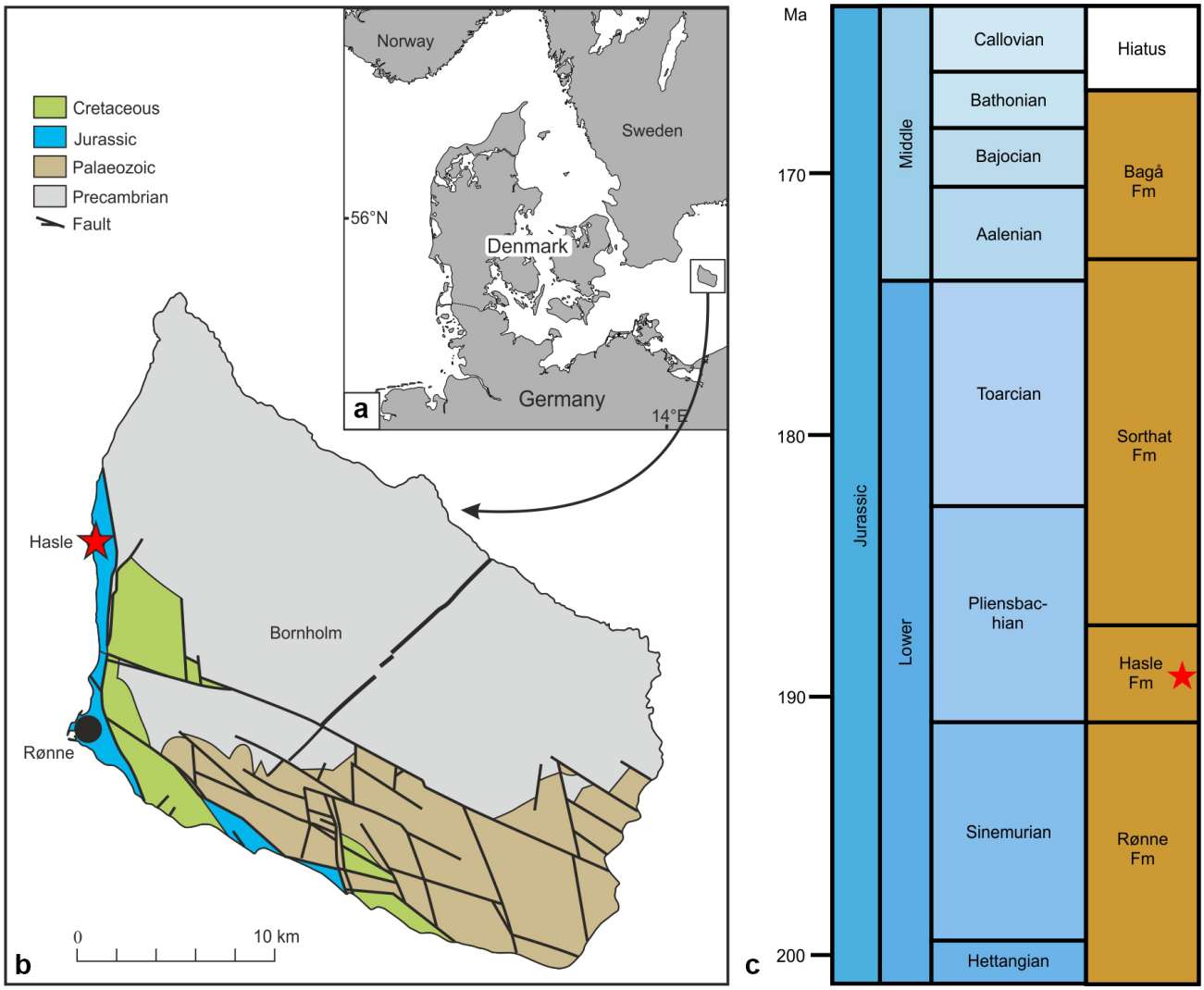

Fig. 1. Bornholm and the Hasle Formation. **a,** Overview map of northern Germany and southern Scandinavia. Note the location of the Danish Island of Bornholm in the southern part of the Baltic Sea. **b,** Simplified geological map of Bornholm, Denmark, with the location of the town of Hasle and type locality of the Hasle Formation indicated by a red star (modified from Graversen 2009, fig. 1). **c,** Middle to Upper Jurassic stratigraphy of Bornholm (modified from Sandersen *et al.* 2014, fig. 3.2). The Hasle Formation is marked by a red star.

at the type locality (Milàn & Mueller-Töwe 2021). The presence of terrestrial vertebrates in the Hasle Formation was first hinted at by a small theropod footprint (Milàn & Surlyk 2015) and, subsequently, by an isolated sauropod tooth (Milàn & Mateus 2024), and, most recently, by nonavian dinosaur bones and two theropod teeth (Molin *et al*. unpublished).

Material and methods

This paper describes and illustrates an isolated tritylodontid tooth (NHMD 1725979) curated in the collections at the Natural History Museum of Denmark, Copenhagen, Denmark (NHMD). X-ray microtomograpy was performed using a Zeiss XRadia Versa XRM520 at the 4D-Imaging Laboratory, Lund University, Sweden. 3001 radiographic projections were acquired, with 6 s exposure for each, over 360° sample rotation using the ×0.4 detector and with the sample at 18.13 mm from the X-ray source and 103.70 mm from the detector, giving a pixel size of 5 μm. The X-ray source was set at 70 kV and 6 W with the manufacturer supplied le3 filter to reduce beam hardening effects. Tomographic reconstructions were done using the Zeiss reconstructor software to yield image volumes with a cubic voxel width of 6 μm that were output as 16-bit TIFF file sequences. These data were segmented and visualised using 3D Slicer 4.11.20200930 (Fedorov *et al*. 2012). NHMD 1725979 was also photographed under an Olympus SZX16 stereomicroscope equipped with an Olympus SC30 digital camera. The morphological terminology (Fig. 2) is primarily based on Panciroli *et al*. (2017), whereas the systematic division of Tritylodontidae into 'basal' and 'derived/advanced' forms follows Watabe *et al*. (2007) and Panciroli *et al*. (2017).

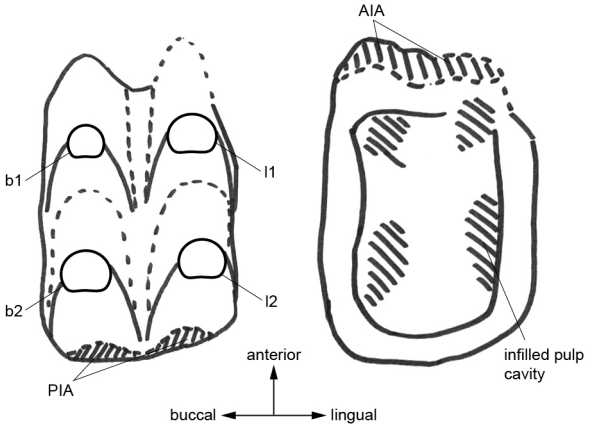

Fig. 2. Descriptive terminology of a left lower tritylodontid postcanine (modified from Panciroli *et al*. 2017, fig. 1). Abbreviations: AIA, anterior interlocking area; b, buccal cusp; l, lingual cusp; PIA, posterior interlocking area.

Systematic palaeontology

Synapsida Osborn, 1903

Cynodontia Owen, 1861

Mammaliamorpha Rowe, 1988

Tritylodontidae Cope, 1884

Remarks on Tritylodontidae. Tritylodontidae includes at least 17 genera (Panciroli *et al*. 2017). These have been sub-divided into basal forms, such as *Oligokyphus* and *Tritylodon* – which first occur in the sedimentary record during the Upper Triassic – Lower Jurassic interval – and derived taxa, such as *Stereognathus*, *Polistodon* and *Bientheroides*, which appear in the Middle Jurassic (e.g., Watabe *et al*. 2007; Panciroli *et al*. 2017). The stratigraphically youngest genera *Xenocretosuchus* and *Montirictus* derive from Lower Cretaceous deposits of eastern Asia [Tatarinov & Matchenko 1999; Matsuoka *et al*. 2016; see also Averianov *et al*. (2017) for a different opinion on the taxonomic status of *Polistodon*, *Xenocretosuchus* and *Montirictus*].

Tritylodontids are distinguishable from other non-mammaliaform cynodonts by their unique tooth morphology (e.g., Sues 1985a, 1986a; Setoguchi *et al*. 1999). The dentition includes two pairs of enlarged incisors, taking the function of canines, and several postcanines with two or three longitudinal rows of cusps (e.g., Sues 1985a, 1986a; Setoguchi *et al*. 1999). Upper postcanines have three rows of six or more cusps with anteriorly curved apices, whereas lower postcanines have two rows of cusps with two or more posteriorly inclined cusps in each row (e.g., Clark & Hopson 1985; Sues 1985a, 1986a, b). V-shaped valleys run between the cusp rows, where the upper and lower teeth meet in occlusion (e.g., Simpson 1928; Kemp 1982; Kermack 1982; Hopson & Barghusen 1986; Sues 1986c). This arrangement creates a dental apparatus that presumably masticated the food when the lower teeth moved in an anteroposterior direction along the upper tooth row (e.g., Kemp 1982; Kermack 1982; Sues 1986c; Velazco *et al*. 2017). Tritylodontids have traditionally been considered as predominantly herbivorous (e.g., Kemp 1982); however, recent studies of dental micro-wear suggest that they instead might have been omnivorous, with a diet consisting of seeds, plants and insects (Hu *et al*. 2009; Kalthoff *et al*. 2019).

Tritylodontidae gen. et sp. indet.

Referred specimen. NHMD 1725979: an isolated tooth-crown (Figs 3, 4).

Description. NHMD 1725979 has experienced some post-depositional abrasion, resulting in that the tooth lacks the root and all cusps are worn (Figs 3, 4a–g). Moreover, the pulp cavities have been infilled with sedimentary matrix (4h–j). The overall anteroposterior length of the fossil is 8.20 mm and the maximum buccolingual width 5.32 mm, resulting in a length/width ratio of 1.54. Because both the posterior interlocking

Fig. 3. Photographs of NHMD 1725979. **a,** Occlusal view (stereo pair). Note slightly offset cusp rows and embayments (arrows) representing the PIA. **b,** Crown base (stereo pair). Note ridged, "enamel-covered" projection (arrow) representing the AIA. **c, d,** NHMD 1725979 in **c,** lingual and **d,** buccal views, respectively.

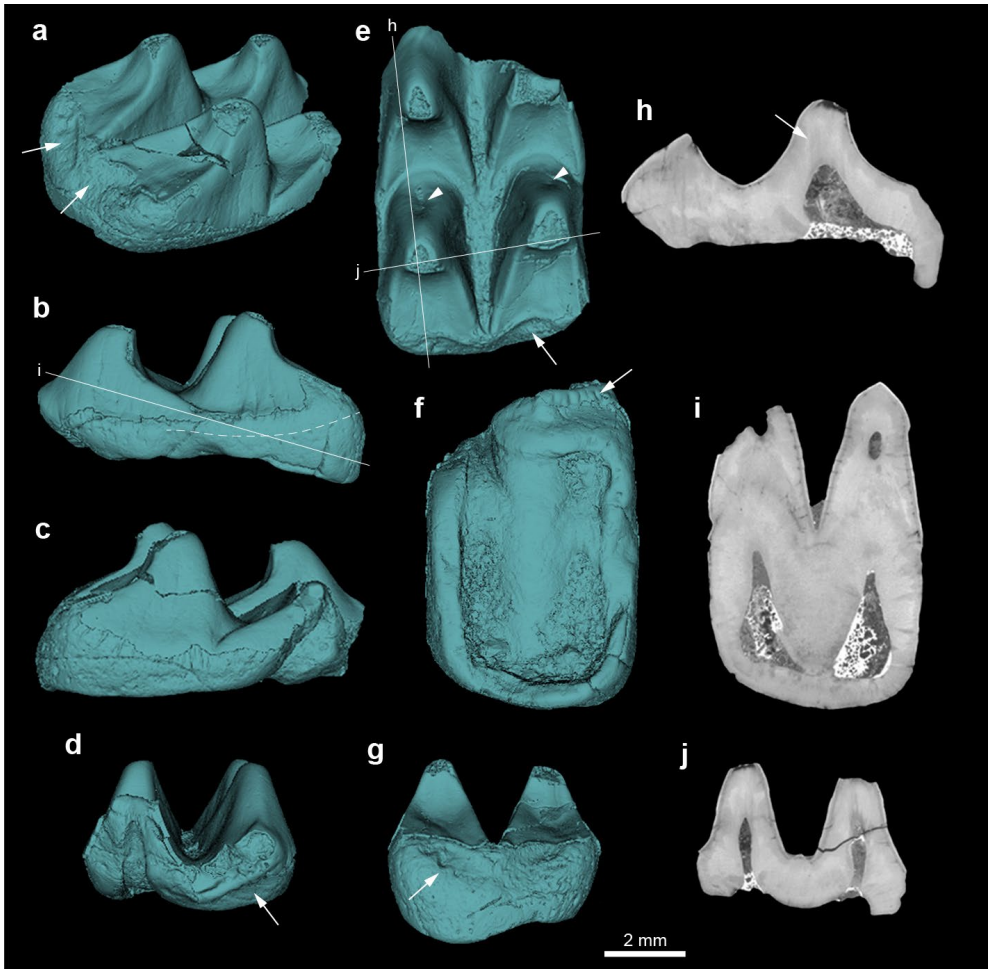

Fig. 4. Digital reconstruction and CT slice data of NHMD 1725979. **a,** Oblique posterolingual view of the tooth. Arrows mark the PIA. **b,** Buccal view of the fossil. The dotted line marks the pseudo-cingulid, while the solid line indicates the orientation of the CT slice depicted in panel **i**. **c,** The tooth depicted in lingual view. **d,** Anterior view of NHMD 1725979. Arrow indicates the AIA. **e,** The fossil in occlusal view. Note shallow depressions on the anterior face of b2 and l2 (arrowheads). Arrow denotes the PIA, while the lines indicate the orientation of the CT slice data depicted in panel **h** and **j**, respectively. **f,** Base of the crown. Arrow marks the AIA. **g,** Posterior view of NHMD 1725979. Arrow denotes the PIA. **h,** Longitudinal CT slice through cusp b2 and parts of b1, showing the pulp cavity of b2. Striations radiating from the pulp cavity likely represent growth lines, and are indicated by an arrow. **i,** Section placed transversely through the cusp bases. The pulp cavities of l2 and b2 can be seen, as well as the beginning of this cavity in b1. **j,** Buccolingual section through b2 and l2. Note prominent pulp cavities.

area (PIA) and parts of the anterior interlocking area (AIA) are preserved, the cusp rows are considered to be complete.

The cusp formula of NHMD 1725979 can be described as '2-2'; i.e., comprising two longitudinal rows of cusps with two principal cusps [lingual (l) 1 and 2, and buccal (b) 1 and 2, respectively] in each row (Figs 2, 3a, 4a, e). The buccal cusp row is located slightly posterior to the lingual one, and the two rows are separated by a V-shaped intercuspal groove (Figs 3a, 4d, e, g). In buccal and lingual aspects, the crescentic cusps are of sub-equal proportions, measuring (as preserved) 2.3 (l2), 2.6 (b1) and 2.6 (b2) mm in height, respectively (l1 is mostly missing; Figs 3c, d, 4b, c). In occlusal view, a shallow depression can be seen on the anterior face of l2 and b2 (Fig. 4e). Buccal and lingual ridges are well developed on all cusps, and those of l1 and b1 embrace the base of l2 and b2, respectively (Figs 3d, 4b). The medial ridges of l1 and b1 reach the intercuspal groove, but do not fuse (Figs 3a, 4e, j). In contrast, the medial ridges of l2 and b2 meet at their basal termination, creating a M-shaped structure adjacent to the PIA (Figs 3a, 4a, e).

The occlusal outline of NHMD 1725979 likely was broadly rhomboidal when the tooth was functional (Figs 3a, 4e). Moreover, even though the lingual half of the anterior edge is broken, it is evident that this margin originally must have been indented (based on traces of a deep sulcus in between the first pair of cusps; Figs 3a, 4e). In buccal view (Fig. 4b), the base of the crown is developed into a weak anteroposterior ridge (a 'pseudo-cingulid' *sensu* Panciroli *et al*. 2017).

The PIA consists of two shallow embayments with faint, longitudinal ridging ('chaotic enamel'; see Panciroli *et al*. 2017) (Fig. 4a). These indentations are separated by the posterior termination of the medial ridges, giving the PIA a slightly M-shaped appearance in occlusal view (Figs 3a, 4e). The preserved portion of the AIA in turn comprises a distinctly ridged, enamel-covered buccolingual projection (Fig. 3b).

Judging from the micro-CT slices, the enamel measures approximately 0.1 mm in thickness. Within the dentine, presumed growth lines can be seen as striations emerging from the pulp cavities and radiating outward towards the enamel (Fig. 4h).

Comparisons and remarks. Given the close morphological similarity between NHMD 1725979 and previously described tritylodontid teeth with a 2-2 cusp formula and V-shaped intercuspal groove (e.g., Lopatin & Agadjanian 2008; Matsuoka *et al*. 2016; Panciroli *et al*. 2017), the fossil from Bornholm is here referred to as a left lower postcanine of that group.

In many basal tritylodontids, there are often small-sized accessory cusps on the lower postcanines in the vicinity of the PIA (e.g., Kemp 1982; Luo & Sun 1994). Such cuspules are, however, lacking in NHMD 1725979, and instead the PIA resembles that of derived taxa (see, e.g., Lopatin & Agadjanian 2008; Panciroli *et al*. 2017). Given that NHMD 1725979 comprises an isolated postcanine that is lacking the root and additionally represents the first tritylodontid remain from Scandinavia, assignment to a specific genus or species is difficult; something that is further compounded by the fact that the general morphology of the tooth compares favourably with derived taxa from the Middle Jurassic to Lower Cretaceous rather than coeval (basal) forms. Therefore, a detailed comparison with all relevant tritylodontid genera follows below.

Oligokyphus – the most widespread tritylodontid during the Upper Triassic – Lower Jurassic interval – is commonly described as having a lower cusp formula of 3-3, where the lingual cusps are slightly larger than the buccal ones (e.g., Kühne 1956; Sues 1985b; Luo & Sun 1994; Fedak *et al*. 2015). However, in some cases, lower teeth assigned to this genus reportedly possess a 2-2 pattern; these accounts probably pertain to more posteriorly located postcanines (Kühne 1956; Sues 1985b; Luo & Sun 1994). In any event, the cusp rows are not offset relative to one another as in NHMD 1725979. The shape of the posterior margin and PIA also differ from those of NHMD 1725979, and lower postcanines of *Oligokyphus* additionally can be equipped with an accessory cusp on the buccal side of the PIA (Kühne 1956; Sues 1985b; Luo & Sun 1994).

Lower teeth of *Tritylodon* have been variously described as having a 3-3 (Panciroli *et al*. 2017) or 2-2 (Kermack 1982) cusp formula. In similarity with *Oligokyphus*, *Tritylodon* does not have offset cusp rows. Furthermore, the PIA of the lower postcanines has a rounded occlusal outline, plus there are both cuspules in the vicinity of the PIA and an anterior cingulum in front of l1 and b1 (contra NHMD 1725979; see Kühne 1943).

Lower postcanines of *Bienotherium* have a cusp formula of 2-2, and the teeth occasionally are equipped with accessory cusps (Young 1940, 1947; Luo & Wu 1994). Even though this pattern matches that of NHMD 1725979 (save for the presence of cuspules), the anterior cusp pair is substantially larger than the posterior one in *Bienotherium* (Young 1947; Luo & Wu 1994). Therefore, NHMD 1725979 cannot be confidently assigned to that genus. The same reasoning can be applied to *Kayentatherium* because this taxon also has larger anterior cusps in the lower postcanines (Kermack 1982; Sues *et al*. 1994).

Various sources (e.g., Luo & Sun 1994; Matsouka & Setoguchi 2000) indicate that lower postcanines of *Lufengia* have a cusp formula of 2-2; others (e.g., Young 1974) state 3-3. Because of this discrepancy,

some authors (e.g., Luo & Wu 1994) have suggested that *Lufengia* has a 3-3 pattern in the first two lower postcanines and a 2-2 pattern further back in the jaw. However, well-preserved material from the Lufeng locality of China described recently by Liu *et al*. (2022), demonstrates that all lower postcanines of this genus have a 2-2 cusp formula. Because the anterior cusps are somewhat larger than the posterior ones, and the posterior crown margin additionally is curved (in occlusal view), NHMD 1725979 cannot be referred to *Lufengia*.

No detailed description of lower postcanines of the Lower Jurassic *Dinnebitodon* has been published to date. The type material includes four lower postcanines with a 2-2 cusp formula (Sues 1986c; Sues *et al*. 1994). Sues (1986b) also mentions the existence of isolated jaw fragments, stating in passing that the lower postcanines have a cusp formula comparable to that of *Kayentatherium*. No figures depicting these remains have been published, however, and size information is currently lacking (other than that *Dinnebitodon* is within the same size range as *Kayentatherium*; Sues 1986b, c). Due to the limited material documented in the scientific literature, NHMD 1725979 cannot be compared with teeth of *Dinnebitodon*.

Published descriptions of lower postcanines assigned to *Yunnanodon* focus mostly on the root morphology (e.g., Cui & Sun 1987). Despite this, it has been noted that the crowns have a 2-2 cusp formula, occasionally accompanied by an accessory cusp (Luo & Wu 1994). Due to the poor documentation of lower postcanines of *Yunnanodon*, NHMD 1725979 cannot be compared with that genus.

Stereognathus, *Bienotheroides* and *Polistodon* are all more advanced tritylodontids (e.g., Panciroli *et al*. 2017), and their lower postcanines bear striking morphological resemblance to NHMD 1725979. This is interesting when considering the time discrepancy between these Middle Jurassic genera and the Pliensbachian NHMD 1725979. *Stereognathus*, *Bienotheroides* and *Polistodon* share a 2-2 cusp formula of their lower postcanines. Moreover, all cusps are of sub-equal size, the posterior border is rather straight, and a deep, V-shaped intercuspal groove separates the two cusp rows from one another (He & Cai 1984; Sun 1984; Matsuoka & Setoguchi 2000; Watabe *et al*. 2007; Avieranov *et al*. 2017; Panciroli *et al*. 2017). *Bienotheroides* is generally not considered to be as specialised as *Stereognathus* and *Polistodon* and is distinguished from the latter by the morphology of the upper dentition, which features a cusp formula of 2-3-3 (Watabe *et al*. 2007). However, there are also morphological differences between lower postcanines of these genera, which can be used for comparative purposes. Firstly, both *Stereognathus* and *Polistodon* have offset cusp rows, where the individual cusps have shifted slightly posteriorly on the buccal side of the crowns (He & Cai 1984; Matsuoka & Setoguchi 2000; Avieranov *et al*. 2017; Panciroli *et al*. 2017); the cusps seem to be more displaced in *Stereognathus* than they are in *Polistodon* (He & Cai 1984; Matsuoka & Setoguchi 2000; Panciroli *et al*. 2017). In contrast, *Bienotheroides* has sub-parallel cusp rows (Young 1982; Sun 1984; Matsuoka & Setoguchi 2000; Watabe *et al*. 2007; Panciroli *et al*. 2017). When comparing the cusp arrangement in *Polistodon* and *Stereognathus* with NHMD 1725979, the two rows in the isolated tooth from Bornholm appear to be more offset than in *Polistodon*, but less so than in *Stereognathus*. Nonetheless, the offset cusp rows result in a slanting of the otherwise rather straight posterior edge in lower postcanines of both genera.

The PIA of *Stereognathus* consists of two deep pockets containing longitudinal ridges and, occasionally, also vestigial cuspules (Avieranov *et al*. 2017; Panciroli *et al*. 2017). These embayments, which are separated by the intercuspal groove, give the PIA an M-shaped occlusal outline (Avieranov *et al*. 2017; Panciroli *et al*. 2017). A similar PIA is present also on teeth of *Bienotheroides*, but seemingly do not exist in teeth of *Polistodon* (Sun 1984; He & Cai 1984). The PIA of *Stereognathus* closely resembles that of NHMD 1725979, with deep embayments and longitudinal ridging. However, cuspules are not present in NHMD 1725979.

The anterior edge of lower postcanines attributed to *Stereognathus* is M-shaped in occlusal view due to a deep depression that separates l1 from b1 (e.g., Averianov *et al*. 2017; Panciroli *et al*. 2017). Conversely, teeth of *Bienotheroides* and *Polistodon* show a less pronounced inclination (He & Cai 1984; Sun 1984; Matsuoka & Setoguchi 2000; Watabe *et al*. 2007). Given that NHMD 1725979 is abraded on the lingual side, it is difficult to determine whether its anterior margin originally was as distinctly M-shaped as it is in *Stereognathus*.

The AIA of *Stereognathus* consist of a slightly convex buccolingual shelf with longitudinal ridging (Averianov *et al*. 2017; Panciroli *et al*. 2017), much like that in NHMD 1725979. Some lower postcanines of *Bienotheroides* have been reported as possessing an accessory cusp at the anterior end of the buccal row (Sun 1984), a feature that cannot be determined in NHMD 1725979 because of extensive wear.

The cusp arrangement also differs between *Bienotheroides* and the more derived genera *Polistodon* and *Stereognathus* (Matsuoka & Setoguchi 2000). While *Bienotheroides* has non-overlapping anterior and posterior cusps (Sun 1984; Matsuoka & Setoguchi 2000), the anterior cusps partially straddle the posterior ones in *Polistodon* and *Stereognathus*, thereby creating a more complex lateral profile (He & Cai 1984; Matsuoka & Setoguchi 2000; Panciroli *et al*. 2017). In addition,

lower postcanines of *Polistodon* and *Stereognathus* are equipped with a pseudo-cingulid that can be seen in buccal view (He & Cai 1984; Panciroli *et al*. 2017). NHMD 1725979 has a cusp arrangement that resembles that in *Polistodon* and *Stereognathus*, as well as a possible pseudo-cingulid (although the latter could be an artefact of preservation).

Lower postcanines of the Upper Jurassic – Lower Cretaceous tritylodontids *Shartegodon*, *Nuurtherium*, *Montirictus*, and *Xenocretosuchus* all have a cusp formula of 2-2. Moreover, the crescentic cusps are of subequal size. The teeth further have a slightly M-shaped anterior edge and a deep, V-shaped intercuspal groove (Tatarinov & Matchenko 1999; Lopatin & Agadjanian 2008; Matsuoka *et al*. 2016; Velazco *et al*. 2017). Teeth of *Shartegodon*, *Montirictus* and *Xenocretosuchus* have offset cusp rows, and accordingly also a slanting posterior edge (Tatarinov & Matchenkov 1999; Lopatin & Agadjanian 2008; Matsuoka *et al*. 2016; Velazco *et al*. 2017). The cusp rows in *Montirictus* seem to be more offset than in *Shartegodon* and *Xenocretosuchus* (Tatarinov & Matchenko 1999; Matsuoka *et al*. 2016; Velazco *et al*. 2017). *Nuurtherium* is described as having cusp b1 offset relative to l1, but not b2 relative to l2 (Velazco *et al*. 2017).

The AIA and PIA are poorly described for *Shartegodon* and *Nuurtherium*. However, according to Panciroli *et al*. (2017), the PIA of these genera resembles that of *Stereognathus*, with two embayments separated by an intercuspal groove. *Montirictus* and *Xenocretosuchus* also share this feature, with similar interlocking properties as in *Stereognathus*, including ridged enamel and a M-shaped PIA in occlusal view (Lopatin & Agadjanian 2008; Matsuoka *et al*. 2016; Panciroli *et al*. 2017). The AIA of *Montirictus* differs somewhat from that of *Stereognathus* (and NHMD 1725979); rather than being developed into a vertically ridged shelf, the AIA of *Montirictus* includes rounded projections with a wrinkled surface (Lopatin & Agadjanian 2008; Matsuoka *et al*. 2016). Vestigial cuspules in the PIA (as described for *Stereognathus*) have also been observed in *Xenocretosuchus* and *Shartegodon* (Panciroli *et al*. 2017). With the exception of cuspules, the PIA of lower postcanines of *Montirictus*, *Xenocretosuchus*, *Shartegodon*, and *Nuurtherium* is very similar to that of NHMD 1725979.

In conclusion, the genera that most closely resemble NHMD 1725979 include *Polistodon*, *Montirictus*, *Nuurtherium*, *Stereognathus*, *Xenocretosuchus*, and *Shartegodon* [note that Averianov *et al*. (2017) synonymised *Polistodon*, *Montirictus* and *Xenocretosuchus* with *Stereognathus*]. Nonetheless, when considering the difficulty in assigning isolated lower postcanines to a specific taxon, the Hasle Formation fossil cannot be placed in any known genus with confidence.

Discussion

The time discrepancy between the Pliensbachian NHMD 1725979 and derived tritylodontids, to which it shares the closest morphological resemblance, is noteworthy. Three possible explanations exist for this incongruity:

1. NHMD 1725979 belongs to one of the genera from the Upper Triassic – Lower Jurassic interval in which lower postcanines are either unknown or poorly described (e.g., *Yunnanodon*, *Dianzhongia* and *Dinnebitodon*);
2. NHMD 1725979 represents a temporally early occurrence of a derived tritylodontid, most likely a member of the *Stereognathus* group. In effect, this would push back the evolutionary history of more advanced tritylodontids from the Middle to Lower Jurassic;
3. NHMD 1725979 represents a new genus and species that has yet to be formally described, which is not entirely unlikely as no previous tritylodontid records exist from Scandinavia.

Hopefully, future discoveries on Bornholm and elsewhere will clarify which of the above listed scenarios is the correct one. Notably, though, NHMD 1725979 shows that the process of cusp reduction in lower postcanines of tritylodontids had been initiated already by the Lower Jurassic [see Panciroli *et al*. (2017) for details].

Traditionally, the Hasle Formation has been interpreted as representing a nearshore, yet fully marine, depositional environment based on sedimentological features (which include well-sorted sandstones and large-scale hummocky cross stratification) and a fossil biota dominated by oceangoing animals (e.g., Gravesen *et al*. 1982; Surlyk & Noe-Nygaard 1986; Koppelhus & Nielsen 1994; Rees 1998). However, recent palaeontological evidence suggests that the Hasle Formation likely was more terrestrially influenced than previously thought. For instance, the discovery of a small theropod footprint (see Milàn & Surlyk 2015) indicates that weathering patterns with strong coastal winds might have contributed to periods with extremely low water stand, which could have created floodplain-like environments. Additional finds of nonavian dinosaur dental and skeletal remains further strengthen this partially revised environmental interpretation (Milàn & Mateus 2024; Molin *et al*. unpublished), as does the tritylodontid tooth described herein.

Conclusions

- A single tooth (NHMD 1725979) from the Lower Jurassic (Pliensbachian) Hasle Formation on the Island of Bornholm, Denmark, is identified as belonging to a tritylodontid synapsid.
- NHMD 1725979 represents the first Scandinavian record of a non-mammaliamorph cynodont, and possibly the oldest record of a derived tritylodontid.
- Together with recent discoveries of nonavian dinosaur remains, NHMD 1725979 strengthens the interpretation that the Hasle Formation fauna contains a substantial terrestrial component.

Acknowledgments

We are grateful to Marianne Falbe Nattestad of Bornholm, who found NHMD 1725979 and brought it to our attention. This work was supported by a project grant (#2020-03542) from the Swedish Research Council to J.L. Comments by journal referees Chang-Fu Zhou and Jiawen Liu helped to improve the paper.

References

Averianov, A.O., Martin, T., Lopatin, A.V., Schultz, J.A., Skutschas, P.P., Rico, S. & Krasnolutskii, S.A. 2017: A tritylodontid synapsid from the Middle Jurassic of Siberia and the taxonomy of derived tritylodontids. Journal of Vertebrate Paleontology 37, e1363767. https://doi.org/10.1080/02724634.2017.1363767

Bonaparte J.F. 1970: Annotated list of the South American Triassic tetrapods. Second Gondwana Symposium, Proceedings and Papers 1, 665–682.

Clark, J.M. & Hopson, J.A. 1985: Distinctive mammal-like reptile from Mexico and its bearing on the phylogeny of the Tritylodontidae. Nature 315, 398–400. https://doi.org/10.1038/315398a0

Cope, E.D. 1884: The Tertiary Marsupialia. The American Naturalist 18, 686–697. https://doi.org/10.1086/273711

Cui, G. & Sun, A. 1987: Postcanine root systems in tritylodontids. Vertebrata PalAsiatica 25, 245–259.

Donovan, D.T. & Surlyk, F. 2003: Lower Jurassic (Pliensbachian) ammonites from Bornholm, Baltic Sea, Denmark. Geological Survey of Denmark and Greenland Bulletin 1, 555–583. https://doi.org/10.34194/geusb.v1.4684

Duffin, C.J. & Milàn, J. 2017: A new myriacanthid holocephalian from the Early Jurassic of Denmark. Bulletin of the Geological Society of Denmark 65, 161–170. https://doi.org/10.37570/bgsd-2017-65-10

Duffin, C.J. & Milàn, J. 2022: Further holocephalian remains from the Hasle Formation (Early Jurassic) of Denmark. Bulletin of the Geological Society of Denmark 70, 139–149. https://doi.org/10.37570/bgsd-2022-70-10

Fedak, T.J., Sues, H.-D. & Olsen, P.E. 2015: First record of the tritylodontid cynodont *Oligokyphus* and cynodont postcranial bones from the McCoy Brook Formation of Nova Scotia, Canada. Canadian Journal of Earth Sciences 52, 244–249. https://doi.org/10.1139/cjes-2014-0220

Fedorov, A. *et al*. 2012: 3D Slicer as an image computing platform for the Quantitative Imaging Network. Magnetic Resonance Imaging 30, 1323–1341. https://doi.org/10.1016/j.mri.2012.05.001

Graversen, O. 2009: Structural analysis of superimposed fault systems of the Bornholm horst block, Tornquist Zone, Denmark. Bulletin of the Geological Society of Denmark 57, 25–49. https://doi.org/10.37570/bgsd-2009-57-02

Gravesen, P., Rolle, F. & Surlyk, F. 1982: Lithostratigraphy and sedimentary evolution of the Triassic, Jurassic and Lower Cretaceous of Bornholm, Denmark. Danmarks Geologiske Undersøgelse Serie B7, 51 pp. https://doi.org/10.34194/serieb.v7.7062

Hammer, W.R. & Smith, N.D. 2008: A tritylodont postcanine from the Hanson Formation of Antarctica. Journal of Vertebrate Paleontology 28, 269–273. https://doi.org/10.1671/0272-4634(2008)28[269:atpfth]2.0.co;2

He, X. & Cai, K. 1984: The tritylodont remains from Dashanpu, Zigong. Journal of Chengdu College of Geology (Special paper on dinosaurian remains of Dashanpu, Zigong, Sichuan [II]), 33–45.

Hennig, E. 1922: Die Säugerzähne des württembergischen Rhät–Lias–Bonebeds. Neues Jahrbuch für Mineralogie, Geologie und Paläontologie 46, 181–267.

Hopson, J.A. & Barghusen H.R. 1986: An analysis of therapsid relationships. In: Hotton, N., Maclean, P.D., Roth, J.J. & Roth E.C. (eds): The ecology and biology of mammal-like reptiles, 83–106. Washington: Smithsonian Institution Press.

Hopson, J.A. & Kitching, J.W. 2001: A probainognathian cynodont from South Africa and the phylogeny of nonmammalian cynodonts. Bulletin of the Museum of Comparative Zoology 156, 5–35. https://doi.org/10.7934/p3187

Hu, Y., Meng, J. & Clark, J.M. 2009: A new tritylodontid from the Upper Jurassic of Xinjiang, China. Acta Palaeontologica Polonica 54, 385–391. https://doi.org/10.4202/app.2008.0053

Höhne, R. 1933: Beiträge zur Stratigraphie, Tektonik und Paläogeographie des südbaltischen Rhät–Lias, insbesondere auf Bornholm. Abhandlungen aus dem Geologisch-Paläontologischen Institut der Universität Greifswald 12, 105 pp.

Kalthoff, D.C., Schulz-Kornas, E., Corfe, I., Martin, T., Mcloughlin, S. & Schultz, J.A. 2019: Complementary approaches to tooth wear analysis in Tritylodontidae (Synapsida, Mammaliamorpha) reveal a generalist diet. PLoS ONE 14, e0220188. https://doi.org/10.1371/journal.pone.0220188

Kemp, T.S. 1982: Mammal-like reptiles and the origin of mammals, 363 pp. London: Academic Press.

Kermack, D. 1982: A new tritylodontid from the Kayenta Forma-

tion of Arizona. Zoological Journal of the Linnean Society 76, 1–17. https://doi.org/10.1111/j.1096-3642.1982.tb01953.x

Kočí, T., Milàn, J., Jacobsen, S.L., Jäger, M. & Bashforth, A. 2024: *Serpula*? *alicecooperi* sp. nov. – a new serpulid from the Lower Jurassic (Pliensbachian) Hasle Formation of Bornholm, Denmark. Bulletin of the Geological Society of Denmark 73, 41–56. https://doi.org/10.37570/bgsd-2023-72-05

Koppelhus, E.B. & Nielsen, L.H. 1994: Palynostratigraphy and palaeoenvironments of the Lower to Middle Jurassic Bagå Formation of Bornholm, Denmark. Palynology 18, 139–194. https://doi.org/10.1080/01916122.1994.9989443

Kühne, W.G. 1943: The dentary of *Tritylodon* and the systematic position of the Tritylodontidae. Journal of Natural History 10, 589–601. https://doi.org/10.1080/00222934308527377

Kühne, W.G. 1956: The Liassic therapsid *Oligokyphus*. Trustees of the British Museum, London, 149 pp. https://doi.org/10.5962/bhl.title.118726

Larsen, O. & Friis, H. 1991: Petrography, diagenesis and pore-water evolution of a shallow marine sandstone (Hasle Formation, Lower Jurassic, Bornholm, Denmark). Sedimentary Geology 72, 269–284. https://doi.org/10.1016/0037-0738(91)90015-6

Liu, J., Wang, L., Beatty, B.L., Zhang, G., Wang, T. & Bi, S. 2022: New material (Tritylodontidae, Mammaliamorpha) from the Lower Jurassic of Lufeng and its implication on the taxonomy of *Lufengia*. Historical Biology 35, 1605–1615. https://doi.org/10.1080/08912963.2022.2104643

Lopatin, A.V. & Agadjanian, A.K. 2008: A tritylodont (Tritylodontidae, Synapsida) from the Mesozoic of Yakutia. Doklady Biological Sciences 419, 107–110. https://doi.org/10.1134/s0012496608020117

Luo, Z.-X., Kielan-Jaworowska, Z. & Cifelli, R.L. 2002: In quest for a phylogeny of Mesozoic mammals. Acta Palaeontologica Polonica 47, 1–78.

Luo, Z. & Sun, A. 1994: *Oligokyphus* (Cynodontia: Tritylodontidae) from the Lower Lufeng Formation (Lower Jurassic) of Yunnan, China. Journal of Vertebrate Paleontology 13, 477–482. https://doi.org/10.1080/02724634.1994.10011526

Luo, Z. & Wu, X.-C. 1994: The small tetrapods of the Lower Lufeng Formation, Yunnan, China. In: Fraser, N.C. & Sues, H-D. (eds): The Shadow of the Dinosaurs – Early Mesozoic Tetrapods, 251–270. Cambridge University Press.

Malling, C. 1911: Hasle-sandstenens alder. Meddelelser fra Dansk Geologisk Forening 3, 629–631.

Malling, C. 1914: De Jespersenske Buelag i Lias paa Bornholm. Meddelelser fra Dansk Geologisk Forening 4, 265–270.

Malling, C. 1920: Den marine Lias og Wealden-Aflejringer paa Bornholm. Meddelelser fra Dansk Geologisk Forening 5, 55–57.

Malling, C. & Grönwall, K.A. 1909: En Fauna i Bornholms Lias. Meddelelser fra Dansk Geologisk Forening 3, 271–316.

Matsuoka, H. & Setoguchi, T. 2000: Significance of Chinese tritylodonts (Synapsida, Cynodontia) for the systematic study of Japanese materials from the Lower Cretaceous Kuwajima Formation, Tetori Group of Shiramine, Ishikawa, Japan. Asian Paleoprimatology 1, 161–176.

Matsuoka, H., Kusuhashi, N. & Corfe, I.J. 2016: A new Early Cretaceous tritylodontid (Synapsida, Cynodontia, Mammaliamorpha) from the Kuwajima Formation (Tetori Group) of central Japan. Journal of Vertebrate Paleontology 36, e1112289. https://doi.org/10.1080/02724634.2016.1112289

Milàn, J. & Bonde, N. 2001: Svaneøgler, nye fund fra Bornholm. Varv 2001, 3–8.

Milàn, J. & Mateus, O. 2024: A turiasaurian (Dinosauria, Sauropoda) tooth from the Pliensbachian Hasle Formation of Bornholm, Denmark, shows an Early Jurassic origin of the Turiasauria. Diversity 16, 12. https://doi.org/10.3390/d16010012

Milàn, J. & Mueller-Töwe, I. 2021: En havkrokodille fra Hasles fjerne fortid. Natur på Bornholm 19, 14–16.

Milàn, J. & Surlyk, F. 2015: An enigmatic, diminutive theropod footprint in the shallow marine Pliensbachian Hasle Formation, Bornholm, Denmark. Lethaia 48, 429–435. https://doi.org/10.37570/bgsd-2023-72-05

Osborn, H.F. 1903: On the primary division of the Reptilia into two sub-classes, Synapsida and Diapsida. Science 17, 275–276. https://doi.org/10.1126/science.17.424.275.c

Owen, R., 1861: Palaeontology or a systematic summary of extinct animals and their geological relations, 463 pp. Edinburgh: Adam and Charles Black.

Panciroli, E., Walsh, S., Fraser, N.C., Brusatte, S.L. & Corfe, I. 2017: A reassessment of the postcanine dentition and systematics of the tritylodontid *Stereognathus* (Cynodontia, Tritylodontidae, Mammaliamorpha), from the Middle Jurassic of the United Kingdom. Journal of Vertebrate Paleontology 37, e1351448.

Rees, J. 1998: Early Jurassic selechians from the Hasle Formation on Bornholm, Denmark. Acta Palaeontologica Polonica 43, 439–452.

Rowe, T. 1988: Definition, diagnosis, and origin of Mammalia. Journal of Vertebrate Paleontology 8, 241–264.

Rowe, T. 1993: Phylogenetic systematics and the early history of mammals. In: Szalay, F.S., Novacek, M.J. & McKenna, M.C. (eds): Mammal phylogeny: Mesozoic differentiation, Multituberculates, monotremes, early Therians, and Marsupials, 129–145. New York: Springer-Verlag.

Ruta, M., Botha-Brink, J., Mitchell, S.A. & Benton, M.J. 2013: The radiation of cynodonts and the ground plan of mammalian morphological diversity. Proceedings of the Royal Society B 280, 1–10.

Sandersen, P.B.E., Rasmussen, E.S., Bjerager, M., Jensen, J.B., Schovsbo, N. & Vosgerau, H. 2014: Skitser til opbygningen af en national 3D geologisk model for Danmark, Forslag til legende for den danske del af den nationale 3D geologiske model. Internal GEUS working paper, Rapport 2, 47 pp.

Setoguchi, T., Matsuoka, H. & Matsuda, M. 1999: New discovery of an Early Cretaceous tritylodontid (Reptilia, Therapsida) from Japan and the phylogenetic reconstruction of Tritylodontidae based on the dental characters. In: Wang Y. & Deng T. (eds): Proceedings of the Seventh Annual Meeting of the Chinese Society of Vertebrate Paleontology, 117–124. Beijing: China Ocean Press.

Simpson, G. 1928: A catalogue of the Mesozoic Mammalia in the Geological Department of the British Museum, 215 pp. Oxford University Press.

Smith, A.S. 2008: Plesiosaurs from the Pliensbachian (Lower Jurassic) of Bornholm, Denmark. Journal of Vertebrate Paleontology 28, 1213–1217. https://doi.org/10.1671/0272-4634-28.4.1213

Sues, H.-D. 1985a: The relationships of the Tritylodontidae (Synapsida). Zoological Journal of the Linnean Society 85, 205–217. https://doi.org/10.1111/j.1096-3642.1985.tb01503.x

Sues, H.-D., 1985b: First record of the tritylodontid *Oligokyphus* (Synapsida) from the Lower Jurassic of western North America. Journal of Vertebrate Paleontology 5, 328–335. https://doi.org/10.1080/02724634.1985.10011869

Sues, H.-D. 1986a: Relationships and biostratigraphic significance of the Tritylodontidae (Synapsida) from the Kayenta Formation of northeastern Arizona. In: Padian, K. (ed.): The beginning of the age of Dinosaurs: Faunal change across the Triassic–Jurassic bwoundary, 279–284. Cambridge University Press.

Sues, H.-D. 1986b: Skull and dentition of two tritylodontid synapsids from the Lower Jurassic of western North America. Bulletin of the Museum of Comparative Zoology 151, 217–268.

Sues, H.-D. 1986c: *Dinnebitodon amarali*, a new tritylodontid (Synapsida) from the Lower Jurassic of western North America. Journal of Paleontology 60, 758–762. https://doi.org/10.1017/s0022336000022277

Sues, H.-D. & Olsen, P. 2015: Stratigraphic and temporal context and faunal diversity of Permian-Jurassic continental tetrapod assemblages from the Fundy rift basin, eastern Canada. Atlantic Geology 51, 139–205. https://doi.org/10.4138/atlgeol.2015.006

Sues, H.-D., Clark, J.M. & Jenkins Jr., F.A. 1994: A review of the Early Jurassic tetrapods from the Glen Canyon Group of the American southwest. In: Fraser, N.C. & Sues, H.-D. (eds) In the shadow of the Dinosaurs – Early Mesozoic Tetrapods, 284–294. Cambridge University Press.

Sun A.L. 1984: Skull morphology of the tritylodont genus *Bienotheroides* of Sichuan. Scientia Sinica Series B 27, 970–984.

Surlyk, F. & Noe-Nygaard, N. 1986: Hummocky cross-stratification from the Lower Jurassic Hasle Formation of Bornholm, Denmark. Sedimentary Geology 46, 259–273. https://doi.org/10.1016/0037-0738(86)90062-x

Tatarinov, L. & Matchenko, E. 1999: A find of an aberrant tritylodont (Reptilia, Cynodontia) in the Lower Cretaceous of the Kemerovo region. Paleontological Journal 33, 422–428.

Velazco, P.M., Buczek, A.J. & Novacek, M.J. 2017: Two new tritylodontids (Synapsida, Cynodontia, Mammaliamorpha) from the Upper Jurassic, southwestern Mongolia. American Museum Novitates 2017, 1–35. https://doi.org/10.1206/3874.1

Watabe, M., Tsubamoto, T. & Tsogtbaatar, K. 2007: A new tritylodontid synapsid from Mongolia. Acta Palaeontologica Polonica 52, 263–274.

Watson, D.M.S. 1942: On Permian and Triassic tetrapods. Geological Magazine 79, 81–116. https://doi.org/10.1017/s0016756800074835

Young, C.C. 1940: Preliminary notes on the Mesozoic mammals of Lufeng, Yunnan, China. Bulletin of the Geological Society of China 20, 93–111. https://doi.org/10.1111/j.1755-6724.1940.mp20001009.x

Young, C.C. 1947: Mammal-like reptiles from Lufeng, Yunnan, China. Proceedings of the Zoological Society of London 1, 537–597. https://doi.org/10.1111/j.1096-3642.1947.tb00537.x

Young, C.C. 1974: New material of therapsids from Lufeng, Yunnan. Vertebrata PalAsiatica 12, 111–114.

Young, C.C. 1982: On a *Bienotherium*-like tritylodont from Szechuan, China. Selected Works of Yang Zhongjian, 10–13.

Instructions to authors

See also www.2dgf.dk/publikationer/bulletin/vejledning.html

The Bulletin publishes articles normally not exceeding 30 printed pages, and short contributions not longer than 4 pages. Longer articles and monographs are also published, but in this case it is advisable to consult the chief editor before submitting long manuscripts. Short contributions may be comments on previously published articles, presentation of current scientific activities, short scientific notes, or book reviews.

Manuscripts with complete sets of illustrations, tables, captions, etc., should be submitted electronically to the chief editor (obe@geus.dk). The **main text** with references and figure captions should be in Word format, figures should be in either pdf, jpeg, or tiff format, and tables should be in Excel or Word format. Word tables should be ordinary text files with tab spacing between table columns; Word's 'table function' is discouraged. Compare published articles for table layout.

Manuscripts will be reviewed by two referees; suggestions of referees are welcome. The final decision on whether or not a manuscript will be accepted for publication rests with the chief editor, acting on the advice of the scientific editors. Articles will be published in the order in which they are accepted and produced for publication.

Manuscript

Language – Manuscripts should be in English. Authors who are not proficient in English should ask an English-speaking colleague for assistance before submission of the manuscript.

Title – Titles should be short and concise, with emphasis on words useful for indexing and information retrieval. An abbreviated title to be used as running title may also be submitted.

Abstract – An abstract in English must accompany all papers. It should be short, factual, and stress new information and conclusions rather than describing the contents of the manuscript. Conclude the abstract with a list of key words.

Main text – Use 1.5 or double spacing throughout and leave wide margins. Italics should be used only in generic and species names and in some Latin abbreviations (e.g. c, *et al.*, ibid., op. cit).

Spelling – Geological units named after localities in Greenland, formal lithostratigraphical units and intrusions named after localities in Greenland remain unchanged even if the eponymous locality names have since been changed in accordance with modern Greenlandic orthography.

References to figures, tables and papers – References to figures and tables in the text should have the form: Fig. 1, Figs 1–3, Table 3 or as (Smith 1969, fig. 3) when the reference is to a figure in a cited paper.

References to papers are given in the form Smith (1969) or (Smith 1969). Combined citations by different authors are separated by a semicolon; two or more papers by same author(s) are separated by commas. Citations are mentioned chronologically and then alphabetically. Use '*et al.*' for three or more authors, e.g. Smith *et al.* (1985).

Reference list

Use the following style:

Smith, A.A. 1989: Geology of the Bulbjerg Formation. Bulletin of the Geological Society of Denmark 38, 119–144. [Note that name of journal is given in full].

Smith, A.A., Jensen, B.B. & MacStuff, C.C. 1987: Sandstones of Denmark, 2nd edition, 533 pp. New York: Springer Verlag. [For more than 10 authors, use first author followed by *et al.*].

Smith, A.A., Jensen, B.B. & MacStuff, C.C. 1992: Characterization of Archean volcanic rocks. In: Hansen, D.D. *et al.* (eds): Geology of Greenland. Geological Survey of Denmark and Greenland Bulletin 40, 1397–1438. [More than three editors – therefore *et al.* form is used].

Sorting – Danish letters æ, ø and å (aa) are treated as ae, o and a (aa), respectively.

References are sorted by:

1) Alphabetically by the first author's surname. 2) Papers by one author: two or more papers are arranged chronologically. 3) Papers by two authors: alphabetically after second author's name. Two or more papers by the same two authors: chronologically. 4) Papers by three or more authors: chronologically. Papers from the same year are arranged alphabetically after second, third, etc. author's name. Authors themselves are responsible for the accuracy and completeness of their references. The reference list must include all, and only, the references cited in the paper (including figures, tables etc).

CrossRef

Please add hyperlinks to Crossref DOI when you create your list of references whenever possible.

Illustrations

May be prepared in either black and white or colour. There is no colour charge. Horizontal illustrations are much to be preferred. Size of smallest letters in illustrations should not be less than 5.5 pt. Remember scale.

All figures (including photographs) should be submitted in electronic form ready for direct reproduction, i.e. having the dimensions of the final figure with a standard resolution of 300 dpi for photographs. Preferred formats are pdf, tiff and jpg.

Size – Width: All widths up to full page width (170 mm) are accepted. Maximum height is 223 mm. Design figure contents to match the preferred figure size.

Captions – Captions to figures and plates must be delivered on separate pages, preferably at the end of the manuscript.

Supplementary data files

Supplementary files are accepted. Such files may provide e.g. analytical data tables, detailed data documentation, illustrations with special effects, or videos.

Proofs

Authors receive page proofs of the article after technical production. The cost of any alterations against the final manuscript will be charged to the author.

Content, vol. 73

Instructions to authors:
See inside the back cover and also www.2dgf.dk/publikationer/bulletin/vejledning.html